Arthritis & Rheumatology

An Official Journal of the American College of Rheumatology
www.arthritisrheum.org and wileyonlinelibrary.com

Editor
S. Louis Bridges, Jr., MD, PhD, *New York*

Deputy Editors
Karen H. Costenbader, MD, MPH, *Boston*
Mariana J. Kaplan, MD, *Bethesda*
Kenneth G. Saag, MD, MSc, *Birmingham*

Co-Editors
Edward M. Behrens, MD, *Philadelphia*
David T. Felson, MD, MPH, *Boston*
Richard F. Loeser Jr., MD, *Chapel Hill*

Editor-in-Chief Emeriti
Richard Bucala, MD, PhD, *New Haven*
Daniel H. Solomon, MD, MPH, *Boston*

Journal Publications Committee
Chair - Betty Tsao, PhD, *Charleston*

Member - ARP Liaison
Cynthia Crowson, PhD, *Stewartville*

Members
Elana Bernstein, MD, MSc, *New York*
Krati Chauhan, MD, PhD, *Burlington*
Himanshu Vashistha, PhD, MBA, *Great Neck*
Marwin Groener, MD, FIT Member, *Baltimore*
Mark Hwang, MD, MS, Member, *Houston*
Eric Roberts, MPH, PhD, ARP Member, *San Francisco*

Editorial Staff
Susan Case, *Vice President, Strategic Marketing, Communications and Publishing, Maryland*
Maggie Parry, *Director, Quality and Production, Georgia*
Brian T. Robinson, *Director, Digital Content, Pennsylvania*
Christy Austin, *Publishing Coordinator, Washington*
Laura Bolte, *Managing Editor, North Carolina*

Associate Editors
Rohit Aggarwal, MD, *Pittsburgh*
Ivona Aksentijevich, MD, PhD, *Bethesda*
Marta Alarcón-Riquelme, MD, PhD, *Stockholm, Sweden*
Elizabeth Arkema, ScD, *Stockholm*
Neil Basu, MD, PhD, *Scotland*
Ashira D. Blazer, MD, MSCI, *Baltimore*
Nunzio Bottini, MD, PhD, *Los Angeles*
John Carrino, MD, MPH, *New York*
Andrew Cope, MD, PhD, *London, UK*
Jeffrey Curtis, MD, MS, MPH, *Birmingham*
Nicola Dalbeth, MBChB, MD, FRCP, *Auckland, NZ*
Maria Danila, MD, MS, *Birmingham*
Christopher Denton, PhD, FRCP, *London, UK*
Doruk Erkan, MD, *New York*
Carol Feghali-Bostwick, PhD, *Charleston*
Richard A. Furie, MD, *Great Neck*
Hassan Ghomrawi, PhD, MPH, *Birmingham*
V. Michael Holers, MD, *Aurora*
J. Michelle Kahlenberg, MD, PhD, *Ann Arbor*
Wan-Uk Kim, MD, PhD, *Seoul, Korea*
Jason S. Knight, MD, PhD, *Ann Arbor*
Carl D. Langefeld, PhD, *Winston-Salem*
Katherine Liao, MD, MPH, *Boston*
Tony R. Merriman, PhD, *Birmingham*
Sara S. McCoy, MD, PhD, *Milwaukee*
Dennis McGonagle, FRCPI, PhD, *Leeds*
Rachel E. Miller, PhD, *Chicago*
Yukinori Okada, MD, PhD, *Osaka, Japan*
Karen B. Onel, MD, *New York*
Dana Orange, MD, MS, *New York*
Janet E. Pope, MD, MPH, FRCPC, *London, Ontario, Canada*
Lisa G. Rider, MD, *Bethesda*
Christopher T. Ritchlin, MD, MPH, *Rochester*
Amr Sawalha, MD, *Pittsburg*
Carla R. Scanzello, MD, PhD, *Philadelphia*
Georg Schett, MD, *Erlangen, Germany*
Gabriela Schmajuk, MD, *Palo Alto*
Raphaèle Seror, MD, PhD, *Becetre, France*
Jasvinder Singh, MD, MPH, *Houston*
Robert F. Spiera, MD, *New York*
Yoshiya Tanaka, MD, PhD, *Kitakyushu, Japan*
Ranjeny Thomas, MBBS, *Queensland*
Fei Wang, PhD, *New York*
Baohong Zhao, PhD, *New York*

Advisory Editors
Hannah C. Ainsworth, PhD, *Winston-Salem*
Matthew C. Baker, MD, MS, *Palo Alto*
Jamie Collins, PhD, *Boston*
Kelsey Collins, PhD, *San Francisco*
Kristen Demoruelle, MD, PhD, *Denver*
Anisha Dua, MD, MPH, *Chicago*
David Fernandez, MD, PhD, *New York*
Shivani Garg, MD, PhD, *New Haven*
Peter Grayson, MD, MSc, *Bethesda*
Lauren Henderson, MD, MMSc, *Boston*
Monique Hinchcliff, MD, MS, *New Haven*
Evelyn Hsieh, MD, PhD, *New Haven*
Deanna P. Jannat-Khah, MSPH, DrPH, *New York*
Vasileios Kyttaris, MD, *Boston*
Kimberly Lakin, MD, MS, *New York*
Lindsay S. Lally, MD, MS, *New York*
Susan MacLauchlan, PhD, *Boston*
Bella Mehta, MBBS, MS, MD, *New York*
Alicia Mueller, MD, PhD, *Stanford*
Julie Paik, MD, MHS, *Baltimore*
Michael Paley, MD, PhD, *St. Louis*
Misti L. Paudel, PhD, MPH, *Boston*
Grant Schulert, MD, PhD, *Cincinnati*
Andrew D Schweitzer, MD, *New York*
Jeffrey A. Sparks, MD, MMSc, *Boston*
Sara K. Tedeschi, MD, MPH, *Boston*
Gaëlle Varkas, MD, PhD, *Ghent*
Fan Zhang, PhD, *Aurora*

AMERICAN COLLEGE OF RHEUMATOLOGY

William Harvey, MD, MSc, *Boston*, **President**
Anne Bass, MD, *New York*, **President-Elect**
Angus Worthing, MD, *Washington, DC,* **Secretary**
Eric Ruderman, MD, *Chicago,* **Treasurer**
Bryce Binstadt, MD, PhD, *Minneapolis,* **Foundation President**
Becki Cleveland, PhD, *Chapel Hill*, **ARP President**
Steven Echard, IOM, CAE, *Atlanta*, **Executive Vice-President**

© 2026 American College of Rheumatology. All rights reserved, including rights for text and data mining and training of artificial technologies or similar technologies. No part of this publication may be reproduced, stored or transmitted in any form or by any means without the prior permission in writing from the copyright holder. Authorization to copy items for internal and personal use is granted by the copyright holder for libraries and other users registered with their local Reproduction Rights Organization (RRO), e.g. Copyright Clearance Center (CCC), 222 Rosewood Drive, Danvers, MA 01923, USA (www.copyright.com), provided the appropriate fee is paid directly to the RRO. This consent does not extend to other kinds of copying or use such as copying for general distribution, for advertising or promotional purposes, for creating new collective works, for resale, or for artificial intelligence tools or technologies. Special requests should be addressed to: permissions@wiley.com.

Access Policy: Subject to restrictions on certain backfiles, access to the online version of this issue is available to all registered Wiley Online Library users 12 months after publication. Subscribers and eligible users at subscribing institutions have immediate access in accordance with the relevant subscription type. Please go to onlinelibrary.wiley.com for details.

The views and recommendations expressed in articles, letters, and other communications published in Arthritis & Rheumatology are those of the authors and do not necessarily reflect the opinions of the editors, publisher, or American College of Rheumatology. The publisher and the American College of Rheumatology do not investigate the information contained in the classified advertisements in this journal and assume no responsibility concerning them. Further, the publisher and the American College of Rheumatology do not guarantee, warrant, or endorse any product or service advertised in this journal.

♾This journal is printed on acid-free paper.

Arthritis & Rheumatology

An Official Journal of the American College of Rheumatology
www.arthritisrheum.org and wileyonlinelibrary.com

VOLUME 78 • October 2026 • NO. 10

In This Issue A15

Journal Club A16

Clinical Connections A17

Special Article

Editorial: The Missing Link in Joint Homeostasis: Telocytes as Master Regulators of the Synovial Lymphatic System
Irene Rosa, Eloisa Romano, and Mirko Manetti 2007

Editorial: Stirring Up Plasma Cells in Systemic Lupus Erythematosus
Georg Schett 2011

Editorial: Targeting Obesity in Psoriatic Arthritis: Is It Time for a Paradigm Change?
Lihi Eder, Rebecca Haberman, and Jose U. Scher 2014

Notes From the Field: Challenges to Research Integrity in Rheumatology: The Threat of Paper Mills, Fraud, and Click Data Science
Tony R. Merriman, Tristan Pascart, and Maria I. Danila 2017

Rheumatoid Arthritis

TWIST1-Mediated Induction of AEBP1 in Fibroblast-Like Synoviocytes Activates Transforming Growth Factor β Signaling to Drive Angiogenesis and Promote Rheumatoid Arthritis
Zhenyu Li, Minglong Cai, Wei Huang, Xi Wen, Yujing Li, Jun Sun, Chen Zhu, Chao Yang, and Zhu Chen 2021

Biologic and Targeted Synthetic Disease-Modifying Antirheumatic Drugs Do Not Arrest Bone Loss in Patients With Rheumatoid Arthritis: A Long-Term Multicenter Observational Study
Takafumi Aritomi, Koshiro Sonomoto, Shingo Nakayamada, Hiroaki Tanaka, Atsushi Nagayasu, Satoshi Kubo, Ippei Miyagawa, Ayako Yamaguchi, Naoaki Ohkubo, Yasuyuki Todoroki, Yurie Satoh-Kanda, Masanobu Ueno, Ryuichiro Kanda, Yuya Fujita, Masashi Funada, Hidenori Sakai, Satsuki Matsunaga, Hiroaki Tanaka, Masayuki Shinojima, Hiroki Kawamura, Kazuki Takahashi, Miyabi Ando, Kazuki Haru, Yusuke Miyazaki, Kentaro Hanami, Masao Nawata, Shunsuke Fukuyo, Keisuke Nakatsuka, Mikiko Tokunaga, Kazuyoshi Saito, and Yoshiya Tanaka 2036

Telocyte Deletion Associated With Loss of Lymphatic Drainage and Exacerbation of Inflammatory-Erosive Arthritis in Mice
Yue Peng, H. Mark Kenney, Sean Lydon, Karen L. de Mesy Bentley, Lianping Xing, Benjamin D. Korman, Christopher T. Ritchlin, and Edward M. Schwarz 2050

Association of Clonal Hematopoiesis With Incident, Late-Onset, Seropositive Rheumatoid Arthritis
Kun Zhao, Yash Pershad, J. Brett Heimlich, Michelle Ormseth, C. Michael Stein, Brian Sharber, Caitlyn Vlasschaert, Alexander G. Bick, and Robert W. Corty 2063

Brief Report: Anti-Carbamylated Protein Antibodies Stabilize Carbamylated Histone H3 to Promote Synovial Activation and Neutrophil Extracellular Trap-Mediated Bone Loss in Rheumatoid Arthritis
Shuichiro Nakabo, Norio Hanata, Eduardo Patino-Martinez, Ronald Holewinski, Ana Barrera-Vargas, Javier Merayo-Chalico, Scott A. Coonrod, David A. Fox, Mariana J. Kaplan, and Carmelo Carmona-Rivera 2074

Osteoarthritis

Brief Report: Per- and Polyfluoroalkyl Substances and Knee Osteoarthritis: Data From the Osteoarthritis Initiative
Jeffrey B. Driban, Lisa B. Rokoff, Bing Lu, Timothy E. McAlindon, Charles B. Eaton, Mary B. Roberts, Diana Mathes, Colleen Lestician, Zhijin Carrie Xu, Zhihua Tina Fan, Shawn P. O'Leary, Ida K. Haugen, Jérémie Sellam, Alice Courties, and Abby F. Fleisch 2082

Psoriatic Arthritis

Ixekizumab With Tirzepatide Achieved Greater Disease Control Than Ixekizumab Alone in Adults With Psoriatic Arthritis and Overweight or Obesity: Results From a Randomized Clinical Trial
Joseph F. Merola, Philip Mease, Alan Kivitz, Naveed Sattar, Laura C. Coates, Daniel Aletaha, Cynthia E. Kartman, Peter Fischer, Luna Sun, Píndaro Martínez-Osuna, Andris Kronbergs, Purvi Prajapati, Anabela Cardoso, Mark C. Genovese, and Alexis Ogdie 2089

Functional Impact of Structural Damage in Psoriatic Arthritis: Insights from a Prospective Cohort Study
Pankti Mehta, Shangyi Gao, Virginia Carrizo Abarza, Fadi Kharouf, Daniel Pereira, Richard J. Cook, Dafna D. Gladman, Vinod Chandran, and Denis Poddubnyy 2102

Systemic Lupus Erythematosus

Dual-Targeting BCMA–CD19 CAR-T Cell Therapy in Systemic Lupus Erythematosus: Single-Cell and Immune Repertoire Analysis Reveals Mechanisms of Immune Reconstitution
Zhenghao He, Weijia Wang, Qianwen Li, Shihao Ding, Mingxia Wang, and Ming Hong 2110

Unveiling Endotypes in Systemic Lupus Erythematosus Through Multiomic Analysis: Insights Into Cardiovascular and Renal Complications
Tomás Cerdó, Laurel Woodridge, Sagrario Corrales, Juan Rafael Muñoz-Castañeda, Ana Isabel Torralbo, Anisur Rahman, Filipa Farinha, Rafaela Ortega Castro, Pedro Segui, Ismael Sanchez-Pareja, Laura Muñoz-Barrera, Christian Merlo, Desiree Ruiz-Vilchez, M. Carmen Ábalos-Aguilera, Pilar Font, Nuria Barbarroja Puerto, PRECISESADS Clinical Consortium, Marta Alarcón-Riquelme, Alejandro Escudero-Contreras, M. Ángeles Aguirre-Zamorano, Carlos Perez-Sanchez, Elizabeth C. Jury, and Chary Lopez-Pedrera 2124

Subsets of Patients With Lupus Identified by Gene Expression Profiles Exhibit Differential Clinical Responsiveness to Baricitinib
Prathyusha Bachali, Amrie Grammer, and Peter E. Lipsky 2138

Autoinflammatory Disease

A Rare *RIPK3* Variant Enhances Necroptosis and Promotes Inflammation in a Still Disease–Like Autoinflammatory Syndrome
Longfang Chen, Qihua Dai, Yu Xiao, Jialin Dai, Mengyan Wang, Yuning Ma, Yujie Shen, Zhimo Xu, Jianfen Meng, Xia Chen, Da Yi, Yue Sun, Hui Shi, Honglei Liu, Xiaobing Cheng, Yutong Su, Junna Ye, Huihui Chi, Zhuochao Zhou, Tingting Liu, Jialin Teng, Chengde Yang, Jinchao Jia, and Qiongyi Hu 2149

Validation of International Classification of Diseases Code–Based Case Definitions of Immune Checkpoint Inhibitor–Associated Inflammatory Arthritis From Administrative Health Data
Manar Elsayed, Zoe Hsu, Finlay A. McAlister, William D. Leslie, Lisa M. Lix, Sasha Bernatsky, Suzanne N. Morin, Michelle M. Graham, Aurore Fifi-Mah, Shahin Jamal, Janet Roberts, and Carrie Ye 2160

Healthcare Delivery

Coverage Generosity of Novel Antirheumatic Drugs in Medicare Advantage and Stand-Alone Part D Plans
Youngmin Kwon, Robert W. Corty, and Stacie B. Dusetzina 2171

Letter

Entering the Era of Somatic Variant Sequencing in Immune Dysregulation: Comment on the Article by Fu et al
Willem Roosens, Catho Colson, Isabelle Meyts, and Rik Schrijvers 2179

Reply
Jinjian Fu, Xiaomin Yu, Jun Wang, Qing Zhou, and Qiong Fu 2181

Cover image: The image on the cover (from Peng et al; pages 2050–2062) shows a mast cell (magenta) is shown in direct physical contact with a telocyte (red) adjacent to a collecting lymphatic vessel (green). This striking three-dimensional image highlights a previously unrecognized cellular partnership within the synovial lymphatic system that may contribute to lymphatic regulation and joint homeostasis.

In this Issue

Highlights from this issue of *A&R* | By Lara C. Pullen, PhD

Long-Term Osteoporosis Progression Under Treatment With DMARDs

Treatment with biologic or targeted synthetic disease-modifying antirheumatic drugs (b/tsDMARDs) may be insufficient to improve bone health and bone mineral density (BMD) in patients with rheumatoid arthritis (RA). Evidence suggests that controlling inflammation may not be sufficient to prevent fractures in this population. A previous prospective study of 1,164 patients with active RA treated with b/tsDMARDs for one year reported stable BMD in patients receiving osteoporosis medication at the start of treatment and BMD decreases in patients who were not. **In this issue, Aritomi et al. (p. 2036)** present a five-year follow-up of 797 of those patients, showing that BMD decreased even when RA activity was controlled by b/tsDMARDs.

p. 2036

Overall, 58% of patients in the long-term study experienced a decrease in T score. T scores decreased significantly in the femoral neck and radius in patients who did not receive osteoporosis treatment (n=645) but not in those who did (n=152). During the study period, the researchers observed 21 new fragility fractures. Surprisingly, neither duration of b/tsDMARD use nor disease activity were associated with BMD maintenance.

Although this real-world study design precludes establishing a causal relationship between b/tsDMARD use and BMD, the authors comment that the observed BMD changes were unlikely to be attributable to measurement error, as differences exceeding the least significant change were observed between patients who did and those who did not receive osteoporosis medication. Rather, the findings suggest that some patients experience BMD loss during treatment with b/tsDMARDs. The authors conclude that managing osteoporosis is an important, independent consideration in patients with RA beyond the control of inflammation.

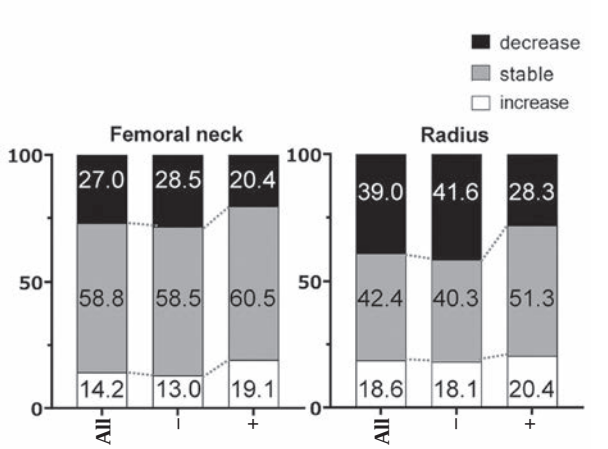


Figure 1A. Proportions of patients with decreased, stable, or increased bone mineral density exceeding the least significant change of the femoral neck and radius in all patients (All), those not receiving osteoporotic drugs at enrollment (–), and those receiving osteoporotic drugs at enrollment (+).

Baricitinib Response in Lupus Endotypes

Clinical features of systemic lupus erythematosus (SLE) do not predict responsiveness to the JAK1 inhibitor baricitinib, leaving clinicians without an important tool for patient management. **In this issue, Bachali et al. (p. 2138)** report a transcriptomic analysis that identified subsets of patients with SLE who are responsive to baricitinib. The study builds upon the group's previously reported machine learning-based approach, which employed transcriptomic data from more than 3,000 patients with SLE using previously derived JAK1, JAK2, and TYK2 gene signature molecules.

p. 2138

The investigators analyzed whole-blood samples from 272 patients with SLE who participated in a phase 2 trial of baricitinib. They classified patients into eight discrete molecular endotypes (A-H) based on baseline gene analysis scores, characterized by progressively increasing immune perturbations. Baseline demographics and SLE Disease Activity Index were similar across endotypes, with modest but significant differences in anti–double-stranded DNA and complement levels.

Significant clinical responses to baricitinib were seen in endotypes D and G. Endotype G, the most baricitinib-responsive subset, was characterized by elevated interferon gene signature, JAK pathway activity, and immunoproteasome expression. Transcriptional changes in this subset were evident as early as week two of treatment, sustained through week 24, and largely associated with clinical response. Patients with endotype D also demonstrated a significant clinical response to baricitinib but exhibited a more restricted transcriptional response pattern than those with endotype G.

Molecular Endotypes in SLE: Cardiovascular Risk and Lupus Nephritis Insights

The high heterogeneity of systemic lupus erythematosus (SLE) complicates its diagnosis and treatment. Previous studies have identified biomarkers of organ involvement, organ damage, or biopsy-proven active lupus nephritis (LN). **In this issue, Cerdó et al. (p. 2124)** report the results of multiomic profiling that integrated immune, vascular, and metabolic pathways associated with cardiovascular (CV) risk and LN to delineate molecular endotypes in patients with SLE. Their results suggest that multiomic profiling can be used as a tool for precision risk stratification in SLE.

p. 2124

Using serum from 199 patients with SLE, the investigators identified metabolomic signatures using machine learning within unsupervised, proteomic-derived clusters. A defined set of molecules consistently distinguished two patient clusters. Patients in cluster 1 showed elevated disease activity, higher rates of LN, hypertension, dyslipidemia, obesity, and abnormal C-reactive protein/erythrocyte sedimentation rate compared with those in cluster 2. The researchers also found 46 proteins upregulated in cluster 1 relative to cluster 2, including well-established immunity mediators and less-characterized proteins associated with NF-κB. Patients in Cluster 1 exhibited elevated creatinine and citrate levels, along with changes in low-density lipoprotein (LDL) lipid profiles.

CV risk in SLE was associated with a distinct molecular signature of inflammatory and immune-mediated proteins together with extensive lipid dysregulation. Renal involvement was associated with an immunometabolic signature characterized by dysregulated proteins involved in immune cell recruitment and renal damage, together with lipid alterations dominated by very low-density lipoprotein and LDL subclasses. In vitro, renal tubular cells treated with serum from patients in cluster 1 (with LN) showed altered expression of 34 inflammatory proteins compared with cells treated with serum from cluster 2 patients (without LN).

Journal Club

A monthly feature designed to facilitate discussion on research methods in rheumatology.

TOGETHER-PsA: Ixekizumab ± Tirzepatide in Patients With PsA and Overweight or Obesity

Merola et al. *Arthritis Rheumatol.* 2026;78:2089–2101.

Overweight and obesity are highly prevalent in patients with psoriatic arthritis (PsA) and are associated with reduced therapeutic response, greater disease severity, and increased comorbidity burden. No randomized controlled trials have previously evaluated the use of biologic and incretin therapy in this population. TOGETHER-PsA was a phase 3b, randomized, 52-week, open-label, blinded-assessor trial (n=271) in adults with active PsA and overweight (body mass index [BMI] ≥27 to <30) with at least one weight-related comorbidity, or obesity (BMI ≥30). Participants were randomized 1:1 to ixekizumab (IXE) or IXE and tirzepatide (TZP). Both groups received diet and exercise counseling.

The trial enrolled a more treatment-refractory population than is typical of PsA pivotal trials, with 69.7% women, a mean screening BMI of 37.6 kg/m², high tender and swollen joint counts (26.7 and 12.3, respectively), 63.1% advanced therapy–experienced, and 18.8% having failed ≥2 classes of advanced therapy. The trial employed a multicomponent primary endpoint—simultaneous achievement of ACR50 and ≥10% weight reduction at week 36—chosen to encompass the key assessments of PsA and obesity/overweight, respectively. PsA disease activity alone, as measured by ACR50, was captured as a key secondary endpoint. Additional non-multiplicity controlled secondary endpoints included patient reported outcomes, quality of life measures, and metabolic outcomes.

At week 36, significantly more patients achieved the primary endpoint with IXE+TZP than with IXE alone (31.7% vs. 0.8%; $P<0.001$). ACR50 was achieved by 33.5% of patients receiving IXE+TZP versus 20.4% receiving IXE alone ($P=0.020$). After four weeks at starting dose (2.5 mg) TZP, ACR50 response was higher in the IXE+TZP group versus IXE (11.1% vs. 3.9%; nominal $P<0.05$), with a mean weight reduction of 2.7% versus 0% in the IXE arm (nominal $P<0.001$). Secondary endpoints at week 36 showed improvements with IXE+TZP compared to IXE alone, including minimal disease activity, HAQ-DI, DAPSA, FACIT-Fatigue, SF-36 physical and mental component scores, and cardiometabolic parameters. Safety profiles were consistent with previous studies for both IXE and TZP.

Questions

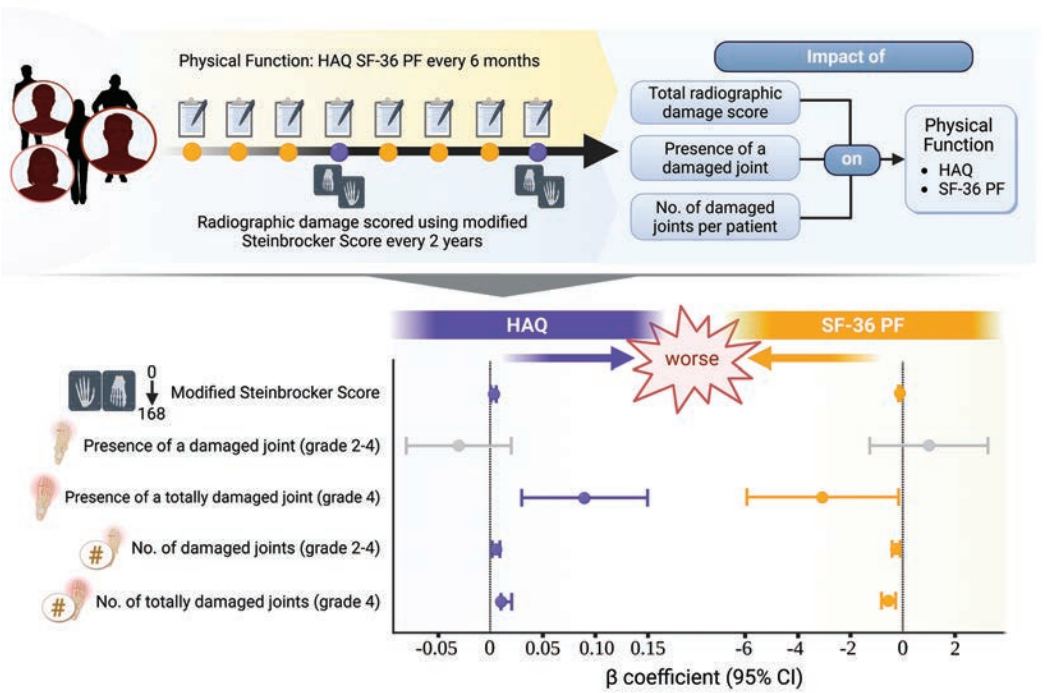
1. **Are the results generalizable to broader populations of patients with PsA and overweight/obesity?**
2. **Would the results be more robust if a less refractory population were enrolled?**
3. **For trials in inflammatory arthritis that incorporate both joint and metabolic endpoints, what is the optimal timing to assess treatment effects, and how should early joint responses observed prior to appreciable weight loss inform endpoint selection and trial design?**

Clinical Connections

Functional Impact of Structural Damage in Psoriatic Arthritis

Mehta et al. *Arthritis Rheumatol.* 2026;78:2102–2109.

CORRESPONDENCE
Denis Poddubnyy, MD, PhD, MSc: denis.poddubnyy@uhn.ca



KEY POINTS

- In PsA, structural damage affects physical function independent of disease activity and demographics.
- Severity of joint damage matters, with even a single joint with complete destruction associated with a clinically significant decline in physical function.
- A strong dose–response relationship was observed between number of completely destroyed joints and physical function. This highlights that cumulative damage, not just individual joint involvement, drives long-term disability in PsA.

SUMMARY

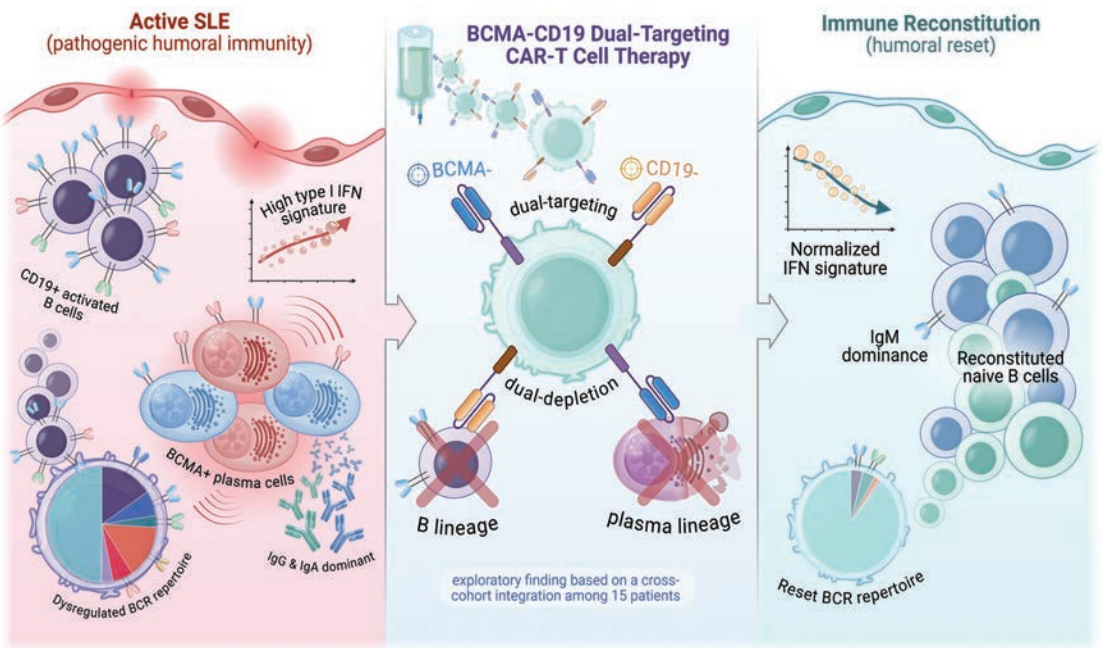
Psoriatic arthritis (PsA) is a chronic inflammatory condition affecting the joints and skin that can lead to permanent structural joint damage over time; however, the precise relationship between joint damage and ability to perform everyday physical tasks has not been well studied in a real-world patient cohort setting. Mehta et al. followed 1,177 patients with PsA at a specialist clinic in Toronto, Canada, over several years, regularly capturing radiographic measures of joint damage and validated questionnaires about physical functioning.

Higher levels of radiographic joint damage were independently associated with worse physical function scores, even after accounting for how many joints were actively swollen, how long a patient had lived with the disease, and whether the patient was male or female. Presence of a joint with modest structural changes did not impair daily functioning significantly. However, when at least one joint had reached complete joint collapse or fusion, patients reported meaningfully worse physical ability. Each additional severely damaged joint was associated with progressively greater functional decline. These findings suggest that patients can compensate for mild to moderate joint damage, but severe and irreversible joint destruction carries real and accumulating consequences for patients' quality of life, underscoring the need for early diagnosis and prevention of damage.

Dual-Targeting BCMA–CD19 CAR-T Cell Therapy in SLE

He et al. *Arthritis Rheumatol.* 2026;78:2110–2123.

CORRESPONDENCE
Ming Hong, PhD: hongming530@126.com



SUMMARY

Cellular therapy has emerged as a promising frontier for refractory cases of systemic lupus erythematosus (SLE), a complex autoimmune disease driven by hyperactive B cells and plasma cells. In a small-scale exploratory study, He et al. analyzed peripheral blood mononuclear cells from five SLE patients who received a novel BCMA–CD19 dual-targeting CAR-T cell therapy. They integrated data from patients treated with CD19 single-targeting CAR-T therapy and healthy controls to evaluate the mechanisms of immune reconstitution at the single-cell transcriptome and immune repertoire levels.

Dual-targeting CAR-T therapy effectively depletes peripheral B cells and shows a tendency toward greater clearance of pathogenic plasma-lineage and plasmablast clusters, which were observed to be partially spared in the CD19 single-targeting comparator. At the molecular level, dual-targeting therapy demonstrated a more pronounced trend in attenuating RIG-I/MDA5 and type I interferon transcriptional programs within B cells, key drivers of SLE pathogenesis. Following the contraction of pathological clones, patients' immune systems were reconstituted with predominantly healthy, naive B cells. These molecular shifts paralleled significant clinical improvement and reduced circulating autoantibody levels. No severe infections or toxicities associated with uncontrolled T cell proliferation from the IL-15 cassette were observed during the follow-up period.

KEY POINTS

- Dual-targeting CAR-T therapy was associated with deeper depletion of plasma-lineage compartments compared with single-targeting therapy.
- Dual-targeting therapy induced greater suppression of RIG-I/MDA5 signaling and type I interferon transcriptional programs in B cells.
- At a median follow-up of 90 days, mean SLEDAI scores dropped significantly, and the B cell receptor repertoire successfully reconstituted toward a more naive profile.
- No severe late-onset infections or uncontrolled T cell proliferation toxicities were observed.

Check for updates

Arthritis & Rheumatology
Vol. 78, No. 10, October 2026, pp 2007–2010
DOI 10.1002/art.70177
© 2026 American College of Rheumatology

American College of Rheumatology
Empowering Rheumatology Professionals

EDITORIAL

The Missing Link in Joint Homeostasis: Telocytes as Master Regulators of the Synovial Lymphatic System

Irene Rosa, PhD, Eloisa Romano, PhD, and Mirko Manetti, PhD

The pathogenesis of rheumatoid arthritis (RA) has traditionally been viewed through the lens of dysregulated adaptive and innate immunity within the synovial microenvironment, focusing primarily on the infiltration of lymphocytes and the proinflammatory secretome of macrophages. However, even with the advent of sophisticated biologics and conventional disease-modifying antirheumatic drugs, nearly 40% of patients with RA fail to achieve primary clinical outcomes, and lasting remission remains elusive for many.[1] Hence, a significant shift in the field has redirected attention toward the synovial lymphatic system (SLS) as a central determinant of joint health.[1] Although it is established that lymphatic drainage is essential for removing catabolic factors, cytokines, and inflammatory cells from the synovium,[1] the mechanisms by which distal joint effusions "communicate" with proximal collecting lymphatic vessels (cLVs) to initiate clearance have remained enigmatic. In this issue of *Arthritis & Rheumatology*, Peng and colleagues present a landmark study that identifies telocytes as the critical sensory network that bridges this gap, demonstrating that their loss directly leads to the collapse of lymphatic drainage and the exacerbation of inflammatory-erosive arthritis in a mouse model of RA.[2]

Telocytes first entered the scene in 2010 and are a unique population of interstitial cells ultrastructurally characterized by a small cell body and extremely long, moniliform cytoplasmic processes—telopodes.[3–5] These telopodes, composed of alternating thin segments (podomers) and dilated portions (podoms), form intricate 3D networks that facilitate long-distance intercellular communication and provide structural support within the stroma of various organs.[3–5] The relevance of telocytes to rheumatology began with the discovery of their presence in the human synovial sublining, particularly concentrated around microvessels and at the boundary of the lining layer.[6] Subsequent studies revealed a severe impairment and loss of the telocyte network in the synovium of patients with RA, a defect that was found to be correlated with disease duration.[7] Interestingly, an experimental study in a rat model showed that telocytes in the infrapatellar fat pad and loose connective tissue are preserved during the progression of osteoarthritis,[8] suggesting that the "telocytopathy" observed in RA is a hallmark of its unique pathobiology.

In this context, the study by Peng et al moves beyond descriptive morphology by leveraging cutting-edge genetic tools to establish a functional role for telocytes in joint-draining lymphatics.[2] Using novel *Efhd1*-CreER^{T2} and *Myoc*-CreER^{T2} inducible transgenic mouse models, the authors identified an extensive network of these stromal cells extending from the ankle synovium to the joint-draining popliteal lymphatic vessels (PLVs).[2] Through transmission electron microscopy and whole-mount immunofluorescence, they discovered that these telocytes are physically integrated with mast cells adjacent to cLVs.[2] This anatomic relationship suggests that telocytes are not merely passive scaffolds, being part of a perilymphatic regulatory system where they may act as mechanical sensors. This discovery complements recent advances in lymphatic physiology, providing a missing link in our understanding of lymphatic pacemaking. Indeed, although it has been recently established that lymphatic muscle cells serve as the innate pacemakers of cLV contractions in response to intraluminal pressure,[9] the signal that initiates these contractions during acute distal tissue edema, such as joint effusions, remained unknown. Peng et al propose a unifying model in which telocytes sense osmotic pressure changes within the joint and signal through their network to perilymphatic mast cells, which in turn degranulate and release factors like histamine that initiate lymphatic muscle cell contractions to clear the excess fluid.[2,10]

The most striking innovation of the study by Peng et al is the functional validation of the proposed model through in vivo cell depletion. By crossing their CreER^{T2} transgenic mouse lines with diphtheria toxin-α floxed mice, the authors achieved a targeted approximately 60% reduction in synovial telocytes.[2] This depletion resulted in a dramatic failure of lymphatic clearance, as

[1]Department of Experimental and Clinical Medicine, University of Florence, Florence, Italy.

Author disclosures are available at https://onlinelibrary.wiley.com/doi/10.1002/art.70177.

Address correspondence via email to Mirko Manetti, PhD, at mirko.manetti@unifi.it.

Submitted for publication March 15, 2026; accepted in revised form April 3, 2026.

measured by indocyanine green near-infrared fluorescence imaging.[2] In the zymosan-induced arthritis model of knee erosive synovitis, the absence of telocytes led to significantly increased synovial volume and exacerbation of focal bone erosions.[2] This mirrors earlier findings that mast cell deficiency or pharmacologic stabilization also compromises lymphatic drainage and worsens experimental arthritis.[11] Taken together, it is highlighted that the telocyte–mast cell tandem is necessary for normal lymphatic function, acting as a primary protective mechanism against joint destruction. Remarkably, Peng and colleagues provide an in-depth mechanistic explanation according to which lymphatic failure in arthritis may be driven by the loss of the telocyte sensory network required to activate the drainage system.[2] As acknowledged by the authors, the reliance on diphtheria toxin-based cell ablation models may suffer from incomplete or variable efficiency, necessitating future gene knockout studies to confirm these findings.

Despite distinctive ultrastructural features, the identification of telocytes has historically been hindered by the lack of specific markers, often leading to their confusion with fibroblasts.[3–5] Telocytes, such as those residing in the synovium, are typically identified by a $CD31^{-}/CD34^{+}$ immunophenotype, distinguishing them from vascular endothelial cells.[4,6] A major strength of the work by Peng et al is the advancement of this knowledge by employing single-cell RNA sequencing (scRNA-seq) to provide a definitive transcriptomic signature.[2] By reanalyzing established scRNA-seq data sets of PLVs in the tumor necrosis factor transgenic (TNF-Tg) mouse model of chronic RA, the authors confirmed that telocytes constitute a distinct $CD31^{-}/CD34^{+}$ mesenchymal population transcriptionally different from adventitial fibroblasts.[2] In fact, these telocytes are specifically characterized by the expression of genes like *Efhd1* and *Myoc*. Interestingly, although telocytes and fibroblasts share several mesenchymal markers, they appear to be spatially and functionally distinct.[2] In particular, the authors observed that telocytes are concentrated near meniscus attachments and around the cLV wall—a spatial organization that is critical for their role as a sensory network for the SLS—whereas $Comp^{+}$ fibroblasts occupy more peripheral regions.[2] Furthermore, high-resolution scanning electron microscopy of PLVs in wild-type mice showed telocytes embedded within a rich extracellular matrix (ECM). In TNF-Tg mice, instead, this perilymphatic ECM was found to undergo significant degeneration accompanied by a marked decrease in the telocyte-to-fibroblast ratio.[2] Hence, the loss of perilymphatic telocytes may contribute to the "collapse phase" of lymphatic failure previously characterized in TNF-Tg mice, where the loss of intrinsic vessel contractions related to altered lymphatic muscle cell populations leads to sudden exacerbations of synovitis.[2,10,12]

Importantly, Peng et al also demonstrate that anti-TNF therapy can partially recover $CD31^{-}/CD34^{+}$ telocytes, suggesting that current biologics may exert some of their efficacy by repairing the SLS sensory network.[2] Thus, it is conceivable that persistent inflammation with chronic exposure to high-cytokine environments, particularly TNF-α, drives telocyte depletion. Moreover, based on a cellular trajectory analysis of the scRNA-seq data, the authors propose that telocytes may have the potential to differentiate into pathologic fibroblast-like synoviocytes in response to both chronic inflammation and a rigid, fibrotic ECM.[2] This provocative hypothesis implies that the disappearance of telocytes in RA synovium may not simply arise from cell degeneration but a phenotypic switch toward the aggressive fibroblasts driving joint destruction in different RA synovial pathotypes, including the fibroid/pauci-immune one that is refractory to all known treatments.[2] Of note, previous reports have suggested that telocytes might transition into profibrotic fibroblasts/myofibroblasts in certain pathologic conditions.[4] Nevertheless, further ultrastructural investigations might clearly help identify degenerative signs in perilymphatic telocytes from affected joints. Finally, it is worth mentioning that early research showed that the inhibition of lymphangiogenesis increases inflammation severity in TNF-Tg mice.[13] In this scenario, we propose that the loss of telocytes, which are spatially close to lymphatic endothelial cells (Figure 1A),[14] might also result into impaired lymphangiogenesis and lymphatic capillary homeostasis, further contributing to synovitis exacerbation. This hypothesis is supported by the evidence that telocytes are exceptionally engaged in paracrine signaling with neighboring cells via the release of extracellular vesicles/exosomes and soluble factors, including proangiogenic growth factors and microRNAs.[3–5]

The therapeutic implications of the Peng et al study are significant. If telocytes are the "gatekeepers" of synovial lymphatic egress, then preserving or restoring their network could be a novel strategy to promote the exit of inflammatory cells from the joint. This aligns with emerging views in other fields, where telocyte loss is seen as a unifying feature of chronic inflammatory and fibrotic diseases like Crohn disease and systemic sclerosis.[15] Interestingly, preliminary studies of Peng et al suggest that moderate exercise can increase the number of synovial telocytes, potentially restoring lymphatic drainage and providing a mechanistic rationale for recent guidelines that integrate exercise into RA management.[10] Moreover, once revealed, the molecular signals by which telocytes communicate with perilymphatic mast cells might represent new drug targets for refractory RA.

In conclusion, the work of Peng et al establishes telocytes as a cornerstone of joint homeostasis. By identifying these cells as the critical sensory network that links joint edema to lymphatic pumping, the authors have provided a new framework for understanding RA pathogenesis and flare (Figure 1B).[2,10] As we move forward, the challenge will be to identify the precise molecular signals that can preserve these delicate cellular networks in the face of autoimmune assault. For now, the discovery of the telocyte–mast cell–lymphatic muscle cell axis stands as a fundamental advance in our understanding of the synovial microenvironment,

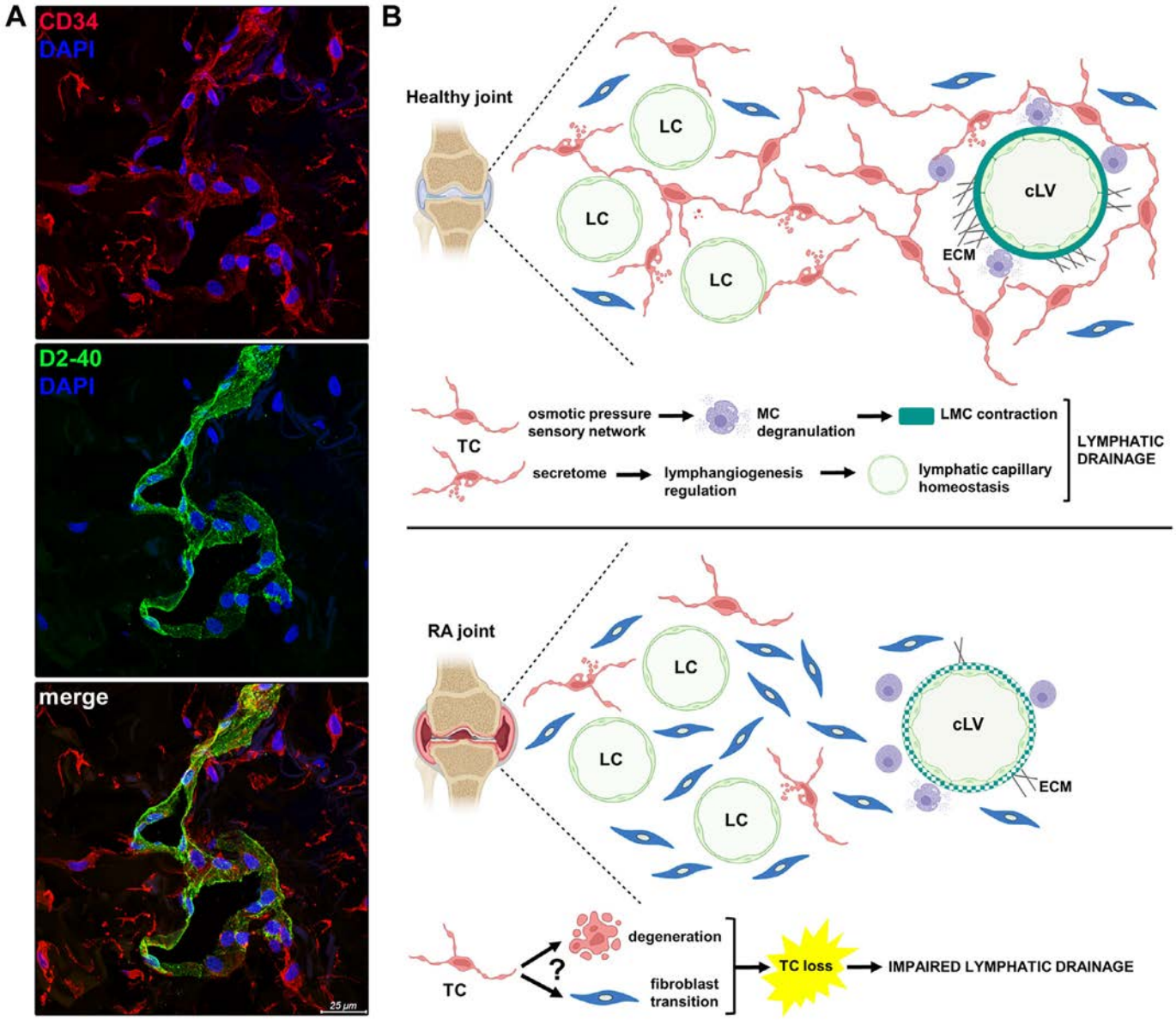


Figure 1. The spatial and functional relationship between TCs and the synovial lymphatic system. (A) Confocal laser scanning microscopy imaging of a 3D network of TCs (immunostained for CD34; red) closely surrounding lymphatic endothelial cells (immunostained for D2-40/podoplanin; green) of an LC. Nuclei are stained blue with DAPI. (B) In healthy joints, TCs form a unique network surrounding synovial LCs and extending around cLVs. The synovial TC network may sense osmotic pressure changes and signal to perilymphatic MCs, which in turn degranulate and release factors (eg, histamine) that initiate LMC contractions to allow lymphatic drainage from the joint. TCs may also contribute to LC homeostasis through paracrine regulation of synovial lymphangiogenesis. In RA-affected joints, synovial TCs are depleted because of cellular degeneration and/or TC-to-fibroblast transition. Together with LMC defects and degeneration of the ECM surrounding cLVs, the loss of TCs results in impaired lymphatic drainage and exacerbation of synovitis. cLV, collecting lymphatic vessel; ECM, extracellular matrix; LC, lymphatic capillary; LMC, lymphatic muscle cell; MC, mast cell; RA, rheumatoid arthritis; TC, telocyte.

promising a future where "unclogging" the joint becomes as vital as suppressing the immune response.

AUTHOR CONTRIBUTIONS

All authors contributed to at least one of the following manuscript preparation roles: conceptualization AND/OR methodology, software, investigation, formal analysis, data curation, visualization, and validation AND drafting or reviewing/editing the final draft. As corresponding author, Dr Manetti confirms that all authors have provided the final approval of the version to be published, and takes responsibility for the affirmations regarding article submission (eg, not under consideration by another journal), the integrity of the data presented, and the statements regarding compliance with institutional review board/Declaration of Helsinki requirements.

REFERENCES

1. Bouta EM, Bell RD, Rahimi H, et al. Targeting lymphatic function as a novel therapeutic intervention for rheumatoid arthritis. Nat Rev Rheumatol 2018;14(2):94–106. PubMed doi:10.1038/nrrheum.2017.205
2. Peng Y, Kenney HM, Lydon S, et al. Telocyte deletion is associated with loss of lymphatic drainage and exacerbation of inflammatory-erosive arthritis in mice. Arthritis Rheumatol 2026;78(10):2050–2062. PubMed doi:10.1002/art.70131
3. Dolbnya A, Ivanova V, Serebryakova O, et al. Telocytes: history, origin, identification, structure, distribution, and functions. Histochem Cell Biol 2025;163(1):86. PubMed doi:10.1007/s00418-025-02413-1
4. Rosa I, Marini M, Manetti M. Telocytes: an emerging component of stem cell niche microenvironment. J Histochem Cytochem 2021; 69(12):795–818. PubMed doi:10.1369/00221554211025489
5. Kondo A, Kaestner KH. Emerging diverse roles of telocytes. Development 2019;146(14):dev175018. PubMed doi:10.1242/dev.175018
6. Rosa I, Marini M, Guasti D, et al. Morphological evidence of telocytes in human synovium. Sci Rep 2018;8(1):3581. PubMed doi:10.1038/s41598-018-22067-5
7. Rosa I, Faussone-Pellegrini MS, Romano E, et al. Impairment in the telocyte/CD34^{+} stromal cell network in human rheumatoid arthritis synovium. J Cell Mol Med 2021;25(4):2274–2278. PubMed doi:10.1111/jcmm.16225
8. Takahashi I, Matsuzaki T, Hoso M. Immunohistochemical study on the distribution of telocytes in the knee joint components in a rat osteoarthritis model. J Phys Ther Sci 2022;34(8):596–601. PubMed doi:10.1589/jpts.34.596
9. Zawieja SD, Pea GA, Broyhill SE, et al. Cellular characterization of the mouse collecting lymphatic vessels reveals that lymphatic muscle cells are the innate pacemaker cells. eLife 2025;12:RP90679. PubMed doi:10.7554/eLife.90679
10. Peng Y, Belcher DJ, Kobryn A, et al. Synovial lymphatic system structure and function in rheumatoid arthritis: lymphatic phases, telocytes, and therapeutic modulation through Eexercise. Curr Opin Rheumatol Published online March 4, 2026. PubMed doi:10.1097/BOR.0000000000001151
11. Peng Y, Kenney HM, de Mesy Bentley KL, et al. Distinct mast cell subpopulations within and around lymphatic vessels regulate lymph flow and progression of inflammatory-erosive arthritis in TNF-transgenic mice. Front Immunol 2023;14:1275871. PubMed doi:10.3389/fimmu.2023.1275871
12. Kenney HM, Wu CL, Loiselle AE, et al. Single-cell transcriptomics of popliteal lymphatic vessels and peripheral veins reveals altered lymphatic muscle and immune cell populations in the TNF-Tg arthritis model. Arthritis Res Ther 2022;24(1):64. PubMed doi:10.1186/s13075-022-02730-z
13. Guo R, Zhou Q, Proulx ST, et al. Inhibition of lymphangiogenesis and lymphatic drainage via vascular endothelial growth factor receptor 3 blockade increases the severity of inflammation in a mouse model of chronic inflammatory arthritis. Arthritis Rheum 2009;60(9):2666–2676. PubMed doi:10.1002/art.24764
14. Rosa I, Marini M, Sgambati E, et al. Telocytes and lymphatic endothelial cells: two immunophenotypically distinct and spatially close cell entities. Acta Histochem 2020;122(3):151530. PubMed doi:10.1016/j.acthis.2020.151530
15. Rosa I, Romano E, Fioretto BS, et al. Pathophysiologic implications and therapeutic potentials of telocytes in multiorgan fibrosis. Curr Opin Rheumatol 2026;38(1):26–37. PubMed doi:10.1097/BOR.0000000000001116

Check for updates

Arthritis & Rheumatology
Vol. 78, No. 10, October 2026, pp 2011–2013
DOI 10.1002/art.70200
© 2026 American College of Rheumatology

American College of Rheumatology
Empowering Rheumatology Professionals

EDITORIAL

Stirring Up Plasma Cells in Systemic Lupus Erythematosus

Georg Schett, MD

Pathogenesis of systemic lupus erythematosus (SLE) is built on an altered B cell and plasma cell activation, leading to an immune response to self-DNA, nucleosomes, and other nuclear antigens.[1] Resetting this pathologic B cell response is crucial to meet the aspirational goal to cure SLE. Deep but reversible depletion of the B cell lineage compartments may provide a path to reset the pathologic immune response in SLE. In this context, chimeric antigen receptor (CAR)–expressing T cells (CAR T cells) are powerful instruments to deplete B cells (through recognizing CD19 on the surface of B cells) or plasma cells (through recognizing BCMA on the surface of plasma cells).[2,3] When CAR T cells bind the antigen-expressing cells, they get activated, kill the target cell, and undergo proliferation, thereby increasing the concentration of the drug. These particular features characterize CAR T cells as "living" drugs. Although the targeting of either CD19 or BCMA by CAR T cells in oncology depends on the type of disease (CD19-recognizing CARs used in non-Hodgkin lymphoma and acute lymphoblastic leukemia; BCMA-recognizing CARs used in multiple myeloma), the most suitable target in rheumatic autoimmune diseases has not been defined to date. It is assumed that individual autoimmune diseases differ in their dependence on memory B cells and short-lived plasmablasts expressing CD19 or long-lived plasma cells expressing BCMA.

In this issue of *Arthritis & Rheumatology*, He et al assessed the molecular response of an autologous dual-targeting CD19/BCMA-directed CAR T cells in patients with refractory SLE.[4] They employed single cell RNA-sequencing analysis for defining the transcriptomic signatures in peripheral blood B cells, plasmablasts, and T cells isolated from five patients with SLE before and after CD19/BCMA-directed CAR T cell treatment. Efficacy data on these patients were published previously[5] showing an improvement of SLE disease activity, although immunosuppression could be stopped for at least over more than one year in all patients with no signs of disease relapse. Transcriptomic signatures were compared to available pretreatment and post-treatment single cell RNA-sequencing data from a previously published study on seven patients with SLE receiving autologous CD19 CAR T cells[6] as well as from data from healthy controls. Follow-up samples were taken from the time of early reconstitution of B cells, when a largely naive B cell compartment reemerges in the patients with SLE treated with CAR T cells.

Patients with SLE showed an increased gene expression in pathways related to interferon and inflammatory signaling, antigen presentation, and T cell activation as compared to healthy controls. This expression signature consistently collapsed after treatment with CD19/BCMA and CD19 CAR T cell therapy. Notably, these effects were not only confined to B cells but were also observed in T cells. Hence, expression of pathways related to type I interferon responses were decreased in both CD4+ and CD8+ T cells after both types of CAR T cell therapy. A more detailed analysis of gene expression in different B cell subtypes showed that memory B cells were decreased after both CD19/BCMA and CD19 CAR T cell therapy, whereas plasma cells were only reduced after CD19/BCMA CAR T cell therapy, suggesting BCMA-associated interference with the plasma cell compartment. The most strongly suppressed pathways in the memory B cell compartment were pattern recognition genes like the cytosolic RNA sensors RIG-I and MDA-5, as well as cytosolic DNA sensor AIM-2, whereas genes associated to Ig synthesis were most suppressed in the plasma cell compartment.

This molecular study, aiming to characterize correlative features of immune reset in patients with SLE treated with autologous dual CD19/BCMA-targeting CAR T cells, provides further insight into the substantial changes in the composition of the B cell but also the T cell compartment after treatment with engineered cells. The reset of the B cell compartment into a non–class-switched naive B cell lineage is in line with previous studies and associated with the loss of the entire activated memory B cell and plasmablast pool, which likely includes autoreactive B cell clones.[4,7] Such B cell repertoire change is a consistent finding

Dr Schett's work was supported by the Deutsche Forschungsgemeinschaft (Leibniz Award and CRC 1755 CASCAID).

[1]Department of Internal Medicine 3-Rheumatology and Immunology, Friedrich-Alexander-Universität Erlangen-Nürnberg and Universitätsklinikum Erlangen, Erlangen, Germany.

Author disclosures are available at https://onlinelibrary.wiley.com/doi/10.1002/art.70200.

Address correspondence via email to Georg Schett, MD, georg.schett@uk-erlangen.de.

Submitted for publication March 4, 2026; accepted in revised form April 15, 2026.

in patients with SLE achieving long-term drug-free remission after CAR T cell therapy.[7,8] Also, and in accordance with this concept of abrogation of autoreactive B cell clones and other antigen-experienced B cell clones, signs of clonal expansion of B cells were abrogated after CD19/BCMA CAR T cell therapy. Notably, RNA-sequencing analyses showed that BCMA targeting substantially influenced the plasma cell compartment in patients with SLE, which is not directly affected by CD19 targeting. This finding could provide an advantage in specific patients, in whom autoantibody production is preferentially anchored in plasma cells.[9] Most interestingly, this study suggests broader normalization of dysregulated immune pathways after treatment, such as the loss of type I interferon response signature in T cells and, additionally, the downregulation of critical RNA/DNA sensor genes.

Although the comparison with the molecular data from CD19-CAR T cell therapy is important and led to interesting results, such as the deeper effect of CD19/BCMA double targeting than CD19 single targeting on the plasma cell lineage, certain additional differences between the two approaches need to be considered: (1) CD19/BCMA CAR T cells were dosed three times higher (3×10^6 cells/kg) than CD19 CAR T cells (1×10^6 cells/kg); (2) CD19/BCMA CAR T cells were manufactured using a "fourth-generation" CAR vector with an interleukin-15 (IL-15) cassette that triggers IL-15 expression when the CAR get activated, which boosts CAR T cell expansion; and (3) the conditioning regimen was based on a mix of cyclophosphamide and fludarabine combination and cyclophosphamide monotherapy in patients treated with CD19/BCMA CAR T cells, whereas in patients treated with CD19 CAR T cells, cyclophosphamide and fludarabine combination was uniformly used as conditioning. Finally, as the authors used a CD19/BCMA double-targeting approach, it remains unclear to what extent the CD19-targeting component contributes to the molecular and clinical effects. Notably, efficacy of BCMA-only targeting CAR T cells and T cell engager therapies has been described in SLE.[3,10]

The effect of the molecular signature of plasma cells by CD19/BCMA CAR T cells shown by the authors raises the question, "which patients profit the most from such deep plasma cell interventions?" Characterization of the appropriate patient population for plasma cell targeting, as it has been done in hemato-oncology, is critical, as BCMA targeting unequivocally leads to a clinically relevant lowering of Igs that needs specific safety precautions (ie, Ig substitutions). Hence, all patients treated with the CD19/BCMA CAR T cells required Ig substitution, and in many patients, the levels of major Ig classes (IgG, IgA, and IgM) fell below their detection limit, requiring substitution. Therefore, selecting the right patients for BCMA-targeted treatment approaches (not necessarily confined to CAR T cell therapy but also considering T cell engagers) is going to be critical. In SLE, previous studies have shown that CD19 monoclonal targeting can induce sustained drug-free remission, suggesting that deep depletion of the memory B cell and the short-lived plasmablast compartments can be sufficient to induce the elimination of the pathogenically relevant B cell populations.[4,6,11] These observations also supported the concept of a continuous extrafollicular production of pathogenic memory B cells (known as double negative 2 cells) and short-lived plasmablasts in SLE that are associated with the generation of anti–double-stranded DNA, antihistone, and antinucleosome antibodies.[12] Notably, however, the pathology of certain forms of SLE and of other autoimmune diseases (eg, certain forms of idiopathic inflammatory myopathy) may be more plasma cell driven and may therefore require targeting of plasma cell antigens such as BCMA. The technological advances to selectively and deeply target certain B cell lineage cells will potentially allow to better stratify different diseases and even individual patients into certain molecular subgroups according to their respective dependency on memory B cells, plasmablasts, and plasma cells. Such molecular stratifications in SLE have been successfully developed with respect to type I interferon signature–based endotypes and therapeutic responses as well B cell–associated endotypes and vaccination responses.[13,14]

In summary, the work of He et al provides a valuable insight into the molecular features of immune reset after combined CD19/BCMA targeting by CAR T cells. These data raise attention as to what extent plasma cells need to be included as targets for CAR T cell therapy and urge to define in which patient autoimmune disease is driven by plasma cells.

AUTHOR CONTRIBUTIONS

The author contributed to all of the following manuscript preparation roles: conceptualization AND/OR methodology, software, investigation, formal analysis, data curation, visualization, and validation AND drafting or reviewing/editing the final draft. As corresponding author, Dr Schett approved the final version to be published and takes responsibility for the affirmations regarding article submission (eg, not under consideration by another journal), the integrity of the data presented, and the statements regarding compliance with institutional review board/Declaration of Helsinki requirements.

REFERENCES

1. Tsokos GC. Systemic lupus erythematosus. N Engl J Med 2011; 365(22):2110–2121. doi:10.1056/NEJMra1100359
2. Müller F, Hagen M, Wirsching A, et al. CD19 CAR-T cells for treatment-refractory autoimmune diseases: the phase 1/2 CASTLE basket trial. Nat Med 2026;32(3):1142–1151. doi:10.1038/s41591-025-04185-6
3. Hu Z, Cai S, Yu Y, et al. BCMA-targeted CAR T cell therapy can effectively induce disease remission in refractory lupus nephritis. Ann Rheum Dis 2025;84(10):1675–1683. doi:10.1016/j.ard.2025.06.2128
4. He Z, Wang W, Li Q, et al. Dual-targeting BCMA-CD19 CAR T-cell therapy in systemic lupus erythematosus: single cell immune repertoire analysis reveals mechanisms of immune reconstitution. Arthritis Rheumatol 2026;78(10):2110–2123. doi:10.1002/art.70117
5. Wang W, He S, Zhang W, et al. BCMA-CD19 compound CAR T cells for systemic lupus erythematosus: a phase 1 open-label clinical trial. Ann Rheum Dis 2024;83(10):1304–1314. doi:10.1136/ard-2024-225785

6. Wilhelm A, Chambers D, Müller F, et al. Selective CAR T cell-mediated B cell depletion suppresses IFN signature in SLE. JCI Insight 2024; 9(12):e179433. doi:10.1172/jci.insight.179433
7. Müller F, Taubmann J, Bucci L, et al. CD19 CAR T-cell therapy in autoimmune disease—a case series with follow-up. N Engl J Med 2024;390(8):687–700. doi:10.1056/NEJMoa2308917
8. Mackensen A, Müller F, Mougiakakos D, et al. Anti-CD19 CAR T cell therapy for refractory systemic lupus erythematosus. Nat Med 2022; 28(10):2124–2132. doi:10.1038/s41591-022-02017-5
9. Müller F, Wirsching A, Hagen M, et al. BCMA CAR T cells in a patient with relapsing idiopathic inflammatory myositis after initial and repeat therapy with CD19 CAR T cells. Nat Med 2025;31(6):1793–1797. doi:10.1038/s41591-025-03718-3
10. Alexander T, Krönke J, Cheng Q, et al. Teclistamab-induced remission in refractory systemic lupus erythematosus. N Engl J Med 2024; 391(9):864–866. doi:10.1056/NEJMc2407150
11. Garantziotis P, Beretta L, Lindblom J, et al; PRECISESADS Clinical Consortium. Differential molecular signatures in response to CD19-CAR T cell therapy compared with conventional pharmacotherapy in systemic lupus erythematosus. Ann Rheum Dis 2026; 85(1):153–163. doi:10.1016/j.ard.2025.06.2132
12. Jenks SA, Cashman KS, Zumaquero E, et al. Distinct effector B cells induced by unregulated Toll-like receptor 7 contribute to pathogenic responses in systemic lupus erythematosus. Immunity 2018;49(4):725–739.e6. doi:10.1016/j.immuni.2018.08.015
13. Cross H, Peng J, McDonnell T, et al; APPLE trial investigators and Childhood Arthritis and Rheumatology Research Alliance (CARRA). Type I interferon endotypes drive divergent clinical trajectories in childhood-onset SLE uncovered through a novel systems immunology approach. Ann Rheum Dis 2026;S0003-4967(25)04605–9. doi:10.1016/j.ard.2025.12.011
14. Faliti CE, Van TTP, Anam FA, et al. Disease-associated B cells and immune endotypes shape adaptive immune responses to SARS-CoV-2 mRNA vaccination in human SLE. Nat Immunol 2025;26(1): 131–145. doi:10.1038/s41590-024-02010-9

Check for updates

American College of Rheumatology
Empowering Rheumatology Professionals

Arthritis & Rheumatology
Vol. 78, No. 10, October 2026, pp 2014–2016
DOI 10.1002/art.70258
© 2026 American College of Rheumatology

EDITORIAL

Targeting Obesity in Psoriatic Arthritis: Is It Time for a Paradigm Change?

Lihi Eder, MD, PhD,[1] Rebecca Haberman, MD,[2] and Jose U. Scher, MD[2,3]

The management of psoriatic arthritis (PsA) has been transformed by advances in understanding immune-mediated disease pathways and by the development of highly effective targeted therapies. Yet, despite this progress, an important and persistent clinical challenge remains insufficiently addressed: the close and complex relationship between psoriatic disease and obesity. Obesity is highly prevalent in people with psoriasis and PsA and is consistently associated with a greater risk of progression from psoriasis to PsA, higher disease activity, poorer quality of life, and reduced response to advanced therapies.[1,2] These observations support the concept of a potential disease modulatory triad linking adiposity, inflammation, and PsA trajectory through both direct and indirect mechanisms. If so, obesity in PsA may represent not only another comorbidity but rather a modifiable therapeutic target.

In this context, the interim results of the TOGETHER-PsA trial reported by Merola et al, in this issue of *Arthritis & Rheumatology*, are timely and potentially practice-shaping.[3] The study addresses a clinically important question: can pharmacologic treatment of obesity, using incretin-based medications, enhance the efficacy of biologic therapy in patients with active PsA and overweight or obesity? In this ongoing open-label, phase 3b randomized controlled trial, patients with active PsA who also met indication for pharmacologic weight loss were randomized to receive tirzepatide (TZP) plus ixekizumab (IXE) or IXE alone. At week 36, the combination of TZP and IXE was associated with superior outcomes across several domains, including the primary end point (American College of Rheumatology 50% improvement indication [ACR50] response plus ≥10% weight reduction); clinically meaningful weight loss; multiple PsA-specific efficacy end points including composite clinical responses, such as ACR50 response; minimal disease activity state (MDA); and objective measures (eg, joint counts, C-reactive protein), as well as patient-reported outcomes including fatigue, physical function, and quality of life. These findings are important because they provide the first comprehensive randomized evidence that targeting adiposity pharmacologically may improve outcomes in PsA beyond those achieved with cytokine inhibition alone, in particular interleukin-17 (IL-17) blockade. Concomitantly, the results raise important questions about how this benefit should be interpreted and how such approach might eventually be integrated into clinical practice.

A central issue is the choice of the primary end point: simultaneous achievement of ACR50 response and at least 10% weight reduction, whereas PsA-specific end points were regarded as only secondary. This choice was justified by the authors by conceptualization of PsA and obesity as coexisting conditions that merit concurrent treatment. Although that framing is understandable and clinically relevant, from the perspective of rheumatology practice, the more pressing question is whether TZP provides additive value for the treatment of PsA itself in the setting of comorbid obesity. As the field advances, caution should be exercised while implementing artificial composite primary end points that combine disparate metrics without a clear mechanistic or established clinical correlate. Although treating both conditions is essential, a combined "success" metric may obscure the distinct immunomodulatory versus metabolic effects of the therapies being studied. Thus, although the study met its primary end point with a substantial 30.9% between-group difference, the PsA-specific outcomes are more informative in assessing the therapeutic role of incretin-based therapy in rheumatology practice.

Viewed through that lens, the results remain encouraging, although more modest. The study demonstrated a statistically significant 13.1% difference in ACR50 response in favor of TZP plus IXE over IXE alone at week 36. Importantly, separation between groups was observed as early as week 4, before substantial weight loss would be expected, raising the possibility that the clinical effect may not be mediated exclusively through weight reduction. Improvement was also seen across most individual ACR components, including more objective measures such as swollen joint count and C-reactive protein. The combined regimen

[1]Department of Medicine, University of Toronto and Women's College Hospital, Toronto, Ontario, Canada; [2]Department of Medicine, Psoriatic Arthritis Center and Division of Rheumatology, NYU Grossman School of Medicine, New York, New York; [3]NYU Colton Center for Autoimmunity, NYU Langone Health, New York, New York.

Author disclosures are available at https://onlinelibrary.wiley.com/doi/10.1002/art.70258.

Address correspondence via email to Lihi Eder, MD, PhD, at lihi.eder@wchospital.ca.

Submitted for publication May 18, 2026; accepted May 19, 2026.

also improved attainment of MDA, a more stringent and recommended treatment target that is achieved in only a minority of patients in both trials and routine practice.

Nevertheless, the size of the PsA-specific treatment effect size (13.1% difference between the two arms) warrants careful perspective. Although statistically significant, the incremental ACR50 response benefit was modest compared with the larger effect sizes observed for IXE versus placebo in pivotal PsA trials (SPIRIT-P1 and SPIRIT-P2 showed a difference approaching 30%).[4,5] This distinction matters. These data do not suggest that incretin-based therapy could replace conventional immune-modulating treatment in very active PsA, as in the present trial. Rather, they support the possibility that such agents may serve as adjunctive therapy in selected patients, particularly those in whom obesity may be an important contributor to persistent disease burden or suboptimal treatment response.

The study population itself may be particularly informative in this regard. Participants had severe obesity, had substantial multimorbidity, and were female-predominant, and over 60% of patients had prior exposure to advanced therapies, features that often characterize patients with more difficult-to-manage disease. The emerging concepts of complex-to-manage and treatment-refractory PsA recognize that persistent symptoms and inadequate treatment response may arise from the interaction of inflammatory activity, obesity, comorbidity, pain amplification, biomechanical factors, and accumulated tissue damage.[6–8] In such patients, escalation of immune modulation alone may be insufficient. The TOGETHER-PsA results therefore raise the important possibility that addressing adiposity in parallel with conventional immune pathways may improve outcomes in a subset of patients with complex or refractory disease.

Yet the findings also caution against overly simplistic assumptions. Most patients treated with TZP achieved clinically meaningful weight loss (84.5% of patients had ≥10% weight reduction), but this did not uniformly translate into corresponding improvement in PsA outcomes. This observation suggests that the relationship between weight loss and musculoskeletal improvement is complex and that adiposity may not be the main driver of PsA activity in some patients. Further analyses and longer follow up are needed to determine whether treatment effects are mediated by reduced biomechanical load, improved physical function and well-being, systemic metabolic changes, or direct immunomodulatory actions of incretin-based therapy. Mediation analyses and studies incorporating imaging, tissue biomarkers, and molecular profiling will be essential to clarify these mechanisms.

Several limitations deserve emphasis. The open-label design may have influenced treatment response and may have contributed to the higher discontinuation in the IXE-alone group (33% vs 15.2%). Critically, the lack of a placebo arm decreases our confidence in interpreting the absolute ACR50 response rates for the IXE monotherapy group, because subjective clinical measures are particularly susceptible to expectation bias in an open-label setting. To better isolate the profound metabolic benefits of weight loss from direct disease-modifying effects on synovio-entheseal structures, an alternative and potentially more clinically relevant trial design could have employed a sequential approach: an initial run-in phase with TZP for several months, followed by the sequential initiation of IXE. Moreover, no subgroup analyses were presented to identify predictors of response, which will be necessary if this approach is to be used more selectively and rationally. Generalizability is currently limited to patients with active polyarticular PsA initiating an IL-17A inhibitor while also meeting indication for pharmacologic weight management. It remains uncertain whether similar benefits would be observed in patients with lower levels of residual disease activity, those with lower body mass index, individuals treated with other classes of biologic or targeted synthetic disease-modifying antirheumatic drugs, or patients in routine care settings. Mechanistically, the study is also limited. Without tissue-based biomarkers, or imaging outcomes, it is not possible to determine what biologic processes underlie the observed clinical benefit. Finally, these are interim data, and longer-term results will be needed to assess durability, safety, persistence, and the broader implications of prolonged treatment.

The larger message from this study is not that incretin-based therapy is ready for routine use as disease-modifying treatment in PsA. Rather, it is that the field may need to think differently about obesity in PsA. For many years, obesity has been recognized primarily as a prognostic factor, a source of comorbidity, and an impediment to treatment response. TOGETHER-PsA suggests that it may also be an actionable therapeutic axis. This is an important conceptual shift.

Before this strategy can be incorporated into practice, several questions must be answered. Will the benefits seen in this trial extend to the broader and more heterogeneous PsA populations encountered in routine care? Which patients are most likely to benefit? What are the long-term trade-offs in safety, tolerability, cost, and persistence? Can these therapies reduce the need for biologic escalation, or are they best viewed as supportive adjuncts? And most importantly, do they modify the underlying disease process, or do they primarily improve symptoms and function through metabolic and biomechanical effects?

These questions are not merely academic. They will determine whether incretin-based therapies in PsA should be regarded as metabolic cotherapy, symptom-modifying adjuncts, or agents with genuine disease-modifying potential. The TOGETHER-PsA trial does not yet resolve that question. But it does move the field forward in an important way by showing that adiposity is not simply background "biologic noise" in PsA. It may be at least partially responsible for the disease process itself and, therefore, should also be addressed as a therapeutic target.

AUTHOR CONTRIBUTIONS

All authors contributed to at least one of the following manuscript preparation roles: conceptualization AND/OR methodology, software,

investigation, formal analysis, data curation, visualization, and validation AND drafting or reviewing/editing the final draft. As corresponding author, Dr Eder confirms that all authors have provided the final approval of the version to be published and takes responsibility for the affirmations regarding article submission (eg, not under consideration by another journal), the integrity of the data presented, and the statements regarding compliance with institutional review board/Declaration of Helsinki requirements.

REFERENCES

1. Haberman RH, Ogdie A, Merola JF, et al. The obesity-inflammation axis in psoriatic disease: mechanisms and therapeutic strategies. Nat Rev Rheumatol 2026;22(3):151–164. doi:https://doi.org/10.1038/s41584-025-01326-6
2. Kumthekar A, Ogdie A. Obesity and psoriatic arthritis: a narrative review. Rheumatol Ther 2020;7(3):447–456. doi:https://doi.org/10.1007/s40744-020-00215-6
3. Merola JF, Mease P, Kivitz A, et al. Ixekizumab with tirzepatide achieved greater disease control than ixekizumab alone in adults with psoriatic arthritis and overweight or obesity: results from a randomized clinical trial. Arthritis Rheumatol 2026;78(10):2089–2101. doi:https://doi.org/10.1002/art.70134
4. Mease PJ, van der Heijde D, Ritchlin CT, et al; SPIRIT-P1 Study Group. Ixekizumab, an interleukin-17A specific monoclonal antibody, for the treatment of biologic-naive patients with active psoriatic arthritis: results from the 24-week randomised, double-blind, placebo-controlled and active (adalimumab)-controlled period of the phase III trial SPIRIT-P1. Ann Rheum Dis 2017;76(1):79–87. doi:https://doi.org/10.1136/annrheumdis-2016-209709
5. Nash P, Kirkham B, Okada M, et al; SPIRIT-P2 Study Group. Ixekizumab for the treatment of patients with active psoriatic arthritis and an inadequate response to tumour necrosis factor inhibitors: results from the 24-week randomised, double-blind, placebo-controlled period of the SPIRIT-P2 phase 3 trial. Lancet 2017;389(10086):2317–2327. doi:https://doi.org/10.1016/S0140-6736(17)31429-0
6. Proft F, Ribeiro AL, Singla S, et al. Consensus definitions of complex-to-manage and treatment-refractory psoriatic arthritis: a GRAPPA initiative. Nat Rev Rheumatol 2026;22(2):132–144. doi:https://doi.org/10.1038/s41584-025-01329-3
7. Fagni F, Motta F, Schett G, et al. Difficult-to-treat psoriatic arthritis: a conceptual approach. Arthritis Rheumatol 2024;76(5):670–674. doi:https://doi.org/10.1002/art.42780
8. Marzo-Ortega H, Harrison SR, Fragoulis GE, et al. EULAR points to consider and consensus definitions for difficult-to-manage and treatment-refractory psoriatic arthritis. Ann Rheum Dis 2026;85(1):61–74. doi:https://doi.org/10.1016/j.ard.2025.10.002

Check for updates

Arthritis & Rheumatology
Vol. 78, No. 10, October 2026, pp 2017–2020
DOI 10.1002/art.70190
© 2026 American College of Rheumatology

American College of Rheumatology
Empowering Rheumatology Professionals

NOTES FROM THE FIELD

Challenges to Research Integrity in Rheumatology: The Threat of Paper Mills, Fraud, and Click Data Science

Tony R. Merriman, PhD,[1,2] Tristan Pascart, MD, PhD,[3] and Maria I. Danila, MD, MSc, MSPH[1,4]

INTRODUCTION

The integrity of biomedical investigation, including rheumatology research, is threatened by deliberate activities from some organizations and researchers. Scientific misconduct and fraud reduces public trust in science and medicine, which influences federal, state, and nongovernmental organization support. Furthermore, the robustness of the science relied upon for medical advances will be eroded, slowing progress and endangering public health. *Arthritis & Rheumatology* has long recognized the critical importance for the readership and wider public to be able to trust the conduct of science.[1] This article seeks to raise awareness in the rheumatology community about the following threats to research integrity and offers recommendations to mitigate their effects: deliberate falsification of data, manuscripts published through paper mills, and "click data science" leading to papers publishing unvalidated or contradictory results using large open access databases.

Intentional scientific fraud is a reality. Although scientific misconduct is not new, its scope and speed are enabled by generative artificial intelligence (AI). We consider fraud to be data synthesis or manipulation with or without the use of generative AI and to include paper mill outputs. One sequela of AI-generated papers results from inclusion of AI hallucinations (in which AI includes incorrect information) and leads to increasing distortion of the scientific literature as more AI-generated papers are included in the AI model training corpus to be included in manuscripts published by paper mills (addressed later in this article).

Illustrating the problem of fraudulent research, an analysis of 50 Cochrane medical reviews raised significant concerns regarding 1 in 17 of the contributing randomized controlled trials.[2] Furthermore, a systematic analysis of >20,000 articles published between 1995 and 2014 identified that 3.8% (approximately 1 in 25) had inappropriately duplicated images (a hallmark of fraudulent science), half of which were clearly deliberate.[3] More than two decades of falsified data have hampered progress toward effective treatments for Alzheimer's disease,[4] at a cost to public health and public and private funding, including failed attempts to replicate results and failed trials. The actions of only a few rogue biomedical scientists, inevitably highlighted in the popular media, have a significant influence on public trust, including discouraging participation in clinical trials. One notable example in rheumatology is a study testing the anti-IgE biologic omalizumab in rheumatoid arthritis: human serum was spiked with mouse antibodies to change negative results to positive findings. This led to retractions of papers in the *Proceedings of the National Academy of Sciences of the United States of America* and *Annals of the Rheumatic Diseases*.[5]

In addition to calculated falsification of research, paper mills are central to the recent increase in degradation in research integrity. Paper mills are businesses that, with large input from generative AI, produce fake papers or click data science, sell authorship, and guarantee publication (including in reputable journals) with the assistance of compromised editors and reviewers.[6] The paper mill industry became infamous in 2023 when many journals of the Hindawi publishing group were infiltrated by paper mills, leading to thousands of retractions and multiple journal closures.[7] Paper mills are abetted by predatory journals that do not conduct quality checks on submissions (eg, publishing articles well outside journal scope) and by hijacked journals (a fake clone of a legitimate journal, 400 of which are currently indexed in Retraction Watch[8]).

The influence of paper mills was noted in a case study of *PLoS One*, which discloses the handling editor of submitted manuscripts.[9] The study highlighted a network of handling editors who facilitated publication of compromised papers at scale. Typically, a specific paper mill targets a set of journals, evolving a new set as target journals are deindexed by Web of Science or

[1]Division of Clinical Immunology and Rheumatology, University of Alabama at Birmingham; [2]Department of Microbiology and Immunology, University of Otago, Dunedin, New Zealand; [3]Department of Rheumatology, Lille Catholic University Hospitals, Lille, France; [4]Geriatric Research Education and Clinical Center, Birmingham Veterans Affairs Medical Center, Birmingham, Alabama.

Author disclosures are available online at https://onlinelibrary.wiley.com/doi/10.1002/art.70190.

Address correspondence via email to Tony R. Merriman, PhD, at trmerriman@uabmc.edu.

Submitted for publication January 6, 2026; accepted in revised form April 6, 2026.

Scopus. An example entity exhibiting features of a paper mill is the Academic Research and Development Association (ARDA) based in Chennai, India. ARDA advertises authorship on manuscripts and thesis and article writing; 33% of target journals listed by ARDA in 2020 eventually were deindexed, compared to the baseline rate of 0.5%.[9] Paper mills invite and bribe journal editors to collaborate. A 2022 "rendezvous" between a journal editor and an unnamed paper mill based in Guangzhou, China, was presented by Sabel et al.[10] The editor (Dr Sabel) was offered $1,000 multiplied by journal impact factor per paper published, with the paper mill offering the journal citations in its fake papers (to increase impact factor). This was in addition to supplying the names of compromised peer reviewers.

The scale of scientific fraud is difficult to estimate, hindered by the ability to unambiguously identify fraudulent papers. Using an empirically developed classification rule, Sabel et al estimated 5.8% (1 in 17) fake papers exist in the biomedical literature.[10] In 2023, 107,800 fake papers were estimated as compared to 5,671 retractions.[10] The total number of scientific publications has been doubling every 15 years, retracted papers every 3.3 years, and estimated paper mill products every 1.5 years.[9] If this trend continues, paper mill products will compose nearly 10% of published papers by 2030.[9]

Another threat to research integrity is the emergence of "click data science", which refers to the practice of using AI methods to generate formulaic low-quality papers from large open access data sets.[11] Click data science is enabled by: ready availability of data sets such as the National Health and Nutrition Examination Survey, UK Biobank, FinnGen, US Food and Drug Administration Adverse Event Reporting System, and Global Disease Burden; machine learning workflows; generative AI; and the paper mill industry have led to a slew of very low-quality papers that collectively pollute the biomedical literature. Click data science includes Mendelian randomization literature, which exploits readily available genome-wide association study summary statistics.[11–13] Data are extracted from an open access data set by an application programming interface, which is then automatically analyzed (eg, multivariate logistic regression of exposure X on phenotype Y in subgroup Z, Mendelian randomization of exposure X on phenotype Y, etc), and the introduction and discussion are written using generative AI (with the formulaic methods and results rewritten each time to evade plagiarism detection).[12]

Contributing to the poor quality of research is overinterpretation of weak data, lack of correction for multiple testing problems, simultaneous testing of different statistical models and different data set stratifications over multiple outcomes, and the presentation of hypotheses as if they were created a priori (this is known as hypothesizing after the results are known, or "HARKing"). The inherent poor quality is worsened by the absence of verification of diagnoses in the large databases and obliviousness to potential biases, confounding, and systematic errors.[14] Click data science also can lead to the growing problem of redundant papers, in which different papers are analyzing the association of the same exposures, with the same outcome in the same data set. More control of data access mechanisms and preregistration of protocols would better balance data availability with more robust science,[13] and better understanding of the pitfalls of large real-world data is needed.[15] Publishers are aware of click data science papers and are introducing policies to prevent their publication; for example, they can require additional work to replicate and

Box 1. Suggested approaches to reduce the negative impact of fraudulent science on health outcomes for people with rheumatic and musculoskeletal diseases

Actions

- Raise awareness about challenges to research integrity.
  - Subscribe to Retraction Watch updates.
  - Be familiar with the Committee on Publication Ethics guidelines on best practices for publication integrity and ethical conduct.
- Publishers must maintain robust policies and procedures to detect fraudulent and click data science papers at submission.
  - Wiley, the publisher of *Arthritis & Rheumatology*, uses six tools: paper mill similarity detection, problematic phrase recognition, author publication behavior, author verification, detection of generative AI content, and checking that a paper is in scope.
- Develop skilled, experienced, and motivated reviewers through formal mentoring of junior researchers.
  - We applaud the work that the American College of Rheumatology Committee on Journal Publications has done through the American College of Rheumatology Journals Peer Review Mentoring Program in this regard.
- Consider compensating reviewers.
  - One hallmark of paper mill activity is inaccurate referencing, particularly in discussion sections, which would be evident to incentivized reviewers.
  - Incentivized specialist reviewers would detect redundant papers.
- Change the current emphasis in academia from quantity to quality of publications.
  - In multi-author, multidisciplinary publications, this would include metrics for appropriate acknowledgment of contribution.
- Consider maintaining a cohort of trusted journals.
  - This would allow the rheumatology community to engage with each other confidently as reviewers, publishing authors, and readers.
- Consider external regulation of academic journals.
  - Example regulatory processes are proposed by Byrne[18] and Tautz and Rainey.[19]
- Acknowledge the conflict of interest inherent when academic institutions investigate their own faculty.
  - Investigation of allegations of scientific misconduct should be performed by independent organizations.
- Consider more severe consequences for fraudulent research.

validate findings.[16] However, it will be important that new requirements do not lead to the unintended consequences of impeding robust research.

The existence in the literature of "zombie" papers (ie, fake papers, those containing fraudulent data, and those based on click data science) will negatively impact public health, and therefore, they need to be purged. The Center for Scientific Integrity, the nonprofit organization that oversees Retraction Watch, has established the Medical Evidence Project, which is aimed toward identifying fake and flawed medical research papers and neutralizing their impact on public health. An analysis of 25,480 retracted papers published over one century revealed that those with serious misconduct took longer to be retracted.[17] Fortunately, science does self-correct over time, with median paper retraction time in medicine being ~600 days.[17] However, in the context of the recent flood of paper mill–generated papers, this lack of alacrity will undoubtedly contribute to impeding progress in biomedical science and, in some cases, affect public health. Another important issue to address is the propagation of fraudulent research by continued ghost citations of retracted papers, with bibliographic databases and journals needing to strengthen retraction notification, including improving the prepublication detection of papers with citations to retracted papers.[17]

CONCLUSIONS

We acknowledge the structural and systemic issues that incentivize the conscious decision to participate in scientific misconduct. Misconduct enabled by paper mills is thriving in a world where increased productivity and citations are perceived as an indicator of academic success and where truth is increasingly regarded as a commodity to be traded for self-interest. What can the rheumatology community do to reduce the negative impact of fraudulent science on health outcomes for people with rheumatic diseases? Detailed in Box 1 there are nine suggested actions: (1) raise awareness; (2) improve publication policies and procedures; (3) promote skilled, experienced, and motivated reviewers; (4) consider compensating reviewers; (5) reduce the emphasis on publication quantity by academic institutions; (6) consideration by the *American College of Rheumatology* the creation of a database of trusted journals; (7) consider external regulation[18,19]; (8) avoid inherent conflict of interest inherent when academic institutions investigate their own faculty; and (9) institute more severe consequences for researchers who deliberately engage in scientific misconduct.

Regarding external regulation, Byrne[18] proposes that academic journals follow the international quality-management standards of the International Organization for Standardization's ISO-9001. This would support establishing a system to document processes put in place to ensure balancing of the interests of consumers of new scientific knowledge against the commercial interests of publishers. Tautz and Rainey[19] propose a journal evaluation system that includes criteria such as an experienced and diverse editorial board with transparent governance, an auditable peer review and publication system with minimum benchmarks, public disclosure of various metrics, and commitment to a code of conduct that rejects predatory practices. The National Institutes of Health Office of Research Integrity (ORI) influences research integrity practices primarily by establishing standards for addressing misconduct. Regarding more severe consequences, the ORI could institute more severe penalties; currently, they typically implement a several-year period of supervision of research activities by the host academic institution. The ORI received 713 allegations of research misconduct in 2024 (https://ori.hhs.gov/blog/ori-announces-release-2024-annual-report). We note that the ORI published only two findings of misconduct in 2025, which is far fewer than the previous average of 12.5 findings per year.

AUTHOR CONTRIBUTIONS

All authors contributed to at least one of the following manuscript preparation roles: conceptualization AND/OR methodology, software, investigation, formal analysis, data curation, visualization, and validation AND drafting or reviewing/editing the final draft. As corresponding author, Dr Merriman confirms that all authors have provided the final approval of the version to be published and takes responsibility for the affirmations regarding article submission (eg, not under consideration by another journal).

REFERENCES

1. Bucala RJ, Solomon DH. Trust in publication: now more than ever. Arthritis Rheumatol 2019;71(10):1593–1594. doi:https://doi.org/10.1002/art.40882
2. Wilkinson J, Heal C, Antoniou GA, et al. Assessing the feasibility and impact of clinical trial trustworthiness checks via an application to Cochrane Reviews: stage 2 of the INSPECT-SR project. J Clin Epidemiol 2025;184:111824. doi:https://doi.org/10.1016/j.jclinepi.2025.111824
3. Bik EM, Casadevall A, Fang FC. The prevalence of inappropriate image duplication in biomedical research publications. MBio 2016;7(3):e00809–e00816. doi:https://doi.org/10.1128/mBio.00809-16
4. Piller C. Doctored: Fraud, Arrogance, and Tragedy in the Quest to Cure Alzheimer's. One Signal Publishers; 2025.
5. Sheldon T. Senior Dutch researcher sacked for manipulating data in rheumatoid arthritis drug trial. BMJ 2013;347:f5267. doi:https://doi.org/10.1136/bmj.f5267
6. Parker L, Boughton S, Bero L, et al. Paper mill challenges: past, present, and future. J Clin Epidemiol 2024;176:111549. doi:https://doi.org/10.1016/j.jclinepi.2024.111549
7. Kincaid E. Hindawi reveals process for retracting more than 8,000 paper mill articles. Retraction Watch. December 19, 2023. Accessed January 2, 2026. https://retractionwatch.com/2023/12/19/hindawi-reveals-process-for-retracting-more-than-8000-paper-mill-articles/
8. Retraction Watch Staff. The Retraction Watch Hijacked Journal Checker now has 400 entries. Retraction Watch. December 26, 2025. Accessed January 5, 2026. https://retractionwatch.com/2025/12/26/retraction-watch-hijacked-journal-checker-now-has-400-entries/

9. Richardson RAK, Hong SS, Byrne JA, et al. The entities enabling scientific fraud at scale are large, resilient, and growing rapidly. Proc Natl Acad Sci U S A 2025;122(32):e2420092122. doi:https://doi.org/10.1073/pnas.2420092122

10. Sabel BA, Knaack E, Gigerenzer G, et al. Fake publications in biomedical science: red-flagging method indicates mass production. Naunyn Schmiedebergs Arch Pharmacol 2026;399(2):2943–2955. doi:https://doi.org/10.1007/s00210-025-04275-9

11. Suchak T, Aliu AE, Harrison C, et al. Explosion of formulaic research articles, including inappropriate study designs and false discoveries, based on the NHANES US national health database. PLoS Biol 2025;23(5):e3003152. doi:https://doi.org/10.1371/journal.pbio.3003152

12. Richardson R, Spick M. Meeting the challenges posed by mass-produced manuscripts and click-data science. Eur Sci Ed 2025;51:e165043. doi:https://doi.org/10.3897/ese.2025.e165043

13. Spick M, Onoja A, Harrison C, et al. Quantifying new threats to health and biomedical literature integrity from rapidly scaled publications and problematic research. J Clin Epidemiol 2026;193:112203. doi:https://doi.org/10.1016/j.jclinepi.2026.112203

14. Costenbader KH, Solomon DH, Bridges SL. Big data may have big pitfalls: ensuring rigor in rheumatic disease epidemiology. Arthritis Rheumatol 2026;78(8):1636–1640. doi:https://doi.org/10.1002/art.70067

15. Jani M, Curtis JR, Hyrich KL. Navigating real-world data sources in rheumatology: opportunities, pitfalls, and practical guidance. Ann Rheum Dis Published online December 22, 2025. doi:https://doi.org/10.1016/j.ard.2025.11.018

16. O'Grady C. Papers based on open health data face bans. Science 2025;390(6770):222–223. doi:https://doi.org/10.1126/science.aed1020

17. Joëts M, Mignon V. Slaying the undead: How long does it take to kill zombie papers? Research Policy 2026;55(2):105401. doi:https://doi.org/10.1016/j.respol.2025.105401

18. Byrne JA. Put pressure on publishers to follow best practice - external regulation is the answer. Nature 2026;649(8095):8. doi:https://doi.org/10.1038/d41586-025-04099-w

19. Tautz D, Rainey PB. An evaluation system for scientific journals. EMBO Rep 2026;27(1):3–4. doi:https://doi.org/10.1038/s44319-025-00649-5

Check for updates

Arthritis & Rheumatology
Vol. 78, No. 10, October 2026, pp 2021–2035
DOI 10.1002/art.70124
© 2026 American College of Rheumatology.

American College of Rheumatology
Empowering Rheumatology Professionals

TWIST1-Mediated Induction of AEBP1 in Fibroblast-Like Synoviocytes Activates Transforming Growth Factor β Signaling to Drive Angiogenesis and Promote Rheumatoid Arthritis

Zhenyu Li, MD,[1] Minglong Cai, MD,[1,2] Wei Huang, MD,[3] Xi Wen, MM,[1] Yujing Li, MD,[1] Jun Sun, PhD,[1,4] Chen Zhu, MD,[3] Chao Yang, PhD,[5] and Zhu Chen, MD[1,4]

Objective. Aggressive fibroblast-like synoviocytes (FLS) drive synovial hyperplasia, extracellular matrix (ECM) remodeling, and pannus formation in rheumatoid arthritis (RA). However, the pathogenic FLS subpopulations and their upstream regulators remain incompletely defined. This study aimed to (i) identify FLS subpopulation(s) responsible for synovial hyperplasia, ECM remodeling, and pannus development, (ii) elucidate the molecular mechanisms regulating their pathogenic activation, and (iii) explore therapeutic strategies targeting FLS activation and pannus-associated neovascularization in RA.

Methods. We integrated bulk RNA sequencing, proteomics, and single-cell transcriptomics to identify pathogenic FLS subpopulation(s) in RA synovium. Functional assays were conducted to assess the effects of adipocyte enhancer-binding protein 1 (AEBP1) and periostin (POSTN) expression on FLS activation, ECM remodeling, and angiogenesis. Bioinformatic analyses and cell biologic experiments were adopted to identify the upstream regulator responsible for AEBP1 expression in FLS. We subsequently investigated the pathologic impact of TWIST1–AEBP1–POSTN axis in a collagen-induced arthritis (CIA) mice model.

Results. We identified a pathogenic $POSTN^+$ FLS subgroup selectively enriched within the sublining layer of synovium that exhibited robust ECM remodeling and fibrogenic features. Mechanistically, we showed that AEBP1 was selectively elevated in these cells, in which it activated transforming growth factor β signaling to drive fibroblast activation, migration, and proliferation. Besides, AEBP1 also induced POSTN expression, which was responsible for neovascularization. Further, inflammatory signalings induced TWIST1 expression, which directly regulated AEBP1 transcription in FLS. Intra-articular modulation of AEBP1 in mice with CIA had opposite effects on synovial hyperplasia, bone erosion, and pannus formation. Moreover, the pharmacological inhibition of TWIST1 by harmine-reduced AEBP1 and POSTN expression, limited the expansion of pathogenic $THY1^+$ FLS, and alleviated joint pathology.

Conclusion. Our study suggests that $POSTN^+$ FLS located in the synovial sublining contribute to RA progression through the TWIST1–AEBP1–POSTN axis. Accordingly, targeting of this axis may offer a novel and effective approach for RA treatment.

INTRODUCTION

Rheumatoid arthritis (RA) is a chronic autoimmune disease characterized by synovial inflammation, hyperplasia, pannus formation, and progressive destruction of cartilage and bone, affecting approximately 0.5% to 1% of the global population.[1,2] Current treatment strategies primarily rely on conventional synthetic disease-modifying antirheumatic drugs (DMARDs) and

Supported by the National Natural Science Foundation of China (grant 82471819 to Dr Chen), the Anhui Provincial Natural Science Foundation (grant 2408085J046 to Dr Chen), the University of Science and Technology of China (USTC) Research Funds of the Double First-Class Initiative (grant YD9110002012 to Dr Chen), the Shaanxi Provincial Scientific and Technological Activities Selective Funding Project for People with study abroad experience (grant 9990401 to Dr Yang), the Key Basic Research Program of Shaanxi (grant 2025SF-YBXM-376 to Dr Yang) and the Basic Scientific Research Funding of Xi'an Jiaotong University (grant xtr052025012 to Dr Yang), .

[1]Department of Rheumatology and Immunology, The First Affiliated Hospital of USTC, Division of Life Sciences and Medicine, USTC, Hefei, China; [2]Department of Dermatology, The First Affiliated Hospital of USTC, Division of Life Sciences and Medicine, USTC, Hefei, China; [3]Department of Orthopedics, The First Affiliated Hospital of USTC, Division of Life Sciences and Medicine, USTC, Hefei, China; [4]National Key Laboratory of Immune Response and Immunotherapy, Division of Life Science and Medicine, USTC, Hefei, China; [5]Department of Rheumatology and Immunology and the MED-X Institute, Center for Immunological and Metabolic Diseases, The First Affiliated Hospital of Xi'an Jiaotong University, Xi'an Jiaotong University, Xi'an, China.

Drs Z. Li, Cai, and Huang contributed equally as first authors.

Additional supplementary information cited in this article can be found online in the Supporting Information section (https://acrjournals.onlinelibrary.wiley.com/doi/10.1002/art.70124).

biologic or targeted synthetic DMARDs (b/tsDMARDs), which predominantly suppress immune cells and inflammatory cytokines. Although b/tsDMARDs have improved outcomes in many patients, therapeutic efficacy remains suboptimal—up to 40% of patients with RA show inadequate responses to specific biologic therapies.[3] One promising avenue involves identifying and selectively targeting disease-driving pathogenic cell subsets within the synovial microenvironment to improve treatment response and halt disease progression.

Fibroblast-like synoviocytes (FLS), as the principal stromal cell type in the synovium, play a central role in maintaining tissue homeostasis under physiologic conditions.[4] Normally, the synovial lining consists of one to three layers of resident cells. In RA, however, FLS undergo pathologic expansion and adopt an aggressive phenotype characterized by increased proliferation, migration, and secretion of pro-inflammatory cytokines and matrix-degrading enzymes. These activated FLS not only perpetuate a chronic inflammatory milieu but also remodel the extracellular matrix (ECM), creating a permissive niche for disease progression. Recent studies have identified a subpopulation of pathogenic FLS within the synovial sublining layer marked by THY1 expression, which is expanded in RA and associated with local joint inflammation.[5] Furthermore, $THY1^+$ FLS interact with vascular endothelial cells through Notch signaling and contribute directly to pathologic angiogenesis and pannus formation.[6] Pannus—a hallmark of RA—is a tumor-like invasive tissue that erodes cartilage and bone. It also creates a pro-inflammatory and pro-angiogenic environment that recruits immune cells and exacerbates synovial inflammation.[7] Despite increasing evidence of FLS heterogeneity, the precise pathogenic FLS subsets and their upstream regulators responsible for synovial angiogenesis and pannus formation in RA are not fully understood.

Adipocyte enhancer-binding protein 1 (AEBP1) was originally identified as a transcriptional repressor involved in adipocyte differentiation.[8] A specific isoform of AEBP1, known as aortic carboxypeptidase-like protein (ACLP), has recently been recognized as a secreted ECM protein with potent profibrotic functions. ACLP promotes fibroblast activation and differentiation, contributing to fibrosis in the lung and heart.[9,10] Additionally, ACLP mediates fibrosis progression in nonalcoholic steatohepatitis (NASH) through Wnt signaling, and its genetic ablation ameliorates fibrosis in both NASH and bleomycin-induced pulmonary fibrosis models.[11,12] Despite this growing evidence of its pathologic roles, the function of AEBP1 and ACLP in RA FLS remains largely unexplored.

In this study, we aimed to identify FLS subpopulation(s) in the pathogenesis of RA, focusing on its effects on FLS behavior, angiogenesis, and the overall severity of arthritis. Specifically, we examined how AEBP1 influenced RA FLS migration, invasion, and proliferation and how AEBP1 expression was regulated by TWIST1, thereby inducing periostin (POSTN) expression and neovascularization. By understanding the mechanistic interactions of these pathways, we elucidated the contribution of the TWIST1–AEBP1–POSTN axis to RA pathology, with the goal of identifying novel therapeutic targets for improving RA treatment strategies.

METHODS

Synovial tissue collection. Synovial tissues from 14 patients with active RA undergoing total knee arthroplasty (diagnosed according to the 2010 American College of Rheumatology/EULAR criteria)[13] and 6 osteoarthritis (OA) controls (patients without RA history) were collected under protocols approved by the Biomedical Ethics Committee of the First Affiliated Hospital of the University of Science and Technology of China with written informed consent. Supplementary Table S1 provides detailed information about the patients involved in the study.

Histologic analysis and FLS culture. Human synovial tissues from patients with RA and OA were fixed, paraffin embedded, and sectioned (4 μm) for immunohistochemistry (IHC) using an anti-AEBP1 antibody (Santa Cruz, USA). FLS of RA synovium and OA synovium were isolated via 0.2% type IV collagenase digestion and cultured in Dulbecco's modified Eagle's medium (DMEM) with 10% fetal bovine serum. Passages four through eight were used.

Flow cytometric sorting. Synovial single-cell suspensions were stained with fluorochrome-conjugated antibodies against CD45 (Brilliant Violet 421, Clone: HI30, BioLegend), CD235a (PE, Clone: HI264, BioLegend), CD31 (PE/Cyanine7, Clone: WM59, BioLegend), PDPN (allophycocyanin, Clone: NC-08, BioLegend), and THY1 (Brilliant Violet 510, Clone: 5E10, BioLegend). Live cells (Zombie NIR^-, BioLegend) were gated as FLS ($CD235a^-CD45^-CD31^-PDPN^+$) and sorted into $THY1^+$ and $THY1^-$ populations (>95% purity) using an FACS Aria III (BD Biosciences) for downstream omics.

Omics analysis. RNA sequencing (RNA-seq) of sorted FLS was performed by OE Biotech Co, Ltd (China). For proteomics, peptides were analyzed using a nanoElute LC system coupled to a trapped ion mobility spectrometry–equipped mass spectrometer (Bruker) operating in diaPASEF mode. Data were processed with Spectronaut (Biognosys Inc; 1% false discovery

Author disclosures and graphical abstract are available at https://onlinelibrary.wiley.com/doi/10.1002/art.70124.

Address correspondence via email to Chen Zhu, at zhuchena@ustc.edu.cn; to Chao Yang, at ychmax@xjtufh.edu.cn; or to Zhu Chen, MD, at doczchen@ustc.edu.cn.

Submitted for publication August 6, 2025; accepted in revised form February 13, 2026.

rate). Public RA/OA single-cell RNA-seq and bulk RNA-seq data (ImmPort: SDY998, https://www.immport.org/shared/study/SDY998) were analyzed using Seurat R package (version 4.0) and DESeq2 R package, respectively.[14]

Quantitative reverse transcriptase–polymerase chain reaction and reverse transcriptase–polymerase chain reaction. For quantitative reverse transcriptase–polymerase chain reaction (qRT-PCR), cDNA synthesis was performed with the BioRT Master Hisensi cDNA First Strand Synthesis Kit (Bioflux), and qPCR amplification was conducted on an ABI Step One system (Applied Biosystems) using Universal qPCR Premix (SYBR Green; Epizyme). Relative expression of target genes was calculated using the $2^{-\Delta\Delta CT}$ method normalized to the reference gene GAPDH (primers in Supplementary Table S2). For reverse transcriptase–polymerase chain reaction (RT-PCR), extracted RNA was reverse transcribed and amplified using the 2× Taq Master Mix (Vazyme) with the primers (primers in Supplementary Table S2).

Western blots. Western blotting followed standard protocols. Polyvinylidene difluoride (PVDF) membranes were probed with primary antibodies including AEBP1 (Santa Cruz, USA), Smad3 (Cell Signaling Technology), p-Smad3 (Cell Signaling Technology), collagen type I (Proteintech), α-SMA (Proteintech), N-Cadherin (Proteintech), vimentin (Proteintech), POSTN (Proteintech), TWIST1 (Proteintech), MMP1 (Epizyme), MMP2 (Epizyme), MMP3 (Epizyme), PDGFRA (Epizyme), PDGFRB (Epizyme), p-P65 (Epizyme), P65 (Epizyme), AKT (Epizyme), and p-AKT (Epizyme) at 4°C overnight and were subsequently probed with horseradish peroxidase (HRP)–conjugated secondary antibodies (Proteintech) at room temperature for one hour. The PVDF membranes were visualized via chemiluminescence on a Tanon Fine-do X6 Imaging System (Tanon) and quantified using ImageJ software.

Cellular assays. Migration and invasion (using Matrigel-coated inserts) were evaluated via Transwell assays after 24 or 48 hours. Scratch wound healing was monitored at 0 and 24 hours. Cell proliferation was measured using an EdU Kit (Epizyme). Endothelial tube formation was assessed by culturing human umbilical vein endothelial cells (HUVECs) on Matrigel for six hours.

Gene modification and conditioned medium. RA FLS were transfected with empty vectors, AEBP1 overexpression (AEBP1-OE) plasmids, or small interfering RNAs (siRNAs) targeting TWIST1/POSTN using Lipofectamine 3000 (Thermo Fisher Scientific) according to the manufacturer's instructions. For conditioned medium (CM), transfected cells were cultured in serum-free DMEM for 24 hours; supernatants were collected, centrifuged, and filtered through a 0.22-μm filter. The CM was aliquoted and stored at –80°C.

Chromatin immunoprecipitation and dual-luciferase assays. Chromatin immunoprecipitation (ChIP) was performed using anti-TWIST1 (Proteintech) or IgG (Proteintech), and enriched AEBP1 promoter regions were quantified by qPCR using specific primers (primers in Supplementary Table S2). For dual-luciferase assays, HEK-293T cells were cotransfected with wild-type/truncated/mutant AEBP1 promoter-luciferase plasmids, TWIST1 overexpression plasmids, and pRL-TK. Luciferase activity was measured after 48 hours.

Collagen-induced arthritis. Male DBA/1 mice (six to eight weeks old) were purchased from Beijing HFK Bio-Technology Co, Ltd. All animal experiments were approved by the Animal Ethics Committee of The First Affiliated Hospital of the University of Science and Technology of China. All mice were housed in a specific pathogen-free animal facility. The food provided to the mice was irradiated, and the water was autoclaved. Mice had free access to food and water. After a one-week acclimation period, the mice were immunized by intradermal injection of Chick type II collagen (Chondrex) emulsified in complete Freund's adjuvant (Chondrex) at the base of the tail. On day 21, a booster injection of Chick type II collagen emulsified in incomplete Freund's adjuvant (Chondrex) was administered at the same site.

For adeno-associated virus (AAV)–AEBP1 injection, mice were randomly assigned to receive an intra-ankle injection of AAV-AEBP1 overexpression (AAV-AEBP1-OE; 1×10^{10} vg/ankle; n = 6) or received an intra-ankle injection of AAV-control (1×10^{10} vg/ankle) on day 14 (n = 6).

For AAV-shAEBP1 injection, mice were randomly assigned to receive an intra-ankle injection of AAV-shAEBP1 (1×10^{10} vg/ankle; n = 6) or received an intra-ankle injection of AAV-control (1×10^{10} vg/ankle) on day 14 (n = 6).

For anti-POSTN antibody injection, mice were randomly assigned to receive an intra-ankle injection of AAV-AEBP1-OE (1×10^{10} vg/ankle; n = 12) or received an intra-ankle injection of AAV-control (1×10^{10} vg/ankle) on day 14 (n = 6). Additionally, anti-POSTN antibody (5 μg/ankle) or IgG control were injected into the ankle joints once a week, starting from day 21 until the end of the experiment.

For pharmacological inhibition experiments, mice were randomly assigned to intraperitoneal injection with harmine (20 mg/kg/day; MedChemExpress; n = 6) starting from day 21, whereas the corresponding control group (n = 6) received an equal volume of vehicle by intraperitoneal injection on the same schedule. The severity of limb swelling was assessed using a 0 to 4 scoring system (0 = normal, 1 = minimal erythema and mild swelling, 2 = moderate erythema and mild swelling, 3 = marked

erythema and severe swelling, without involvement of the digits, 4 = maximal swelling, with digit involvement).

Flow cytometry of mice joints. Flow cytometry of mouse ankle joints was performed as previously described.[15] Briefly, the joints were dissected from 3 mm above the ankle to the middle of the paw. The tissues were digested in 2-mL RPMI medium containing 2% fetal calf serum and 1-mg/mL collagenase D (Sigma-Aldrich) at 37°C for one hour. The digested suspension was then passed through a 70-μm cell strainer, followed by red blood cell lysis using red blood cell lysis buffer for five minutes. The cells were stained with Zombie NIR Dye (BioLegend) for 15 minutes, washed, and incubated with anti-CD16/CD32 blocking antibody (BioLegend) at room temperature for 10 minutes. Then, the cells were incubated in the dark with CD45 (Brilliant Violet 510, Clone: 30F11, BioLegend), CD31 (PE/Dazzle 594, Clone: 390 BioLegend), PDPN (PE/Cyanine7, Clone: 8.1.1, BioLegend), and THY1.2 (Brilliant Violet 605, Clone: 53-2.1, BioLegend) for 30 minutes. After incubation, flow cytometric analysis was performed using CytoFLEX S (Beckman Coulter). Data were analyzed with CytExpert version 2.5 (Beckman Coulter).

Histologic analysis of mice joints. At day 42 post modeling, ankle joints were fixed in 4% paraformaldehyde, decalcified with 10% EDTA, and sectioned (4 μm) for hematoxylin and eosin and Safranin O/Fast Green staining. Collagen-induced arthritis (CIA) histopathological features (including synovial hyperplasia, inflammation, cartilage destruction, and bone erosion) were evaluated using a standard 0 to 4 scoring system.

IHC and immunofluorescence of mice joints. Joint sections underwent citrate buffer antigen retrieval. For IHC, sections were probed with anti-AEBP1, detected via HRP/diaminobenzidine reagent, and counterstained with hematoxylin. For immunofluorescence (IF), sequential dual-target labeling was performed using a tyramide signal amplification kit (Recordbio) with intermediate peroxidase quenching and secondary antigen retrieval, followed by DAPI counterstaining for nuclei.

Micro–computed tomography. Ankle joints and hind paws were scanned using a nanoVoxel-1000 micro–computed tomography system (Sanying; 100 kV, 80 μA). Joint structural damage was quantified by calculating bone volume fraction (bone volume/total volume [BV/TV]) and trabecular thickness (Tb.Th) using Dragonfly software (version 2022.1).

Statistical analysis. GraphPad Prism was used for statistical analysis and figure generation. Comparisons between two groups were conducted using an unpaired two-tailed Student's *t*-test, whereas multiple-group comparisons were performed using one-way analysis of variance. Each experiment was repeated at least three times. Data are presented as mean ± SD, and a P value < 0.05 was considered statistically significant.

RESULTS

POSTN$^+$ FLS are expanded in RA and enriched for ECM remodeling signatures. To investigate FLS heterogeneity, we sorted THY1$^+$ and THY1$^-$ FLS from RA synovium for bulk RNA-seq and proteomic profiling (Gating strategy shown in Supplementary Figure S1A). Consistent with previous findings, PRG4 was highly expressed in THY1$^-$ FLS, whereas NOTCH3 was enriched in THY1$^+$ FLS (Figure 1A).[6] Gene ontology (GO) analysis revealed that THY1$^+$ FLS were highly enriched in ECM organization pathways (Figure 1B).

Reanalysis of public single-cell RNA-seq data from Zhang et al identified four major FLS subsets, among which a POSTN$^+$ subset (marked by COL1A1, AEBP1, COL1A2, SPARC, COL3A1) was substantially expanded in RA compared to OA synovium (Figure 1C-F).[14] Notably, AEBP1 expression was highest in POSTN$^+$ cluster (Figure 1G), which also exhibited strong ECM pathway enrichment (Figure 1H, 1I), mirroring our bulk THY1$^+$ FLS data.

Integrating our bulk RNA-seq and proteomics data sets confirmed that AEBP1 was significantly up-regulated at both messenger RNA (mRNA) and protein levels in THY1$^+$ FLS (Figure 1J). Furthermore, cross–cell-type analysis demonstrated that AEBP1-OE in RA synovium was strictly FLS-specific, with no significant upregulation in immune cells (Figure 1K, 1L). Consequently, we prioritized AEBP1 to investigate its contribution to FLS pathology and RA.

The ECM-associated isoform of AEBP1 is predominantly expressed in RA FLS and promotes RA FLS activation. AEBP1 exists as a short nuclear repressor and a long ECM-associated isoform (ACLP).[8,16,17] RT-PCR and Western blotting revealed that RA FLS predominantly express ACLP, whereas the short isoform was undetectable (Figure 2A, 2B). Furthermore, AEBP1 mRNA and protein levels were significantly elevated in RA FLS versus OA FLS (Figure 2B, Supplementary Figure S1B). Immunohistochemistry and multiplexed IF confirmed AEBP1 predominantly localizes to the sublining region of RA synovium, specifically within THY1$^+$ and PDPN$^+$ FLS populations (Figure 2C, 2D). Thus, ACLP is the dominant functional isoform in RA FLS.

Functionally, AEBP1-OE significantly enhanced RA FLS migration, invasion, and proliferation (Figure 2E–H). Recombinant ACLP (rACLP) treatment and AEBP1 siRNA knockdown corroborated these pro-activation effects of AEBP1 (Figure 2I–K, Supplementary Figure S2A–E), suggesting that AEBP1 promotes FLS activation via an autofeedback mechanism.

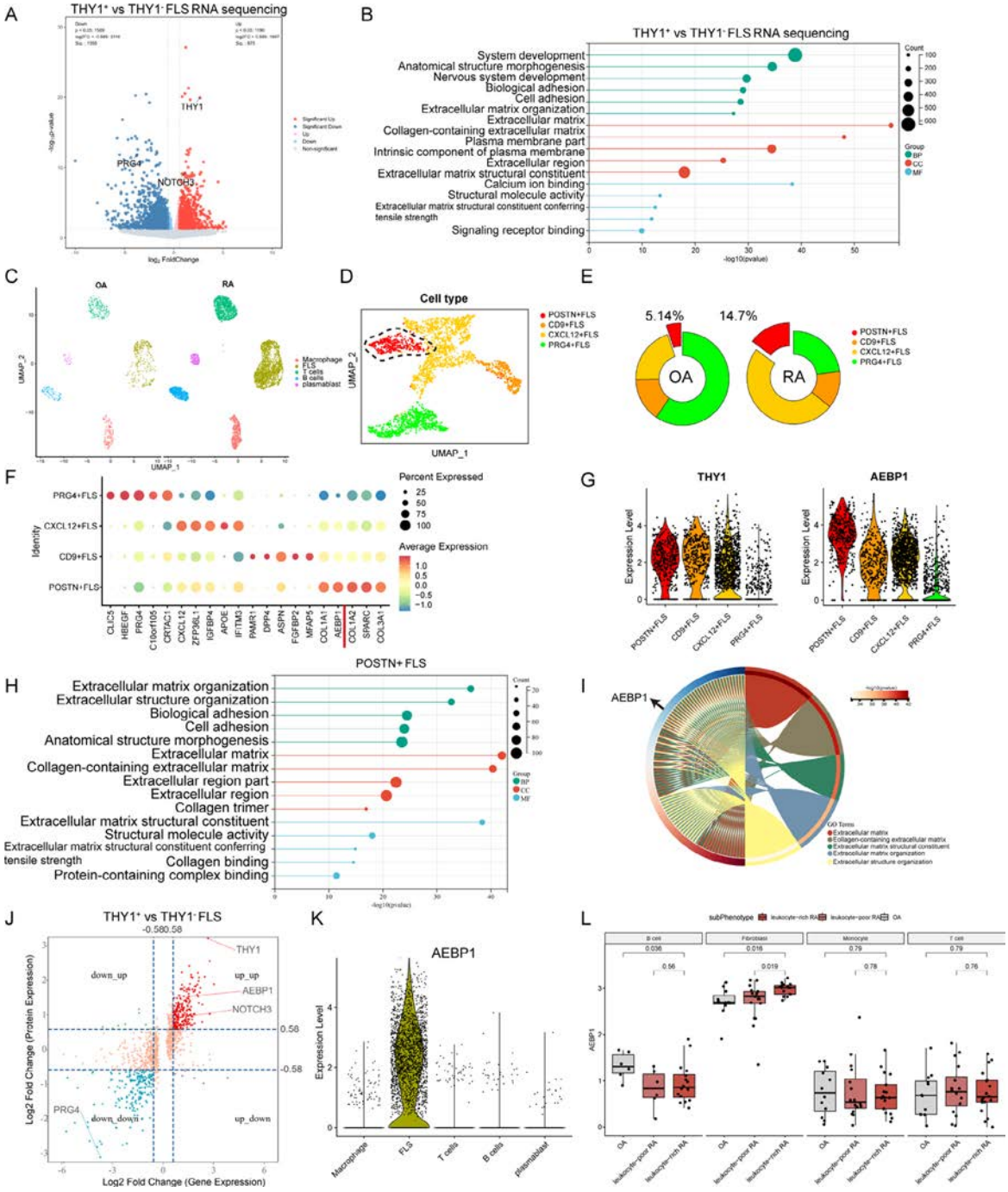


Figure 1. POSTN$^+$ FLS are enriched in RA synovium and ECM remodeling features. (A) Volcano plot showing differential expression between THY1$^+$ and THY1$^-$ FLS. (B) GO analysis of up-regulated genes indicating ECM-related enrichment in THY1$^+$ FLS. (C) UMAP projection showing diverse cell populations in synovial tissue. (D) UMAP projection showing four FLS subsets: POSTN$^+$ FLS, CD9$^+$ FLS, CXCL12$^+$ FLS, PRG4$^+$ FLS. (E) Pie chart showing the increased proportion of POSTN$^+$ FLS in RA versus OA. (F) Dot plot showing the marker genes of POSTN$^+$ FLS, CD9$^+$ FLS, CXCL12$^+$ FLS, PRG4$^+$ FLS. (G) Violin plots confirming the high AEBP1 expression in POSTN$^+$ FLS cluster. (H, I) GO enrichment analysis of POSTN$^+$ FLS indicates ECM and collagen pathway activation. (J) Distribution of genes with a significant change in both mRNA level and protein expression level in THY1$^+$ FLS versus THY1$^-$ FLS. (K) Violin plot of single-cell RNA-seq showing AEBP1 expression is FLS-specific in RA synovium. (L) Bulk RNA-seq revealing the up-regulation of AEBP1 in FLS of leukocyte-rich RA synovium. AEBP1, adipocyte enhancer-binding protein 1; BP, biological process; CC, cellular component; ECM, extracellular matrix; FLS, fibroblast-like synoviocytes; GO, gene ontology; MF, molecular function; mRNA, messenger RNA; OA, osteoarthritis; POSTN, periostin; RA, rheumatoid arthritis; RNA-seq, RNA sequencing; UMAP, uniform manifold approximation and projection.

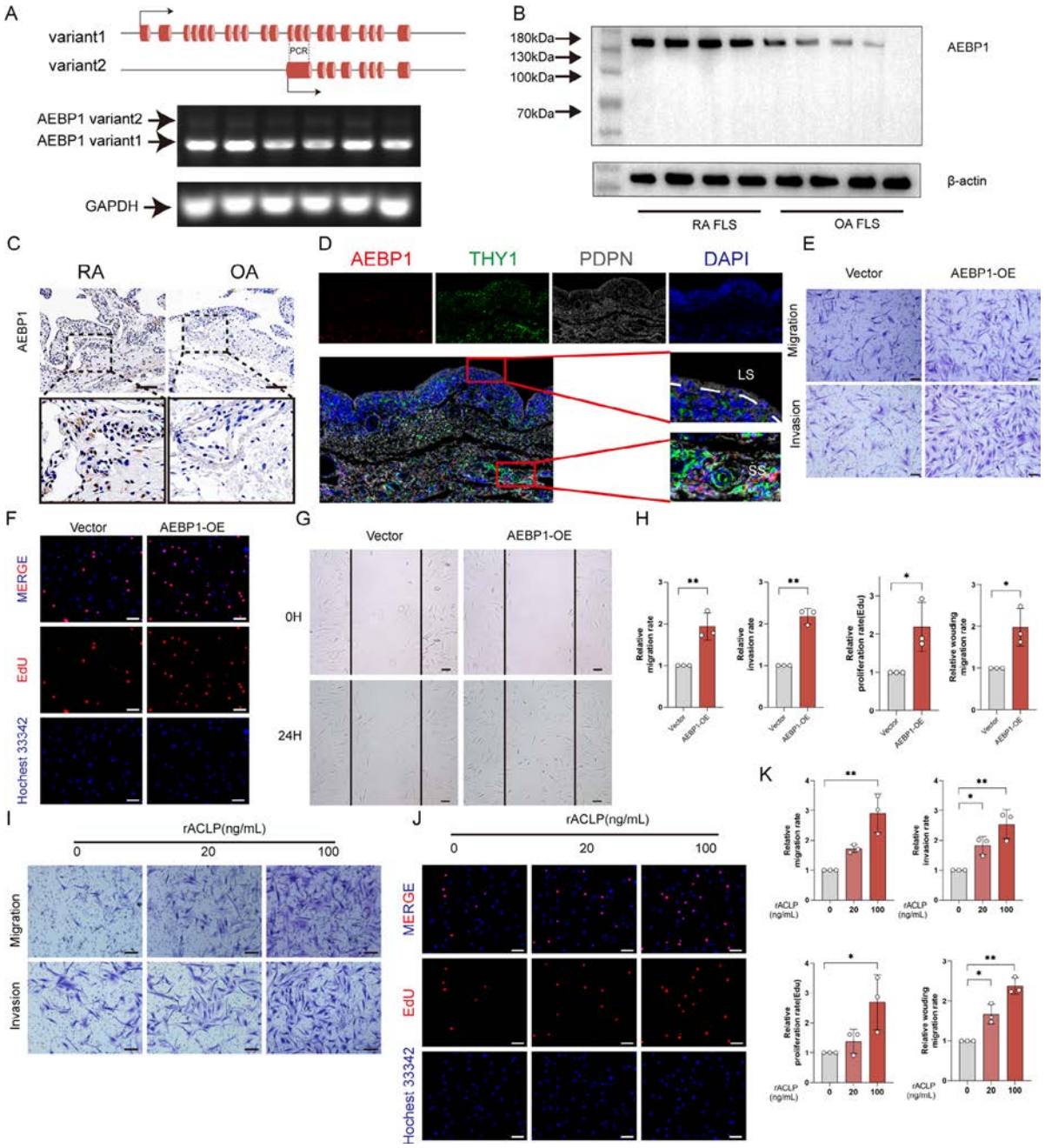


Figure 2. ACLP is the predominant AEBP1 isoform in RA FLS and promotes FLS activation. (A) RT-PCR demonstrates that RA FLS primarily express the long ECM-associated isoform of AEBP1 (ACLP). (B) Western blot analysis confirms elevated AEBP1 protein levels in RA FLS compared to OA FLS. (C) IHC reveals increased AEBP1 expression localized to the sublining region of RA synovium. Scale = 100 μm. (D) Multiplexed IF staining performed on RA synovium to assess the expression of AEBP1 (red) in relation to THY1 (green, a marker for sublining markers), PDPN (gray, a marker for both lining and sublining markers), and DAPI (blue, nuclear stain). Scale = 100 μm. (E–H) The overexpression of AEBP1 prompts the migration, invasion, and proliferation of RA FLS, n = 3. (I–K) rACLP treatment prompts the migration, invasion, and proliferation of RA FLS, n = 3. Scale = 100 μm. $^{*}P < 0.05$, $^{**}P < 0.01$. ACLP, aortic carboxypeptidase-like protein; AEBP1, adipocyte enhancer-binding protein 1; ECM, extracellular matrix; FLS, fibroblast-like synoviocytes; IF, immunofluorescence; IHC, immunohistochemistry; LS, lining synovium; OA, osteoarthritis; OE, overexpression; PCR, polymerase chain reaction; RA, rheumatoid arthritis; rACLP, recombinant ACLP; RT, reverse transcriptase; SS, sublining synovium. Color figure can be viewed in the online issue, which is available at http://onlinelibrary.wiley.com/doi/10.1002/art.70124/abstract.

AEBP1 activates RA FLS via transforming growth factor β signaling and induces epithelial-mesenchymal transition–associated fibrogenic phenotypes. RNA-seq of AEBP1-overexpressing RA FLS revealed significant differential gene expression (Figure 3A). GO and Hallmark analyses, supported by gene set enrichment analysis, indicated robust enrichment in ECM, epithelial-mesenchymal transition (EMT), and transforming growth factor β (TGFβ) signaling pathways (Figure 3B–E). Similar enrichment was observed in POSTN$^+$ and THY1$^+$ FLS subpopulations (Supplementary Figure S3A–C). Consistent with ACLP directly activating TGFβ receptors,[10] AEBP1-OE increased SMAD3 phosphorylation, which was effectively blocked by the TGFβ receptor inhibitor LY2109761 (Supplementary Figure S3D). Furthermore, siRNA knockdown revealed that rACLP activates TGFβ signaling primarily through transforming growth factor β receptor type II (TGFβRII; Supplementary Figure S4A), aligning with previous findings on TGFβRII in fibroblast pathogenesis.[10,18]

Investigating EMT and ECM remodeling, we found AEBP1-OE significantly up-regulated fibrotic (COL1A1, α-SMA) and EMT-associated (vimentin, N-cadherin) markers, which was reversed by LY2109761, TGFβ receptor inhibition (Supplementary Figure S3E, S3F). Similarly, rACLP treatment promoted SMAD3 phosphorylation (Supplementary Figure S3G) and up-regulated these markers in a TGFβ-dependent manner (Supplementary Figure S3H–J). Thus, AEBP1-induced fibrogenic activation relied on TGFβ signaling.

Additionally, AEBP1-OE promoted the expression of key migration/invasion factors (MMP1, MMP3, CDH11; Supplementary Figure S4B) and the proliferation receptor PDGFRA (Supplementary Figure S4C). Similarly, rACLP up-regulated these migration/invasion factors and was blocked by the TGFβ receptor inhibitor LY2109761 (Supplementary Figure S4D). Survival pathways (AKT, NF-κB) were not significantly involved (Supplementary Figure S4E, S4F). These findings suggest that AEBP1 promotes FLS migration, invasion, and proliferation via the modulation of MMPs, CDH-11, and PDGFRA expression.

AEBP1 induces POSTN in FLS driving angiogenesis during the pathogenesis of RA. Pathologic pannus formation requires aberrant synovial angiogenesis. CM from AEBP1-overexpressing RA FLS (AEBP1-OE-CM) significantly enhanced HUVECs proliferation and tube formation (Figure 3F, 3G). However, rACLP treatment directly failed to elicit this response (Supplementary Figure S5A, S5B), indicating that AEBP1-activated FLS secreted pro-angiogenic factors.

Intersecting three transcriptomic data sets and established pro-angiogenic genes identified POSTN as the sole shared pro-angiogenic mediator (Figure 3H). POSTN was up-regulated parallel to AEBP1 in our bulk RNA-seq and proteomic analyses (Figure 3I) and in the RA leukocyte-enriched subgroup (Figure 3J). Single-cell RNA-seq data specifically enriched POSTN in the POSTN$^+$ FLS subpopulation (Figure 3K, Supplementary Figure S5C, S5D). AEBP1-overexpressing RNA-seq confirmed this high POSTN expression (Figure 3A, Supplementary Figure S5E).

Mechanistically, AEBP1 induced POSTN protein expression dependently on TGFβ receptor activation (Supplementary Figure S5F–H). Functionally, silencing POSTN in AEBP1-overpressing FLS abrogated the CM's pro-angiogenic effect (Figure 3L, Supplementary Figure S5I). Recombinant human POSTN promoted tube formation (Supplementary Figure S6A, S6B), and POSTN neutralization suppressed AEBP1-OE-CM–induced angiogenesis (Supplementary Figure S6C, S6D). Thus, POSTN critically mediates AEBP1-induced angiogenesis in RA.

AEBP1 aggravates arthritis severity and promotes synovial angiogenesis through POSTN in mice with CIA. To assess the function of AEBP1 in vivo, mice with CIA received intra-articular AAV-AEBP1 or control vectors on day 14 (Figure 4A). By day 42, IHC confirmed robust synovial AEBP1-OE (Figure 4B). AEBP1-overexpressing mice exhibited significantly elevated arthritis scores, hind paw swelling, and bone erosion (Figure 4C–F). Histologic and IF analyses revealed exacerbated inflammation, joint destruction (Figure 4G–I), increased POSTN expression, and enhanced vascular density in AEBP1-overexpressing mice (Figure 4J). Additionally, AEBP1-OE increased the THY1$^+$/THY1$^-$ FLS ratio (Figure 4K, 4L; gating strategy shown in Supplementary Figure S7A), with AEBP1 localizing predominantly around PDPN$^+$ FLS (Supplementary Figure S7B).

Conversely, AEBP1 knockdown via AAV-shAEBP1 significantly alleviated arthritis severity, synovial inflammation, and vascularization (Supplementary Figure S8A–H). Crucially, administering a neutralizing anti-POSTN antibody to AAV-AEBP1–treated mice reduced vascular density and ameliorated the arthritis (Supplementary Figure S9A–F). These in vivo findings confirmed POSTN as a pivotal mediator of AEBP1-induced neovascularization and joint pathology.

TWIST1 is responsible for AEBP1 expression in RA FLS. BNC2, SNAI2, and TWIST1 were identified as potential upstream regulators of AEBP1 using JASPAR predictions and co-expression analyses (Figure 5A). TWIST1 exhibited the most significant differential expression across FLS subsets (Figure 5B, 5C). Moreover, bulk RNA-seq data from Zhang et al revealed that TWIST1 was significantly up-regulated in leukocyte-enriched RA FLS (Figure 5D), showing a similar expression trend to AEBP1.[14] Additionally, Western blot analysis further confirmed that TWIST1 expression was significantly higher in RA FLS than in OA FLS (Figure 5E).

Four putative TWIST1 binding sites were predicted in the AEBP1 promoter using JASPAR (Figure 5F). ChIP-qPCR and

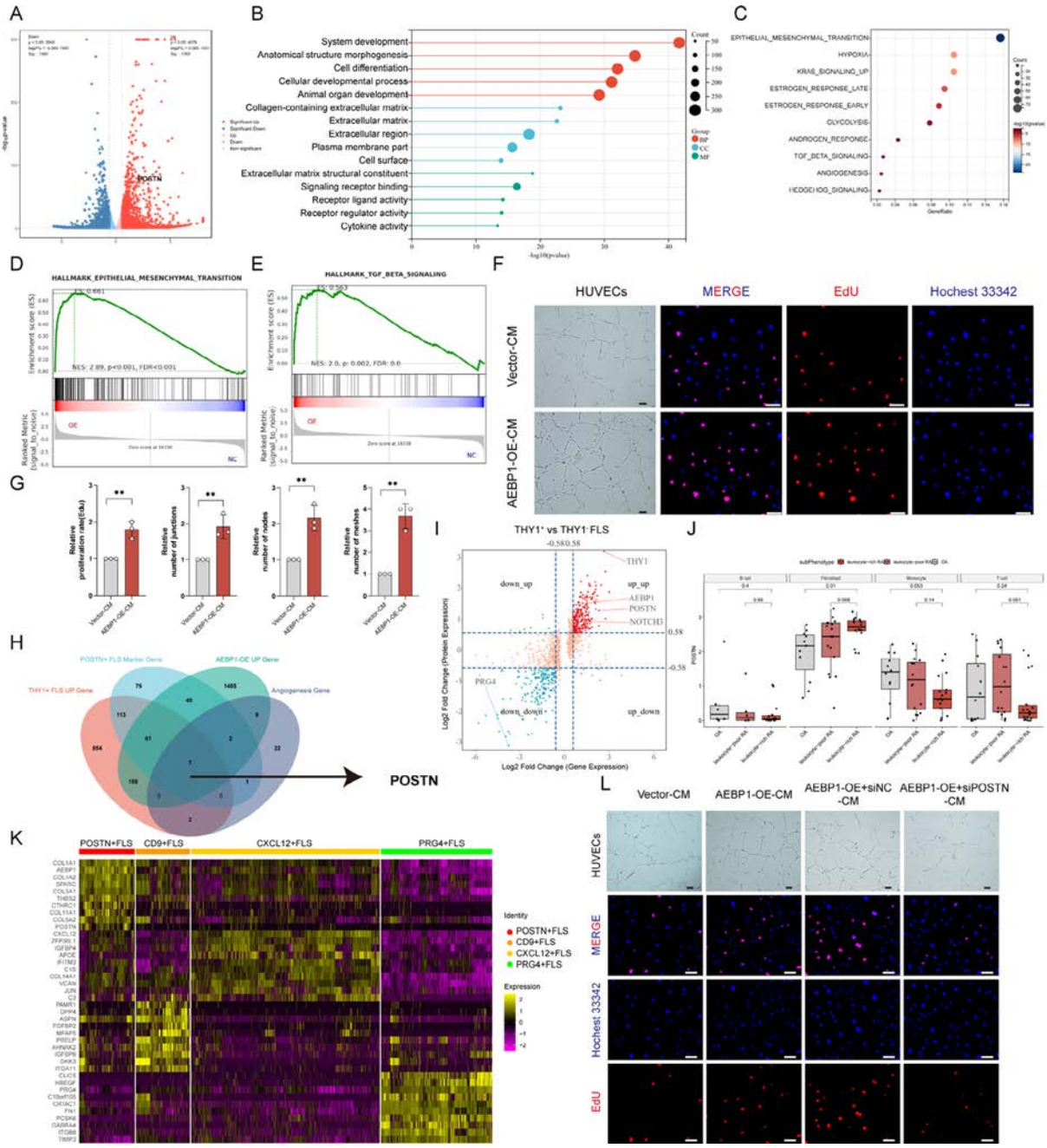


Figure 3. AEBP1 induces RA FLS activation and promotes EMT-like fibrogenic and pro-angiogenic phenotypes via TGFβ signaling. (A) Volcano plot showing differentially expressed genes in AEBP1-OE RA FLS versus vector controls. (B) GO enrichment analysis reveals up-regulation of ECM-related pathways. (C–E) Hallmark and GSEA analysis shows enrichment in TGFβ signaling and EMT gene signatures. (F, G) CM from AEBP1-OE RA FLS promotes HUVEC proliferation and tube formation, n = 3. (H) Venn diagram of four intersecting gene sets identifies POSTN as a shared, angiogenesis-related target. (I) Distribution of POSTN in both mRNA level and protein expression level in $THY1^+$ FLS versus $THY1^-$ FLS. (J) Bulk RNA-seq revealing the up-regulation of POSTN in FLS of leukocyte-rich RA synovium. (K) The heat map of genes of four FLS subsets ($POSTN^+$ FLS, $CD9^+$ FLS, $CXCL12^+$ FLS, $PRG4^+$ FLS) of single-cell RNA-seq. (L) POSTN knockdown abolishes AEBP1-OE-CM mediated angiogenic effects of RA FLS in HUVECs, n = 3. Scale = 100 μm $^{**}P < 0.01$. AEBP1, adipocyte enhancer-binding protein 1; AEBP1-OE-CM, CM from AEBP1-overexpressing RA FLS; BP, biological process; CC, cellular component; CM, conditioned medium; ECM, extracellular matrix; EMT, epithelial-mesenchymal transition; FDR, false discovery rate; FLS, fibroblast-like synoviocytes; GO, gene ontology; GSEA, gene set enrichment analysis; HUVEC, human umbilical vein endothelial cell; MF, molecular function; mRNA, messenger RNA; NES, normalized enrichment score; OA, osteoarthritis; OE, overexpressing; POSTN, periostin; RA, rheumatoid arthritis; RNA-seq, RNA sequencing; si, small interfering; TGFβ, transforming growth factor β. Color figure can be viewed in the online issue, which is available at http://onlinelibrary.wiley.com/doi/10.1002/art.70124/abstract.

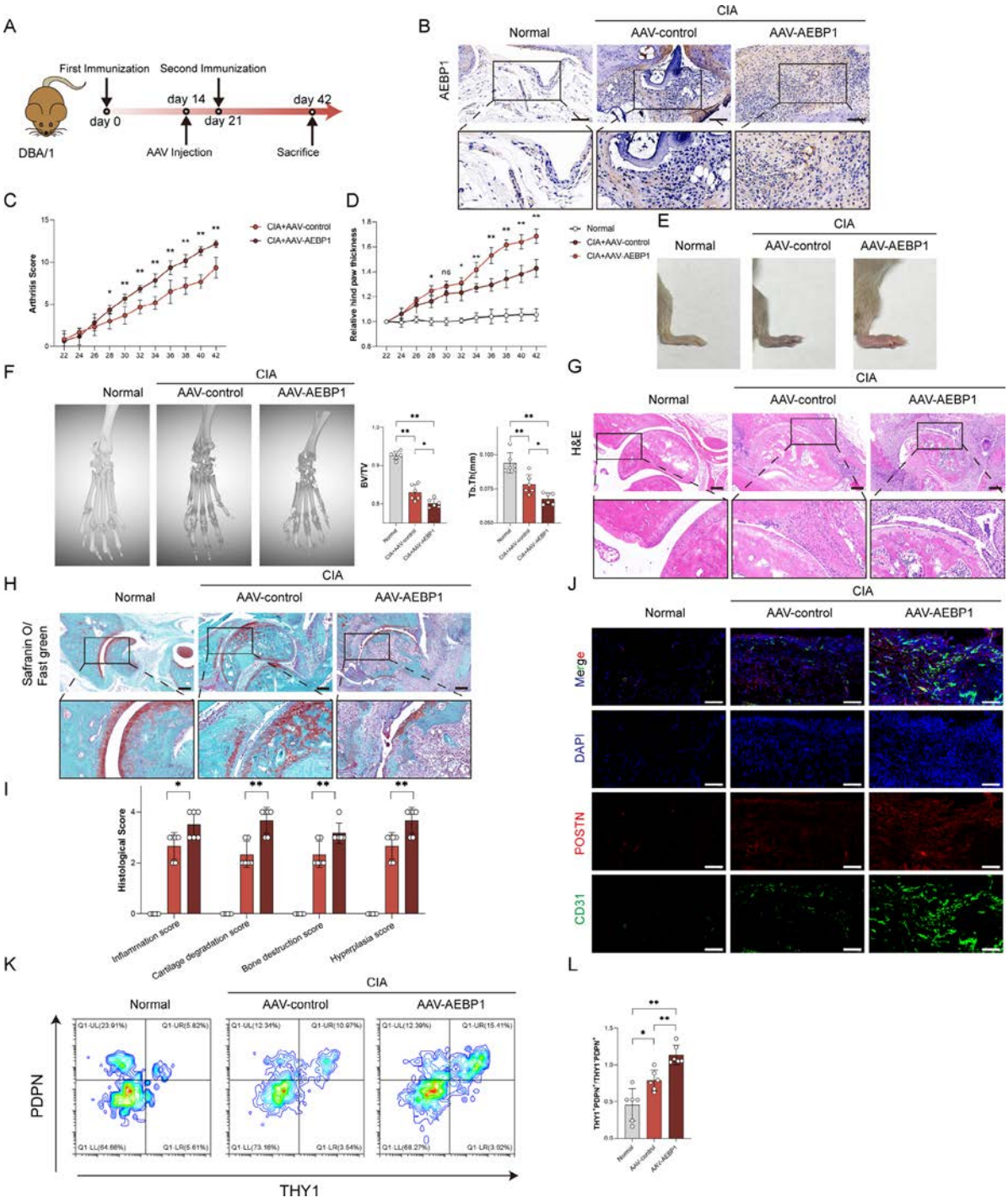


Figure 4. Intra-articular AEBP1 overexpression exacerbates joint pathology and enhances angiogenesis in mice with CIA. (A) Schematic drawing of AAV injection into ankle joints of mice with CIA. (B) IHC confirms AEBP1 overexpression in synovial tissues, scale = 100 μm, n = 6. (C, D) AAV-AEBP1–treated mice show increased arthritis scores and hind paw thickness, n = 6. (E) Representative joint images from normal, CIA +AAV-control, and CIA+AAV-AEBP1 mice. (F) Micro-CT reveals greater bone erosion and destruction in AEBP1-overexpressing joints, n = 6. (G–I) H&E and Safranin O/Fast green staining demonstrate the synovial inflammation, cartilage degradation, bone destruction, and hyperplasia in each group, scale = 200 μm, n = 6. (J) IF staining shows the POSTN expression and vascular density in the joints of each group, scale = 100 μm, n = 6. (K, L) Flow cytometry indicates the $THY1^{+}/THY1^{-}$ FLS ratio of joints of each group, n = 6. $^{*}P < 0.05$, $^{**}P < 0.01$. AAV, adeno-associated virus; AEBP1, adipocyte enhancer-binding protein 1; BV/TV, bone volume/total volume; CIA, collagen-induced arthritis; CT, computed tomography; FLS, fibroblast-like synoviocytes; H&E, hematoxylin and eosin; IF, immunofluorescence; IHC, immunohistochemistry; LL, lower left; LR, lower right; ns, no significance; POSTN, periostin; Q1, quadrant gate 1; Tb.Th, trabecular thickness; UL, upper left; UR, upper right. Color figure can be viewed in the online issue, which is available at http://onlinelibrary.wiley.com/doi/10.1002/art.70124/abstract.

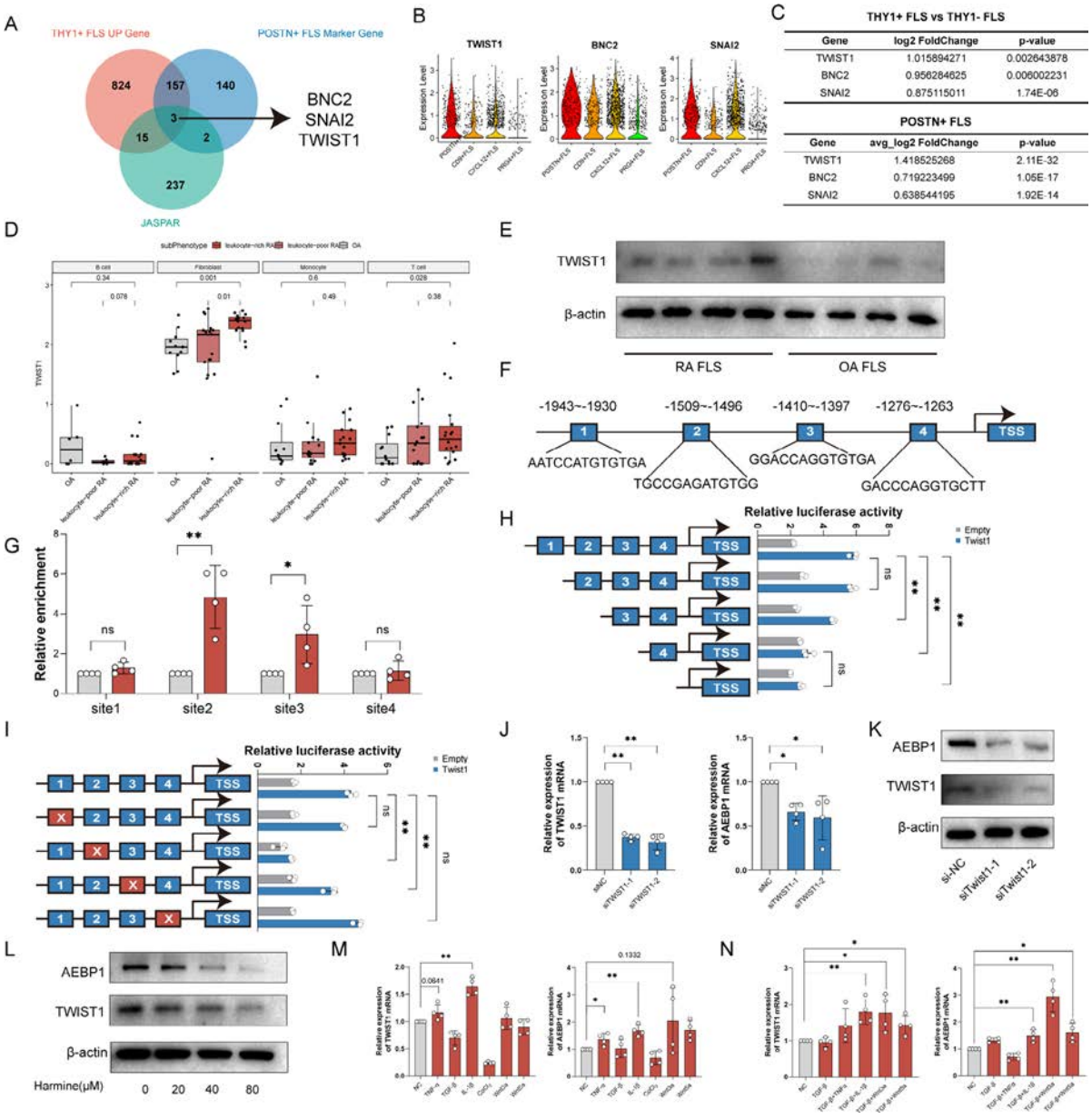


Figure 5. TWIST1 directly regulates AEBP1 transcription and may serve as a therapeutic target in RA FLS. (A) Venn diagram showing the prediction of TWIST1, SNAI2, and BNC2 binding to the AEBP1 promoter. (B, C) TWIST1 shows the most significant differential expression across FLS subsets. (D) Bulk RNA-seq data confirm TWIST1 up-regulation in FLS of RA leukocyte-rich synovium. (E) Western blot verifies higher TWIST1 protein expression in RA FLS versus OA FLS. (F) Four predicted TWIST1 binding sites in the AEBP1 promoter. (G) ChIP-qPCR identifies specific enrichment at Site2 and Site3, n = 4. (H, I) Dual-luciferase assays show TWIST1-driven AEBP1 promoter activation is abolished by (H) Site2/3 deletion or (I) mutation, n = 3. (J–K) siRNA knockdown of TWIST1 reduces AEBP1 mRNA (n = 4) and protein expression (n = 3). (L) Harmine treatment suppresses both TWIST1 and AEBP1 protein levels in RA FLS, n = 3. (M, N) qPCR of TWIST1 and AEBP1 in RA FLS treated with indicated cytokines alone (M) or combined with TGFβ (N) (doses: TNFα/TGFβ/IL-1β 10 ng/mL, $CoCl_2$ 150 μM, Wnt3a/5a 100 ng/mL), n = 4. $^{*}P < 0.05$, $^{**}P < 0.01$. AEBP1, adipocyte enhancer-binding protein 1; ChIP, chromatin immunoprecipitation; FLS, fibroblast-like synoviocytes; IL-1β, interleukin-1β; mRNA, messenger RNA; ns, no significance; OA, osteoarthritis; POSTN, periostin; qPCR, quantitative polymerase chain reaction; RA, rheumatoid arthritis; RNA-seq, RNA sequencing; si, small interfering; TGFβ, transforming growth factor β; TNFα, tumor necrosis factor α; TSS, transcription start site. Color figure can be viewed in the online issue, which is available at http://onlinelibrary.wiley.com/doi/10.1002/art.70124/abstract.

dual-luciferase assays confirmed that TWIST1 bound AEBP1 promoter specifically at Site2 and Site3 to activate the promoter activity (Figure 5G–I). Knockdown of TWIST1 by siRNA reduced AEBP1 mRNA and protein levels in RA FLS (Figure 5J, 5K). Similarly, suppression of TWIST1 by harmine, which can induce TWIST1 degradation,[19] effectively reduced AEBP1 expression in FLS (Figure 5L). Considering harmine has been extensively studied for its inhibition of DYRK (a Ser/Thr kinase), inhibition of DYRK

by harmine can regulate pathways such as MAPK and Spry2, which are involved in RA FLS function.[20] To rule out potential off-target effects of harmine on inhibiting DYRK function, we employed a highly selective DYRK inhibitor EHT 1610 in our in vitro experiments. Interestingly, we observed that AEBP1 expression showed an increasing trend at both the mRNA and protein levels following EHT 1610 treatment, suggesting that DYRK may suppress rather than promote AEBP1 expression (Supplementary Figure S10A, S10B). Besides, EHT 1610 did not induce TWIST1 degradation (Supplementary Figure S10B); we thus believed that harmine exerted its effects primarily through TWIST1 degradation, leading to the modulation of AEBP1 expression and FLS function in RA.

Next, to explore the upstream regulators of TWIST1–AEBP1 signaling, we treated RA FLS with various cytokines, including tumor necrosis factor α (TNFα), TGFβ, interleukin-1β (IL-1β), $CoCl_2$, Wnt3a, and Wnt5a, and analyzed their effects on TWIST1 and AEBP1 expression by qPCR. Our results showed that TNFα and IL-1β significantly up-regulated TWIST1 expression in RA FLS (Figure 5M). However, only IL-1β significantly up-regulated AEBP1 expression, indicating that IL-1β is a critical regulator of AEBP1 in RA FLS (Figure 5M). Additionally, we treated RA FLS with TGFβ in combination with other cytokines and found that Wnt3a and Wnt5a synergized with TGFβ, further enhancing TWIST1–AEBP1 activation. These findings suggested that signaling crosstalk between Wnt/β-catenin and TGFβ signaling may contribute to RA FLS pathology (Figure 5N).

To investigate additional regulatory factors that influence POSTN expression, we treated RA FLS with various cytokines, including TNFα, TGFβ, IL-1β, $CoCl_2$, Wnt3a, Wnt5a, and rACLP and assessed POSTN expression. Our results demonstrated that TGFβ and rACLP could promote POSTN expression, supporting the role of TGFβ and rACLP as key regulators of POSTN production in RA FLS (Figure S10C).

Regulation of TWIST1 activity mitigates the progression of RA. Evaluating the therapeutic potential of targeting TWIST1, we administered the TWIST1 inhibitor harmine (20 mg/kg/day, intraperitoneal injection) to mice with CIA (Figure 6A). Harmine was well-tolerated in vivo without overt organ toxicity (Supplementary Figure S11). Importantly, harmine-treated mice exhibited significantly lower arthritis scores, reduced paw swelling, and increased bone volume fraction (BV/TV) and Tb.Th (Figure 6B–F). Histologic staining confirmed marked reductions in inflammation, cartilage degradation, bone destruction, and synovial hyperplasia in harmine-treated mice (Figure 6G–I). IHC analysis confirmed a corresponding reduction in AEBP1 expression after harmine treatment (Figure 6J). Furthermore, IF analysis showed the down-regulation of POSTN expression and vascular density in the harmine-treated group (Figure 6K). Flow cytometric analysis of synovial tissues revealed that harmine treatment significantly reduced the ratio of $THY1^+$ FLS/$THY1^-$ FLS (Figure 6L, 6M). Together, these findings suggest that inhibition of TWIST1 by harmine effectively suppresses synovial fibroblast activation, vascular pannus formation, and joint destruction in the CIA model and that targeting TWIST1 in FLS may represent a promising therapeutic strategy to halt the progression of RA.

DISCUSSION

RA is an immune-mediated inflammatory disease characterized by the infiltration of immune cells and the proliferation of FLS. However, the mechanisms by which these distinct FLS subtypes contribute to RA pathogenesis remain unclear. By integrating multi-omics and functional assays, we identified AEBP1 as a marker for a distinct, profibrotic $THY1^+$ FLS subset.

Although $THY1^+$ FLS are considered inflammatory FLS,[5,6] our bulk RNA-seq data showed that $THY1^+$ FLS represented a lack of canonical inflammatory signals. A disease-enriched $POSTN^+$ subpopulation within $THY1^+$ FLS was identified by single-cell RNA-seq and characterized by ECM remodeling and fibrotic genes including COL1A1, COL1A2, and AEBP1. This fibrogenic predominance likely masks inflammatory signals in bulk sequencing, as pro-inflammatory signatures actually segregated into a distinct $CXCL12^+$ FLS subset.[21] These findings highlight the dual nature of RA pathogenesis driven by both immune dysregulation and stromal remodeling. Fibrotic activation of FLS, previously underappreciated, may play a critical role in promoting synovial hyperplasia and persistent inflammation. We propose that under chronic inflammatory conditions, cycles of failed tissue repair result in persistent fibrotic reprogramming of FLS, leading to sustained expansion and pannus formation.

Originally identified as a transcriptional repressor in macrophages,[8] AEBP1 has since been implicated in fibrosis and other pathologies.[22–25] Our transcriptomic analyses showed that *AEBP1* expression is highly restricted to FLS in RA. Functional studies confirmed that *AEBP1* predominantly existed as the ECM-associated isoform that induced hallmark features of myofibroblast activation. RNA-seq data further revealed that *AEBP1* activated TGFβ signaling and EMT-like programs, supporting a pseudo-EMT process similar to that observed in epithelial fibrosis. ACLP has been reported to potentiate TGFβ signaling through directly activating TGFβ receptor.[10,18,26] Our results confirmed the activation of the TGFβ signaling pathway by ACLP. Although previous studies have demonstrated that global deficiency of *Aebp1* in mice or pathogenic variants in human *AEBP1* result in connective tissue laxity, hyperextensibility, and impaired wound healing,[27,28] our findings suggest that sustained up-regulation of *AEBP1* under chronic inflammation shifts its role from tissue repair to pathogenic remodeling. This prolonged fibrogenic signaling likely promotes ECM deposition in the sublining layer, thereby facilitating FLS expansion and immune cell infiltration.

Synovial angiogenesis is another key driver of pannus progression. In our study, CM from AEBP1-overexpressing FLS

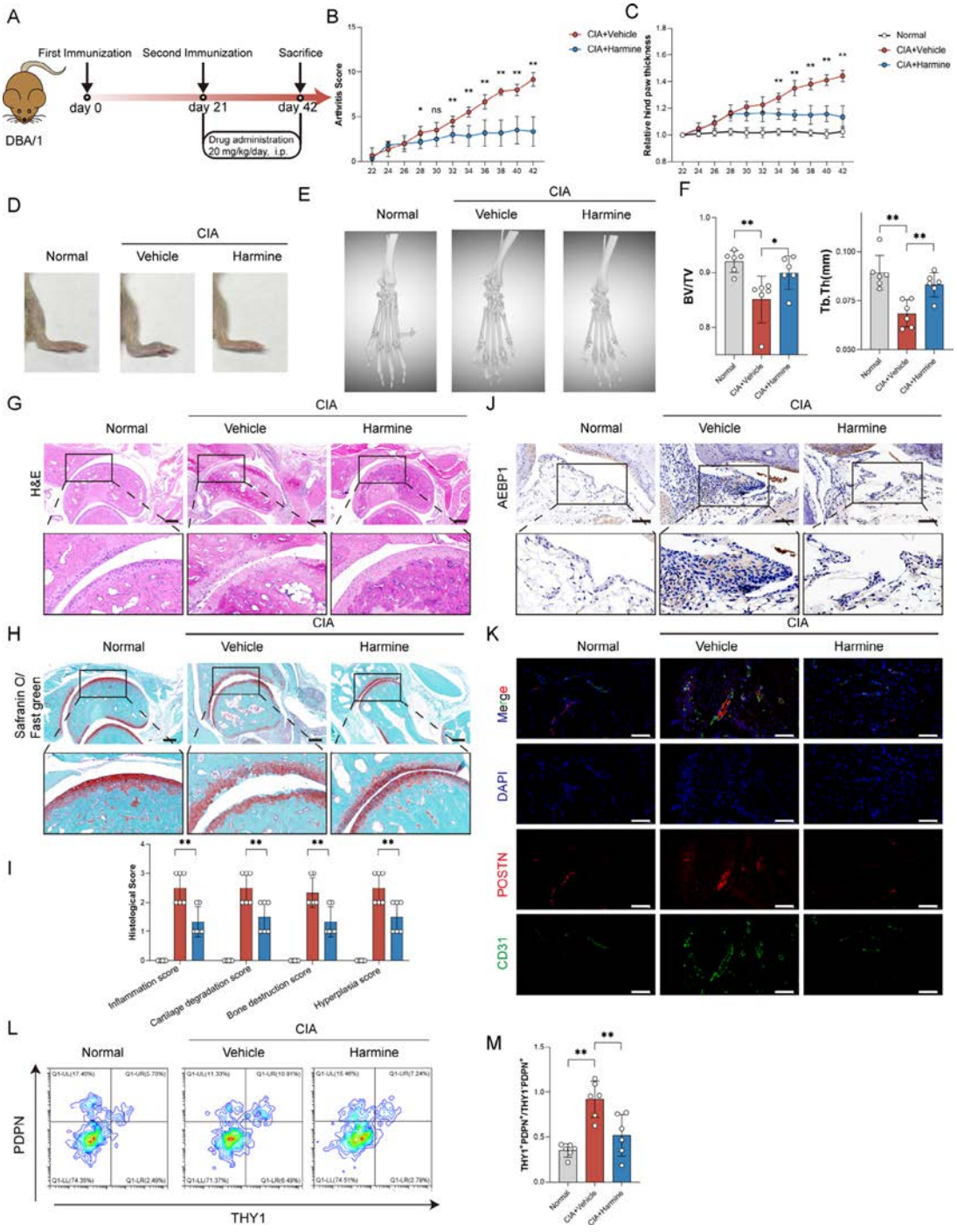


Figure 6. Harmine suppresses the TWIST1–AEBP1–POSTN axis and mitigates joint pathology in the CIA model. (A) Schematic drawing of harmine administration in mice with CIA. (B, C) Harmine reduces clinical arthritis scores and hind paw thickness, n = 6. (D) Representative joint images from normal, CIA+vehicle, and CIA+harmine-treated mice. (E, F) Micro-CT analysis shows bone volume fraction (BV/TV) and Tb.Th in each group, n = 6. (G–I) H&E and Safranin O/Fast green staining show the scores of synovial inflammation, cartilage degradation, bone destruction, and hyperplasia in each group, scale = 200 μm, n = 6. (J) IHC shows AEBP1 expression in the synovium of each group, scale = 100 μm, n = 6. (K) IF staining shows POSTN expression and vascular density in the joints of each group, scale = 100 μm, n = 6. (L, M) Flow cytometry demonstrates the $THY1^{+}$/$THY1^{-}$ FLS ratio of the joints of each group, n = 6. $^{*}P < 0.05$, $^{**}P < 0.01$. AEBP1, adipocyte enhancer-binding protein 1; BV/TV, bone volume/total volume; CIA, collagen-induced arthritis; CT, computed tomography; FLS, fibroblast-like synoviocytes; H&E, hematoxylin and eosin; IF, immunofluorescence; IHC, immunohistochemistry; i.p., intraperitoneal injection; LL, lower left; LR, lower right; ns, no significance; POSTN, periostin; Q1, quadrant gate 1; UL, upper left, UR, upper right; Tb.Th, trabecular thickness. Color figure can be viewed in the online issue, which is available at http://onlinelibrary.wiley.com/doi/10.1002/art.70124/abstract.

significantly promoted endothelial tube formation in vitro. However, recombinant ACLP (the secreted ECM isoform of AEBP1) alone failed to elicit a direct pro-angiogenic effect, suggesting that ACLP may instead promote angiogenesis indirectly by inducing the secretion of pro-angiogenic factors. Transcriptomic profiling eventually revealed that POSTN was a key downstream effector of AEBP1, with well-established roles in promoting angiogenesis and endothelial cell function.[29–32] POSTN itself has been previously reported as a canonical downstream effector of TGFβ signaling in multiple fibrotic contexts and tumor microenvironment.[33–36] We confirmed that AEBP1-induced POSTN expression was dependent on TGFβ signaling. Furthermore, synovial tissue from mice with AEBP1-overexpressing CIA showed elevated POSTN levels in vivo. Eventually, POSTN knockdown or neutralization attenuated AEBP1-driven angiogenesis in vitro and in vivo. These findings establish POSTN as a functional mediator of AEBP1-driven angiogenesis, linking matrix remodeling and vascular expansion in RA.

Besides, we identified TWIST1 as the critical transcriptional driver of AEBP1 in RA FLS and CIA mice. Though TWIST1 has been extensively studied in cancer metastasis and organ fibrosis,[37–41] its role in RA has remained largely unexplored. In this study, we showed that TWIST1 was highly expressed in RA FLS, but not in macrophages, and that silencing TWIST1 down-regulated AEBP1. Harmine, a β-carboline alkaloid derived from Peganum harmala and other plant sources, has been shown to suppress TWIST1 expression and to promote its proteasomal degradation.[19] Recent studies have demonstrated the therapeutic potential of harmine in fibrotic and inflammatory conditions via inhibition of TWIST1 activities.[39,41–43] Notably, pharmacological inhibition of TWIST1 with harmine reduced AEBP1 and POSTN expression, decreased the proportion of $THY1^+$ FLS in the synovium, ameliorated synovial inflammation, prevented pannus formation, and mitigated joint damage in mice with CIA, providing proof-of-concept for therapeutic targeting of TWIST1 for mitigating the pathogenesis of RA. As reported in previous studies, POSTN and TWIST1 play a crucial role in RA FLS migration and invasion.[44] In this study, we demonstrated that harmine selectively affected TWIST1-driven fibroblast activation, and it may offer a more tissue-specific approach to RA treatment without broadly affecting immune function.

Our findings indicate that IL-1β, Wnt3a, and Wnt5a are crucial upstream regulators of the TWIST1–AEBP1 signaling axis in RA FLS. We observed that IL-1β significantly up-regulated TWIST1, whereas Wnt3a and Wnt5a acted synergistically with TGFβ to further enhance this signaling axis. These results highlight the complex interplay between inflammatory cytokines and TGFβ signaling in the regulation of AEBP1 expression and RA pathogenesis. Future studies will be conducted to explore how the synergistic effects of these signaling pathways contribute to synovial remodeling and fibrosis in RA.

Study limitations include the lack of a conditional *Aebp1* knockout model, as global deletion of *Aebp1* causes perinatal lethality and impairs tissue homeostasis.[28] Although AEBP1 may aid early tissue repair, sustained overexpression likely drives maladaptive fibrosis, warranting future temporal studies to clarify these dual roles. Although AEBP1 is predominantly expressed in FLS, its potential extracellular immunomodulatory effects on other synovial cells require further investigation to fully map its pathogenic scope in RA.[24,45]

In summary, we identified $POSTN^+$ FLS subset in RA with dual fibrogenic and pro-angiogenic activity. This subset, orchestrated by the TWIST1–AEBP1–POSTN axis, played a central role in pannus formation and structural remodeling of the joint. Given the limitations of current RA therapies in targeting stromal components, the TWIST1–AEBP1–POSTN axis represents a promising therapeutic candidate.

AUTHOR CONTRIBUTIONS

All authors contributed to at least one of the following manuscript preparation roles: conceptualization AND/OR methodology, software, investigation, formal analysis, data curation, visualization, and validation AND drafting or reviewing/editing the final draft. As corresponding authors, Drs Zhu, Yang, and Chen confirm that all authors have provided the final approval of the version to be published and take responsibility for the affirmations regarding article submission (eg, not under consideration by another journal), the integrity of the data presented, and the statements regarding compliance with institutional review board/Declaration of Helsinki requirements.

REFERENCES

1. Bottini N, Firestein GS. Duality of fibroblast-like synoviocytes in RA: passive responders and imprinted aggressors. Nat Rev Rheumatol 2013;9(1):24–33. doi:https://doi.org/10.1038/nrrheum.2012.190
2. Tobón GJ, Youinou P, Saraux A. The environment, geo-epidemiology, and autoimmune disease: rheumatoid arthritis. Autoimmun Rev 2010;9(5):A288–A292. doi:https://doi.org/10.1016/j.autrev.2009.11.019
3. Buch MH. Defining refractory rheumatoid arthritis. Ann Rheum Dis 2018;77(7):966–969. doi:https://doi.org/10.1136/annrheumdis-2017-212862
4. Bartok B, Firestein GS. Fibroblast-like synoviocytes: key effector cells in rheumatoid arthritis. Immunol Rev 2010;233(1):233–255. doi:https://doi.org/10.1111/j.0105-2896.2009.00859.x
5. Croft AP, Campos J, Jansen K, et al. Distinct fibroblast subsets drive inflammation and damage in arthritis. Nature 2019;570(7760):246–251. doi:https://doi.org/10.1038/s41586-019-1263-7
6. Wei K, Korsunsky I, Marshall JL, et al; Accelerating Medicines Partnership Rheumatoid Arthritis & Systemic Lupus Erythematosus (AMP RA/SLE) Consortium. Notch signalling drives synovial fibroblast identity and arthritis pathology. Nature 2020;582(7811):259–264. doi:https://doi.org/10.1038/s41586-020-2222-z
7. Dakin SG, Coles M, Sherlock JP, et al. Pathogenic stromal cells as therapeutic targets in joint inflammation. Nat Rev Rheumatol 2018;14(12):714–726. doi:https://doi.org/10.1038/s41584-018-0112-7
8. He GP, Muise A, Li AW, et al. A eukaryotic transcriptional repressor with carboxypeptidase activity. Nature 1995;378(6552):92–96. doi:https://doi.org/10.1038/378092a0

9. Kattih B, Boeckling F, Shumliakivska M, et al. Single-nuclear transcriptome profiling identifies persistent fibroblast activation in hypertrophic and failing human hearts of patients with longstanding disease. Cardiovasc Res 2023;119(15):2550–2562. doi:https://doi.org/10.1093/cvr/cvad140
10. Tumelty KE, Smith BD, Nugent MA, et al. Aortic carboxypeptidase-like protein (ACLP) enhances lung myofibroblast differentiation through transforming growth factor β receptor-dependent and -independent pathways. J Biol Chem 2014;289(5):2526–2536. doi:https://doi.org/10.1074/jbc.M113.502617
11. Schissel SL, Dunsmore SE, Liu X, et al. Aortic carboxypeptidase-like protein is expressed in fibrotic human lung and its absence protects against bleomycin-induced lung fibrosis. Am J Pathol 2009;174(3):818–828. doi:https://doi.org/10.2353/ajpath.2009.080856
12. Teratani T, Tomita K, Suzuki T, et al. Aortic carboxypeptidase-like protein, a WNT ligand, exacerbates nonalcoholic steatohepatitis. J Clin Invest 2018;128(4):1581–1596. doi:https://doi.org/10.1172/JCI92863
13. Aletaha D, Neogi T, Silman AJ, et al. 2010 Rheumatoid arthritis classification criteria: an American College of Rheumatology/European League Against Rheumatism collaborative initiative. Arthritis Rheum 2010;62(9):2569–2581. doi:https://doi.org/10.1002/art.27584
14. Zhang F, Wei K, Slowikowski K, et al; Accelerating Medicines Partnership Rheumatoid Arthritis and Systemic Lupus Erythematosus (AMP RA/SLE) Consortium. Defining inflammatory cell states in rheumatoid arthritis joint synovial tissues by integrating single-cell transcriptomics and mass cytometry. Nat Immunol 2019;20(7):928–942. doi:https://doi.org/10.1038/s41590-019-0378-1
15. Chen Z, Andreev D, Oeser K, et al. Th2 and eosinophil responses suppress inflammatory arthritis. Nat Commun 2016;7(1):11596. doi:https://doi.org/10.1038/ncomms11596
16. Sekiguchi S, Yorozu A, Okazaki F, et al. ACLP activates cancer-associated fibroblasts and inhibits CD8+ T-cell infiltration in oral squamous cell carcinoma. Cancers (Basel) 2023;15(17):4303. doi:https://doi.org/10.3390/cancers15174303
17. Yorozu A, Yamamoto E, Niinuma T, et al. Upregulation of adipocyte enhancer-binding protein 1 in endothelial cells promotes tumor angiogenesis in colorectal cancer. Cancer Sci 2020;111(5):1631–1644. doi:https://doi.org/10.1111/cas.14360
18. Kim H, Kim MJ, Moon SA, et al. Aortic carboxypeptidase-like protein, a putative myokine, stimulates the differentiation and survival of bone-forming osteoblasts. FASEB J 2023;37(8):e23104. doi:https://doi.org/10.1096/fj.202300140R
19. Yochum ZA, Cades J, Mazzacurati L, et al. A first-in-class TWIST1 inhibitor with activity in oncogene-driven lung cancer. Mol Cancer Res 2017;15(12):1764–1776. doi:https://doi.org/10.1158/1541-7786.MCR-17-0298
20. Guo X, Zhang D, Zhang X, et al. Dyrk1A promotes the proliferation, migration and invasion of fibroblast-like synoviocytes in rheumatoid arthritis via down-regulating Spry2 and activating the ERK MAPK pathway. Tissue Cell 2018;55:63–70. doi:https://doi.org/10.1016/j.tice.2018.10.002
21. Micheroli R, Elhai M, Edalat S, et al. Role of synovial fibroblast subsets across synovial pathotypes in rheumatoid arthritis: a deconvolution analysis. RMD Open 2022;8(1):e001949. doi:https://doi.org/10.1136/rmdopen-2021-001949
22. Ju G, Xing T, Xu M, et al. AEBP1 promotes papillary thyroid cancer progression by activating BMP4 signaling. Neoplasia 2024;49:100972. doi:https://doi.org/10.1016/j.neo.2024.100972
23. Kim SW, Muise AM, Lyons PJ, et al. Regulation of adipogenesis by a transcriptional repressor that modulates MAPK activation. J Biol Chem 2001;276(13):10199–10206. doi:https://doi.org/10.1074/jbc.M010640200
24. Majdalawieh A, Zhang L, Fuki IV, et al. Adipocyte enhancer-binding protein 1 is a potential novel atherogenic factor involved in macrophage cholesterol homeostasis and inflammation. Proc Natl Acad Sci U S A 2006;103(7):2346–2351. doi:https://doi.org/10.1073/pnas.0508139103
25. Sinha S, Renganathan A, Nagendra PB, et al. AEBP1 down regulation induced cell death pathway depends on PTEN status of glioma cells. Sci Rep 2019;9(1):14577. doi:https://doi.org/10.1038/s41598-019-51068-1
26. Jager M, Lee MJ, Li C, et al. Aortic carboxypeptidase-like protein enhances adipose tissue stromal progenitor differentiation into myofibroblasts and is upregulated in fibrotic white adipose tissue. PLoS One 2018;13(5):e0197777. doi:https://doi.org/10.1371/journal.pone.0197777
27. Blackburn PR, Xu Z, Tumelty KE, et al. Bi-allelic alterations in AEBP1 lead to defective collagen assembly and connective tissue structure resulting in a variant of Ehlers-Danlos syndrome. Am J Hum Genet 2018;102(4):696–705. doi:https://doi.org/10.1016/j.ajhg.2018.02.018
28. Layne MD, Yet SF, Maemura K, et al. Impaired abdominal wall development and deficient wound healing in mice lacking aortic carboxypeptidase-like protein. Mol Cell Biol 2001;21(15):5256–5261. doi:https://doi.org/10.1128/MCB.21.15.5256-5261.2001
29. Zhu M, Fejzo MS, Anderson L, et al. Periostin promotes ovarian cancer angiogenesis and metastasis. Gynecol Oncol 2010;119(2):337–344. doi:https://doi.org/10.1016/j.ygyno.2010.07.008
30. Liu Y, Li F, Gao F, et al. Periostin promotes tumor angiogenesis in pancreatic cancer via Erk/VEGF signaling. Oncotarget 2016;7(26):40148–40159. doi:https://doi.org/10.18632/oncotarget.9512
31. Pang L, Dunterman M, Xuan W, et al. Circadian regulator CLOCK promotes tumor angiogenesis in glioblastoma. Cell Rep 2023;42(2):112127. doi:https://doi.org/10.1016/j.celrep.2023.112127
32. Zhang Z, Nie F, Chen X, et al. Upregulated periostin promotes angiogenesis in keloids through activation of the ERK 1/2 and focal adhesion kinase pathways, as well as the upregulated expression of VEGF and angiopoietin-1. Mol Med Rep 2015;11(2):857–864. doi:https://doi.org/10.3892/mmr.2014.2827
33. Liu B, Wu T, Lin B, et al. Periostin-TGF-β feedforward loop contributes to tumour-stroma crosstalk in liver metastatic outgrowth of colorectal cancer. Br J Cancer 2024;130(3):358–368. doi:https://doi.org/10.1038/s41416-023-02516-3
34. Tirunavalli SK, Kuncha M, Sistla R, et al. Targeting TGF-β/periostin signaling by sesamol ameliorates pulmonary fibrosis and improves lung function and survival. J Nutr Biochem 2023;116:109294. doi:https://doi.org/10.1016/j.jnutbio.2023.109294
35. Yue H, Li W, Chen R, et al. Stromal POSTN induced by TGF-β1 facilitates the migration and invasion of ovarian cancer. Gynecol Oncol 2021;160(2):530–538. doi:https://doi.org/10.1016/j.ygyno.2020.11.026
36. Um JE, Park JT, Nam BY, et al. Periostin-binding DNA aptamer treatment attenuates renal fibrosis under diabetic conditions. Sci Rep 2017;7(1):8490. doi:https://doi.org/10.1038/s41598-017-09238-6
37. Kang Y, Massagué J. Epithelial-mesenchymal transitions: twist in development and metastasis. Cell 2004;118(3):277–279. doi:https://doi.org/10.1016/j.cell.2004.07.011
38. Qin Q, Xu Y, He T, et al. Normal and disease-related biological functions of Twist1 and underlying molecular mechanisms. Cell Res 2012;22(1):90–106. doi:https://doi.org/10.1038/cr.2011.144
39. Sun L, Liu L, Jiang J, et al. Transcription factor Twist1 drives fibroblast activation to promote kidney fibrosis via signaling proteins Prrx1/TNC. Kidney Int 2024;106(5):840–855. doi:https://doi.org/10.1016/j.kint.2024.07.028
40. Mammoto T, Jiang A, Jiang E, et al. Role of Twist1 phosphorylation in angiogenesis and pulmonary fibrosis. Am J Respir Cell

Mol Biol 2016;55(5):633–644. doi:https://doi.org/10.1165/rcmb.2016-0012OC

41. Zhang Y, Wang J, Sun H, et al. TWIST1+FAP+ fibroblasts in the pathogenesis of intestinal fibrosis in Crohn's disease. J Clin Invest 2024;134(18):e179472. doi:https://doi.org/10.1172/JCI179472
42. Liu L, Ning X, Wei L, et al. Twist1 downregulation of PGC-1α decreases fatty acid oxidation in tubular epithelial cells, leading to kidney fibrosis. Theranostics 2022;12(8):3758–3775. doi:https://doi.org/10.7150/thno.71722
43. Nafie E, Lolarga J, Lam B, et al. Harmine inhibits breast cancer cell migration and invasion by inducing the degradation of Twist1. PLoS One 2021;16(2):e0247652. doi:https://doi.org/10.1371/journal.pone.0247652
44. You S, Yoo SA, Choi S, et al. Identification of key regulators for the migration and invasion of rheumatoid synoviocytes through a systems approach. Proc Natl Acad Sci U S A 2014;111(1):550–555. doi:https://doi.org/10.1073/pnas.1311239111
45. Majdalawieh A, Zhang L, Ro HS. Adipocyte enhancer-binding protein-1 promotes macrophage inflammatory responsiveness by up-regulating NF-kappaB via IkappaBalpha negative regulation. Mol Biol Cell 2007;18(3):930–942. doi:https://doi.org/10.1091/mbc.e06-03-0217

Check for updates

American College of Rheumatology
Empowering Rheumatology Professionals

Arthritis & Rheumatology
Vol. 78, No. 10, October 2026, pp 2036–2049
DOI 10.1002/art.70125
© 2026 American College of Rheumatology.

Biologic and Targeted Synthetic Disease-Modifying Antirheumatic Drugs Do Not Arrest Bone Loss in Patients With Rheumatoid Arthritis: A Long-Term Multicenter Observational Study

Takafumi Aritomi, MD,[1,2] Koshiro Sonomoto, MD, PhD,[1,3,4] Shingo Nakayamada, MD, PhD,[1,5] Hiroaki Tanaka, MD, PhD,[1,6] Atsushi Nagayasu, MD,[1,7] Satoshi Kubo, MD, PhD,[1,8] Ippei Miyagawa, MD, PhD,[1,9,10] Ayako Yamaguchi, MD, PhD,[1,2,11,12] Naoaki Ohkubo, MD, PhD,[1,13,14] Yasuyuki Todoroki, MD, PhD,[1,9,15] Yurie Satoh-Kanda, MD, PhD,[1,16] Masanobu Ueno, MD, PhD,[1] Ryuichiro Kanda, MD,[1] Yuya Fujita, MD,[1,17] Masashi Funada, MD,[1] Hidenori Sakai, MD,[1,18] Satsuki Matsunaga, MD,[1,19] Hiroaki Tanaka, MD,[1,20] Masayuki Shinojima, MD,[1,21] Hiroki Kawamura, MD,[1,22] Kazuki Takahashi, MD,[1,23] Miyabi Ando, MD,[1,24] Kazuki Haru, MD,[1,25] Yusuke Miyazaki, MD, PhD,[1,26] Kentaro Hanami, MD, PhD,[27] Masao Nawata, MD, PhD,[28] Shunsuke Fukuyo, MD, PhD,[1,26] Keisuke Nakatsuka, MD, PhD,[29] Mikiko Tokunaga, MD, PhD,[30] Kazuyoshi Saito, MD, PhD,[31] and Yoshiya Tanaka, MD, PhD[1,9]

Objective. Osteoporosis causes fractures that further increase the disease burden of rheumatoid arthritis (RA); however, osteoporosis treatment rates remain low. Although several studies have reported that biologic or targeted synthetic disease-modifying antirheumatic drugs (b/tsDMARDs) can prevent or improve osteoporosis in RA, our large-scale, real-world study showed that one-year b/tsDMARDs use did not arrest osteoporosis progression. This study aimed to examine longer-term changes in bone mineral density (BMD).

Methods. BMD was observed for up to five years in patients receiving b/tsDMARDs for active RA. The primary endpoint was change in BMD (T score), and the secondary endpoint was change in T score–related factors.

Results. In total, 797 patients (antiosteoporosis–, n = 645; antiosteoporosis+, n = 152) were included, with a median 3.1-year follow-up (2,489 patient-years). Clinical Disease Activity Index (CDAI) improved in both groups (antiosteoporosis– 26.0 to 6.6; antiosteoporosis+ 24.4 to 6.8). T scores decreased significantly in the femoral neck and radius in the antiosteoporosis– group but not in the antiosteoporosis+ group (antiosteoporosis–: mean change –0.11 to –0.33, both $P < 0.001$; antiosteoporosis+ –0.01 to –0.10, $P = 0.830$ and 0.071, respectively). Overall, 460 patients (58%) experienced a decrease in T score. A high baseline T score correlated with a subsequent decrease, whereas longer osteoporosis treatment duration correlated with an increase. Unexpectedly, the duration of b/tsDMARD use and mean CDAI during observation were not associated with BMD maintenance.

Conclusion. Even when RA activity was controlled with b/tsDMARDs, BMD still decreased. This study emphasizes the importance of considering osteoporosis as an independent aspect of RA, beyond inflammation control.

INTRODUCTION

Rheumatoid arthritis (RA) is an autoimmune disease characterized by inflammatory polyarthritis followed by irreversible joint damage. RA is associated with para-articular osteoporosis due to localized inflammation; however, systemic osteoporosis is also common,[1,2] with a prevalence rate approximately twice that in the general population.[3] Osteoporosis leads to fractures, which

Supported in part by a grant-in-aid for scientific research (19K17919) from the University of Occupational and Environmental Health, Japan and through the University of Occupational and Environmental Health, Japan for Advanced Research.

[1]First Department of Internal Medicine, School of Medicine, University of Occupational and Environmental Health Japan, Kitakyushu, Japan; [2]Department of Laboratory and Transfusion Medicine, Hospital of the University of Occupational and Environmental Health Japan, Kitakyushu, Japan; [3]Department of Clinical Nursing, School of Health Sciences, University of Occupational and Environmental Health Japan, Kitakyushu, Japan; [4]Department of Rheumatology, Shunan Memorial Hospital, Kudamatsu, Japan; [5]Department of Rheumatology, Saiseikai Yahata General Hospital, Kitakyushu, Japan; [6]Department of Medical Informatics and Management, Hospital of the University of Occupational and Environmental Health Japan, Kitakyushu, Japan; [7]Department of Infectious Disease Medicine, School of Medicine, University of Occupational and Environmental Health Japan, Kitakyushu, Japan; [8]Department of Rheumatology, Kyusyu Rosai Hospital, Kitakyushu, Japan; [9]Department of Molecular Targeted Therapeutics, University of

further reduce physical function, thereby placing an additional burden on patients with RA, who already experience a decline in physical function.[4] Factors promoting RA-related systemic osteoporosis include aging, menopause, smoking, decreased physical activity, the use of glucocorticoids (GCs), comorbidities such as chronic kidney disease or diabetes, and chronic inflammation.[1,5–9] Therefore, the multifactorial nature of osteoporosis should be considered in its management because these factors are likely to increase with global aging, making appropriate management of osteoporosis in RA increasingly important. Although its importance has long been recognized, treatment rates remain suboptimal.[6–10] Even among GC users, who are particularly at risk of osteoporosis and fractures, only 38% to 60% receive therapy.[6]

Achieving remission is known to correlate with less osteoporosis.[11] Accordingly, the American College of Rheumatology recommends a treat-to-target approach for its numerous benefits and its potential to protect against osteoporosis.[12] Biologic or targeted synthetic disease-modifying antirheumatic drugs (b/tsDMARDs) effectively control arthritis in RA and suppress local joint damage, which also improve osteoporosis in the para-articular region. Because inflammation is considered one of the multiple causes of systemic osteoporosis in RA,[1,5–9] it has been hypothesized that suppressing inflammation with b/tsDMARDs may also benefit systemic bone loss. This hypothesis has prompted several small-scale studies, which reported that b/tsDMARDs can stabilize or even improve systemic osteoporosis.[13–28] However, recent studies have shown that although the use of b/tsDMARDs has increased and the remission rate has nearly doubled, the fracture rate has also risen.[29,30] This suggests that b/tsDMARD use or inflammation control may be insufficient to improve osteoporosis.

This raises a key clinical question: can b/tsDMARDs truly arrest osteoporosis progression? Answering this question could help rheumatologists reaffirm the importance of managing osteoporosis in RA. To address this issue, we recently reported the results from a relatively large real-world study.[31] We analyzed 1,164 patients with active RA who were treated with b/tsDMARDs for one year without antiosteoporotic drugs. Despite a marked reduction in disease activity, bone mineral density (BMD) of the femoral neck and radius significantly decreased. These findings suggest that b/tsDMARD use and/or control of RA inflammation alone may be insufficient to manage osteoporosis in RA. Although the importance of osteoporosis management in RA is widely recognized, our results highlight the need for continued awareness of bone health because treatment rates remain low. However, long-term outcomes remain unclear. The present study is the extension of our previous work and reports the five-year follow-up results on the long-term effects of b/tsDMARDs on bone metabolism.

PATIENTS AND METHODS

Study design and participants. This study is a multicenter, prospective, observational study on bone metabolism conducted as part of FIRST registry[32,33] and an extension of our previous study on osteoporosis.[31] Patients with active RA who met the 2010 classification criteri[34]a and initiated their first b/tsDMARD between August 2013, when tumor necrosis factor inhibitors (TNFi), interleukin-6 receptor inhibitors (IL-6Ri), CTLA4-Ig, and JAK inhibitors (JAKi) became available in Japan, and July 2022 were enrolled. To reflect real-world clinical practice, all consecutive patients were enrolled. Patients provided informed consent to participate in this study at the introduction of b/tsDMARDs.

In accordance with the FIRST registry framework, patients visited the Hospital of the University of Occupational and Environmental Health (UOEH) at the start of treatment (week 0), at 2 weeks, at 26 weeks, at 52 weeks, and annually afterwards for up to five years to undergo the evaluations described below. During this time, patients received treatments, including treatments for RA, at local medical facilities. No restrictions were placed on medical interventions, including b/tsDMARDs and osteoporosis medications. FIRST registry is a multicenter cohort study involving 27 medical institutions within a 150-km radius.[32] In Japan, the average distance to rheumatologists is relatively short, so 150 km is considered far. Patients can visit UOEH for annual evaluations; however, those living a considerable distance away may

Occupational and Environmental Health, Japan, Kitakyushu, Japan; [10]Department of Rheumatology, Kokura Memorial Hospital, Kitakyushu, Japan; [11]Department of Rheumatology, Fukuoka Shin Mizumaki Hospital, Kitakyushu, Japan; [12]Department of Rheumatology, Shin-Kokura Hospital, Kitakyushu, Japan; [13]Department of Environmental Epidemiology, University of Occupational and Environmental Health Japan, Kitakyushu, Japan; [14]Department of Rheumatology, Obase Hospital, Kanda, Japan; [15]Department of Rheumatology, Steel Memorial Yawata Hospital, Kitakyushu, Japan; [16]Department of Rheumatology, Tochiku Hospital, Kitakyushu, Japan; [17]Department of Rheumatology, Ashiya Central Hospital, Kitakyushu, Japan; [18]Department of Rheumatology, Yamaguchi-ken Saiseikai Shimonoseki General Hospital, Shimonoseki, Japan; [19]Department of Rheumatology, Yamaguchi Rosai Hospital, Sanyo-Onoda, Japan; [20]Department of Rheumatology, Hagiwara Central Hospital, Kitakyushu, Japan; [21]Department of Rheumatology, Kenai Memorial Hospital, Kitakyushu, Japan; [22]Department of Rheumatology, Ohira Medical Care Hospital, Kitakyushu, Japan; [23]Department of Rheumatology, Hosoe Clinic, Shimonoseki, Japan; [24]Department of Rheumatology, Sasaki Hospital, Kitakyushu, Japan; [25]Department of Rheumatology, Yoshino Hospital, Kitakyushu, Japan; [26]Department of Rheumatology and Diabetology, Wakamatsu Hospital of the University of Occupational and Environmental Health Japan, Kitakyushu, Japan; [27]Department of Rheumatology and Diabetology, Kitakyushu General Hospital, Kitakyushu, Japan; [28]Department of Rheumatology, Kokura Rheumatology Clinic, Kitakyushu, Japan; [29]Department of Internal Medicine, Japan Community Health care Organization Fukuoka Yutaka Central Hospital, Nogata, Japan; [30]Hakataeki Minami Tokunaga Clinic, Fukuoka, Japan; [31]Department of Clinical Immunology and Rheumatology, Tobata General Hospital, Kitakyushu, Japan.

Additional supplementary information cited in this article can be found online in the Supporting Information section (https://acrjournals.onlinelibrary.wiley.com/doi/10.1002/art.70125).

Author disclosures and graphical abstract are available at https://onlinelibrary.wiley.com/doi/10.1002/art.70125.

Address correspondence via email to Yoshiya Tanaka, MD, PhD, at tanaka@med.uoeh-u.ac.jp.

Submitted for publication October 6, 2025; accepted in revised form February 24, 2026.

choose to visit a nearby participating institution for annual evaluations. When patients do not visit UOEH, clinical indices and concomitant medications are reported. However, items requiring specific equipment, such as BMD, are missing. In this study, such cases were treated as censored.

Clinical data, medications, and adverse events were recorded at enrollment and follow-up. The occurrence of fractures was obtained from the medical records entered by the attending physician. The following b/tsDMARDs were used: TNFi (infliximab, etanercept, adalimumab, golimumab, certolizumab pegol, and ozoralizumab), IL-6Ri (tocilizumab and sarilumab), CTLA4-Ig (abatacept), and JAKi (tofacitinib, baricitinib, peficitinib, upadacitinib, and filgotinib).

BMD measurement. During regular evaluations, BMD was measured at the femoral neck and one-third radius at UOEH, typically at week 0, week 26, week 52, and annually thereafter. Total hip BMD was derived from images obtained during femoral neck assessment through post hoc analysis. BMD, T score, and *Z* score values were recorded. An allowance of 45 days was given before and after the measurement of BMD. Least significant change (LSC) in BMD was determined based on the recommendations of the International Society for Clinical Bone Mineral Density[35]; the cut-off value was >0.029 g/cm^2 for the femoral neck and >0.011 g/cm^2 for the one-third radius using the Horizon A (Horizon, Marlborough, MA) device. The diagnosis of osteoporosis was made according to the World Health Organization criteria.[36] In our previous study, we did not measure lumbar spine BMD to avoid overestimation associated with degenerative lumbar disease or vertebral compression fractures and to reflect the constraints of the Japanese health care system.[31] The present study is an extension of that work and we used the same assessment framework. In the prior study, bone turnover markers were evaluated; however, no significant association with changes in BMD was observed.[31] Because BMD is the primary measure used in fracture risk assessment,[37,38] bone turnover markers were not evaluated in this study.

Endpoints. The primary endpoint was the change in T score before and after the observation period. The secondary endpoints were (1) change in *Z* score and BMD before and after the observation period; (2) percentage of participants who showed changes in BMD beyond the LSC; and (3) factors associated with changes in T score.

Ethical considerations. This study complied with the Declaration of Helsinki and was approved by the Ethics Committee of the UOEH (UOEHCRB21-068, approved on July 28, 2021). Appropriate consent was obtained from all participants in accordance with the Ministry of Health, Labour, and Welfare's "Ethical Guidelines for Medical and Health Research Involving Human Subjects." The retrospective inclusion of opt-outs was also approved.

Statistical analysis. Continuous variables were expressed as means ± SD and categorical variables as frequencies (%). Between-group comparisons of continuous variables were performed using *t*-tests or Mann-Whitney *U*-tests, and categorical variables were compared using chi-square tests or Fisher exact tests. When indicated, differences in patient characteristics were adjusted using inverse probability of treatment weighting (IPTW) based on propensity scores. Changes before and after the observation period were evaluated using a paired *t*-test. To evaluate the mean change from baseline, one-sample *t*-tests were performed under the null hypothesis of no change. Comparisons among three or more groups were performed using one-way analysis of variance for continuous variables and chi-square tests for categorical variables. False discovery rate (FDR) correction with Benjamini-Hochberg method was performed for multiple comparisons. In addition, univariate and multivariate analyses were performed to identify factors associated with the change in T score of the femoral neck and radius.

Furthermore, to explore heterogeneity in BMD change patterns, we performed clustering based on longitudinal BMD data using a Gaussian mixture model and performed trajectory analysis. Statistical significance level was set at $P < 0.05$. Statistical analyses were performed using JMP Pro version 18 (SAS Institute Inc, Cary, NC). Gaussian mixture models were computed using the scikit-learn library in Python.

Data availability statement. The datasets used and analyzed during the current study are available from the corresponding author on reasonable request.

RESULTS

A total of 1,447 patients with RA receiving their first b/tsDMARD treatment provided informed consent and participated in this study (all enrolled patients) (Table 1, Supplementary Figure S1). All participants were Asian patients. Patients were included in the analysis if their BMD was measured at week 0 and at least once more after 26 weeks or longer. Because this was a real-world clinical study, there were some issues such as the lack of adequate baseline BMD data, no follow-up visits during the study period, and missing BMD data. Approximately 45% of the 1,447 patients enrolled dropped out and ultimately, 797 participants were included in the study (target group). The most common reason for withdrawal was loss to follow-up. There were limited differences in the patient characteristics between all enrolled patients and the target group, and random censoring was presumed (data available if requested). Supplementary Table S1 shows the percentage of missing data in the target group.

Table 1. Baseline characteristics of the participants according to antiosteoporosis drug use*

Characteristics	All enrolled patients (N = 1,447)	Target group (n = 797)	Antiosteoporosis− (n = 645)	Antiosteoporosis+ (n = 152)	*P* values
Age, mean ± SD, years	62.4 ± 14.1	61.4 ± 14.0	59.4 ± 14.0	69.8 ± 10.1	**<0.001**
Women, %	75.3	77.2	74.1	90.1	**<0.001**
BMI, mean ± SD, kg/m^2	22.4 ± 4.0	22.8 ± 3.9	22.6 ± 4.0	21.5 ± 3.5	**0.004**
Disease duration, mean ± SD, months	72.0 ± 106.9	60.9 ± 91.2	52.1 ± 82.6	98.0 ± 114.0	**<0.001**
RA stage I/II/III/IV, %					**<0.001**
Stage I	34.5	36.6	38.8	27.6	
Stage II	45.0	45.9	47.5	39.5	
Stage III	11.5	10.3	8.7	17.1	
Stage IV	9.0	7.1	5.0	15.8	
RF positive, %	75.6	72.2	72.9	69.5	0.438
ACPA positive, %	68.8	65.4	65.3	66.0	0.884
Concomitant MTX use, %	70.9	74.2	76.9	62.5	**<0.001**
MTX dose in user, mean ± SD, mg/week	12.3 ± 3.7	12.4 ± 3.7	12.7 ± 3.6	11.8 ± 3.8	0.474
Concomitant GC use, (%)	22.9	22.0	14.9	52.0	**<0.001**
GC dose in user, mean ± SD, PSL mg/day	11.3 ± 13.7	9.1 ± 10.6	9.6 ± 10.5	8.5 ± 10.7	0.461
b/tsDMARD, %					**<0.001**
TNFi	41.5	46.8	50.7	30.3	
IL-6Ri	29.2	26.5	24.6	34.2	
CTLA4-Ig	22.3	20.7	18.0	32.2	
JAKi	7.0	6.0	6.7	3.3	
CRP, mean ± SD, mg/dl	2.5 ± 3.6	2.5 ± 3.5	2.5 ± 3.7	2.3 ± 2.9	0.206
ESR, mean ± SD, mm/h	50.1 ± 31.0	50.4 ± 31.2	49.7 ± 31.6	53.6 ± 29.3	0.097
CDAI, mean ± SD	25.4 ± 12.9	25.7 ± 12.8	26.0 ± 13.0	24.4 ± 11.6	0.170
HAQ, mean ± SD	1.2 ± 0.8	1.2 ± 0.8	1.2 ± 0.8	1.2 ± 0.8	0.392
ILD, %	11.0	10.0	9.1	12.5	0.235
Femoral neck T score, mean ± SD	−1.61 ± 1.10	−1.58 ± 1.06	−1.43 ± 1.04	−2.22 ± 0.85	**<0.001**
Radius T score, mean ± SD	−1.13 ± 2.33	−0.96 ± 2.23	−0.60 ± 2.13	−2.49 ± 1.95	**<0.001**
Menopause in women, %	71.9	70.9	64.0	94.9	**<0.001**
Osteoporosis, %	–	31.7	25.0	60.5	**<0.001**
History of bone fracture, %	15.2	18.1	12.7	40.8	**<0.001**
Diabetes, %	16.6	16.7	16.1	19.1	0.379
eGFR <60 mL/min/m^2, %	20.2	18.7	16.1	29.6	**<0.001**
Emphysema, %	4.4	4.5	4.5	4.6	0.954
Smoking, %					0.037
Current	16.0	16.2	18.5	6.1	
Past	22.9	22.0	22.3	21.1	
Never	61.1	61.8	59.2	72.8	

* Data are shown for the overall (all enrolled patients) and analysis cohorts (target group), those not receiving antiosteoporotic drug at enrollment (antiosteoporosis−), and those receiving antiosteoporotic drug at enrollment (antiosteoporosis+). *P* values indicate comparisons between antiosteoporosis (−) and antiosteoporosis (+) groups. Bolded values are $P < 0.05$ after false discovery rate correction. ACPA, anticitrullinated protein antibody; BMI, body mass index; b/tsDMARD, biologic and targeted synthetic disease-modifying antirheumatic drug; CDAI, Clinical Disease Activity Index; CRP, C-reactive protein; eGFR, estimated glomerular filtration rate; ESR, erythrocyte sedimentation rate; GC, glucocorticoid; HAQ, Health Assessment Questionnaire; ILD, interstitial lung disease; IL-6Ri, interleukin-6 receptor inhibitor; JAKi, JAK inhibitor; MTX, methotrexate; PSL, prednisolone; RA, rheumatoid arthritis; RF, rheumatoid factor; TNFi, tumor necrosis factor inhibitor.

The mean age of the target group (Table 1) was 61.4 years, 77.2% were women, and the mean duration of RA was 60.9 months. RA stage I or II accounted for >80% of cases. The rate of concomitant methotrexate (MTX) use was 74.2% (mean dose [among users only] 12.4 mg/week), and the rate of concomitant GC use was 22.0% (mean dose [among users only] prednisolone equivalent 9.1 mg/day). The mean Clinical Disease Activity Index (CDAI) was 25.7, indicating high disease activity. The menopausal rate for women was 70.9%. In the target group, the incidence of osteoporosis was 31.7%, the proportion of patients with a history of fracture was 18.1%, the incidence of diabetes was 16.7%, the proportion of patients with estimated glomerular filtration rate (eGFR) <60 was 18.7%, the incidence of emphysema was 4.5%, and the proportion of current smokers was 16.2%. Of the patients who met the diagnostic criteria for osteoporosis at baseline, 36.4% were receiving osteoporosis treatment (data available if requested). Of the study participants, 152 were receiving osteoporosis treatment (antiosteoporosis+ group) and 645 were not receiving treatment (antiosteoporosis– group). Compared with the antiosteoporosis– group, the antiosteoporosis+ group was older (69.8 vs 59.4 years) and had more women (90.1% vs 74.1%), a longer RA duration (98.0 vs 52.1 months),

more advanced RA stage (stages III+IV 32.9% vs 13.7%), less MTX use (62.5% vs 76.9%), more GC use (52.0% vs 14.9%), more menopausal and fracture histories (menopausal history 94.9% vs 64.0%; fracture history 40.8% vs 12.7%), and a higher proportion of those with reduced eGFR (eGFR <60 29.6% vs 16.1%).

Details of the first b/tsDMARDs use are as follows: TNFi were used by 373 patients, IL-6Ri were used by 211 patients, CTLA4-Ig were used by 165 patients, and JAKi were used by 48 patients (Supplementary Figure S1; Supplementary Table S2). This study was based on real-world clinical data, and patient characteristics varied between formulations, including T scores. There were no remarkable differences in RA disease activity at the time of the first b/tsDMARD initiation among the four groups (CDAI 23.1–26.8).

In the antiosteoporosis+ group (N = 152), osteoporosis treatments used at baseline were as follows: bisphosphonates (72.4%), active vitamin D (38.8%), denosumab (11.2%), selective estrogen receptor modulators (4.6%), and parathyroid hormone (3.3%) (Supplementary Table S3). In addition, multiple drugs were used concomitantly in some cases.

Changes in the endpoints (RA disease activity, osteoporosis comorbidity rate, osteoporosis treatment, BMD, T score, and *Z* score) during the observation period are shown in Table 2, Supplementary Table S4, and Supplementary Figure S2. The follow-up period for the target group (Table 2, left) was 2,489 person-years (median 3.1 years). b/tsDMARDs were interrupted or discontinued due to real-world settings, and patients received b/tsDMARDs for 83.3% of the observation period. Disease activity significantly improved from high to low in terms of the CDAI score (mean CDAI 25.7–6.6, $P < 0.001$). Meanwhile, T scores of the femoral neck and radius both decreased (femoral neck −1.58 to −1.67; radius −0.96 to −1.25; both $P < 0.001$) (Table 2; Supplementary Figure S2). The T scores for the total hip, assessed alongside the femoral neck, also decreased, from −1.14 to −1.21 ($P < 0.001$) (Supplementary Table S4). The percent change and yearly percent change in BMD reproduced this pattern. A significant decrease in BMD was observed in the antiosteoporosis− group, whereas bone mass was maintained in the antiosteoporosis+ group. Regarding the secondary endpoint, the *Z* score, there was an increase in the femoral neck (−0.27 to −0.20, $P < 0.001$) but there was no significant change in the radius (0.73–0.69, $P = 0.065$). The *Z* score at the total hip decreased significantly (−0.22 to −0.32, $P < 0.001$).

The incidence of osteoporosis increased from 31.7% to 34.6% ($P < 0.001$). During the observation period, 21 new cases of fragility fractures (2.6%) occurred (Table 2).

When stratified by osteoporosis medication use at baseline, the CDAI improved in the antiosteoporosis− (Table 2, middle) and antiosteoporosis+ groups (Table 2, right) (antiosteoporosis− 26.0 to 6.6, antiosteoporosis+ 24.4 to 6.8, both $P < 0.001$). In the antiosteoporosis− group, the rate of osteoporosis treatment increased to 45.6% during the observation period, with the average duration of 1.1 years. However, the T scores for the femoral neck and radius were significantly reduced (femoral neck −1.43 to −1.54; radius −0.60 to −0.93; both $P < 0.001$). Meanwhile, in the antiosteoporosis+ group, the average duration of osteoporosis treatment was 3.1 years, and no change in T score was observed (femoral neck −2.22 to −2.21, $P = 0.830$; radius −2.49 to −2.59, $P = 0.071$). This pattern was also observed in the total hip. Specifically, bone density decreased significantly in the antiosteoporosis− group, whereas it remained unchanged in the antiosteoporosis+ group (Supplementary Table S4).

To further support our findings, we conducted a sensitivity analysis. Baseline patient characteristics were adjusted using IPTW based on propensity scores (Supplementary Table S5). The absolute standardized mean differences indicated that IPTW achieved adequate balance of the covariates (Supplementary Figure S3). Following IPTW adjustment, favorable bone mass outcomes were consistently observed for BMD and T score in the antiosteoporosis+ group compared with the antiosteoporosis− group (Supplementary Table S6).

Regarding *Z* score, the antiosteoporosis− group showed an increase in the femoral neck (−0.23 to −0.18, $P = 0.007$) but a decrease in the radius (0.91 to 0.81, $P = 0.04$) (Table 2). Meanwhile, the antiosteoporosis+ group showed an increase in both the femoral neck and radius (femoral neck −0.45 to −0.30, $P < 0.001$; radius −0.03 to 0.18, $P = 0.003$).

Furthermore, the incidence of osteoporosis increased in the antiosteoporosis− group (25.0% to 27.8%, $P < 0.001$) but not in the antiosteoporosis+ group (60.5 to 63.8, no significant difference after FDR). In summary, in the antiosteoporosis− group, the *Z* score increased depending on the site, but the T score decreased in both sites, resulting in an increase in osteoporosis.

The change in BMD beyond the measurement error is termed the LSC.[35] The percentages of patients who showed changes in BMD exceeding the LSC in the target group (Figure 1A, left bars) were as follows: in the femoral neck, BMD increased (white) in 14.2%, remained stable (gray) in 58.8%, and decreased (black) in 27.0%; and in the radius, BMD increased in 18.6%, remained stable in 42.4%, and decreased in 39.0%. In the antiosteoporosis+ group (right bars), the rate of BMD increase in the femoral neck was higher (19.1% vs 13.0%) and the rate of decrease was lower (20.4% vs 28.5%) compared to the antiosteoporosis− group (middle bars). The results were similar for the radius (BMD increase 20.4% vs 18.1%, BMD decrease 28.3% vs 41.6%).

Changes in femoral neck and radius T scores over three years were shown in a Sankey diagram (Figure 1B). Based on the T scores of both sites, the baseline and three-year status were compared. Change patterns were visually classified into the following: [A] Stable high T score >−2.5: T score > −2.5 throughout the observation period; [B] Decreased T score ≤−2.5 and T score deteriorated from >−2.5 to ≤−2.5 during the observation period;

Table 2. Changes in CDAI and bone mass scores during the observation period*

Variables	Target group (N = 797)			Antiosteoporosis− (n = 645)			Antiosteoporosis+ (n = 152)		
	First visit	Last visit	*P* value	First visit	Last visit	*P* value	First visit	Last visit	*P* value
Observation period, n (median, min–max), person-years	2,489 (3.1, 0.4–5.5)			2,020 (3.1, 0.4–5.5)			469 (3.0, 0.5–5.5)		
Duration of b/tsDMARDs use, %	83.3			82.1			88.2		
CDAI, mean ± SD	25.7 ± 12.8	6.6 ± 8.3	**<0.001**	26.0 ± 13.0	6.6 ± 8.5	**<0.001**	24.4 ± 11.6	6.8 ± 7.5	**<0.001**
Mean CDAI. mean ± SD	8.2 ± 6.7			8.2 ± 6.8			8.4 ± 6.3		
Osteoporosis, %	31.7	34.6	**<0.001**	25.0	27.8	**<0.001**	60.5	63.8	0.025
Antiosteoporotic drug use, %	19.1	56.0	**<0.001**	0	45.6	**<0.001**	100	100	–
Antiosteoporotic drug duration, mean ± SD, years	1.5 ± 1.9			1.1 ± 1.7			3.1 ± 1.7		
New fracture, % (n)	2.6 (21)			1.4 (9)			7.9 (12)		
Vertebra, % (n)	1.5 (12)			0.8 (5)			4.6 (7)		
Distal radius, % (n)	0.1 (1)			0 (0)			0.7 (1)		
Hip, % (n)	1.0 (8)			0.6 (4)			3.3 (5)		
Femoral neck, mean ± SD									
BMD	0.628 ± 0.126	0.618 ± 0.119	**<0.001**	0.646 ± 0.125	0.634 ± 0.118	**<0.001**	0.550 ± 0.098	0.550 ± 0.100	0.884
Change in BMD, %	−1.2 ± 6.6		**<0.001**	−1.5 ± 6.4		**<0.001**	0.3 ± 7.4		0.601
Yearly % change in BMD, %	−0.7 ± 3.9		**<0.001**	−0.9 ± 3.8		**<0.001**	0.0 ± 4.5		0.978
T score	−1.58 ± 1.06	−1.67 ± 0.99	**<0.001**	−1.43 ± 1.04	−1.54 ± 0.98	**<0.001**	−2.22 ± 0.85	−2.21 ± 0.85	0.830
Z score	−0.27 ± 1.02	−0.20 ± 0.99	**<0.001**	−0.23 ± 1.03	−0.18 ± 1.00	**0.007**	−0.45 ± 0.95	−0.30 ± 0.95	**<0.001**
Radius, mean ± SD									
BMD	0.602 ± 0.132	0.588 ± 0.132	**<0.001**	0.625 ± 0.126	0.608 ± 0.128	**<0.001**	0.509 ± 0.117	0.503 ± 0.113	0.040
Change in BMD, %	−2.3 ± 6.3		**<0.001**	−2.7 ± 6.2		**<0.001**	−0.8 ± 6.6		0.170
Yearly % change in BMD, %	−1.0 ± 3.1		**<0.001**	−1.1 ± 3.2		**<0.001**	−0.4 ± 2.8		0.091
T score	−0.96 ± 2.23	−1.25 ± 2.21	**<0.001**	−0.60 ± 2.13	−0.93 ± 2.16	**<0.001**	−2.49 ± 1.95	−2.59 ± 1.88	0.071
Z score	0.73 ± 1.70	0.69 ± 1.66	0.065	0.91 ± 1.65	0.81 ± 1.64	**0.004**	−0.03 ± 1.71	0.18 ± 1.65	**0.003**

* Changes in CDAI, bone mass, and treatment status between the first and last visits in all patients (target group), those not receiving antiosteoporotic drug at enrollment (antiosteoporosis−), and those receiving antiosteoporotic drug at enrollment (antiosteoporosis+). The percent change in BMD was calculated by dividing the difference in BMD between the first and last visits by the baseline BMD and expressing it as a percentage. The yearly percent change in BMD was calculated by dividing the percent change in BMD by the observational period (years). *P* values indicate comparisons between first and last visits within each group calculated using a paired *t*-test. Bolded values are $P < 0.05$ after false discovery rate correction. BMD, bone mineral density; b/tsDMARD, biologic or targeted synthetic disease-modifying antirheumatic drug; CDAI, Clinical Disease Activity Index.

[C] Recovered from T score ≤−2.5: T score improved from ≤−2.5 to >−2.5 during the observation period; [D] Stable low T score ≤−2.5 and T score ≤−2.5 throughout the observation period. In the target group (left), T score improvement [C] was 4.3%, whereas T score deterioration [B] was 8.9%. The same was true for the antiosteoporosis− group (middle), with an improvement in [C] of 3.1% and a deterioration in [B] of 9.0%. Meanwhile, in the antiosteoporosis+ group (right), improvement [C] and deterioration in [B] were both 8.5%. Patient backgrounds based on the T score change patterns for groups [A] to [D] are shown in Supplementary Table S7. Although there were differences in age, disease duration, concomitant GC rate, menopausal rate, baseline T score, and concomitant osteoporosis treatment rate, patients with a T score improvement [C] had lower baseline T scores than did patients with T score deterioration [B] (femoral neck T score −2.23 vs −1.64, radius T score −0.93 vs −1.02), and a higher rate of concomitant osteoporosis medication at the start and throughout the observation period (antiosteoporotic drug use: baseline 42.9% vs 20.7%, entire period 92.9% vs 72.4%). Of note, all four groups maintained low disease activity

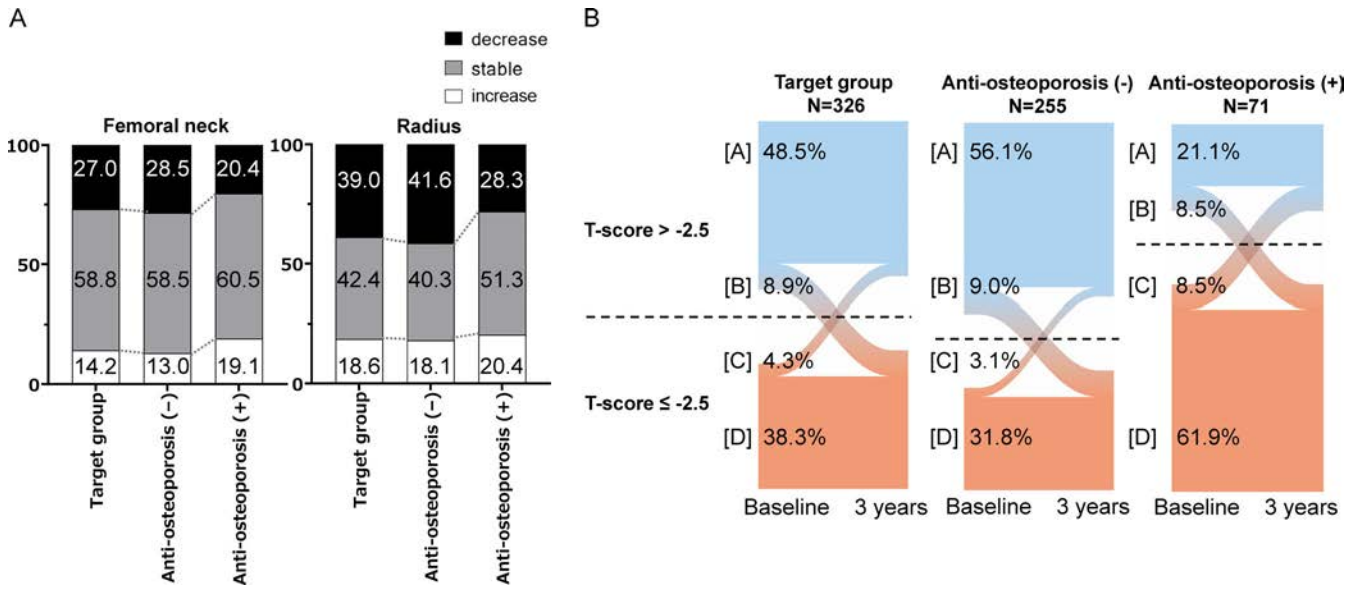


Figure 1. Changes in bone mineral density and transitions in T score categories. (A) Bone mineral density changes beyond the least significant change. Proportions of patients with increased, stable, or decreased bone mineral density exceeding the least significant change of the femoral neck and radius in all patients (target group), those not receiving antiosteoporotic drug at enrollment (antiosteoporosis–), and those receiving anti-osteoporotic drug at enrollment (antiosteoporosis+). The least significant change, reflecting device-specific precision error, was set at >0.029 g/cm^2 for the femoral neck and >0.011 g/cm^2 for the radius. (B) Sankey diagram showing transitions in T score categories from baseline to three years. Changes over time are shown for the entire cohort (target group, N = 797), as well as subgroups based on the use of antiosteoporotic drugs at baseline. Each patient was further classified into one of the following four T score change patterns: [A] Stable high T-score >−2.5: T-scores remained >−2.5 throughout the observation: [B] Decreased to T-score ≤−2.5: T-scores decreased from >−2.5 to ≤−2.5: [C] Recovered from T score ≤−2.5: T scores recovered from ≤−2.5 to >−2.5: [D] Stable low T score ≤−2.5: T-scores remained ≤−2.5. Percentages represent the proportion of patients in each category within each group.

during the observation period (average CDAI scores 5.1–7.0). These results suggest that the concomitant use of osteoporosis medications is important for maintaining BMD.

Furthermore, univariate and multivariate analyses were performed to explore factors associated with T score changes (Table 3). Multivariate analysis was adjusted for background factors such as patient background, complications, RA treatment, and osteoporosis treatment. In multivariate analysis, for both femoral neck (left) and radius T score change (right), a longer period of osteoporosis treatment was associated with an increased T score, and a higher baseline T score was associated with a decreased T score. Longer use of b/tsDMARDs was not correlated with suppressed bone loss. Consistent with the above findings, cumulative CDAI values were not associated with BMD maintenance in both sites.

As a sensitivity analysis to explore factors correlated with BMD change, a trajectory analysis was performed using a Gaussian mixture model to cluster BMD into trajectory groups (Figure 2). In the femoral neck, five trajectory groups were established: group 1 had 135 patients, group 2 had 200 patients, group 3 had 194 patients, group 4 had 149 patients, and group 5 had 117 patients. T scores increased significantly in 335 patients (42%) belonging to groups 1 (mean T score change 0.27) and 2 (mean T score change 0.10) but decreased significantly in 450 patients (58%) belonging to groups 3, 4, and 5 (mean T score change −0.17, −0.38, and −0.27, respectively). Additionally, the radius was divided into four groups: group 1 had 214 patients, group 2 had 249 patients, group 3 had 185 patients, and group 4 had 148 patients. Group 1 (27%) showed an increase in T score (mean change in T score 0.27), whereas groups 2, 3, and 4 (73%) showed a decrease (mean change −0.17, −0.73, −0.75, respectively).

We compared background factors in each group. For femoral neck (Table 4), the elevated T score groups (groups 1 and 2) had a lower baseline femoral neck T score than the decreased T score groups (groups 3–5) (−1.98 and −1.89 for groups 1 and 2 vs −1.47, −1.05, and −1.46 for groups 3, 4, and 5, respectively), a higher rate of osteoporosis treatment at baseline and overall (baseline: 25.9% and 21.3% for groups 1 and 2 vs 15.5%, 12.1%, and 17.9% for groups 3, 4, and 5, respectively; overall: 68.1% and 71.0% for groups 1 and 2 vs 51.5%, 34.9%, and 49.6% for groups 3, 4, and 5, respectively), and a longer duration of treatment (duration, 1.9 years and 2.4 years for groups 1 and 2 vs 1.4, 0.7, and 0.5 years for groups 3, 4, and 5, respectively). For the radius, the patients were divided into elevated (group 1) and decreased T score groups (groups 2, 3, and 4)

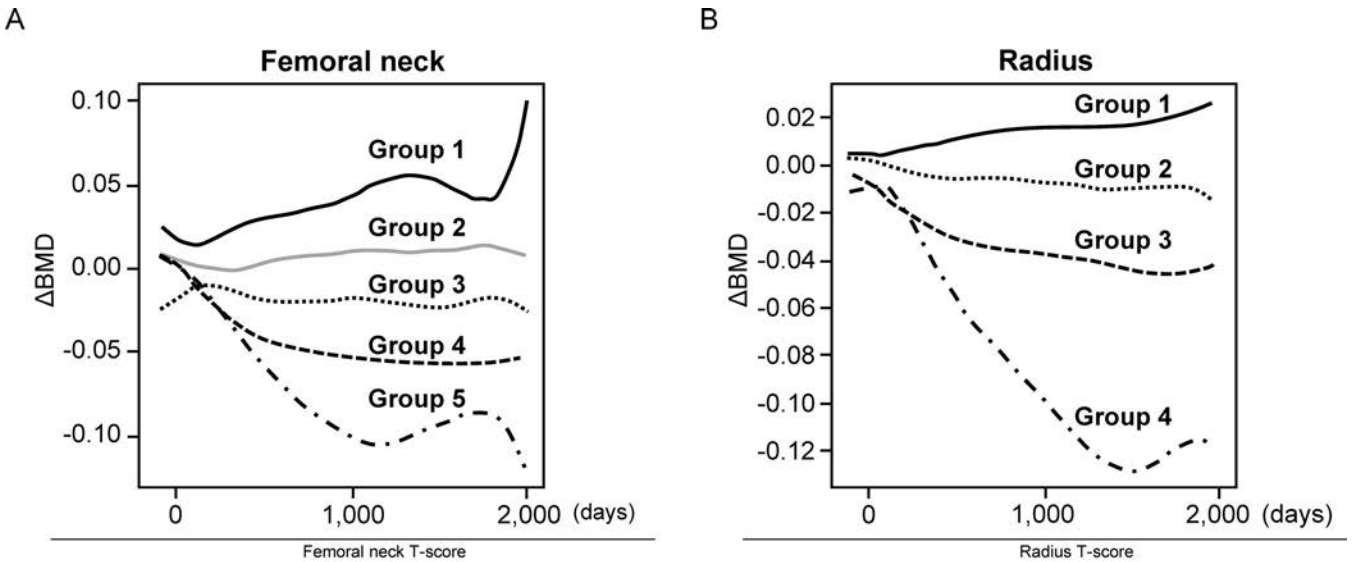
Table 3. Factors associated with changes in T score*

Variables	ΔT score femoral neck				ΔT score radius			
	Univariate		Multivariate		Univariate		Multivariate	
	β	*P* value	β	*P* value	β	*P* value	β	*P* value
Age	0.098	0.006	−0.002	0.188	−0.041	0.259	**−0.014**	**<0.001**
Women	0.048	0.173	−0.075	0.113	−0.005	0.892	−0.015	0.872
Disease duration	0.073	0.040	0.000	0.948	0.115	0.001	0.000	0.194
BMI	−0.086	0.016	0.002	0.490	−0.039	0.283	0.011	0.114
RA stage I and II	0.092	0.010	−0.002	0.955	0.088	0.014	0.017	0.843
MTX use	0.022	0.534	−0.013	0.702	−0.079	0.028	−0.014	0.844
GC use	−0.003	0.931	−0.009	0.791	0.043	0.232	0.096	0.148
eGFR	−0.047	0.189	0.000	0.448	−0.025	0.493	−0.001	0.675
Smoking	0.076	0.032	−0.051	0.090	0.021	0.568	−0.039	0.517
Diabetes	0.066	0.063	−0.032	0.385	0.040	0.267	−0.069	0.340
Emphysema	−0.015	0.683	0.048	0.435	−0.027	0.452	0.147	0.235
ILD	0.008	0.826	0.007	0.875	−0.058	0.109	0.129	0.153
Menopause	−0.109	0.002	−0.020	0.628	0.045	0.210	**−0.253**	**0.002**
History of fractures	−0.113	0.001	0.015	0.671	−0.107	0.003	0.045	0.529
New fracture	0.004	0.920	**−0.149**	**0.038**	0.022	0.543	0.077	0.595
CRP	−0.070	0.049	−0.003	0.538	−0.059	0.099	−0.001	0.942
Cumulative CRP	0.000	0.009	0.000	0.083	0.000	<0.001	**0.000**	**0.032**
RF titer	0.009	0.808	0.000	0.859	−0.025	0.484	0.000	0.280
ACPA titer	−0.013	0.720	0.000	0.899	−0.017	0.630	0.000	0.666
CDAI	−0.017	0.635	0.001	0.488	−0.079	0.029	−0.002	0.391
Cumulative CDAI	0.000	0.406	0.000	0.871	0.000	<0.001	0.000	0.212
HAQ	−0.021	0.557	−0.027	0.238	−0.039	0.287	0.066	0.151
Cumulative HAQ	0.000	0.205	0.000	0.230	0.000	0.025	0.000	0.176
Duration of b/tsDMARDs	0.022	0.006	0.062	0.233	0.003	0.860	0.119	0.254
TNFi	0.000	0.163	−0.049	0.275	0.000	0.108	**−0.206**	**0.021**
IL-6Ri	0.000	0.029	−0.081	0.055	0.000	0.175	**−0.198**	**0.018**
CTLA4-Ig	0.000	<0.001	−0.020	0.635	0.000	0.088	0.002	0.983
JAKi	0.000	0.831	−0.039	0.377	0.000	0.479	−0.090	0.303
Switching of b/tsDMARDs	0.077	0.031	−0.011	0.805	0.107	0.003	0.045	0.616
Duration of antiosteoporotic drug	0.296	<0.001	**0.034**	**<0.001**	0.180	<0.001	**0.083**	**<0.001**
Bisphosphonate use	−0.224	<0.001	0.012	0.721	−0.099	0.006	−0.017	0.808
Denosumab use	−0.211	<0.001	0.056	0.107	−0.068	0.059	0.089	0.195
Femoral neck T score, baseline	−0.343	<0.001	**−0.098**	**<0.001**	−0.114	0.002	0.049	0.158
Radius T score, baseline	−0.222	<0.001	0.002	0.809	−0.190	<0.001	**−0.109**	**<0.001**

* Bold indicates statistical significance. Univariate and multivariate regression analyses were performed to identify factors associated with ΔT score of the femoral neck and radius. β-coefficients and *P* values are shown for each variable. ACPA, anticyclic citrullinated peptide antibody; BMI, body mass index; b/tsDMARD, biologic and targeted synthetic disease-modifying antirheumatic drug; CDAI, Clinical Disease Activity Index; CRP, C-reactive protein; eGFR, estimated glomerular filtration rate; GC, glucocorticoid; HAQ, Health Assessment Questionnaire; ILD, interstitial lung disease; IL-6Ri, interleukin-6 receptor inhibitor; JAKi, JAK inhibitor; MTX, methotrexate; RA, rheumatoid arthritis; RF, rheumatoid factor; TNFi, tumor necrosis factor inhibitor; ΔT score, changes in T score.

(Supplementary Table S8). Groups 1 and 2 showed similar characteristics compared to groups 3 and 4, including a lower baseline T score (group 1: −1.13, group 2: −1.09), a higher use of osteoporosis medications at baseline and overall (baseline: 21.5% for group 1, 21.3% for group 2; overall: 60.7% for group 1, 61.8% for group 2), and a longer duration of medication use (duration: 1.8 years for group 1, 1.9 years for group 2 vs 1.2 years for group 3, 0.6 years for group 4). Therefore, the characteristics of the groups with elevated radius T scores were unclear. This analysis also found that average CDAI did not explain the increase or decrease in femoral and radial BMD.

During the observation period, 21 new fragility fractures (2.6%) were observed (Table 2; Supplementary Table S9). Patients with new fractures, compared with those without new fractures, were more likely to be older women (mean age 73.4 vs 61.1, women 85.7% vs 76.9%), postmenopausal women (88.9% vs 76.9%), patients with reduced renal function (eGFR <60 mL/min/m^2 38.1% vs 18.2%), patients receiving GCs (concomitant use 38.1% vs 21.5%, mean dose 4.6 mg/day vs 3.9 mg/day), or patients with fracture history (61.9% vs 16.9%). Furthermore, patients with new fractures were more likely to be at high fracture risk, with lower baseline T scores (femoral neck T score baseline −2.26 vs −1.56; radius T score baseline −2.37 vs −0.93). No obvious differences in fracture sites were observed between the antiosteoporosis− and antiosteoporosis+ groups (Table 2).



Femoral neck T-score

	First visit	Last visit	mean change	*P* value
Group 1, N=135	-1.98 ± 1.08	-1.71 ± 1.06	0.27 ± 0.35	< 0.001
Group 2, N=200	-1.89 ± 0.91	-1.79 ± 0.90	0.10 ± 0.17	< 0.001
Group 3, N=194	-1.47 ± 1.00	-1.64 ± 1.00	-0.17 ± 0.16	< 0.001
Group 4, N=149	-1.05 ± 1.05	-1.43 ± 1.04	-0.38 ± 0.26	< 0.001
Group 5, N=117	-1.46 ± 1.00	-1.73 ± 0.93	-0.27 ± 0.47	< 0.001

Radius T-score

	First visit	Last visit	mean change	*P* value
Group 1, N=214	-1.13 ± 2.45	-0.86 ± 2.46	0.27 ± 0.44	< 0.001
Group 2, N=249	-1.09 ± 2.25	-1.26 ± 2.21	-0.17 ± 0.29	< 0.001
Group 3, N=185	-0.77 ± 1.99	-1.49 ± 1.97	-0.73 ± 0.50	< 0.001
Group 4, N=148	-0.75 ± 2.11	-1.50 ± 2.06	-0.75 ± 1.15	< 0.001

Figure 2. Trajectory of bone mineral density. Bone mineral density change (ΔBMD) trajectories identified using Gaussian mixture modeling. ΔBMD indicates change from baseline over time (days). Data in the tables are presented as mean ± SD. *P* values indicate comparisons between the first and last visits within each group.

DISCUSSION

In our recent one-year prospective study of 1,164 patients with active RA receiving their first b/tsDMARD, BMD decreased in the group not receiving osteoporosis medication at the start of treatment[31] but remained stable in the group receiving such therapy. The present study extends those findings with up to five years of follow-up. To better reflect actual clinical practice, we also considered changes to or discontinuation of b/tsDMARDs, as well as changes in concomitant medications. Our results, examined by grouping based on antiosteoporosis at baseline and by multivariable analysis without grouping the patients, as well as by trajectory analysis with grouping based on BMD trajectory, repeatedly demonstrated the impact of antiosteoporosis. Although the reduction in BMD was numerically modest, it contrasted with previous studies reporting that biologic therapy improves osteoporosis. Namely, b/tsDMARD treatment improved RA disease activity but did not arrest BMD loss when osteoporosis medication was not used sufficiently. Neither duration of b/tsDMARD use nor disease activity during the study (eg, cumulative CDAI) was associated with BMD maintenance. In contrast, the longer duration of osteoporosis treatment maintained and increased BMD in some patients. It is understandable that BMD declines in patients with controlled disease activity who are not receiving antiosteoporotic therapy because inflammation is only one of several factors that contribute to RA-related osteoporosis.[1,5–9] Although the importance of managing osteoporosis is widely recognized, it is not widely implemented in clinical practice. This study reiterates the necessity of addressing osteoporosis as an independent component of RA management, in addition to inflammation control.

The BMD changes observed in this study were unlikely attributable to measurement error because differences exceeding the LSC were observed between patients who did and who did not receive osteoporosis medication. The yearly BMD change rate was –0.9% in patients not treated with osteoporosis medication at enrollment. This rate exceeds the placebo group rates reported in osteoporosis drug trials, which ranged from –0.2% to –0.4% per year.[39–41] Despite the differences in patient populations between this study and osteoporosis drug development trials, the rapid rate of BMD loss observed in this study is a notable finding. However, the clinical impact of these BMD changes on fractures, the primary outcome of osteoporosis management, remains unclear. Indeed, patients in the antiosteoporosis– group had relatively preserved baseline BMD and experienced more rapid bone mass loss during follow-up. Nevertheless, they exhibited a lower fracture incidence than patients receiving antiosteoporosis treatment. This observation underscores the need for further investigation into the relationship between BMD changes and fracture risk in this cohort. However, the fracture incidence observed in this study was lower than that reported in previous

Table 4. Patient characteristics of femoral neck bone mineral density–based trajectory groups*

Characteristics	Group 1 (n = 135)	Group 2 (n = 200)	Group 3 (n = 194)	Group 4 (n = 149)	Group 5 (n = 117)	*P* value
Observation period, mean ± SD, years	2.9 ± 1.6	4.0 ± 1.2	3.4 ± 1.5	3.2 ± 1.5	1.4 ± 1.4	<0.001[a]
Age, mean ± SD, years	63.7 ± 13.4	61.9 ± 13.4	59.9 ± 14.6	59.5 ± 13.6	62.7 ± 14.6	0.037
Women, %	80.7	75.2	76.8	75.2	67.5	0.038
BMI, mean ± SD, kg/m^2	21.7 ± 4.2	22.2 ± 3.4	22.2 ± 3.4	23.4 ± 4.5	22.4 ± 4.2	0.004[a]
Disease duration, mean ± SD, months	74.7 ± 103.9	55.5 ± 78.4	60.3 ± 90.6	55.4 ± 83.1	60.1 ± 103.7	0.358
RA stages, %						0.009[a]
Stage I	37.0	31.0	40.7	44.3	30.8	
Stage II	40.0	51.5	44.8	38.8	54.7	
Stage III	11.1	12.0	8.8	13.4	5.1	
Stage IV	11.9	5.5	5.7	4.0	9.4	
RF positive, %	74.1	70.3	66.5	72.5	76.9	0.302
ACPA positive, %	68.1	63.4	60.3	63.5	71.6	0.301
Concomitant MTX use, %	77.8	75.9	78.4	77.2	57.3	<0.001[a]
Concomitant GC use, %	22.0	21.3	23.1	18.1	25.6	0.645
CRP baseline, mean ± SD, mg/dl	2.4 ± 3.1	2.2 ± 3.0	2.3 ± 3.7	3.0 ± 3.9	2.7 ± 3.7	0.186
Average CRP during the observation, mean ± SD, mg/dl	0.4 ± 0.6	0.4 ± 0.9	0.4 ± 0.7	0.7 ± 1.4	1.1 ± 1.7	<0.001[a]
CDAI baseline, mean ± SD	24.7 ± 14.1	25.8 ± 13.2	24.9 ± 12.8	25.9 ± 12.3	25.9 ± 12.0	0.485
Average CDAI during the observation, mean ± SD	7.4 ± 5.5	7.3 ± 6.4	7.8 ± 6.1	7.9 ± 7.1	12.0 ± 7.6	<0.001[a]
HAQ baseline, mean ± SD	1.2 ± 0.8	1.2 ± 0.8	1.1 ± 0.8	1.3 ± 0.8	1.3 ± 0.8	0.356
Average HAQ during the observation, mean ± SD	0.8 ± 0.7	0.6 ± 0.6	0.7 ± 0.7	0.7 ± 0.7	0.9 ± 0.7	**0.001**[a]
ILD, %	8.9	7.5	6.7	10.7	19.7	0.003[a]
Menopause in women, %	85.3	79.8	72.5	75.3	75.3	0.251
Femoral neck T score, baseline, mean ± SD	−1.98 ± 1.08	−1.89 ± 0.91	−1.47 ± 1.00	−1.05 ± 1.05	−1.46 ± 1.00	<0.001[a]
Radius T score, baseline, mean ± SD	−1.52 ± 2.29	−1.30 ± 2.23	−0.78 ± 2.18	−0.26 ± 1.97	−0.86 ± 2.28	<0.001[a]
Femoral neck ΔT score during the observation, mean ± SD	0.27 ± 0.26	0.10 ± 0.17	−0.17 ± 0.16	−0.38 ± 0.26	−0.27 ± 0.47	<0.001[a]
Radius ΔT score during the observation, mean ± SD	−0.06 ± 0.59	−0.17 ± 0.62	−0.37 ± 0.72	−0.49 ± 0.94	−0.38 ± 0.79	<0.001[a]
Antiosteoporotic drug use, baseline, %	25.9	21.3	15.5	12.1	17.9	0.011[a]
Antiosteoporotic drug use during the whole period, %	68.1	71.0	51.5	34.9	49.6	<0.001[a]
Duration of b/tsDMARDs use, mean ± SD, years	2.4 ± 1.5	3.3 ± 1.5	2.7 ± 1.5	2.4 ± 1.5	1.2 ± 1.2	<0.001[a]
Duration of antiosteoporotic use, mean ± SD, years	1.9 ± 2.0	2.4 ± 2.1	1.4 ± 1.8	0.7 ± 1.3	0.5 ± 1.0	<0.001[a]
History of fractures, %	26.0	21.0	16.5	9.4	17.1	0.006[a]
New fracture, %	1.5	3.0	3.1	2.0	3.4	0.833
Diabetes, %	11.1	16.0	13.4	22.1	22.2	0.034
eGFR <60 mL/min/m^2, baseline	20.0	15.5	17.0	18.1	26.5	0.161
Emphysema, %	3.7	5.0	4.1	2.7	7.7	0.371
Smoking, %						0.039
Current	9.8	14.8	16.1	17.5	24.6	
Past	20.5	18.4	22.9	24.8	25.4	
Never	69.7	66.8	60.9	57.7	50.0	

* Characteristics and treatment history of patients classified into five groups based on changes in femoral bone mass, using Gaussian mixture modeling. Statistical comparisons across groups were conducted using one-way analysis of variance or Pearson's chi-square test, with false discovery rate–adjusted *P* values. ACPA, anticyclic citrullinated peptide antibody; BMI, body mass index; b/tsDMARD, biologic and targeted synthetic disease-modifying antirheumatic drugs; CDAI, Clinical Disease Activity Index; CRP, C-reactive protein; eGFR, estimated glomerular filtration rate; GC, glucocorticoid; HAQ, Health Assessment Questionnaire; ILD, interstitial lung disease; MTX, methotrexate; RA, rheumatoid arthritis; RF, rheumatoid factor; ΔT score, changes in T score.
[a] $P < 0.05$ after false discovery rate correction was considered statistically significant.

RA fracture studies. With 21 events, the incidence was 8.4 per 1,000 person-years, compared with previous RA fracture study rates ranging from 13.0 to 21.0 per 1,000 person-years.[42–44] The limited number of fracture events prevented a robust evaluation of fracture outcomes.

Our findings suggest that some patients experience BMD loss during treatment with b/tsDMARDs. This may increase their risk of developing osteoporosis over time, underscoring the importance of osteoporosis-focused care. However, prior studies have not reported a consensus on the necessity and optimal frequency of regular BMD assessments. Studies conducted primarily on the general population have reported that changes in BMD do not always correlate with fracture risk; therefore, they do not recommend routine screening.[45–48] In contrast, other studies propose screening every one to two years for high-risk populations, including patients with RA.[49–51] Although the former

perspective is useful for evaluating screening strategies at the population level, the latter reflects a more clinically oriented, personalized medicine approach.

Notably, evidence from fracture outcome studies indicates that controlling inflammation alone may not be enough to prevent fractures in RA. If b/tsDMARDs use and inflammation control alone were sufficient to improve osteoporosis, one would expect increased use of b/tsDMARDs and improved clinical outcomes to reduce fracture rates in patients with RA. However, a recent Japanese RA cohort study reported that fracture rates increased over time despite higher b/tsDMARD use and remission rates.[29] A Spanish study found that fractures were 1.5 times more common in patients with RA than in the general population, and GC use contributed to fractures though disease activity and b/tsDMARDs did not.[30] These observations support the notion that b/tsDMARDs use and inflammation control alone may not adequately prevent bone loss or fractures in RA, highlighting the need for multifactorial management.

In light of these findings, BMD remains a useful osteoporosis management tool because it involves relatively low radiation exposure.[52] For high-risk patients, regular BMD assessments may therefore provide a clinical benefit with an acceptable level of physical burden. Taken together, these findings suggest that osteoporosis prevention requires more attention and implementation as the global population ages.

Although our results did not demonstrate the beneficial effects of b/tsDMARDs on bone health, other studies have reported improvements in BMD in patients with RA.[53,54] The differences between those studies and this study may be due to differences in the analyzed population, race, and lifestyle. A Taiwanese study reported that BMD was maintained after the introduction of b/tsDMARDs.[53] When comparing their population and ours, calcium intakes were considered comparable (587 and 533 mg/day, respectively).[55] However, compared with their cohort, participants in our study were older (mean 61.4 vs 56.4 years) and more likely to smoke (16.2% vs 5.0%). Additionally, 19% of our participants were receiving treatment for osteoporosis at baseline, whereas the Taiwanese study did not provide this information, which may have been higher in their cohort. These differences may have led to different results. Similarly, a Japanese observational study reported increased fracture rates despite the increased use of b/tsDMARDs,[29] whereas a German study showed decreased fracture rates.[54] However, differences in populations, such as calcium intake (533 vs 1,068 mg/day)[55] and osteoporosis prevalence (12.8% vs 6.6%),[56,57] may have led to conflicting results regarding fractures.

Other studies[13–28] are relatively small in scale and may not adequately describe confounding factors with significant effects on osteoporosis, such as menopause, GC use, concomitant use of osteoporosis medications, and comorbidities (eg, chronic kidney disease, emphysema). Therefore, these findings should be interpreted carefully. In contrast, our study included a larger sample size and controlled for several confounding factors.

Although the reasons for discrepancies among studies remain unclear, our findings suggest that a considerable proportion (ie, 58% in this study) of patients experience bone loss despite adequate inflammation control with b/tsDMARDs. These findings support the concept that greater attention to osteoporosis is needed in patients with RA.[7,9,10]

In the present study, changes in *Z* score were evaluated. The T score was compared with the average for young adults, and the *Z* score was compared with the average for people of the same age and sex.[58] Therefore, a decline in *Z* scores over time indicates a greater decrease in bone density than would be expected with aging alone. The *Z* score decreased in the group in which osteoporosis medications were never used throughout the study period (data available if requested). This finding indicates that patients with RA may experience bone loss beyond age-related changes without antiosteoporosis therapy, even with sufficient inflammation control. Accordingly, the observed increase in *Z* score is likely attributable to the initiation of osteoporosis medications during the observation period, rather than the use of b/tsDMARDs.

This study observed 21 new fragility fractures, and the characteristics of these patients were consistent with known risk factors for osteoporotic fractures.[59] In our cohort, patients receiving osteoporosis therapy generally maintained BMD. However, some patients experienced fractures despite receiving therapy, which may partly reflect their higher baseline fracture risk. These results imply that, although improving the rate of osteoporosis management is important, optimizing treatment for each patient may be equally crucial.

Several limitations should be acknowledged. The main limitation of this study is its single-arm, real-world design, which precludes establishing a causal relationship between b/tsDMARDs and BMD. As with other observational studies, randomizing patients to conventional synthetic DMARDs (csDMARDs) and b/tsDMARDs was ethically challenging. Although a csDMARD control group could be constructed from real-world data in theory, substantial differences in patient characteristics would make adequate statistical adjustment problematic. Therefore, as with other real-world studies, our work could not overcome these limitations. Because medication use was unrestricted, some patients in antiosteoporosis– group-initiated osteoporosis therapy to maximize patient benefit. However, their treatment duration was short and BMD was not stabilized, whereas longer therapy was associated with BMD maintenance. Thus, this variation is unlikely to affect the conclusion that b/tsDMARDs and inflammation control alone are insufficient to arrest osteoporosis progression. Second, data on fragility fractures during the observation period were based on patient self-reporting and physician records. Thus, asymptomatic fractures were not captured. Although the validity of patient-reported fracture records has

previously been demonstrated,[60] the effectiveness of b/tsDMARDs in preventing fractures cannot be determined from the present results. Third, a lack of detailed information on dosage and adherence to antiosteoporosis precluded a detailed comparison of drug-specific treatment effects.

Despite these limitations, our findings provide real-world insights into bone health management in RA and highlight the importance of ongoing attention to osteoporosis. In conclusion, bone mass decreased in the group without concomitant osteoporosis medication even after the introduction of b/tsDMARDs, whereas concomitant osteoporosis treatment helped maintain BMD. Although the decrease in BMD in the group not receiving osteoporosis medication became more "age-appropriate," managing osteoporosis remains important. Regular evaluation and appropriate interventions for osteoporosis in patients with RA are considered necessary.

ACKNOWLEDGMENTS

The authors thank the medical staff of all participating institutions for providing the study data, with special thanks to Hiroko Yoshida, Yoko Saito, Yuki Itose, and Ayumi Maruyama of the FIRST registry supporting team for the excellent data management.

AUTHOR CONTRIBUTIONS

All authors contributed to at least one of the following manuscript preparation roles: conceptualization AND/OR methodology, software, investigation, formal analysis, data curation, visualization, and validation AND drafting or reviewing/editing the final draft. As corresponding author, Dr Y. Tanaka confirms that all authors have provided the final approval of the version to be published and takes responsibility for the affirmations regarding article submission (eg, not under consideration by another journal), the integrity of the data presented, and the statements regarding compliance with institutional review board/Declaration of Helsinki requirements.

REFERENCES

1. Tanaka Y. Managing osteoporosis and joint damage in patients with rheumatoid arthritis: an overview. J Clin Med 2021;10(6):1241. doi:https://doi.org/10.3390/jcm10061241
2. Heinlen L, Humphrey MB. Skeletal complications of rheumatoid arthritis. Osteoporos Int 2017;28(10):2801–2812. doi:https://doi.org/10.1007/s00198-017-4170-5
3. Haugeberg G, Uhlig T, Falch JA, et al. Bone mineral density and frequency of osteoporosis in female patients with rheumatoid arthritis: results from 394 patients in the Oslo County Rheumatoid Arthritis register. Arthritis Rheum 2000;43(3):522–530. doi:https://doi.org/10.1002/1529-0131(200003)43:3<522:AID-ANR7>3.0.CO;2-Y
4. Sattui SE, Saag KG. Fracture mortality: associations with epidemiology and osteoporosis treatment. Nat Rev Endocrinol 2014;10(10):592–602. doi:https://doi.org/10.1038/nrendo.2014.125
5. Baker R, Narla R, Baker JF, et al. Risk factors for osteoporosis and fractures in rheumatoid arthritis. Best Pract Res Clin Rheumatol 2022;36(3):101773. doi:https://doi.org/10.1016/j.berh.2022.101773
6. Schmajuk G, Tonner C, Trupin L, et al. Variations in radiographic procedure use for Medicare patients with rheumatoid arthritis. Arthritis Care Res (Hoboken) 2017;69(5):642–648. doi:https://doi.org/10.1002/acr.22988
7. Lindner L, Callhoff J, Alten R, et al. Osteoporosis in patients with rheumatoid arthritis: trends in the German National Database 2007-2017. Rheumatol Int 2020;40(12):2005–2012. doi:https://doi.org/10.1007/s00296-020-04593-6
8. Kareem R, Botleroo RA, Bhandari R, et al. The impact of rheumatoid arthritis on bone loss: links to osteoporosis and osteopenia. Cureus 2021;13(8):e17519. doi:https://doi.org/10.7759/cureus.17519
9. Dulcey L, Theran J, Villamizar D, et al. Ab1008 characterization of the risk of osteoporosis in a cohort of rheumatic patients during 10 years of follow-up. Ann Rheum Dis 2022;81:1628. doi:https://doi.org/10.1136/annrheumdis-2022-eular.329
10. Audet T, Carrier N, Boire G, et al. Management of osteoporosis in patients with rheumatoid arthritis: insights from a Canadian academic division of rheumatology. J Rheumatol 2025;52(suppl 2):109. doi:https://doi.org/10.3899/jrheum.2025-0314.135
11. Smolen JS, Breedveld FC, Burmester GR, et al. Treating rheumatoid arthritis to target: 2014 update of the recommendations of an international task force. Ann Rheum Dis 2016;75(1):3–15. doi:https://doi.org/10.1136/annrheumdis-2015-207524
12. Fraenkel L, Bathon JM, England BR, et al. 2021 American College of Rheumatology guideline for the treatment of rheumatoid arthritis. Arthritis Rheumatol 2021;73(7):1108–1123. doi:https://doi.org/10.1002/art.41752
13. Vis M, Voskuyl AE, Wolbink GJ, et al; OSTRA Study Group. Bone mineral density in patients with rheumatoid arthritis treated with infliximab. Ann Rheum Dis 2005;64(2):336–337. doi:https://doi.org/10.1136/ard.2003.017780
14. Lange U, Teichmann J, Müller-Ladner U, et al. Increase in bone mineral density of patients with rheumatoid arthritis treated with anti-TNF-alpha antibody: a prospective open-label pilot study. Rheumatology (Oxford) 2005;44(12):1546–1548. doi:https://doi.org/10.1093/rheumatology/kei082
15. Seriolo B, Paolino S, Sulli A, et al. Bone metabolism changes during anti-TNF-alpha therapy in patients with active rheumatoid arthritis. Ann NY Acad Sci 2006;1069(1):420–427. doi:https://doi.org/10.1196/annals.1351.040
16. Vis M, Havaardsholm EA, Haugeberg G, et al. Evaluation of bone mineral density, bone metabolism, osteoprotegerin and receptor activator of the NFkappaB ligand serum levels during treatment with infliximab in patients with rheumatoid arthritis. Ann Rheum Dis 2006;65(11):1495–1499. doi:https://doi.org/10.1136/ard.2005.044198
17. Marotte H, Pallot-Prades B, Grange L, et al. A 1-year case-control study in patients with rheumatoid arthritis indicates prevention of loss of bone mineral density in both responders and nonresponders to infliximab. Arthritis Res Ther 2007;9(3):R61. doi:https://doi.org/10.1186/ar2219
18. Chopin F, Garnero P, le Henanff A, et al. Long-term effects of infliximab on bone and cartilage turnover markers in patients with rheumatoid arthritis. Ann Rheum Dis 2008;67(3):353–357. doi:https://doi.org/10.1136/ard.2007.076604
19. Wijbrandts CA, Klaasen R, Dijkgraaf MG, et al. Bone mineral density in rheumatoid arthritis patients 1 year after adalimumab therapy: arrest of bone loss. Ann Rheum Dis 2009;68(3):373–376. doi:https://doi.org/10.1136/ard.2008.091611
20. Hoff M, Kvien TK, Kälvesten J, et al. Adalimumab reduces hand bone loss in rheumatoid arthritis independent of clinical response: subanalysis of the PREMIER study. BMC Musculoskelet Disord 2011;12(1):54. doi:https://doi.org/10.1186/1471-2474-12-54
21. Dischereit G, Tarner IH, Müller-Ladner U, et al. Infliximab improves bone metabolism and bone mineral density in rheumatoid arthritis and ankylosing spondylitis: a prospective 2-year study. Clin

Rheumatol 2013;32(3):377–381. doi:https://doi.org/10.1007/s10067-012-2128-8

22. Krieckaert CL, Nurmohamed MT, Wolbink G, et al. Changes in bone mineral density during long-term treatment with adalimumab in patients with rheumatoid arthritis: a cohort study. Rheumatology (Oxford) 2013;52(3):547–553. doi:https://doi.org/10.1093/rheumatology/kes320
23. Kume K, Amano K, Yamada S, et al. The effect of tocilizumab on bone mineral density in patients with methotrexate-resistant active rheumatoid arthritis. Rheumatology (Oxford) 2014;53(5):900–903. doi:https://doi.org/10.1093/rheumatology/ket468
24. Briot K, Rouanet S, Schaeverbeke T, et al. The effect of tocilizumab on bone mineral density, serum levels of Dickkopf-1 and bone remodeling markers in patients with rheumatoid arthritis. Joint Bone Spine 2015;82(2):109–115. doi:https://doi.org/10.1016/j.jbspin.2014.10.015
25. Chen YM, Chen HH, Huang WN, et al. Tocilizumab potentially prevents bone loss in patients with anticitrullinated protein antibody-positive rheumatoid arthritis. PLoS One 2017;12(11):e0188454. doi:https://doi.org/10.1371/journal.pone.0188454
26. Tada M, Inui K, Sugioka Y, et al. Abatacept might increase bone mineral density at femoral neck for patients with rheumatoid arthritis in clinical practice: AIRTIGHT study. Rheumatol Int 2018;38(5):777–784. doi:https://doi.org/10.1007/s00296-017-3922-z
27. Chen MH, Yu SF, Chen JF, et al. Different effects of biologics on systemic bone loss protection in rheumatoid arthritis: an interim analysis of a three-year longitudinal cohort study. Front Immunol 2021;12:783030. doi:https://doi.org/10.3389/fimmu.2021.783030
28. Hamar A, Szekanecz Z, Pusztai A, et al. Effects of one-year tofacitinib therapy on bone metabolism in rheumatoid arthritis. Osteoporos Int 2021;32(8):1621–1629. doi:https://doi.org/10.1007/s00198-021-05871-0
29. Furuya T, Inoue E, Yamanaka H, et al. Increasing fracture incidence over 13 years in patients with rheumatoid arthritis from the IORRA cohort. J Bone Miner Metab 2025;43(4):411–418. doi:https://doi.org/10.1007/s00774-025-01598-8
30. Guañabens N, Olmos JM, Hernández JL, et al; OsteoResSer Working Group of the Spanish Society of Rheumatology. Vertebral fractures are increased in rheumatoid arthritis despite recent therapeutic advances: a case-control study. Osteoporos Int 2021;32(7):1333–1342. doi:https://doi.org/10.1007/s00198-021-05824-7
31. Sonomoto K, Nakayamada S, Fujino Y, et al. Biological/targeted synthetic DMARDs do not arrest bone loss in patients with rheumatoid arthritis: a multicenter prospective observational study. Rheumatology (Oxford) 2024;63(8):2239–2248. doi:https://doi.org/10.1093/rheumatology/kead579
32. Sonomoto K, Nakayamada S, Tanaka H, et al. Real-world safety and efficacy of targeted therapies in rheumatoid arthritis: a 5-year, 5130-case follow-up from first registry. Rheumatol Ther 2025;12(3):561–580. doi:https://doi.org/10.1007/s40744-025-00762-w
33. Sonomoto K, Tanaka Y. Targeted therapies for rheumatoid arthritis in super-elderly society: insights from FIRST registry, Japan. Int J Rheum Dis 2025;28(4):e70232. doi:https://doi.org/10.1111/1756-185X.70232
34. Aletaha D, Neogi T, Silman AJ, et al. 2010 Rheumatoid arthritis classification criteria: an American College of Rheumatology/European League Against Rheumatism collaborative initiative. Arthritis & Rheumatism 2010;62(9):2569–2581. doi: https://doi.org/10.1002/art.27584
35. Jankowski LG, Warner S, Gaither K, et al. Cross-calibration, least significant change and quality assurance in multiple dual-energy x-ray absorptiometry scanner environments: 2019 ISCD official position. J Clin Densitom 2019;22(4):472–483. doi:https://doi.org/10.1016/j.jocd.2019.09.001
36. Assessment of fracture risk and its application to screening for postmenopausal osteoporosis. Report of a WHO Study Group. World Health Organ Tech Rep Ser 1994;843:1–129.
37. Kanis JA, McCloskey EV, Johansson H, et al. A reference standard for the description of osteoporosis. Bone 2008;42(3):467–475. doi:https://doi.org/10.1016/j.bone.2007.11.001
38. Morris HA, Eastell R, Jorgensen NR, et al; IFCC-IOF Working Group for Standardisation of Bone Marker Assays (WG-BMA). Clinical usefulness of bone turnover marker concentrations in osteoporosis. Clin Chim Acta 2017;467:34–41. doi:https://doi.org/10.1016/j.cca.2016.06.036
39. Cummings SR, Black DM, Thompson DE, et al. Effect of alendronate on risk of fracture in women with low bone density but without vertebral fractures: results from the Fracture Intervention Trial. JAMA 1998;280(24):2077–2082. doi:https://doi.org/10.1001/jama.280.24.2077
40. Harris ST, Watts NB, Genant HK, et al; Vertebral Efficacy With Risedronate Therapy (VERT) Study Group. Effects of risedronate treatment on vertebral and nonvertebral fractures in women with postmenopausal osteoporosis: a randomized controlled trial. JAMA 1999;282(14):1344–1352. doi:https://doi.org/10.1001/jama.282.14.1344
41. Eastell R, Lang T, Boonen S, et al; HORIZON Pivotal Fracture Trial. Effect of once-yearly zoledronic acid on the spine and hip as measured by quantitative computed tomography: results of the HORIZON Pivotal Fracture Trial. Osteoporos Int 2010;21(7):1277–1285. doi:https://doi.org/10.1007/s00198-009-1077-9
42. Shin A, Park EH, Dong YH, et al. Comparative risk of osteoporotic fracture among patients with rheumatoid arthritis receiving TNF inhibitors versus other biologics: a cohort study. Osteoporos Int 2020;31(11):2131–2139. doi:https://doi.org/10.1007/s00198-020-05488-9
43. Abtahi S, Cordtz R, Dreyer L, et al. Biological disease-modifying antirheumatic drugs and osteoporotic fracture risk in patients with rheumatoid arthritis: a Danish cohort study. Am J Med 2022;135(7):879–888.e3. doi:https://doi.org/10.1016/j.amjmed.2022.01.017
44. Tronstad I, Hoff M, Horn J, et al. Rheumatoid arthritis, disease-modifying antirheumatic drugs and risk of major osteoporotic fracture: prospective data from the HUNT Study, Norway. RMD Open 2024;10(1):e003919. doi:https://doi.org/10.1136/rmdopen-2023-003919
45. Ahmed LA, Emaus N, Berntsen GK, et al. Bone loss and the risk of non-vertebral fractures in women and men: the Tromsø study. Osteoporos Int 2010;21(9):1503–1511. doi:https://doi.org/10.1007/s00198-009-1102-z
46. Berry SD, Samelson EJ, Pencina MJ, et al. Repeat bone mineral density screening and prediction of hip and major osteoporotic fracture. JAMA 2013;310(12):1256–1262. doi:https://doi.org/10.1001/jama.2013.277817
47. Leslie WD, Majumdar SR, Morin SN, et al. Why does rate of bone density loss not predict fracture risk? J Clin Endocrinol Metab 2015;100(2):679–683. doi:https://doi.org/10.1210/jc.2014-3777
48. Crandall CJ, Larson J, Wright NC, et al. Serial bone density measurement and incident fracture risk discrimination in postmenopausal women. JAMA Intern Med 2020;180(9):1232–1240. doi:https://doi.org/10.1001/jamainternmed.2020.2986
49. Gourlay ML, Fine JP, Preisser JS, et al; Study of Osteoporotic Fractures Research Group. Bone-density testing interval and transition to osteoporosis in older women. N Engl J Med 2012;366(3):225–233. doi:https://doi.org/10.1056/NEJMoa1107142
50. Hwang J, Lee EK, Ahn JK, et al. Bone-density testing interval and transition to osteoporosis in patients with rheumatoid arthritis. Osteoporos Int 2017;28(1):231–237. doi:https://doi.org/10.1007/s00198-016-3703-7

51. LeBoff MS, Greenspan SL, Insogna KL, et al. The clinician's guide to prevention and treatment of osteoporosis. Osteoporos Int 2022; 33(10):2049–2102. doi:https://doi.org/10.1007/s00198-021-05900-y
52. Njeh CF, Fuerst T, Hans D, et al. Radiation exposure in bone mineral density assessment. Appl Radiat Isot 1999;50(1):215–236. doi:https://doi.org/10.1016/S0969-8043(98)00026-8
53. Chen JF, Hsu CY, Yu SF, et al. The impact of long-term biologics/target therapy on bone mineral density in rheumatoid arthritis: a propensity score-matched analysis. Rheumatology (Oxford) 2020;59(9):2471–2480. doi:https://doi.org/10.1093/rheumatology/kez655
54. Oelzner P, Mueller PH, Hoffmann T, et al. Significant decrease of osteoporosis and osteoporotic fractures in rheumatoid arthritis within a period of 24 years: experiences of a single centre. RMD Open 2024; 10(3):e004564. doi:https://doi.org/10.1136/rmdopen-2024-004564
55. Balk EM, Adam GP, Langberg VN, et al; International Osteoporosis Foundation Calcium Steering Committee. Global dietary calcium intake among adults: a systematic review. Osteoporos Int 2017; 28(12):3315–3324. doi:https://doi.org/10.1007/s00198-017-4230-x
56. Tamaki J, Fujimori K, Ikehara S, et al; Working Group of Japan Osteoporosis Foundation. Estimates of hip fracture incidence in Japan using the National Health Insurance Claim Database in 2012-2015. Osteoporos Int 2019;30(5):975–983. doi:https://doi.org/10.1007/s00198-019-04844-8
57. Kanis JA, Norton N, Harvey NC, et al. SCOPE 2021: a new scorecard for osteoporosis in Europe. Arch Osteoporos 2021;16(1):82. doi:https://doi.org/10.1007/s11657-020-00871-9
58. Cummings SR, Bates D, Black DM. Clinical use of bone densitometry: scientific review. JAMA 2002;288(15):1889–1897. doi:https://doi.org/10.1001/jama.288.15.1889
59. Gregson CL, Armstrong DJ, Bowden J, et al. UK clinical guideline for the prevention and treatment of osteoporosis. Arch Osteoporos 2022;17(1):58. doi:https://doi.org/10.1007/s11657-022-01061-5
60. Baleanu F, Moreau M, Kinnard V, et al. What is the validity of self-reported fractures? Bone Rep 2020;12:100256. doi:https://doi.org/10.1016/j.bonr.2020.100,256

Check for updates

American College of Rheumatology
Empowering Rheumatology Professionals

Arthritis & Rheumatology
Vol. 78, No. 10, October 2026, pp 2050–2062
DOI 10.1002/art.70131
© 2026 American College of Rheumatology.

Telocyte Deletion Associated With Loss of Lymphatic Drainage and Exacerbation of Inflammatory-Erosive Arthritis in Mice

Yue Peng, PhD,[1,2] H. Mark Kenney, MD, PhD,[1,2] Sean Lydon, MS,[2] Karen L. de Mesy Bentley, MS,[1,2] Lianping Xing, B.Med, PhD,[1,2] Benjamin D. Korman, MD,[1,3] Christopher T. Ritchlin, MD, MPH,[1,3] and Edward M. Schwarz, PhD[1,2]

Objective. Patients with rheumatoid arthritis (RA) have lymphatic defects characterized by loss of collecting lymphatic vessel (cLV) contractions of unknown etiology. To elucidate underlying mechanisms, we generated transgenic mice with lymphatic-specific inducible genetics and studied joint-draining lymphatics in zymosan-induced arthritis (ZIA).

Methods. We crossed novel *Efhd1*-CreER^{T2} and *Myoc*-CreER^{T2} mice to Ai9 tdTomato (tdT) reporter mice to assess tamoxifen-induced transgene expression via single-cell RNA sequencing, whole-mount immunofluorescent microscopy (WMIFM), and immunohistochemistry. We applied electron and confocal microscopy of popliteal lymphatic vessels (PLVs) to examine α smooth muscle actin positive lymphatic muscle cells, mast cell tryptase–positive mast cells, and CD31^{-}/CD34^{+} cells. We crossed *Efhd1*-CreER^{T2} and *Myoc*-CreER^{T2} mice to diphtheria toxin-alphafloxed mice to examine: (1) tamoxifen-induced targeted cell deletion; (2) lymphatic function via near-infrared imaging of injected indocyanine green; and (3) effects on ZIA in the knee via longitudinal ultrasound, micro–computed tomography, and histology.

Results. Multimodal microscopy discovered the presence of peri-PLV spindle-shaped cells with elongated cytoplasmic extensions physically integrated into mast cells. Gene expression studies confirmed these cells are consistent with telocytes, and WMIFM demonstrated peri-PLV tdT^{+} telocyte networks extending from capillaries in the ankle synovium to cLV near the knee. In vivo telocyte depletion decreased lymphatic drainage and exacerbated synovitis and focal erosions in ZIA.

Conclusion. Telocyte networks extend from the synovium into mast cells proximal to joint-draining cLVs, and telocyte loss is associated with synovial lymphatic system (SLS) defects and exacerbated joint pathology from inflammatory-erosive arthritis. Thus, SLS telocytes are a novel drug target for RA, and interventions that maintain telocytes (eg, exercise) may improve lymphatic function.

INTRODUCTION

Lymphatic dysfunction is a critical factor in joint inflammation, damage, and flare, in patients with rheumatoid arthritis (RA),[1] and lymphadenopathy has been documented in 41% to 82% of patients with RA.[2] Thus, understanding the mechanisms that control collecting lymphatic vessel (cLV) contractions, which are responsible for the majority of lymph transport,[3] is critical for the development of novel interventions. Although recent advances elucidated mechanisms of intraluminal pressure-induced intrinsic cLV pacemaking by lymphatic muscle cells (LMCs),[4] how resting cLV become activated in response to acute edema in distal tissues and how cLV contractility is lost in lymphedema remains unknown.[5]

Supported by NIH grants F30-AG-076326 (to Dr Kenney), T32-GM-007356 (to Dr Kenney), R01-AG-084707 (to Dr Xing), R01-AR-069000 (to Mr Ritchlin), R01-AR-056702 (to Dr Schwarz), and P30-AR-069655 (to Dr Schwarz).

[1]Center for Musculoskeletal Research, University of Rochester Medical Center, Rochester, New York; [2]Department of Pathology & Laboratory Medicine, University of Rochester Medical Center, Rochester, New York; [3]Division of Allergy, Immunology, Rheumatology, Department of Medicine, University of Rochester Medical Center, Rochester, New York.

Additional supplementary information cited in this article can be found online in the Supporting Information section (https://acrjournals.onlinelibrary.wiley.com/doi/10.1002/art.70131).

Author disclosures and graphical abstract are available at https://onlinelibrary.wiley.com/doi/10.1002/art.70131.

Address correspondence via email to Edward M. Schwarz, PhD, at edward_schwarz@urmc.rochester.edu.

Submitted for publication November 13, 2025; accepted in revised form February 24, 2026.

Functional studies in RA animal models demonstrated that the loss of vascular endothelial growth factor C (VEGF-C) signaling together with decreased lymphangiogenesis exacerbates inflammatory-erosive arthritis,[6] whereas VEGF-C therapy ameliorates inflammatory arthritis by increasing lymphangiogenesis.[7] Additionally, we observed the loss of cLV contractions during arthritic progression in the setting of chronic joint inflammation.[8] Based on the knowledge that mast cells regulate LMC contractility,[9] and evidence supporting proinflammatory and catabolic roles for mast cells in RA,[10] we investigated mast cell effects on joint-draining lymphatics and inflammatory-erosive arthritis in tumor necrosis factor-transgenic (TNF-tg) mice[11] and their wild-type (WT) littermates. We found that popliteal lymphatic vessels (PLVs) are surrounded by an expanded frequency of mast cell tryptase–positive (MCT^+)/mast cell protease-1–positive ($MCPT1^+$)/$MCPT4^+$ mast cells in TNF-tg mice, and the percentage of peri-PLV degranulating mast cells was inversely correlated with lymphatic clearance.[12] We also identified a unique population of MCT^+/$MCPT1^-$/$MCPT4^-$ mast cells embedded within the PLV cellular architecture, but the function of these cells remains unknown.[12] Genetic and pharmacologic mast cell loss of function experiments in TNF-tg mice demonstrated severe lymphatic defects, which were associated with exacerbated inflammatory-erosive arthritis, and led us to conclude that MCT^+/$MCPT1^-$/$MCPT4^-$ mast cells embedded within PLVs are required for normal lymphatic function.[12] However, how these mast cells integrate into the synovial lymphatic system (SLS) remains to be elucidated.

To address this, we developed conditional-inducible transgenic mice for genetic gain and loss of function studies in LMCs based on single-cell RNA sequencing (scRNAseq) studies of PLV and associated adventitial cells that identified three specifically expressed genes (*Efhd1, Myoc*, and *Pla1a*).[13] We then generated three transgenic mouse lines in which a $CreER^{T2}$ cassette was knocked into these genes, and the resulting animals were crossed to B6.Cg-*Gt(ROSA)26Sor*$^{tm9(CAG\text{-}tdTomato)Hze}$/J (Ai9)[14] and B6.129P2-*Gt(ROSA)26Sor*$^{tm1(DTA)Lky}$/J (diphtheria toxin subunit A [DTA])[15] mice for lineage tracing and loss of function studies, respectively. Herein, we describe the construction of these models and the serendipitous finding of tamoxifen-inducible gene expression in peri-PLV spindle-shaped cells with very long cytoplasmic extensions that were physically integrated into mast cells, although there was no expression in the predicted LMC population,[13] which has been further described in more recent scRNAseq studies.[4] We hypothesized the identified peri-PLV spindle-shaped cells to be telocytes, which are unique mesenchymal cells found in most tissues and are characterized by a small cell body and long, thin cytoplasmic extensions called telopodes.[16] Of note are the various telocyte functions that include extracellular matrix (ECM) synthesis for tissue structural support, cell-to-cell communication, regulation of immune responses, and pacemaking of smooth muscle contractions.[17] These novel mice were used to test the hypotheses that (1) networks of contiguous telocytes extend from the ankle synovium to PLVs, (2) telocytes are distinct from PLV adventitial fibroblasts, and (3) loss of telocytes decreases lymphatic drainage and exacerbates inflammatory-erosive arthritis.

MATERIALS AND METHODS

Mouse models. All animal research was conducted with Institutional Animal Care and Use Committee approval. Three transgenic mouse strains were generated with P2A-$CreER^{T2}$ cassettes, which were knocked into C57BL/6NTac mice via CRISPR/Cas-mediated genome engineering (Taconic Biosciences, Germantown, NY) as described in Figure 1, and the polymerase chain reaction primers for genotyping are presented in Supplementary Table 1. Ai9 strain #007909,[14] $DTA^{flox/-}$ strain #009669,[15] and c-$Kit^{-/-}$ strain #030764[12] mice were purchased from The Jackson Laboratory (Bar Harbor, ME). Mice were anesthetized with 1% to 3% isoflurane for in vivo studies and euthanized with a lethal dose of ketamine/xylazine cocktail (intraperitoneal) followed by cervical dislocation.

Whole-mount immunofluorescent microscopy and immunohistochemistry. PLVs were harvested, fixed, stained, and imaged as previous described[12] using the following antibodies: anti–α smooth muscle actin (αSMA; AlexaFluor 488 conjugate; ThermoFisher Scientific Cat# 53-9760-82, diluted at 1:100), anti-human MCT (Bioss Antibodies Cat# BSM-52533R; 1:100 dilution), anti-human MCT (Bioss Antibodies Cat# BSM-52533R; 1:100 dilution), secondary antibodies (Alexa Fluor 647 Conjugate; Cell Signaling Technology Cat#4414; 1:500 dilution), and Fc blocker (Alexa Fluor 647 Conjugate; Cell Signaling Technology Cat#4414; 1:500 dilution). Counterstaining used DAPI (ThermoFisher Scientific Cat# R37606). IHC was performed on optimal cutting temperature–frozen cryosections or paraffin-embedded tissue sections, as previously described.[18] The following primary antibodies were used: anti-CD34 (Abcam Cat# ab81289; 1:50 dilution), anti-CD31 (Thermo Fisher Cat# MA1-40074; 1:50), anti-COMP (Abcam Cat# ab231977; 1:125), anti-CD117 (c-Kit) (Thermo Fisher Cat# 14-1172-81; 1:100), and antimyocilin (Abcam Cat# ab41552; 1:50). Secondary antibodies included Alexa Fluor 555–conjugated antirabbit IgG (Cell Signaling Technology Cat# 4413; 1:1000), fluorescein isothiocyanate (FITC)–conjugated goat antirat IgG (Jackson ImmunoResearch Cat# 112-096-003; 1:200), Alexa Fluor 647–conjugated donkey antirat IgG (Jackson ImmunoResearch Cat# 712-606-153; 1:500), and FITC-conjugated goat antirabbit IgG (Jackson ImmunoResearch Cat# 111-096-047; 1:100).

Histochemistry and histomorphometry. For histochemistry of knees and quantification of synovitis and osteoclasts, lower limbs of the mice were processed for paraffin-

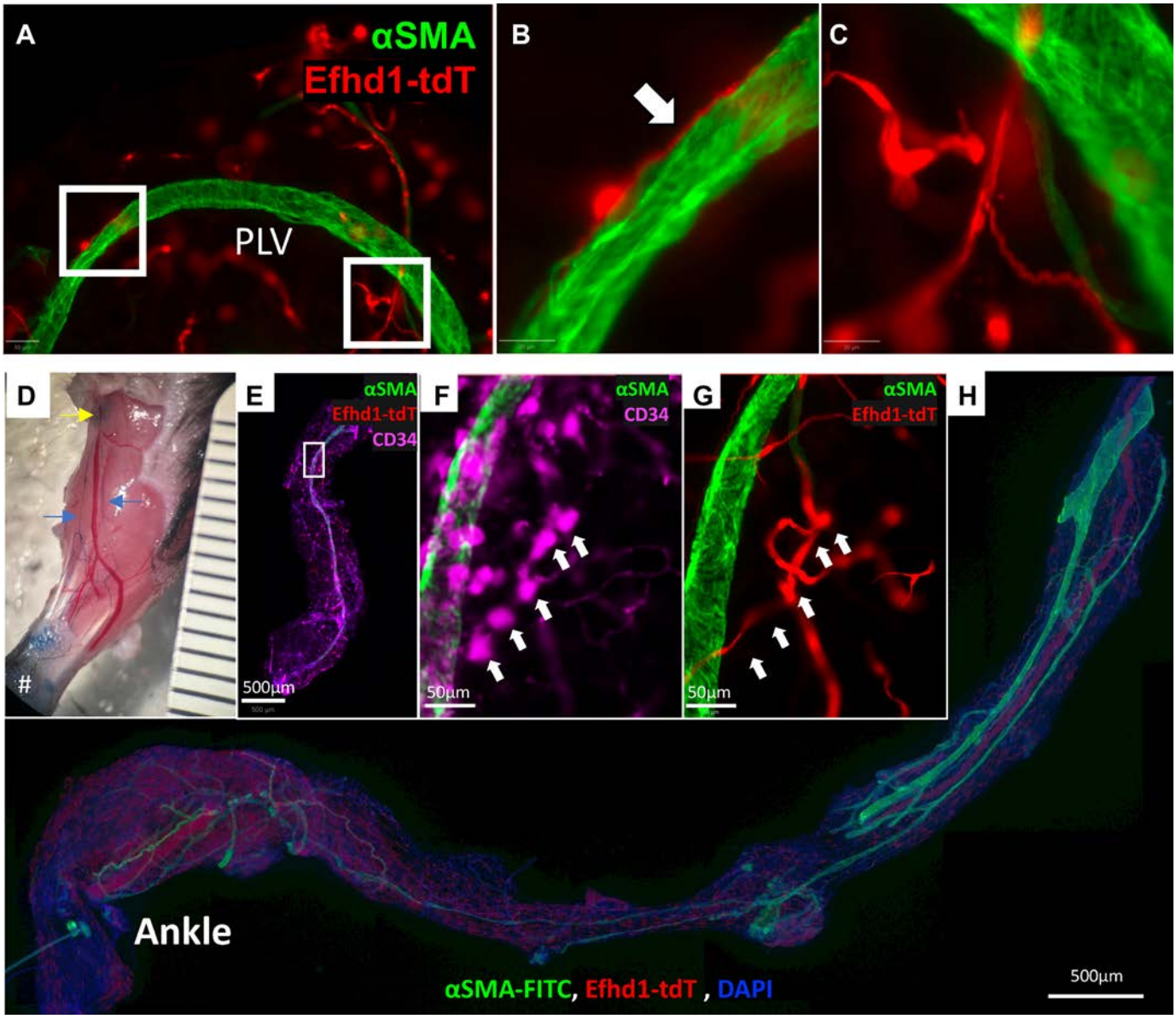


Figure 1. Efhd1-CreER^{T2} targets two populations of PLV adventitial cells that are adjacent to mast cells. (A) Whole-mount immunofluorescent microscopy of PLV from tamoxifen-treated Efhd1-CreER$^{+/-}$ × Ai9$^{+/-}$ mice was performed as described in Figure 1 and a 4× image is shown with 10× images of the boxed ROIs highlighting (B) a tdT^{+} telocyte-like cell with its telopode (arrow) aligned along the surface of the PLV and (C) a network of tdT^{+} cells in the adipose tissue adjacent to the vessels. (D) Evan's blue dye was injected into the footpad of a tamoxifen-treated *Efhd1*-CreER^{T2} × Ai9 mouse to image the PLVs for dissection, and the tissue was immunostained with fluorescent antibodies against CD34 and αSMA and counterstained with DAPI. (E–G) Low-power and high-power confocal microscopy images of the ROI (box) confirm immunostaining of the mast cells elaborating the tdT^{+} network along the PLV (green). (H) Eight fluorescent low-power images of an immunostained full-length PLV with associated tissues were stitched together to imaging telocyte networks that extend from capillaries in the ankle synovium to a collecting lymphatic vessel near the knee. The box indicates the ROI shown in parts E–G. αSMA, α smooth muscle actin; FITC, fluorescein isothiocyanate; PLV, popliteal lymphatic vessel; ROI, region of interest; tdT, tdTomato. Color figure can be viewed in the online issue, which is available at http://onlinelibrary.wiley.com/doi/10.1002/art.70131/abstract.

embedded demineralized sections stained with hematoxylin and eosin or for tartrate-resistant acid phosphatase (TRAP) as previously described.[19] All slides were scanned with an Olympus VS120 (full slide scans available upon request), and histomorphometry for synovial area was quantified with Visiopharm (Hoersholm, Denmark) as previously described.[20]

Electron microscopy. Transmission electron microscopy (TEM) was performed as previously described[8] using a Hitachi 7650 Transmission Electron Microscope with an AMT NanoSprint 12-megapixel digital camera was used to image the grids. Telocytes were identified and distinguished from adventitial fibroblasts and LMCs by well-established morphologic criteria as described

in Supplementary Figure 1. Scanning electron microscopy (SEM) was performed as previously described[21] using a Zeiss Auriga Field Emission SEM. Three SEM micrographs per sample group were randomly chosen for descriptive analysis.

scRNAseq. In silico analyses of previously published scRNAseq datasets of WT and TNF-tg PLVs (GEO; accession number GSE190999)[13] were performed using Seurat (v5.0.1) to generate uniform manifold approximation and projections (UMAPs) of the mesenchymal cells. Other data supporting the findings of this study are available from the corresponding author upon reasonable request. Individual gene expression within this UMAP was performed with FeaturePlot in Seurat. Pseudotime predictions analysis of the scRNAseq data from WT and TNF-tg PLVs was performed with Monocle 3 to generate UMAPs with heatmaps of the hypothesized cellular differentiation and the telocyte:fibroblast ratio.

Near-infrared indocyanine imaging and quantification of lymphatic function. Near-infrared indocyanine (NIR-ICG) imaging and quantification of lymphatic clearance from the footpad was performed as previously described[12] using an IVIS Live Animal Imaging System (Caliper Life Sciences Inc.). The ratio of the fluorescence difference and baseline fluorescence was used to define lymphatic clearance function, which reflects the lymphatic vessel's ability to remove extra fluid from the footpad.

Zymosan-induced arthritis model. Female 8-week-old *Efhd1*-CreER$^{+/-}$ × DTA$^{f/-}$ mice and WT littermate controls received intraperitoneal injections of tamoxifen (0.1 mg/g body weight) for 5 consecutive days to induce *Efhd1*-driven DTA expression and telocyte depletion. Two weeks after the initiation of tamoxifen treatment, mice were anesthetized and received a single intra-articular injection of 180 mcg zymosan (Sigma-Aldrich, St. Louis, MO) in 6 µL phosphate-buffered saline (PBS) into the knee joint cavity. Control mice received PBS alone. Knee joint inflammation was monitored by high-resolution ultrasound imaging (Vevo 3100, VisualSonics) performed before zymosan injection (baseline) and on days 2, 7, and 14 after injection. Analysis of knee joint inflammation was performed using Amira to measure synovial volume, as described before.[22] On days 13 to 15, mice were euthanized, and knee joints were harvested, fixed in 4% paraformaldehyde, micro–computed tomography (CT) scanned, and processed for histologic analysis.

Micro-CT analysis. Micro-CT scanning and 3D reconstruction were performed as previously described[23] using identical imaging settings and parameters. To assess articular erosions, 2D projections were generated from the articular surface of the femoral trochlea, which articulates with the tibia. Erosive lesions were manually annotated using QuPath (v0.5.0), and the cumulative erosion area was normalized to the total projected area of the distal femur (region of interest [ROI]). The erosion percentage (erosion area/ROI) was used as a quantitative measure of joint damage.

Statistics. All statistical analyses were performed using GraphPad Prism (version 9.1.1, GraphPad Software, Boston, MA, USA) and R (version 4.3.2). Additional analyses and data visualization including zymosan-induced arthritis (ZIA) model readouts were conducted using the R package ggpubr (version 0.6.0). Two-group comparisons were assessed using unpaired two-tailed Student's *t*-tests, and multiple group comparisons were performed using one-way or two-way analysis of variance as appropriate. A P value <0.05 was considered statistically significant.

RESULTS

Generation of novel CreER^{T2} mouse models for genetic targeting of telocytes in the SLS. We recently described scRNAseq analysis of lymphatic vessels in which we identified *Efhd1, Myoc*, and *Pla1a* as PLV-selective genes.[13] Based on these findings, we generated three knock-in mouse lines in which a *CreER^{T2}* cassette was inserted into these genes of embryonic stem cells, and the resulting mice were crossed to Ai9 reporter mice to assess tamoxifen-induced in vivo gene targeting (Figure 1A–C). Ex vivo whole-mount immunofluorescent microscopy (WMIFM) revealed the absence of tdTomato (tdT)$^+$ cells in Ai9$^{+/-}$ negative controls and the presence of elongated tdT$^+$ cells that were preferentially clustered in networks around PLVs vs blood vessels from tamoxifen-treated *Efhd1*-CreER$^{+/-}$ × Ai9$^{+/-}$ and *Myoc*-CreER$^{+/-}$ × Ai9$^{+/-}$ mice (Figure 1D). Tamoxifen treatment of younger mice (P10–P13) resulted in a similar pattern of PLV adventitial tdT$^+$ cells, suggesting that they maintain their identity from early postnatal development (Supplementary Figure 2). These tdT$^+$ cells were not found in tissues from tamoxifen-treated *Pla1a*-CreER$^{+/-}$ × Ai9$^{+/-}$ mice, and these mice were not further analyzed.

Interrogation of the PLV WMIFM revealed two distinct tdT$^+$ populations of fibroblastic cells that contained very long dendritic processes phenotypically consistent with telopodes (Figure 2A). One population extended longitudinally along the PLV (Figure 2B), and the other existed in telocyte arrays within adipose tissue adjacent to PLVs (Figure 2C). To gain a holistic insight into the extent of tdT$^+$ cell arrays along the PLV, we performed WMIFM on tissues from tamoxifen-treated *Efhd1*-CreER^{T2} × Ai9 mice with antibodies against αSMA and CD34 to label the vascular smooth muscle and mast cells. Confocal images of soft-tissue extending from the ankle to the knee containing the PLVs were reconstructed in 3D and stitched together (Figure 2D–H). The high-power images confirmed the presence of tdT$^+$ cell arrays adjacent to PLVs that contained CD34$^+$ cells with a mast cell

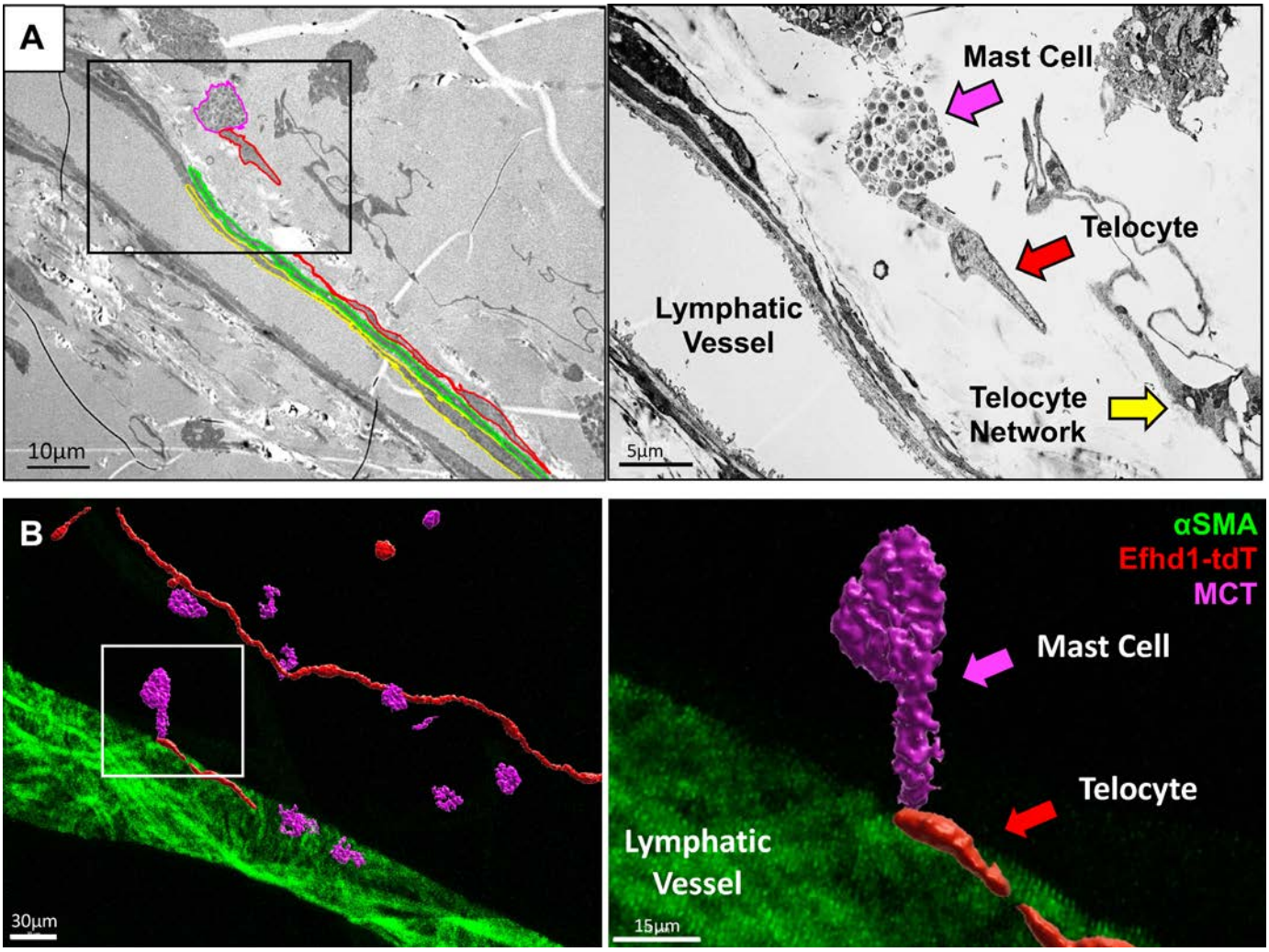


Figure 2. Transmission electron microscopy and whole-mount immunofluorescent microscopy imaging of pre-PLV mast cells physically integrated into telocyte arrays. (A) Transmission electron microscopy was performed on the PLVs described in Figure 2, and a representative 1,000× image is shown highlighting the endothelium (yellow) and smooth muscle (green) layers, cells with telocyte ultrastructural morphology (red), and a mast cell (magenta). A high-power 5,000× image of the boxed region is shown highlighting the telocyte-like cell (red arrow) physically integrated into a mast cell (purple arrow) and remnants of a network of cells (yellow arrow). (B) PLV with tdT^+ cells (red) were labeled with fluorescent antibodies against αSMA (green) and MCT (magenta) for whole-mount immunofluorescent confocal microscopy, and a representative 3D rendering is shown. Note: several mast cells are tethered to the tdT^+ telocyte-like cell network (Supplementary Video 1). The magnified image of the boxed region of interest illustrates the physical integration, as the distance between the mast cell and tdT^+ telocyte-like cell is <500 nm. αSMA, α smooth muscle actin; MCT, mast cell tryptase; PLV, popliteal lymphatic vessel; tdT, tdTomato. Color figure can be viewed in the online issue, which is available at http://onlinelibrary.wiley.com/doi/10.1002/art.70131/abstract.

morphology. The low-resolution images revealed the networks of tdT^+ cells that paralleled the vessels from the ankle synovium to cLV.

Previous investigations of lymphatic dysfunction revealed an enrichment of mast cells around lymphatic vessels,[12] which prompted us to examine these distinct tdT^+ cells and their interactions within the peri-PLV tissue more closely. Scrutiny of TEM images of PLVs revealed elongated cells in tamoxifen-treated *Efhd1*-$CreER^{+/-}$ × $Ai9^{+/-}$ and *Myoc*-$CreER^{+/-}$ × $Ai9^{+/-}$ mice with morphologic characteristics consistent with the tdT^+ cells identified by WMIFM (Figure 3A). Moreover, these cells have characteristic ultrastructural features of telocytes[16] (ie, spindle-shaped polygonal cells with a large single nucleus and scant cytoplasm and thinly attenuated cytoplasmic extensions). These cells were found to form intimate contacts with mast cells in what appears to be specialized junctional structures at their plasma membrane interfaces, suggesting active intercellular communication (Figure 3A). To validate these observations and better characterize the spatial relationships between telocytes and mast cells, we conducted 3D immunofluorescent confocal microscopy. This analysis demonstrated that mast cells form direct contacts with the two tdT^+ telocyte-like populations (Figure 3B; Supplementary Video 1). The spatial distribution and interaction patterns observed through 3D confocal imaging precisely matched our

WMIFM and TEM observations, confirming that both mural and peri-PLV telocyte populations engage in direct cellular interactions with mast cells. Taken together, these findings suggest a previously unrecognized cellular partnership between telocytes and mast cells along lymphatic vessels, potentially representing a novel signaling axis in cLV regulation.

To provide additional confirmation that the tdT^{+} cells are telocytes, we reanalyzed our published scRNAseq data on murine

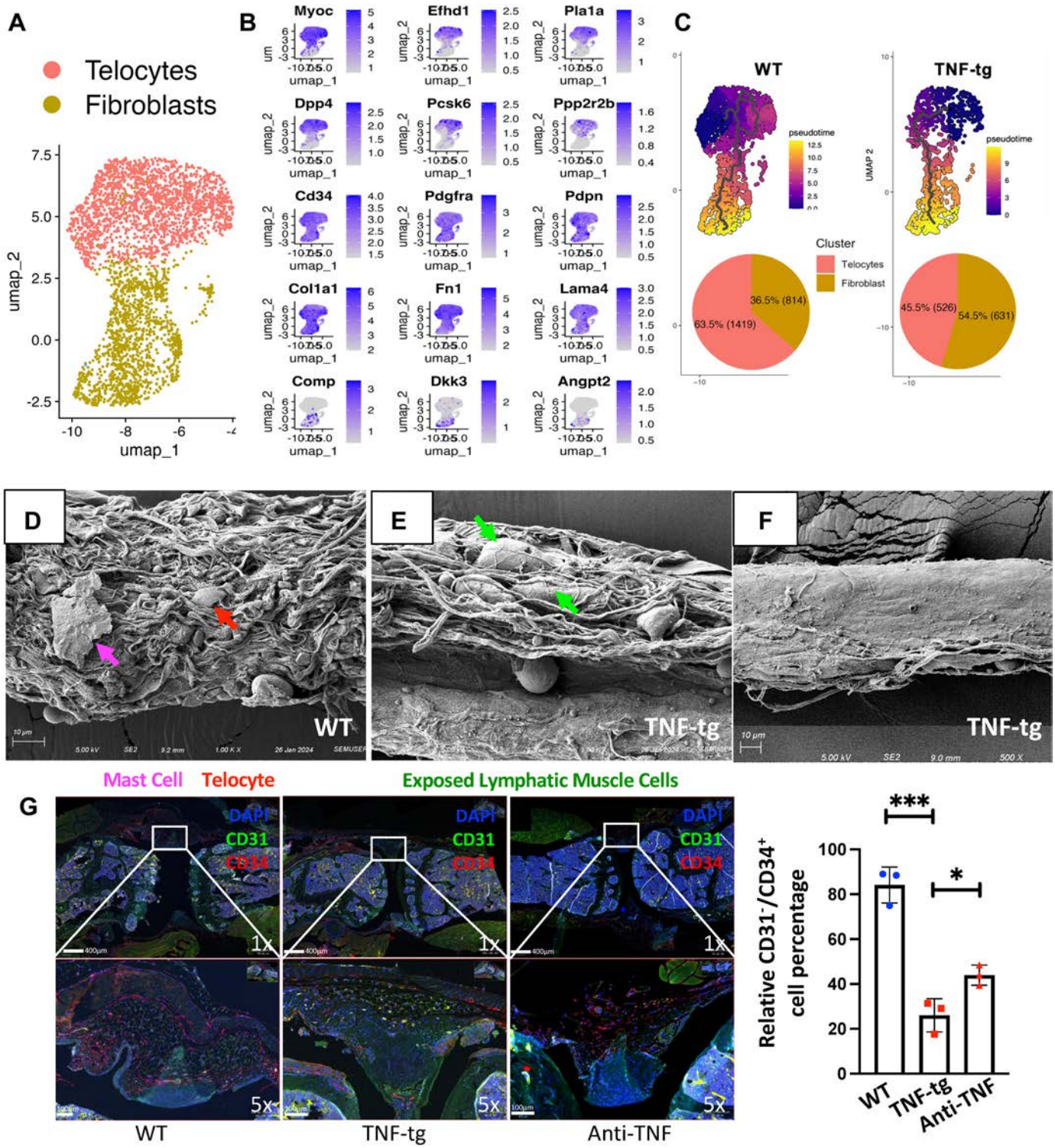


Figure 3. Legend on next page.

PLV-associated cells[13] to identify the *Pdgfrα*$^{+}$/*Cd34*$^{+}$ population known to contain telocytes and adventitial fibroblasts,[4] which produced a UMAP of these closely related populations (Figure 4A). To characterize their transcriptome distinctions and similarities, we generated UMAPs of known marker genes selectively expressed in either one cell type or both telocytes and fibroblasts. The results confirmed that the *Myoc, Efhd1, Pla1a, Dpp4, Pcsk6*, and *Ppp2r2b* genes[4] are preferentially expressed in PLV-associated telocytes (Figure 4B). The results also confirmed that (1) the pan marker genes *CD34, Pdgfra*, and *Pdpn* have equivocal expression in both PLV-associated telocytes and fibroblasts; (2) both cell types produce ECM gene products including *Col1a1, Fn1*, and *Lama4*; and (3) *Comp, Dkk3*, and *Angpt2* are specific marker genes for PLV-associated fibroblasts. We also performed a cellular trajectory analysis of the scRNAseq data from WT and TNF-tg PLVs using Monocle 3, which predicts that telocytes have the potential to differentiate into fibroblasts (Figure 4C top). Moreover, we found that there was a 47.7% decrease in the proportion of telocytes relative to fibroblasts in TNF-tg mice relative to their WT littermates (Figure 4C bottom). To further confirm that our transgenic mice label synovial telocytes rather than endothelial cells and fibroblasts, we performed multicolor immunohistochemistry (IHC) on ankle and knee sections from tamoxifen-treated *Efhd1*-CreER^{T2} mice and found that the tdT+ cells are Cd34+ and negative for the endothelial cell marker CD31 and the fibroblast marker Comp (Supplementary Figure 3).

To elucidate synovial perilymphatic telocyte loss in TNF-tg mice, we performed SEM of PLVs and IHC on knee synovium. SEM of WT PLVs revealed cell bodies embedded within a very rich ECM structure and associated mast cells on top of this ECM (Figure 4D). These cells appear to correspond to the telocytes extended longitudinally along the PLV (Figure 2B). In contrast, SEM of TNF-tg PLVs displayed varying degrees of ECM degeneration (Figure 4E and F; Supplementary Figure 4), which is consistent with their contractility defects observed ex vivo.[24] Consistent with the loss of CD31^{-}/CD34^{+} telocytes observed in RA synovium determined by IHC,[25] we also observed a significant decrease in CD31^{-}/CD34^{+} cells in the synovium of TNF-tg mice receiving placebo treatment compared with WT and their partial recovery from the TNF-tg mice receiving 6 weeks of anti-TNF treatment[21] (Figure 4G).

Given that telocytes are also known to express c-Kit,[16] a critical gene for mast cells, we examined if c-Kit is also required for telocyte development and survival and performed IHC on joints from mast cell deficient *Kit*$^{W\text{-}sh/W\text{-}sh}$ (c-Kit$^{-/-}$) mice. The results demonstrated similar levels of synovial CD31^{-}/CD34^{+} cells compared with WT mice (Supplementary Figure 4), which supports the notion that lymphatic dysfunction in these animals[12] is likely because of the loss of mast cells rather than telocytes, which also express c-Kit. Additionally, we found tdT^{+} cells in tendon, skin hair follicles, and within the ganglion cell layer of the retina, but no tdT^{+} cells were found among the c-Kit^{+} interstitial cells of Cajal in intestine (Supplementary Figure 5). Therefore, despite the absence of definitive markers or functional assays to prove telocyte identity, the preponderance of our ultrastructural, histologic, and gene expression data show that the *Myoc*-CreER^{T2} mice target tamoxifen-induced gene expression to telocyte subtypes in some but not all tissue types.

In vivo depletion of telocytes decreases lymphatic function and exacerbates inflammatory arthritis. To test the hypothesis that in vivo depletion of *Myoc* and *Efhd1* expressing telocytes in the SLS are critical for lower-limb lymphatic function in mice, we generated an inducible depletion model by crossing the telocyte-specific CreER mice with DTA^{floxed} mice, followed by tamoxifen treatment to induce DTA in vivo depletion of the gene targeted cells as outlined in Figure 5A. To estimate in vivo depletion efficiency in these models, we performed WMIFM on PLVs and IHC knee joints from tamoxifen-treated double and single (control) transgenic mice and assessed CD31^{-}/CD34^{+} cells. WMIFM of PLVs demonstrated a dramatic DTA elimination of telocytes on the vessel surface and the arrayed telocytes in the adjacent adipose tissue (Figure 5B). IHC analysis of the knees confirmed an approximately 60% reduction in the number of CD31^{-}/CD34^{+} synoviocytes (Figure 5C and D). As these telocytes are physically integrated into mast cells, we repeated the WMIFM experiment and reimaged the PLVs after staining with toluidine blue and fast green (Supplementary Figure 6). The results

Figure 3. Transcriptome confirmation of PLV-associated telocytes and the loss of PLV ECM and telocytes in TNF-tg mice. (A) Published single-cell RNA sequencing data on PLV-associated cells from mice[13] were reanalyzed to identify the Pdgfrα^{+}/Cd34^{+} population known to contain telocytes and adventitial fibroblasts,[4] and a color-coated UMAP of these populations associated with WT PLV is presented to demonstrate their proportions. (B) UMAPs of known marker genes selectively expressed in one cell type or both telocytes and fibroblasts are shown to further define these populations. (C) Monocle-3 analysis of the single-cell RNA sequencing data was performed to generate UMAPs with pseudotime predictions (heat maps), hypothesized telocyte differentiation into fibroblasts (lines within the UMAPs), and the 52.3% decrease in the telocyte:fibroblast ratio in TNF-tg mice relative to their WT littermates ($P < 10^{15}$ via Fisher test). (D) Representative 5,000× scanning electron microscopy image of a PLV from a WT mouse with intact ECM structure, associated mast cell (magenta arrow), and an apparent telocyte cell body (red arrow) embedded in the ECM. Representative 5,000× scanning electron microscopy images of PLVs from TNF-tg mice, (E) one with partial ECM loss and exposed LMCs (green arrows), and (F) one with extensive ECM and LMC loss. (G) Immunohistochemistry was performed on knees from WT TNF-tg mice receiving placebo or anti-TNF treatment from a prior study,[21] and representative fluorescent microscopy images are shown with quantification of the CD31^{-}/CD34^{+} cells as a percentage of synoviocytes (n = 3; $P < 0.001$ *t*-test). ECM, extracellular matrix; PLV, popliteal lymphatic vessel; TNF-tg, tumor necrosis factor-transgenic; UMAP, uniform manifold approximation and projection; WT, wild-type.

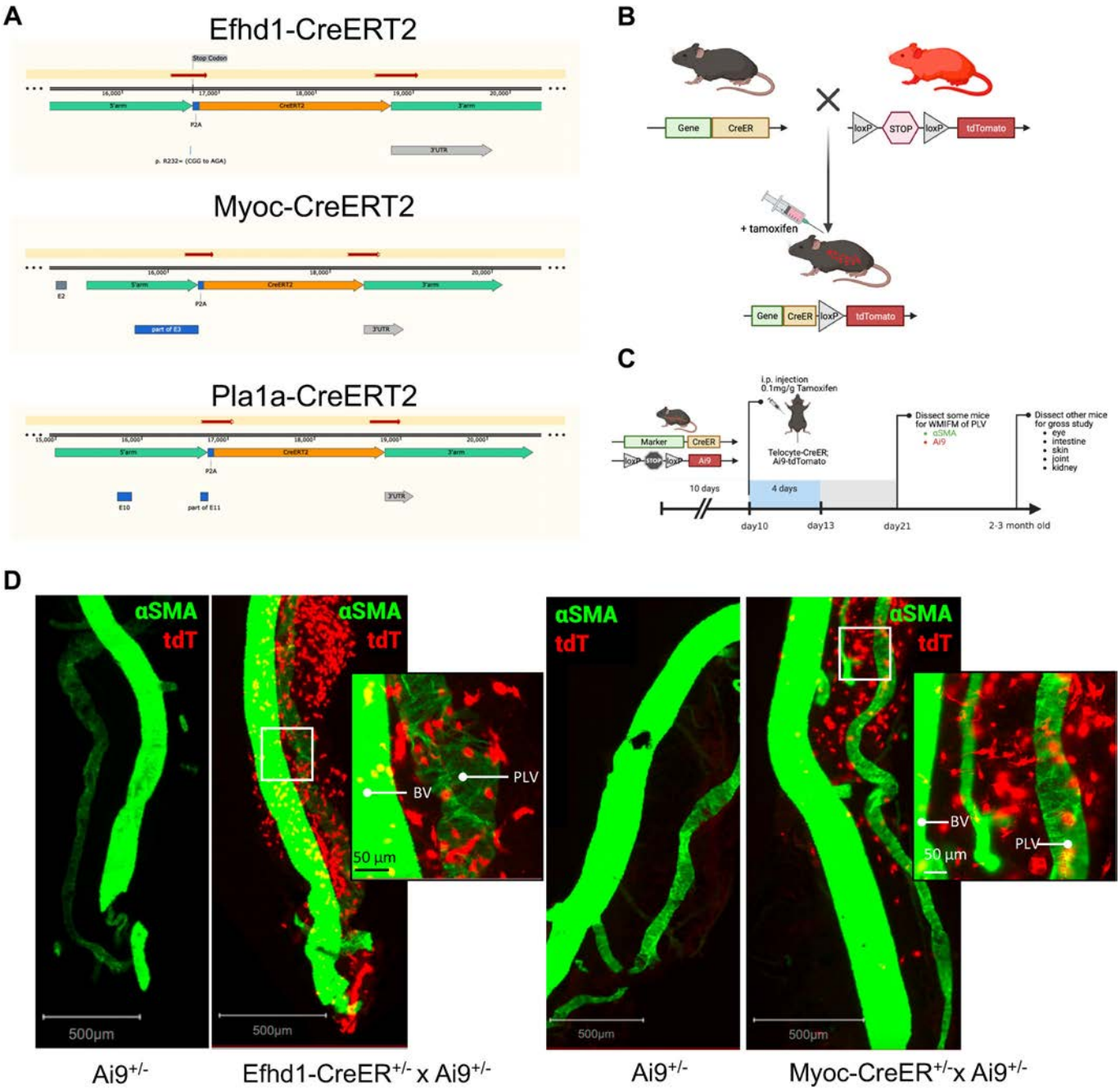


Figure 4. Similarities between synovial and PLV-associated tdT$^+$ cells with a telocyte phenotype and their distinctions from fibroblasts. (A) Experimental workflow showing tamoxifen treatment of Efhd1-CreER$^{+/-}$ × Ai9$^{+/-}$ mice followed by tissue harvest, cell isolation, and subsequent analyses. (B) Flow cytometric analysis of knee and ankle synovial tissues revealing distinct tdT^{high} and tdT^{low} populations (red arrows). (C) Uniform manifold approximation and projections showing expression of telocyte and fibroblast marker genes in knee synovial cells, matching the expression patterns observed in Figure 3B. (D) Representative immunofluorescence images of knee and ankle sections from tamoxifen-treated Efhd1-CreER$^{+/-}$ × Ai9$^{+/-}$ mice stained for Comp (green) and DAPI (blue), demonstrating distinct spatial localization of telocytes near the meniscus attachment sites while fibroblasts (Comp$^+$) occupy peripheral regions. Images at 1× magnification with 5× magnification of boxed region are shown with parallel hematoxylin and eosin brightfield images. αSMA, α smooth muscle actin; BV, blood vessel; PLV, popliteal lymphatic vessel; tdT, tdTomato; WMIFM, whole-mount immunofluorescent microscopy. Color figure can be viewed in the online issue, which is available at http://onlinelibrary.wiley.com/doi/10.1002/art.70131/abstract.

confirmed highly efficient depletion of the brightly staining CD34$^+$ spindle-shaped cells (telocytes) without affecting the dimly staining CD34$^+$ larger round mast cells, which was confirmed by the brightfield imaging.

We repeated this experiment to assess telocyte depletion effects on lymphatic drainage. Cohorts of single and double transgenic mice underwent NIR-ICG imaging before tamoxifen treatment and 6 hours following the last tamoxifen injection. We

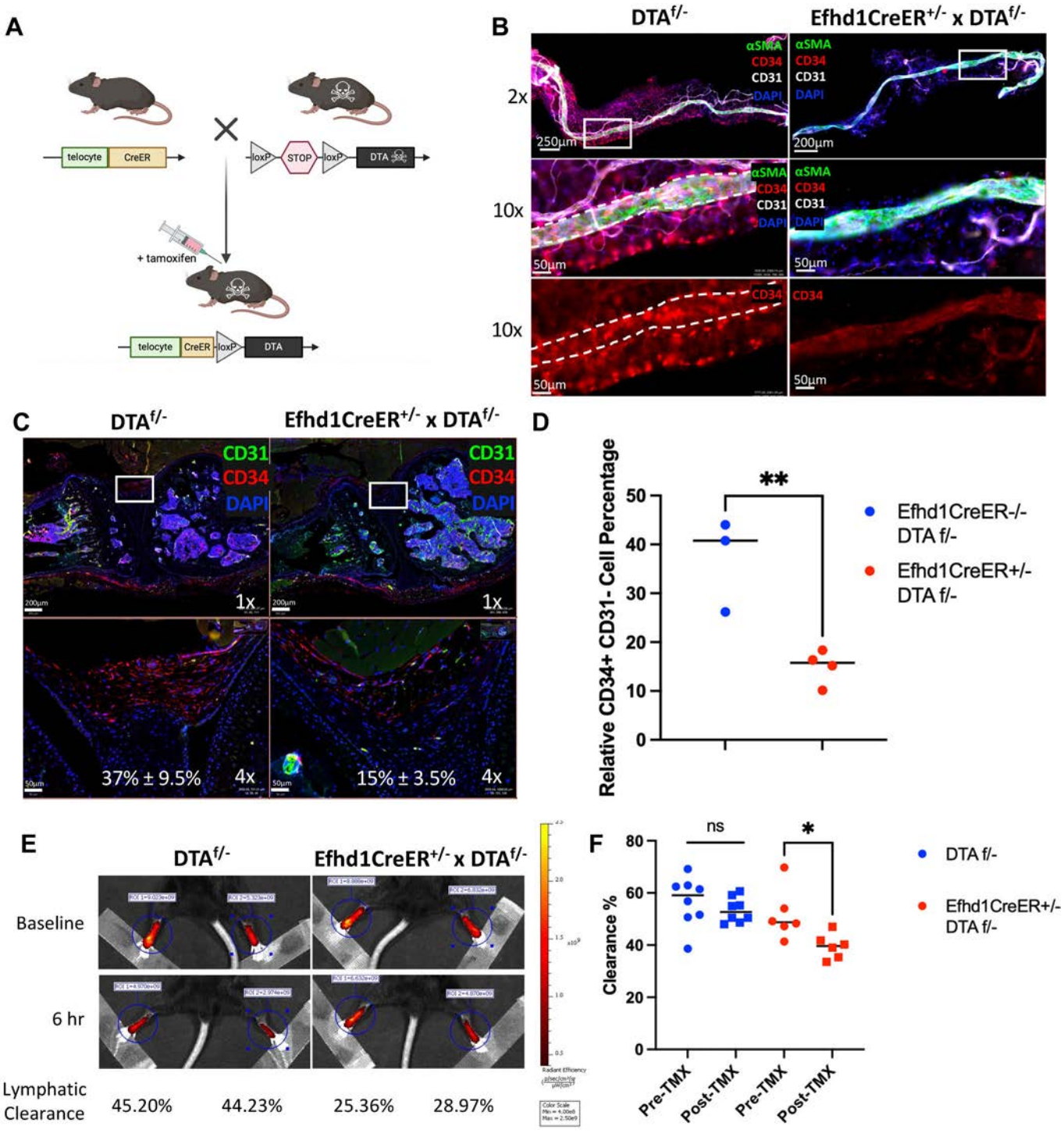


Figure 5. In vivo depletion of telocytes decreases lymphatic function. (A) Schematic illustration of the tamoxifen-induced telocyte deletion model generated by crossing Efhd1-CreER^{T2} mice with DTA-floxed mice. The efficiency of in vivo telocyte deletion following tamoxifen treatment was assessed via (B) whole-mount immunofluorescent microscopy of popliteal lymphatic vessels and (C) immunohistochemistry of knee synovium with quantification of the relative telocyte percentage as described in Figure 3, from the double transgenic mice and their DTA$^{f/-}$ littermates. (D) Histomorphometric quantification of relative telocyte percentage (n = 3; *P < 0.5 or ***P < 0.001*** vs placebo-treated tumor necrosis factor-transgenic via t-test). (E) Lymphatic clearance in tamoxifen-treated Efhd1-CreER$^{+/-}$ × DTA$^{f/-}$ mice and their DTA$^{f/-}$ littermate controls was assessed via near-infrared indocyanine imaging, and representative In Vivo Imaging System images of the indocyanine injected into the footpads at the time of injection (baseline) and 6 hours later are shown with the heatmap of the signal intensity and percent lymphatic clearance for each foot. (F) Data on the percent lymphatic clearance of the cohort before and after tamoxifen injection are presented for each mouse with the mean for the group (n ≥ 6; P < 0.05 via t-test). Similar results were obtained in experiments with Myoc- CreER$^{+/-}$ × DTA$^{f/-}$ mice (data not shown). αSMA, α smooth muscle actin; DTA, diphtheria toxin A; Max, maximum; Min, minimum; ns, not significant; TMX, tamoxifen. Color figure can be viewed in the online issue, which is available at http://onlinelibrary.wiley.com/doi/10.1002/art.70131/abstract.

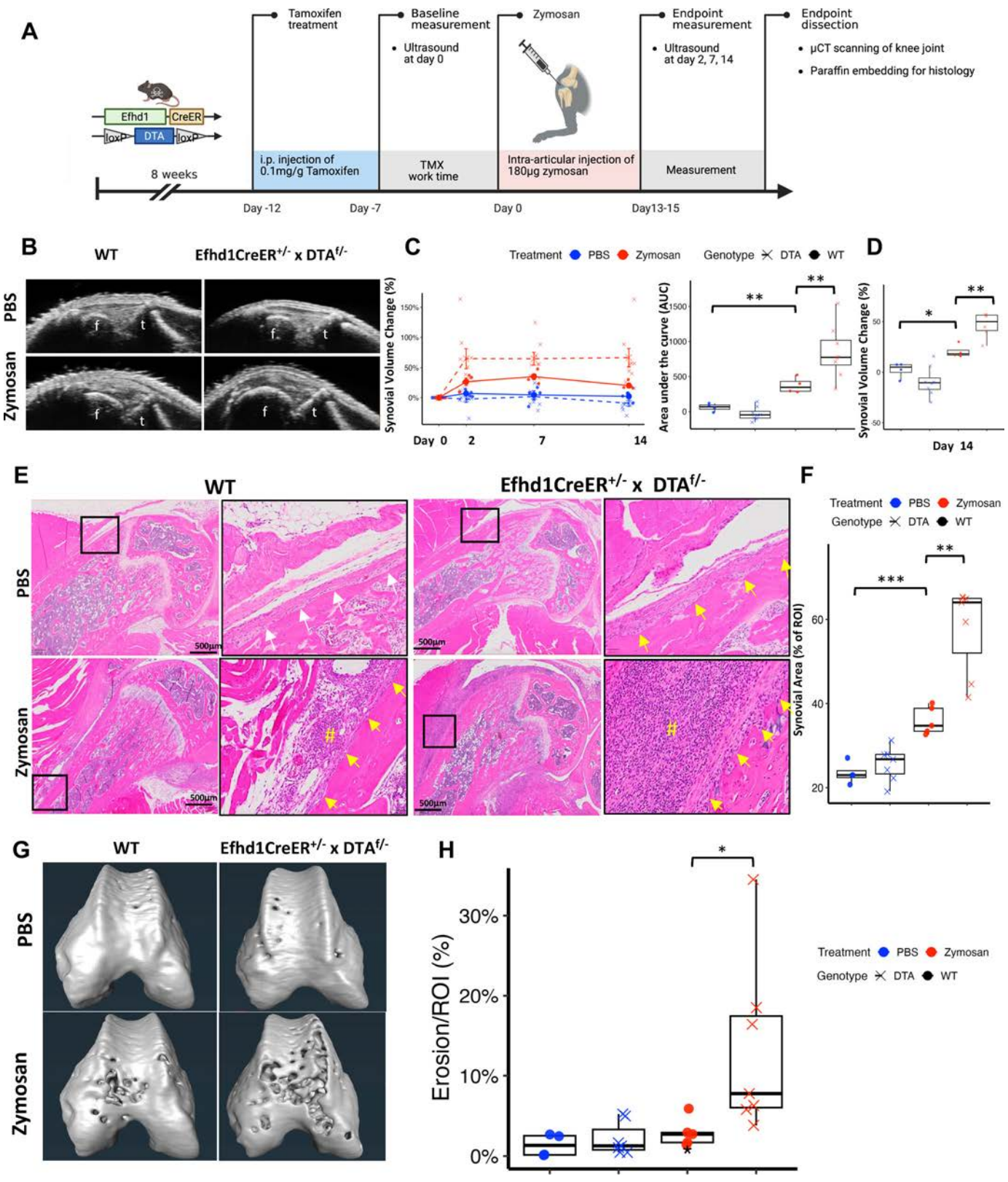


Figure 6. Legend on next page.

observed no tamoxifen effects on DTA$^{f/-}$ mice contrasted with a significant reduction of ICG clearance in the tamoxifen-treated double transgenic mice (Figure 5E and F). These findings support our hypothesis that SLS telocytes regulate synovial lymphatic clearance, although these results are confounded by our inability to assess systemic effects and DTA deletion of nontelocytes (eg, fibroblasts that differentiated from telocytes after tamoxifen treatment).

To assess the effects of lymphatic dysfunction following telocyte deletion on acute joint inflammation, we used the ZIA model[26] as outlined in Figure 6A. Longitudinal ultrasound confirmed a 10-fold increase in synovial volume following knee injection with zymosan versus PBS controls (Figure 6B–D). Moreover, zymosan induced 3.2-fold greater synovitis in telocyte-depleted mice, and although this acute synovitis commenced resolution in WT mice after 7 days (Figure 6C), the increased synovial volume was unabated at day 14 in telocyte-depleted mice (Figure 6D). Histology of the knee joints corroborated the imaging results demonstrating increased pannus tissue in knees with ZIA from mice with depleted telocytes (Figure 6E and F). Remarkably, the histology also revealed resorbed cortical bone surfaces in the DTA and zymosan groups (Figure 6E). To assess telocyte depletion and ZIA effects on focal erosions and osteoclast numbers, we performed histomorphometry and micro-CT analyses on these femurs. The results showed increased numbers of TRAP+ osteoclasts on resorbed cortical bone surfaces in some of the femurs from zymosan-treated mice (Figure 6). Surprisingly, we also observed large numbers of osteoclasts in some femurs from telocyte-depleted mice injected with PBS. Micro-CT further demonstrated that acute ZIA failed to induce focal erosions in the knees of WT mice within 14 days, whereas it induced extensive erosions in the patellar groove of telocyte-depleted mice at this time point (Figure 6G and H). Together with our lymphatic readouts, these data demonstrate that telocyte depletion reduces lymphatic function, and upon challenge with acute inflammatory arthritis, leads to more persistent inflammation, exacerbated synovitis, and rapid focal cortical bone loss.

DISCUSSION

RA is a complex immune-mediated inflammatory disorder with divergent mechanisms of disease progression, major unmet clinical needs remain for a large fraction of patients with RA who fail to achieve remission and approximately 30% who are refractory to all current therapies.[27,28] With this in mind, we focused on the autoimmune independent pathologies of inflammatory-erosive arthritis observed in TNF-tg mice.[29] This research led to the discovery of the SLS,[30] an interactive network critical for joint homeostasis,[31] which is dysfunctional in RA and osteoarthritis, and this altered function correlates with disease progression and flare.[1] Here we present the first evidence that telocytes physically associated with peri-PLV mast cells are integral to the SLS (Figures 2 and 3) and may be responsible for communicating joint drainage needs to inactive cLVs. This emerging hypothesis is predicated on similar lymphatic defects and exacerbated inflammatory-erosive arthritis observed in mice deficient in mast cells[12] and telocytes (Figures 5 and 6), suggesting that these cells may serve as novel targets for treating patients with RA.

In contrast to the circulatory system, which is responsible for blood flow and where development, regulation, and repair have been defined in great cellular and molecular detail, many fundamental questions about lymphatics remain open, including critical questions about the mechanisms that control cLV contractions.[32] To address lymphatic contraction mechanisms, Zawieja et al used conditional-inducible CreER^{T2} transgenic mice to assess the innate pacemaking potential of mast cells, telocytes, pericytes, fibroblasts, and LMCs in cLVs ex vivo.[4] Taken together with other studies, these results support a longstanding model of LMCs as the intrinsic pacemaker of cLVs.[33,34] However, although these studies largely explain the mechanisms responsible for intraluminal pressure-dependent spontaneous cLV contractions, they do not provide information on the initiating signal for distal tissue LMC contractions in response to edema (eg, joint effusions).

Here, we present the first evidence that telocytes are a component of the SLS, and that they exist as a network of integrated cells that parallel lymphatic vessels from the synovium, which terminate in mast cells adjacent to LMCs in joint-draining cLVs. We

Figure 6. Telocyte depletion increases severity and duration of synovial inflammation from zymosan-induced arthritis. (A) Experimental design and workflow in which 8-week-old female WT and Efhd1-CreER$^{+/-}$ × DTA$^{f/-}$ mice received tamoxifen treatment to introduce telocyte depletion in DTA double-transgenics. Knee injections of zymosan or PBS were given at age 10 weeks followed by knee ultrasound before knee injection and on days 2, 7, and 14 after knee injection. Mice were euthanized on day 15, and knee joints were harvested for histology. (B) Representative day 14 knee ultrasound images of the synovial volume between the femur and tibia that were quantified longitudinally ([C] AUC values with mean ± SD; $P < 0.01$, ANOVA) and before euthanization on day 14 ([D]; $^{**}P \leq 0.01$ via ANOVA). (E) Representative hematoxylin and eosin–stained joint histology obtained at 10× magnification with magnified ROI (box) highlighting nonresorbed cortical bone surfaces in PBS WT (white arrows) versus resorbed cortical bone surface in all other groups (yellow arrows), and the zymosan-induced arthritis pannus tissue (#). (F) Quantification of the synovial area is reported as the percentage of ROI, as described in the Methods section. Data are presented with the mean ± SD ($^{**}P < 0.01$ via ANOVA). Similar results were obtained in experiments with Myoc-CreER$^{+/-}$ × DTA$^{f/-}$ mice (data not shown). (G) Three-dimensional renderings of the distal femur μCT scans, with quantification of the focal erosions ([H]; $^{*}P \leq 0.05$ via ANOVA). Data are presented for each femur with mean ± SD. ANOVA, analysis of variance; AUC, area under the curve; DTA, diphtheria toxin subunit A; f, femur; μCT, micro–computed tomography; PBS, phosphate-buffered saline; ROI, region of interest; t, tibia; TMX, tamoxifen; WT, wild-type. Color figure can be viewed in the online issue, which is available at http://onlinelibrary.wiley.com/doi/10.1002/art.70131/abstract.

also demonstrate that these telocytes can be efficiently deleted in *Efhd1*-CreER^{T2} × DTA^{floxed} mice following tamoxifen treatment without affecting peri-PLV mast cells, and these telocyte-depleted mice display lymphatic clearance defects and exacerbated ZIA. We also present several preliminary findings that must be addressed in future studies. Notable among these limitations are potential off-target effects of our transgenic mouse models when performing systemic tamoxifen delivery experiments. As our models may target cells in tissues that were not studied exhaustively and we confirmed targeting to nontelocytes known to express Efhd1 (eg, renal tubule cells[35]; Supplementary Figure 7), conclusions about telocyte-specific effects need to be tempered. Additionally, the DTA-induced telocyte ablation strategy used in this study may be subject to incomplete or variable ablation efficiency, which is a common limitation of DTA-based cell ablation models. Thus, formal gene knockout studies are warranted to confirm these findings. We also report some preliminary results that need to be followed up in future studies. The first is our variable findings of increased osteoclasts in femurs of mice with DTA-deleted target cells (Supplementary Figure 6), which warrants prospective studies to determine if these preliminary observations are significant.

There are also technical challenges that need to be overcome. This study exclusively investigated PLVs that drain the ankle, whereas the knee joint that was studied in the ZIA experiments drains to the inguinal and iliac lymph nodes. Although concerns about this disconnect are somewhat abated by studies that demonstrated lymphatic dysfunction in mice with inflammatory arthritis occurs in series of the low limb in both lymphatic vessels and lymph nodes[36] such that assessment of PLV is predictive of lymphatic function along the ipsilateral axis, technology that allows for longitudinal assessment of lymph transport to deep lymphatics is needed. We also conclude that this technical shortcoming contributed to the highly variable NIR-ICG assessments of lymphatic drainage of PBS- versus zymosan-injected knees, which were confounded by effects of multiple intra-articular injections (data not shown). Thus, faithful measurement of lymphatic drainage from the knee will likely require technical innovations (eg, assessing large-molecule translocation from the joint to iliac lymph nodes). Additionally, we note that this study does not directly compare telocytes or mast cells in lymphoid tissues between control and ZIA conditions, nor does it assess lymphatic function under ZIA conditions. Thus, these open questions need to be addressed in future studies.

In summary, we find that telocytes embedded in the ECM around PLVs are lost in TNF-tg mice with inflammatory arthritis and can be partially recovered by anti-TNF therapy (Figure 4G), and telocyte networks adjacent to PLVs are integrated into mast cells (Figure 3). Furthermore, telocyte deletion decreases lymphatic function (Figure 5) and exacerbates ZIA (Figure 6). Based on these discoveries, we propose a unifying model to explain the functions of telocytes within the SLS. This model posits three testable hypotheses that are the focus of our future directions. The first is the existence of connected telocyte networks that parallel lymphatic vessels from the synovial lymphatic capillaries to mast cell elaborated cLVs, which is supported by our WMIFM images (Figure 2H) and can be further tested by high-resolution light-sheet microscopy to confirm the tdT^{+} cells in the array are physically associated. The second is that telocytes sense osmotic pressure in joints (eg, ankle) and signal through the telocyte network to the peri-PLV mast cells that degranulate and initiate LMC contractions in response. Experiments to test this will require generation of double transgenic mice in which the *Efhd1*-CreER^{T2} are crossed to mice with telocyte- or mast cell–specific Ca^{2+} reporter probes for intravital microscopy studies following ankle stimulations. Finally, we propose that RA fibroblast-like synoviocytes are derived from telocytes that differentiate in response to chronic inflammation and adherence to rigid ECM in inflamed joints. This could be tested via lineage tracing studies with tamoxifen-treated *Efhd1*-CreER^{T2} × Ai9 mice and genetic EFHD1 gain and loss of function studies, which could provide the field with a novel molecular target to treat pauci-immune RA and lymphedema that is refractory to all known treatments.

ACKNOWLEDGMENTS

We would like to thank the faculty and staff at the Genomics Research Center (RRID SCR_012359) and Histology, Biochemistry, Electron Microscopy Resource (RRID SCR_012366) in the Center for Advanced Resource Technologies and Molecular Imaging Core at the University of Rochester Medical Center.

AUTHOR CONTRIBUTIONS

All authors contributed to at least one of the following manuscript preparation roles: conceptualization AND/OR methodology, software, investigation, formal analysis, data curation, visualization, and validation AND drafting or reviewing/editing the final draft. As corresponding author, Dr Schwarz confirms that all authors have provided the final approval of the version to be published and takes responsibility for the affirmations regarding article submission (eg, not under consideration by another journal), the integrity of the data presented, and the statements regarding compliance with institutional review board/Declaration of Helsinki requirements.

REFERENCES

1. Bouta EM, Bell RD, Rahimi H, et al. Targeting lymphatic function as a novel therapeutic intervention for rheumatoid arthritis. Nat Rev Rheumatol 2018;14(2):94–106. doi:https://doi.org/10.1038/nrrheum.2017.205
2. Calgüneri M, Oztürk MA, Ozbalkan Z, et al. Frequency of lymphadenopathy in rheumatoid arthritis and systemic lupus erythematosus. J Int Med Res 2003;31(4):345–349. doi:https://doi.org/10.1177/147323000303100415
3. Scallan JP, Zawieja SD, Castorena-Gonzalez JA, et al. Lymphatic pumping: mechanics, mechanisms and malfunction. J Physiol 2016;594(20):5749–5768. doi:https://doi.org/10.1113/JP272088
4. Zawieja SD, Pea GA, Broyhill SE, et al. Cellular characterization of the mouse collecting lymphatic vessels reveals that lymphatic muscle

cells are the innate pacemaker cells. *eLife* 2025;12:RP90679. doi:https://doi.org/10.7554/eLife.90679.4

5. Azhar SH, Lim HY, Tan BK, et al. The unresolved pathophysiology of lymphedema. Front Physiol 2020;11:137. doi:https://doi.org/10.3389/fphys.2020.00137
6. Guo R, Zhou Q, Proulx ST, et al. Inhibition of lymphangiogenesis and lymphatic drainage via vascular endothelial growth factor receptor 3 blockade increases the severity of inflammation in a mouse model of chronic inflammatory arthritis. Arthritis Rheum 2009;60(9):2666–2676. doi:https://doi.org/10.1002/art.24764
7. Zhou Q, Guo R, Wood R, et al. Vascular endothelial growth factor C attenuates joint damage in chronic inflammatory arthritis by accelerating local lymphatic drainage in mice. Arthritis Rheum 2011;63(8):2318–2328. doi:https://doi.org/10.1002/art.30421
8. Bouta EM, Kuzin I, de Mesy Bentley K, et al. Brief report: treatment of tumor necrosis factor-transgenic mice with anti-tumor necrosis factor restores lymphatic contractions, repairs lymphatic vessels, and may increase monocyte/macrophage egress. Arthritis Rheumatol 2017;69(6):1187–1193. doi:https://doi.org/10.1002/art.40047
9. Pal S, Nath S, Meininger CJ, et al. Emerging roles of mast cells in the regulation of lymphatic immuno-physiology. Front Immunol 2020;11:1234. doi:https://doi.org/10.3389/fimmu.2020.01234
10. Nigrovic PA, Lee DM. Mast cells in inflammatory arthritis. Arthritis Res Ther 2005;7(1):1–11. doi:https://doi.org/10.1186/ar1446
11. Keffer J, Probert L, Cazlaris H, et al. Transgenic mice expressing human tumour necrosis factor: a predictive genetic model of arthritis. EMBO J 1991;10(13):4025–4031. doi:https://doi.org/10.1002/j.1460-2075.1991.tb04978.x
12. Peng Y, Kenney HM, de Mesy Bentley KL, et al. Distinct mast cell subpopulations within and around lymphatic vessels regulate lymph flow and progression of inflammatory-erosive arthritis in TNF-transgenic mice. Front Immunol 2023;14:1275871. doi:https://doi.org/10.3389/fimmu.2023.1275871
13. Kenney HM, Wu CL, Loiselle AE, et al. Single-cell transcriptomics of popliteal lymphatic vessels and peripheral veins reveals altered lymphatic muscle and immune cell populations in the TNF-Tg arthritis model. Arthritis Res Ther 2022;24(1):64. doi:https://doi.org/10.1186/s13075-022-02730-z
14. Madisen L, Zwingman TA, Sunkin SM, et al. A robust and high-throughput Cre reporting and characterization system for the whole mouse brain. Nat Neurosci 2010;13(1):133–140. doi:https://doi.org/10.1038/nn.2467
15. Voehringer D, Liang HE, Locksley RM. Homeostasis and effector function of lymphopenia-induced "memory-like" T cells in constitutively T cell-depleted mice. J Immunol 2008;180(7):4742–4753. doi:https://doi.org/10.4049/jimmunol.180.7.4742
16. Popescu LM, Faussone-Pellegrini MS. TELOCYTES - a case of serendipity: the winding way from interstitial cells of Cajal (ICC), via interstitial Cajal-like cells (ICLC) to TELOCYTES. J Cell Mol Med 2010;14(4):729–740. doi:https://doi.org/10.1111/j.1582-4934.2010.01059.x
17. Kondo A, Kaestner KH. Emerging diverse roles of telocytes. Development 2019;146(14):dev175018. doi:https://doi.org/10.1242/dev.175018
18. Kawamoto T, Kawamoto K. Preparation of thin frozen sections from nonfixed and undecalcified hard tissues using Kawamoto's film method (2020). Methods Mol Biol 2021;2230:259–281. doi:https://doi.org/10.1007/978-1-0716-1028-2_15
19. Bell RD, Slattery PN, Wu EK, et al. iNOS dependent and independent phases of lymph node expansion in mice with TNF-induced inflammatory-erosive arthritis. Arthritis Res Ther 2019;21(1):240. doi:https://doi.org/10.1186/s13075-019-2039-z
20. Bell RD, Wu EK, Rudmann CA, et al. Selective sexual dimorphisms in musculoskeletal and cardiopulmonary pathologic manifestations and mortality incidence in the tumor necrosis factor-transgenic mouse model of rheumatoid arthritis. Arthritis Rheumatol 2019;71(9):1512–1523. doi:https://doi.org/10.1002/art.40903
21. Kenney HM, Peng Y, Bell RD, et al. Persistent popliteal lymphatic muscle cell coverage defects despite amelioration of arthritis and recovery of popliteal lymphatic vessel function in TNF-Tg mice following anti-TNF therapy. Sci Rep 2022;12(1):12751. doi:https://doi.org/10.1038/s41598-022-16884-y
22. Bouta EM, Ju Y, Rahimi H, et al. Power Doppler ultrasound phenotyping of expanding versus collapsed popliteal lymph nodes in murine inflammatory arthritis. PLoS One 2013;8(9):e73766. doi:https://doi.org/10.1371/journal.pone.0073766
23. Kenney HM, Peng Y, Chen KL, et al. A high-throughput semi-automated bone segmentation workflow for murine hindpaw micro-CT datasets. Bone Rep 2022;16:101167. doi:https://doi.org/10.1016/j.bonr.2022.101167
24. Scallan JP, Bouta EM, Rahimi H, et al. *Ex vivo* demonstration of functional deficiencies in popliteal lymphatic vessels from TNF-transgenic mice with inflammatory arthritis. Front Physiol 2021;12:745096. doi:https://doi.org/10.3389/fphys.2021.745096
25. Rosa I, Faussone-Pellegrini MS, Romano E, et al. Impairment in the telocyte/CD34^{+} stromal cell network in human rheumatoid arthritis synovium. J Cell Mol Med 2021;25(4):2274–2278. doi:https://doi.org/10.1111/jcmm.16225
26. Bernotiene E, Palmer G, Talabot-Ayer D, et al. Delayed resolution of acute inflammation during zymosan-induced arthritis in leptin-deficient mice. Arthritis Res Ther 2004;6(3):R256–R263. doi:https://doi.org/10.1186/ar1174
27. Alivernini S, Firestein GS, McInnes IB. The pathogenesis of rheumatoid arthritis. Immunity 2022;55(12):2255–2270. doi:https://doi.org/10.1016/j.immuni.2022.11.009
28. Gravallese EM, Firestein GS. Rheumatoid arthritis - common origins, divergent mechanisms. N Engl J Med 2023;388(6):529–542. doi:https://doi.org/10.1056/NEJMra2103726
29. Li P, Schwarz EM. The TNF-alpha transgenic mouse model of inflammatory arthritis. Springer Semin Immunopathol 2003;25(1):19–33. doi:https://doi.org/10.1007/s00281-003-0125-3
30. Liang Q, Zhang L, Xu H, et al. Lymphatic muscle cells contribute to dysfunction of the synovial lymphatic system in inflammatory arthritis in mice. Arthritis Res Ther 2021;23(1):58. doi:https://doi.org/10.1186/s13075-021-02438-6
31. Bouta EM, Li J, Ju Y, et al. The role of the lymphatic system in inflammatory-erosive arthritis. Semin Cell Dev Biol 2015;38:90–97. doi:https://doi.org/10.1016/j.semcdb.2015.01.001
32. Davis MJ, Zawieja SD. Pacemaking in the lymphatic system. J Physiol Published online March 23, 2024. doi:https://doi.org/10.1113/JP284752
33. Van Helden DF. Pacemaker potentials in lymphatic smooth muscle of the guinea-pig mesentery. J Physiol 1993;471(1):465–479. doi:https://doi.org/10.1113/jphysiol.1993.sp019910
34. Van Helden DF, Zhao J. Lymphatic vasomotion. Clin Exp Pharmacol Physiol 2000;27(12):1014–1018. doi:https://doi.org/10.1046/j.1440-1681.2000.03368.x
35. Meng K, Hu Y, Wang D, et al. EFHD1, a novel mitochondrial regulator of tumor metastasis in clear cell renal cell carcinoma. Cancer Sci 2023;114(5):2029–2040. doi:https://doi.org/10.1111/cas.15749
36. Li J, Zhou Q, Wood RW, et al. CD23(+)/CD21(hi) B-cell translocation and ipsilateral lymph node collapse is associated with asymmetric arthritic flare in TNF-Tg mice. Arthritis Res Ther 2011;13(4):R138. doi:https://doi.org/10.1186/ar3452

Check for updates

Arthritis & Rheumatology
Vol. 78, No. 10, October 2026, pp 2063–2073
DOI 10.1002/art.70133
© 2026 The Author(s). *Arthritis & Rheumatology* published by Wiley Periodicals LLC on behalf of American College of Rheumatology.
This is an open access article under the terms of the Creative Commons Attribution License, which permits use, distribution and reproduction in any medium, provided the original work is properly cited.

American College of Rheumatology
Empowering Rheumatology Professionals

Association of Clonal Hematopoiesis With Incident, Late-Onset, Seropositive Rheumatoid Arthritis

Kun Zhao, PhD,[1] Yash Pershad, BS,[1] J. Brett Heimlich, MD, PhD,[2] Michelle Ormseth, MD, MSCI,[3] C. Michael Stein, MB, ChB,[1] Brian Sharber, MS,[1] Caitlyn Vlasschaert, MD, PhD,[4] Alexander G. Bick, MD, PhD,[1] and Robert W. Corty, MD, PhD[3]

Objective. Clonal hematopoiesis (CH), defined by acquired driver mutations in hematopoietic stem cells, is associated with many inflammatory diseases of aging. We investigated whether CH and its subtypes, CH of indeterminate potential (CHIP) and mosaic chromosomal alteration (mCA), are associated with incident rheumatoid arthritis (RA) and whether complement modifies these associations.

Methods. CHIP was detected in NIH All of Us, Vanderbilt BioVU, and UK Biobank; mCA was detected in UK Biobank. A harmonized, high-specificity phenotyping algorithm was applied across biobanks to identify participants with seropositive and seronegative RA (SPRA and SNRA). Age-scale survival models assessed the effect of CH on risk of incident RA. Effect modification was tested with interaction models with genetically predicted complement protein levels.

Results. Among 612,989 participants, 30,840 had CHIP, 1,535 had incident SPRA, and 1,090 had incident SNRA. CHIP was associated with an increased risk of incident SPRA (pooled hazard ratio [HR] 1.26; confidence interval [CI] 1.03–1.52; $P = 2.3 \times 10^{-2}$), driven primarily by *DNMT3A*-mutated CHIP and late-onset RA (HR 1.45; CI 1.13–1.96; $P = 3.6 \times 10^{-3}$) but not SNRA. Autosomal mCA and mosaic loss of chromosome Y (mLOY) were associated with an increased risk of incident SPRA (HR 2.12 and 2.85; CI 1.18–3.8 and 1.57–5.19; $P = 1.2 \times 10^{-2}$ and 6.1×10^{-4}) but not SNRA. Higher genetically predicted levels of C1r and C1s attenuated the CHIP–SPRA association.

Conclusion. Age-related CH, including *DNMT3A*-CHIP, autosomal mCA, and mLOY, are risk factors for incident SPRA but not SNRA, supporting a genotype- and serostatus-specific link between somatic mutation and RA, with the classical complement pathway as a potential modifier.

INTRODUCTION

Rheumatoid arthritis (RA) is a systemic, autoimmune disease characterized by chronic inflammation and heterogeneous clinical trajectories across age, serologic status, and treatment response.[1] RA primarily affects older adults, though people of all ages can be affected.[2] RA with onset at the age of 60 years or older has been termed late-onset RA (LORA).[3] LORA has a distinct genetic profile, higher levels of inflammatory cytokines, and inferior response to therapy.[4–7] The mechanisms driving LORA remain incompletely understood. There is a pressing need for advancements in the diagnosis and care of LORA as its incidence is increasing over time.[2] The pathogenesis of seropositive RA (SPRA; defined by presence of rheumatoid factor [RF] or anti–cyclic citrullinated peptide antibodies) involves antigen-driven clonal selection on lymphocytes.[8] But the role of clonal selection among hematopoietic stem cells, a common phenomenon in older adults, remains much less explored.

The two most common forms of clonal hematopoiesis (CH) are CH of indeterminate potential (CHIP) and mosaic

Supported by the NIH (grants DP5-OD-029586, R01-AG-088657, and R01-AG-083736), the Burroughs Wellcome Fund, the Edward P. Evans Foundation, the RUNX1 Research Program, the Pew Charitable Trusts, and a Hevolution/American Federation for Aging Research New Investigator Award. Dr Pershad's work was supported by the Vanderbilt University Medical Center Brock Family Endowment and Young Ambassador Award (AGB), the Arthritis National Research Foundation and Rheumatology Research Foundation (RWC), and the NIH (grant F30-AG-099331).

[1]Division of Genetic Medicine and Clinical Pharmacology, Department of Medicine, Vanderbilt University Medical Center, Nashville, Tennessee; [2]Division of Cardiovascular Medicine, Department of Medicine, Vanderbilt University Medical Center, Nashville, Tennessee; [3]Division of Rheumatology, Department of Medicine, Vanderbilt University Medical Center, Nashville, Tennessee; [4]Department of Medicine, Queen's University, Kingston, Ontario, Canada.

Additional supplementary information cited in this article can be found online in the Supporting Information section (https://acrjournals.onlinelibrary.wiley.com/doi/10.1002/art.70133).

Author disclosures and graphical abstract are available at https://onlinelibrary.wiley.com/doi/10.1002/art.70133.

Address correspondence via email to Robert W. Corty, MD, PhD, at robert.corty@vumc.org.

Submitted for publication January 19, 2026; accepted in revised form March 3, 2026.

chromosomal alteration (mCA). CHIP is defined by the clonal expansion of hematopoietic stem cells carrying a small somatic mutation in a leukemogenic gene.[9–11] Seventy-five percent of CHIP cases are driven by mutation in one of three epigenetic regulators, *DNMT3A*, *TET2*, and *ASXL1*.[12] CHIP is rarely observed among people in their 40s and younger (<1%) but is present in ~15% of individuals in their 70s.[12] Although typically asymptomatic, CHIP skews hematopoiesis toward myelopoiesis, causes chronic inflammation, and confers elevated risks for myeloid neoplasms, cardiovascular disease, giant cell arteritis, gout, and all-cause mortality.[10,13–15] mCA, the other form of CH, is defined by large-scale chromosomal gain, loss, or copy-neutral loss of heterozygosity of the autosomes or sex chromosomes (ie, mosaic loss of chromosome X, known as mLOX, and mosaic loss of chromosome Y, known as mLOY). mCA is also common among older adults, can be asymptomatic, and confers risk for a distinct, but less well understood, set of diseases of aging.[16,17]

Recent investigations have begun to elucidate the relationship between CH and RA. Hiitola et al found that CHIP is associated with prevalent RA in a genotype- and seropositivity-specific manner, noting that the rate of *DNMT3A* CHIP is elevated among patients with SPRA and the rate of *TET2* CHIP is elevated among patients with seronegative RA (SNRA).[18] But disease ascertainment was based solely on diagnosis codes, an approach that has been found to have specificity of around 55%.[19–21] Similarly, Uchiyama et al highlighted the critical importance of age at disease onset, reporting that male participants with LORA are enriched for mLOY compared to age-matched controls but participants with young-onset RA are paradoxically depleted for mLOY compared to matched controls.[22] However, both studies used only cross-sectional data, limiting insights into the time course of the relationship. Furthermore, studies to date have offered limited insight into the mechanistic link between CH, which heightens innate immune activation, and RA, which has prominent adaptive immune features. The complement system functionally links the innate and adaptive immune system.[23] Notably, C3d-tagged antigens stimulate B cell activation ~10,000 times more efficiently than nontagged antigens.[23] Thus, we hypothesize that the complement pathway may influence the association between CH and RA.

To address these questions, we performed a meta-analysis across three large biobanks: the NIH All of Us Research Program (AoU), Vanderbilt's BioVU, and the UK Biobank (UKB). We leveraged extensive electronic health records (EHR) and genetic sequencing data to study over 600,000 research participants. We employed established bioinformatic pipelines for CH detection, a rigorous RA phenotyping strategy, and longitudinal study design to (1) identify high-confidence cases of SPRA and SNRA, (2) comprehensively characterize the effects of CHIP and mCA on risk of incident SPRA and SNRA, (3) dissect the effects of CHIP on risk for cardiovascular disease and death among research participants with RA, and (4) test for effect modification by genetically predicted complement protein levels.

METHODS

Study cohorts. De-identified data were obtained from three biobanks with linked EHR and either whole exome or whole genome sequencing (WES/WGS): AoU, BioVU, and UKB. AoU is a population sample in which participants provide a blood sample at a time of their choosing, whereas BioVU is a hospital-based cohort, enriched for participants with chronic disease, in which blood samples left over after clinical testing were used for sequencing, and UKB is a prospectively designed study in which participants were invited to the assessment center on a medically arbitrary date.

Inclusion, exclusion, and case ascertainment. Inclusion and exclusion criteria and RA disease ascertainment criteria were applied consistently across the biobanks.

Inclusion criteria. Research participants were included in the study only if they had (1) adequate genetic data for CHIP ascertainment, (2) adequate clinical data for RA disease ascertainment (two or more diagnosis codes spanning a year or more, one or more laboratory value, and one or more medication prescription), and (3) adequate engagement with the health care system that RA would likely be diagnosed if it were present (ie, five or more total diagnosis codes).

Exclusion criteria. Research participants were excluded if they were aged <40 years at the time of the blood sample used for DNA sequencing because CHIP is very rare among the young.[11,24] Similarly, research participants were excluded if they had prevalent hematologic cancer (defined by diagnosis codes in Supplementary Table 1).[9] As smoking is a risk factor for both CH and RA, smoking status was a critical covariate. It was inferred from questionnaires administered to all participants in AoU, BioVU, and UKB, and participants who did not answer were excluded.

Follow-up. Health records in AoU and BioVU are updated approximately annually to include all available data; thus, follow-up is until last available diagnosis code. In UKB, ambulatory records are kept by general practitioners and are available for approximately 45% of the cohort with a truncation date in 2016 as described in the UKB data showcase, defining the censoring date for participants with no diagnosis of RA. Only participants with available primary care data were included in the study (Figure 1).

RA ascertainment. We used a combination of diagnosis codes, laboratory data, and medication prescription to identify research participants with RA. This approach has been found to have sensitivity and specificity of approximately 85% and 99%, respectively.[19,25–27]

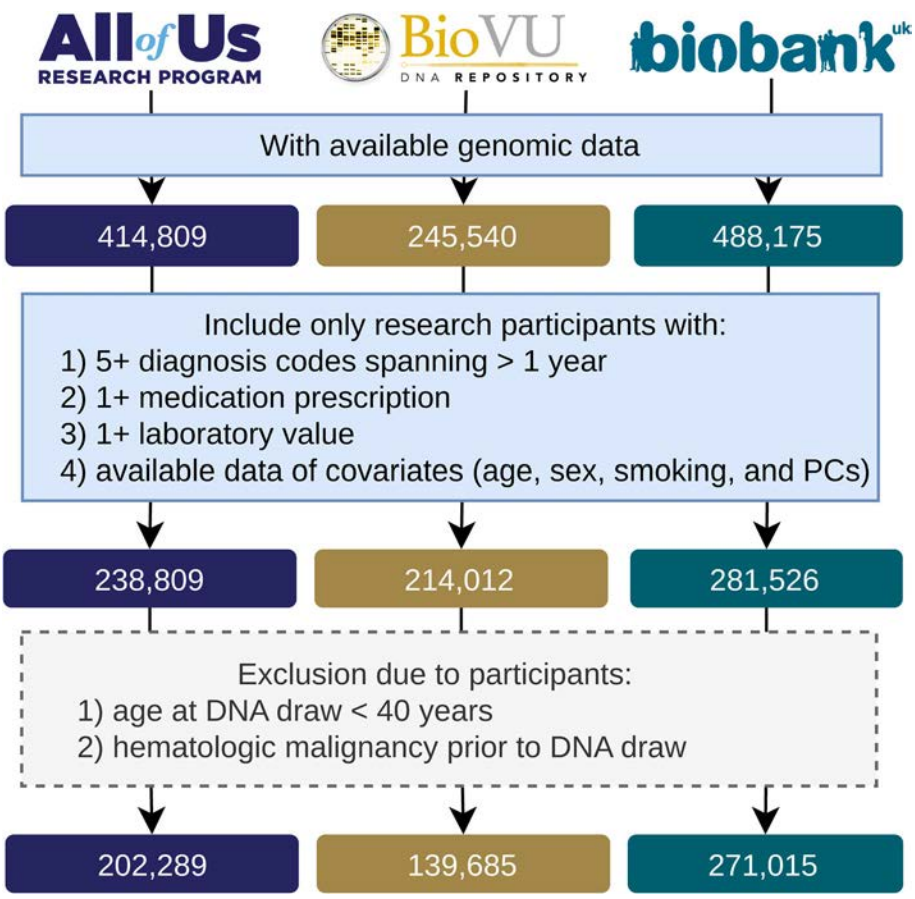


Figure 1. Flow diagram summarizing inclusion and exclusion in the All of Us Research Program, Vanderbilt BioVU, and UK Biobank. PC, principle component.

Diagnosis codes. For BioVU, in which diagnoses are recorded by *International Classification of Diseases, Ninth Revision* (ICD-9) and ICD-10 codes, codes matching "M05" were considered SPRA, codes matching "M06" were considered SNRA (excluding "M06.1" and "M06.4"), and codes matching "714.0" were considered RA not otherwise specified. For AoU and UKB, in which diagnoses are recorded in the Systematized Nomenclature of Medicine vocabulary, relevant codes were identified with a search strategy described in the Supplementary Appendix that resulted in a code list provided in Supplementary Table 2.

Medications. The list of disease-modifying antirheumatic drugs (DMARDs) was defined as the combination of conventional synthetic DMARDs, biologic DMARDs, and targeted synthetic DMARDs (Supplementary Table 3).

Laboratory values. We identified concepts that capture RF and anti–cyclic citrullinated peptide (anti-CCP) and developed a careful parsing method to assign each result as either positive or negative, as detailed in the Supplementary Appendix. Each participant was considered seropositive by laboratory values if they had a positive RF or anti-CCP results, negative if they had a result for at least one with no positive results, and not applicable otherwise.

Date of disease onset. Participants with RA were considered to have developed the disease on the date the diagnosis code first appeared in their medical records. Cases were considered as "prevalent" when diagnosed on or before the date of the blood sample used for DNA sequencing and "incident" when diagnosed after the blood sample.

Osteoarthritis controls. Controls with osteoarthritis were identified in BioVU as participants with phecode MS_708 and no instances of M05 or M06.

CHIP detection. Based on genetic sequencing data availability, CHIP calling was performed with WGS for AoU (depth ~40×) and BioVU (depth ~35×) and with WES for UKB (depth ~40×). For each cohort, the same CHIP-defining somatic single nucleotide variants and short indels were identified per established variant detection methods as we have previously described.[28,29] Briefly, 74 genes known to harbor CHIP-driving variants were screened for somatic variants using the *Mutect2* to identify putative CHIP variants (Supplementary Table 4).[10,30,31] The variant allele fraction of the CHIP clone was visualized with violin plots.

mCA detection. mCA detection in UKB was previously described. In brief, mCAs in blood DNA genotyping intensity data were detected using a validated statistical phasing-based approach.[32]

Genetically predicted complement protein levels. To investigate the mechanistic role of the classical complement pathway without the confounding effects of active inflammation or reverse causation, we used genetically predicted protein levels as a proxy for stable, lifelong systemic exposure. Briefly, we retrieved genetic effect estimates from the INTERVAL study and summed the genotypes of participants of European ancestry weighted by those effects as detailed in the Supplementary Appendix.[33]

Genetic principal components. Genetic principal components were retrieved from each biobank's central data repository, in which they have been deposited for wide dissemination after applying standard bioinformatic tools to variant tables as detailed in the Supplementary Appendix.[34–36]

Survival models for incident RA. To estimate the CHIP-associated risk of incident RA, Cox proportional hazards models were used. Because the three biobanks obtained the blood draw used to define CHIP status at times with different health contexts and empirically at a wide range of ages, implying a wide range of baseline risk for age-associated conditions such as RA, two time scales were evaluated: the "time-since-blood-draw" scale and the "age" scale.[37,38] Using the Grambsch–Therneau test, the proportional hazards assumption was violated in BioVU and AoU on the "time-since-blood-draw" scale, but on the "age" scale, no proportional hazards violations were observed (Supplementary Table 7).[39] Therefore, all time-to-event analyses were conducted on the age scale. Using the age scale, each participant entered the risk pool at the age at which the blood sample was drawn and exited the risk pool at the age they were diagnosed with RA (event) or the end of the available follow-up data (censoring). All time-to-event analyses included covariates of biologic sex, smoking status, and genetic principal components (PC1–PC5). Age-scale time-to-event analysis accounts for the effect of age comprehensively and nonparametrically, so no parametric correction for age effects on risk for RA was appropriate.[37] The model described here was applied for both SPRA and SNRA, first estimating the effect of all CHIP and then CHIP driven by each of the three most common drivers (*DNMT3A*, *TET2*, and *ASXL1*). Estimated hazard ratios and their confidence intervals (CIs) were visualized with forest plots. A nonparametric time-to-event modeling approach was considered but, due to the critical need for covariate adjustment, was not selected for analysis.

Logistic regression models for prevalent RA. To estimate the CHIP-associated odds of prevalent RA, logistic regression was used. Covariates were biologic sex, smoking status, genetic principal components (PC1–PC5), and participant's age at the time of blood draw. As described in the previous paragraph, the model described here was applied to both SPRA and SNRA, first estimating the effect of all CHIP and then CHIP driven by each of the three most common drivers. Estimated odds ratios (ORs) and their CIs were visualized with forest plots.

Survival models for all-cause mortality. Among participants with RA, the impact of CHIP on all-cause mortality was assessed using age-scale Cox proportional hazards models, adjusting sex, smoking status, and genetic principal components (PC1–PC5), as mentioned in the previous paragraph. Kaplan–Meier curves were generated to visually compare survival across CHIP and non-CHIP groups, and differences were assessed using the log-rank test. Empirical survival fraction over time was visualized with Kaplan–Meier plots, and estimated hazard ratios and their CIs were visualized with forest plots.

Meta-analysis combining results from three biobanks. Inverse variance-weighted meta-analysis is a statistical method that can improve the precision of effect estimates by combining information across studies. Specifically, it weights the effect estimated in each study proportional to the inverse of its variance.[40] The across-studies degree of heterogeneity (I^2 statistic) was used to determine whether the random or fixed effect model was used: in cases in which $I^2 > 50\%$, the random effect model was used; otherwise the fixed effects model was used, consistent with generally accepted practice.[40] Meta-analyses were visualized with forest plots.

Effect modification by genetically predicted complement levels. We tested for effect modification by modifying the age-scale survival analysis described earlier in this section to include an interaction term between CHIP status and genetically predicted complement levels.

Multiple hypothesis testing corrections. Multiple hypothesis testing correction was performed using the Bonferroni method when five or fewer hypotheses were tested, as in the analyses of how specific CHIP driver genes affect the risk or odds of RA and risk of death, and the Benjamini–Hochberg method when six or more hypotheses were tested, as in the analyses of effect modification by predicted complement levels.[41,42]

Data availability statement. Primary data from the UKB and NIH All Of Us biobanks are public, whereas primary data from BioVU require an institutional account at Vanderbilt University Medical Center. Processed data including CHIP calls, mCA calls, covariates, and phenotype ascertainment will be shared upon request after requester completion of relevant data security and privacy trainings.

Table 1. Sociodemographic characteristics of the three cohorts studied, separately and in aggregate*

	NIH All of Us (n = 202,289)	BioVU (n = 139,685)	UK Biobank (n = 271,015)	Total (N = 612,989)
Age at blood sample, median (IQR), y	61.1 (52.2–69.5)	58.9 (50.3–68.0)	58.0 (50.0–63.0)	58.0 (50.8–66.3)
Women, n (%)	120,600 (59.6)	75,085 (53.4)	150,584 (55.6)	346,269 (56.5)
Ever smoked, n (%)	87,733 (43.4)	50,459 (36.1)	121,336 (44.8)	259,528 (42.3)
Race, n (%)				
White	121,558 (60.1)	116,082 (83.0)	260,119 (96.0)	497,759 (81.2)
Black or AA	33,775 (16.7)	14,713 (10.5)	3,769 (1.4)	52,257 (8.5)
East Asian	3,971 (2.0)	1,761 (1.3)	7,127 (2.6)	12,859 (2.1)
With clonal hematopoiesis, n (%)				
Overall CHIP	10,799 (5.4)	11,321 (8.1)	8,720 (3.2)	30,840 (5.0)
DNMT3A	5,582 (2.8)	5,399 (3.9)	5,390 (2.0)	16,371 (2.7)
TET2	2,181 (1.1)	2,989 (2.1)	1,313 (0.5)	6,483 (1.1)
ASXL1	888 (0.4)	1,319 (0.9)	1,022 (0.4)	3,229 (0.5)
With prevalent SPRA or SNRA, n (%)				
SPRA	1,523 (0.75)	1,758 (1.26)	689 (0.25)	3,970 (0.65)
SNRA	862 (0.43)	1,286 (0.92)	394 (0.15)	2,542 (0.41)
With incident SPRA or SNRA, n (%)				
SPRA	217 (0.10)	1,101 (0.79)	217 (0.08)	1,535 (0.25)
SNRA	139 (0.07)	798 (0.57)	153 (0.06)	1,090 (0.18)
Years of follow-up, median (IQR)	2.1 (0.5–4.0)	4.3 (1.7–10.3)	12.3 (11.6–13.1)	8.6 (2.3–12.3)

* AA, African American; CHIP, clonal hematopoiesis of indeterminate potential; IQR, interquartile range; SNRA, seronegative rheumatoid arthritis; SPRA, seropositive rheumatoid arthritis.

RESULTS

Sociodemographic characteristics. After applying the unified inclusion and exclusion criteria, a total of 612,989 participants were included across the three biobanks: 202,289 from AoU, 139,685 from BioVU, and 271,015 from UKB (Figure 1). Their sociodemographic characteristics are presented in Table 1. Across cohorts, participants were middle-aged to older adults at the time of blood sample collection, with median ages ranging from 58.0 to 61.1 years. Women composed over half of each cohort (53.4%–59.6%). Smoking history was common across all three cohorts, with the highest prevalence observed in UKB. AoU and BioVU included more racially diverse participants, whereas UKB was predominantly White.

CHIP. Across the three cohorts, a total of 30,840 participants (5.0%) had one or more detectable CHIP mutation(s), with rates of 5.4% in AoU, 8.1% in BioVU, and 3.2% in UKB ($P < 0.001$ for differences across cohorts). CHIP carriers were, on average, older than noncarriers (mean age 65.8 vs 58.4 years, $P < 0.001$). Most CHIP clones were driven by mutations in *DNMT3A* (48%), *TET2* (21%), and *ASXL1* (10%), which together accounted for 79% of all detected driver mutations (Supplementary Figure S1). The aggregate meta-cohort and each individual cohort demonstrated an increase in the rate of CHIP with age, but the absolute frequency differed across biobanks, with BioVU showing the highest prevalence at all age groups (Supplementary Figures S2A and S2B).

Prevalent and incident RA. SPRA and SNRA were identified in 3,970 (0.65%) and 2,542 (0.41%) of the combined cohort, respectively. Prevalent SPRA (first diagnosed before the blood draw in which CHIP status was ascertained) occurred in 1,523 (0.75%), 1,758 (1.26%), and 689 (0.25%) participants in AoU, BioVU, and UKB, respectively. Prevalent SNRA occurred in 862 (0.43%), 1,286 (0.92%), and 394 (0.15%) participants in AoU, BioVU, and UKB, respectively. Incident SPRA (first diagnosed after the blood draw in which CHIP status was ascertained) occurred in 217 (0.10%), 1,101 (0.79%), and 217 (0.08%) participants in AoU, BioVU, and UKB, respectively, whereas incident SNRA occurred in 139 (0.07%), 798 (0.57%), and 153 (0.06%) participants in AoU, BioVU, and UKB, respectively.

CHIP is associated with increased risk of incident SPRA but not SNRA. In a three-cohort meta-analysis, a subtype-specific relationship between CHIP and risk of incident RA was observed, with a clear distinction between SPRA and SNRA. CHIP was associated with increased risk of incident SPRA (pooled hazard ratio [HR] 1.26; 95% CI 1.03–1.52; $P = 2.3 \times 10^{-2}$; $I^2 = 14\%$; Figure 2A). Gene-stratified analyses revealed that this association was primarily driven by *DNMT3A*-CHIP (HR 1.45; 95% CI 1.13–1.96; $P = 3.6 \times 10^{-3}$). This association was considered statistically significant because it met the corrected *P* value of 0.05 divided by 3 assigned by the Bonferroni method due to the three genes tested. By contrast, *TET2*-CHIP was not associated with incident SPRA (Figure 2A, Supplementary Figure S3) nor was *ASXL1*-CHIP, though effect heterogeneity limited their interpretability (Figure 2A, Supplementary Figure S3). Neither overall CHIP nor any specific CHIP driver gene was associated with incident SNRA (Figure 2B, Supplementary Figure S4). The distribution of CHIP driver mutations and their variant allele fractions was similar between individuals who developed

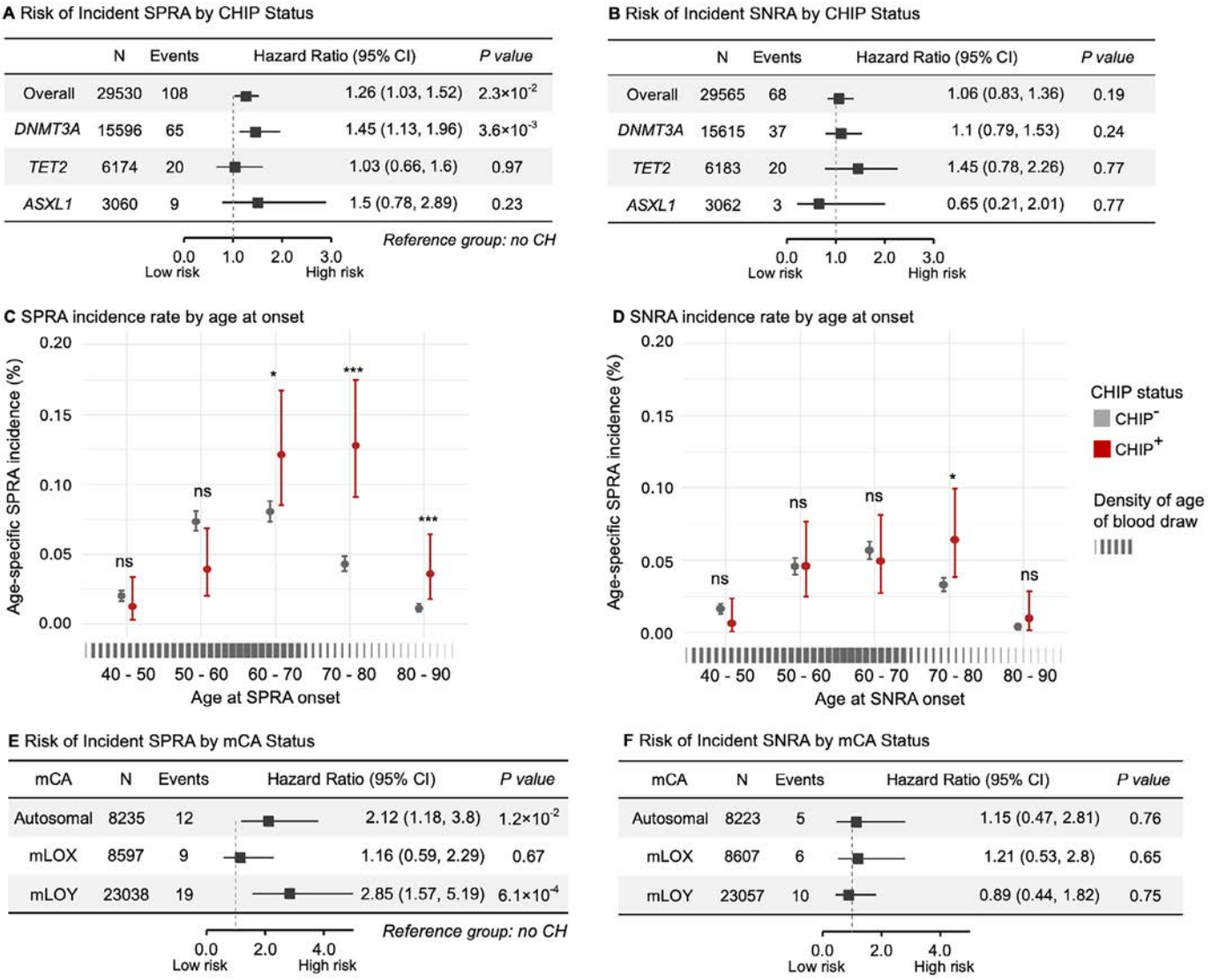


Figure 2. Association of CH with incident SPRA and SNRA. Forest plots show three-biobank meta-analytic effects of CHIP and subtypes on risk of incident (A) SPRA and (B) SNRA after correcting for biologic sex, smoking status, and five genetic principal components. "N" indicates the number of CH carriers and "Events" indicates the number of incident SPRA/SNRA cases among CH carriers. Incidence of (C) SPRA and (D) SNRA was calculated by decade and compared across CHIP status. Gray bars along the bottom of panels C and D indicate relative frequency of the blood draws from which CHIP status was inferred, where darker areas indicate the ages when more participants had blood draws performed. Forest plots show the mCA-associated risk of incident (E) SPRA and (F) SNRA after correcting for biologic sex, smoking status, and five genetic principal components in UKB. $^{*}P < 0.05$, $^{***}P < 0.0005$. CH, clonal hematopoiesis; CHIP, clonal hematopoiesis of indeterminate potential; CI, confidence interval; mCA, mosaic chromosomal alteration; mLOX, mosaic loss of chromosome X; mLOY, mosaic loss of chromosome Y; ns, not significant; SNRA, seronegative rheumatoid arthritis; SPRA, seropositive rheumatoid arthritis; UKB, UK Biobank.

SPRA and those who developed SNRA (Supplementary Figure S5A–D).

CHIP is associated with late-onset SPRA but not early-onset SPRA. The association of CHIP with incident but not prevalent SPRA presented an apparent conflict. We investigated further by examining the incidence of SPRA by decade and comparing it to the age when blood samples were taken for DNA sequencing (Figure 2C, 2D). Most blood samples were taken in middle age, and CHIP carriers exceeded noncarriers in SPRA incidence only in older age. The largest CHIP-associated difference in SPRA incidence was observed among research participants age 70 to 80 years, an RA subtype that has been termed LORA ($P < 0.005$; Figure 2C).[22] In contrast, there was no difference in SPRA incidence by CHIP status among people aged <60 years, suggesting that early-onset RA is largely unrelated to CHIP.

Autosomal mCAs and mLOY are associated with increased risk of incident SPRA but not SNRA. Survival analyses in UKB (the only biobank in which mCA data are

available) revealed striking associations with SPRA but none for SNRA. Autosomal mCA was associated with an increased risk of incident SPRA (HR 2.12; 95% CI 1.18–3.80; $P = 1.2 \times 10^{-2}$; Figure 2E). Among male participants, mLOY was associated with an increased risk of SPRA (HR 2.85; 95% CI 1.57–5.19; $P = 6.1 \times 10^{-4}$; Figure 2E). No significant association was observed between mLOX and risk of SPRA among female participants (HR 1.16; 95% CI 0.59–2.29) nor between any class of mCA and incident SNRA (Figures 2E and 2F).

Systemic inflammation in CHIP$^+$ and CHIP$^-$ SPRA. Given the association between CHIP and incident SPRA, we sought to assess whether participants with CHIP developed a subtype of SPRA with higher levels of systemic inflammation as manifested in the C-reactive protein (CRP) level. Therefore, we compared the last CRP measurement before diagnosis of incident SPRA between patients with and without CHIP and compared them to controls without CHIP who developed osteoarthritis. SPRA groups exhibited substantially higher CRP levels than osteoarthritis controls ($P < 0.001$). CRP levels were numerically higher in CHIP$^+$ SPRA compared with CHIP$^-$ SPRA participants (median 14.7 vs 13.1 mg/L; $P = 0.048$; Supplementary Figure S6).

CH is not associated with prevalent RA. In contrast to the clear associations between CH and incident SPRA, there was no association between CH and prevalent RA, neither SPRA nor SNRA (Supplementary Figure S7A and S7B). In a meta-analysis across the three cohorts, the odds of having prevalent SPRA did not differ between CHIP carriers and noncarriers, nor

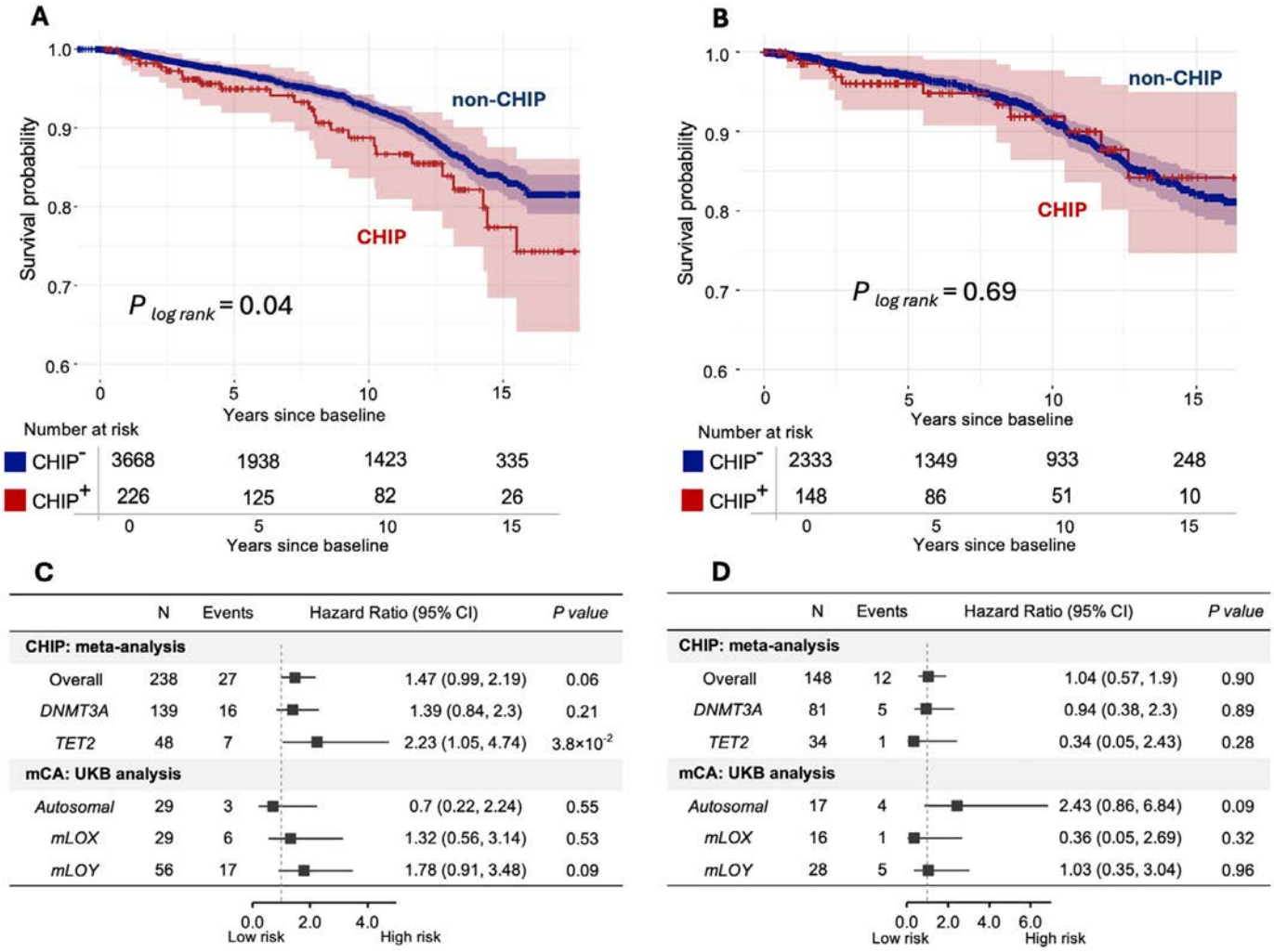


Figure 3. The association between CH and mortality among participants with RA. Kaplan–Meier plots of overall survival for patients with prevalent (A) SPRA and (B) SNRA, stratified by CHIP status. Cox regression was performed to evaluate the association between CH with all-cause mortality among patients with (C) SPRA and (D) SNRA, correcting for effects of biologic sex, smoking status, and five genetic principal components. CH, clonal hematopoiesis; CHIP, clonal hematopoiesis of indeterminate potential; CI, confidence interval; mCA, mosaic chromosomal alteration; mLOX, mosaic loss of chromosome X; mLOY, mosaic loss of chromosome Y; RA, rheumatoid arthritis; SNRA, seronegative rheumatoid arthritis; SPRA, seropositive rheumatoid arthritis; UKB, UK Biobank.

was *DNMT3A*-, *TET2*-, or *ASXL1*-CHIP associated with increased SPRA prevalence. Similarly, in UKB, none of autosomal mCA, mLOX, or mLOY was enriched among people with prevalent SPRA. Similar patterns were observed for prevalent SNRA, with no significant associations for overall CHIP, individual driver genes, or any mCA type.

CHIP and all-cause mortality among patients with SPRA and SNRA. Differential mortality is of absolute interest and could also explain the apparent conflict between incident and prevalent RA described previously; therefore, we examined the risk of all-cause mortality among research participants with prevalent SPRA and SNRA with or without CHIP. In the overall study population, CHIP, both overall and by individual driver genes, was associated with increased mortality risk (Supplementary Figure S8). Among individuals with SPRA, CHIP carriers had shorter survival than noncarriers by the log-rank test (P = 0.04; Figure 3A). Age-scale survival analysis revealed that overall CHIP was not significantly associated with mortality (HR 1.47; 95% CI 0.99–2.19), but *TET2*-CHIP was associated with an increased risk of mortality (HR 2.23; 95% CI 1.05–4.74; $P = 3.8 \times 10^{-2}$; Figure 3C). Analysis of other common CHIP drivers and mCA among participants with SPRA found no association with mortality (Figure 3C). In contrast to SPRA, neither CHIP nor any subtype nor any mCA was associated with mortality among participants with SNRA (Figures 3B and 3D).

Genetically predicted C1s and C1r modify the effect of CHIP on risk of SPRA. To investigate the role of classical complement in modifying the CHIP-associated risk for SPRA, we performed age-scale survival analysis with an interactive effect between genetically predicted complement levels and CH status.

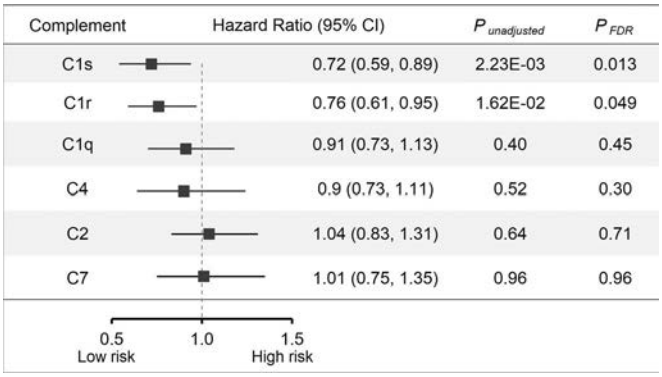


Figure 4. Effect modification of CHIP–SPRA association by genetically predicted complement levels. Forest plots show the interaction between CHIP and genetically predicted complement protein levels on incident SPRA risk from Cox models after correcting for biologic sex, smoking status, and five genetic principal components. P values are shown before and after FDR correction. CHIP, clonal hematopoiesis of indeterminate potential; CI, confidence interval; FDR, false discovery rate; SPRA, seropositive rheumatoid arthritis.

These analyses revealed effect modification between CHIP and C1s ($P = 2.2 \times 10^{-3}$, adjusted P [P_{adj}] = 0.013) and C1r ($P = 1.6 \times 10^{-2}$, P_{adj} = 0.049), indicating that higher genetically predicted complement levels attenuate the CHIP-associated risk of SPRA. In contrast, no significant interaction effect was observed for SPRA and any other complement components ($P \geq 0.4$; Figure 4). A sensitivity analysis conducted only among people with CHIP examined the effect of genetically predicted complement levels on risk of SPRA and observed consistent effects (C1s: OR 0.81, 95% CI 0.69–0.95, $P = 1.1 \times 10^{-2}$; C1r: OR 0.79, 95% CI 0.66–0.94, $P = 9.9 \times 10^{-3}$; Supplementary Figure S9).

DISCUSSION

Our three-biobank meta-analysis found that CHIP was associated with an increased risk of incident SPRA, driven primarily by an increase in *DNMT3A*-CHIP–associated, late-onset SPRA. Furthermore, participants with *TET2*-CHIP and SPRA had an increased risk of all-cause mortality compared to participants with SPRA alone. Effect modification analysis found genetically predicted levels of classical complement proteins C1r and C1s may modify the CHIP-associated risk of SPRA. In UKB, autosomal mCA and mLOY were associated with an increased risk of SPRA.

The association between CHIP and incident SPRA with absence of association between CHIP and prevalent SPRA presents an apparent conflict. Straightforwardly, this observation may be the result of the reality that CHIP rarely occurs before middle age and RA generally onsets in older adulthood. However, results presented here suggest that differential survival may explain part of the enigma, with CHIP$^+$ patients with SPRA less likely to survive to the date of enrollment. Intriguingly, a final possibility is that the treatments rendered for RA may cause CHIP clones to shrink or resolve, as has been observed experimentally in nonhuman primates for one RA treatment, tocilizumab, though this phenomenon has not been observed in humans.[43]

Throughout this study, all analyses relating to SNRA were null. Due to the low incidence of SNRA (Table 1), this study had 80% power to detect a CHIP-associated hazard ratio for SNRA of 1.5, substantially larger than the 1.3 HR that could be detected with 80% power for SPRA. Furthermore, though CHIP has a well-known association with all-cause mortality that robustly replicated in the cohorts studied here (HR 1.35; $P = 9.4 \times 10^{-17}$; Supplementary Figure S8), there was no statistically significant CHIP–mortality association among people with prevalent SNRA. This negative result was most likely due to the study's ~10% power to detect a CHIP-associated effect with hazard ratio 1.35 among the 2,542 people with prevalent SNRA rather than a CHIP-mortality rescue phenomenon associated with SNRA. In summary, discordant results between SPRA and SNRA may reflect lack of power, biologic differences between SPRA and SNRA, or

the difficulty of studying SNRA with a biobank approach due to the high susceptibility for misclassification.

Negative effect modification by genetically predicted levels of early classical complement proteins C1r and C1s suggests that the classical pathway may buffer, rather than amplify, the CHIP-associated risk of SPRA. One explanation is that higher baseline C1r and C1s activity promotes more efficient opsonization and clearance of apoptotic and cellular debris, limiting dysregulated inflammatory signaling in the context of CHIP. These results motivate targeted mechanistic studies to test whether complement-mediated clearance pathways attenuate CHIP-associated risk for RA and other inflammatory diseases of aging. We note that circulating levels of complement components, particularly C4, are strongly influenced by gene copy number variation. Due to the lack of a C4 copy number genome-wide association study, the genetic instrument approach applied here is not feasible to assess how copy number variation influences the CHIP-associated risk for RA. Direct measurement of C4 copy number could be performed to more comprehensively define the role of the classical complement pathway in CHIP-associated RA risk. The strong association between mLOY and incident SPRA is consistent with prior work on prevalent SPRA.[22] Still, it was observed only in one biobank and merits replication in other biobanks. Similarly, the association between autosomal mCA and SPRA was statistically sound but merits replication. If these effects were found to be consistent across cohorts, mechanistic studies could begin to determine the pathways that relate these larger scale somatic genetic changes to RA.

The strengths of this study include its large sample size, considering >1 million research participants for inclusion and exclusion and ultimately studying 612,989. The large sample size permitted use of a phenotyping approach that prioritized specificity over sensitivity, as is critical for valid inference of uncommon outcomes. The phenotyping approach combined diagnosis codes, laboratory values, and medication prescriptions, yielding an estimated 99% specificity and overcoming a critical weakness of recent biobank-based work on CH and RA in which researcher ascertained RA status strictly from billing codes.[18,19,25,44] This study also made use of the longitudinal follow-up data in each biobank to conduct age-scale survival analysis, suggesting that CH may *cause* RA, rather than vice versa.

This study also has notable limitations. First, because general-purpose genetic sequencing was used to infer CHIP status, the ascertainment was neither sensitive nor specific.[24] Imperfect CHIP calls increase the risk of false-negative studies and attenuate the discernable risk but do not increase the risk of false-positive associations.[24] Furthermore, the size of a CHIP clone can have profound implications for health outcomes but cannot be estimated with general-purpose sequencing.[13,45] To address these weaknesses will require dedicated CHIP sequencing in the baseline samples of a cohort that has been followed longitudinally.

Second, the heterogeneity of biobank designs might complicate direct comparison of results across cohorts. Although sequencing depths were similar, recruitment strategies and the timing of blood sample collection differed. These differences likely contributed to the higher baseline prevalence of CHIP observed in the hospital-based BioVU cohort compared to the population-based AoU or UKB cohorts. To address this heterogeneity and the resulting differences in baseline risk, we used survival analyses on the age scale. This approach accounts for age-related risk nonparametrically and, importantly, satisfied the proportional hazards assumption across all biobanks, whereas the time-on-study scale did not.[46]

Third, because incident SPRA and SNRA are uncommon and our approach prioritized specificity over sensitivity, there were few events among participants with each kind of CH. A cohort in which more participants had CH or more participants developed RA would provide more powerful statistical inference. Relatedly, patients can move between health care systems in the United States, and electronic medical records may not always be accurately transferred with them. Therefore, some participants in BioVU and AoU who were adjudicated as incident cases may have truly been prevalent cases, misclassified due to missing medical records.

In conclusion, SPRA is a complex autoimmune disease with antigen-driven clonal proliferation of lymphocytes as a core pathophysiologic process. This study suggests that the pro-inflammatory, antigen-independent clonal proliferation of hematopoietic stem cells such as CHIP and mCA also play a role in SPRA pathogenesis. The classical complement cascade may modify the role of CH in RA pathogenesis. Work into mechanisms by which *DNMT3A*-CHIP, mCA, and mLOY drive the increased risk of SPRA merits attention as these insights might guide development of early interventions for patients with CHIP to avoid SPRA or precision interventions for patients with SPRA based on their CHIP status.

AUTHOR CONTRIBUTIONS

All authors contributed to at least one of the following manuscript preparation roles: conceptualization AND/OR methodology, software, investigation, formal analysis, data curation, visualization, and validation AND drafting or reviewing/editing the final draft. As corresponding author, Dr Corty confirms that all authors have provided the final approval of the version to be published and takes responsibility for the affirmations regarding article submission (eg, not under consideration by another journal), the integrity of the data presented, and the statements regarding compliance with institutional review board/Declaration of Helsinki requirements.

REFERENCES

1. Gravallese EM, Firestein GS. Rheumatoid arthritis - common origins, divergent mechanisms. N Engl J Med 2023;388(6):529–542. doi:10.1056/NEJMra2103726
2. Conrad N, Misra S, Verbakel JY, et al. Incidence, prevalence, and co-occurrence of autoimmune disorders over time and by age, sex, and

socioeconomic status: a population-based cohort study of 22 million individuals in the UK. Lancet 2023;401(10391):1878–1890. doi:10.1016/S0140-6736(23)00457-9

3. Kojima M, Sugihara T, Kawahito Y, et al. Consensus statement on the management of late-onset rheumatoid arthritis. Mod Rheumatol 2024;34(6):1095–1102. doi:10.1093/mr/roae011
4. Mena-Vázquez N, Lisbona-Montañez JM, Redondo-Rodriguez R, et al. Inflammatory profile of incident cases of late-onset compared with young-onset rheumatoid arthritis: a nested cohort study. Front Med (Lausanne) 2022;9:1016159. doi:10.3389/fmed.2022.1016159
5. Sugitani N, Tanaka E, Inoue E, et al. Higher risk of poor functional outcome and unfavourable clinical events for late-onset rheumatoid arthritis: results from the IORRA cohort. Rheumatology (Oxford) 2025;64(5):2541–2549. doi:10.1093/rheumatology/keae673
6. Zimba O, Baimukhamedov C, Kocyigit BF. Late-onset rheumatoid arthritis: clinical features, diagnostic challenges, and treatment approaches. Rheumatol Int 2025;45(6):152. doi:10.1007/s00296-025-05908-1
7. Arnold MB, Bykerk VP, Boire G, et al; CATCH Investigators. Are there differences between young- and older-onset early inflammatory arthritis and do these impact outcomes? An analysis from the CATCH cohort. Rheumatology (Oxford) 2014;53(6):1075–1086. doi:10.1093/rheumatology/ket449
8. Banda NK, Deane KD, Bemis EA, et al. Analysis of complement gene expression, clinical associations, and biodistribution of complement proteins in the synovium of early rheumatoid arthritis patients reveals unique pathophysiologic features. J Immunol 2022;208(11):2482–2496. doi:10.4049/jimmunol.2101170
9. Steensma DP, Bejar R, Jaiswal S, et al. Clonal hematopoiesis of indeterminate potential and its distinction from myelodysplastic syndromes. Blood 2015;126(1):9–16. doi:10.1182/blood-2015-03-631747
10. Jaiswal S, Natarajan P, Silver AJ, et al. Clonal hematopoiesis and risk of atherosclerotic cardiovascular disease. N Engl J Med 2017;377(2):111–121. doi:10.1056/NEJMoa1701719
11. Jaiswal S, Fontanillas P, Flannick J, et al. Age-related clonal hematopoiesis associated with adverse outcomes. N Engl J Med 2014;371(26):2488–2498. doi:10.1056/NEJMoa1408617
12. Bick AG, Weinstock JS, Nandakumar SK, et al; NHLBI Trans-Omics for Precision Medicine Consortium. Inherited causes of clonal haematopoiesis in 97,691 whole genomes. Nature 2020;586(7831):763–768. doi:10.1038/s41586-020-2819-2
13. Ezzat D, Uddin MM, Xue L, et al. Clonal hematopoiesis and cardiovascular outcomes in older women. J Am Coll Cardiol 2025;86(15):1093–1106. doi:10.1016/j.jacc.2025.07.058
14. Robinette ML, Weeks LD, Kramer RJ, et al. Association of somatic TET2 mutations with giant cell arteritis. Arthritis Rheumatol 2024;76(3):438–443. doi:10.1002/art.42738
15. Agrawal M, Niroula A, Cunin P, et al. TET2-mutant clonal hematopoiesis and risk of gout. Blood 2022;140(10):1094–1103. doi:10.1182/blood.2022015384
16. Lin S-H, Brown DW, Rose B, et al. Incident disease associations with mosaic chromosomal alterations on autosomes, X and Y chromosomes: insights from a phenome-wide association study in the UK Biobank. Cell Biosci 2021;11(1):143. doi:10.1186/s13578-021-00651-z
17. Zhao K, Pershad Y, Poisner HM, et al. Genetic drivers and clinical consequences of mosaic chromosomal alterations in 1 million individuals. medRxiv Preprint posted online March 6, 2025. doi:10.1101/2025.03.05.25323443
18. Hiitola E, Korhonen J, Kokkonen H, et al; FinnGen. Clonal hematopoiesis is associated with distinct rheumatoid arthritis phenotypes. Sci Adv 2025;11(18):eadt9846. doi:10.1126/sciadv.adt9846
19. Kronzer VL, Williamson KA, Hanson AC, et al. Quantifying and improving rheumatoid arthritis algorithm performance in biobank settings. Semin Arthritis Rheum 2025;72:152668. doi:10.1016/j.semarthrit.2025.152668
20. Ng B, Aslam F, Petersen NJ, et al. Identification of rheumatoid arthritis patients using an administrative database: a Veterans Affairs study. Arthritis Care Res (Hoboken) 2012;64(10):1490–1496. doi:10.1002/acr.21736
21. Singh JA, Holmgren AR, Noorbaloochi S. Accuracy of Veterans Administration databases for a diagnosis of rheumatoid arthritis. Arthritis Rheum 2004;51(6):952–957. doi:10.1002/art.20827
22. Uchiyama S, Ishikawa Y, Ikari K, et al. Mosaic loss of chromosome Y characterises late-onset rheumatoid arthritis and contrasting associations of polygenic risk score based on age at onset. Ann Rheum Dis 2025;84(8):1313–1323. doi:10.1016/j.ard.2025.01.034
23. Walport MJ. Complement. Second of two parts. N Engl J Med 2001;344(15):1140–1144. doi:10.1056/NEJM200104123441506
24. Corty R, Pershad Y, Vlasschaert C, et al. Detection of clonal hematopoiesis of indeterminate potential via genome or exome sequencing profoundly underestimates disease associations. medRxiv Preprint posted online August 16, 2025. doi:10.1101/2025.08.11.25333294
25. Saka-Herrán C, Bennett J, Alkabti Y, et al. Accuracy of diagnostic codes and algorithms used to identify rheumatoid arthritis and juvenile idiopathic arthritis in administrative claims and electronic health records: systematic review and meta-analysis. Arthritis Care Res (Hoboken) Published online October 16, 2025. doi:10.1002/acr.25662
26. Liao KP, Cai T, Gainer V, et al. Electronic medical records for discovery research in rheumatoid arthritis. Arthritis Care Res (Hoboken) 2010;62(8):1120–1127. doi:10.1002/acr.20184
27. Chung CP, Rohan P, Krishnaswami S, et al. A systematic review of validated methods for identifying patients with rheumatoid arthritis using administrative or claims data. Vaccine 2013;31(suppl 10):K41–K61. doi:10.1016/j.vaccine.2013.03.075
28. Vlasschaert C, Mack T, Heimlich JB, et al. A practical approach to curate clonal hematopoiesis of indeterminate potential in human genetic data sets. Blood 2023;141(18):2214–2223.
29. Zhao K, Hsu CC, Pershad Y, et al. Interleukin-17 receptor-A signalling: atheroprotective role in JAK2 clonal haematopoiesis. Eur Heart J 2025;46(48):5292–5295. doi:10.1093/eurheartj/ehaf737
30. McKenna A, Hanna M, Banks E, et al. The Genome Analysis Toolkit: a MapReduce framework for analyzing next-generation DNA sequencing data. Genome Res 2010;20(9):1297–1303. doi:10.1101/gr.107524.110
31. Van der Auwera GA, O'Connor BD. Genomics in the Cloud: Using Docker, GATK, and WDL in Terra. O'Reilly Media, Inc; 2020.
32. Loh P-R, Genovese G, McCarroll SA. Monogenic and polygenic inheritance become instruments for clonal selection. Nature 2020;584(7819):136–141. doi:10.1038/s41586-020-2430-6
33. Xu Y, Ritchie SC, Liang Y, et al. An atlas of genetic scores to predict multi-omic traits. Nature 2023;616(7955):123–131. doi:10.1038/s41586-023-05844-9
34. Avery C, Babanejad M, Baker J, et al. Genome sequencing of 35,024 predominantly African ancestry persons addresses gaps in genomics and healthcare. medRxiv Preprint posted online November 2, 2025. doi:10.1101/2025.10.30.25338549
35. Privé F, Luu K, Blum MGB, et al. Efficient toolkit implementing best practices for principal component analysis of population genetic data. Bioinformatics 2020;36(16):4449–4457. doi:10.1093/bioinformatics/btaa520
36. Sharma S, Nagar SD, Pemu P, et al; SEEC Consortium. Genetic ancestry and population structure in the All of Us Research Program

cohort. Nat Commun 2025;16(1):4123. doi:10.1038/s41467-025-59351-8

37. Cologne J, Hsu WL, Abbott RD, et al. Proportional hazards regression in epidemiologic follow-up studies: an intuitive consideration of primary time scale. Epidemiology 2012;23(4):565–573. doi:10.1097/EDE.0b013e318253e418
38. Thiébaut ACM, Bénichou J. Choice of time-scale in Cox's model analysis of epidemiologic cohort data: a simulation study. Stat Med 2004;23(24):3803–3820. doi:10.1002/sim.2098
39. Grambsch PM, Therneau TM. Proportional hazards tests and diagnostics based on weighted residuals. Biometrika 1994;81(3):515–526. doi:10.1093/biomet/81.3.515
40. Rao G, Lopez-Jimenez F, Boyd J, et al; American Heart Association Council on Lifestyle and Cardiometabolic Health; Council on Cardiovascular and Stroke Nursing; Council on Cardiovascular Surgery and Anesthesia; Council on Clinical Cardiology; Council on Functional Genomics and Translational Biology; and Stroke Council. Methodological standards for meta-analyses and qualitative systematic reviews of cardiac prevention and treatment studies: a scientific statement from the American Heart Association. Circulation 2017;136(10):e172–e194. doi:10.1161/CIR.0000000000000523
41. Benjamini Y, Hochberg Y. Controlling the false discovery rate: a practical and powerful approach to multiple testing. J R Stat Soc Series B Stat Methodol 1995;57(1):289–300. doi:10.1111/j.2517-6161.1995.tb02031.x
42. Sedgwick P. Multiple hypothesis testing and Bonferroni's correction. BMJ 2014;349:g6284. doi:10.1136/bmj.g6284
43. Shin T-H, Zhou Y, Chen S, et al. A macaque clonal hematopoiesis model demonstrates expansion of TET2-disrupted clones and utility for testing interventions. Blood 2022;140(16):1774–1789. doi:10.1182/blood.2021014875
44. Zhang J, Zhou C, Guan S. Association between rheumatoid arthritis and clonal hematopoiesis: a Mendelian randomization study. Twin Res Hum Genet 2024;27(3):169–173. doi:10.1017/thg.2024.24
45. Zhao K, Shen X, Liu H, et al. Somatic and germline variants and coronary heart disease in a Chinese population. JAMA Cardiol 2024;9(3):233–242. doi:10.1001/jamacardio.2023.5095
46. Vyas MV, Fang J, Kapral MK, et al. Choice of time-scale in time-to-event analysis: evaluating age-dependent associations. Ann Epidemiol 2021;62:69–76. doi:10.1016/j.annepidem.2021.06.006

Check for updates

Arthritis & Rheumatology
Vol. 78, No. 10, October 2026, pp 2074–2081
DOI 10.1002/art.70158
Published 2026. This article is a U.S. Government work and is in the public domain in the USA. *Arthritis & Rheumatology* published by Wiley Periodicals LLC on behalf of American College of Rheumatology.
This is an open access article under the terms of the Creative Commons Attribution-NonCommercial License, which permits use, distribution and reproduction in any medium, provided the original work is properly cited and is not used for commercial purposes.

American College of Rheumatology
Empowering Rheumatology Professionals

BRIEF REPORT

Anti-Carbamylated Protein Antibodies Stabilize Carbamylated Histone H3 to Promote Synovial Activation and Neutrophil Extracellular Trap-Mediated Bone Loss in Rheumatoid Arthritis

Shuichiro Nakabo, MD, PhD,[1] Norio Hanata, MD, PhD,[1] Eduardo Patino-Martinez, PhD,[1] Ronald Holewinski, PhD,[2] Ana Barrera-Vargas, MD,[3] Javier Merayo-Chalico, MD,[4] Scott A. Coonrod, MD,[5] David A. Fox, MD,[6] Mariana J. Kaplan, MD,[1] and Carmelo Carmona-Rivera, PhD[1]

Objective. Carbamylation, a nonenzymatic post-translational modification, contributes to rheumatoid arthritis (RA) pathogenesis. Anti-carbamylated protein antibodies (anti-CarP) occur in around 50% of patients with RA and associate with greater joint damage. Neutrophil extracellular traps (NETs) are a major source of carbamylated autoantigens. We sought to study how carbamylation and anti-CarP antibodies promote joint pathology.

Methods. NETs were generated with calcium ionophore and analyzed for carbamylation by immunofluorescence, flow cytometry, and mass spectrometry. Enzymatic pathways were interrogated using pharmacologic inhibitors and peptidyl arginine deiminase (PAD)2/4 deficient mice. Degradation kinetics of carbamylated histone H3 (carH3) were evaluated with neutrophil elastase (NE) and anti-CarP IgG from patients with RA. Toll-like receptor 4 (TLR4) activation was quantified using a HEK293 reporter line. RA fibroblast-like synoviocytes (FLS) were stimulated with carH3 or carH3-IgG immune complexes (ICs) and profiled by RNA-sequencing and enzyme-linked immunosorbent assay.

Results. Histone carbamylation, especially of H3, occurred during NETosis and was independent of peptidylarginine deiminase-4, myeloperoxidase, NE, or oxidative pathways. CarH3 was rapidly degraded by NE, but anti-CarP antibodies protected it from proteolysis. NETs exposed to anti-CarP IgG triggered stronger TLR4 activation and enhanced osteoclastogenesis. In FLS, carH3 and particularly carH3-ICs induced robust up-regulation of pro-inflammatory genes and cytokine secretion (interleukin [IL-]6, IL-8, MCP-1, GM-CSF). Transcriptomic analysis revealed enrichment of immune activation, chemotaxis, and angiogenesis pathways, most pronounced with carH3-IC.

Conclusion. Anti-CarP antibodies stabilize carH3 within NETs, amplifying its pro-inflammatory and osteoclastogenic activity. The resulting carH3-IgG ICs potently activate FLS, linking humoral immunity to tissue inflammation and bone destruction in RA. These findings identify carH3 stabilization as a potential therapeutic target in antibody-mediated joint damage.

Supported in part by the Intramural Research Program of the National Institutes of Health (ZIA-AR-041199) and KAKENHI (#25K19593).

[1]Systemic Autoimmunity Branch, National Institute of Arthritis and Musculoskeletal and Skin Diseases, National Institutes of Health, Bethesda, Maryland; [2]Frederick National Laboratory for Cancer Research, National Institutes of Health, Bethesda, Maryland; [3]Department of Medical Education, Instituto Nacional de Ciencias Médicas y de la Nutrición, Salvador Zubirán, Mexico City, Mexico; [4]Department of Immunology and Rheumatology, Instituto Nacional de Ciencias Médicas y de la Nutrición, Salvador Zubirán, Mexico City, Mexico; [5]Baker Institute for Animal Health, College of Veterinary Medicine, Cornell University, Ithaca, New York; [6]Division of Rheumatology and Clinical Autoimmunity Center of Excellence, Department of Internal Medicine, University of Michigan, Ann Arbor, Michigan.

Dr Nakobo's current address is the Department of Advanced Medicine for Rheumatic Diseases, Kyoto University, Kyoto, Japan.

Additional supplementary information cited in this article can be found online in the Supporting Information section (https://acrjournals.onlinelibrary.wiley.com/doi/10.1002/art.70158).

Author disclosures and graphical abstract are available at https://onlinelibrary.wiley.com/doi/10.1002/art.70158.

Address correspondence via email to Carmelo Carmona-Rivera, PhD at carmelo.carmona-rivera@nih.gov.

Submitted for publication October 22, 2025; accepted in revised form February 20, 2026.

INTRODUCTION

Rheumatoid arthritis (RA) is a chronic autoimmune disease characterized by synovial inflammation, cartilage destruction, and periarticular bone erosion that affects approximately 1% of the global population.[1] A hallmark of RA is the presence of autoantibodies targeting post-translationally modified (PTM) proteins, most notably anti-citrullinated protein antibodies (ACPAs), which can precede clinical onset by years and correlate with disease severity.[1,2] In addition to citrullination, carbamylation, which is a nonenzymatic modification of lysine residues mediated by cyanate, has emerged as another critical PTM in RA. Approximately 40% to 50% of patients with RA develop anti-carbamylated protein (anti-CarP) antibodies, and their presence associates with greater joint damage, bone erosion, and death.[2–5]

Neutrophils, which are abundant in RA synovial tissue, play a central role in both inflammation and tissue injury.[6,7] Through the formation of neutrophil extracellular traps (NETs), which are web-like structures composed of DNA, histones, and granule enzymes such as myeloperoxidase (MPO) and neutrophil elastase (NE), neutrophils externalize modified autoantigens, including citrullinated and carbamylated proteins.[8,9] Excessive NET formation or defective clearance has been implicated in autoimmune pathology, including RA.

We and others have shown that NETs are enriched in RA synovial lesions and contain carbamylated proteins capable of stimulating both innate and adaptive immune responses.[3,4,7,9] Carbamylated NETs can promote osteoclastogenesis, driving bone resorption independently of the canonical RANKL pathway through Toll-like receptor 4 (TLR4)-dependent activation by NET-derived DNA, histones, and NE.[10]

Despite these insights, key questions remain regarding how carbamylated proteins within NETs are generated, stabilized, and rendered immunogenic. Although MPO-mediated cyanate production likely contributes to protein carbamylation, the role of NE in processing and degrading carbamylated NET proteins, particularly histones, remains unclear. We hypothesized that anti-CarP antibodies may stabilize carbamylated histones by shielding them from NE-mediated degradation, thereby sustaining proinflammatory and osteoclastogenic signaling in RA.

In this study, we demonstrate that anti-CarP antibodies protect carbamylated histone H3 (carH3) from elastase–mediated degradation, promoting the persistence of carH3–IgG immune complexes (ICs) that enhance fibroblast activation and osteoclast differentiation. These findings define a novel mechanism linking neutrophil-derived PTMs, humoral immunity, and bone destruction in RA, and reveal previously unrecognized mechanisms by which anti-CarP antibodies amplify osteoimmune pathology.

MATERIALS AND METHODS

Human study population. Participants diagnosed with RA fulfilled the 2010 classification criteria established by the American College of Rheumatology.[11,12] All participants provided written informed consent and were enrolled in a study protocol approved by the Ethics Committee of the Instituto Nacional de Ciencias Médicas y de la Nutrición Salvador Zubirán (INCMNSZ, reference number 1243). Healthy control participants were recruited through public advertisement. Peripheral blood was collected into EDTA tubes and samples were fractionated by Ficoll-Paque Plus (GE Healthcare) density gradient centrifugation. Neutrophils were subsequently isolated by dextran sedimentation followed by hypotonic lysis of erythrocytes, as described in past protocols.[6,9]

Isolation of mouse neutrophil. Mouse neutrophils were isolated from bone marrow extracted from femurs and tibias using a negative selection approach with the Mouse Neutrophil Isolation Kit (Miltenyi Biotec). Breeding pairs of PAD2/4 double-knockout (DKO) mice were provided by Dr Scott Coonrod (Cornell University), whereas wild-type (WT) (C57BL/6J) and MPO-deficient mice were obtained from The Jackson Laboratory. All animals were maintained under specific pathogen-free conditions. Experimental procedures adhered to the guidelines set forth by the National Institutes of Health (NIH) and were approved by the Animal Care and Use Committee of the National Institute of Arthritis and Musculoskeletal and Skin Diseases (NIAMS) under protocol number A022-08-03.

Histone purification. Neutrophil histones were purified using the Histone Purification Mini Kit (Active Motif) following the manufacturer's protocol.

Immunofluorescence analysis. Immunofluorescence analysis was performed as previously described.[9] In brief, neutrophils were fixed overnight in 4% paraformaldehyde at 4°C, washed, permeabilized by 0.2% Triton-X100 for 10 minutes (for intracellular carbamylated protein staining), and blocked with 0.2% porcine gelatin for 30 minutes. Cells were then incubated with primary antibodies for 1 hour at 37°C in a humid chamber, which was followed by secondary antibody incubation for 30 minutes. Nuclei were counterstained with Hoechst (1:1000) and after final washes, coverslips were mounted using ProLong Gold (Invitrogen). Images were captured using a Leica microscope.

Mass spectrometry. Detection of carbamylation was done as previously described.[9] Briefly, extracted histones from neutrophils treated with calcium ionophore were separated by sodium dodecyl sulfate–polyacrylamide gel electrophoresis (SDS-PAGE), stained with Coomassie blue, and processed for in-gel trypsin digestion. The resulting peptides were analyzed by nanoLC-MS/MS using an Ultimate 3000 system coupled to an Orbitrap Lumos Tribrid mass spectrometer. Peptides were

separated on an EASY-Spray C18 column with a 65-minute acetonitrile gradient. MS data were acquired in data-dependent mode and processed using Proteome Discoverer (v2.4) with Byonic for identification of carbamylated and citrullinated peptides, applying strict search parameters and an false discovery rate (FDR) threshold of less than 2%. Neutral loss of isocyanic acid from carbamylated peptides was also examined.

Statistical analysis. Statistical analyses and graph generation were performed using GraphPad Prism 9.5.1 (GraphPad Software). Data are expressed as mean ± SEM. Normality was assessed with the Shapiro-Wilk test. Depending on data distribution, comparisons were made using two-tailed unpaired *t*-tests or nonparametric tests (Mann-Whitney for two groups; one-way analysis of variance or Kruskal-Wallis with post hoc analysis for multiple groups). Exact *P* values are provided in the figure legends. Data will be shared upon request.

RESULTS

Neutrophil histone carbamylation during NETosis is independent of PAD, MPO, and oxidative pathways. We previously demonstrated that NETs from activated neutrophils of patients with RA contain carbamylated proteins.[9] Here, we examined whether carbamylation occurs in resting neutrophils, how it changes after activation, and which enzymatic pathways contribute to this process.

Immunofluorescence of unstimulated peripheral blood human neutrophils revealed a nuclear carbamylation signal predominantly localized to euchromatin (decondensed) regions (Figure 1A). Following calcium ionophore (A23187) stimulation, nuclear carbamylation increased markedly and colocalized with DNA throughout the nucleus (Figure 1B). Time-course imaging showed that carbamylation peaked before full NET release and declined as chromatin was expelled (Figure 1C), indicating that carbamylation is an intrinsic neutrophil feature that diminishes during NET extrusion.

Mass spectrometry identified multiple carbamylated histone peptides, particularly histone H3, confirming histones as major carbamylation targets in NETs (Figure 1D). Flow cytometry demonstrated that approximately 10% of neutrophils were carbamylation-positive at baseline, rising to around 20% after ionophore stimulation (Figure 1E).

To determine whether certain peptidyl arginine deiminases (PAD2/PAD4) mediate this modification, we used both pharmacologic and genetic approaches. Treatment with the pan-PAD inhibitor Cl-amidine did not affect carbamylation frequency (Figure 1F). Likewise, bone- marrow neutrophils from PAD2/PAD4 DKO mice exhibited robust carbamylation after ionophore stimulation. In contrast, citrullinated histone H3 was increased in WT but absent in PAD2/4-deficient neutrophils, confirming antibody specificity and the distinct nature of the two PTMs (Figure 1G). Thus, histone carbamylation occurs independently of PAD activity and is mechanistically distinct from citrullination.

Because MPO and NE are key drivers of NET formation, we next tested whether they influence carbamylation. Inhibiting MPO (4-aminobenzoic acid hydrazide [4-ABAH]) or NE (alvelestat) during calcium ionophore stimulation did not reduce carbamylation (Figure 1F and I). Similarly, neutrophils from MPO-deficient mice retained carbamylation capacity (Figure 1H), indicating that MPO is dispensable. Inhibition of NADPH oxidase with diphenyleneiodonium or the antioxidant treatment with N-acetylcysteine likewise had no effect on carbamylation (Supplementary Figure 1). Collectively, these results demonstrate that nuclear histone carbamylation is an intrinsic neutrophil process that increases during NET formation and occurs independently of PAD enzymes, MPO, NE, and oxidative pathways.

Anti-CarP antibodies protect carbamylated histone H3 from neutrophil elastase–mediated degradation. Because histone H3 emerged as a principal target of carbamylation and carbamylation levels declined during NET formation, we next examined the stability of carH3. Neutrophils were stimulated with calcium ionophore, and purified histones were analyzed by Western blot. Immunoblotting with an anti-carbamylation antibody revealed a loss of intact carH3 (15–20 kDa) and the appearance of a lower MW fragment (~10 kDa), consistent with proteolytic cleavage. Probing for total histone H3 confirmed this degradation pattern (Figure 2A).

To identify the protease responsible, we inhibited MPO and NE using 4-ABAH and alvelestat, respectively. MPO inhibition had no effect, whereas NE inhibition markedly reduced carH3 degradation, preserving the intact 20–15 kDa band and reducing the 10 kDa fragment (Figure 2A), implicating NE in carH3 proteolysis during NET formation.

A time-course comparison of unmodified and carH3 exposed to NE further demonstrated that carH3 was degraded rapidly, within one minute, whereas unmodified histone H3 persisted for up to 60 minutes (Figure 2B). Pre-incubation of carH3 with an anti-carbamylated lysine (carLys) antibody delayed degradation, with intact protein detectable up to 10 minutes, suggesting that masking carbamylated lysines can partially block NE recognition (Figure 2B). Similarly, carbamylated histone H4 was more susceptible to NE-mediated degradation than its unmodified counterpart (Supplementary Figure 2).

To determine whether anti-CarP antibodies from patients with RA exert similar protective effects, recombinant carH3 was incubated with IgG purified from anti-CarP$^+$ or anti-CarP$^-$ RA sera. CarH3 was significantly protected from degradation in the presence of anti-CarP$^+$ IgGs (Figure 2C). Finally, when neutrophils were stimulated with calcium ionophore in the presence of IgGs from anti-CarP$^+$ or anti-CarP$^-$ in patients with RA, NETs generated with anti-CarP$^+$ IgGs contained higher levels of intact histone H3 than those incubated with anti-CarP$^-$ IgG (Figure 2D and E). IgGs isolated from anti-CarP$^-$ patients exhibited elevated ACPA

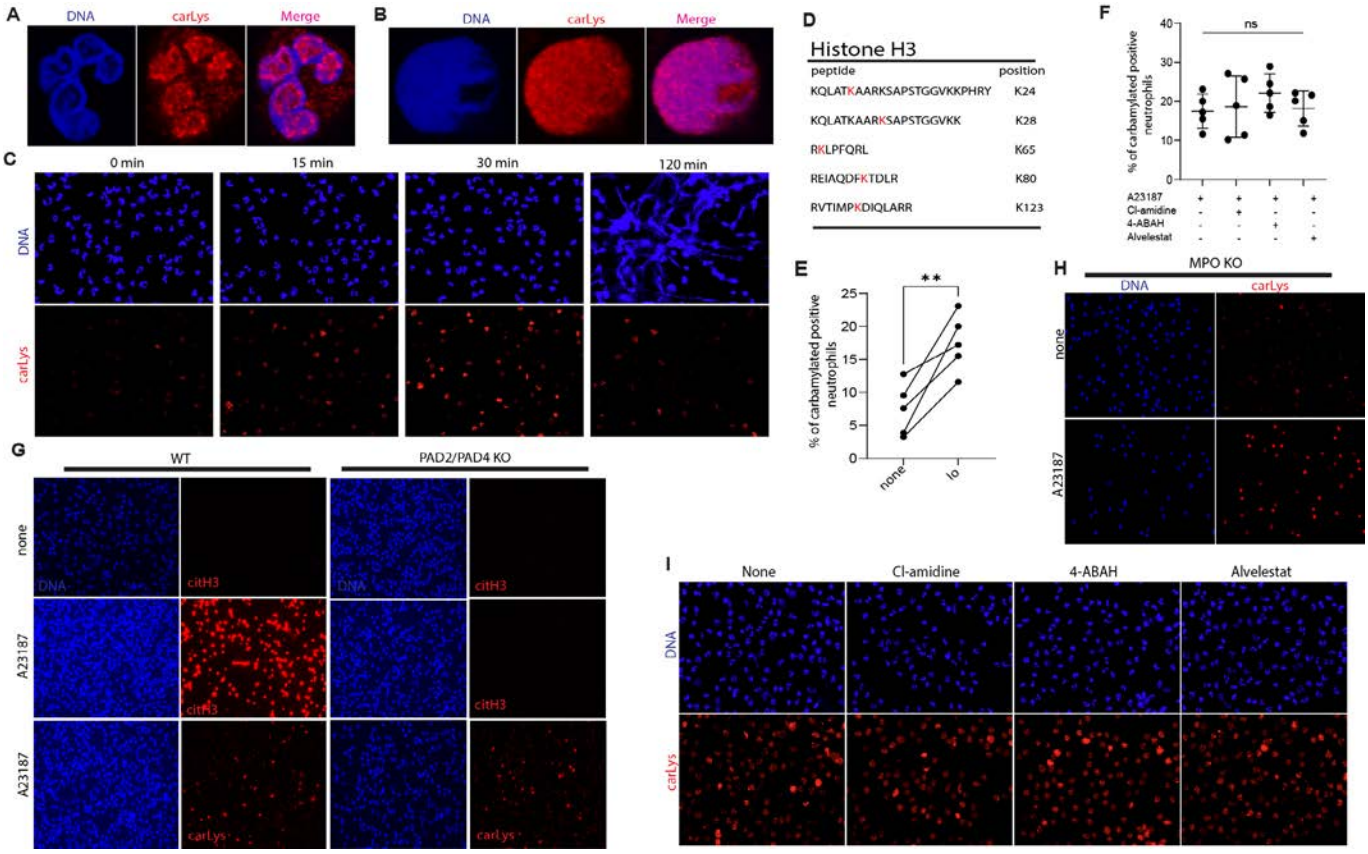


Figure 1. Intrinsic carbamylation of histones in neutrophils. Immunofluorescence of purified neutrophils from healthy donors at steady state (A) and after two hours of stimulation with calcium ionophore A23187 (B). Images were acquired at 63× original magnification. (C) Time-course analysis of histone carbamylation in neutrophils stimulated with calcium ionophore. Red, carbamylated lysines; blue, DNA. Images are representative of four independent experiments and were acquired at 40× original magnification. (D) Mass spectrometry of isolated neutrophil nuclei following calcium ionophore stimulation. Red marks indicate carbamylated lysines and their peptide positions. (E) Flow cytometry quantification of carbamylation-positive neutrophils at baseline and after stimulation with calcium ionophore. Data represent mean ± SEM from five independent experiments; statistical significance assessed by Mann-Whitney U test. (F) Flow cytometric analysis of neutrophils pretreated with inhibitors of PAD (Cl-amidine), MPO (4-ABAH), or NE (alvelestat) followed by stimulation with calcium ionophore. Data represent the mean ± SEM from five independent experiments. Mann-Whitney U test was used for statistical analysis. (G) and (H) Immunofluorescence of bone marrow neutrophils from WT, PAD2/PAD4 DKO, or MPO KO mice following stimulation with calcium ionophore. Histone carbamylation and/or citrullination were assessed. Images are representative of three independent experiments. Images were acquired at 20× original magnification. (I) Representative immunofluorescence images of human neutrophils stimulated with calcium ionophore in the presence or absence of Cl-amidine, 4-ABAH, or alvelestat, showing histone carbamylation. 4-ABAH, 4-aminobenzoic acid hydrazide; carLys, carbamylated lysine; DKO, double knockout; MPO, myeloperoxidase; NE, neutrophil elastase; PAD, peptidylarginine deiminase; WT, wild-type.

titers (see Supplementary Table 1), indicating that the effects observed in these experiments are unlikely to be confounded by ACPAs.

Collectively, these findings demonstrate that carbamylation increases histone susceptibility to NE-mediated degradation and that anti-CarP antibodies can stabilize carbamylated histone H3 both in vitro and during NET formation, preserving it as a potential autoantigen within the RA inflammatory environment.

Anti-CarP antibodies enhance the pro-osteoclastogenic and pro-inflammatory effects of carbamylated histone H3. We previously showed that levels of carH3 are elevated in RA and correlate with anti-CarP antibody titers.[9,10] Carbamylated NETs (cNETs) promote rapid osteoclastogenesis through carH3-dependent TLR4 activation.[10] Based on these observations, we hypothesized that anti-CarP antibodies stabilize carH3, protecting it from degradation and enhancing its ability to activate TLR4 and drive bone resorption.

To test this, purified NETs were incubated with IgG from patients with RA who were positive or negative for anti-CarP antibodies. NETs exposed to anti-CarP^{+} IgG induced significantly greater TLR4 activation in a HEK-Blue reporter assay compared with NETs treated with anti-CarP^{-} IgG (Figure 3A), consistent with antibody-mediated protection of carH3 from elastase degradation.

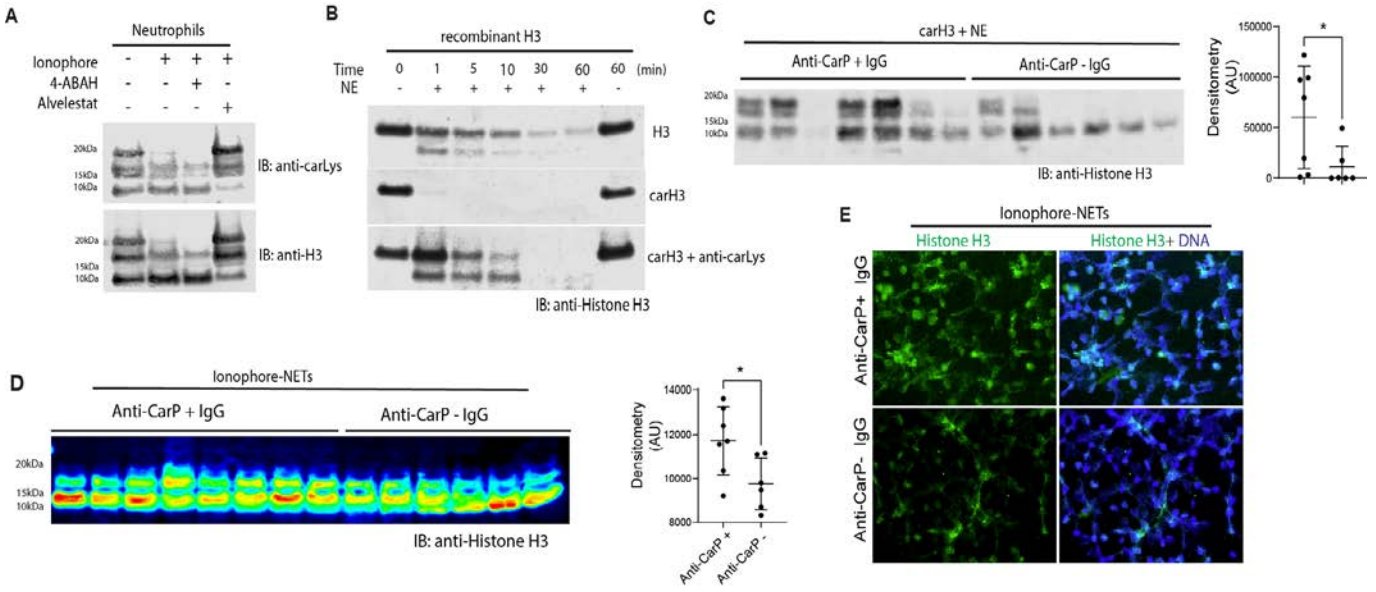


Figure 2. Anti-CarP antibodies protect carbamylated histone h3 from neutrophil elastase–mediated degradation. (A) Western blot analysis of total histone H3 and carbamylated histone H3 (carH3) from neutrophils stimulated with calcium ionophore in the presence or absence of MPO (4-ABAH) and/or NE (alvelestat) inhibitors. A ~10 kDa band indicates degraded histone fragments, whereas bands around 15–20 kDa represent intact histone H3. (B) Time-course degradation assay of recombinant histone H3 and carH3 in vitro, with or without anti-carbamylated lysine antibodies and/or recombinant NE. (C) Representative Western blot showing degradation of in vitro carH3 by recombinant NE in the presence of purified IgG from anti-CarP$^+$ (n = 7) or anti-CarP$^-$ (n = 6) patients with RA. Densitometric quantification of histone remnants is shown in the panel to the right. Data represent the mean ± SEM. Mann-Whitney U test was used for statistical analysis. *P < 0.05. (D) Western blot analysis of histones from calcium ionophore-induced NETs incubated with purified IgG from anti-CarP$^+$ (n = 7) or anti-CarP$^-$ (n = 6) patients with RA. Densitometry of histone remnants is shown to the right. Data represent the mean ± SEM. Mann-Whitney U test was used for statistical analysis. *P < 0.05. (E) Representative immunofluorescence images of NETs generated with calcium ionophore in the presence or absence of IgG from anti-CarP$^+$ or anti-CarP$^-$ patients with RA. Histones are stained green; DNA is stained in blue. Images are representative of three independent experiments and acquired at 40× original magnification. 4-ABAH, 4-aminobenzoic acid hydrazide; anti-CarP, anti-carbamylated protein; carH3, carbamylated histone H3; carLys, carbamylated lysine; MPO, myeloperoxidase; NE, neutrophil elastase; NETs, neutrophil extracellular traps; RA, rheumatoid arthritis.

We next evaluated the functional consequence of this effect on osteoclastogenesis. CD14$^+$ monocytes cultured with cNETs differentiated into osteoclasts, an effect significantly amplified by the presence of purified IgG from anti-CarP$^+$ patients with RA and reduced with exposure to anti-CarP$^-$ IgG (Figure 3B). These findings suggest that anti-CarP antibodies potentiate cNET-driven osteoclast differentiation, likely through stabilization of carH3 and enhanced TLR4 signaling.

To assess the impact of carH3 on fibroblast-like synoviocytes (FLS) activation, we stimulated osteoarthritis-derived FLS (OA FLS), chosen for their immunologically naïve baseline, with carH3 or carH3–IgG ICs. Quantitative polymerase chain reaction analysis showed induction of *IL6* and *IL8* by carH3, which was further potentiated by carH3-IgG ICs (Figure 3C). Similar changes were also observed in RA-derived FLS at 24 hours, although with a lesser magnitude, which we believe reflects their pre-activated or "primed" state (Supplementary Figure 3A). RNA-sequencing profiling confirmed broad transcriptional activation by both stimuli relative to unstimulated controls (Figure 3D). CarH3 up-regulated pro-inflammatory (*IL6*, *TNFAIP3*, *NFKBIZ*), chemotactic (*CXCL1*, *CXCL5*, and *CXCL8*) and matrix-remodeling (*MMP1*, *PTGS2*) genes, whereas carH3-IC elicited a stronger response, further enhancing expression of *IL6*, *CXCL13*, *TNFAIP6*, and additional *CXCL/CCL* chemokines (Figure 3D).

Gene ontology analysis revealed that carH3 stimulation enriched for pathways related to innate immune activation and granulocyte migration (Figure 3E), whereas carH3-IC additionally activated antimicrobial, inflammatory, leukocyte migration, and lipid-response pathways (Figure 3F). Direct comparison showed that IC formation amplified networks linked to immune modulation, angiogenesis, and antiviral responses (Figure 3G and H). These transcriptional changes translated into enhanced cytokine secretion, with enzyme-linked immunosorbent assay demonstrating increased release of interleukin (IL)-6, IL-8, MCP-1, and GM-CSF in OA FLS, most prominently in response to carH3–IC (Figure 3I). IL-6 and IL-8 were also significantly elevated in RA-derived FLS treated with carH3–IgG complexes, indicating that the effect extends to pre-activated, disease-relevant synovial fibroblasts (Supplementary Figure 3B).

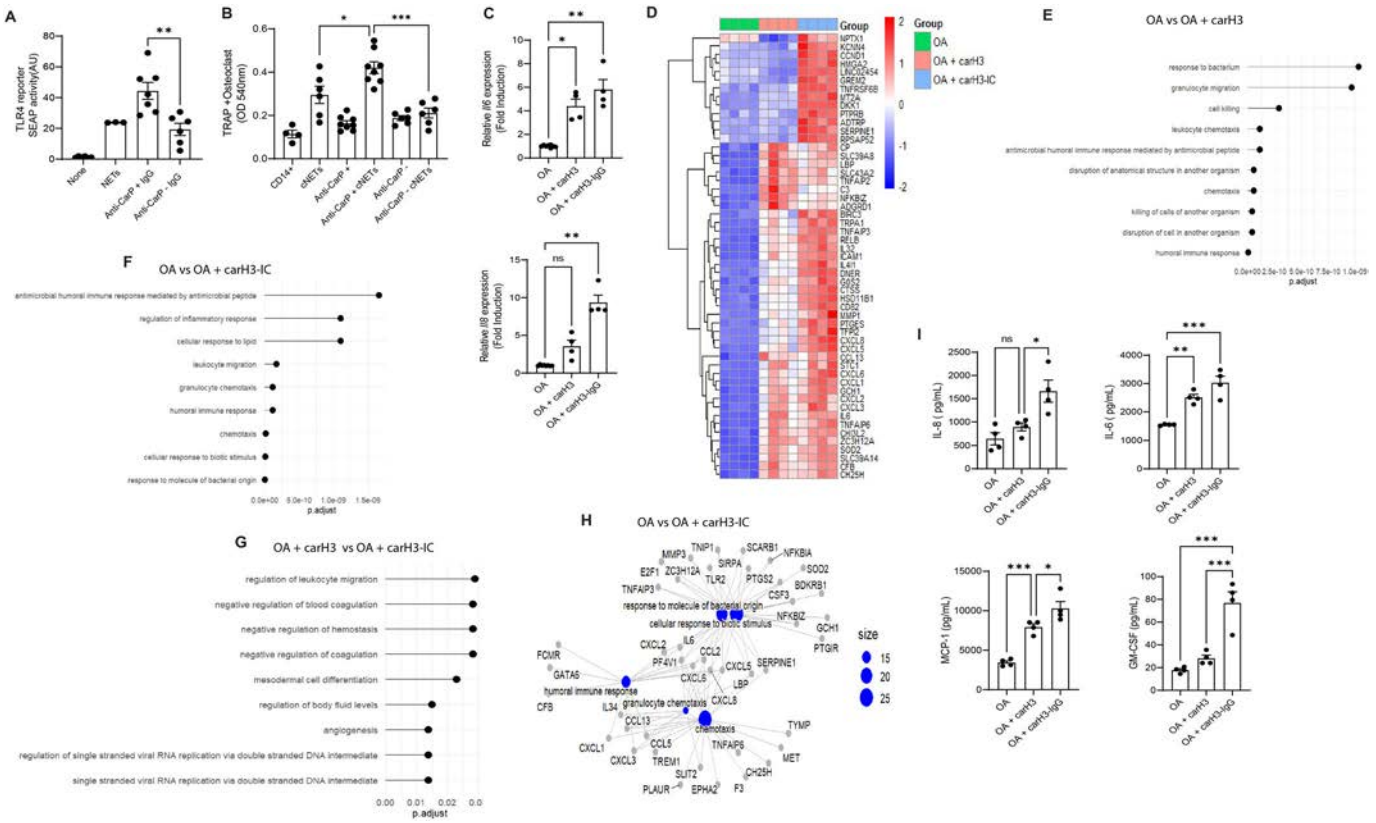


Figure 3. Carbamylated histone H3–IgG ICs trigger osteoclastogenesis and inflammatory responses in FLS. (A) SEAP-TLR4 reporter assay measuring TLR4 activation by calcium ionophore-induced NETs incubated with purified IgG from anti-CarP^{+} or (n = 7) or anti-CarP^{-} (n = 6) patients with RA. Results are shown as mean ± SEM. Mann-Whitney U test was used; $P < 0.01$. (B) Quantification of TRAP-positive osteoclasts by colorimetric assay (OD at 540 nm) following incubation of CD14^{+} monocytes with cNETs and purified IgG from anti-CarP^{+} or anti-CarP^{-} patients with RA (n = 4–8). Data are presented as mean ± SEM. Mann-Whitney U test was used; $^{*}P < 0.05$, $^{***}P < 0.001$. (C) Quantitative PCR analysis of IL-6 and IL-8 mRNA levels in OA FLS treated for 24 hours with carH3 or carH3–IgG ICs (n = 4 per group). Kruskal-Wallis test was used; $^{*}P < 0.05$, $^{**}P < 0.01$. (D) Heatmap showing differentially expressed genes in OA FLS following treatment with carH3 or carH3–IgG ICs for 24 hours. (E) Gene Ontology enrichment analysis of differentially expressed genes in OA FLS treated with carH3. (F) Dot plot showing significantly enriched biologic pathways in OA FLS treated with carH3–IgG ICs (adjusted P value <0.05). (G) Dot plot comparing enriched biologic pathways between OA FLS treated with carH3 alone vs carH3–IgG ICs (adjusted P value <0.05). (H) Network diagram representing up-regulated genes and pathways in OA FLS stimulated with carH3–IgG ICs. (I) ELISA quantification of IL-8, IL-6, MCP-1, and GM-CSF levels in the supernatant of OA FLS treated with carH3 or carH3–IgG ICs (n = 4 per group). Kruskal-Wallis test was used; $^{*}P < 0.05$, $^{**}P < 0.01$, $^{***}P < 0.001$. anti-CarP, anti-carbamylated protein; cNETs, carbamylated neutrophil extracellular traps; ELISA, enzyme-linked immunosorbent assay; FLS, fibroblast-like synoviocytes; ICs, immune complexes; IL, interleukin; mRNA, messenger RNA; NETs, neutrophil extracellular traps; OA, osteoarthritis; OD, optical density; PCR, polymerase chain reaction; RA, rheumatoid arthritis; SEAP, secreted embryonic alkaline phosphatase; TLR4, Toll-like receptor 4; TRAP, tartrate-resistant acid phosphatase.

Together, these results indicate that anti-CarP antibodies amplify the inflammatory and osteoclastogenic effects of carH3. By stabilizing carH3 and promoting the formation of carH3–IgG ICs, they potentiate TLR4-dependent signaling, FLS activation, and cytokine production, thereby linking humoral autoimmunity to joint inflammation and bone destruction in RA.

DISCUSSION

RA is characterized by chronic synovial inflammation and progressive bone erosion, with neutrophils playing a central role, particularly in the early stages of disease.[1] Although neutrophils have traditionally been viewed as transient amplifiers of inflammation, their direct contribution to bone destruction has been less clearly defined. Our findings reveal a previously unrecognized mechanism linking NETs, PTMs, and humoral autoimmunity in RA. Specifically, we show that anti-CarP antibodies stabilize carH3 within NETs, protecting it from NE-mediated degradation and thereby amplifying its proinflammatory and osteoclastogenic functions.

This stabilization mechanism expands the functional repertoire of autoantibodies beyond their classical role in IC formation. By preserving their cognate antigen, anti-CarP antibodies sustain innate immune activation and extend the lifespan of NET-derived

autoantigens. In doing so, they transform NET components from transient byproducts of neutrophil death into persistent inflammatory drivers, thereby linking antibody specificity directly to the perpetuation of joint damage.

We previously identified carH3 as a prominent NET-associated antigen elevated in patients with RA that promotes osteoclast differentiation through TLR4 activation.[10] Here, we uncover an additional layer of regulation, showing that anti-CarP antibodies functionally potentiate this process by preventing NE-mediated degradation. As a result, carH3 persists longer within the inflammatory microenvironment, maintaining its capacity to engage TLR4 and promote osteoclast differentiation. This suggests that anti-CarP antibodies not only serve as biomarkers of autoimmune reactivity but also act as amplifiers of joint inflammation and bone destruction by stabilizing immunostimulatory PTMs within NETs.

Functionally, this stabilization may have key consequences for RA pathogenesis. We previously demonstrated that carbamylated NETs induce a rapid, RANKL-independent form of osteoclastogenesis driven by TLR4 signaling.[10] Here, we show that protection of carH3 by anti-CarP antibodies further enhances TLR4 activation and osteoclast differentiation. Monocytes exposed to NETs in the presence of anti-CarP$^+$ IgG undergo more robust osteoclastogenesis, whereas FLS stimulated with carH3–IgG ICs up-regulate IL-6, IL-8, MCP-1, and GM-CSF, adopting a proinflammatory, chemotactic, and matrix-remodeling phenotype. Together, these findings position anti-CarP antibodies not only as disease markers but also as functional effectors that sustain and amplify NET-driven inflammation and tissue destruction.

Our findings also underscore the broader immunogenic complexity of PTM within NETs.[2,5] The co-existence of native, citrullinated, and carbamylated proteins likely contributes to spreading epitope and the diversity of autoantibody responses in RA. Although anti-CarP and ACPA antibodies display limited cross-reactivity, they may cooperate to intensify inflammation and tissue damage, particularly when localized within the same NET structures.[4,5] Unlike ACPAs, which promote osteoclastogenesis primarily via Fcγ receptor– and RANKL-dependent pathways,[2] anti-CarP antibodies appear to act through Fc-independent stabilization of NET antigens and TLR4-mediated signaling. These complementary mechanisms may help explain the additive pathogenicity observed in patients harboring both ACPA and anti-CarP responses.

This work also highlights the technical and conceptual challenges in dissecting PTM biology in vivo. Unlike citrullination, which is enzymatically mediated by PADs, carbamylation is a non-enzymatic process with no known specific catalyst or inhibitor. The absence of selective tools to modulate carbamylation or neutralize carbamylated histones has limited functional dissection of these pathways. Future approaches such as site-specific PTM mapping, advanced proteomics, and targeted cyanate scavenging strategies could clarify the temporal and spatial interplay of PTMs in RA and other autoimmune settings.

Beyond the neutrophil compartment, the concurrent activation of other synovial components suggests that anti-CarP–carH3 interactions may orchestrate multicellular inflammatory circuits within the RA synovium. These interactions may contribute to persistent inflammation, angiogenesis, and tissue remodeling, which are all hallmarks of chronic joint pathology. The persistence of carbamylated antigens stabilized by autoantibodies provides an additional mechanistic explanation for the chronicity and self-sustaining nature of synovial inflammation.

Taken together, our study identifies a novel immune–bone interface in RA in which anti-CarP antibodies preserve the inflammatory potential of NETs by stabilizing carbamylated histones, prolonging TLR4 activation, monocyte-driven osteoclastogenesis, and synovial inflammation. This model positions NETs and their modified cargo not only as triggers of autoimmunity but also as direct effectors of joint damage and tissue injury. Therapeutically, these insights suggest that disrupting the stabilization of carbamylated histones or blocking their recognition by anti-CarP antibodies may attenuate downstream inflammatory and osteoclastogenic cascades. Similar to the development of PAD inhibitors targeting citrullination, strategies that limit cyanate formation, neutralize carbamylated proteins, or selectively degrade pathogenic NETs may hold promises for mitigating both systemic inflammation and local bone erosion in RA.

ACKNOWLEDGMENTS

This research was supported in part by the Intramural Research Program of the NIH (ZIAAR041199) and KAKENHI (#25K19593). We also thank the NIAMS Office of Science and Technology and Dr Kan Jiang for technical support. The contributions of the NIH author(s) were made as part of their official duties as NIH federal employees, are in compliance with agency policy requirements, and are considered Works of the United States Government. However, the findings and conclusions presented in this paper are those of the author(s) and do not necessarily reflect the views of the NIH or the US Department of Health and Human Services.

AUTHOR CONTRIBUTIONS

All authors contributed to at least one of the following manuscript preparation roles: conceptualization AND/OR methodology, software, investigation, formal analysis, data curation, visualization, and validation AND drafting or reviewing/editing the final draft. As corresponding author, Dr Carmona-Rivera confirms that all authors have provided the final approval of the version to be published and takes responsibility for the affirmations regarding article submission (eg, not under consideration by another journal), the integrity of the data presented, and the statements regarding compliance with institutional review board/Declaration of Helsinki requirements.

REFERENCES

1. Holers VM. Autoimmunity to citrullinated proteins and the initiation of rheumatoid arthritis. Curr Opin Immunol 2013;25(6):728–735. doi: https://doi.org/10.1016/j.coi.2013.09.018

2. Trouw LA, Rispens T, Toes REM. Beyond citrullination: other post-translational protein modifications in rheumatoid arthritis. Nat Rev Rheumatol 2017;13(6):331–339. doi:https://doi.org/10.1038/nrrheum.2017.15
3. Shi J, Knevel R, Suwannalai P, et al. Autoantibodies recognizing carbamylated proteins are present in sera of patients with rheumatoid arthritis and predict joint damage. Proc Natl Acad Sci U S A 2011;108(42):17372–17377. doi:https://doi.org/10.1073/pnas.1114465108
4. Castellanos-Moreira R, Rodríguez-García SC, Gomara MJ, et al. Anti-carbamylated proteins antibody repertoire in rheumatoid arthritis: evidence of a new autoantibody linked to interstitial lung disease. Ann Rheum Dis 2020;79(5):587–594. doi:https://doi.org/10.1136/annrheumdis-2019-216709
5. Pruijn GJ. Citrullination and carbamylation in the pathophysiology of rheumatoid arthritis. Front Immunol 2015;6:192. doi:https://doi.org/10.3389/fimmu.2015.00192
6. Khandpur R, Carmona-Rivera C, Vivekanandan-Giri A, et al. NETs are a source of citrullinated autoantigens and stimulate inflammatory responses in rheumatoid arthritis. Sci Transl Med 2013;5(178):178ra40. doi:https://doi.org/10.1126/scitranslmed.3005580
7. Wright HL, Lyon M, Chapman EA, et al. Rheumatoid arthritis synovial fluid neutrophils drive inflammation through production of chemokines, reactive oxygen species, and neutrophil extracellular traps. Front Immunol 2021;11:584116. doi:https://doi.org/10.3389/fimmu.2020.584116
8. Papayannopoulos V, Metzler KD, Hakkim A, et al. Neutrophil elastase and myeloperoxidase regulate the formation of neutrophil extracellular traps. J Cell Biol 2010;191(3):677–691. doi:https://doi.org/10.1083/jcb.201006052
9. O'Neil LJ, Barrera-Vargas A, Sandoval-Heglund D, et al. Neutrophil-mediated carbamylation promotes articular damage in rheumatoid arthritis. Sci Adv 2020;6(44):eabd2688. doi:https://doi.org/10.1126/sciadv.abd2688
10. O'Neil LJ, Oliveira CB, Wang X, et al. Neutrophil extracellular trap-associated carbamylation and histones trigger osteoclast formation in rheumatoid arthritis. Ann Rheum Dis 2023;82(5):630–638. doi:https://doi.org/10.1136/ard-2022-223568
11. Britsemmer K, Ursum J, Gerritsen M, et al. Validation of the 2010 ACR/EULAR classification criteria for rheumatoid arthritis: slight improvement over the 1987 ACR criteria. Ann Rheum Dis 2011;70(8):1468–1470. doi:https://doi.org/10.1136/ard.2010.148619
12. Aletaha D, Neogi T, Silman AJ, et al. 2010 rheumatoid arthritis classification criteria: an American College of Rheumatology/European League Against Rheumatism collaborative initiative. Arthritis Rheum 2010;62:2569–81.

Check for updates

Arthritis & Rheumatology
Vol. 78, No. 10, October 2026, pp 2082–2088
DOI 10.1002/art.70154
© 2026 The Author(s). *Arthritis & Rheumatology* published by Wiley Periodicals LLC on behalf of American College of Rheumatology.
This is an open access article under the terms of the Creative Commons Attribution-NonCommercial License, which permits use, distribution and reproduction in any medium, provided the original work is properly cited and is not used for commercial purposes.

American College of Rheumatology
Empowering Rheumatology Professionals

BRIEF REPORT

Per- and Polyfluoroalkyl Substances and Knee Osteoarthritis: Data From the Osteoarthritis Initiative

Jeffrey B. Driban, PhD,[1] Lisa B. Rokoff, PhD,[2] Bing Lu, MD, DrPH,[3] Timothy E. McAlindon, MD, MPH,[4] Charles B. Eaton, MD, MS,[5,6,7] Mary B. Roberts, MS,[5,6,7] Diana Mathes, BS,[8] Colleen Lestician, BS,[8] Zhijin Carrie Xu, PhD,[8] Zhihua Tina Fan, PhD,[8] Shawn P. O'Leary, BS,[8] Ida K. Haugen, MD, PhD,[9,10] Jérémie Sellam, MD, PhD,[11] Alice Courties, MD, PhD,[11] and Abby F. Fleisch, MD, MPH[2,12]

Objective. To examine whether concentrations of specific per- and polyfluoroalkyl substances (PFAS) and a mixture of PFAS relate to incident knee osteoarthritis (KOA) and knee pain progression.

Methods. Among a case-cohort sample from the OA Initiative (n = 1,878), we examined associations of serum concentrations of eight PFAS with odds of developing over the subsequent 48 months (1) symptomatic KOA and (2) a clinically meaningful change in the Western Ontario and McMaster Universities OA Index knee pain score. We used weighted logistic regression to assess single PFAS (continuous and quartiles) and quantile g-computation to assess the PFAS mixture in relation to our outcomes, accounting for sociodemographics.

Results. Fifty-eight percent of participants were female with a mean age of 62 years and body mass index of 28.6 kg/m^2. Participants with higher perfluorooctanoic acid (continuous) had greater odds of incident symptomatic KOA (odds ratio [OR] per interquartile range [IQR] 1.12, 95% confidence interval [CI] 1.04–1.21). Participants in the highest quartiles of perfluorononanoic acid (PFNA) had greater odds of incident symptomatic KOA [OR for the third quartile 1.63, 95% CI 1.29–2.07; fourth quartile 1.55, 95% CI 1.19–2.01). Perfluorooctanoic acid may have a nonlinear relationship with the greatest chance of incident symptomatic KOA with serum concentrations between 5.19 and 6.88 ng/mL (OR 1.55, 95% CI 1.21–1.97). Participants with greater perfluorooctanoic acid and PFNA (continuous) had greater odds of knee pain progression (OR per IQR: perfluorooctanoic acid 1.10, 95% CI 1.03–1.18; PFNA 1.06, 95% CI 1.01–1.11). Mixture models showed perfluorooctanoic acid and PFNA were among the PFAS with the strongest positive weights for both outcomes.

Conclusion. In a large cohort at risk for KOA, higher perfluorooctanoic acid and PFNA serum concentrations may be associated with a greater likelihood of symptomatic KOA incidence and knee pain progression.

INTRODUCTION

The prevalence of knee osteoarthritis (KOA) in the United States has doubled since the mid-20th century.[1] This finding that cannot be fully accounted for by increased life expectancy or obesity,[1] suggesting a potential contribution of environmental factors.[2]

Per- and polyfluoroalkyl substances (PFAS) are synthetically produced water-, grease-, or stain-resistant chemicals used in a

Supported by grants from the National Institute of Arthritis and Musculoskeletal and Skin Diseases, NIH (awards R01-AR-081791 and R24-AR-085006). Dr Fleisch's work was supported by a grant from the National Institutes of Environmental Health Sciences, NIH (R01-ES-30101).

[1]Department of Population and Quantitative Health Sciences, UMass Chan Medical School, Worcester, Massachusetts; [2]Center for Interdisciplinary and Population Health Research, MaineHealth Institute for Research, Westbrook, Maine; [3]Department of Public Health Sciences, UConn Health, Farmington, Connecticut; [4]Division of Rheumatology, Department of Medicine, UMass Chan Medical School, Worcester, Massachusetts; [5]Center for Primary Care and Prevention, Kent Hospital, Pawtucket, Rhode Island; [6]Department of Family Medicine, Warren Alpert Medical School Brown University, Rhode Island; [7]Department of Epidemiology, Brown University School of Public Health, Providence, Rhode Island; [8]Environmental and Chemical Laboratory Services, Public Health & Environmental Laboratories, New Jersey Department of Health, Ewing; [9]Center for Treatment of Rheumatic and Musculoskeletal Diseases (REMEDY), Diakonhjemmet Hospital, Oslo, Norway; [10]Faculty of Medicine, University of Oslo, Oslo, Norway; [11]Department of Rheumatology, Saint-Antoine Hospital, Assistance Publique–Hôpitaux de Paris (AP-HP), Centre de Recherche Saint-Antoine (CRSA) Inserm UMRS-938, Sorbonne Université, Paris, France; [12]Pediatric Endocrinology and Diabetes, Maine Medical Center, Portland.

Additional supplementary information cited in this article can be found online in the Supporting Information section (https://acrjournals.onlinelibrary.wiley.com/doi/10.1002/art.70154).

Author disclosures are available at https://onlinelibrary.wiley.com/doi/10.1002/art.70154.

Address correspondence via email to Jeffrey B. Driban, PhD, at jeffrey.driban@umassmed.edu.

Submitted for publication November 24, 2025; accepted in revised form March 9, 2026.

wide range of products (eg, food packaging and water-resistant fabric).[3] These compounds are universally detectable in the US population and have long biologic half-lives of 2 to 8 years. PFAS may exacerbate OA development by increasing inflammation, adiposity, and bone loss. Cross-sectional studies have demonstrated an association of serum PFAS, particularly perfluorooctanoic acid, with self-reported OA diagnosis.[4,5]

An important next step is to examine the longitudinal associations of PFAS with specific types of OA using high-quality symptomatic and radiographic assessments. Our recent longitudinal study found possible associations of perfluorodecanoic acid (PFDA) and perfluorononanoic acid (PFNA) with symptomatic hand OA.[6] Herein, we investigate the extent to which specific PFAS and a mixture of PFAS, capturing the overall joint effect and accounting for the correlations among PFAS compounds, relate to KOA incidence and knee pain progression.

MATERIAL AND METHODS

Study sample. We leveraged a case-cohort sample of participants from the OA Initiative (OAI), which we previously described.[6] The OAI cohort comprised 4,796 individuals aged 45 to 79 years, recruited from 2004 to 2006 at four sites in the United States. The OAI staff primarily recruited participants who had or were at high risk for symptomatic KOA. Participants attended annual OAI visits, which included knee radiographs and knee pain assessments, for the first 48 months.

We selected a random sample of 1,351 to represent the eligible cohort among OAI participants with hand radiographs and no radiographic evidence of pathology other than hand OA.[6] We then selected an additional 549 "cases" based on the development of at least one of seven hand OA outcomes at the 48-month follow-up visit.[6] Among the 1,900 participants in the original case-cohort sample, 1,878 had baseline serum samples for PFAS assays.

PFAS measurement. We measured PFAS in archived serum from the OAI baseline examination (2004–2006). We sent samples without a freeze-thaw cycle to the New Jersey Department of Health's Environmental and Chemical Laboratory Service for PFAS measurement.

The laboratory performed analysis in singlicate for 12 PFAS, using a high-throughput online solid-phase extraction (Spark Holland, Emmen, the Netherlands) system and a highly sensitive tandem mass spectrometer (MS/MS; Sciex QTrap 6500, Framingham, MA; iChromQtrap). The PFAS included perfluorooctanoic acid, perfluorooctane sulfonic acid (PFOS), PFDA, perfluorohexane sulfonic acid, 2-(N-methyl-perfluorooctane sulfonamido) acetic acid, PFNA, perfluoroundecanoic acid (PFUnA), perfluorododecanoic acid, perfluoro-2-proproxypropanoic acid, 4,8-dioxa-3H-perfluorononanoic acid, 9-chlorohexadecafluoro-3-oxanone-1-sulfonic acid, and perfluoroheptanesulfonic acid. The laboratory established the validity of their methods[7,8] and reported the limits of detection (LODs, ranging from 0.001 to 0.025 ng/mL).[7,8]

Incident symptomatic KOA. Participants received annual bilateral weight-bearing, fixed-flexion posterior-anterior knee radiographs. Central readers provided Kellgren-Lawrence grades (0–4) for public release (κ coefficients 0.70–0.78).

Frequent knee pain was assessed with a standardized question (answer: yes or no), "During the last 12 months, have you had pain, aching, or stiffness in or around your right knee on most days for at least 1 month? By most days, we mean more than half the days of a month." The same question was asked for the left knee.

We classified a participant as having symptomatic KOA if they had a knee with a Kellgren-Lawrence grade ≥2 (definite osteophyte) and frequent knee pain. Incident symptomatic KOA was defined as someone without symptomatic KOA in either knee at baseline but who developed symptomatic KOA in at least one knee by 48 months after baseline.

Clinically meaningful within-participant change in knee pain (knee pain progression). The OAI administered knee-specific Western Ontario and McMaster Universities OA Index (WOMAC) questionnaires, a validated tool for assessing KOA symptom severity (pain scale 0–20). We defined knee pain progression as an increase in pain severity of >2 units[9] in either knee between any two consecutive follow-up visits (eg, baseline to 12 months and 12–24 months). In analyses of knee pain progression, we excluded five participants who only completed the questionnaire at baseline and 48 months (ie, had no follow-up between the first and last visits).

Covariates. Participants reported date of birth, race (open-ended question), and education. The OAI questionnaire asked, "What is your gender, male or female?" At baseline, study staff measured weight and height, which were used to calculate body mass index (BMI; kg/m^2). Among women, we estimated menopause status at baseline based on the self-reported last natural period or age at hysterectomy; premenopause: last natural period within past 12 months; perimenopause: last natural period 1 to 4 years ago or hysterectomy <5 years before baseline; and postmenopause: last natural period or hysterectomy ≥5 years before baseline.

Statistical analyses. We a priori included PFAS with 60% detectability in samples, ensuring consistency with prior studies.[3,10] Eight PFAS met this threshold (Table 1). In cases where PFAS were below the LOD, we replaced those values with the LOD / $\sqrt{2}$.[3,10]

We examined the linearity of associations of single PFAS with KOA using generalized additive models. Some models indicated

Table 1. Associations of baseline serum PFAS concentration with development of symptomatic KOA by 48 months after baseline (N = 1,307)*

PFAS, ng/mL	Odds ratio (95% confidence interval) of KOA (27% cases)[a]		
	Model 1[b]	Model 2[c]	Model 3[d]
PFOS			
IQR (8.90)	0.99 (0.91–1.08)	0.95 (0.87–1.04)	0.95 (0.86–1.04)
Q1 (0.10–9.00)	Reference	Reference	Reference
Q2 (9.01–12.73)	1.18 (0.93–1.49)	1.13 (0.89–1.44)	1.12 (0.88–1.43)
Q3 (12.74–17.90)	1.11 (0.88–1.40)	1.06 (0.83–1.36)	1.04 (0.81–1.33)
Q4 (17.91–85.50)	1.04 (0.82–1.33)	0.95 (0.74–1.22)	0.94 (0.73–1.22)
Perfluorooctanoic acid			
IQR (3.01)	**1.14 (1.06–1.23)**	**1.12 (1.04–1.21)**	**1.09 (1.01–1.18)**
Q1 (0.33–3.87)	Reference	Reference	Reference
Q2 (3.88–5.18)	1.03 (0.81–1.31)	1.02 (0.80–1.30)	1.03 (0.80–1.32)
Q3 (5.19–6.88)	**1.58 (1.25–2.01)**	**1.55 (1.21–1.97)**	**1.51 (1.17–1.93)**
Q4 (6.89–66.30)	**1.30 (1.02–1.66)**	1.22 (0.95–1.56)	1.14 (0.88–1.47)
PFNA			
IQR (0.74)	**1.06 (1.00–1.12)**	1.04 (0.98–1.10)	1.03 (0.97–1.09)
Q1 (0.07–0.76)	Reference	Reference	Reference
Q2 (0.77–1.05)	1.21 (0.95–1.55)	1.19 (0.93–1.53)	1.14 (0.89–1.47)
Q3 (1.06–1.50)	**1.70 (1.34–2.15)**	**1.63 (1.29–2.07)**	**1.53 (1.20–1.95)**
Q4 (1.51–13.40)	**1.64 (1.27–2.10)**	**1.55 (1.19–2.01)**	**1.42 (1.09–1.85)**
PFHxS			
IQR (2.62)	1.00 (0.94–1.05)	0.98 (0.93–1.04)	0.99 (0.94–1.05)
Q1 (0.10–1.96)	Reference	Reference	Reference
Q2 (1.97–2.97)	0.92 (0.72–1.17)	0.83 (0.65–1.07)	0.87 (0.67–1.12)
Q3 (2.98–4.58)	1.13 (0.90–1.43)	1.07 (0.84–1.36)	1.16 (0.90–1.49)
Q4 (4.59–66.70)	1.12 (0.88–1.42)	1.03 (0.81–1.32)	1.12 (0.87–1.44)
MeFOSAA			
IQR (0.46)	0.96 (0.90–1.03)	0.95 (0.88–1.01)	0.95 (0.88–1.01)
Q1 (0.03–0.25)	Reference	Reference	Reference
Q2 (0.26–0.43)	1.18 (0.93–1.49)	1.18 (0.92–1.50)	1.19 (0.93–1.52)
Q3 (0.44–0.72)	1.17 (0.93–1.48)	1.16 (0.92–1.48)	1.20 (0.94–1.52)
Q4 (0.73–16.30)	1.02 (0.80–1.30)	0.97 (0.76–1.24)	0.97 (0.75–1.24)
PFHpS			
IQR (0.34)	**1.15 (1.05–1.27)**	1.09 (0.99–1.21)	1.07 (0.96–1.19)
Q1 (<LOD–0.21)	Reference	Reference	Reference
Q2 (0.22–0.36)	1.11 (0.88–1.41)	1.03 (0.80–1.31)	1.02 (0.79–1.30)
Q3 (0.37–0.55)	1.15 (0.90–1.47)	1.03 (0.80–1.33)	0.99 (0.76–1.28)
Q4 (0.56–2.97)	**1.52 (1.20–1.92)**	**1.36 (1.06–1.75)**	1.25 (0.97–1.62)
PFDA			
IQR (0.25)	1.01 (0.94–1.08)	0.99 (0.92–1.07)	1.00 (0.93–1.08)
Q1 (<LOD–0.15)	Reference	Reference	Reference
Q2 (0.16–0.25)	0.93 (0.73–1.18)	0.97 (0.76–1.24)	0.88 (0.69–1.14)
Q3 (0.26–0.40)	**1.35 (1.07–1.70)**	**1.39 (1.10–1.76)**	**1.29 (1.01–1.64)**
Q4 (0.41–3.54)	1.26 (0.99–1.61)	1.27 (0.99–1.63)	1.28 (0.99–1.65)
PFUnA			
IQR (0.24)	1.06 (0.99–1.13)	1.04 (0.96–1.11)	1.05 (0.98–1.13)
Q1 (<LOD–0.08)	Reference	Reference	Reference
Q2 (0.09–0.16)	1.01 (0.80–1.29)	0.99 (0.78–1.26)	0.97 (0.76–1.24)
Q3 (0.17–0.32)	1.19 (0.94–1.51)	1.21 (0.96–1.54)	1.19 (0.93–1.52)
Q4 (0.33–3.41)	1.27 (1.00–1.61)	1.21 (0.94–1.54)	1.27 (0.99–1.63)

* Bolded estimates indicate $P < 0.05$. We used inverse probability weighting to account for oversampling of hand osteoarthritis cases with the case-cohort study design. IQR, interquartile range; KOA, knee osteoarthritis; LOD, limit of detection; MeFOSAA, 2-(N-methyl-perfluorooctane sulfonamido) acetic acid; PFAS, per- and polyfluoroalkyl substances; PFDA, perfluorodecanoic acid; PFHpS, perfluoroheptanesulfonic acid; PFHxS, perfluorohexane sulfonic acid; PFNA, perfluorononanoic acid; PFOS, perfluorooctane sulfonic acid; PFUnA, perfluoroundecanoic acid; Q, quartile.

[a] Excluding n = 571 participants who had symptomatic KOA at baseline.

[b] Model 1: unadjusted.

[c] Model 2: adjusted for gender/menopause status (male, premenopausal female, perimenopausal female, or postmenopausal female), race (Black, yes/no), education level (college graduate, yes/no), and age at baseline.

[d] Model 3: model 2 + body mass index at baseline.

possible nonlinear associations; hence, we represented PFAS in the following ways: (1) a continuous variable per interquartile range (IQR) increment and (2) a categorical variable by quartiles.

We first ran unadjusted logistic models. Then, we ran adjusted models; using prior literature on PFAS and KOA, we a priori adjusted for gender/menopause status (male; female, premenopause; female, perimenopause; and female, postmenopause), race (Black, yes/no), education (college graduate, yes/no), and age at baseline (continuous). In a further adjusted model, we included baseline BMI (continuous), as body weight could be a confounder or mediator between PFAS exposure and KOA development, thereby complicating interpretation. Given the sparse missingness of adjustment covariates (<0.5%), we used single imputation to replace missing values with the overall mode (for race and education), age group–specific mode (for menopause status), or gender-specific median (for BMI). For all models, we used sampling weights to account for the case-cohort study design. Specifically, because we selected the case-cohort based on hand OA, hand OA cases received a weight of 1, and noncases received a weight of 1 / sampling fraction.[11]

Knee pain can vary frequently; hence, we performed a sensitivity analysis with a more conservative criterion to define persistent knee pain progression: an increase in the WOMAC pain score of >2 units in either knee between any two consecutive follow-up visits, followed by no change or further increase in the same knee at the next follow-up visit. We conducted this analysis among participants with complete WOMAC pain score data for at least one knee at all follow-up visits (n = 1,788, 4.5% with persistent pain progression).

Because humans are exposed to multiple, not single, PFAS concurrently, we also evaluated the joint effects of the PFAS mixture on our outcomes. We used quantile-based g-computation, a mixtures approach that (1) allows for estimation of the joint effect of an exposure mixture on an outcome and (2) generates output of individual weights for each component in the mixture, taking into account collinearity with other exposures.[12] The overall effect estimates reflect a simultaneous quartile increase in all PFAS in the mixture on the odds of our outcomes.

We used SAS for data management and performed all statistical analyses in R version 4.5.1 (Core Team, 2018). The data and codebook will be shared by the corresponding author upon request.

RESULTS

Participant characteristics. Fifty-eight percent of participants were female, and 83% were White. On average, participants were aged 62 ± 9 years with a mean ± SD BMI of 28.6 ± 4.7 kg/m^2. Of 1,307 participants without symptomatic KOA at baseline, 359 developed symptomatic KOA, and 434 participants of 1,873 with available data developed meaningful knee pain progression. Supplemental Tables S1 and S2 provide detailed descriptions of the eligible participants and a comparison of participants with and without each outcome.

Symptomatic KOA. When we represented PFAS concentrations as continuous variables, participants with higher perfluorooctanoic acid had greater odds of incident symptomatic KOA (odds ratio [OR] per IQR 1.12, 95% confidence interval [CI] 1.04–1.21) in the covariate-adjusted model (model 2), and this finding was consistent in the perfluorooctanoic acid model additionally adjusted for BMI (model 3; Table 1). When we represented perfluorooctanoic acid concentrations in quartiles, participants in the third quartile (5.19–6.88 ng/mL) had greater odds of incident symptomatic KOA (OR vs first quartile 1.55, 95% CI 1.21–1.97) in the covariate-adjusted model (model 2). When we represented PFNA concentrations in quartiles, participants in the highest quartiles had greater odds of incident symptomatic KOA (OR vs first quartile: third quartile 1.63, 95% CI 1.29–2.07; fourth quartile 1.55, 95% CI 1.19–2.01) in the covariate-adjusted model (model 2). These findings were slightly attenuated, but statistically significant, in the model that additionally included BMI (model 3; Table 1). We observed no other consistent associations between individual PFAS and incident symptomatic KOA. The overall PFAS mixture was associated with greater odds of KOA (OR 1.17, 95% CI 1.03–1.33 per quartile increase in the mixture; Figure 1). Consistent with the single-PFAS models, PFNA and perfluorooctanoic acid had weights in the positive-scaled direction (ie, higher odds; Figure 1).

Knee pain progression. When we represented PFAS concentrations as continuous variables, participants with greater perfluorooctanoic acid and PFNA had greater odds of knee pain progression in the covariate-adjusted model (model 2); however, the CIs for PFNA included the null after adjusting for BMI (model 3; Table 2). The association between perfluorooctanoic acid and knee pain progression was statistically significant for those in the highest tertile (>6.89 ng/mL) (OR vs first quartile 1.28, 95% CI 1.03–1.59) in the covariate-adjusted model (model 2); however, this association was attenuated after adjusting for BMI (model 3). When we represented PFNA and PFDA in quartiles, we detected nonmonotonic associations (models 2 and 3). Specifically, participants in the middle PFNA quartiles had approximately 16% to 26% lower odds of knee pain progression than those in the lowest quartile (models 1–3; Table 2). In contrast, participants in the highest PFNA quartile had increased odds of knee pain progression (models 1–3), which was only statistically significant in the unadjusted model (model 1). Participants in the middle PFDA quartiles had approximately 32% to 50% lower odds of knee pain progression than those in the lowest quartile (models 1–3). Finally, participants in the higher PFUnA quartiles had approximately 21% to 27% lower odds of knee pain progression than those in the lowest quartile (models 2 and 3). No other individual PFAS or

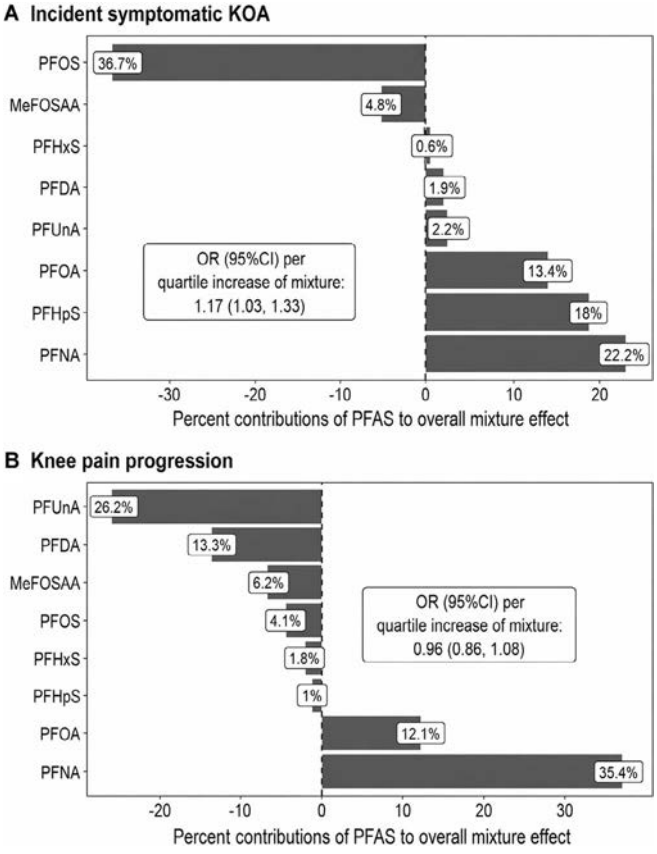


Figure 1. Odds of (A) incident symptomatic KOA and (B) knee pain progression per quartile increase of all PFAS in the mixture simultaneously, and the percent contribution of each PFAS to the overall mixture (calculated using quantile g-computation output and accounting for the scaled effect size in each direction; ie, [absolute value of scaled directional effect / sum of the absolute values of scaled positive and negative effects] × PFAS weight × 100). Models are adjusted for gender/menopause status (male, premenopausal female, perimenopausal female, or postmenopausal female), race (Black, yes/no), education level (college graduate, yes/no), and age at baseline. Models incorporated inverse probability weighting to account for oversampling of hand osteoarthritis cases with the case-cohort study design. CI, confidence interval; KOA, knee osteoarthritis; MeFOSAA, 2-(N-methyl-perfluorooctane sulfonamido) acetic acid; OR, odds ratio; PFAS, per- and polyfluoroalkyl substances; PFDA, perfluorodecanoic acid; PFHpS, perfluoroheptanesulfonic acid; PFHxS, perfluorohexane sulfonic acid; PFNA, perfluorononanoic acid; PFOA, perfluorooctanoic acid; PFOS, perfluorooctane sulfonic acid; PFUnA, perfluoroundecanoic acid.

the overall PFAS mixture were associated with knee pain progression. Consistent with the single-PFAS models, PFNA and perfluorooctanoic acid had the strongest and only weights in the positive-scaled direction in the mixture approach (Table 2, Figure 1).

Our sensitivity analysis with persistent knee pain progression as the outcome (Supplemental Table S3) was less powered but supported our primary findings for perfluorooctanoic acid (model 2) with a modestly stronger, statistically significant OR for perfluorooctanoic acid (eg, continuous OR 1.18 vs 1.10). Other reported findings were typically attenuated.

DISCUSSION

In a large cohort at high risk for KOA, serum concentrations of perfluorooctanoic acid and PFNA were associated with developing symptomatic KOA and knee pain progression. Specifically, the odds of developing symptomatic KOA were greatest for perfluorooctanoic acid concentrations between 5.19 and 6.88 ng/mL and PFNA concentrations ≥1.06 ng/mL (models 1–3). Furthermore, greater perfluorooctanoic acid concentrations (especially >6.89 ng/mL; model 2) and PFNA (especially >1.51 ng/mL; model 1) were associated with knee pain progression; however, these associations were attenuated after further adjustments (ie, for BMI [model 3] and any covariate [models 2 and 3], respectively). In the mixture analyses, which account for correlations among PFAS, perfluorooctanoic acid and PFNA consistently had the strongest weights in the positive-scaled direction (greater odds) for developing either outcome. We found no consistent evidence that other PFAS related to a greater chance of KOA incidence or progression.

Our findings complement prior cross-sectional studies that observed adults with higher serum concentrations of perfluorooctanoic acid, but not PFOS, have greater odds of self-reported OA.[4,5] Self-reported OA is strongly influenced by KOA—the most prevalent OA phenotype.[13] However, PFAS may influence OA phenotypes differently; hand joints may be more sensitive to systemic factors (eg, inflammatory perturbations) than weight-bearing joints such as the knees, leading to distinct responses to PFAS. Indeed, our current findings are partially consistent with our prior longitudinal findings that participants with greater serum concentrations of PFNA and PFDA are more likely to develop symptomatic hand OA.[6] Collectively, our results and prior studies suggest that perfluorooctanoic acid may have a phenotypically specific association with KOA rather than hand OA. Furthermore, PFNA is consistently associated with incident symptomatic knee and hand OA. Both perfluorooctanoic acid and PFNA have a long carbon chain and a carboxylic acid functional group. Their biologic activity may differ from PFAS with different functional groups or carbon chain lengths.[14]

By examining multiple PFAS, both individually and as a mixture, our work advances the prior literature, which focused on PFOS and perfluorooctanoic acid. We found that perfluorooctanoic acid and PFNA are associated with developing symptomatic KOA in both single-PFAS and mixture models. Serum concentrations of perfluorooctanoic acid and PFNA moderately correlate (r_s = 0.52)[6]; however, the mixture analyses highlight the unique roles of each PFAS in relation to KOA outcomes.

A strength of our study was our ability to adjust for BMI. The associations we observed of perfluorooctanoic acid and PFNA

Table 2. Associations of baseline serum PFAS concentration with clinically meaningful knee pain progression (change in WOMAC Pain score (>2-unit) between any two visits from baseline and 48 months [N = 1,873])

	Odds ratio (95% confidence interval) of a >2-unit change[a] in WOMAC score (23% cases)		
PFAS, ng/mL	Model 1[b]	Model 2[c]	Model 3[d]
PFOS			
IQR (8.90)	1.03 (0.95–1.11)	0.97 (0.89–1.05)	0.97 (0.89–1.05)
Q1 (0.10–9.00)	Reference		Reference
Q2 (9.01–12.73)	1.11 (0.90–1.38)	1.14 (0.92–1.42)	1.12 (0.90–1.40)
Q3 (12.74–17.90)	1.18 (0.95–1.46)	1.15 (0.92–1.43)	1.11 (0.89–1.39)
Q4 (17.91–85.50)	1.18 (0.95–1.46)	1.08 (0.86–1.35)	1.08 (0.86–1.36)
Perfluorooctanoic acid			
IQR (3.01)	**1.10 (1.03–1.17)**	**1.10 (1.03–1.18)**	**1.08 (1.01–1.15)**
Q1 (0.33–3.87)	Reference	Reference	Reference
Q2 (3.88–5.18)	0.89 (0.71–1.10)	0.95 (0.76–1.19)	0.94 (0.75–1.18)
Q3 (5.19–6.88)	1.08 (0.87–1.33)	1.18 (0.95–1.46)	1.15 (0.92–1.43)
Q4 (6.89–66.30)	1.22 (0.99–1.50)	**1.28 (1.03–1.59)**	1.19 (0.96–1.49)
PFNA			
IQR (0.74)	**1.12 (1.07–1.17)**	**1.06 (1.01–1.11)**	1.05 (1.00–1.10)
Q1 (0.07–0.76)	Reference	Reference	Reference
Q2 (0.77–1.05)	0.81 (0.65–1.01)	**0.79 (0.64–0.99)**	**0.76 (0.60–0.94)**
Q3 (1.06–1.50)	0.84 (0.68–1.04)	**0.79 (0.63–0.98)**	**0.74 (0.59–0.92)**
Q4 (1.51–13.40)	**1.49 (1.22–1.82)**	1.20 (0.96–1.48)	1.13 (0.91–1.40)
PFHxS			
IQR (2.62)	**0.94 (0.89–1.00)**	0.96 (0.90–1.01)	0.97 (0.91–1.03)
Q1 (0.10–1.96)	Reference	Reference	Reference
Q2 (1.97–2.97)	0.95 (0.78–1.18)	1.01 (0.81–1.25)	1.01 (0.81–1.26)
Q3 (2.98–4.58)	0.81 (0.65–1.00)	0.87 (0.70–1.09)	0.92 (0.73–1.16)
Q4 (4.59–66.70)	1.03 (0.84–1.26)	1.13 (0.91–1.41)	1.21 (0.97–1.50)
MeFOSAA			
IQR (0.46)	0.97 (0.91–1.03)	0.95 (0.89–1.01)	0.95 (0.89–1.01)
Q1 (0.03–0.25)	Reference	Reference	Reference
Q2 (0.26–0.43)	1.16 (0.95–1.43)	1.23 (1.00–1.52)	1.23 (1.00–1.53)
Q3 (0.44–0.72)	0.87 (0.70–1.08)	0.91 (0.73–1.13)	0.92 (0.74–1.15)
Q4 (0.73–16.30)	0.99 (0.81–1.22)	1.00 (0.81–1.24)	1.00 (0.80–1.24)
PFHpS			
IQR (0.34)	1.00 (0.92–1.09)	0.96 (0.87–1.06)	0.94 (0.85–1.04)
Q1 (<LOD–0.21)	Reference	Reference	Reference
Q2 (0.22–0.36)	0.81 (0.65–1.01)	0.84 (0.67–1.05)	0.81 (0.65–1.01)
Q3 (0.37–0.55)	1.14 (0.92–1.40)	1.21 (0.97–1.51)	1.12 (0.90–1.40)
Q4 (0.56–2.97)	1.03 (0.83–1.26)	1.00 (0.80–1.26)	0.93 (0.74–1.17)
PFDA			
IQR (0.25)	**1.09 (1.03–1.15)**	1.00 (0.94–1.06)	1.00 (0.94–1.07)
Q1 (<LOD–0.15)	Reference	Reference	Reference
Q2 (0.16–0.25)	**0.57 (0.46–0.71)**	**0.54 (0.43–0.68)**	**0.50 (0.40–0.63)**
Q3 (0.26–0.40)	**0.68 (0.55–0.84)**	**0.62 (0.50–0.77)**	**0.59 (0.47–0.73)**
Q4 (0.41–3.54)	1.14 (0.93–1.38)	0.88 (0.71–1.09)	0.89 (0.72–1.10)
PFUnA			
IQR (0.24)	**1.10 (1.04–1.16)**	1.02 (0.96–1.08)	1.03 (0.97–1.09)
Q1 (<LOD–0.08)	Reference	Reference	Reference
Q2 (0.09–0.16)	**0.77 (0.63–0.96)**	**0.75 (0.61–0.93)**	**0.74 (0.60–0.92)**
Q3 (0.17–0.32)	0.88 (0.71–1.08)	**0.79 (0.64–0.98)**	**0.79 (0.63–0.98)**
Q4 (0.33–3.41)	0.94 (0.77–1.16)	**0.73 (0.58–0.90)**	**0.76 (0.61–0.95)**

* Bolded estimates indicate $P < 0.05$. We used inverse probability weighting to account for oversampling of hand osteoarthritis cases with the case-cohort study design. IQR, interquartile range; LOD, limit of detection; MeFOSAA, 2-(N-methyl-perfluorooctane sulfonamido) acetic acid; PFAS, per- and polyfluoroalkyl substances; PFDA, perfluorodecanoic acid; PFHpS, perfluoroheptanesulfonic acid; PFHxS, perfluorohexane sulfonic acid; PFNA, perfluorononanoic acid; PFOS, perfluorooctane sulfonic acid; PFUnA, perfluoroundecanoic acid; Q, quartile; WOMAC, Western Ontario and McMaster Universities Osteoarthritis Index.

[a] Based on Conaghan et al,[9] we classified a meaningful within-patient change as WOMAC scores (scaled 0–10) that correlated with a two-category change in the Patient's Global Assessment of osteoarthritis (>2 units in WOMAC score) in either knee between any two follow-up visits; excluding n = 5 participants who only had scores available at baseline and at 48-month follow-up.

[b] Model 1: unadjusted.

[c] Model 2: adjusted for gender/menopause status (male, premenopausal female, perimenopausal female, or postmenopausal female), race (Black, yes/no), education level (college graduate, yes/no), and age at baseline.

[d] Model 3: model 2 + body mass index at baseline.

with KOA outcomes remained statistically significant after adjusting for BMI, although they were often attenuated, suggesting that the relationships of these PFAS with KOA outcomes are not fully explained by BMI, either as a confounder or mediator.

The OAI provided a unique opportunity to investigate the relationships between PFAS and OA in a well-characterized cohort with longitudinal data. Our study is the first to examine PFAS and KOA. It is reassuring that our perfluorooctanoic acid findings complement prior cross-sectional studies. The age of this cohort enabled us to observe a high incidence rate during a 48-month period (27% had incident symptomatic KOA). Despite these strengths, our study had limitations. First, the purposeful recruitment of people aged 45 to 79 years with risk factors for OA could influence the generalizability of our results. Furthermore, although the OAI is a rich data set, we were unable to adjust for some potential confounders (eg, occupational factors or environmental exposures) that could be considered in future studies. We also assessed knee pain progression using clinically meaningful within-participant change in knee pain[9] during a 12-month interval. However, given that KOA symptoms vary frequently, it remains uncertain whether PFAS is associated with sustained, long-term progression of knee pain. We also acknowledge that the KOA analyses were not planned but informed by our prior work.[6] Finally, as in most epidemiologic studies of PFAS, we relied on PFAS concentrations in blood samples as a marker of PFAS exposure, which reflects only part of their total body burden. Furthermore, we were unable to analyze short-chain PFAS because they tend to have shorter half-lives and are undetectable on routine biomonitoring.[15] Future studies using animal models could clarify the health impacts of total PFAS body burden, PFAS in specific tissues (eg, articular cartilage and subchondral bone), and short-chain PFAS.

In conclusion, in a large prospective cohort of adults at risk for KOA, we found that serum concentrations of perfluorooctanoic acid and PFNA may be associated with developing symptomatic KOA and knee pain progression. Although our findings require replication in large, prospective cohorts, they raise the possibility that clinical monitoring for patients with PFAS exposure may warrant inclusion of KOA.

AUTHOR CONTRIBUTIONS

All authors contributed to at least one of the following manuscript preparation roles: conceptualization AND/OR methodology, software, investigation, formal analysis, data curation, visualization, and validation AND drafting or reviewing/editing the final draft. As corresponding author, Dr Driban confirms that all authors have provided the final approval of the version to be published and takes responsibility for the affirmations regarding article submission (eg, not under consideration by another journal), the integrity of the data presented, and the statements regarding compliance with institutional review board/Declaration of Helsinki requirements.

REFERENCES

1. Wallace IJ, Worthington S, Felson DT, et al. Knee osteoarthritis has doubled in prevalence since the mid-20th century. Proc Natl Acad Sci U S A 2017;114(35):9332–9336. doi:https://doi.org/10.1073/pnas.1703856114
2. Deprouw C, Courties A, Fini JB, et al. Pollutants: a candidate as a new risk factor for osteoarthritis-results from a systematic literature review. RMD Open 2022;8(2):8. doi:https://doi.org/10.1136/rmdopen-2021-001983
3. Botelho JC, Kato K, Wong L-Y, et al. Per- and polyfluoroalkyl substances (PFAS) exposure in the U.S. population: NHANES 1999-March 2020. Environ Res 2025;270:120916. doi:https://doi.org/10.1016/j.envres.2025.120916
4. Uhl SA, James-Todd T, Bell ML. Association of osteoarthritis with perfluorooctanoate and perfluorooctane sulfonate in NHANES 2003-2008. Environ Health Perspect 2013;121(4):447–452. doi:https://doi.org/10.1289/ehp.1205673
5. Innes KE, Ducatman AM, Luster MI, et al. Association of osteoarthritis with serum levels of the environmental contaminants perfluorooctanoate and perfluorooctane sulfonate in a large Appalachian population. Am J Epidemiol 2011;174(4):440–450. doi:https://doi.org/10.1093/aje/kwr107
6. Driban JB, Rokoff LB, Lu B, et al. Per- and polyfluoroalkyl substances and hand osteoarthritis: data from the Osteoarthritis Initiative. Arthritis Rheumatol 2026;78(5):1076–1087. doi:https://doi.org/10.1002/art.70026
7. Yu CH, Patel B, Palencia M, et al. A sensitive and accurate method for the determination of perfluoroalkyl and polyfluoroalkyl substances in human serum using a high performance liquid chromatography-online solid phase extraction-tandem mass spectrometry. J Chromatogr A 2017;1480:1–10. doi:https://doi.org/10.1016/j.chroma.2016.11.063
8. Yu CH, Riker CD, Lu SE, et al. Biomonitoring of emerging contaminants, perfluoroalkyl and polyfluoroalkyl substances (PFAS), in New Jersey adults in 2016-2018. Int J Hyg Environ Health 2020;223(1):34–44. doi:https://doi.org/10.1016/j.ijheh.2019.10.008
9. Conaghan PG, Dworkin RH, Schnitzer TJ, et al. WOMAC meaningful within-patient change: results from 3 studies of tanezumab in patients with moderate-to-severe osteoarthritis of the hip or knee. J Rheumatol 2022;49(6):615–621. doi:https://doi.org/10.3899/jrheum.210543
10. Rokoff LB, Rifas-Shiman SL, Aris IM, et al. Mid-childhood plasma concentrations of per- and polyfluoroalkyl substances, modifiable lifestyle factors, and bone mineral density through late adolescence. Environ Sci Technol 2024;58(45):19970–19980. doi:https://doi.org/10.1021/acs.est.4c08480
11. Prentice RL. A case-cohort design for epidemiologic cohort studies and disease prevention trials. Biometrika 1986;73:1–11.
12. Keil AP, Buckley JP, O'Brien KM, et al. A quantile-based g-computation approach to addressing the effects of exposure mixtures. Environ Health Perspect 2020;128(4):47004. doi:https://doi.org/10.1289/EHP5838
13. Steinmetz JD, Culbreth GT, Haile LM, et al; GBD 2021 Osteoarthritis Collaborators. Global, regional, and national burden of osteoarthritis, 1990-2020 and projections to 2050: a systematic analysis for the Global Burden of Disease Study 2021. Lancet Rheumatol 2023;5(9):e508–e522. doi:https://doi.org/10.1016/S2665-9913(23)00163-7
14. Wolf CJ, Schmid JE, Lau C, et al. Activation of mouse and human peroxisome proliferator-activated receptor-alpha (PPARα) by perfluoroalkyl acids (PFAAs): further investigation of C4-C12 compounds. Reprod Toxicol 2012;33(4):546–551. doi:https://doi.org/10.1016/j.reprotox.2011.09.009
15. Centers for Disease Control and Prevention. National Report on Human Exposure to Environmental Chemicals. Accessed November 20, 2025. https://www.cdc.gov/environmental-exposure-report/

Check for updates

Arthritis & Rheumatology
Vol. 78, No. 10, October 2026, pp 2089–2101
DOI 10.1002/art.70134
© 2026 Eli Lilly and Company and The Author(s). *Arthritis & Rheumatology* published by Wiley Periodicals LLC on behalf of American College of Rheumatology.
This is an open access article under the terms of the Creative Commons Attribution-NonCommercial License, which permits use, distribution and reproduction in any medium, provided the original work is properly cited and is not used for commercial purposes.

American College of Rheumatology
Empowering Rheumatology Professionals

Ixekizumab With Tirzepatide Achieved Greater Disease Control Than Ixekizumab Alone in Adults With Psoriatic Arthritis and Overweight or Obesity: Results From a Randomized Clinical Trial

Joseph F. Merola, MD, MMSc, FAAD, FACR,[1] Philip Mease, MD,[2] Alan Kivitz, MD, MACR,[3] Naveed Sattar, FMedSci,[4] Laura C. Coates, MBChB, PhD,[5] Daniel Aletaha, MD, MS, MBA,[6] Cynthia E. Kartman, RN,[7] Peter Fischer, MD,[7] Luna Sun, PhD,[7] Píndaro Martínez-Osuna, MD,[7] Andris Kronbergs, PhD,[7] Purvi Prajapati, PhD,[7] Anabela Cardoso, MD,[7] Mark C. Genovese, MD,[7] and Alexis Ogdie, MD, MSCE[8]

Objective. Overweight or obesity is prevalent in 72% to 82% of individuals with psoriatic arthritis (PsA). We assessed the efficacy and safety of ixekizumab (IXE) concomitantly administered with tirzepatide (TZP) compared with IXE alone in adult participants with active PsA and overweight with at least one weight-related comorbidity or obesity.

Methods. TOGETHER-PsA (ClinicalTrials.gov identifier: NCT06588296) is a phase 3b, randomized, 52-week trial in adults with active PsA and overweight (body mass index [BMI] ≥27 to <30) with at least one weight-related comorbidity or obesity (BMI ≥30) using US-approved doses for IXE and TZP. The primary end point was simultaneous achievement of 50% improvement in American College of Rheumatology response criteria (ACR50) and ≥10% weight reduction at 36 weeks. Key secondary outcomes included ACR50. Additional secondary outcomes and patient-reported outcomes (PROs) were assessed. Safety was assessed as adverse events (AEs), treatment-emergent AEs, and serious AEs.

Results. A total of 271 participants were randomized (IXE + TZP, n = 138; IXE, n = 133). The primary end point was achieved with significant improvements in the IXE + TZP arm (31.7%) compared to IXE alone (0.8%) ($P < 0.001$). Greater improvements in ACR50 were demonstrated in IXE + TZP (33.5%) versus IXE alone (20.4%) ($P = 0.02$), with significant early separation at week 4 (nominal $P < 0.05$). IXE + TZP demonstrated nominally significant improvements in ACR20 ($P < 0.001$), minimal disease activity ($P < 0.05$), and absolute Psoriasis Area and Severity Index score ($P < 0.01$) compared to IXE alone. IXE + TZP demonstrated significant improvements in PROs, including Health Assessment Questionnaire–Disability Index (Δ −0.2; nominal $P < 0.001$) and Functional Assessment of Chronic Illness Therapy–Fatigue (improvement of 3.8; nominal $P < 0.01$) compared to IXE alone. Safety profiles were consistent with previous studies for each drug.

Conclusion. Participants with active PsA and complex inflammatory-metabolic disease achieved clinically meaningful improvement of PsA, physical function, weight reduction, and quality of life when treated with IXE + TZP compared to IXE alone, with no new safety concerns.

ClinicalTrials.gov identifier NCT06588296.
Supported by Eli Lilly and Company.
[1]Department of Dermatology and Department of Medicine, Division of Rheumatology, University of Texas Southwestern Medical Center and O'Donnell School of Public Health, Dallas; [2]Department of Rheumatology, Providence-Swedish Medical Center and University of Washington, Seattle; [3]Altoona Center for Clinical Research, Duncansville, Pennsylvania; [4]School of Cardiovascular and Metabolic Health, University of Glasgow, Glasgow, United Kingdom; [5]Nuffield Department of Orthopaedics, Rheumatology, and Musculoskeletal Sciences, University of Oxford, Oxford, United Kingdom; [6]Division of Rheumatology, Department of Internal Medicine III, Medical University of Vienna, Vienna, Austria; [7]Eli Lilly and Company, Indianapolis, Indiana; [8]Perelman School of Medicine, University of Pennsylvania, Philadelphia.

Lilly provides access to all individual participant data collected during the trial, after anonymization, with the exception of pharmacokinetic or genetic data. Data are available to request six months after the indication studied has been approved in the United States and European Union and after primary publication acceptance, whichever is later. No expiration date of data requests is currently set once data are made available. Access is provided after a proposal has been approved by an independent review committee identified for this purpose and after receipt of a signed data sharing agreement. Data and documents, including the study protocol, statistical analysis plan, clinical study

INTRODUCTION

Psoriatic arthritis (PsA) is a chronic, immune-mediated inflammatory disease characterized by synovitis, enthesitis, dactylitis, spondylitis, and coexisting psoriasis (PsO). Additionally, up to 30% to 40% of individuals with PsO develop PsA.[1,2] These manifestations contribute to joint pain, swelling, and potential irreversible structural damage when inadequately treated.[3] Patients with enthesitis, dactylitis, or substantial peripheral involvement often experience poorer general health and reduced quality of life (QoL).[4] PsA is further complicated by a higher burden of cardiometabolic comorbidities, including obesity, hypertension, dyslipidemia, diabetes mellitus, cardiovascular disease (CVD), and nonalcoholic fatty liver disease compared to the general population.[3,5]

Overweight or obesity is disproportionately prevalent in PsA compared with the general population, with estimates ranging[6] from 72% to 82% (Curtis J, et al: unpublished observations). Obesity is associated with increased prevalence of PsA up to two-fold higher compared to those with normal weight, which highlights obesity as a key modifiable risk factor[7] (Curtis J, et al: unpublished observations). Obesity promotes a chronic, low-grade inflammatory state through adipokine release and up-regulation of cytokines such as tumor necrosis factor α (TNFα), interleukin-17 (IL-17), and IL-6,[8] while mechanical stress at entheseal sites and reduced physical activity exacerbate musculoskeletal symptoms. Conversely, inflammation associated with PsA can contribute to weight gain and increased cardiovascular risk, emphasizing the link between these conditions.[9,10]

The coexistence of obesity and active PsA is clinically important, as higher body weight is associated with increased disease activity, attenuated response to biologic therapies, reduced likelihood of achieving minimal disease activity (MDA), and greater cardiovascular morbidity.[11] Obesity has been shown to negatively influence treatment response to biologics, such as TNFα inhibitors[12] and IL-17 inhibitors, although ixekizumab (IXE) maintains efficacy across body mass index (BMI) categories despite reduced absolute response rates in individuals with obesity.[13] Weight loss of ≥5% has been associated with improved PsA outcomes, including higher rates of MDA and reductions in proinflammatory mediators.[14–16] Consequently, major international guidelines (American College of Rheumatology [ACR]/National Psoriasis Foundation, the Group for Research and Assessment of Psoriasis and Psoriatic Arthritis [GRAPPA], the EULAR) advocate for assessment and management of obesity as part of comprehensive PsA care.[17–19]

IXE, a humanized monoclonal antibody targeting IL-17A,[20] is an established therapy for PsA, demonstrating efficacy in biologic-naïve and TNF inhibitor–experienced populations, superiority over adalimumab in a head-to-head trial, and sustained long-term benefit.[21–28] Tirzepatide (TZP), a long-acting dual glucose-dependent insulinotropic polypeptide receptor and glucagon-like peptide 1 (GLP-1) receptor agonist,[29] is approved for treatment of overweight in the presence of at least one weight-related comorbid condition or obesity and produces substantial, durable weight reduction accompanied by improvements in cardiometabolic risk factors and physical function.[30–33] TZP has also demonstrated anti-inflammatory effects, including reductions in high-sensitivity C-reactive protein (hsCRP) and IL-6 levels.[34] TZP has demonstrated superiority to semaglutide in participants with obesity and without diabetes mellitus in reduction in body weight and waist circumference at 72 weeks.[35]

Given the interplay between obesity, systemic inflammation, and PsA disease activity, use of an IL-17A inhibitor with an effective weight loss therapy may offer additive clinical benefits. IXE and TZP were used to treat two comorbid conditions, PsA and overweight/obesity, in this trial. Therefore, a multicomponent primary end point of simultaneous achievement of 50% improvement in ACR response criteria (ACR50)[36] and at least a 10% weight reduction at week 36 was selected to incorporate clinically meaningful end points for both diseases to evaluate the overall treatment benefits, and key secondary end points were selected to correspond to individual disease outcomes.

Therefore, this trial tested the efficacy and safety of IXE and TZP used concomitantly compared to IXE alone in participants with active PsA and overweight with at least one weight-related comorbidity or obesity.

METHODS

Trial design. TOGETHER-PsA is an ongoing 52-week, phase 3b, randomized, multicenter, open-label trial (ClinicalTrials.gov identifier NCT06588296) conducted in the United States, including Puerto Rico (Figure S1). This trial was designed to assess the treatment of IXE and concomitantly administered TZP (IXE + TZP) at the maximum tolerated dose (MTD) or IXE in participants with active PsA and overweight (BMI ≥27 to <30) in the presence of at least one weight-related comorbidity or obesity (BMI ≥30). All participants received individualized counseling from a dietician or equivalent delegate for a healthy diet and exercise. To minimize potential bias due to observed efficacy, a blinded assessor

report, and blank or annotated case report forms, will be provided in a secure data sharing environment. For details on submitting a request, see the instructions provided at www.vivli.org.

Additional supplementary information cited in this article can be found online in the Supporting Information section (https://acrjournals.onlinelibrary.wiley.com/doi/10.1002/art.70134).

Author disclosures and graphical abstract are available at https://onlinelibrary.wiley.com/doi/10.1002/art.70134.

Address correspondence via email to Mark C. Genovese, MD, at Mark.Genovese@lilly.com.

Submitted for publication February 3, 2026; accepted in revised form March 13, 2026.

completed assessments of tender joint count (TJC), swollen joint count (SJC), the Leeds Enthesitis Index, dactylitis count, the Psoriasis Area and Severity Index (PASI), and body surface area. To minimize interobserver variation, the same assessor was used to perform all the assessments of a participant, whenever possible. The primary outcome was assessed at week 36. After the week 36 visit, if the patient failed to demonstrate at least 20% improvement in TJC and SJC, the investigator could adjust the background standard-of-care therapy and use rescue medications.

IXE and TZP were administered according to the approved US prescribing information for each drug.[22,30] IXE was administered as a 160-mg subcutaneous (SC) injection at week 0, followed by 80 mg once every four weeks or the PsO-approved dosing for those with coexistent moderate-to-severe PsO. TZP was administered as an SC injection once weekly, with a starting dose of 2.5 mg for four weeks and dose escalation by 2.5-mg increments every four weeks to achieve MTD (5, 10, or 15 mg). From week 32 onward, the permitted maintenance dose was 5, 10, or 15 mg.

All participants were required to provide written informed consent before entering the trial. The trial was conducted according to the protocol and in line with consensus ethical principles derived from international guidelines, including the Declaration of Helsinki and Council for International Organizations of Medical Sciences International Ethical Guidelines, applicable International Council for Harmonisation Good Clinical Practice Guidelines, and applicable laws and regulations. The protocol, protocol amendments, informed consent form, investigator brochure, and other relevant documents were reviewed and approved by the institutional review board/independent ethics committee before initiation of the trial. The trial was registered at ClinicalTrials.gov (identifier NCT06588296).

Participants. TOGETHER-PsA enrolled participants between 18 and 80 years of age with signs and/or symptoms or documented diagnosis of PsA for a minimum of six months and currently fulfilling the Classification of Psoriatic Arthritis (CASPAR) criteria.[37] Participants were required to have active PsA, defined as having at least 3 or more of 68 tender joints and at least 3 or more of 66 swollen joints. Participants were also required to have overweight with at least one weight-related comorbidity (hypertension, dyslipidemia, obstructive sleep apnea, CVD, or type 2 diabetes mellitus [T2DM]) or obesity.

Key exclusion criteria included failure of more than three distinct classes of advanced therapies, prior use of IXE or TZP, and/or previous failure of or intolerance to an IL-17 inhibitor or GLP-1 receptor agonist. Participants were permitted to use background standard of care. Full details on prior and concomitant therapies, as well as full eligibility criteria, are provided in the Supplementary Material (see Tables S1–S3 and study protocol). Race and ethnicity were self-reported by participants using fixed selection categories.

Outcomes. The primary efficacy end point was simultaneous achievement of ACR50 and at least 10% weight reduction at week 36. Key secondary end points were achievement of ACR50, simultaneous achievement of ACR20 and at least 5% weight reduction, and achievement of at least 10% weight reduction at week 36. These end points were multiplicity controlled. Achievement of ACR50 over time was also assessed as a nongated end point.

Additional secondary end points that were not adjusted for multiplicity included Disease Activity Index for Psoriatic Arthritis (DAPSA)[38], MDA,[39] ACR20, ACR70, and ACR subcomponents. Dermatologic end points included PASI,[40] PASI75, PASI90, PASI100, and absolute PASI change from baseline (CFB).

Additional patient-reported outcomes (PROs), including CFB measurements for Functional Assessment of Chronic Illness Therapy–Fatigue (FACIT-F), Psoriatic Arthritis Impact of Disease (PsAID) total score, and Short-Form 36 Version 2 Health Survey (SF-36) mental component score (MCS) and physical component score (PCS), were evaluated. Metabolic outcomes assessed were BMI, body weight, glucose, hemoglobin A_{1c} (HbA_{1c}), lipids (namely, low-density lipoprotein cholesterol, high-density lipoprotein cholesterol, total cholesterol, and triglycerides), and systolic and diastolic blood pressure.

Safety assessments included incidence of adverse events (AEs). Treatment-emergent AEs (TEAEs), AEs of special interest, serious AEs (SAEs), and gastrointestinal (GI) AEs were assessed. Laboratory assessments were conducted according to the protocol.

Statistical analysis. Participants with active PsA and overweight or obesity were randomly assigned in a 1:1 ratio to either IXE + TZP or IXE (N = 271). Stratification factors for randomization were sex, treatment history (advanced therapy [biologic disease-modifying antirheumatic drug (bDMARD) and targeted synthetic DMARD (tsDMARD), except apremilast] naïve vs advanced therapy experienced), and BMI category (BMI ≥27 to <30 vs ≥30) at screening. The sample size was based on the primary end point assuming response rates were 46% and 4% for IXE + TZP and IXE, respectively. Using the two-sided chi-square test with an α of 0.05, a trial with an overall sample size of 250 has >90% power to detect such a treatment difference. Multiplicity-adjusted analyses were performed on the primary and key secondary objectives to control the overall family-wise Type 1 error rate at a two-sided α level of 0.05. The graphical multiple testing procedure was used as previously described.[41,42] This approach is a closed testing procedure; hence, it strongly controls the family-wise error rate across all hypotheses.[43]

Efficacy outcomes were assessed in the modified intent-to-treat (mITT) population, consisting of all randomly assigned participants with PsA and overweight with weight-related comorbidities or obesity. This mITT population was used to answer our key scientific question, which was to assess the treatment

efficacy difference between IXE and IXE with concomitantly administered TZP as an adjunct to a reduced-calorie diet and increased physical activity in the randomly assigned participants with active PsA and overweight in the presence of at least one weight-related comorbid condition or active PsA and obesity, had they continued taking their randomized treatment without prohibited medication use.

The hypothetical strategy[44] with intercurrent events of treatment discontinuation or initiation of prohibited medication was used to address this scientific question. This primary estimand[44] assessed average treatment effects of IXE + TZP and IXE under the condition that all participants who had undergone randomization continued receiving their randomized trial intervention for the entire treatment duration without initiation of prohibited medication. Data collected after an intercurrent event were excluded from the analyses and handled using multiple imputation. Imputations were performed separately by treatment arm to allow for differences in correlation patterns, dropout rates, and treatment responses between groups. The imputation model included stratification factors (sex, prior advanced treatment use, and BMI category), baseline values, and all available outcome data collected before the intercurrent event. All postbaseline visits up to week 36 were imputed simultaneously.

For binary outcomes, logistic regression was used as the working model to estimate unconditional risk difference with stratification variables included as covariates.[45] For continuous end points that were used for primary and key secondary end point derivation, analysis of covariance (ANCOVA) with robust variance was performed: the model included treatment, baseline value, and stratification variables as fixed factors. For continuous end points that were not used in derivation and had more than one postbaseline data collection per schedule of activities up to week 36, mixed model for repeated measures analysis was used: the model included treatment group, baseline value, randomization stratification factors, visit, and treatment interaction as fixed effects. For those with only one postbaseline data collection up to week 36, last observation carried forward was applied when early discontinuation data were available and ANCOVA was used.

Safety outcomes were assessed using the modified safety population, defined as mITT participants who were exposed to at least one dose of any of the trial treatments. Participants were included according to the trial intervention they received irrespective of adherence to trial drug.

RESULTS

Baseline characteristics and patient demographics. In keeping with the Consolidated Standards of Reporting Trials guidelines for reporting randomized trials,[46] the TOGETHER-PsA participant flow diagram is provided (Figure 1). Of 405 participants screened, the mITT population was composed of 271 participants (IXE + TZP, n = 138; IXE, n = 133). An additional eight participants without a specified weight-related comorbidity were excluded from the mITT population. In the mITT population, 116 (84.1%) completed IXE + TZP treatment and 89 (66.9%) completed IXE treatment (Figure 1). For the IXE + TZP treatment arm, 78.9% of participants with reported dosing data had TZP 15 mg, 8.3% TZP 10 mg, and 9.2% TZP 5 mg as their MTD.

The summary of baseline demographics and disease characteristics by treatment group is shown in Table 1. Overall, 69.7% of participants were female; the mean age was 55.0 (SD 11.9) years, the mean baseline weight was 106.1 (SD 24.8) kg, the mean screening BMI was 37.6 (SD 7.6), the mean FACIT-F score was 27.1 (SD 11.7), and the mean duration since PsA diagnosis was 8.9 (SD 9.8) years. Further, 71.6% of the participants had coexistent PsO, of which 4.4% had moderate-to-severe PsO and were assigned the approved PsO dosing regimen. Overall, 63.1% of participants were advanced therapy experienced (inclusive of prior exposure to bDMARD and tsDMARD, with the exception of apremilast; see Table S4), while 18.8% had failed two or more classes of advanced therapy.

Efficacy outcomes. The primary outcome and all key secondary outcomes were achieved. ACR50 and at least 10% weight reduction was statistically significant at week 36 with IXE + TZP (31.7%) versus 0.8% with IXE alone (treatment difference 30.9% [95% confidence interval (CI) 22.6%–39.1%]; $P < 0.001$) (Figure 2). From the key secondary outcomes, 69.7% of participants achieved simultaneous ACR20 and at least 5% weight reduction with IXE + TZP versus 10.3% with IXE alone (treatment difference 59.5% [95% CI 49.8%–69.2%]; $P < 0.001$) (Figure 2). Furthermore, 33.5% of participants achieved ACR50 with IXE + TZP versus 20.4% with IXE alone (treatment difference 13.1% [95% CI 2.1%–24.1%]; $P = 0.020$). Improvements in ACR50 were seen as early as week 4, with a significant difference between IXE + TZP and IXE alone (nominal $P < 0.05$), as shown in Figure 3. In addition, 84.5% achieved at least 10% weight reduction with IXE + TZP versus 4.5% with IXE alone (treatment difference 80.0% [95% CI 72.2%–87.9%]; $P < 0.001$) (Figure 2). Clinically significant improvements were observed for percentage CFB in body weight for the IXE + TZP treatment group versus IXE alone (Figure S2).

Additional prespecified nongated clinically relevant secondary outcomes showed improvements in IXE + TZP and IXE treatment arms, with higher responses in IXE + TZP compared to IXE alone. Significantly more participants achieved ACR20 response (71.3% vs 48.5%, treatment difference 22.8 [95% CI 10.0–35.6]; $P < 0.001$), MDA (26.3% vs 15.3%, treatment difference 11.0% [95% CI 1.3–20.6]; $P < 0.05$), and CFB in DAPSA (–32.4 vs –23.7, treatment difference –8.7 [95% CI –12.7 to –4.7]; $P < 0.001$) with IXE + TZP compared to IXE, with numerical improvements noted in ACR70 response in IXE + TZP compared to IXE alone (15.7% vs 8.4%, treatment difference 7.3 [95% CI –0.3 to 14.9]; $P = 0.060$). For the dermatologic outcomes, there

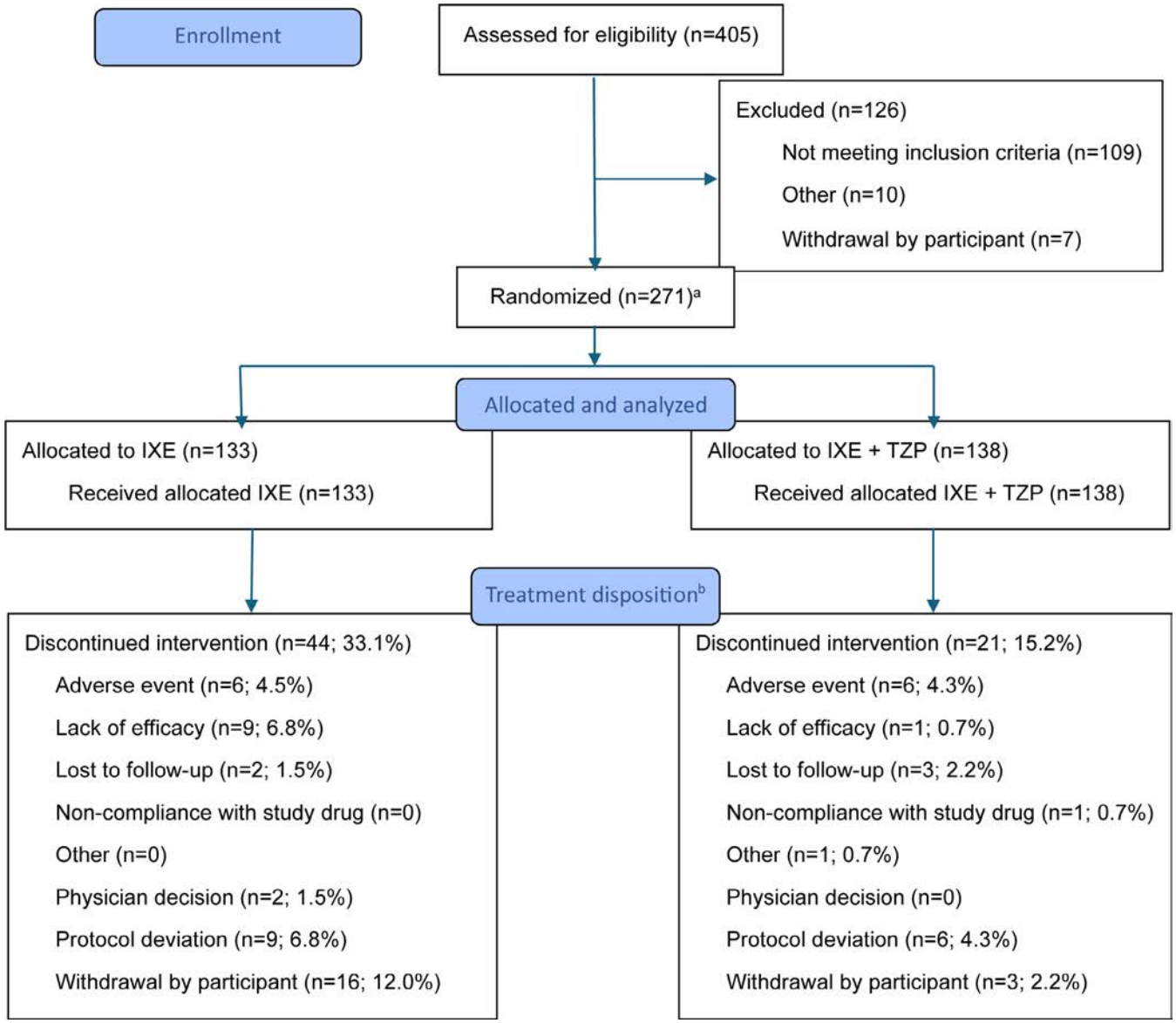


Figure 1. Flow of participants in the TOGETHER-PsA trial through week 36. Data from the modified intent-to-treat population up to the week 36 visit. [a]A total of 279 participants were randomized. Among them, eight participants did not have weight-related comorbidity due to early change in inclusion criteria and were excluded from the modified intent-to-treat population and the modified safety population. [b]One participant ongoing in the IXE + TZP arm. Although more participants in the IXE alone arm discontinued study intervention due to lack of efficacy compared to the IXE + TZP arm, no consistent pattern of discontinuation was identified for withdrawal by participant. Reasons for withdrawal included personal circumstances such as moving, scheduling conflicts, personal issues unrelated to the trial, and concern with study procedures, and only three participants suggested specifically that they wanted to pursue glucagon-like peptide-1 receptor agonist therapy. Discontinuation due to lack of efficacy did not delineate whether it was due to psoriatic disease activity or lack of weight loss. IXE, ixekizumab; TZP, tirzepatide.

was a significant difference in CFB between both treatment groups for absolute PASI score ($P < 0.01$). In participants with body surface area ≥3% at baseline, numerically higher response rates were achieved for the IXE + TZP treatment group compared to IXE alone for PASI75, PASI90, and PASI100 (Table 2).

There were improvements from baseline for the ACR core components and PROs with IXE + TZP and IXE alone. Among ACR components, significant differences were observed in the IXE + TZP arm in mean CFB for each of the following: TJC 68, SJC 66, patient global assessment of disease activity numerical rating scale, Health Assessment Questionnaire disability index (HAQ DI), and hsCRP (all nominal $P < 0.001$), with a significant difference also observed for physician global assessment of disease activity (nominal $P < 0.01$). Numerical improvements were observed in patient pain visual analog scale (VAS) in the IXE + TZP arm compared with IXE alone. Among PROs, significant improvements were observed in the CFB scores for FACIT-F, PsAID, and SF-36 MCS and PCS with IXE + TZP versus IXE alone (Table 2). The IXE + TZP arm had

Table 1. Key baseline demographics and disease characteristics*

Parameter	IXE (n = 133)	IXE + TZP (n = 138)	Total (N = 271)
Age, mean (SD), y	54.8 (11.9)	55.3 (11.8)	55.0 (11.9)
Female, n (%)	92 (69.2)	97 (70.3)	189 (69.7)
Baseline weight, mean (SD), kg	107.6 (24.4)	104.6 (25.2)	106.1 (24.8)
Screening BMI, mean (SD)[a]	38.3 (7.4)	37.0 (7.8)	37.6 (7.6)
Screening BMI category, n (%)[a]			
BMI ≥27 to <30[b]	14 (10.5)	20 (14.5)	34 (12.5)
BMI ≥30	119 (89.5)	118 (85.5)	237 (87.5)
Race, n (%)			
White	109 (82.0)	119 (86.2)	228 (84.1)
Black or African American	6 (4.5)	3 (2.2)	9 (3.3)
Asian	2 (1.5)	4 (2.9)	6 (2.2)
Multiple	3 (2.3)	2 (1.4)	5 (1.8)
Ethnicity, n (%)			
Hispanic or Latino	35 (26.3)	36 (26.1)	71 (26.2)
Non-Hispanic or non-Latino	97 (72.9)	98 (71.0)	195 (72.0)
Time since PsA diagnosis, mean (SD), y	8 (8.3)	10 (11.0)	8.9 (9.8)
csDMARDs experienced, n (%)			
No	63 (47.4)	59 (42.8)	122 (45.0)
Yes	70 (52.6)	79 (57.2)	149 (55.0)
csDMARDs inadequate response, n (%)			
No	95 (71.4)	93 (67.4)	188 (69.4)
Yes	38 (28.6)	45 (32.6)	83 (30.6)
DMARDs experienced, n (%)			
No	25 (18.8)	18 (13.0)	43 (15.9)
Yes	108 (81.2)	120 (87.0)	228 (84.1)
No. of prior advanced therapies by class, n (%)[c]			
0	51 (38.3)	49 (35.5)	100 (36.9)
1	60 (45.1)	60 (43.5)	120 (44.3)
2	15 (11.3)	24 (17.4)	39 (14.4)
>2	7 (5.3)	5 (3.6)	12 (4.4)
Treatment history, n (%)			
Advanced therapy experienced[d]	82 (61.7)	89 (64.5)	171 (63.1)
Advanced therapy naïve	51 (38.3)	49 (35.5)	100 (36.9)
Advanced therapies inadequate response, n (%)			
No	79 (59.4)	80 (58.0)	159 (58.7)
Yes	54 (40.6)	58 (42.0)	112 (41.3)
Participants with specific disease characteristics			
PsO, n (%)[e]	98 (73.7)	96 (69.6)	194 (71.6)
PASI total score, mean (SD)	3.3 (5.9)	3.2 (4.7)	3.3 (5.3)
BSA, mean (SD)	8.1 (15.1)	7.8 (12.3)	7.9 (13.7)
BSA ≥3%	75 (56.4)	76 (55.1)	151 (55.7)
sPGA, mean (SD)	2 (1.0)	2 (1.0)	2 (1.0)
Moderate-to-severe plaque PsO, n (%)[f]	7 (5.3)	5 (3.6)	12 (4.4)
Dactylitis count >0, n (%)	46 (34.6)	46 (33.3)	92 (33.9)
Baseline disease and quality of life scores			
TJC (68 joints), mean (SD)	27.9 (17.7)	25.5 (15.8)	26.7 (16.8)
SJC (66 joints), mean (SD)	12.8 (10.6)	11.9 (9.0)	12.3 (9.8)
PhGADA NRS, mean (SD)	6.2 (1.9)	6.3 (1.8)	6.2 (1.8)
PaGADA NRS, mean (SD)	6.6 (2.0)	6.5 (1.8)	6.5 (1.9)
Patient-reported pain VAS, mean (SD)	60.6 (22.5)	57 (21.6)	58.8 (22.1)
HAQ DI total score, mean (SD)	1.3 (0.6)	1.3 (0.6)	1.3 (0.6)
hsCRP (mg/L), mean (SD)	7.9 (11.4)	8.0 (14.7)	7.9 (13.2)
DAPSA, mean (SD)	55.4 (24.3)	47.2 (22.7)	51.3 (23.8)
LEI >0, n (%)[g]	110 (82.7)	111 (80.4)	221 (81.5)
FACIT-F, mean (SD)	27.3 (11.6)	27.0 (11.9)	27.1 (11.7)
PsAID-12 score, mean (SD)	5.9 (1.8)	5.8 (2.0)	5.9 (1.9)
SF-36 MCS, mean (SD)	48.8 (12.2)	48.4 (10.8)	48.6 (11.5)
SF-36 PCS, mean (SD)	33.1 (9.0)	32.8 (9.0)	33.0 (9.0)
EQ-5D 5L, mean (SD)	0.65 (0.16)	0.67 (0.15)	0.66 (0.15)
Metabolic characteristics			
Hypertension, n (%)	76 (57.1)	89 (64.5)	165 (60.9)
Dyslipidemia, n (%)	60 (45.1)	61 (44.2)	121 (44.6)

(Continued)

Table 1. (*Cont'd*)

Parameter	IXE (n = 133)	IXE + TZP (n = 138)	Total (N = 271)
Obstructive sleep apnea, n (%)	21 (15.8)	13 (9.4)	34 (12.5)
CVD, n (%)	11 (8.3)	13 (9.4)	24 (8.9)
T2DM, n (%)	16 (12.0)	14 (10.1)	30 (11.1)
Systolic blood pressure, mean (SD), mm Hg	132.5 (14.9)	130.3 (13.1)	131.4 (14.0)
Diastolic blood pressure, mean (SD), mm Hg	83.1 (9.3)	82.1 (7.7)	82.6 (8.5)
LDL cholesterol, mean (SD), mg/dL	107 (36.5)	104.1 (36.7)	105.5 (36.6)
HDL cholesterol, mean (SD), mg/dL	50.2 (12.9)	51.0 (12.6)	50.6 (12.7)
Total cholesterol, mean (SD), mg/dL	188.8 (41.5)	185.6 (38.3)	187.1 (39.9)
Triglycerides, mean (SD), mg/dL	161 (80.3)	156.9 (87.3)	158.9 (83.8)
Glucose, mean (SD), mg/dL	101.3 (23.5)	106.8 (40.0)	104.2 (33.2)
HbA_{1c}, mean (SD), %	5.8 (0.7)	5.8 (0.8)	5.8 (0.7)

* Baseline characteristics and disease characteristics are shown for the mITT (efficacy) population. BMI, body mass index; BSA, body surface area; csDMARD, conventional synthetic disease-modifying antirheumatic drug; CVD, cardiovascular disease; DAPSA, Disease Activity Index for Psoriatic Arthritis; DMARD, disease-modifying antirheumatic drug; EQ-5D 5L, European Quality of Life–5 dimensions 5 level; FACIT-F, Functional Assessment of Chronic Illness Therapy–Fatigue; HAQ DI, Health Assessment Questionnaire disability index; HbA_{1c}, hemoglobin A_{1c}; HDL, high-density lipoprotein; hsCRP, high-sensitivity C-reactive protein; IXE, ixekizumab; LDL, low-density lipoprotein; LEI, Leeds Enthesitis Index; MCS, mental component score; mITT, modified intent-to-treat; NRS, numerical rating scale; PaGADA, patient's global assessment of disease activity; PASI, Psoriasis Area and Severity Index; PCS, physical component score; PhGADA, physician's global assessment of disease activity; PsA, psoriasis arthritis; PsAID-12, Psoriatic Arthritis Impact of Disease 12; PsO, psoriasis; SF-36, 36-Item Short Form Health Survey; SJC, swollen joint count; sPGA, static physician's global assessment; T2DM, type 2 diabetes mellitus (non–insulin dependent); TJC, tender joint count; TZP tirzepatide; VAS, visual analog scale.
[a] Screening BMI used because it is the stratification variable.
[b] Comorbidity requirement.
[c] Prior therapies are categorized by drug class for stratification. Prior exposure to apremilast was not considered an advanced therapy. Patients using more than one drug of the same class were counted once here.
[d] Inclusive of prior exposure to biologic DMARDs and targeted synthetic DMARDs, with the exception of apremilast.
[e] Evaluated in participants with PsO, as qualitatively assessed by the investigator, at baseline.
[f] Moderate-to-severe plaque PsO was defined as having minimum BSA involvement of 10%, an sPGA score of ≥3 in the overall assessment (plaque thickness or induration, erythema, and scaling) of PsO on a severity scale of 0 to 4, and a PASI score ≥12. If applicable, participants must fulfill the above definition of moderate-to-severe plaque PsO at visit 2 to receive the PsO dosing regimen.
[g] Evaluated in participants with enthesitis, as qualitatively assessed by the investigator, at baseline.

higher responses than IXE alone in achieving 50% improvement in all individual components of ACR50 at week 36 (Figure S3).

Nominally statistically significant improvements were observed in metabolic outcomes in the IXE + TZP treatment group compared with the IXE treatment group for BMI, body weight, systolic blood pressure, glucose, HbA_{1c}, total cholesterol, and triglycerides (Table 2).

Safety outcomes. Overall, 73.7% of participants reported at least one TEAE, with the majority being mild to moderate in severity (Table 3). The most commonly reported TEAEs were GI AEs, including nausea (IXE + TZP: 29.7%; IXE: 3.0%;), diarrhea (IXE + TZP: 18.1%; IXE: 3.8%), constipation (IXE + TZP: 16.7%; IXE: 3.0%), and vomiting (IXE + TZP: 10.9%; IXE: 0.8%), which were more prevalent in the IXE + TZP arm compared to IXE alone. The incidence of injection site reactions (ISRs) was similar in both arms (IXE + TZP: 15.2%; IXE: 16.7%). SAEs were lower in the IXE + TZP arm compared to the IXE arm (3.6% vs 7.6%). There were no deaths (Table 3) or other significant differences in SAEs between treatment arms (Table S5). Discontinuation from study treatment due to an AE was similar in both arms (IXE + TZP: 5.1%; IXE: 5.3%) (Table 3).

DISCUSSION

This is the first randomized controlled trial to provide a robust assessment of concomitant use of an incretin therapy approved for weight loss (TZP) with a biologic (IXE) in patients with active PsA and overweight or obesity. The comprehensive body of evidence from this trial demonstrated improvements across and beyond both primary and all key secondary end points, indicating the concomitant use of IXE + TZP yielded meaningful benefits across all major domains of psoriatic disease, including clinical manifestations (TJC), acute-phase reactants (hsCRP), physical function (HAQ DI), PROs, QoL (SF-36 and FACIT-F), and cardiometabolic and weight-related parameters, surpassing the efficacy observed with IXE alone in this population.

The multicomponent primary objective requiring simultaneous achievement of ACR50 and at least a 10% weight reduction was statistically significant and clinically relevant given the high prevalence of overweight and obesity in the PsA population. These data suggest that PsA may be considered a weight-related comorbidity.

The improvement in ACR50 at week 36 as a key secondary composite measure suggests direct improvement of psoriatic disease activity with IXE + TZP versus IXE monotherapy. Furthermore, the statistically significant improvement as early as

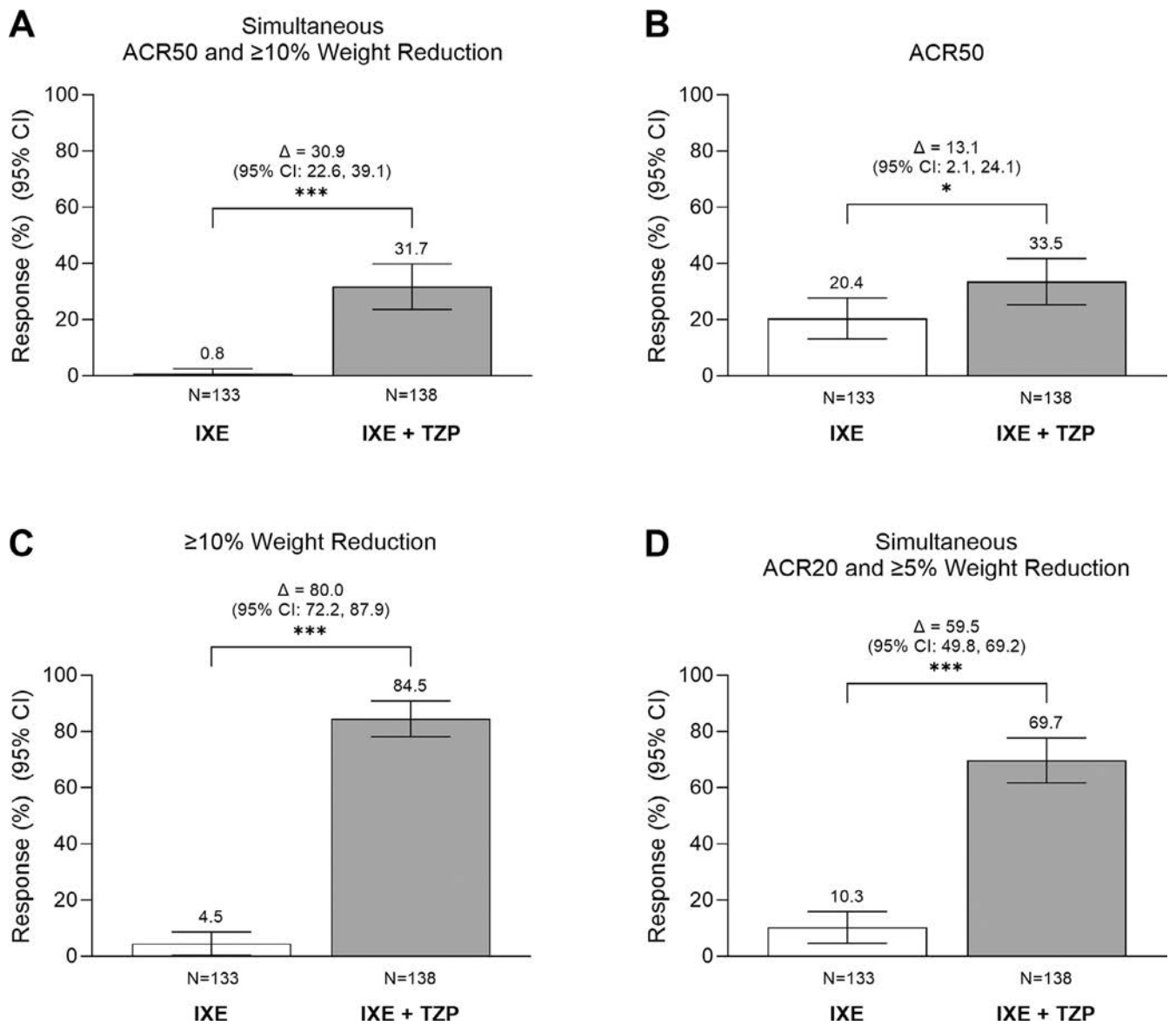


Figure 2. IXE with TZP demonstrated superiority in primary and key secondary outcomes versus IXE alone at week 36. Data are shown for (A) the primary outcome and (B–D) key secondary outcomes. Hypothetical estimand was used with multiple imputation. Logistic regression (with treatment, screening body mass index category, sex, and treatment history as factors) was used as a working model to estimate unconditional risk difference. Primary and key secondary outcomes were controlled for multiplicity. Δ = treatment difference of IXE + TZP versus IXE. *$P < 0.05$; ***$P < 0.001$. ACR20/50, 20%/50% improvement in American College of Rheumatology response criteria; CI, confidence interval; IXE, ixekizumab; TZP, tirzepatide.

week 4 observed in ACR50 at a nominal level and in numerical reductions in hsCRP levels with IXE + TZP versus IXE before clinically meaningful weight loss suggests a weight-independent benefit of TZP on PsA disease measures.

The impact in key domains of PsA was demonstrated by improvements in measurements of individual ACR components for both treatment groups, with significant improvements observed in the IXE + TZP arm versus IXE alone, except for pain VAS. In addition, significant improvements in PROs, such as HAQ DI and fatigue, and in QoL, such as PsAID, are meaningful outcomes of the concomitant IXE + TZP treatment, which are impactful for patients. The improvement in physical function (as measured by HAQ DI) is considered clinically meaningful with IXE + TZP, exceeding the well-defined HAQ DI minimally clinical important difference of −0.35.[4] A significant difference in the reduction of DAPSA CFB was observed in the IXE + TZP arm compared to IXE alone. Furthermore, significantly more patients treated with IXE + TZP versus IXE alone achieved MDA at week 36, a comprehensive aim and recommended goal for the management of patients with PsA.[17,18,39] The observed weight loss and improvement of systolic blood pressure, total cholesterol, triglycerides, HbA_{1c}, and glucose in the IXE + TZP arm are

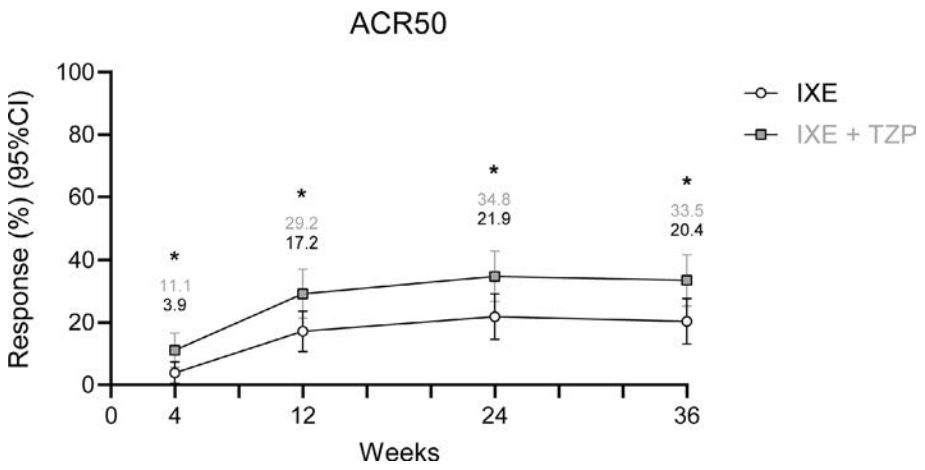


Figure 3. IXE and TZP showed significantly higher ACR50 responses versus IXE alone at week 4 and over time through week 36. Hypothetical estimand was used with multiple imputation. Logistic regression (with treatment, screening body mass index category, sex, and treatment history as factors) was used as a working model to estimate unconditional risk difference. Error bars represent 95% CIs for group-specific estimates. Statistical significance was assessed using formal tests of the between-group difference, not visual inspection of interval overlap. The week 36 end point was the only multiplicity-controlled time point. *$P < 0.05$. ACR50, 50% improvement in American College of Rheumatology response criteria; CI, confidence interval; IXE, ixekizumab; TZP, tirzepatide.

consistent with those reported for TZP in the SURMOUNT trials[31,32] and are additional considerations in the comprehensive treatment of PsA given the high prevalence and burden of overweight and obesity and greater risks for worse cardiovascular outcomes in PsA.

PsO end points were not the focus of TOGETHER-PsA because enrollment criteria did not include a requirement for participants to have PsO, although PsO is considered as a contributor to meeting CASPAR requirements. Only a minority of participants (4.4%) had moderate-to-severe PsO per protocol definition. Although assessments of PsO are limited, significant change in PASI from baseline and numerical improvements in PASI75/90/100 were observed, which may suggest an improved effect in the skin domain of the disease with the concomitant treatment. A specific trial of IXE + TZP to treat PsO (ClinicalTrials.gov identifier NCT06588283) is underway.

The participants in TOGETHER-PsA represent a more difficult to treat cohort than historical pivotal trials of current approved therapies for several reasons. At screening, 87.5% of patients had obesity (BMI ≥30), and the mean BMI was high at 37.6, which is associated with poor outcomes and negatively impacts response to biologics.[47] In addition, there was a high proportion of women among the participants in this trial at 69.7%. Women with PsA have consistently demonstrated lower efficacy responses compared with men, particularly with respect to the effectiveness of TNF inhibitors as reflected by lower remission rates.[48,49] Further, women present with higher disease burden at diagnosis, such as longer symptom duration and less favorable PROs, than men.[50] Furthermore, this trial recruited patients with failure of up to three classes of advanced therapies, including bDMARDs and/or tsDMARDs, which led to 18.8% of participants with previous failure of at least two classes of advanced therapy, representing a high proportion of patients with high unmet need.

Given the unique and complex inflammatory-metabolic disease of the study population in TOGETHER-PsA, the focus on the incremental benefit of the concomitant use of TZP with IXE compared with IXE alone, rather than the overall numerical improvement in composite measures of disease activity, is more meaningful for patient care, especially the changes in PROs, including fatigue, and in body weight (plus accompanying cardiometabolic improvements), with a near seven-unit difference in BMI seen by 36 weeks. For that reason, but also in general, it is challenging to directly compare numerical improvements in these measurements of PsA in this trial versus historical ones. However, given the high proportion (72%–82%) of patients with PsA with overweight or obesity[6] (Curtis J, et al: unpublished observations), the results of this trial are relevant to many patients with PsA.

AEs were consistent with established drug profiles. No unexpected safety concerns were observed for the IXE + TZP treatment arm, with fewer SAEs in the IXE + TZP arm compared with IXE alone (Table S4). The frequency of GI AEs in the IXE + TZP arm was generally comparable to that in trials that investigated TZP alone for weight management,[31,32] with nausea, diarrhea, constipation, and vomiting being the most common TEAEs in the IXE + TZP arm. Discontinuations due to GI AEs in the IXE + TZP arm (2.9%) were comparable to those observed in the weight management trial (SURMOUNT-1). ISRs have been associated with IXE administration in patients with PsA.[23,24] In our analysis, the frequency of ISRs was similar in both treatment arms and higher than that observed in conventional TZP trials, which could be attributed to the administration of IXE. Furthermore, the

Table 2. Additional secondary outcomes at week 36*

Parameter	IXE (n = 133)[a]	IXE + TZP (n = 138)[a]	Treatment difference (95% CI)	*P* value
Composite measures and enthesitis assessments				
ACR20	48.5 (38.4 to 58.6)	71.3 (63.4 to 79.1)	22.8 (10.0 to 35.6)	<0.001
ACR70	8.4 (3.6 to 13.2)	15.7 (9.6 to 21.8)	7.3 (−0.3 to 14.9)	0.060
MDA	15.3 (9.2 to 21.5)	26.3 (18.8 to 33.8)	11.0 (1.3 to 20.6)	0.026
DAPSA (CFB)	−23.7	−32.4	−8.7 (−12.7 to −4.7)	<0.001
Enthesitis (adjusted mean CFB)	−0.9	−1.6	−0.7 (−1.1 to −0.3)	0.002
Dermatologic outcomes[b]				
PASI75	52.5 (40.3 to 64.8)	64.4 (52.8 to 76.0)	11.9 (−5.5 to 29.2)	0.177
PASI90	35.6 (24.2 to 47.0)	52.2 (40.1 to 64.2)	16.6 (−0.0 to 33.1)	0.050
PASI100	26.6 (16.5 to 36.8)	36.9 (25.9 to 47.8)	10.2 (−4.7 to 25.2)	0.179
Absolute PASI (CFB)[c]	−3.3	−4.3	−0.9 (−1.6 to −0.2)	0.008
ACR components				
TJC 68	−12.1	−16.9	−4.8 (−7.6 to −2.1)	<0.001
SJC 66	−7.2	−9.7	−2.5 (−3.9 to −1.1)	<0.001
Patient assessment of arthritis pain VAS	−21.9	−25.3	−3.4 (−8.8 to 2.0)	0.217
PaGADA NRS	−2.1	−3.0	−1.0 (−1.5 to −0.4)	<0.001
PhGADA NRS	−3.3	−4.0	−0.7 (−1.2 to −0.2)	0.009
HAQ DI	−0.3	−0.5	−0.2 (−0.3 to −0.1)	<0.001
hsCRP (mg/L)	−0.44	−1.79	−1.35 (−2.10 to −0.61)	<0.001
PROs				
FACIT-F	4.8	8.6	3.8 (1.4 to 6.1)	0.002
PsAID total score	−2.0	−2.7	−0.7 (−1.2 to −0.2)	0.005
SF-36				
MCS	0.4	3.1	2.7 (0.1 to 5.2)	0.041
PCS	6.2	9.7	3.5 (1.5 to 5.6)	<0.001
Metabolic outcomes				
BMI	−0.45	−6.72	−6.27 (−6.93 to −5.62)	<0.001
Body weight, %	−1.1	−18.0	−16.9 (−18.6 to −15.2)	<0.001
Glucose, mg/dL	8.5	−15.3	−23.7 (−30.9 to −16.6)	<0.001
HbA_{1c}, %	0.1	−0.6	−0.7 (−0.9 to −0.5)	<0.001
HDL cholesterol, mg/dL	−0.29	−0.039	0.25 (−1.48 to 1.98)	0.777
LDL cholesterol, mg/dL	−2.52	−2.71	−0.19 (−9.97 to 9.60)	0.970
Total cholesterol, mg/dL	−0.80	−11.03	−10.24 (−19.0 to −1.52)	0.021
Triglycerides, mg/dL	2.5	−36.2	−38.8 (−51.8 to −25.7)	<0.001
Systolic blood pressure, mm Hg	−3.93	−10.81	−6.88 (−10.31 to −3.46)	<0.001
Diastolic blood pressure, mm Hg	−2.84	−4.69	−1.85 (−4.16 to 0.45)	0.114

* Hypothetical estimand was used. Nominal *P* values were reported. ACR20/70, 20%/70% improvement in American College of Rheumatology response criteria; BMI, body mass index; CFB, change from baseline; CI, confidence interval; DAPSA, Disease Activity Index for Psoriatic Arthritis; FACIT-F, Functional Assessment of Chronic Illness Therapy–Fatigue; HAQ DI, Health Assessment Questionnaire disability index; HbA_{1c}, hemoglobin A_{1c}; HDL, high-density lipoprotein; hsCRP, high-sensitivity C-reactive protein; IXE, ixekizumab; LDL, low-density lipoprotein; MCS, mental component score; MDA, minimal disease activity; NRS, numerical rating scale; PaGADA, patient global assessment of disease activity; PASI75/90/100, Psoriasis Area Severity Index criteria for 75%/90%/100% improvement; PCS, physical component score; PhGADA, physician global assessment of disease activity; PRO, patient-reported outcome; PsAID, Psoriatic Arthritis Impact of Disease; SF-36, 36-item Short Form Health Survey; SJC, swollen joint count; TJC, tender joint count; TZP, tirzepatide; VAS, visual analog scale.
[a] Data are presented as response % (95% CI) or as CFB.
[b] Assessed in participants with ≥3% body surface area at baseline: IXE, n = 75; IXE + TZP, n = 76.
[c] Post hoc.

frequency of upper respiratory tract infections was lower than that in historical SPIRIT phase 3 trials.

The limitations of this trial include the open-label approach for sites, participants, and the sponsor, mitigated with the use of blinded joint and skin assessors. An open-label design was selected to reflect real-world clinical practice given the likelihood that participants would be able to ascertain their treatment allocation based on early weight loss for those receiving

Table 3. Summary of safety outcomes*

Parameter	IXE (N = 132),[a] n (%)	IXE + TZP (N = 138), n (%)
TEAEs	95 (72.0)	104 (75.4)
Mild	40 (30.3)	42 (30.4)
Moderate	49 (37.1)	58 (42.0)
Severe	6 (4.5)	4 (2.9)
Most frequent TEAEs by PT[b]		
Nausea	4 (3.0)	41 (29.7)
Diarrhea	5 (3.8)	25 (18.1)
Constipation	4 (3.0)	23 (16.7)
ISR	22 (16.7)	21 (15.2)
Vomiting	1 (0.8)	15 (10.9)
Sinusitis	3 (2.3)	9 (6.5)
Urinary tract infection	4 (3.0)	9 (6.5)
Dizziness	1 (0.8)	8 (5.8)
Headache	1 (0.8)	8 (5.8)
Upper respiratory tract infection	7 (5.3)	5 (3.6)
SAEs	10 (7.6)	5 (3.6)
Deaths	0	0
Discontinued from study treatment due to AE	7 (5.3)	7 (5.1)
Discontinuation due to GI AEs	1 (0.8)	4 (2.9)
Abdominal pain upper	0	1 (0.7)
Colitis ulcerative	0	1 (0.7)
Diarrhea	0	1 (0.7)
Nausea	0	1 (0.7)
Colitis[c]	1 (0.8)	0
AEs of special interest		
Hypersensitivity reactions	0	0
ISRs[d]	24 (18.2)	21 (15.2)
Hypoglycemia for those with T2DM at baseline	0	1 (0.7)
Severe/serious hypoglycemia	0	0
Pancreatitis	0	0
Serious/severe GI AEs	1 (0.8)	1 (0.7)
Upper abdominal pain	0	1 (0.7)
Nausea	0	1 (0.7)
Colitis[c]	1 (0.8)	0
Infections and infestations	49 (37.1)	51 (37.0)
Opportunistic infections	2 (1.5)	2 (1.4)
Suicidal ideation	1 (0.8)	0
Inflammatory bowel disease	1 (0.8)	1 (0.7)

* Data from the modified safety population up to the cutoff date. AEs are represented as MedDRA version 28.1 PTs. AE, adverse event; GI, gastrointestinal; ISR, infection site reaction; IXE, ixekizumab; N, number of participants in the patient population; n, number of participants with at least one event reported; PT, preferred term; SAE, serious adverse event; T2DM, type 2 diabetes mellitus; TEAE, treatment-emergent adverse event; TZP, tirzepatide.
[a] One participant was randomized but did not receive the study treatment.
[b] AEs occurring in ≥5% of participants.
[c] Reported as colitis with ulceration, which could not be definitively confirmed as inflammatory bowel disease. Study drug was withdrawn.
[d] ISRs are a cluster of individual AE PTs.

TZP. We also observed that more participants in the IXE alone arm discontinued study intervention due to lack of efficacy and withdrawal by participant, the latter of which showed no consistent pattern of discontinuation. Because this was an open-label trial, reasons for discontinuation due to lack of efficacy were captured at a high level and did not systematically ascertain whether insufficient response was driven by inadequate joint improvement, lack of weight loss, or a combination of both.

This trial did not include patients with a normal BMI or patients with overweight with a BMI of 25 to <27 to follow the TZP approved label at the time of protocol development. This trial did not evaluate participants if they had any prior or current inadequate response to IL-17 inhibitor(s), which will be addressed in an ongoing trial (ClinicalTrials.gov identifier NCT06864026) in PsA that includes participants currently taking IXE and evaluates the addition of TZP. Lastly, it should be noted that this trial was conducted solely in the United States in contrast to historical IXE large, global phase 3 PsA trials.

Concomitant administration of IXE and TZP was superior to IXE alone in achieving key efficacy outcomes by 36 weeks, as well as improvement in ACR50 as early as 4 weeks of treatment in patients with complex inflammatory-metabolic disease, with no new safety concerns. Specifically, these results highlight improvements in rheumatic and dermatologic disease activity end points, weight and cardiometabolic end points, biomarkers and laboratory measures, and overall health of patients, as evidenced by significant improvements in PROs and QoL.

This is the first randomized controlled trial of TZP and IXE in patients with PsA and overweight or obesity that addresses the comprehensive management needs of this patient population with a positive meaningful impact in multiple domains of PsA disease, including disease control and its comorbidities. These data strengthen the EULAR and GRAPPA treatment guidelines, which recommend that clinicians consider comorbidities in the patient's treatment approach to achieve low disease activity or remission.[18,19]

Additional studies are warranted to evaluate a possible anti-inflammatory effect of TZP in PsA. The addition of TZP to IXE represents a potential paradigm shift to optimize comprehensive clinical outcomes and patient QoL in the appropriate patient population.

ACKNOWLEDGMENTS

The authors would like to thank all the participants and investigators who took part in this trial. The authors would also like to thank Mathijs C. Bunck, MD, PhD, of Eli Lilly and Company for his significant contribution to the trial design and development, as well as medical expertise, and Ann Leung, MS, Yurong Chen, PhD, Fangui Sun, PhD, and Jordan Bauer, MS, for their considerable contributions to statistical analysis.

AUTHOR CONTRIBUTIONS

All authors contributed to at least one of the following manuscript preparation roles: conceptualization AND/OR methodology, software, investigation, formal analysis, data curation, visualization, and validation AND drafting or reviewing/editing the final draft. As corresponding author, Dr Genovese confirms that all authors have provided the final

approval of the version to be published and takes responsibility for the affirmations regarding article submission (eg, not under consideration by another journal), the integrity of the data presented, and the statements regarding compliance with institutional review board/Declaration of Helsinki requirements.

ROLE OF THE STUDY SPONSOR

Eli Lilly and Company contributed to the trial design, data collection, data analysis, data interpretation, preparation of the manuscript, and the decision to submit the paper for publication. All authors had full access to all of the data in the trial and had final responsibility for the decision to submit for publication. All authors critically revised the manuscript. Medical writing support was provided by Alexandre Chappard, PhD, Amelia Torcello Gomez, PhD, Himanshi Bhatia, PhD, and Nancy Tan, PharmD, all of Eli Lilly and Company. Publication of this article was not contingent upon approval by Eli Lilly and Company.

REFERENCES

1. Mease PJ, Armstrong AW. Managing patients with psoriatic disease: the diagnosis and pharmacologic treatment of psoriatic arthritis in patients with psoriasis. Drugs 2014;74(4):423–441. doi:10.1007/s40265-014-0191-y
2. Kharouf F, Gladman DD. Advances in the management of psoriatic arthritis in adults. BMJ 2024;387:e081860. doi:10.1136/bmj-2024-081860
3. Williams JC, Hum RM, Rogers K, et al. Metabolic syndrome and psoriatic arthritis: the role of weight loss as a disease-modifying therapy. Ther Adv Musculoskelet Dis 2024;16:1759720X241271886. doi:10.1177/1759720X241271886
4. Walsh JA, Ogdie A, Michaud K, et al. Impact of key manifestations of psoriatic arthritis on patient quality of life, functional status, and work productivity: findings from a real-world study in the United States and Europe. Joint Bone Spine 2023;90(3):105534. doi:10.1016/j.jbspin.2023.105534
5. Ruiz-Ponce M, Cuesta-López L, López-Montilla MD, et al. Decoding clinical and molecular pathways of liver dysfunction in psoriatic arthritis: impact of cumulative methotrexate doses. Biomed Pharmacother 2023;168:115779. doi:10.1016/j.biopha.2023.115779
6. Eder L, Thavaneswaran A, Chandran V, et al. Obesity is associated with a lower probability of achieving sustained minimal disease activity state among patients with psoriatic arthritis. Ann Rheum Dis 2015;74(5):813–817. doi:10.1136/annrheumdis-2013-204448
7. Haberman RH, Ogdie A, Merola JF, et al. The obesity-inflammation axis in psoriatic disease: mechanisms and therapeutic strategies. Nat Rev Rheumatol 2026;22(3):151–164. doi:10.1038/s41584-025-01326-6
8. Kumthekar A, Ogdie A. Obesity and psoriatic arthritis: a narrative review. Rheumatol Ther 2020;7(3):447–456. doi:10.1007/s40744-020-00215-6
9. Porta S, Otero-Losada M, Kölliker Frers RA, et al. Adipokines, cardiovascular risk, and therapeutic management in obesity and psoriatic arthritis. Front Immunol 2021;11:590749. doi:10.3389/fimmu.2020.590749
10. Jamnitski A, Symmons D, Peters MJ, et al. Cardiovascular comorbidities in patients with psoriatic arthritis: a systematic review. Ann Rheum Dis 2013;72(2):211–216. doi:10.1136/annrheumdis-2011-201194
11. Klingberg E, Bilberg A, Björkman S, et al. Weight loss improves disease activity in patients with psoriatic arthritis and obesity: an interventional study. Arthritis Res Ther 2019;21(1):17. doi:10.1186/s13075-019-1810-5
12. di Minno MN, Peluso R, Iervolino S, et al. Obesity and the prediction of minimal disease activity: a prospective study in psoriatic arthritis. Arthritis Care Res (Hoboken) 2013;65(1):141–147. doi:10.1002/acr.21711
13. Eder L, Odhav S, Korkosz M, et al. FRI0430 Ixekizumab improves the signs and symptoms of psoriatic arthritis regardless of sex, duration of disease, or body mass index in two randomized, phase 3 clinical trials [abstract]. Ann Rheum Dis 2019;78(suppl 2):904–905. doi:10.1136/annrheumdis-2019-eular.1474
14. Di Minno MN, Peluso R, Iervolino S, et al; CaRRDs Study Group. Weight loss and achievement of minimal disease activity in patients with psoriatic arthritis starting treatment with tumour necrosis factor α blockers. Ann Rheum Dis 2014;73(6):1157–1162. doi:10.1136/annrheumdis-2012-202812
15. Leung YY, Eder L, Orbai AM, et al. Association between obesity and likelihood of remission or low disease activity status in psoriatic arthritis applying index-based and patient-based definitions of remission: a cross-sectional study. RMD Open 2023;9(3):e003157. doi:10.1136/rmdopen-2023-003157
16. Landgren AJ, Jonsson CA, Bilberg A, et al. Serum IL-23 significantly decreased in obese patients with psoriatic arthritis six months after a structured weight loss intervention. Arthritis Res Ther 2023;25(1):131. doi:10.1186/s13075-023-03105-8
17. Singh JA, Guyatt G, Ogdie A, et al. 2018 American College of Rheumatology/National Psoriasis Foundation guideline for the treatment of psoriatic arthritis. Arthritis Rheumatol 2019;71(1):5–32. doi:10.1002/art.40726
18. Coates LC, Soriano ER, Corp N, et al; GRAPPA Treatment Recommendations domain subcommittees. Group for Research and Assessment of Psoriasis and Psoriatic Arthritis (GRAPPA): updated treatment recommendations for psoriatic arthritis 2021. Nat Rev Rheumatol 2022;18(8):465–479. doi:10.1038/s41584-022-00798-0
19. Gossec L, Kerschbaumer A, Ferreira RJO, et al. EULAR recommendations for the management of psoriatic arthritis with pharmacological therapies: 2023 update. Ann Rheum Dis 2024;83(6):706–719. doi:10.1136/ard-2024-225531
20. Liu L, Lu J, Allan BW, et al. Generation and characterization of ixekizumab, a humanized monoclonal antibody that neutralizes interleukin-17A. J Inflamm Res 2016;9:39–50. doi:10.2147/JIR.S100940
21. Blauvelt A, Chiricozzi A. The immunologic role of IL-17 in psoriasis and psoriatic arthritis pathogenesis. Clin Rev Allergy Immunol 2018;55(3):379–390. doi:10.1007/s12016-018-8702-3
22. Eli Lilly and Company. Taltz highlights of prescribing information. 2024. Updated August 2024. https://pi.lilly.com/us/taltz-uspi.pdf
23. Mease PJ, van der Heijde D, Ritchlin CT, et al; SPIRIT-P1 Study Group. Ixekizumab, an interleukin-17A specific monoclonal antibody, for the treatment of biologic-naive patients with active psoriatic arthritis: results from the 24-week randomised, double-blind, placebo-controlled and active (adalimumab)-controlled period of the phase III trial SPIRIT-P1. Ann Rheum Dis 2017;76(1):79–87. doi:10.1136/annrheumdis-2016-209709
24. Nash P, Kirkham B, Okada M, et al; SPIRIT-P2 Study Group. Ixekizumab for the treatment of patients with active psoriatic arthritis and an inadequate response to tumour necrosis factor inhibitors: results from the 24-week randomised, double-blind, placebo-controlled period of the SPIRIT-P2 phase 3 trial. Lancet 2017;389(10086):2317–2327. doi:10.1016/S0140-6736(17)31429-0
25. Mease PJ, Smolen JS, Behrens F, et al; SPIRIT H2H study group. A head-to-head comparison of the efficacy and safety of ixekizumab and adalimumab in biological-naïve patients with active psoriatic arthritis: 24-week results of a randomised, open-label, blinded-assessor trial. Ann Rheum Dis 2020;79(1):123–131. doi:10.1136/annrheumdis-2019-215386

26. Orbai AM, Gratacós J, Turkiewicz A, et al. Efficacy and safety of ixekizumab in patients with psoriatic arthritis and inadequate response to TNF inhibitors: 3-year follow-up (SPIRIT-P2). Rheumatol Ther 2021; 8(1):199–217. doi:10.1007/s40744-020-00261-0
27. Chandran V, van der Heijde D, Fleischmann RM, et al. Ixekizumab treatment of biologic-naïve patients with active psoriatic arthritis: 3-year results from a phase III clinical trial (SPIRIT-P1). Rheumatology (Oxford) 2020;59(10):2774–2784. doi:10.1093/rheumatology/kez684
28. Smolen JS, Sebba A, Ruderman EM, et al. Efficacy and safety of ixekizumab with or without methotrexate in biologic-naïve patients with psoriatic arthritis: 52-week results from SPIRIT-H2H study. Rheumatol Ther 2020;7(4):1021–1035. doi:10.1007/s40744-020-00250-3
29. Coskun T, Sloop KW, Loghin C, et al. LY3298176, a novel dual GIP and GLP-1 receptor agonist for the treatment of type 2 diabetes mellitus: from discovery to clinical proof of concept. Mol Metab 2018;18: 3–14. doi:10.1016/j.molmet.2018.09.009
30. Eli Lilly and Company. Zepbound highlights of prescribing information. 2025. Updated September 2025. https://pi.lilly.com/us/zepbound-uspi.pdf
31. Jastreboff AM, Aronne LJ, Ahmad NN, et al; SURMOUNT-1 Investigators. Tirzepatide once weekly for the treatment of obesity. N Engl J Med 2022;387(3):205–216. doi:10.1056/NEJMoa2206038
32. Garvey WT, Frias JP, Jastreboff AM, et al; SURMOUNT-2 investigators. Tirzepatide once weekly for the treatment of obesity in people with type 2 diabetes (SURMOUNT-2): a double-blind, randomised, multicentre, placebo-controlled, phase 3 trial. Lancet 2023; 402(10402):613–626. doi:10.1016/S0140-6736(23)01200-X
33. Wadden TA, Chao AM, Machineni S, et al. Tirzepatide after intensive lifestyle intervention in adults with overweight or obesity: the SURMOUNT-3 phase 3 trial. Nat Med 2023;29(11):2909–2918. doi: 10.1038/s41591-023-02597-w
34. Sattar N, Verma S, Sourij H, et al. Abstract 4139912: Inflammatory biomarkers in people treated with tirzepatide living with overweight or obesity, without and with T2D: a post-hoc analysis from SURMOUNT-1 and SURMOUNT-2 [abstract]. Circulation 2024;150-(suppl 1). doi:10.1161/circ.150.suppl_1.4139912
35. Aronne LJ, Horn DB, le Roux CW, et al; SURMOUNT-5 Trial Investigators. Tirzepatide as compared with semaglutide for the treatment of obesity. N Engl J Med 2025;393(1):26–36. doi:10.1056/NEJMoa2416394
36. Felson DT, Anderson JJ, Boers M, et al. American College of Rheumatology. Preliminary definition of improvement in rheumatoid arthritis. Arthritis Rheum 1995;38(6):727–735. doi:10.1002/art.1780380602
37. Taylor W, Gladman D, Helliwell P, et al; CASPAR Study Group. Classification criteria for psoriatic arthritis: development of new criteria from a large international study. Arthritis Rheum 2006;54(8):2665–2673. doi:10.1002/art.21972
38. Ogdie A, Coates LC, Mease P. Measuring outcomes in psoriatic arthritis. Arthritis Care Res (Hoboken) 2020;72(suppl 10):82–109. doi:10.1002/acr.24242
39. Coates LC, Fransen J, Helliwell PS. Defining minimal disease activity in psoriatic arthritis: a proposed objective target for treatment. Ann Rheum Dis 2010;69(1):48–53. doi:10.1136/ard.2008.102053
40. Mease PJ. Measures of psoriatic arthritis: tender and swollen joint assessment, Psoriasis Area and Severity Index (PASI), Nail Psoriasis Severity Index (NAPSI), Modified Nail Psoriasis Severity Index (mNAPSI), Mander/Newcastle Enthesitis Index (MEI), Leeds Enthesitis Index (LEI), Spondyloarthritis Research Consortium of Canada (SPARCC), Maastricht Ankylosing Spondylitis Enthesis Score (MASES), Leeds Dactylitis Index (LDI), Patient Global for Psoriatic Arthritis, Dermatology Life Quality Index (DLQI), Psoriatic Arthritis Quality of Life (PsAQOL), Functional Assessment of Chronic Illness Therapy-Fatigue (FACIT-F), Psoriatic Arthritis Response Criteria (PsARC), Psoriatic Arthritis Joint Activity Index (PsAJAI), Disease Activity in Psoriatic Arthritis (DAPSA), and Composite Psoriatic Disease Activity Index (CPDAI). Arthritis Care Res (Hoboken) 2011;63-(suppl 11):S64–S85.
41. Bretz F, Posch M, Glimm E, et al. Graphical approaches for multiple comparison procedures using weighted Bonferroni, Simes, or parametric tests. Biom J 2011;53(6):894–913. doi:10.1002/bimj.201000239
42. Bretz F, Maurer W, Brannath W, et al. A graphical approach to sequentially rejective multiple test procedures. Stat Med 2009;28(4): 586–604. doi:10.1002/sim.3495
43. Alosh M, Bretz F, Huque M. Advanced multiplicity adjustment methods in clinical trials. Stat Med 2014;33(4):693–713. doi:10.1002/sim.5974
44. European Medicines Agency. ICH E9 (R1) Addendum on Estimands and Sensitivity Analysis in Clinical Trials to the Guideline on Statistical Principles for Clinical Trials. Committee for Medicinal Products for Human Use; 2020.
45. US Food and Drug Administration. Adjusting for Covariates in Randomized Clinical Trials for Drugs and Biological Products Guidance for Industry. US Department of Health and Human Services; 2023.
46. Hopewell S, Chan AW, Collins GS, et al. CONSORT 2025 statement: updated guideline for reporting randomised trials. BMJ 2025;389: e081123. doi:10.1136/bmj-2024-081123
47. Højgaard P, Glintborg B, Kristensen LE, et al. The influence of obesity on response to tumour necrosis factor-α inhibitors in psoriatic arthritis: results from the DANBIO and ICEBIO registries. Rheumatology (Oxford) 2016;55(12):2191–2199. doi:10.1093/rheumatology/kew326
48. Siebert S, Sattar N, Ferguson LD. Weighing in on obesity and psoriatic arthritis - time to move beyond association to robust randomised trials. Joint Bone Spine 2025;92(5):105904. doi:10.1016/j.jbspin.2025.105904
49. Baciu T, Neagu AE, Saulescu IC, et al. Unveiling sex-related variability in psoriatic arthritis: a call for personalized care. J Clin Med 2025; 14(12):4124. doi:10.3390/jcm14124124
50. Passia E, Vis M, Coates LC, et al. Sex-specific differences and how to handle them in early psoriatic arthritis. Arthritis Res Ther 2022;24(1): 22. doi:10.1186/s13075-021-02680-y

Check for updates

Arthritis & Rheumatology
Vol. 78, No. 10, October 2026, pp 2102–2109
DOI 10.1002/art.70145
© 2026 The Author(s). *Arthritis & Rheumatology* published by Wiley Periodicals LLC on behalf of American College of Rheumatology.
This is an open access article under the terms of the Creative Commons Attribution-NonCommercial-NoDerivs License, which permits use and distribution in any medium, provided the original work is properly cited, the use is non-commercial and no modifications or adaptations are made.

American College of Rheumatology
Empowering Rheumatology Professionals

Functional Impact of Structural Damage in Psoriatic Arthritis: Insights from a Prospective Cohort Study

Pankti Mehta, MBBS, MD, DM,[1,2,3] Shangyi Gao, BSc, MSc,[1] Virginia Carrizo Abarza, MD,[1,2] Fadi Kharouf, MD,[1,2,4] Daniel Pereira, BSc,[1] Richard J. Cook, BSc, MMath, PhD,[5] Dafna D. Gladman, MD, FRCPC, OC,[1,2,3] Vinod Chandran, MBBS, MD, DM, PhD,[1,2,3,6] and Denis Poddubnyy, MD, PhD, MSc[1,2,3]

Objective. To examine the association between radiographic structural damage and physical function (PF) in psoriatic arthritis (PsA).

Methods. Data were analyzed from a large longitudinal PsA cohort. PF was measured using the Health Assessment Questionnaire (HAQ, 0–3) and Short Form-36 PF subscale (SF-36, 0–100); radiographic joint damage was measured using the modified Steinbrocker score (mSS, 0–168). Associations between PF and mSS were analyzed using linear mixed models. We also evaluated the impact of the presence of any damaged joint (grade 2–4), joint damage by individual grades, and the number of damaged joints (grade 2–4) per patient on PF.

Results. Of 1,177 patients (mean ± SD age 44.61 ± 12.76 years; 55.8% men), baseline mSS was 2 (interquartile range [IQR] 0–8.5), HAQ was 0.62 (IQR 0.12–1.12), and SF-36 PF was 60 (IQR 35–85). Higher mSS was significantly associated with worse SF-36 PF (β = −0.10; 95% confidence interval [CI] −0.15 to −0.05) and HAQ (β = 0.003; 95% CI 0.002 to 0.004) after controlling for swollen joint count, sex, and disease duration. The number of damaged joints was associated with worse SF-36 PF (β = −0.23; 95% CI −0.38 to −0.08) and HAQ (β = 0.005; 95% CI 0.002 to 0.009). The presence of a damaged joint (grade 2–4) alone did not impact PF. However, the presence of a joint with grade 4 destruction was associated with substantially worse SF-36 PF (β = −3.04; 95% CI −5.93 to −0.15) and HAQ (β = 0.09; 95% CI 0.03 to 0.15). Increasing counts of grade 4 joints demonstrated a strong dose response with SF-36 PF (β = −0.54; 95% CI −0.81 to −0.26) and HAQ (β = 0.01; 95% CI 0.01 to 0.02).

Conclusion. Radiographic structural damage, particularly severe joint destruction, is independently associated with impaired PF in PsA, highlighting the importance of early detection and prevention of damage.

INTRODUCTION

Persistent articular inflammation in psoriatic arthritis (PsA) disrupts the balance between destructive and reparative mechanisms in cartilage and bone. This results in classical radiographic findings including erosions, joint space narrowing (JSN), and new bone formation.[1] PsA significantly impacts quality of life, physical function (PF), and work disability, which are believed to reflect both disease activity and structural joint damage.[2] Structural damage can be observed as early as 2 years into the disease course[3,4] and is a predictor of future damage.[5]

One of the primary therapeutic goals in PsA is to prevent or inhibit structural damage progression while optimizing functional status and quality of life.[6] Radiographic assessment provides an objective means to monitor structural damage over time and remains a standard approach in clinical trials of PsA.[7–10]

Current research recommendations highlight the need to define prognostic factors, including the relationship between structural damage and functional outcomes.[11] Although it is

[1]Gladman Krembil Psoriatic Arthritis Program, Centre for Prognosis Studies in the Rheumatic Diseases, Schroeder Arthritis Institute, Krembil Research Institute, University Health Network, Toronto, Ontario, Canada; [2]Division of Rheumatology, Department of Medicine, University of Toronto, Toronto, Ontario, Canada; [3]Institute of Medical Science, University of Toronto, Toronto, Ontario, Canada; [4]Rheumatology Unit, Department of Medicine, Hadassah Medical Center and Faculty of Medicine, Hebrew University of Jerusalem, Israel; [5]Department of Statistics and Actuarial Science, University of Waterloo, Waterloo, Ontario, Canada; [6]Department of Laboratory Medicine and Pathobiology, University of Toronto, Toronto, Ontario, Canada.

Additional supplementary information cited in this article can be found online in the Supporting Information section (https://acrjournals.onlinelibrary.wiley.com/doi/10.1002/art.70145).

Author disclosures and graphical abstract are available at https://onlinelibrary.wiley.com/doi/10.1002/art.70145.

Address correspondence via email to Denis Poddubnyy, MD, PhD, MSc, at denis.poddubnyy@uhn.ca.

Submitted for publication November 24, 2025; accepted in revised form February 4, 2026.

widely accepted that structural damage is linked to poor functional outcomes, only one study to date has quantitatively evaluated this relationship using the modified Sharp-van der Heijde (mSvdH) scoring system.[4] Importantly, that study was limited to a clinical trial database, which may not fully capture real-world variability. The analyses adjusted only for disease activity, leaving other potential confounders, like demographics, unaccounted for. This gap complicates the interpretation of radiographic changes, as it remains unclear whether observed changes translate to clinically meaningful functional gains, especially in large, real-world cohorts with long-term follow-up.[12–14]

With the advent of biologic disease-modifying antirheumatic drugs (bDMARDs) and targeted synthetic (ts) DMARDs, the prevalence of severe joint damage has declined.[15] This raises an important question of the precise contribution of radiographic progression to the PF impairment. Addressing this is crucial, as structural damage is generally irreversible and a major contributor to permanent disability.

Therefore, we hypothesized that structural damage is independently associated with PF. We aimed to study the impact of structural damage on PF in PsA in a large, real-world cohort of PsA.

PATIENTS AND METHODS

Setting. This was a longitudinal observational cohort study conducted at the Gladman Krembil PsA Program, Schroeder Arthritis Institute, Toronto, Ontario, Canada.[16] Since 1978, patients with PsA have been systematically observed at 6- to 12-month intervals, with clinical, laboratory, and radiographic data collected using a standardized protocol. The assessments include detailed medical history, physical examination, evaluation of disease activity, patient-reported outcomes, and laboratory tests. Radiographs of the hands, feet, pelvis, and cervical and lumbar spine are performed biennially. More than 99% of patients in the cohort meet the Classification Criteria for PsA.[1] All patients enrolled in the cohort up to May 15, 2025, with at least one PF assessment within 3 months of the radiographs were included.

Assessments. Demographic characteristics (age, sex, and disease duration), body weight, comorbidities (Charlson comorbidity index), smoking status (current smoker, ex-smoker, or never smoker), clinical features (66 swollen joint count [SJC66], 68 tender joint count, enthesitis, dactylitis, and nail involvement), disease activity (Psoriasis Area and Severity Index and clinical Disease Activity index for PsA),[17] patient-reported outcomes (Health Assessment Questionnaire [HAQ] and Medical Outcomes Survey Short Form-36 [SF-36]), laboratory values (erythrocyte sedimentation rate and C-reactive protein), radiographic features (number of joints with erosions, sacroiliitis, syndesmophytes, and modified Steinbrocker score [mSS]), and treatment (nonsteroidal anti-inflammatory drugs and conventional synthetic DMARDs, bDMARDs, and tsDMARDs) were retrieved from the database.

Structural damage in peripheral joints was evaluated on radiographs. All radiographs are reviewed in separate consensus reading sessions by at least two experienced readers (DDG, VC, and DP [Poddubnyy]) independent of clinical assessments. Radiographs were scored using the mSS system (range 0–168),[18–20] which is a radiographic scoring system that evaluates specific joints of the hands and feet. It includes 30 joints of the hands (bilateral wrists, metacarpophalangeal, proximal interphalangeal, and distal interphalangeal [DIP]) and 12 joints of the feet (metatarsophalangeal and first interphalangeal joints). Each joint is assigned a score from 0 to 4 based on the severity of damage:

- 0: Normal
- 1: Minimal damage (soft tissue swelling or juxta-articular osteopenia)
- 2: Moderate damage (presence of erosion)
- 3: Severe damage (presence of erosion with JSN)
- 4: Total joint destruction (complete joint destruction with erosions all along the joint line, arthritis mutilans, subluxation, or ankylosis)

It has excellent interobserver and good intraobserver reliability.[18] PF was assessed using the HAQ (0–3) and the SF-36 PF subscale (0–100).[21,22] Multiple visits per patient were assessed over the follow-up.

Statistical analysis. Baseline characteristics at the time of study enrollment were described using descriptive statistics. Quantitative variables were described as mean ± SD or median (interquartile range [IQR]) if there was evidence for nonnormality. Qualitative variables were summarized in terms of frequencies and percentages.

We assessed the association between PF measures (SF-36 PF and HAQ) and the mSS using univariable and multivariable linear mixed models (LMMs) with random intercepts with PF as the outcome. LMM were used to account for repeated measurements within the same patient over follow-up by incorporating patient-specific random intercepts, thereby allowing for studying association between observations from the same individual. The multivariable models were adjusted for covariates, including SJC66 at the time of the radiographs, sex, and disease duration of PsA, as visualized by a directed acyclic graph (Supplementary Figure 1).[23,24] Age was not included in the multivariable model because of collinearity with disease duration. We included SJC66 as an objective measure of articular disease activity.

Additionally, we assessed the presence of joint damage (at least one joint graded as 2, 3, or 4) and the number of damaged joints per patient (graded as 2, 3, or 4 to include erosion, JSN, and total joint destruction) for their association with SF-36 PF and HAQ using univariable and multivariable LMMs with random effects. These were adjusted for SJC66, sex, and disease

duration of PsA at the time of radiographs. These models were also repeated to determine associations between presence of different grades of joint damage (at least one joint graded as 2 [erosion], 2 and 3 [erosion and JSN], or 4 [total joint destruction]) and number of joints per patient with different grades of damage (grade 2 [erosion], grades 2 and 3 [erosion and JSN], and grade 4 [complete destruction]) and SF-36 and HAQ. Statistical analyses were conducted using SAS version 9.3 (SAS Institute, Cary, NC, USA) and R version 4.2.3. *P* values of <0.05 were deemed statistically significant, and results were expressed as β estimate with 95% confidence intervals (CIs).

Consent and ethics. We obtained ethics approval from the University Health Network Research Ethics Board (08-0630). All patients provided informed consent at enrollment. The data underlying this article will be shared upon reasonable request to the corresponding author.

RESULTS

A total of 1,177 patients were included in the study with a median of 2 (IQR 1–3) visits per patient over follow-up. The mean ± SD age at enrollment was 44.6 ± 12.8 years, and 657 (55.8%) were male. The mean ± SD age at PsA onset was 38.8 ± 13.5 years. At baseline, the median SJC66 was 2 (IQR 0–5), with dactylitis present in 316 patients (26.9%), enthesitis in 253 (23.7%), and axial disease in 326 (28%). The mean ± SD mSS was 9.7 ± 21.2, with a median of 2 (IQR 0–8.5). The median HAQ score was 0.6 (IQR 0.1–1.1), and the median SF-36 PF score was 60 (IQR 35–85) (Table 1).

Association of mSS with PF. In univariable analysis, mSS was significantly associated with SF-36 PF (β = –0.12; 95% CI –0.17 to –0.07) (Table 2). In multivariable analysis, the mSS was significantly associated with SF-36 PF (β = –0.10; 95% CI –0.15 to –0.05), SJC66 (β = –1.51; 95% CI –1.75 to 1.28), male sex (β = 12.50; 95% CI 9.53 to 15.46), and disease duration (β = –0.14; 95% CI –0.25 to –0.04). Similarly, mSS was significantly associated with HAQ (β = 0.003; 95% CI 0.002–0.005) in univariable analysis (Table 2). In multivariable analysis, HAQ was associated with mSS (β = 0.003; 95% CI 0.002 to 0.004), SJC66 (β = 0.04; 95% CI 0.03–0.04), male sex (β = –0.30; 95% CI –0.37 to –0.24), and disease duration (β = 0.005; 95% CI 0.003 to 0.007) (Figure 1).

Association between the presence of joint damage with PF. The presence of at least one joint with grades 2, 3, or 4 damage was not associated with SF-36 PF in both univariable (β = –0.58; 95% CI –2.87 to 1.71) and multivariable analysis (β = 1.00, 95% CI –1.25 to 3.25). Similarly, the presence of a joint with grades 2, 3, or 4 damage was not significantly associated with HAQ in both univariable (β = 0.016; 95% CI –0.03 to 0.06) and multivariable analysis (β = –0.03, 95% CI –0.08 to 0.02) (Figure 2).

The presence of at least one joint exhibiting total joint destruction was associated with poorer SF-36 PF scores on univariable analysis (β = –5.16; 95% CI –8.07 to –2.25) and multivariable analysis (β = –3.04; 95% CI –5.93 to –0.15). Similarly, it was significantly associated with HAQ in both univariable (β = 0.15; 95% CI 0.09–0.22) and multivariable analysis (β = 0.09; 95% CI 0.03–0.15). Separate analyses of the presence of grade 2 and grades 2 and 3 damage were not associated with PF (Supplementary Tables 1–3).

Table 1. Baseline characteristics of patients at enrollment*

Characteristics (N = 1,177)	Data
Demographics	
Age, mean (SD), y	44.61 (12.76)
Male sex, n (%)	657 (55.8)
Age at onset of PsA, mean (SD), y	38.84 (13.50)
Age at onset of psoriasis, mean (SD), y	28.82 (14.76)
Duration of PsA, median [IQR], y	2.69 [0.71–8.19]
Ever smoking, n (%)	490 (42.3)
Body mass index, mean (SD)	28.90 (6.25)
Charlson comorbidity index, median [IQR]	1.00 [1.00–1.00]
Clinical features	
66-Swollen joint count, median [IQR]	2.00 [0.00–5.00]
68-Tender joint count, median [IQR]	4.00 [1.00–10.00]
Dactylitis, n (%)	316 (26.9)
Enthesitis, n (%)	253 (21.7)
Nail disease, n (%)	663 (56.4)
Axial disease, n (%)	326 (28.0)
Disease activity, median [IQR]	
PASI score	1.70 [0.00–4.50]
DAPSA	17.00 [9.80–29.22]
Patient-reported outcomes, median [IQR]	
HAQ	0.62 [0.12–1.12]
SF-36 PF	60.00 [35.00–85.00]
SF-36 PCS	37.06 [28.72–47.79]
SF-36 MCS	48.48 [37.55–56.37]
Radiographic features	
Erosions, n (%)	591 (51.3)
Radiographic damaged joint count, median [IQR]	1.00 [0.00–4.00]
Modified Steinbrocker score, median [IQR]	2.00 [0.00–8.50]
Syndesmophytes, n (%)	137 (11.8)
Sacroiliitis, n (%)	253 (21.8)
Laboratory variables, n (%)	
Abnormal ESR[a]	492 (42.4)
Abnormal CRP[b]	493 (49.3)
HLA B*27	157 (16.0)
HLA C*06	261 (26.7)
Treatment, n (%)	
Conventional synthetic DMARDs	451 (38.3)
NSAIDs	773 (65.7)
Biologic DMARDs	115 (9.8)
Targeted synthetic DMARDs	6 (0.5)

* CRP, C-reactive protein; DAPSA, Disease Activity in Psoriatic Arthritis; DMARD, disease-modifying antirheumatic drug; ESR, erythrocyte sedimentation rate; HAQ, Health Assessment Questionnaire; IQR, interquartile range; MCS, mental component score; NSAID, nonsteroidal anti-inflammatory drug; PASI, Psoriasis Area and Severity Index; PCS, physical component score; PF, physical function; PsA, psoriatic arthritis; SF, Short Form.
[a] ESR > 20 mm; [b]CRP > 6 mg/L.

Table 2. Results of the association between SF-36 PF and HAQ and with physical function using univariable linear mixed models*

	SF-36 PF			HAQ		
	Estimate	95% CI	*P* value	Estimate	*P* value 95% CI	*P* value
Modified Steinbrocker score (0–168)	−0.12	−0.17 to −0.07	<0.001	0.003	0.002 to 0.005	<0.001
Presence of a damaged joint (grade 2,3, or 4 vs 1 or 0)	−0.58	−2.87 to 1.71	0.620	0.016	−0.03 to 0.06	0.529
Number of damaged joints (grade 2, 3, or 4)	−0.32	−0.47 to −0.18	<0.001	0.008	0.005 to 0.012	<0.001
Presence of a severely damaged joint (grade 4 vs 0, 1, 2, or 3)	−5.16	−8.07 to −2.25	<0.001	0.15	0.01 to 0.22	<0.001
Number of severely damaged joints (grade 4)	−0.63	−0.91 to −0.35	<0.001	0.017	0.01 to 0.02	<0.001
SJC (0–66)	−1.59	−1.83 to −1.36	<0.001	0.04	0.03 to 0.04	<0.001
Sex, male	12.64	9.61 to 15.67	<0.001	−0.31	−0.38 to −0.24	<0.001
Duration of PsA, y	−0.09	−0.19 to 0.01	0.07	0.004	0.002 to 0.006	<0.001
Age, y	−0.13	−0.25 to −0.02	0.03	0.003	−0.31 to −0.08	0.06

* CI, confidence interval; HAQ, Health Assessment Questionnaire; PF, physical function; PsA, psoriatic arthritis; SF-36, Short Form-36; SJC, swollen joint count.

Association of the number of damaged joints with PF. The number of damaged joints (graded 2, 3, or 4) per patient was significantly associated with SF-36 PF in univariable analysis (β = –0.3; 95% CI –0.47 to –0.18) and multivariable analysis (β = –0.23; 95% CI –0.38 to –0.08). Similarly, the number of damaged joints (graded 2, 3, or 4) was significantly associated with HAQ in univariable (β = 0.008; 95% CI 0.005–0.012) and multivariable analysis (β = 0.005; 95% CI 0.002–0.009) (Figure 3).

This association was stronger when the number of totally damaged joints (grade 4) per patient was studied with SF-36 PF in both univariable (β = –0.63; 95% CI –0.91 to –0.35) and multivariable analysis (β = –0.54; 95% CI –0.81 to –0.26). Similarly, the number of totally damaged joints (grade 4) was associated with HAQ in both univariable (β = 0.017; 95% CI 0.01–0.02) and multivariable analysis (β = 0.01; 95% CI 0.01–0.02). Separate analyses of the number of grades 2 and 3 joints per patient were not associated with PF (Supplementary Tables 4–6).

DISCUSSION

In this study, we could demonstrate an association between mSS and PF. After adjusting for disease activity, sex, and disease duration, we noted a small but statistically significant decrease in PF with increasing mSS. However, disease activity and sex emerged as the most prominent contributors to functional impairment. Importantly, both the presence of a single severely damaged joint and the cumulative number of severely damaged

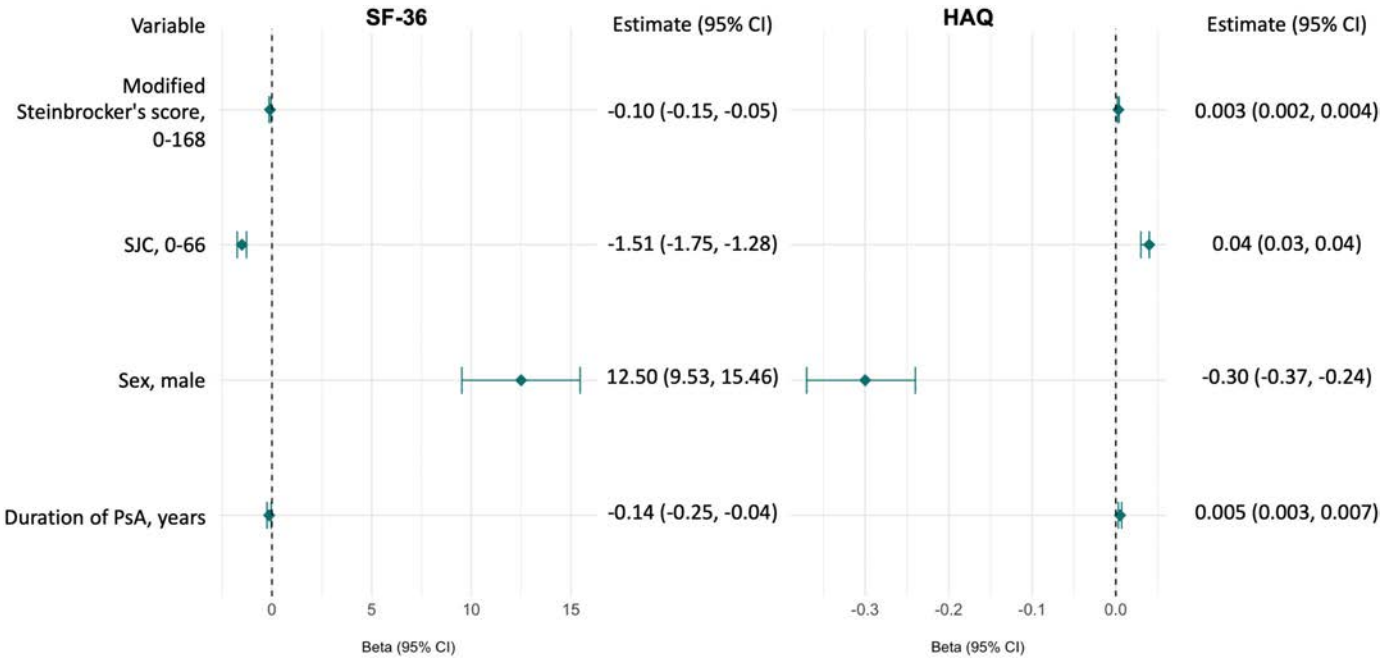


Figure 1. Results of the association between modified Steinbrocker score and physical function using multivariable linear mixed models. CI, confidence interval; HAQ, Health Assessment Questionnaire; PsA, psoriatic arthritis; SF-36, Short Form-36; SJC, swollen joint count.

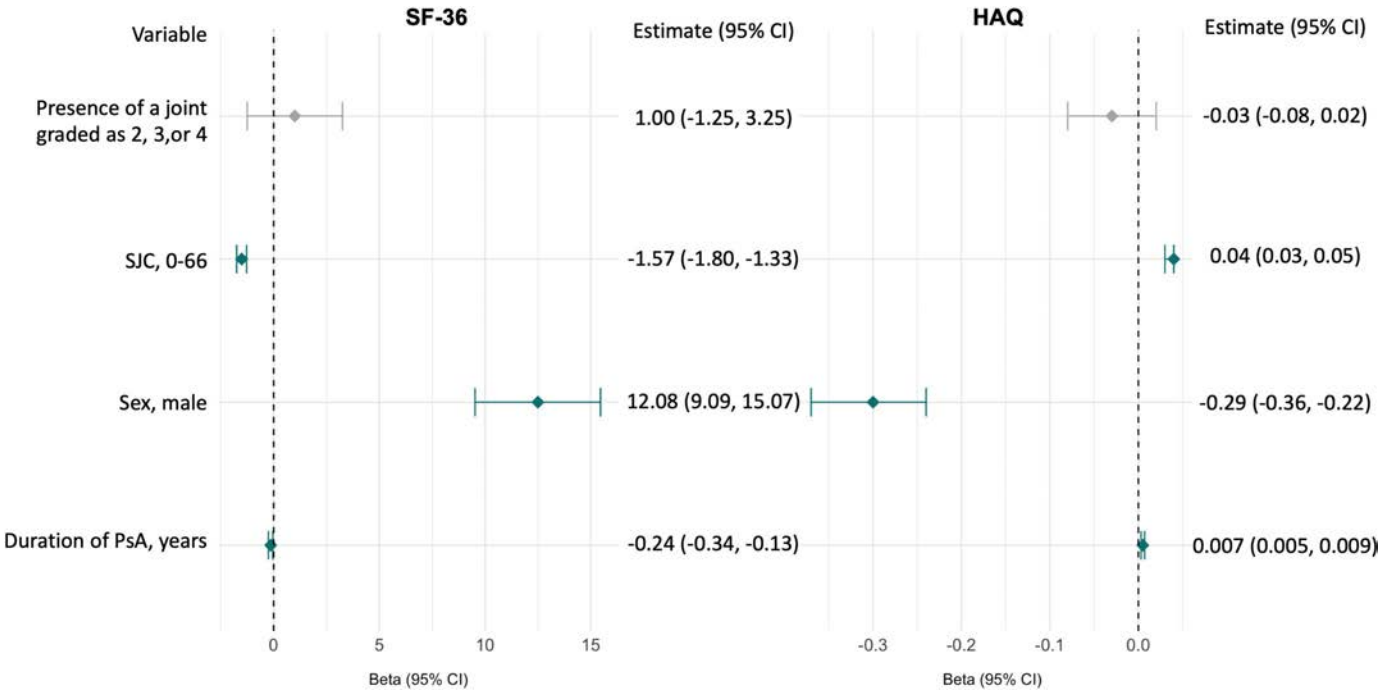


Figure 2. Results of the association between the presence of a damaged joint (grade 2, 3, or 4 vs 0 or 1) with physical function using multivariable linear mixed models. CI, confidence interval; HAQ, Health Assessment Questionnaire; PsA, psoriatic arthritis; SF-36, Short Form-36; SJC, swollen joint count. Color figure can be viewed in the online issue, which is available at http://onlinelibrary.wiley.com/doi/10.1002/art.70145/abstract.

joints were significantly associated with poorer PF in individuals with PsA, highlighting novel quantitative insights into structural damage burden in real-world cohorts.

Our analysis showed that a 1-unit increase in the mSS was associated with a 0.10-point worsening in the SF-36 PF score and a 0.003-point deterioration in HAQ scores. Although these

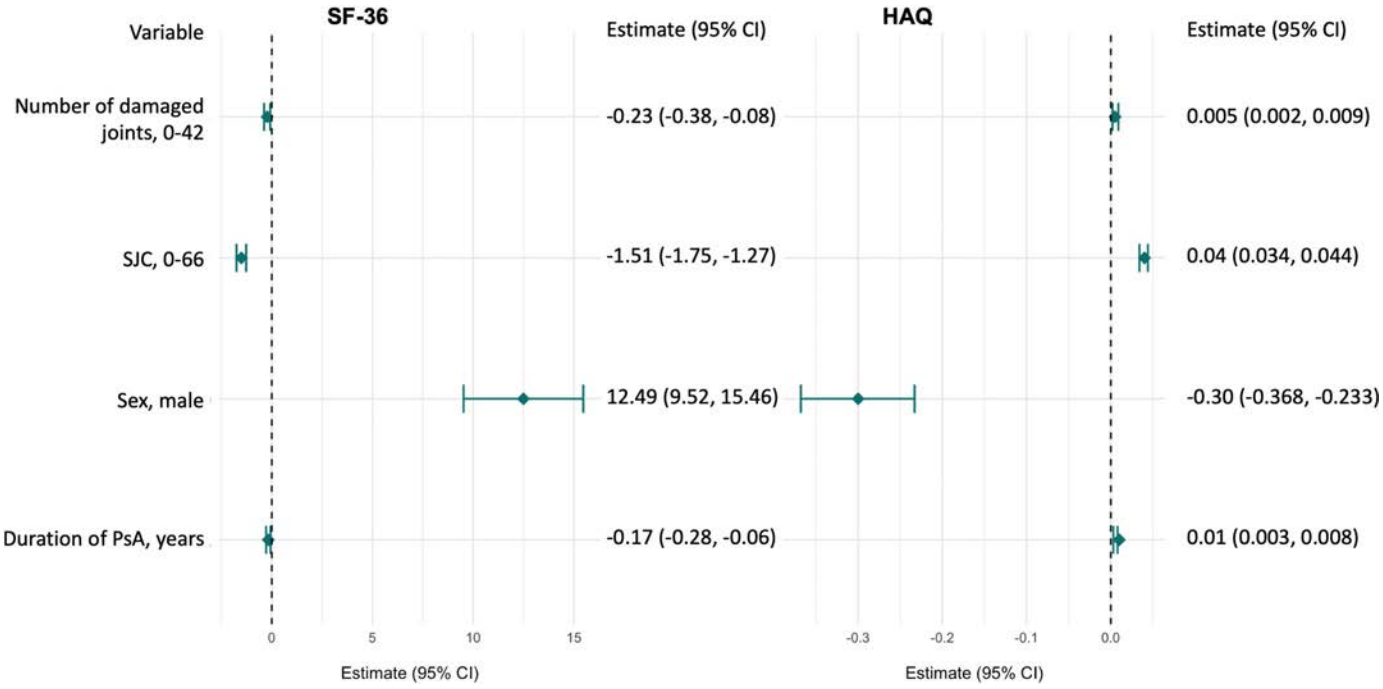


Figure 3. Results of the association between the number of damaged joints (grade 2, 3, or 4) per patient with physical function using multivariable linear mixed models. CI, confidence interval; HAQ, Health Assessment Questionnaire; PsA, psoriatic arthritis; SF-36, Short Form-36; SJC, swollen joint count. Color figure can be viewed in the online issue, which is available at http://onlinelibrary.wiley.com/doi/10.1002/art.70145/abstract.

changes are modest, they were statistically significant and independent of disease activity. To contextualize this, increases of 10, 50, and 100 units in mSS would correspond to worsening of SF-36 PF by 1, 5, and 10 points, respectively, and worsening of HAQ by 0.03, 0.15, and 0.3 points. A similar relationship was previously observed in a post hoc analysis of a phase 3 trial of golimumab in PsA, in which a 1-unit increase in the modified mSvdH score was linked to a 0.002-point increase in HAQ. Thus, mSvdH scores of 10, 50, and 100 would correspond to predicted HAQ scores of 0.02, 0.1, and 0.2, respectively.[13] It is important to note that such high radiographic scores are rarely encountered in clinical practice.

An earlier study from our cohort reported that HAQ scores remained relatively stable over time in patients with increasing joint damage but no ongoing inflammation, up to a damaged joint count of 21.[25,26] This pattern may be because of the different ways in which inflammation and structural damage affect PF. Inflammation impacts PF through pain, joint stiffness, and systemic symptoms such as fatigue, often resulting in rapid and noticeable declines in function. In contrast, joint damage typically leads to mechanical limitations that develop gradually, allowing time for patients to adapt and compensate. As a result, the perceived effect on PF may be less immediate. Nonetheless, in our analysis, the impact of structural damage on PF persisted even after adjusting for disease activity, underscoring its independent contribution to disability. Given that radiographic damage can occur as early as 6 months after PsA onset, early and aggressive disease control is essential to prevent long-term functional decline.[3,27]

In addition to structural damage, we found that longer disease duration and female sex were significantly associated with reduced PF. Among these, female sex had the strongest association, consistent with prior studies identifying it as a key determinant of disability.[28] This association persisted even after adjusting for disease activity, suggesting potential sex-based differences in pain perception. Experimental data in spondyloarthritis support the influence of hormonal and immune response differences on pain processing.[29] Sociocultural factors may also contribute; for example, women often perform fine-motor tasks that place greater strain on the hands and joints and men typically have greater muscle mass, which may confer some physical resilience.

We found that the presence of any damaged joint (grades 2, 3, or 4) was not associated with impaired PF, whereas the presence of a severely damaged joint (grade 4) showed a clear meaningful effect. This may reflect the functional importance of the specific joint involved; for instance, low-grade damage to DIP joints may have less impact on PF than similar damage to the wrist. Alternatively, it is possible that only complete joint destruction, rather than milder forms of damage, has substantial functional consequences. The presence of even a single grade-4 joint was associated with significantly worse PF. The reduction in SF-36 PF (–3.04 points) approaches the established minimum clinically important difference of 5 points, and the HAQ worsening of 0.09 is similarly meaningful.[30,31] Moreover, increasing counts of grade-4 joints demonstrated a strong dose response relationship, with each additional destroyed joint associated with further functional decline (SF-36 PF = –0.63; HAQ = +0.02). These results align with prior studies showing that cumulative structural damage drives impairments in PF.[25]

PF is a core domain in PsA clinical trials and is incorporated into most composite indices and response criteria.[32] The significant association we observed between radiographic damage and PF reinforces the need to include patient-reported outcomes when assessing treatment efficacy. Unlike disease activity, the disability related to structural damage is irreversible, highlighting the importance of its prevention.

A major strength of our study is the use of data from a well-characterized, prospectively observed, real-world PsA cohort. We used two complementary measures of PF (SF-36 PF and HAQ) to robustly examine the relationship with radiographic damage. Long-term follow-up data enabled meaningful assessment of structural progression and its impact.

However, this study has limitations. We focused on peripheral joint damage, without accounting for axial involvement. Additionally, the mSS does not include evaluation of larger joints such as the shoulders, elbows, hips, and knees, which are not routinely imaged because of potential confounding by conditions such as osteoarthritis. Nevertheless, we believe the mSS is a useful surrogate for global joint damage in PsA. Although PF was measured through patient-reported outcomes that may be influenced by unmeasured variables, our use of two distinct tools and multivariable adjustment aimed to mitigate this issue. Sex and disease activity were strongly associated with PF, which may obscure the independent impact of mSS on minimal clinically important difference for SF-36 PF and HAQ.

In conclusion, structural joint damage, as quantified by the mSS, is independently associated with impaired PF in PsA, even after adjusting for disease activity and other confounders. A 1-unit increase in mSS is associated with a 0.10-point decline in SF-36 PF and a 0.003-point increase in HAQ. Both the presence of even a single severely damaged joint and the cumulative damage burden significantly contribute to reduced function. These findings emphasize the need for early diagnosis and effective intervention to prevent irreversible disability in PsA.

ACKNOWLEDGMENTS

The Gladman Krembil PsA Program is funded by a grant from the Krembil Foundation and the Schroeder Arthritis Institute.

AUTHOR CONTRIBUTIONS

All authors contributed to at least one of the following manuscript preparation roles: conceptualization AND/OR methodology, software,

investigation, formal analysis, data curation, visualization, and validation AND drafting or reviewing/editing the final draft. As corresponding author, Dr Poddubnyy confirms that all authors have provided the final approval of the version to be published and takes responsibility for the affirmations regarding article submission (eg, not under consideration by another journal), the integrity of the data presented, and the statements regarding compliance with institutional review board/Declaration of Helsinki requirements.

REFERENCES

1. Taylor W, Gladman D, Helliwell P, et al; CASPAR Study Group. Classification criteria for psoriatic arthritis: development of new criteria from a large international study. Arthritis Rheum 2006;54(8):2665–2673. doi:https://doi.org/10.1002/art.21972
2. Walsh JA, Ogdie A, Michaud K, et al. Impact of key manifestations of psoriatic arthritis on patient quality of life, functional status, and work productivity: findings from a real-world study in the United States and Europe. Joint Bone Spine 2023;90(3):105534. doi:https://doi.org/10.1016/j.jbspin.2023.105534
3. Kane D, Stafford L, Bresnihan B, et al. A prospective, clinical and radiological study of early psoriatic arthritis: an early synovitis clinic experience. Rheumatology (Oxford) 2003;42(12):1460–1468. doi:https://doi.org/10.1093/rheumatology/keg384
4. Kerschbaumer A, Baker D, Smolen JS, et al. The effects of structural damage on functional disability in psoriatic arthritis. Ann Rheum Dis 2017;76(12):2038–2045. doi:https://doi.org/10.1136/annrheumdis-2017-211433
5. Bond SJ, Farewell VT, Schentag CT, et al. Predictors for radiological damage in psoriatic arthritis: results from a single centre. Ann Rheum Dis 2007;66(3):370–376. doi:https://doi.org/10.1136/ard.2006.056457
6. Coates LC, Soriano ER, Corp N, et al; GRAPPA Treatment Recommendations domain subcommittees. Group for Research and Assessment of Psoriasis and Psoriatic Arthritis (GRAPPA): updated treatment recommendations for psoriatic arthritis 2021. Nat Rev Rheumatol 2022;18(8):465–479. doi:https://doi.org/10.1038/s41584-022-00798-0
7. Mease P, van der Heijde D, Landewé R, et al. Secukinumab improves active psoriatic arthritis symptoms and inhibits radiographic progression: primary results from the randomised, double-blind, phase III FUTURE 5 study. Ann Rheum Dis 2018;77(6):890–907. doi:https://doi.org/10.1136/annrheumdis-2017-212687
8. Wang SH, Yu CL, Wang TY, et al. Biologic disease-modifying antirheumatic drugs for preventing radiographic progression in psoriatic arthritis: a systematic review and network meta-analysis. Pharmaceutics 2022;14(10):2140. doi:https://doi.org/10.3390/pharmaceutics14102140
9. Gottlieb AB, McInnes IB, Rahman P, et al. Low rates of radiographic progression associated with clinical efficacy following up to 2 years of treatment with guselkumab: results from a phase 3, randomised, double-blind, placebo-controlled study of biologic-naïve patients with active psoriatic arthritis. RMD Open 2023;9(1):e002789. doi:https://doi.org/10.1136/rmdopen-2022-002789
10. Ritchlin CT, Coates LC, Mease PJ, et al. The effect of guselkumab on inhibiting radiographic progression in patients with active psoriatic arthritis: study protocol for APEX, a phase 3b, multicenter, randomized, double-blind, placebo-controlled trial. Trials 2023;24(1):22. doi:https://doi.org/10.1186/s13063-022-06945-y
11. Gossec L, Kerschbaumer A, Ferreira RJO, et al. EULAR recommendations for the management of psoriatic arthritis with pharmacological therapies: 2023 update. Ann Rheum Dis 2024;83(6):706–719. doi:https://doi.org/10.1136/ard-2024-225531
12. Kavanaugh A, Antoni CE, Gladman D, et al. The Infliximab Multinational Psoriatic Arthritis Controlled Trial (IMPACT): results of radiographic analyses after 1 year. Ann Rheum Dis 2006;65(8):1038–1043. doi:https://doi.org/10.1136/ard.2005.045658
13. Kavanaugh A, van der Heijde D, McInnes IB, et al. Golimumab in psoriatic arthritis: one-year clinical efficacy, radiographic, and safety results from a phase III, randomized, placebo-controlled trial. Arthritis Rheum 2012;64(8):2504–2517. doi:https://doi.org/10.1002/art.34436
14. Mease PJ, Kivitz AJ, Burch FX, et al. Etanercept treatment of psoriatic arthritis: safety, efficacy, and effect on disease progression. Arthritis Rheum 2004;50(7):2264–2272. doi:https://doi.org/10.1002/art.20335
15. Koc GH, Kok MR, do Rosario Y, et al. Determinants of radiographic progression in early psoriatic arthritis: insights from a real-world cohort. RMD Open 2024;10(2):e004080. doi:https://doi.org/10.1136/rmdopen-2024-004080
16. Gladman DD, Chandran V. Observational cohort studies: lessons learnt from the University of Toronto Psoriatic Arthritis Program. Rheumatology (Oxford) 2011;50(1):25–31. doi:https://doi.org/10.1093/rheumatology/keq262
17. Schoels M, Aletaha D, Funovits J, et al. Application of the DAREA/DAPSA score for assessment of disease activity in psoriatic arthritis. Ann Rheum Dis 2010;69(8):1441–1447. doi:https://doi.org/10.1136/ard.2009.122259
18. Rahman P, Gladman DD, Cook RJ, et al. Radiological assessment in psoriatic arthritis. Br J Rheumatol 1998;37(7):760–765. doi:https://doi.org/10.1093/rheumatology/37.7.760
19. van der Heijde D, Sharp J, Wassenberg S, et al. Psoriatic arthritis imaging: a review of scoring methods. Ann Rheum Dis 2005;64(Suppl 2)(suppl 2):ii61–ii64. doi:https://doi.org/10.1136/ard.2004.030809
20. van der Heijde D, Gladman DD, Kavanaugh A, et al. Assessing structural damage progression in psoriatic arthritis and its role as an outcome in research. Arthritis Res Ther 2020;22(1):18. doi:https://doi.org/10.1186/s13075-020-2103-8
21. Blackmore MG, Gladman DD, Husted J, et al. Measuring health status in psoriatic arthritis: the Health Assessment Questionnaire and its modification. J Rheumatol 1995;22(5):886–893.
22. Husted JA, Gladman DD, Farewell VT, et al. Validating the SF-36 health survey questionnaire in patients with psoriatic arthritis. J Rheumatol 1997;24(3):511–517.
23. Dagitty: graphical analysis of causal diagrams. Accessed December 27, 2025. https://www.dagitty.net/
24. Digitale JC, Martin JN, Glymour MM. Tutorial on directed acyclic graphs. J Clin Epidemiol 2022;142:264–267. doi:https://doi.org/10.1016/j.jclinepi.2021.08.001
25. Husted JA, Tom BD, Farewell VT, et al. A longitudinal study of the effect of disease activity and clinical damage on physical function over the course of psoriatic arthritis: does the effect change over time? Arthritis Rheum 2007;56(3):840–849. doi:https://doi.org/10.1002/art.22443
26. Husted JA, Tom BD, Farewell VT, et al. Description and prediction of physical functional disability in psoriatic arthritis: a longitudinal analysis using a Markov model approach. Arthritis Rheum 2005;53(3):404–409. doi:https://doi.org/10.1002/art.21177
27. Haroon M, Gallagher P, FitzGerald O. Diagnostic delay of more than 6 months contributes to poor radiographic and functional outcome in psoriatic arthritis. Ann Rheum Dis 2015;74(6):1045–1050. doi:https://doi.org/10.1136/annrheumdis-2013-204858
28. Coates LC, van der Horst-Bruinsma IE, Lubrano E, et al. Sex-specific differences in patients with psoriatic arthritis: a systematic review. J Rheumatol 2023;50(4):488–496. doi:https://doi.org/10.3899/jrheum.220386

29. Bidad K, Gracey E, Hemington KS, et al. Pain in ankylosing spondylitis: a neuro-immune collaboration. Nat Rev Rheumatol 2017;13(7):410–420. doi:https://doi.org/10.1038/nrrheum.2017.92
30. Cella D, Yount S, Rothrock N, et al; PROMIS Cooperative Group. The Patient-Reported Outcomes Measurement Information System (PROMIS): progress of an NIH Roadmap cooperative group during its first two years. Med Care 2007;45(5)(suppl 1):S3–S11. doi: 10.1097/01.mlr.0000258615.42478.55
31. Cella D, Riley W, Stone A, et al; PROMIS Cooperative Group. The Patient-Reported Outcomes Measurement Information System (PROMIS) developed and tested its first wave of adult self-reported health outcome item banks: 2005-2008. J Clin Epidemiol 2010;63(11):1179–1194. doi: https://doi.org/10.1016/j.jclinepi.2010.04.011
32. Orbai AM, de Wit M, Mease P, et al. International patient and physician consensus on a psoriatic arthritis core outcome set for clinical trials. Ann Rheum Dis 2017;76(4):673–680. doi:https://doi.org/10.1136/annrheumdis-2016-210242

Check for updates

American College of Rheumatology
Empowering Rheumatology Professionals

Arthritis & Rheumatology
Vol. 78, No. 10, October 2026, pp 2110–2123
DOI 10.1002/art.70117
© 2026 American College of Rheumatology.

Dual-Targeting BCMA–CD19 CAR-T Cell Therapy in Systemic Lupus Erythematosus: Single-Cell and Immune Repertoire Analysis Reveals Mechanisms of Immune Reconstitution

Zhenghao He, PhD,[1,2] Weijia Wang, MD,[3] Qianwen Li, PhD,[2] Shihao Ding, MD,[3] Mingxia Wang, MD,[4] and Ming Hong, PhD[3]

Objective. To investigate peripheral immune reconstitution following BCMA–CD19 dual-targeting CAR-T therapy in patients with systemic lupus erythematosus (SLE).

Methods. Single-cell RNA sequencing and parallel B cell receptor (BCR) and T cell receptor sequencing were performed on peripheral blood mononuclear cells from five patients with SLE before infusion and after peripheral B cell reconstitution (median 90 days postinfusion). These data were integrated with public datasets from seven patients with SLE treated with CD19 single-targeting CAR-T and three healthy controls for comparative analysis (total N = 15 subjects; 176,182 single cells analyzed).

Results. Dual-targeting CAR-T induced marked depletion of B-lineage populations, including plasma-lineage clusters that persisted after CD19 therapy. Specifically, cluster 2 decreased from 10.70% to 2.67% and cluster 3 from 9.55% to 3.12% in the dual-targeting cohort, whereas cluster 3 increased (6.78%–12.19%) in the single-targeting comparator. In B cells, dual targeting produced greater suppression of RIG-I/MDA5 and type I interferon transcriptional programs than single-targeting therapy. BCR repertoires shifted toward an IGHM-dominant (49.83%–89.19%, $P < 0.05$), naïve-biased profile, with contraction of pre-enriched class-switched clones and restoration of diversity toward healthy-like profiles. Clinical improvement was significant (mean SLE Disease Activity Index decreased from 9.6 to 2.4, $P < 0.05$), paralleling these molecular changes.

Conclusion. BCMA–CD19 dual CAR-T therapy was associated with deeper depletion of plasma-lineage compartments and a tendency toward more pronounced reversal of SLE-associated molecular signatures. This exploratory finding suggests a potential advantage of dual targeting in achieving a more comprehensive humoral reset in SLE, which warrants further direct comparative studies to determine clinical superiority.

INTRODUCTION

Systemic lupus erythematosus (SLE) is a systemic autoimmune disease driven in large part by B cell hyperactivation, autoantibody production, and immune-complex–mediated organ injury.[1–3] Although conventional immunosuppression and biologics benefit many patients, a subset remains refractory or intolerant, motivating new targeted therapies.[4,5] B cell–directed CAR-T therapy has shown efficacy in hematologic malignancies and is being explored for antibody-mediated autoimmune diseases.[6–8] Recently, Müller et al reported promising results from the phase 1 and 2 CASTLE basket trial using CD19 CAR-T cells,[9] further validating this approach.

CD19 is broadly expressed across B-lineage cells, whereas BCMA is enriched on plasma cells, including long-lived plasma cells.[10] CD19-directed CAR-T effectively depletes B cells but can spare some plasma cell compartments that lose CD19 expression and sustain autoantibody production[11–13]; dual

Supported by Medical Science Research Foundation of Guangdong Province of China (grants A2024293 and A2024431).

[1]Department of Plastic Surgery, Zhongshan People's Hospital, Zhongshan, Guangdong, People's Republic of China; [2]Department of Dermatology, Second Xiangya Hospital, Hunan Key Laboratory of Medical Epigenomics, Clinical Medical Research Center of Major Skin Diseases and Skin Health of Hunan Province, Central South University, Changsha, Hunan, People's Republic of China; [3]Institute of Advanced Diagnostic and Clinical Medicine, Zhongshan People's Hospital, Zhongshan, Guangdong, People's Republic of China; [4]Department of Rheumatology and Immunology, Zhongshan People's Hospital, Zhongshan, Guangdong, People's Republic of China.

Drs He, W. Wang, and Li are co-first authors and contributed equally to this work.

Additional supplementary information cited in this article can be found online in the Supporting Information section (https://acrjournals.onlinelibrary.wiley.com/doi/10.1002/art.70117).

Author disclosures and graphical abstract are available at https://onlinelibrary.wiley.com/doi/10.1002/art.70117.

Address correspondence via email to Ming Hong, PhD, at hongming530@126.com.

Submitted for publication December 8, 2025; accepted in revised form February 13, 2026.

targeting of CD19 and BCMA therefore offers a mechanistic rationale to achieve deeper depletion of pathogenic humoral immune cell compartments and more durable immune resetting in SLE.[14,15]

Here, we applied single-cell transcriptomics together with parallel B and T cell receptor (BCR/TCR) repertoire profiling to map peripheral immune reconstitution after BCMA–CD19 dual-targeting CAR-T in SLE and to place these findings in the context of healthy controls (HCs) and a CD19-only CAR-T cohort. We specifically evaluated B-lineage and plasma-lineage compartments, type I interferon (IFN)–related programs, and clonal repertoire features. In our cohort, dual targeting was associated with depletion of plasma-lineage clusters and suppression of B cell IFN-associated pathways. Because cross-cohort comparisons can be influenced by batch, protocol, patient selection, and sampling-window differences despite harmonized processing, we present such contrasts as exploratory and emphasize within-cohort pre-to-post changes.

MATERIALS AND METHODS

Patient cohort and sample collection. Five patients with SLE (P1–P5) received BCMA–CD19 CAR-T cell therapy. Detailed clinical characteristics are provided in Supplementary Table 1 and our prior report.[11] Peripheral blood mononuclear cell (PBMC) samples were collected before and after treatment. Post-sampling was performed at the time of peripheral B cell reconstitution; the median time to reconstitution sampling was 90 days (range 60–120 days). B cell absolute counts at this time point are provided in Supplementary Table 2. Raw data are deposited at the GEO (GSE304878).

For comparative analysis, we downloaded single-cell RNA-sequencing (scRNA-seq) data (dataset GSE267645), TCR data (GSE267639), and BCR data (GSE267642) from the GEO database for HC subjects.[16] To compare the therapeutic effects of dual-targeting versus single-targeting therapy, we integrated publicly available data (GSE263931) from a cohort of patients with refractory SLE treated with a canonical second-generation CD19 CAR (MB-CART19.1), as described by Wilhelm et al.[17] The single-targeting construct used an FMC63-derived scFv, a CD8-derived hinge region, a TNFRSF19-derived transmembrane domain, and 4-1BB and CD3-ζ signaling domains. T cells for this comparator were expanded in the presence of interleukin-7 (IL-7) and IL-15. Samples from this cohort included those collected before therapy (SPRE) and after early peripheral B cell reconstitution (SPOST; median 149 days, range 70–233 days postinfusion).[17]

CAR-T cell therapy design and manufacturing. The design principles, construction methods, and manufacturing processes for BCMA–CD19 dual-targeting CAR-T cells have been extensively described in our previous study.[11] Briefly, the construct incorporates an IL-15 expression cassette to provide intrinsic cytokine support and enhance T cell persistence and functionality. The CAR transgene was delivered by a replication-deficient lentiviral vector, and T cells were manufactured under the institutional good manufacturing practice–equivalent protocol.

scRNA-seq and immune repertoire sequencing library preparation. Single-cell 5′ transcriptome and V(D)J libraries were generated from PBMCs using the 10× Genomics Chromium Single Cell 5′ platform and sequenced on an Illumina NovaSeq system with a paired-end 150-bp configuration. Detailed protocols are provided in the Supplementary Methods.

scRNA-seq data analysis. Raw FASTQ files were processed with CellRanger. Downstream analyses were conducted in Seurat (version 5) with Harmony for batch correction and scRepertoire (version 1.8) for clonotype analysis, and differential expression and pathway enrichment were performed using clusterProfiler. Quality control metrics and parameter settings are detailed in the Supplementary Methods.

BCR and TCR sequencing analysis. V(D)J sequence assembly and paired clonotype calling for antigen receptor repertoires were performed using the cellranger vdj function of CellRanger software (10× Genomics) with default parameters. The analysis of TCR/BCR diversity and clonality was conducted with the scRepertoire package[18] (version 1.8.0). Subsequently, the scRepertoire package and the Seurat package were used to map T and B cells harboring TCR/BCR clonotypes onto a precomputed T-distributed stochastic neighbor embedding dimensionality reduction plot.

Differential expression and pathway enrichment analysis. Differential gene expression analysis was conducted using the FindMarkers function in the Seurat package. Functional enrichment analysis for Gene Ontology and KEGG pathways of differentially expressed genes (DEGs) across different sample groups and cell clusters was performed using the clusterProfiler package[19] (version 4.9.0.002). Statistical significance was determined by a P value <0.05, serving as the threshold for identifying enriched biologic processes, molecular functions, and cellular components.

Statistical analysis. Descriptive statistical analyses were conducted on the patient characteristics. All statistical analyses were performed using R software, with comprehensive details provided in the respective figure legends. It was considered statistically significant at a P value threshold of <0.05.

Data availability statement. All data generated and/or analyzed during this study are included in this article and its supplementary materials or are available from public databases.

Specifically, scRNA-seq data (GSE267645), TCR data (GSE267639), and BCR data (GSE267642) for normal control samples, as well as scRNA-seq data and TCR data (GSE263931) for CD19 CAR-T cell–treated patients with SLE before and after treatment, were downloaded from the GEO database. The scRNA-seq and immune repertoire dataset produced in the course of this study is accessible via the GEO database under accession number GSE304878. The raw data from this study will be made available to the research community upon reasonable request. Detailed analysis steps (normalization and integration, clustering and annotation, and repertoire processing) with software versions and key parameters are provided in Supplementary Methods. Analysis scripts are available from the corresponding author upon reasonable request.

Ethics approval. This study protocol received approval from the ethics committee of Zhongshan People's Hospital and strictly adhered to the ethical principles of the Declaration of Helsinki concerning human research. All patients participating in the study fully understood and signed written informed consent forms before undergoing any study-related procedures.

RESULTS

Single-cell transcriptome profiling of PBMCs from patients with SLE reveals subtype dynamics and B cell pathway regulation after dual-targeting BCMA–CD19 CAR-T therapy. We profiled PBMCs from five patients with SLE (before and after at peripheral B cell reconstitution after BCMA–CD19 dual-targeting CAR-T) and integrated publicly available data from seven patients with SLE treated with CD19 CAR-T (SPRE and SPOST collected after early B cell reconstitution) and three HCs (Figure 1A). After quality control (QC), 176,182 cells were analyzed (HC 23,788, before 45,608, after 41,214, SPRE 36,483, SPOST 29,089) and clustered into 28 discrete clusters (Figure 1B). Using canonical markers, we annotated eight major compartments: classical monocytes (CD14, CD68, and LYZ), nonclassical monocytes (FCGR3A and CX3CR1), megakaryocytes (PF4, PPBP, and ITGA2B), natural killer (NK) cells (GNLY, NKG7, KLRD1, and GZMB), $CD4^+$ T cells (CD3D, CD3E, and CD4), $CD8^+$ T cells (CD3D, CD3E, CD8A, and CD8B), B cells (MS4A1, CD19, and CD79A), and plasma cells (JCHAIN, IGHA1, and XBP1) (Figure 1C and 1D).

Composition analysis showed disease- and treatment-associated shifts (Figure 1E). Compared with HC, pre-SLE samples had expanded B cells (before 9.79% vs HC 5.04%; mean 892.8 vs 399.3 cells/sample) and plasma cells (before 1.12% vs HC 0.01%; mean 102.2 vs 0.7 cells/sample). After dual targeting, these populations decreased: B cells declined from before (9.79%) to after (7.93%) (Figure 1E), corresponding to a reduction in absolute counts from a mean of 892.8 to 653.4 cells per sample. Similarly, plasma cells declined from before (1.12%) to after (0.24%), with the mean cell count per sample dropping from 102.2 to 19.6 (Supplementary Table 3), consistent with prior clinical and serologic improvement; cohort mean SLE Disease Activity Index decreased from 9.6 at baseline to 2.4 (paired test, $P < 0.05$), and circulating autoantibody and Ig levels (including ANA and IgA) were significantly reduced after therapy (paired tests with Holm correction, $P < 0.05$; Supplementary Figure 1). Regarding B-lineage cells, the dual-targeting cohort showed a deeper sustained reduction in plasma cells compared to B cells. This is expected because B cells reconstitute from bone marrow precursors more rapidly than plasma cells, which are effectively depleted by the BCMA-targeting component. Notably, the overall B cell fraction is highly time dependent, especially around the phase of peripheral B cell reconstitution, and therefore is not a robust efficacy biomarker across cohorts. In the CD19 single-targeting comparator, postsampling occurred after early B cell reconstitution, so the bulk B cell fraction can increase at SPOST despite clinical improvement; our cross-study inferences thus prioritize subset composition, pathway readouts, and BCR repertoire remodeling rather than total B cell percentages.

We performed differential expression and pathway enrichment across three contrasts: disease versus healthy (before + SPRE vs HC), dual-targeting response (before vs after), and single-targeting response (SPRE vs SPOST) (Figure 1F; Supplementary Figure 2). Disease versus healthy revealed broad activation: IFN and inflammatory signaling, antigen presentation, and T cell activation. Both CAR-T modalities reversed many SLE-associated programs across cell types, attenuating inflammatory and IFN modules, consistent with system-level immune dampening after B-lineage depletion. Within B cells, the dual-targeting cohort showed an apparently stronger attenuation of type I IFN–related pathways (type I IFN signaling, cellular response to type I IFN, and RIG-I/MDA5 signaling) than the CD19-only cohort (Figure 1F); given timing differences around B cell reconstitution, we interpret this signal as exploratory and emphasize concordant changes at the subset (eg, plasma-lineage clusters 2/3) and repertoire levels.

Unique transcriptomic features and therapeutic responses of $CD4^+$ and $CD8^+$ T cell subsets. We subclustered T cells to examine finer remodeling. $CD4^+$ T cells partitioned into eight clusters, and we performed differential expression analysis across clusters (Supplementary Figures 3A and 3B). Compared with HC, $CD4^+$ subsets of before + SPRE group broadly up-regulated type I IFN programs ("type I interferon signaling pathway," "response to type I interferon," and "type I interferon production"), along with T cell activation and antiviral modules (Supplementary Figure 4A). Both single- and dual-targeting CAR-T markedly down-regulated these IFN, activation and proliferation, and antiviral pathways (Supplementary Figures 3C and 4B).

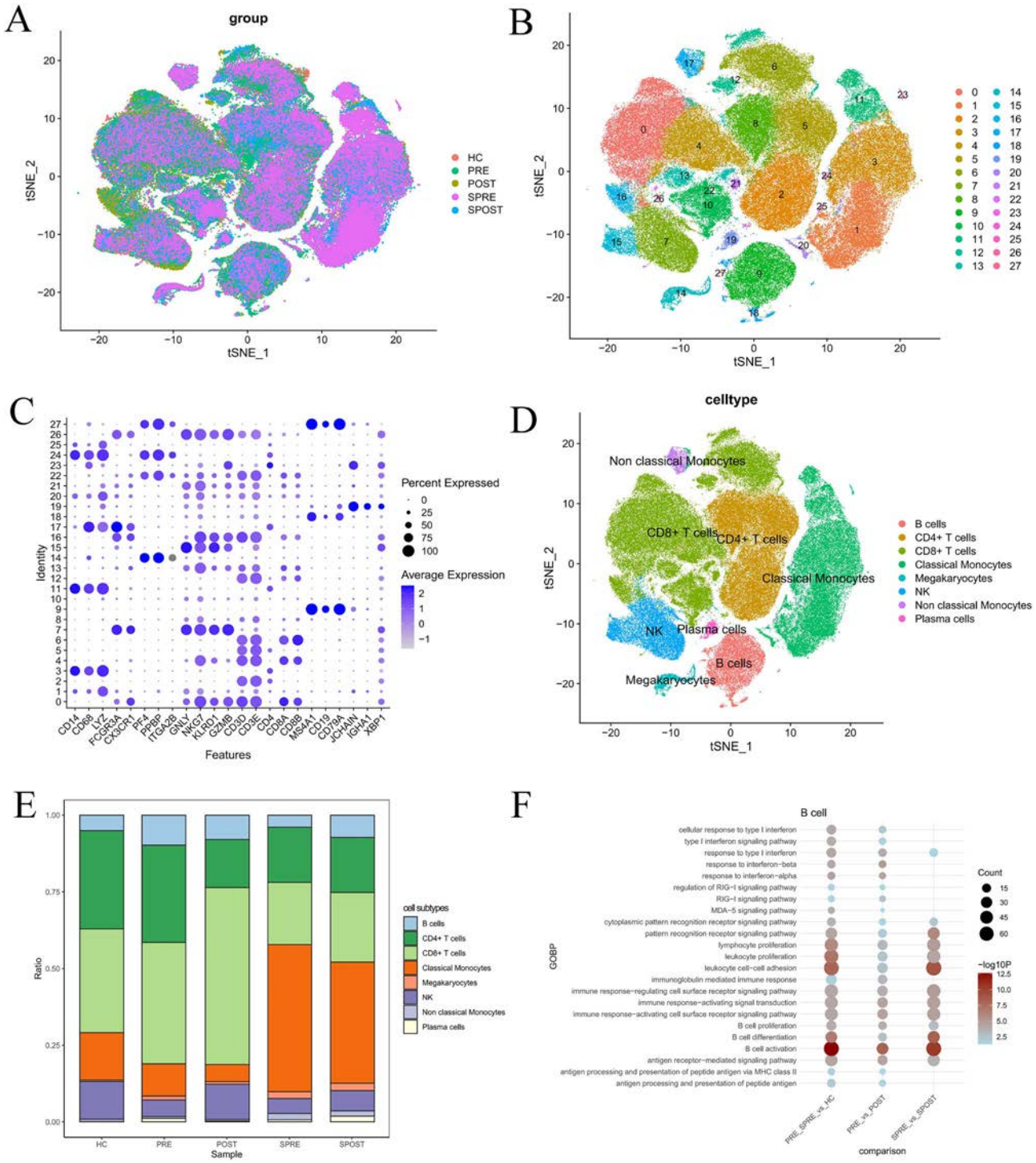


Figure 1. Single-cell transcriptome analysis of peripheral blood mononuclear cells from patients with systemic lupus erythematosus treated with dual-targeting CAR-T reveals cell subtype dynamics and B cell pathway-specific regulation. (A) tSNE embedding of all peripheral blood mononuclear cells, colored by clinical group. (B) Dimensionality reduction analysis clustered all peripheral blood mononuclear cells into 28 clusters, with points colored to distinguish different clusters. (C) Expression levels of cell markers across various clusters. (D) Cell clusters annotated into eight cell subtypes based on cell markers. (E) Proportion of each cell subtype in peripheral blood mononuclear cells across different groups. (F) B cell enrichment pathway changes displayed according to the grouping comparisons described in the text. HC, healthy control; NK, natural killer; PRE, pre–CAR-T treatment; POST, post–CAR-T treatment; SPOST, post–CD19 single-targeting CAR-T treatment; SPRE, pre-CD19 single-targeting CAR-T treatment; tSNE, T-distributed stochastic neighbor embedding.

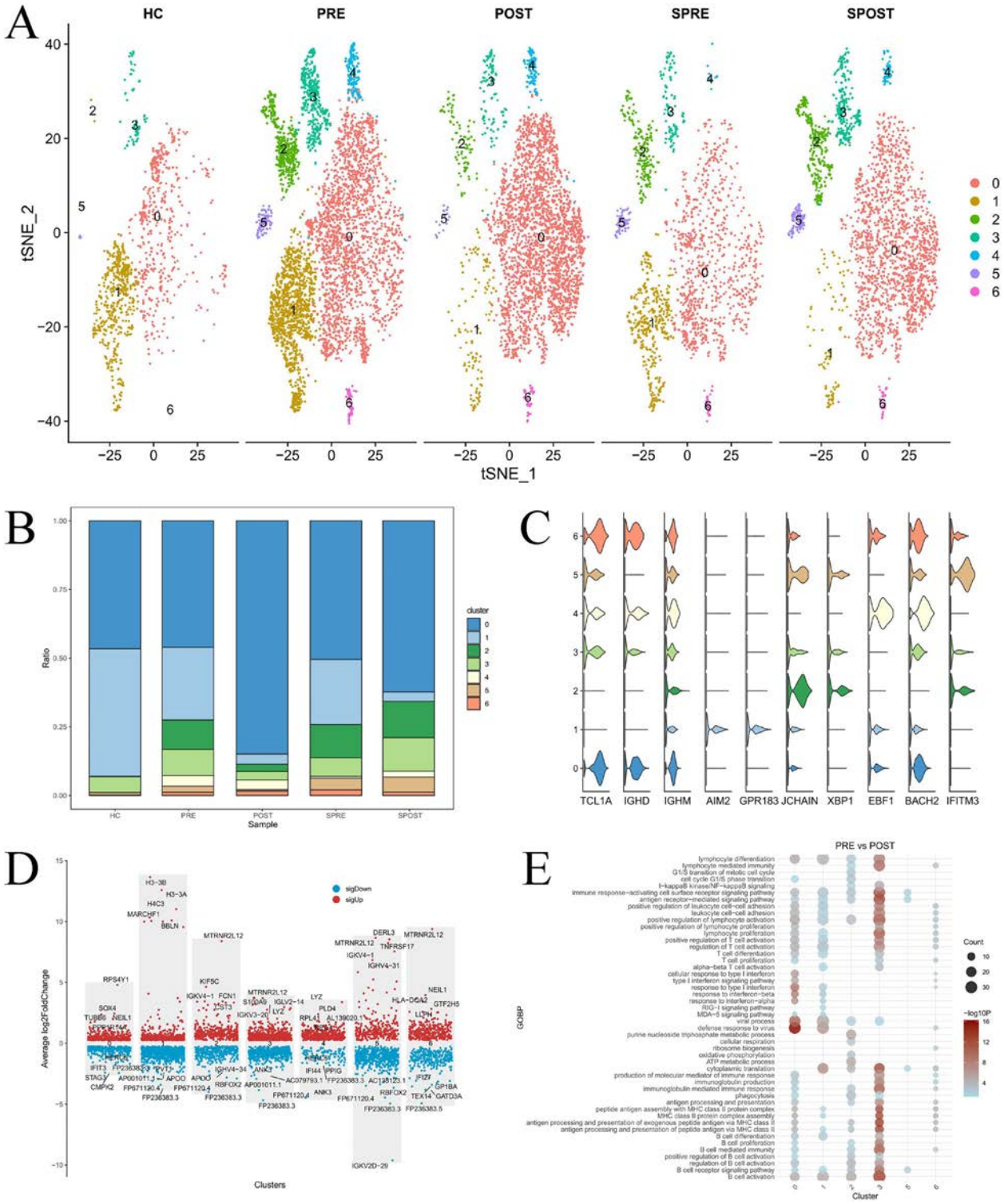


Figure 2. B cell and plasma cell subtype clustering and pathway regulation characteristics after dual-targeting treatment. (A) tSNE dimensionality reduction visualization showing the distribution of seven B cell and plasma cell clusters, with points colored to distinguish different clusters. (B) Proportion of each cluster in various groups. (C) Expression levels of cell markers across various clusters. (D) Heatmap showing differentially expressed genes for seven clusters in PRE and POST groups, with color representing gene expression levels. (E) PRE versus POST group enriched pathways for differentially expressed genes in each cluster. HC, healthy control; PRE, pre–CAR-T treatment; POST, post–CAR-T treatment; SPOST, post–CD19 single-targeting CAR-T treatment; SPRE, pre-CD19 single-targeting CAR-T treatment; tSNE, T-distributed stochastic neighbor embedding. Color figure can be viewed in the online issue, which is available at http://onlinelibrary.wiley.com/doi/10.1002/art.70117/abstract.

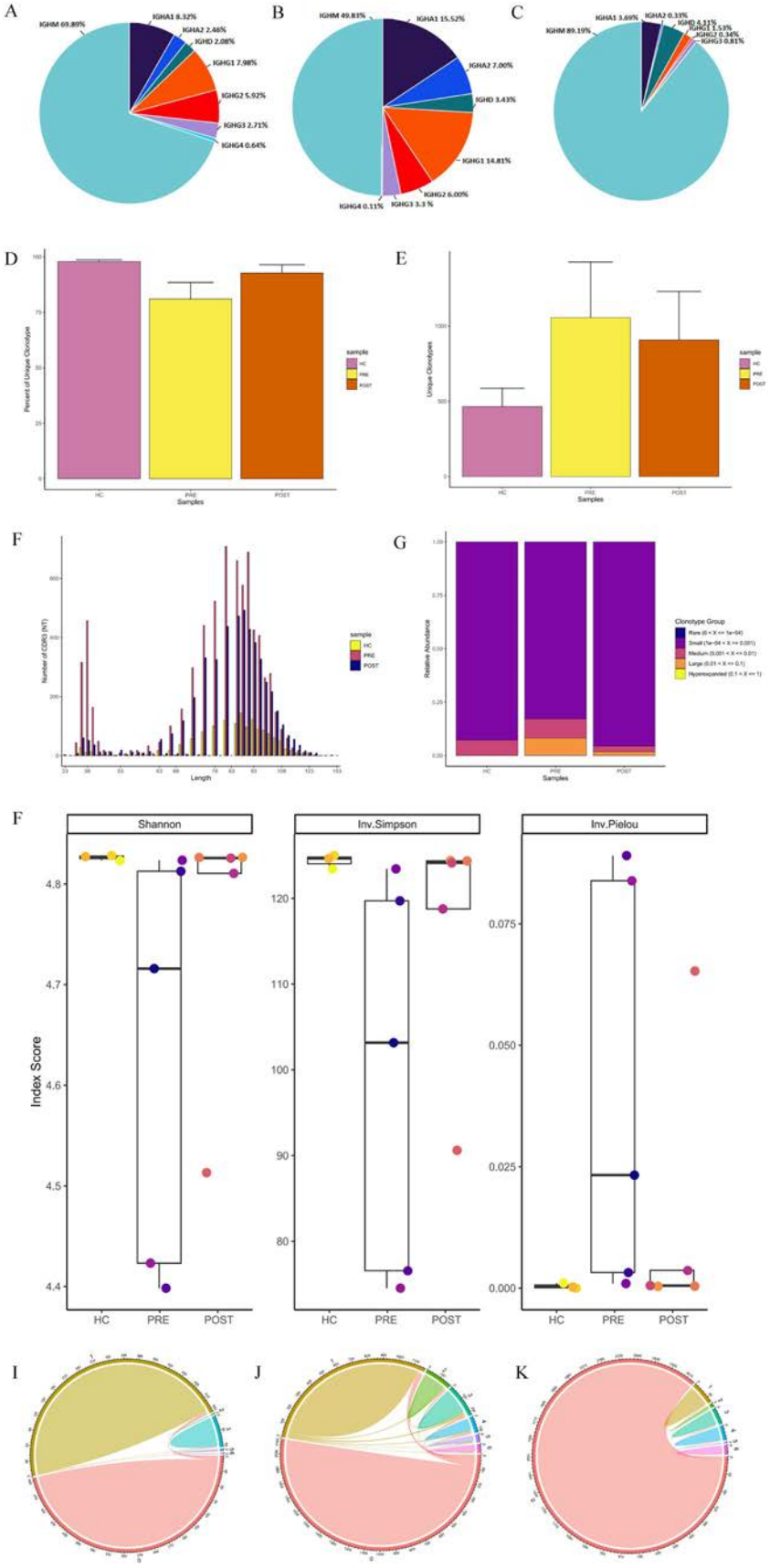


Figure 3. Legend on next page.

$CD8^+$ T cells formed 12 clusters and performed differential expression analysis across clusters (Supplementary Figures 3D and 3E). $CD8^+$ subsets of before + SPRE group showed enrichment for cytotoxicity, antigen processing and presentation, activation, and IFN responses (NK-mediated cytotoxicity, antigen processing and presentation of endogenous peptide antigen, cellular response to type I IFN, and response to IFN-γ) (Supplementary Figure 4C). Post–CAR-T (both arms), these hyperactive $CD8^+$ programs, including cytotoxicity, antigen presentation, activation circuits, and type I/II IFN signatures, were comprehensively suppressed (Supplementary Figures 3F and 4D), indicating broad normalization of T cell hyperfunction. Meanwhile, we also analyzed the TCR profiles in each group and found that dominant large clones existed in the after group, which were mainly concentrated in cluster 0 and cluster 2 (Supplementary Figure 5).

Dual-targeting CAR-T therapy induces profound remodeling of B cell and plasma cell compartments. Extracted B cells and plasma cells yielded seven clusters (Figure 2A). Cluster-level proportions revealed differential depletion (Figures 2B); cluster 1 fell dramatically after both therapies, from before (26.47%) to after (3.66%) in the dual-targeting cohort (paired *t*-test, Holm-adjusted $P < 0.05$; Supplementary Figure 1) and from SPRE (23.70%) to SPOST (3.40%) in the single-targeting cohort. Clusters 2 and 3 were depleted only by dual targeting. Specifically, cluster 2 decreased from before (10.70%) to after (2.67%); in the single-targeting cohort cluster 2 changed from SPRE (12.09%) to SPOST (13.21%), indicating that single targeting spared this CD19-low or negative subset, consistent with the expected antigen expression profile. Cluster 3 decreased from before (9.55%) to after (3.12%), whereas in the single-targeting cohort, cluster 3 increased from SPRE (6.78%) to SPOST (12.19%). Cluster annotation used TCL1A/IGHD (naïve, cluster 0), AIM2/GPR183 (memory, cluster 1), and JCHAIN/XBP1 (plasma cells, clusters 2 and 3) (Figure 2C). Taken together, these features, JCHAIN/XBP1 plasma identity and selective depletion only with dual targeting, support annotating clusters 2 and 3 as disease-linked plasma-lineage subsets in our dataset. After dual targeting, clusters showed coordinated downregulation of cell cycle (G1 and S transition), lymphocyte activation, NF-κB signaling, type I IFN–related signaling, and metabolic pathways (ATP metabolism and oxidative phosphorylation); plasma clusters (2 and 3) showed the strongest suppression of Ig synthesis and proliferation, whereas memory B (cluster 1) showed attenuation of pattern-recognition (MDA5 and RIG-I) pathways (Figures 2D and 2E).

BCMA–CD19 CAR-T therapy drives comprehensive BCR repertoire reconstruction. BCR repertoire profiling (HC, before, and after; Figure 3A–3C) showed isotype reversion after dual targeting; HC repertoire was IGHM dominant (69.89%) with other isotypes <10%, the before group exhibited class-switching (IGHM 49.83%, IGHA1 15.52%, and IGHG1 14.81%), and the after group reverted to IGHM dominance (89.19%) with other isotypes <5%, indicating restoration toward a naïve-biased repertoire (paired *t*-test, Holm-adjusted $P < 0.05$; Supplementary Figure 1). Percent unique clonotype was slightly lower in before than HC and after (Figure 3D), but raw unique clonotype counts were highest in before, intermediate in after, and lowest in HC (Figure 3E). CDR3 nucleotide length distributions showed before-specific enrichments at 38 nt and 83 to 93 nt; after shifted toward HC patterns with reduced abundance at those ranges (Figure 3F). Clonotype-size categories revealed before had increased medium ($0.001 < X \leq 0.01$) and large ($0.01 < X \leq 0.1$) clones, whereas HC and after were dominated by small clones ($1 \times 10^{-4} < X \leq 0.001$) (Figure 3G). Diversity metrics (Shannon, InvSimpson, and InvPielou) indicated lower Shannon and InvSimpson in before and higher indices in HC and after; InvPielou was higher in before, consistent with dominant disease-associated clones and reduced evenness (Figure 3H). Chord diagrams of clonotype sharing showed HC with balanced intercluster connections, before with denser interconnections, and after with fewer and thinner chords, consistent with depletion of expanded disease clones (Figures 3I–3K). Across cell types and repertoire measures, dual-targeting BCMA–CD19 CAR-T depleted disease-linked B and plasma cell subsets (notably clusters 2 and 3), rebalanced isotype distributions (restoring IGHM dominance), reduced IFN and activation programs, and reconstructed the BCR repertoire toward a healthier state, changes that align with clinical and serologic improvement after peripheral B cell reconstitution (Supplementary Figure 1).

Figure 3. Regulatory effects of dual-targeting CAR-T therapy on B cell receptor repertoire characteristics in patients with SLE. (A–C) BCR IGH isotype distribution in each group: (A) HC, (B) PRE, and (C) POST. (D) Comparison of the percent of unique clonotype. (E) Comparison of unique B cell receptor clonotypes. (F) Histogram of CDR3 nucleotide lengths, where yellow represents the HC group, pink represents the PRE group, and blue represents the POST group. (G) Relative abundance of each clonotype group in each group. (H) B cell receptor diversity indices among groups. A higher Shannon index indicates more clonal types with more uniform abundance distribution, a higher InvSimpson index means weaker influence of dominant clones and more stable overall diversity, and a higher InvPielou index suggests that a few clones dominate (ie, reduced evenness). (I–K) B cell receptor clonotype interconnection analysis between B cell and plasma cell clusters using chord diagrams, showing the distribution of unique and shared clonotypes among groups: (I) HC group, (J) PRE group, and (K) POST group. HC, healthy control; IGH, Ig heavy chain; PRE, pre–CAR-T treatment; POST, post–CAR-T treatment; SPOST, post–CD19 single-targeting CAR-T treatment; SPRE, pre-CD19 single-targeting CAR-T treatment; tSNE, T-distributed stochastic neighbor embedding. Color figure can be viewed in the online issue, which is available at http://onlinelibrary.wiley.com/doi/10.1002/art.70117/abstract.

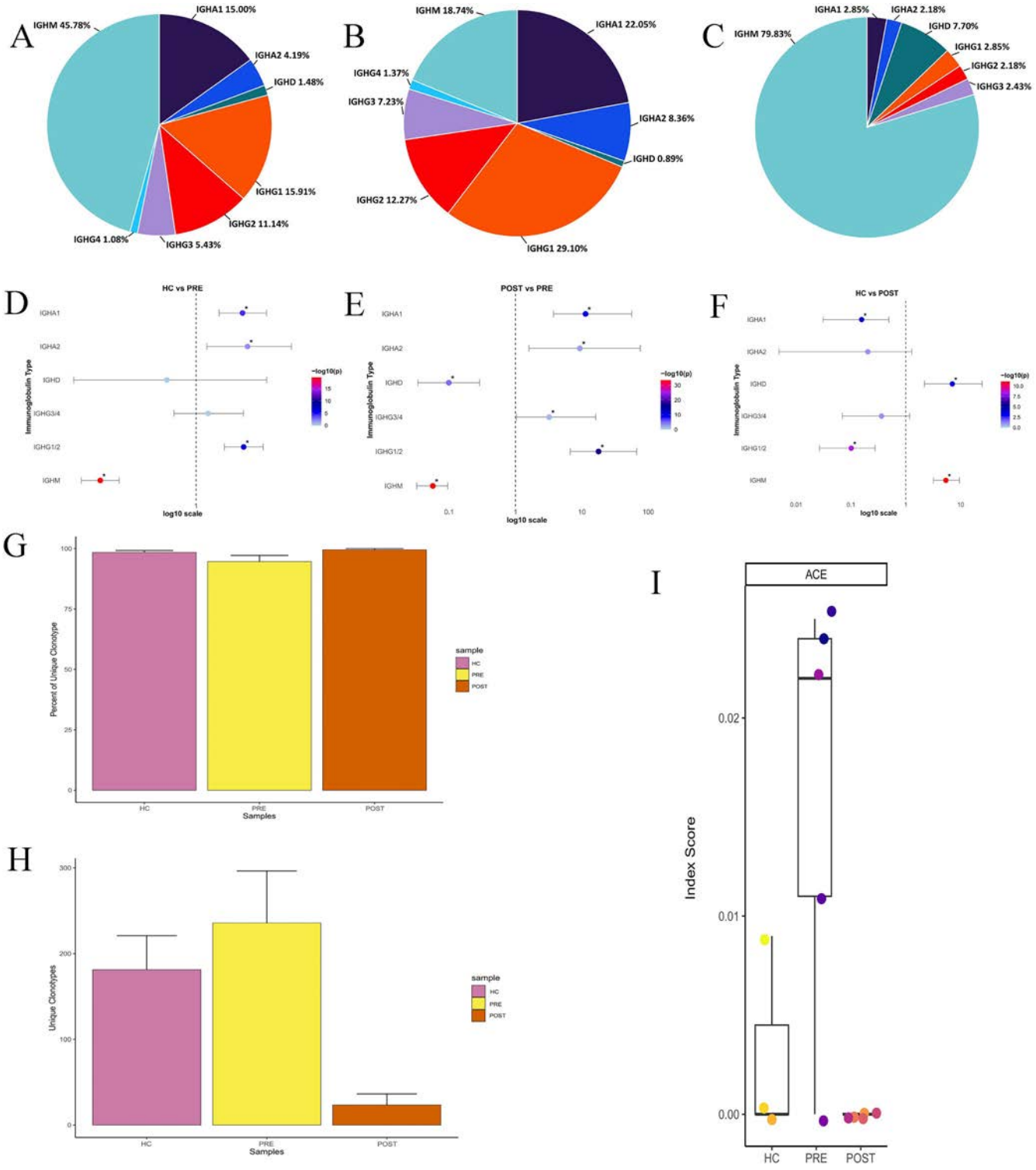


Figure 4. Ig isotype class-switching and clonal expansion cluster 1 (clusters 1 as defined in Figure 2). (A–C) IGH isotype proportion analysis in cluster 1, with (A) for HC group, (B) for PRE group, and (C) for POST group. (D–F) Forest plots comparing differences in Ig isotypes between two groups. The left side represents higher expression in the first group, and the right side represents higher expression in the second group. Dot colors reflect statistical significance, with red indicating smaller *P* values. (G) Comparison of the percent of unique clonotype. (H) Comparison of unique B cell receptor clonotypes. (I) ACE richness for cluster 1 B cell receptor clonotypes. Boxplots summarize per-patient ACE estimates in HC, PRE, and POST. Higher ACE indicates greater expected richness of unobserved and rare clonotypes (higher potential repertoire richness); values near zero indicate little unseen richness. ACE, Abundance-based Coverage Estimator; HC, healthy control; IGH, Ig heavy chain; PRE, pre–CAR-T treatment; POST, post–CAR-T treatment. Color figure can be viewed in the online issue, which is available at http://onlinelibrary.wiley.com/doi/10.1002/art.70117/abstract.

Characterization of changes in the cluster 1 before and after CAR-T therapy. Cluster 1, as defined in Figure 2, decreased after both treatments but was relatively abundant in HC. DEG and enrichment analyses linked cluster 1 to AIM2; AIM2 expression was higher in SLE (before and SPRE) than HC (Supplementary Figures 6A and 6B), suggesting that in SLE, these memory B cells aberrantly express AIM2 and may sense endogenous double-stranded DNA, promoting activation. After single or dual CAR-T, the expression level of AIM2 decreased in cluster 1, and SLE-related pathways were significantly suppressed (Supplementary Figure 6C). BCR features in cluster 1: IGHV families IGHV3, IGHV4, and IGHV1 were most abundant across groups (Supplementary Figure 6D), and IGHD and IGHJ patterns were shown in Supplementary Figures 6E and 6F.

VJ chord diagrams (HC, before, and after groups; Supplementary Figure 7A-C) show VJ recombination differences in cluster 1's IGHV/IGHJ regions, with chord thickness indicating recombination frequency. HC group had dominant V genes (IGHV3–23, IGHV3–7, IGHV4–39, and IGHV3–33), J genes (IGHJ4, IGHJ6, IGHJ5, and IGHJ3), and pairings (eg, IGHV3–23-IGHJ4); before group showed increased V/J counts, with top V (IGHV3–33, IGHV3–23, IGHV4–34, and IGHV4–39), J (IGHJ4, IGHJ3, IGHJ6, and IGHJ5), and pairings (eg, IGHV3–33-IGHJ4); and after group normalized, with V/J usages approaching HC levels with key V (IGHV3–33, IGHV3–15, IGHV4–61, and IGHV3–23), J (IGHJ4, IGHJ6, IGHJ3, and IGHJ5), and pairings (eg, IGHV3–33-IGHJ4). CDR3 length in cluster 1 showed before enrichments at 38 nt and 78 to 93 nt; after had far fewer CDR3 sequences than before or HC (Supplementary Figure 7D).

The IGH isotype composition of cluster 1 was as follows: in HC, IGHM (45.78%), IGHA1 (15.00%), IGHG1 (15.91%), and IGHG2 (11.14%); in before, IGHM (18.74%), IGHA1 (22.05%), and IGHG1 (29.10%); in after, IGHM (79.83%), with concurrent declines in other isotypes (Figures 4A–4C). Ratio analyses confirmed significant differences ($P < 0.05$) in multiple isotypes among HC, before, and after groups, including both HC-to-before, HC-to-after, and before-to-after transitions (Figures 4D–4F). The percent unique clonotype showed no significant group differences (Figure 4G), whereas absolute counts of unique clonotypes followed the order before > HC > after (Figure 4H). Abundance-based Coverage Estimator richness for cluster 1 clonotypes was highest in before, intermediate in HC, and minimal in after, indicating loss of rare and unobserved clonotypes after dual targeting (Figure 4I).

Dual-targeting CAR-T therapy selectively targets disease-linked plasma-lineage clusters (2 and 3) and their immune repertoires. The disease-linked plasma-lineage clusters (clusters 2 and 3, as defined in Figure 2) contained abundant clones in before, which were markedly reduced in after and approached HC levels (Figure 5A). DEG and pathway enrichment for these clusters showed substantial suppression of SLE-related pathways after dual targeting, a pattern not seen with single targeting (Figure 5B). Regarding BCR features in clusters 2 and 3, the IGHV3, IGHV4, and IGHV1 families dominated with intergroup shifts (Figure 5C), whereas IGHD and IGHJ patterns were further detailed in Figures 5D and 5E.

VJ chord diagrams for clusters 2 and 3 (Supplementary Figure 8A-C) show VJ recombination differences in IGHV/IGHJ segments, with chord thickness indicating recombination frequency: HC group had dominant V genes (IGHV3–33, IGHV1–18, IGHV3–11, and IGHV4–61), J genes (IGHJ4, IGHJ6, IGHJ3, and IGHJ5), and pairings (eg, IGHV3–33-IGHJ4); before group showed increased V/J counts, with top V (IGHV4–34, IGHV3–33, IGHV3–66, and IGHV4–61), J (IGHJ4, IGHJ5, IGHJ3, and IGHJ2), and pairings (eg, IGHV4–34-IGHJ5); and after group normalized, with V/J counts declining substantially (remaining higher than HC) with key V (IGHV3–33, IGHV3–23, IGHV4–39, and IGHV1–18), J (IGHJ4, IGHJ5, IGHJ6, and IGHJ3), and pairings (eg, IGHV3–33-IGHJ4). CDR3 nucleotide length distributions in clusters 2 and 3 were as follows: HC had multipeak, dispersed distribution; before showed enrichment in 72 to 102 nt; after had fewer sequences than before, although the distribution remained slightly higher than HC, indicating that full normalization was not achieved (Supplementary Figure 8D).

IGH isotype composition in clusters 2 and 3 differed significantly across HC, before, and after (Figures 6A–6C): HC exhibited an IGHM-dominant profile (65.50%) with low, balanced IGHA1 (6.06%), IGHG1 (8.14%), and IGHG2 (5.11%); before showed class-switch activation (IGHM dropped to 37.90%; IGHA1 increased to 24.84%; IGHG1 increased to 14.61%), reflecting disease-linked plasma cell dysregulation; and after displayed IGHM rebound (56.21%) and reduced other isotypes, shifting toward IGHM dominance. Ratio analyses (Figures 6D–6F) revealed significant alterations ($P < 0.05$) in multiple Ig isotypes, including HC–before differences in IGHA1, IGHG3/4 and IGHM, before–after transitions characterized by declines in IGHA2 and IGHG1/2 with concomitant IGHM elevation, and HC–after changes in IGHA1, IGHG1/2, and IGHM.

In clonotype analyses, the percent of unique clonotype was slightly lower in before than in HC and after (Figure 6G). However, raw counts of unique clonotypes were highest in before, lower in HC, and lowest in after (Figure 6H). Diversity indices (Figure 6I) showed lower Shannon and InvSimpson and higher InvPielou in before vs HC and after, consistent with disease-associated clonal dominance reducing diversity and evenness in active SLE. After showed diversity and evenness shifting toward healthy patterns, indicating immune reconstitution post dual-targeting CAR-T.

Flow cytometry confirms preferential plasmablast depletion and B cell reconstitution. Flow cytometric analysis of a representative paired sample (patient P5) from the PBMCs used for scRNA-seq showed remodeling of the peripheral B cell

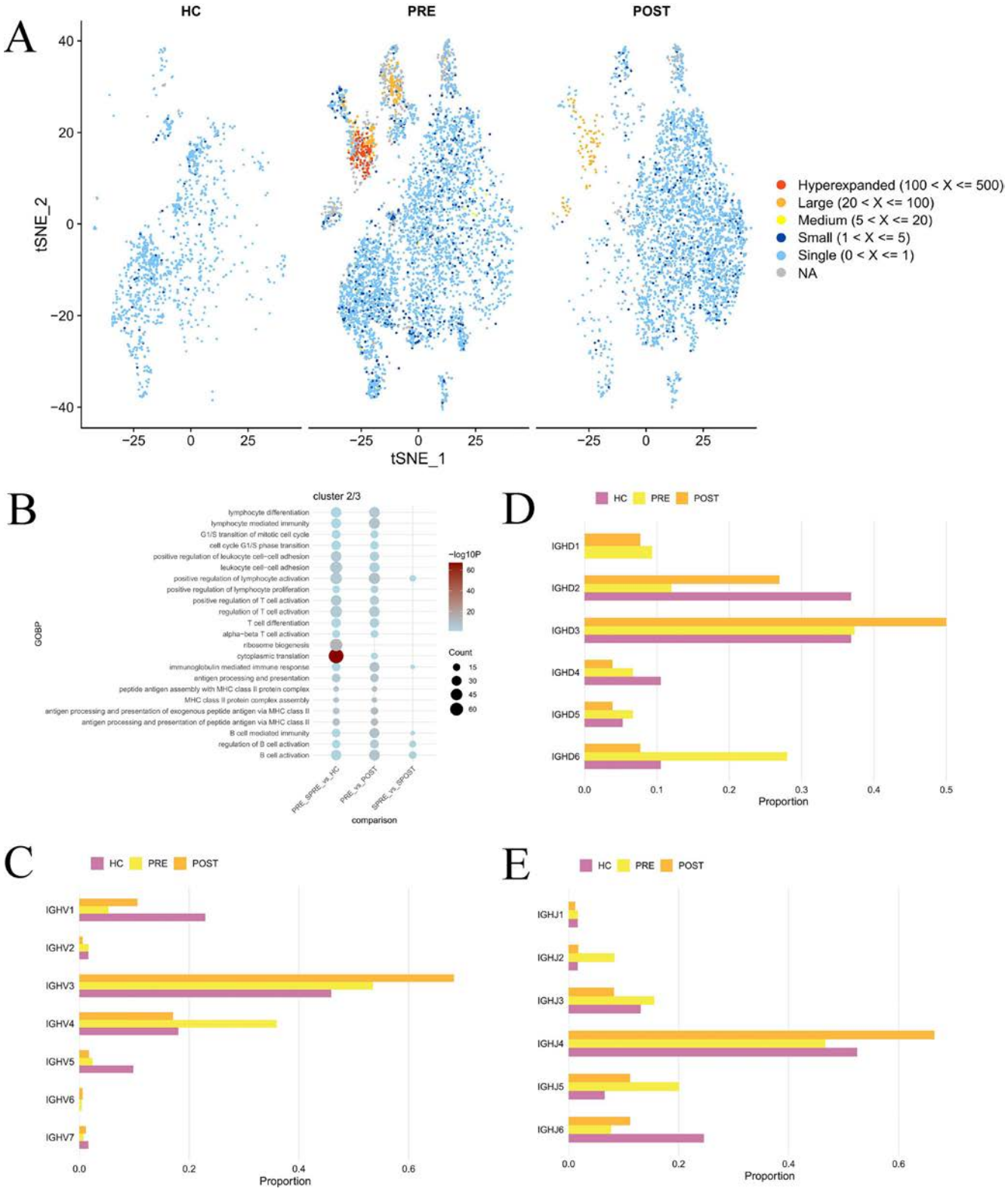


Figure 5. BCR characteristics, pathway regulation, and B cell receptor heavy chain region analysis in clusters 2 and 3. (A) tSNE visualization showing the distribution of B cell receptors in HC, PRE, and POST groups, with colors indicating clonotype types. (B) Pathway enrichment analysis results for differentially expressed genes in clusters 2 and 3 across various groups. (C) Proportional distribution of IGHV in HC, PRE, and POST groups. (D) Proportional distribution of IGHD in HC, PRE, and POST groups. (E) Proportional distribution of IGHJ in HC, PRE, and POST groups. HC, healthy control; IGH, Ig heavy chain; IGHD, Ig heavy chain diversity region; IGHJ, Ig heavy chain joining region; IGHV, Ig heavy chain variable region; NA, not applicable; PRE, pre–CAR-T treatment; POST, post–CAR-T treatment; tSNE, T-distributed stochastic neighbor embedding. Color figure can be viewed in the online issue, which is available at http://onlinelibrary.wiley.com/doi/10.1002/art.70117/abstract.

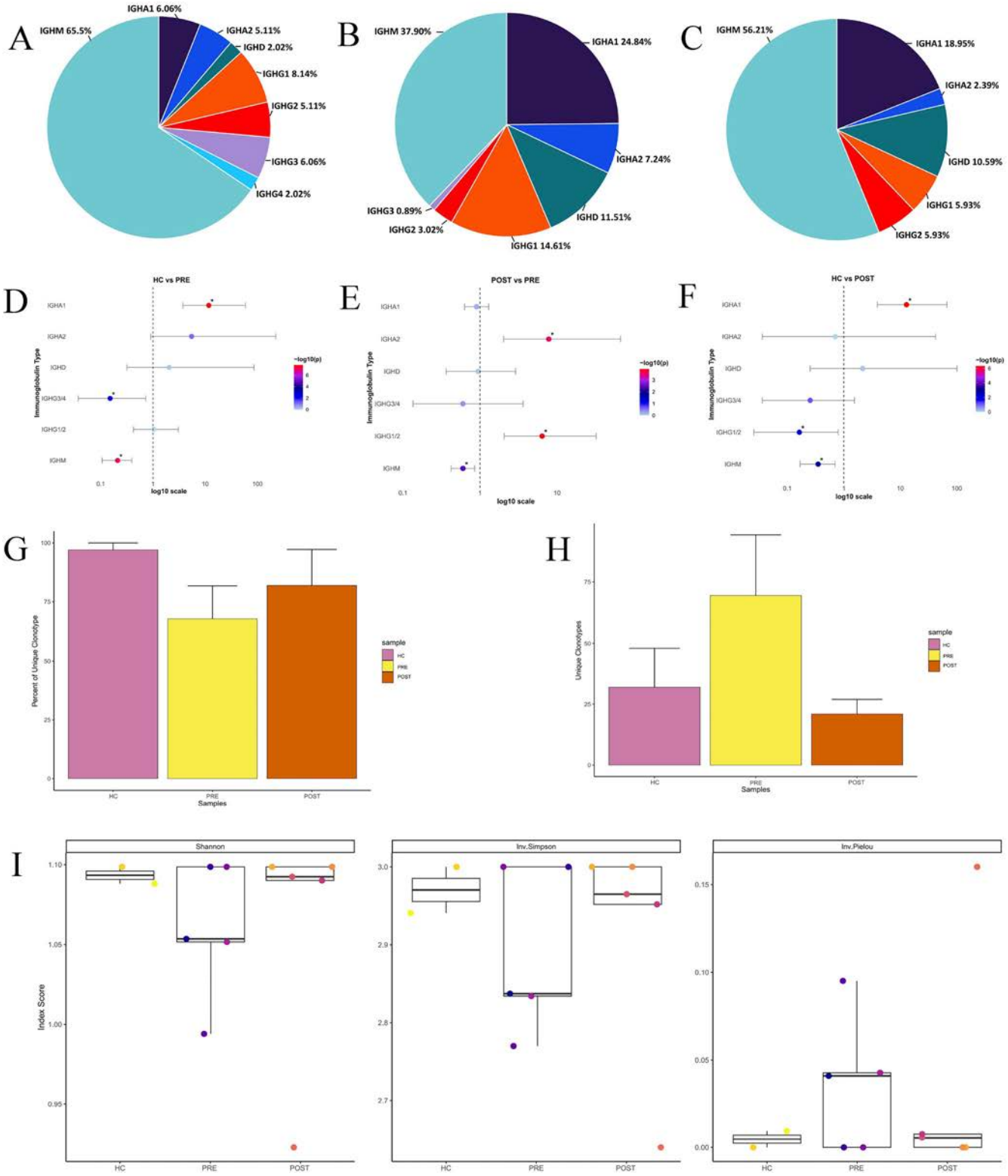


Figure 6. Ig isotype class-switching and clonal expansion in clusters 2 and 3 (clusters 2 and 3 as defined in Figure 2). (A–C) IGH isotype proportion analysis in clusters 2 and 3, with (A) for HC group, (B) for PRE group, and (C) for POST group. (D–F) Forest plots comparing differences in Ig isotypes between two groups. The left side represents higher expression in the first group, and the right side represents higher expression in the second group. Dot colors reflect statistical significance, with red indicating smaller *P* values. (G) Comparison of the percent of unique clonotype. (H) Comparison of unique B cell receptor clonotypes. (I) B cell receptor diversity indices (Shannon, InvSimpson, and InvPielou) in clusters 2 and 3. A higher Shannon index indicates more clonal types with more uniform abundance distribution, a higher InvSimpson index means weaker influence of dominant clones and more stable overall diversity, and a higher InvPielou index suggests that a few clones dominate (ie, reduced evenness). HC, healthy control; IGH, Ig heavy chain; PRE, pre–CAR-T treatment; POST, post–CAR-T treatment. Color figure can be viewed in the online issue, which is available at http://onlinelibrary.wiley.com/doi/10.1002/art.70117/abstract.

composition (Supplementary Figure 9). Consistent with the scRNA-seq findings, the data showed a preferential depletion of the plasma-lineage compartment. Specifically, whereas the total CD19+ B cell frequency (as a fraction of lymphocytes) showed only a modest increase post-treatment, the B cell compartment composition underwent profound remodeling. The CD19+CD27 – naïve B cell fraction expanded, consistent with a shift toward a naïve-biased composition. Conversely, the CD19+CD27+CD38+ plasmablast fraction decreased, consistent with depletion of circulating, short-lived plasma-lineage cells. These flow cytometric data align with the single-cell observation of XBP1+ plasma-lineage cell depletion and B cell repertoire restoration toward a naïve phenotype. However, we note that because PBMCs only reflect circulating cells, these flow data do not directly quantify changes in tissue-resident long-lived plasma cells.

DISCUSSION

Using single-cell transcriptomics and immune repertoire sequencing, we characterized immune remodeling after BCMA–CD19 dual-targeting CAR-T in patients with SLE. In our cohort, dual targeting remodeled the B-lineage compartment, with changes in memory B cells (cluster 1) and selective contraction of plasma-lineage and plasmablast subsets (clusters 2 and 3) that appeared less affected in the CD19-only dataset.[17] Although plasma-lineage and plasmablast subsets are plausible contributors to circulating autoantibodies, our data do not directly prove that these specific cells are the dominant pathogenic reservoir; longitudinal serologic correlation and bone marrow sampling are required in our future study to link cell-type depletion to sustained autoantibody loss and relapse risk.[20] A recent CD19–CAR-T study reported B cell depletion and reduced type I IFN signaling.[21] In exploratory cross-cohort contrasts, our analysis suggests that inclusion of a BCMA-targeting component is associated with more complete impact on plasma-lineage subsets that were less affected under CD19-only conditions, and this, together with more pronounced attenuation of RIG-I/MDA5 and type I IFN pathways in B cells, may underlie the broader immunomodulation observed. Given the time-dependent nature of bulk B cell percentages during reconstitution, we therefore focus on the concordant and more stable signals at the subset (especially plasma-lineage clusters 2 and 3), pathway, and repertoire levels.

After dual targeting, the B cell compartment reconstituted toward naïve dominance (cluster 0), comprising >80% of B cells. This shift was corroborated by an increased IGHM proportion in the IGH isotype distribution. IGHM predominance is consistent with reconstitution of an immature and naïve B cell pool, following depletion of memory and plasma cell populations; this shift reduces the reservoir for autoreactive, class-switched antibodies. Immune reconstitution may support long-term remission by reducing autoreactive pools and permitting generation of new B cells.[17,22] Notably, these molecular observations align with our phase 1 trial findings and corroborate clinical findings from our trial.[11] Overall, BCMA–CD19 CAR-T was associated with plasma cell reduction, contraction of disease-associated clones, and attenuation of type I IFN programs; these early BCR and transcriptional shifts may therefore serve as mechanistic biomarkers of the depth and quality of response.

At the BCR repertoire level, dual targeting markedly reduced clonal expansions and dominant clones. CDR3-length peaks enriched in the before group (eg, 38, 78, and 83 nt) were diminished after treatment, reflecting clearance of autoantigen-driven clones; reduced enrichment at these lengths supports loss of disease-associated clonotypes. Although BCR diversity did not fully recover to HC levels after treatment, its close similarity to a healthy state indicates the positive effects of the therapy and the potential for immune system self-repair.[23]

Beyond the direct effects on B cells and plasma cells, this study also observed a broad impact of CAR-T therapy on T cell subsets. The DEG pathways of both $CD4^+$ and $CD8^+$ T cells showed a trend toward normalization after treatment, which may reflect an overall improvement in the immune microenvironment following B cell clearance.[24] Meanwhile, the emergence of dominant TCR clones concentrated in specific T cell clusters (see Supplementary Figures 3–5 for the full granularity). We emphasize that these T cell findings are descriptive and intended as a resource; although consistent with broader immune normalization after B cell depletion, our cohort lacks orthogonal functional assays to attribute mechanisms, such as those driven by CAR-T persistence, endogenous antigen responses, or simple homeostatic proliferation. Future work with antigen-specific assays, CAR transgene detection in sorted T cells, and longitudinal phenotyping will be required for mechanistic resolution.

Pathway analysis showed stronger regulation of RIG-I/MDA5 and type I IFN signaling in B cells after dual targeting versus single targeting. The type I IFN signaling pathway plays a critical role in SLE pathogenesis, and its abnormal activation is closely associated with disease activity.[24,25] However, causality remains to be demonstrated, and functional experiments (eg, ex vivo stimulation with RIG-I/MDA5 ligands and measurement of serum IFNα/IFN signature scores before and after) are needed to confirm whether dual targeting directly suppresses IFN production or secondarily reduces IFN responses by removing IFN-producing B and plasma cell reservoirs. The stronger suppression of these pathways may contribute to the broader immunomodulatory profile observed, although causality remains to be established. Cluster 1 was associated with AIM2 overexpression in SLE and declined after CAR-T, implicating AIM2-linked signaling as a therapy target.[26] The significant decrease in cluster 1 proportion and AIM2 expression after CAR-T treatment suggests that this cell subset and its mediated signaling pathways are key targets for CAR-T therapy in SLE.

Our study has several important limitations, including small sample size, limited follow-up, and the use of heterogeneous

public comparators; larger, randomized, and longer-term studies will be required to robustly assess safety, durability, CAR-T persistence, and mechanistic effects. Cross-cohort contrasts are constrained by methodologic differences, including batch effects, library chemistry, sequencing depth, and sampling timing (our after group at peripheral B cell reconstitution versus the CD19-only cohort sampled after early repopulation). Furthermore, the absence of immune repertoire data in the public single-targeting dataset precluded detailed BCR comparisons between the two therapeutic modalities. We mitigated these issues by applying uniform QC and reprocessing with the same reference and normalization, stand Harmony-based integration; however, residual confounding cannot be excluded, and we therefore frame all cross-study statements as exploratory and hypothesis generating. The BCMA–CD19 construct used here differs from the CD19-only comparator at multiple levels (fourth-generation dual-targeting with an IL-15 cassette versus a canonical second-generation CD19 CAR with 4-1BB costimulation), and such design differences may influence T cell expansion and persistence, cytokine production, and the capacity to deplete plasma-lineage cells. Regarding safety, in our extended clinical follow-up, no related major late adverse events have been observed to date; nevertheless, we will continue prospective monitoring.

Our clinical work with the BCMA–CD19 CAR demonstrated rapid in vivo expansion and detectability by flow cytometry from day 2 through at least day 50 postinfusion, indicating short-term survival and proliferation; importantly, durable clinical control was observed with symptom-free, medication-free remission (MFR) lasting 46 months (P1), 25 months (P2), and ≥1 year in nine patients with lupus nephritis, accompanied at 12-month follow-up by negative autoantibodies and normalized complement. By contrast, the CD19-only cohort sampled in the after group after early B cell repopulation (9–28 weeks) did not detect circulating CAR-T cells at that stage; the report notes drug-free remission after reconstitution but does not provide longer MFR durations, and follow-up did not exceed one year. Taken together, these differences in construct design (IL-15 vs none), target biology (BCMA inclusion), and follow-up horizon provide context for interpreting persistence-related signals in our dataset and for why plasma-lineage depletion may appear deeper with dual targeting.

Although dual-targeting BCMA–CD19 CAR-T extends depletion to plasma-lineage compartments, it carries potential risks, including prolonged hypogammaglobulinemia and infection susceptibility. In our cohort (P1–P5), we observed no severe late-onset infections during the follow-up period, although rigorous monitoring of Ig levels and infectious titers remains critical. The depletion of plasma cells may also impact pre-existing vaccine immunity, necessitating re-vaccination strategies postreconstitution. Furthermore, although the IL-15 cassette enhances persistence, we did not observe toxicity associated with uncontrolled T cell proliferation.

In summary, our single-cell and repertoire analyses provide preliminary evidence that BCMA–CD19 dual-targeting CAR-T induces broad remodeling of the peripheral B cell compartment and reduces disease-associated IFN signaling in SLE. Cross-cohort contrasts should be considered exploratory given differences in batch, protocol, patient selection, and sampling timing, despite harmonized processing. These findings warrant further controlled studies to determine clinical efficacy, safety, and the mechanistic basis of these immune changes.

ACKNOWLEDGMENTS

We thank all patients who participated in this study. We thank Shanghai Tengyun Biotechnology Co, Ltd for developing Hiplot Pro platform (https://hiplot.com.cn/) and providing technical assistance and valuable tools for data analysis and visualization. We thank Dr Ting Lan, Dr Ziji Lu, and Dr Qinglian Jiang for their kind help on flow cytometric analysis. The authors declare that a generative artificial intelligence tool, specifically ChatGPT (OpenAI), was used exclusively for the purpose of refining the English language, improving clarity, and correcting grammatical errors in the final draft of the manuscript. The use of this tool was strictly limited to language editing, and it was not employed for generating scientific content, data, analysis, or interpretation. The authors confirm that all text refined by the artificial intelligence was meticulously reviewed, critically evaluated, and verified for scientific accuracy and integrity. The authors retain full responsibility for the entire content of this submission.

AUTHOR CONTRIBUTIONS

All authors contributed to at least one of the following manuscript preparation roles: conceptualization AND/OR methodology, software, investigation, formal analysis, data curation, visualization, and validation AND drafting or reviewing/editing the final draft. As corresponding author, Dr Hong confirms that all authors have provided the final approval of the version to be published and takes responsibility for the affirmations regarding article submission (eg, not under consideration by another journal), the integrity of the data presented, and the statements regarding compliance with institutional review board/Declaration of Helsinki requirements.

REFERENCES

1. Schett G, Nagy G, Krönke G, et al. B-cell depletion in autoimmune diseases. Ann Rheum Dis 2024;83(11):1409–1420. doi:https://doi.org/10.1136/ard-2024-225727
2. Durcan L, O'Dwyer T, Petri M. Management strategies and future directions for systemic lupus erythematosus in adults. Lancet 2019; 393(10188):2332–2343. doi:https://doi.org/10.1016/S0140-6736(19)30237-5
3. Jesus D, Matos A, Henriques C, et al. Derivation and validation of the SLE Disease Activity Score (SLE-DAS): a new SLE continuous measure with high sensitivity for changes in disease activity. Ann Rheum Dis 2019;78(3):365–371. doi:https://doi.org/10.1136/annrheumdis-2018-214502
4. Han EJ, Ahn JS, Chae YJ, et al. Immunomodulatory roles of Faecalibacterium prausnitzii and Akkermansia muciniphila in autoimmune diseases: mechanistic insights and therapeutic potential. Clin Rev Allergy Immunol 2025;68(1):77. doi:https://doi.org/10.1007/s12016-025-09093-8

5. Patiño-Martinez E, Kaplan MJ. Immunometabolism in systemic lupus erythematosus. Nat Rev Rheumatol 2025;21(7):377–395. doi: https://doi.org/10.1038/s41584-025-01267-0
6. Hagen M, Müller F, Wirsching A, et al. Local immune effector cell-associated toxicity syndrome in CAR T-cell treated patients with autoimmune disease: an observational study. Lancet Rheumatol 2025; 7(6):e424–e433. doi:https://doi.org/10.1016/S2665-9913(25)00091-8
7. Müller F, Taubmann J, Bucci L, et al. CD19 CAR T-cell therapy in autoimmune disease - a case series with follow-up. N Engl J Med 2024;390(8):687–700. doi:https://doi.org/10.1056/NEJMoa2308917
8. Mougiakakos D, Meyer EH, Schett G. CAR T cells in autoimmunity: game changer or stepping stone? Blood 2025;145(17):1841–1849. doi:https://doi.org/10.1182/blood.2024025413
9. Müller F, Hagen M, Wirsching A, et al. CD19 CAR-T cells for treatment-refractory autoimmune diseases: the phase 1/2 CASTLE basket trial. Nat Med 2026;32(3):1142–1151. doi:https://doi.org/10.1038/s41591-025-04185-6
10. Müller F, Wirsching A, Hagen M, et al. BCMA CAR T cells in a patient with relapsing idiopathic inflammatory myositis after initial and repeat therapy with CD19 CAR T cells. Nat Med 2025;31(6):1793–1797. doi:https://doi.org/10.1038/s41591-025-03718-3
11. Wang W, He S, Zhang W, et al. BCMA-CD19 compound CAR T cells for systemic lupus erythematosus: a phase 1 open-label clinical trial. Ann Rheum Dis 2024;83(10):1304–1314. doi:https://doi.org/10.1136/ard-2024-225785
12. Kaulen LD, Martinez-Lage M, Abramson JS, et al. Clinical presentation, management, and outcome of TIAN in CNS lymphoma treated with CD19-CAR T-cell therapy. Blood 2025;146(16):1902–1913. doi:https://doi.org/10.1182/blood.2025028964
13. Taubmann J, Müller F, Yalcin Mutlu M, et al. CD19 chimeric antigen receptor T cell treatment: unraveling the role of B cells in systemic lupus erythematosus. Arthritis Rheumatol 2024;76(4):497–504. doi: https://doi.org/10.1002/art.42784
14. Bulliard Y, Freeborn R, Uyeda MJ, et al. From promise to practice: CAR T and Treg cell therapies in autoimmunity and other immune-mediated diseases. Front Immunol 2024;15:1509956. doi:https://doi.org/10.3389/fimmu.2024.1509956
15. Vukovic J, Abazovic D, Vucetic D, et al. CAR-engineered T cell therapy as an emerging strategy for treating autoimmune diseases. Front Med (Lausanne) 2024;11:1447147. doi:https://doi.org/10.3389/fmed.2024.1447147
16. Paran FJ, Oyama R, Khasawneh A, et al. BCR, not TCR, repertoire diversity is associated with favorable COVID-19 prognosis. Front Immunol 2024;15:1405013. doi:https://doi.org/10.3389/fimmu.2024.1405013
17. Wilhelm A, Chambers D, Müller F, et al. Selective CAR T cell-mediated B cell depletion suppresses IFN signature in SLE. JCI Insight 2024; 9(12):e179433. doi:https://doi.org/10.1172/jci.insight.179433
18. Borcherding N, Bormann NL, Kraus G. scRepertoire: an R-based toolkit for single-cell immune receptor analysis. F1000 Res 2020;9: 47. doi:https://doi.org/10.12688/f1000research.22139.1
19. Wu T, Hu E, Xu S, et al. clusterProfiler 4.0: a universal enrichment tool for interpreting omics data. Innovation (Camb) 2021;2(3):100141. doi: https://doi.org/10.1016/j.xinn.2021.100141
20. Stockfelt M, Teng YKO, Vital EM. Opportunities and limitations of B cell depletion approaches in SLE. Nat Rev Rheumatol 2025;21(2): 111–126. doi:https://doi.org/10.1038/s41584-024-01210-9
21. Garantziotis P, Beretta L, Lindblom J, et al; PRECISESADS Clinical Consortium. Differential molecular signatures in response to CD19-CAR T cell therapy compared with conventional pharmacotherapy in systemic lupus erythematosus. Ann Rheum Dis 2026; 85(1):153–163. doi:https://doi.org/10.1016/j.ard.2025.06.2132
22. Alsuliman T, Marjanovic Z, Rimar D, et al. Harnessing the potential of CAR-T cell in lupus treatment: from theory to practice. Autoimmun Rev 2024;23(12):103687. doi:https://doi.org/10.1016/j.autrev.2024.103687
23. Bashford-Rogers RJM, Bergamaschi L, McKinney EF, et al. Analysis of the B cell receptor repertoire in six immune-mediated diseases. Nature 2019;574(7776):122–126. doi:https://doi.org/10.1038/s41586-019-1595-3
24. Kansal R, Richardson N, Neeli I, et al. Sustained B cell depletion by CD19-targeted CAR T cells is a highly effective treatment for murine lupus. Sci Transl Med 2019;11(482):eaav1648. doi:https://doi.org/10.1126/scitranslmed.aav1648
25. Eloranta ML, Rönnblom L. Cause and consequences of the activated type I interferon system in SLE. J Mol Med (Berl) 2016;94(10):1103–1110. doi:https://doi.org/10.1007/s00109-016-1421-4
26. Yang M, Long D, Hu L, et al. AIM2 deficiency in B cells ameliorates systemic lupus erythematosus by regulating Blimp-1-Bcl-6 axis-mediated B-cell differentiation. Signal Transduct Target Ther 2021;6(1):341. doi:https://doi.org/10.1038/s41392-021-00725-x

Check for updates

Arthritis & Rheumatology
Vol. 78, No. 10, October 2026, pp 2124–2137
DOI 10.1002/art.70127
© 2026 The Author(s). *Arthritis & Rheumatology* published by Wiley Periodicals LLC on behalf of American College of Rheumatology.
This is an open access article under the terms of the Creative Commons Attribution-NonCommercial-NoDerivs License, which permits use and distribution in any medium, provided the original work is properly cited, the use is non-commercial and no modifications or adaptations are made.

American College of Rheumatology
Empowering Rheumatology Professionals

Unveiling Endotypes in Systemic Lupus Erythematosus Through Multiomic Analysis: Insights Into Cardiovascular and Renal Complications

Tomás Cerdó, PhD,[1] Laurel Woodridge, PhD,[2] Sagrario Corrales, MSc,[1] Juan Rafael Muñoz-Castañeda, PhD,[1] Ana Isabel Torralbo, BSc,[1] Anisur Rahman, MD, PhD,[2] Filipa Farinha, MD, PhD,[2] Rafaela Ortega Castro, MD, PhD,[1] Pedro Segui, MD,[1] Ismael Sanchez-Pareja, MSc,[1] Laura Muñoz-Barrera, MSc,[1] Christian Merlo, BSc,[1] Desiree Ruiz-Vilchez, MSc,[1] M. Carmen Ábalos-Aguilera, BSc,[1] Pilar Font, MD, PhD,[1] and Nuria Barbarroja Puerto, PhD,[1] PRECISESADS Clinical Consortium, Marta Alarcón-Riquelme, MD, PhD,[3,4] Alejandro Escudero-Contreras, MD, PhD,[1] M. Ángeles Aguirre-Zamorano, MD, PhD,[1] Carlos Perez-Sanchez, PhD,[1,5] Elizabeth C. Jury, PhD,[2] and Chary Lopez-Pedrera, PhD[1]

Objective. Systemic lupus erythematosus (SLE) shows clinical and molecular heterogeneity, and cardiovascular (CV) complications and lupus nephritis (LN) remain leading causes of morbidity and mortality. This study investigated whether omic profiling can reveal molecular endotypes linked to these outcomes.

Methods. Serum from 199 patients with SLE underwent proximity extension assay–based proteomics and targeted nuclear magnetic resonance metabolomics. Unsupervised clustering was performed on proteomic data, followed by integrative multiomic factor analysis, logistic regression, and machine learning models. Cohorts with SLE from the University College London, a subset with expanded Olink Reveal panel and untargeted metabolomics, and in vitro (human umbilical vein endothelial cell and HK2) and ex vivo (rat kidneys) models exposed to patient sera were used for validation and mechanistic exploration.

Results. Proteomic clustering identified two molecular subgroups (cluster 1 and cluster 2). Compared with cluster 2, cluster 1 showed damage burden and increased rates of LN (1.8-fold), hypertension (3-fold), dyslipidemia (2-fold), obesity (8-fold), and abnormal C-reactive protein/erythrocyte sedimentation rate (4-fold), consistent with CV risk. A total of 47 inflammatory and organ-damage proteins and multiple metabolites were increased in cluster 1. Neural network models based on metabolites and clinical variables discriminated clusters (area under the curve = 0.77), highlighting citrate and lipoproteins as key features. Multiomic analyses and external cohorts confirmed reproducibility and enrichment in pathways related to leukocyte trafficking, endothelial stress, and nephritis. In vitro, serum from patients with SLE induced NF-κB activation in rat kidneys compared with controls, supporting a proinflammatory effect.

Conclusion. Multiomic profiling delineates molecular endotypes in SLE, integrating immune, vascular, and metabolic pathways associated with CV risk and LN, supporting their potential for precision risk stratification.

INTRODUCTION

Systemic lupus erythematosus (SLE) is a complex autoimmune disease with heterogeneous clinical manifestations and unpredictable progression, complicating diagnosis and treatment.[1] It affects multiple organs, particularly the skin, joints, and kidneys, and the cardiovascular (CV) system. Lupus nephritis (LN) and CV complications are major contributors to SLE-related morbidity and mortality.

Supported by the Instituto de Salud Carlos III (ISCIII) and European Union (grant PI24/00959); Health Outcomes-Oriented Cooperative Research Networks (grants RD21/0002/0033 and RD24/0007/0019), granted by the ISCIII and funded by the European Union – NextGenerationEU, via Mecanismo de Recuperación y Resiliencia and Plan de Recuperación, Transformación y Resiliencia (PRTR); and Fundacion Andaluza de Reumatología; and Ministerio de Ciencia, Innovación y Universidades (grant PID2022-141500OA-I00). Dr Cerdó's work was supported by the Sara Borrell program of the ISCIII (grant CD21/00187). Author Muñoz-Barrera's work was supported by the ISCIII (grant FI22/00299). Drs Puerto and Perez-Sanchez's work was supported by the MINECO Ramon y Cajal program (grants RYC2021-033828-I and RyC-2017-23437) and the European Union NextGenerationEU/PRTR. Dr Jury's work was supported by the London Interdisciplinary Biosciences PhD Consortium (grant BB/M009513/1) through a PhD studentship. Dr Lopez-Pedrera's work was supported by the Spanish Junta de Andalucía (Nicolas Monardes program).

[1]Instituto Maimónides de Investigación Biomédica de Córdoba, Hospital Reina Sofía, University of Córdoba, Cordoba, Spain; [2]Centre for Rheumatology Research, Division of Medicine, University College London, London, United Kingdom; [3]Center for Genomics and Oncological Research, Granada, Spain; [4]Institute for Environmental Medicine, Karolinska Institutet, Stockholm, Sweden; [5]Department of Cell Biology, Immunology and

SLE-associated CV disease (CVD)—including early atherosclerosis, stroke, and thrombosis—arises from a multifactorial interplay of genetic predispositions (eg, STAT4, IRF5, PDGF, HAS2, ITGAM, SLC5A11), epigenetic changes (eg, DNA methylation, microRNAs, splicing), classical CV risk factors (hyperlipidemia, hypertension, obesity), autoimmunity (autoantibodies, immune cell dysregulation), complement activation, oxidative stress, endothelial dysfunction, and proinflammatory mediators.[2–4] LN occurs in ~40% of patients and entails renal inflammation with potential long-term organ damage.[5] Its variable clinical presentation challenges early detection and risk stratification. Traditional markers (proteinuria, serum creatinine) often fail to fully capture disease severity or dynamics.[6]

Recent evidence supports the utility of molecular biomarkers—including anti–double-stranded DNA (dsDNA), anti-Smith antibodies, and others—in assessing disease activity and organ involvement. Yet, the clinical heterogeneity of SLE remains a barrier to effective management, emphasizing the need for deeper insights into its molecular basis. Identifying discrete molecular endotypes may enable personalized therapies.

Multiomic strategies offer a powerful framework for deciphering the complex biology of SLE. Unlike static genomic data, the proteome and metabolome dynamically reflect the disease state, allowing the discovery of active pathways driving pathology. Their integration enables more accurate interpretation of disease processes, uncovering phenotype-specific molecular signatures and candidate biomarkers for stratification and prognosis.[7]

This study aims to enhance the molecular characterization of SLE by analyzing serum proteomic and metabolomic profiles in a well-defined patient cohort. We focus on signatures linked to inflammation, organ damage, CV risk, and LN. Complementary in vitro and ex vivo experiments—using human umbilical vein endothelial cells (HUVECs), HK2 cells, and rat kidney slices—model the endothelial and renal responses to patient serum. Advanced data analysis, including machine learning (ML), supports the classification of molecular subgroups and integrates multiomic profiles to inform patient stratification, pathophysiologic understanding, and therapeutic decision-making.

MATERIALS AND METHODS

Patients. A total of 199 patients fulfilling the revised American College of Rheumatology criteria for SLE were included across three cohorts.[8] The first cohort (n = 100) belonged to the European multicenter cross-sectional PRECISESADS Innovative Medicines Initiative study (NCT02890121; Supplementary Table 1), conducted in accordance with Good Clinical Practice guidelines and the Declaration of Helsinki, with informed consent obtained from all participants. Peripheral blood was collected in the morning after an eight-hour fast. There were no significant differences in steroid exposure between cluster 1 (23 of 48 patients) and cluster 2 (23 of 52 patients; $P = 0.866$). Two additional independent cohorts comprising 99 patients with SLE (58 with CV risk and 41 with LN) were recruited from the rheumatology clinic at University College London (UCL) Hospital following approval by local ethics committees (15-LO-2065, 11-LO-0330, and 06/Q0505/79) and written informed consent. Peripheral venous blood samples were processed to obtain serum and stored at –80°C until use.

Circulating inflammatory profile. Protein levels of 184 markers—92 proinflammatory and 92 organ-damage mediators—were measured in PRECISESADS serum using the sensitive proximity extension assay (PEA) technology (Cobiomic Bioscience; https://cobiomicbioscience.com/wp-content/uploads/2025/07/Target-96-Inflammation.pdf). Additionally, proteome assays were performed in a subset of six samples (cluster 1, n = 5; cluster 2, n = 5) using PEA technology, analyzing 1,034 proteins from the Reveal panel (https://cobiomicbioscience.com/wp-content/uploads/2025/10/olink-reveal.pdf).

Serum metabolomics. Measures of 228 serum biomarkers were performed with an established nuclear magnetic resonance spectroscopy platform (Nightingale Health; https://research.nightingalehealth.com/uploads/documents/Nightingale-Blood-Analysis_List-of-Biomarkers.pdf). Moreover, an untargeted metabolomic study of the metabolite profile was conducted in a small subset of samples (cluster 1, n = 5; cluster 2, n = 5) by high-resolution liquid chromatography mass spectrometry using both ESI-positive and -negative ionization modes at the UCAI Metabolomics Facility of Instituto Maimónides de Investigación Biomédica de Córdoba, detecting 5,237 metabolites.

Treatment of HUVECs with serum from patients with SLE with high or low disease severity to identify the differential effects promoted on endothelial dysfunction. HUVECs were treated for 24 hours at 37°C with 15% serum from patients with high or low disease severity. Cells

Physiology, Agrifood Campus of International Excellence, University of Córdoba, Cordoba, Spain.

Drs Perez-Sanchez, Jury, and Lopez-Pedrera contributed equally to this work.

Additional supplementary information cited in this article can be found online in the Supporting Information section (https://acrjournals.onlinelibrary.wiley.com/doi/10.1002/art.70127).

Author disclosures and graphical abstract are available at https://onlinelibrary.wiley.com/doi/10.1002/art.70127.

Address correspondence via email to Tomás Cerdó, PhD, at tomas.craez@imibic.org; or Chary Lopez-Pedrera, PhD, at md2lopem@uco.es.

Submitted for publication July 1, 2025; accepted in revised form February 20, 2026.

were lysed with radioimmunoprecipitation assay (RIPA) buffer, and proteome assays of 92 CV-related proteins were performed using PEA technology (https://cobiomicbioscience.com/wp-content/uploads/2025/07/Target-96-Cardiovascular-II.pdf).

Treatment of the renal cell line HK2 with serum from patients with cluster 1 or cluster 2 lupus to identify the differential effects associated with kidney damage. HK2 proximal tubular cells were exposed to 15% serum from patients with cluster 1 and cluster 2 at 37°C for 24 hours. Cells were lysed with RIPA buffer, and proteome assays of 92 inflammation-related proteins were performed using PEA technology (https://cobiomicbioscience.com/wp-content/uploads/2025/07/Target-96-Inflammation.pdf).

Ex vivo experiments on kidney slices from rats and p65 immunofluorescence in renal tissue. These experiments assessed the effects of serum from patients with cluster 1 and cluster 2 on renal and vascular inflammation through p65 expression. Kidneys from euthanized male Wistar rats were aseptically harvested, and renal slices were cultured for six hours with culture medium supplemented with 15% serum from healthy controls or patients with cluster 1 or cluster 2 at 37°C and 5% CO_2. Experiments were performed by authors JRM-C and AIT under blinded conditions; they received patient sera without knowledge of their origin or cluster assignment. Only authors TC and CL-P were aware of the identity of the sera analyzed. Finally, proteome assays in homogenized kidney slices were then performed by PEA technology, analyzing 48 proteins from the mouse cytokine panel, which is compatible with rat samples (https://cobiomicbioscience.com/wp-content/uploads/2025/07/Target-48-Mouse-Cytokine.pdf).

Renal slices were fixed in paraformaldehyde, paraffin embedded, and sectioned (3–4 μm) for p65 immunofluorescence. After deparaffinization, antigen retrieval in citrate buffer (pH 6) and permeabilization, sections were incubated overnight at 4°C with an anti-p65 primary antibody, followed by Alexa Fluor 647–conjugated secondary antibody. Nuclei were counterstained with DAPI. Negative controls were performed by omitting the primary antibody. Images were acquired by fluorescence microscopy and analyzed using Fiji/ImageJ software.

Data analysis. Statistical analyses were performed using SPSS version 25.0 (IBM), R (with multiple analytical packages), GraphPad Prism 9, and MetaboAnalyst version 6. The significance threshold was set at $P < 0.05$ or false discovery rate (FDR) ≤0.05 when multiple-testing correction was applied. Data distribution and variance homogeneity were assessed before hypothesis testing, and nonparametric methods were used when appropriate.

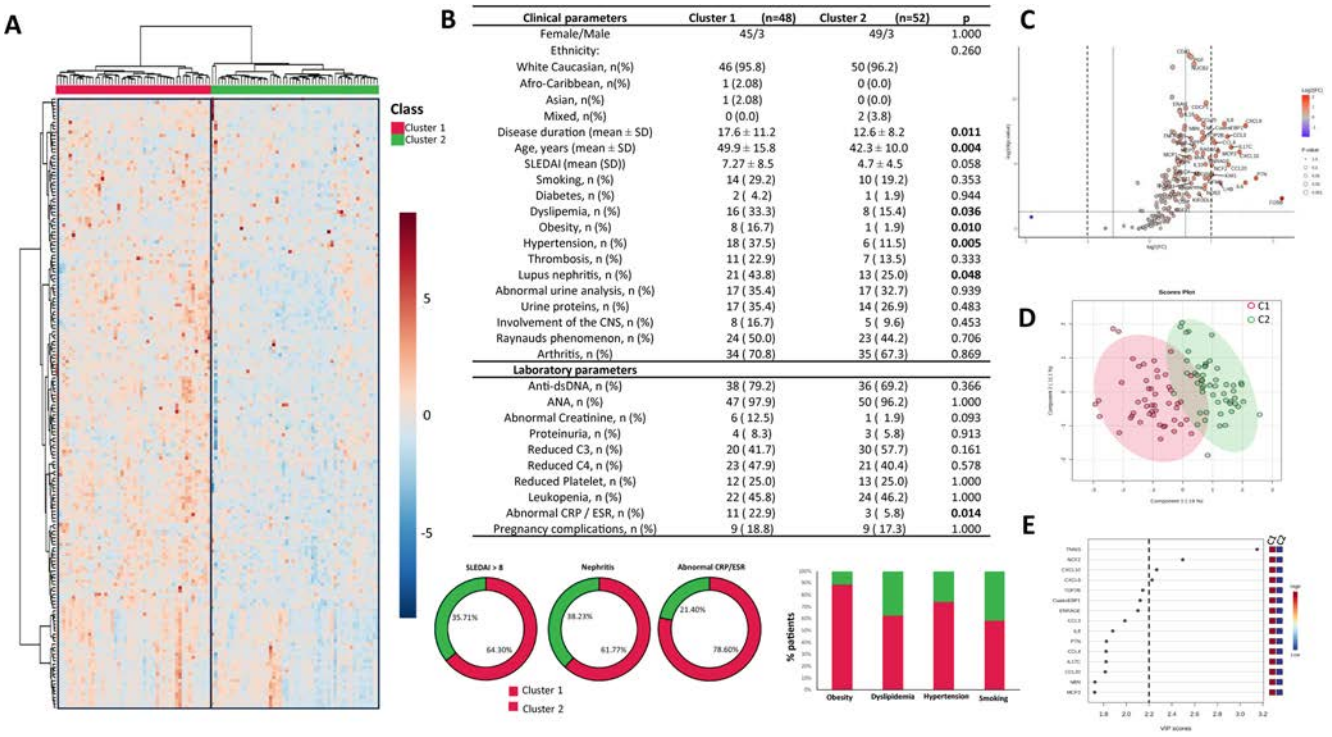
MetaboAnalyst was employed for unsupervised clustering analyses (including hierarchical clustering and partial least squares discriminant analysis [PLS-DA]) and for metabolomic data exploration, whereas functional and network enrichment analyses were performed using STRING and Metascape. Multiomic data integration was conducted using the multiomic factor analysis (MOFA) framework, with log2 normalization and view scaling applied to adjust variance across omics layers before model training. Predictive modeling was performed using univariate logistic regression and six supervised ML algorithms: support vector machine, generalized linear model with lasso regularization, boosted logistic regression, XGBoost, neural network, and random forest. Models were evaluated through 10-fold cross-validation.

Metabolite features with >10% missing data were excluded, and the remaining missing values were imputed using k-nearest neighbors (k = 5). Highly correlated metabolites ($r > 0.95$) were removed to reduce redundancy. Pearson correlation analyses were conducted to examine associations between clinical and molecular variables and visualized in R using the circlize and qgraph packages. The data sets generated and analyzed during the current study will be shared upon reasonable request from the corresponding author. PRECISESADS Clinical Consortium members are listed in Appendix A.

RESULTS

Unsupervised clustering of circulating inflammatory and organ-damage proteomes stratifies patients with SLE into two distinctive molecular subgroups, which also exhibit relevant metabolic alterations linked to their clinical profiles. To determine the relative contribution of each omic layer, we first applied an MOFA integrating proteomic and metabolomic data. Proteomics emerged as the dominant driver of variance (44.9%) across patients, exerting a stronger discriminatory power compared to metabolomics (4.8%; Supplementary Figure 1). Based on this, we performed unsupervised clustering of circulating inflammatory and organ-damage proteomes in patients with SLE (Supplementary Table 1), identifying two molecular subgroups with distinct clinical features (Figure 1A). Cluster 1 showed elevated disease activity (Systemic Lupus Erythematosus Disease Activity Index [SLEDAI] > 5), longer disease duration, abnormal C-reactive protein/erythrocyte sedimentation rate, and a higher prevalence of CV risk factors (obesity, hypertension, dyslipidemia, statin use) and LN compared to cluster 2 (Figure 1B).

At the molecular level, patients with cluster 1 overexpressed 47 proteins ($P < 0.05$, fold change ≥ 1.5, FDR) versus cluster 2 (Figure 1C), with the top six (CD40, prostaglandin F [PGF], ENAH, NUCB2, CDCP1, interleukin-18 [IL-18]) linked to inflammation. PLS-DA confirmed subgroup separation (Figure 1D), highlighting TINNI3, NCF2, CXCL10, and CXCL9 as key drivers (variable importance in projection plot > 2.2; Figure 1E). To ensure that the observed molecular differences between clusters are not



Clinical parameters	Cluster 1 (n=48)	Cluster 2 (n=52)	p
Female/Male	45/3	49/3	1.000
Ethnicity:			0.260
White Caucasian, n(%)	46 (95.8)	50 (96.2)	
Afro-Caribbean, n(%)	1 (2.08)	0 (0.0)	
Asian, n(%)	1 (2.08)	0 (0.0)	
Mixed, n(%)	0 (0.0)	2 (3.8)	
Disease duration (mean ± SD)	17.6 ± 11.2	12.6 ± 8.2	**0.011**
Age, years (mean ± SD)	49.9 ± 15.8	42.3 ± 10.0	**0.004**
SLEDAI (mean (SD))	7.27 ± 8.5	4.7 ± 4.5	0.058
Smoking, n (%)	14 (29.2)	10 (19.2)	0.353
Diabetes, n (%)	2 (4.2)	1 (1.9)	0.944
Dyslipemia, n (%)	16 (33.3)	8 (15.4)	**0.036**
Obesity, n (%)	8 (16.7)	1 (1.9)	**0.010**
Hypertension, n (%)	18 (37.5)	6 (11.5)	**0.005**
Thrombosis, n (%)	11 (22.9)	7 (13.5)	0.333
Lupus nephritis, n (%)	21 (43.8)	13 (25.0)	**0.048**
Abnormal urine analysis, n (%)	17 (35.4)	17 (32.7)	0.939
Urine proteins, n (%)	17 (35.4)	14 (26.9)	0.483
Involvement of the CNS, n (%)	8 (16.7)	5 (9.6)	0.453
Raynauds phenomenon, n (%)	24 (50.0)	23 (44.2)	0.706
Arthritis, n (%)	34 (70.8)	35 (67.3)	0.869
Laboratory parameters			
Anti-dsDNA, n (%)	38 (79.2)	36 (69.2)	0.366
ANA, n (%)	47 (97.9)	50 (96.2)	1.000
Abnormal Creatinine, n (%)	6 (12.5)	1 (1.9)	0.093
Proteinuria, n (%)	4 (8.3)	3 (5.8)	0.913
Reduced C3, n (%)	20 (41.7)	30 (57.7)	0.161
Reduced C4, n (%)	23 (47.9)	21 (40.4)	0.578
Reduced Platelet, n (%)	12 (25.0)	13 (25.0)	1.000
Leukopenia, n (%)	22 (45.8)	24 (46.2)	1.000
Abnormal CRP / ESR, n (%)	11 (22.9)	3 (5.8)	**0.014**
Pregnancy complications, n (%)	9 (18.8)	9 (17.3)	1.000

Figure 1. Proteomic analysis. (A) Unsupervised heatmap of patients. High disease severity subgroup (cluster 1 [C1]) is colored in red (n = 48) and low disease severity subgroup (C2) is colored in green (n = 52). (B) Clinical and analytical profiles of patients from C1 and C2. The figure represents the most important and significant variables between both subgroups. (C) Volcano plot showing 47 significant proteins between C1 and C2 ($P < 0.05$, fold change [FC] ≥1.5 on the linear scale, corresponding to $|\log2(FC)| \geq 0.58$, false discovery rate adjusted). The x-axis represents log2-transformed FCs. (D) Partial least squares discriminant analysis (PLS-DA) summarizing the differences among the protein profiles C1 (red) and C2 (green). (E) Variable importance in projection plot (VIP): proteins identified by sparse variant PLS-DA in descending order of importance. The graph represents the relative contribution of these proteins to the variance between the two subgroups. The blue and red boxes on the right indicate whether the protein levels are increased (red) or decreased (blue) in the serum of patients across subgroups. ANA, antinuclear antibody; CNS, central nervous system; CRP, C-reactive protein; dsDNA, double-stranded DNA; ESR, erythrocyte sedimentation rate; SLEDAI, Systemic Lupus Erythematosus Disease Activity Index.

biased by disease duration, we fitted linear models adjusted for age and disease duration. All proteins remained significantly associated with cluster assignment except FGF21, which was excluded (Supplementary Table 2).

Protein–protein interaction analysis via STRING revealed 46 nodes and 238 edges ($P < 1.0 \times 10^{-16}$; Supplementary Figure 2A). Enrichment analysis showed up-regulated proteins involved in inflammatory pathways (leukocyte chemotaxis/migration, inflammatory response, myeloid leukocyte migration, and neutrophil chemotaxis), CV mechanisms (fluid shear stress, atherosclerosis, blood pressure regulation, and lipid metabolism), and nephritis-related pathways (interferon γ and IL-17 regulation; Supplementary Figure 2B). Comparison with healthy donors (HDs; Supplementary Figure 3) revealed that the proteomic profile of cluster 2 was more similar to HDs than to cluster 1, the latter characterized by a markedly higher number of up-regulated inflammatory and organ damage–related proteins.

To validate the findings in an independent cohort, matched proteomic data from the UCL cohort were analyzed using the same Olink panels and analytical pipeline applied in PRECISESADS. Unsupervised clustering and principal components analysis identified two molecular subgroups (cluster 1, n = 16; cluster 2, n = 20) with clinical features closely mirroring those observed in PRECISESADS (Supplementary Figure 4A–C; Supplementary Table 3). A substantial subset of proteins distinguishing the clusters in PRECISESADS showed concordant changes in UCL, including IL-18, CXCL9, CXCL10, CD40, CDCP1, PGF, NCF2, NUCB2, TNNI3, and FGF23 (Supplementary Figure 4D). Network and functional enrichment analyses highlighted pathways related to immune activation, endothelial/vascular stress, and nephritis (Supplementary Figure 4E–F).

These findings indicate that the proteomic endotypes defined in PRECISESADS are reproducible in an independent cohort and that the associated metabolomic and proteomic signatures represent robust, cross-cohort molecular traits. In order to explore molecular differences between the two proteomic-defined clusters, a metabolomic analysis was performed on matched patient samples. Significant changes in the abundance of 13 serum metabolites were identified (Figure 2A). A total of

12 metabolites were up-regulated in cluster 1 (Figure 2A), with the top 3 being creatinine (P = 0.0034), citrate (P = 0.0037), and medium low-density lipoprotein (LDL) triglycerides (TGs; P = 0.012). Only one metabolite was down-regulated in cluster 1, isoleucine (P = 0.014).

To investigate whether metabolite levels were independently associated with subgroup classification, univariate logistic regressions were conducted for each serum metabolite. These models were adjusted for relevant clinical, demographic, and treatment covariates, including disease duration, age, and SLEDAI score. This analysis identified six metabolites—acetoacetate, citrate, creatinine, large LDL TGs, LDL TGs, and medium LDL TGs—that were significantly up-regulated in the patients with cluster 1 compared to cluster 2 (Figure 2B and C).

Next, six supervised ML models were trained and validated to discriminate between cluster 1 and cluster 2. Given the high degree of correlation among metabolites, homology reduction was applied (see the Materials and Methods section), resulting in a data set of 111 nonredundant metabolites. The same clinical variables used in logistic regression were also included as features (Figure 2B). The best-performing model, based on accuracy, specificity, and F1 score, was the neural network (Figure 2D and E; Supplementary Table 4). This model achieved an area under the receiver operating characteristic curve of 0.77 (Figure 2D), with a sensitivity of 70.92% and specificity of 73.08%.

Top features included citrate, mycophenolate mofetil use, very low–density lipoprotein (VLDL) particle size, pyruvate, and alanine. Citrate, acetoacetate, and creatinine—also significant in logistic regression—ranked among the top 20 features (Figure 2E), further supporting their relevance in distinguishing patients with cluster 1 from cluster 2. To determine if metabolites identified by the neural network model reflected metabolic differences between cluster 1 and cluster 2, a metabolite set enrichment analysis was performed (Figure 2E and F). Pathways

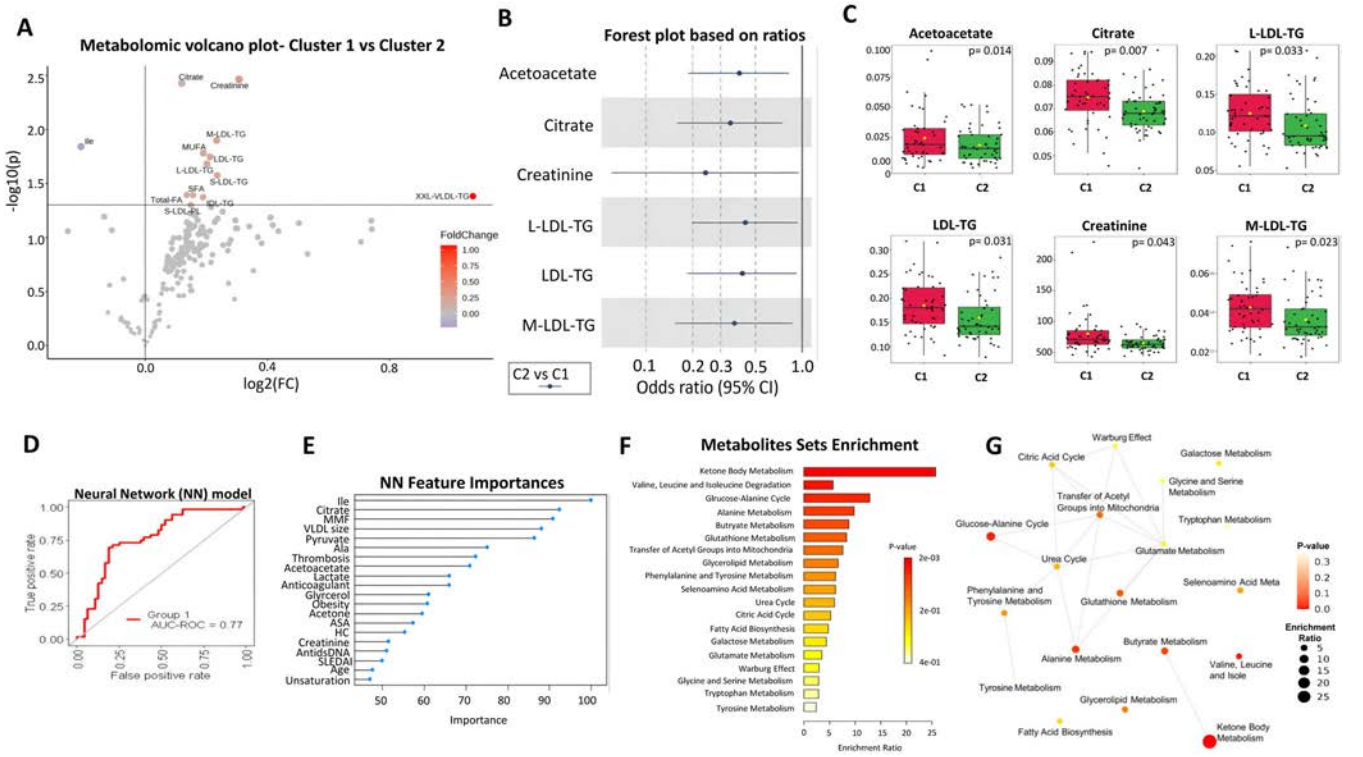


Figure 2. Metabolomic analysis using proteomic clusters. (A) Volcano plot shows 13 metabolites up-regulated and 1 metabolite down-regulated in cluster 1 (C1) versus C2 (fold change [FC] 1 $P \leq 0.05$). (B) Forest plot showing odds ratios (ORs) and 95% confidence intervals (CIs) of serum lipids comparing all patients in the C2 to the C1 (reference group) by logistic regression analysis adjusted for disease duration, age, SLEDAI score, sex, smoking, diabetes, dyslipidemia, obesity, anti–double-stranded DNA (dsDNA), hypertension, thrombosis, lupus nephritis, statin, steroids, prednisone, acetylsalicylic acid (ASA), anticoagulant, azathioprine, immunosuppressant, mycophenolate mofetil (MMF), antimalarials, hydroxychloroquine (HC), methotrexate, nonsteroidal anti-inflammatory. ORs below 1 denote metabolites that are increased in C1 versus C2. (C) Significant metabolites from the Forest plot. (D) Receiver operating characteristic (ROC) curves for neural network (NN) model. (E) Variable importance plot of the NN analysis, in which the variables are ordered top to bottom as most to least important in classifying between C1 and C2. (F) Enrichment analysis using the Small Molecule Pathway Database (SMPDB). Pathways with a significant enrichment P <0.05 are shown (–log10[P value]). Enrichment ratio is indicated along the y-axis. (G) Network of metabolic pathways derived from the SMPDB. Nodes are sized using the –log10(P value) and colored on a red-to-yellow gradient. The larger and redder the node, the greater the significance of the P value. Ala, alanine; AUC, area under the curve; FA, fatty acid; IDL, intermediate-density lipoprotein; L, large; LDL, low-density lipoprotein; M, medium; MUFA, monounsaturated FA; PL, phospholipids; S, small; SFA, saturated FA; SLEDAI, Systemic Lupus Erythematosus Disease Activity Index; TG, triglyceride; VLDL, very low–density lipoprotein; XXL, extra-extra large. Color figure can be viewed in the online issue, which is available at http://onlinelibrary.wiley.com/doi/10.1002/art.70127/abstract.

related to amino acid and lipid metabolism were enriched in cluster 1, including "ketone body metabolism" ($P = 0.002$) and "valine, leucine, and isoleucine degradation" ($P = 0.04$; Figure 2F). Network analysis confirmed the connections among these pathways (Figure 2E).

To validate and extend our previous findings, we performed a massively parallel multiomic analysis in 10 patients (5 with cluster 1 and 5 with cluster 2), detecting 1,034 proteins (Olink proteomics) and 5,237 metabolites (mass spectrometry). First, MOFA (Supplementary Figure 5A) revealed that proteomics explained the majority of variance (39.25%), whereas metabolomics contributed 1.30%, consistent with the initial observations. Next, volcano plot analysis of proteomics data (fold change ≥ 2, $P < 0.05$; Supplementary Figure 5B) identified 340 proteins up-regulated in clusters 1 and 2 down-regulated in cluster 1. Metabolomics volcano analysis (fold change ≥ 2, $P < 0.05$; Supplementary Figure 5C) revealed 228 metabolites enriched in cluster 1 and 119 down-regulated. Significant proteins and metabolites from these analyses were then correlated (FDR-adjusted $P < 0.05$), yielding 2,467 significant correlations, predominantly positive (Supplementary Figure 5D).

Finally, biologic process enrichment analysis (STRING) of the 150 proteins involved in significant correlations highlighted relevant functional pathways (Supplementary Figure 5E), such as immune system processes, immune response and cytokine-mediated signaling, and functional classification of the 84 metabolites involved in significant correlations (Supplementary Figure 5F) delineated inflammation-linked metabolic signatures, including tryptophan/indole signaling, bile acid–mediated immunoregulation, lipid signaling/inflammation, and core energy metabolism.

Omics integration reveals specific biomarker signatures associated with CV risk and LN. Considering the impact of CVD risk (CVD risk$^+$/CVD risk$^-$) and LN (SLE-LN$^+$/SLE-LN$^-$) in SLE, we investigated molecular biomarkers to classify patients using a supervised approach.

Molecular CVD risk signature. Patients from the PRECISESADS cohort were classified based on the presence (CVD risk$^+$, n = 24) or absence (CVD risk$^-$, n = 76) of dyslipidemia and hypertension. The group with CVD risk was older, had longer disease duration, higher disease activity (SLEDAI > 8), and greater diabetes prevalence (Supplementary Table 5). This group showed up-regulation of 23 circulating inflammatory and organ damage–related proteins (top 5: LHB, ADGRG1, TNFRSF9, IL-4, and PLIN1), with only pleiotrophin (PTN) down-regulated. Additionally, 71 significant metabolites were identified, mainly lipids and subclasses of high-density lipoprotein, LDL, and intermediate-density lipoprotein (Figure 3A). Multiple significant correlations (Pearson, $P < 0.05$) linked proteins related to chemotaxis, immune activation, and inflammation (eg, CXCL9, CD40, IL-4) with proatherogenic metabolites (Figure 3B). These findings were validated in an independent UCL cohort (22 with CVD risk and 36 without CVD risk) with comparable clinical features (Supplementary Table 5), in which 60 metabolites were significantly up-regulated in patients with CVD risk (Figure 4A). Comparison between PRECISESADS and UCL cohorts identified 49 overlapping significant metabolites of 71 (69% concordance; Figure 4B and C), confirming a robust metabolic signature associated with CV risk in lupus.

Molecular LN signature. The PRECISESADS cohort included 34 patients with LN and 66 patients without LN (Supplementary Table 6). Differential analysis of serum proteome and metabolome revealed 27 up-regulated proteins related to inflammation and organ damage (top 5: CX3CL1, IL-2RB, CRH, and urokinase plasminogen activator [uPA]) and six down-regulated proteins (FES, FKBP1B, WAS, BID, TNFSF24, and PRKAB1). Additionally, 40 metabolites, mainly LDL and VLDL subclasses linked to cholesterol metabolism, inflammation, and fatty acids, were significantly increased. Correlation analysis showed multiple positive associations (Pearson, $P < 0.05$) among proteins related to renal damage (FGF23, BID, ENTPD6, TNFSF14, and uPA) and proatherogenic/proinflammatory metabolites (LDL, VLDL subclasses, GlycA, monounsaturated fatty acid, and remnant-C), indicating a coordinated proteomic–metabolomic profile in patients with LN (Figure 3C and D).

Validation in a UCL cohort (29 with LN, 12 without LN) with similar clinical features (Supplementary Table 6) identified 93 up-regulated metabolites (Figure 4D) in patients with LN. Cross-cohort comparison showed 35 overlapping metabolites (87.5% of PRECISESADS altered metabolites), confirming a robust metabolomic signature associated with LN (Figure 4E and F).

Integrated correlation networks reveal distinct protein–metabolite interactions associated with CV risk and LN in SLE. To further explore the biologic connections between omics data and disease severity in patients with SLE, we constructed integrated correlation networks based on proteins and metabolites significantly associated with CVD risk and LN. For the group with CV risk, the network was built using 23 proteins and 49 overlapping metabolites identified in the subgroup with CVD risk. Significant correlations (Pearson, $P < 0.01$) were found between common metabolites and five key proteins: CCL11, CXCL6, CES2, PLIN1, and RARRES1 (Supplementary Figure 6A). Expression analysis revealed that all molecules were up-regulated in patients with cluster 1 compared to cluster 2, except for RARRES1, which showed down-regulation (Supplementary Figure 6B).

Similarly, in the cohort with LN, a correlation network was developed using 23 proteins and 49 metabolites significantly associated with LN. Significant associations (Pearson, $P < 0.01$) were observed between common metabolites and five proteins: LIFR, AMN, BID, ENTPD6, and IL-7 (Supplementary Figure 6C). Most proteins were up-regulated in cluster 1 compared to cluster 2, whereas BID exhibited an opposite regulation pattern, being

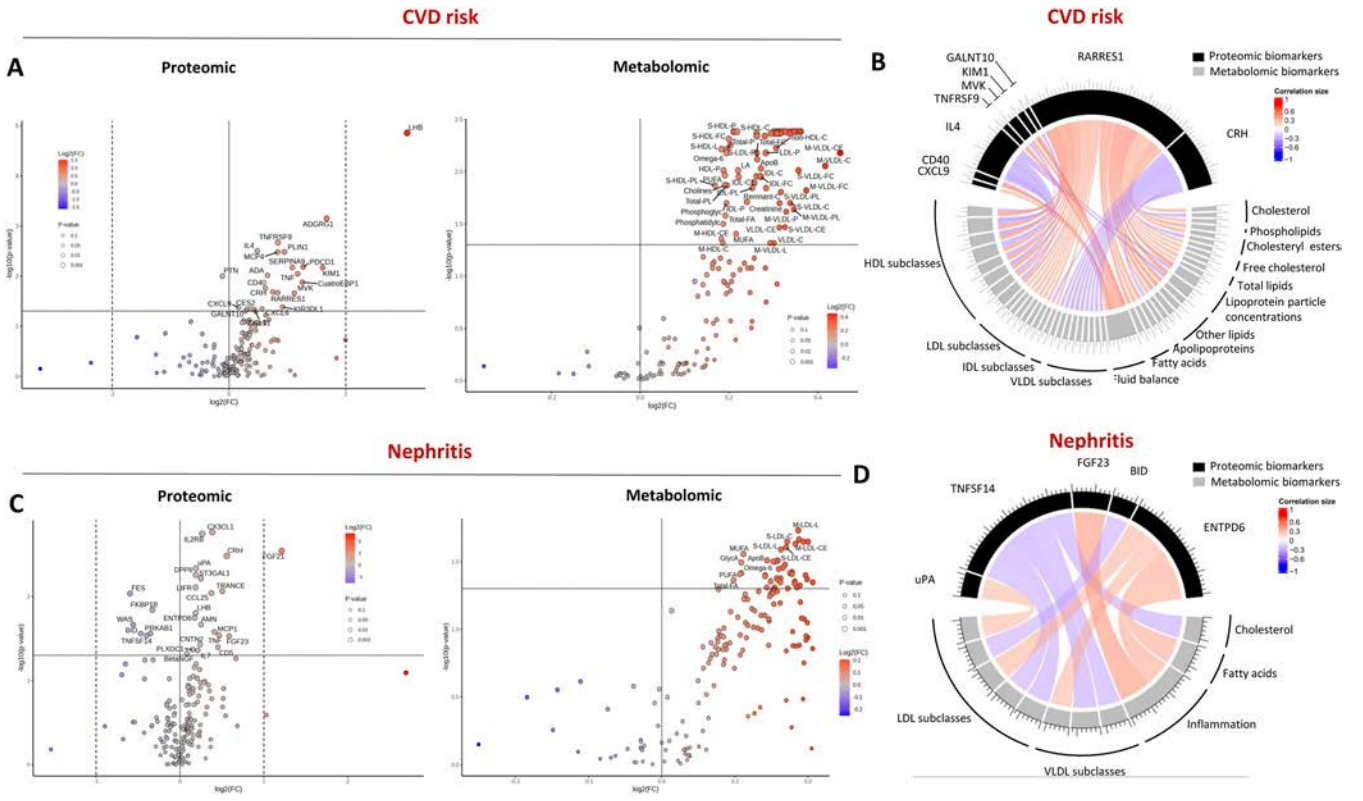


Figure 3. Cardiovascular (CV) risk and lupus nephritis studies. (A) Volcano plots show 23 significant circulating inflammatory and organ-damage proteins and 71 significantly up-regulated metabolites in patients with CV disease (CVD). Proteomic and metabolomic differences are displayed as log2-transformed fold changes (FCs). Thresholds correspond to an FC ≥2 on the linear scale (|log2[FC]| ≥ 1) for proteins and metabolites, with FDR-adjusted P <0.05 for metabolites and nominal P <0.05 for proteins. Dashed vertical lines indicate the linear-scale FC thresholds; for proteins, no significant down-regulated proteins were detected, but the line is included for clarity. (B) Circular plots display the results of protein-driven (black) and metabolite-driven (gray) integration of omics in the CV risk study. (C) Volcano plots show 6 down-regulated and 21 up-regulated significant circulating inflammatory and organ-damage proteins, as well as 40 significantly up-regulated metabolites in patients with lupus nephritis risk. Thresholds and dashed vertical lines are defined as in panel A. (D) Circular plots display the results of protein-driven (black) and metabolite-driven (gray) integration of omics in the lupus nephritis study. In the center of each circular plot, significant correlation coefficients (Pearson, P < 0.05) are visualized through links connecting the two correlated omics. Links are colored according to the sign of the correlation coefficient: red for positive correlations and blue for negative correlations. The thickness of the links increases with the absolute value of the correlation coefficients. C, cholesterol; CE, cholesteryl ester; CRH, corticotropin-releasing hormone; FA, fatty acid; HDL, high-density lipoprotein; IDL, intermediate-density lipoprotein; L, large; LDL, low-density lipoprotein; M, medium; P, particles; PL, phospholipids; PUFA, polyunsaturated FA; S, small; uPA, urokinase plasminogen activator; VLDL, very low–density lipoprotein. Color figure can be viewed in the online issue, which is available at http://onlinelibrary.wiley.com/doi/10.1002/art.70127/abstract.

down-regulated in the group in cluster 1 (Supplementary Figure 6D). These integrated protein–metabolite networks highlight distinct molecular signatures linked to disease severity in patients with SLE with CV risk and LN, offering insight into the underlying biologic mechanisms and potential therapeutic targets.

The direct contribution of the altered circulating molecular profile observed in patients with lupus to CV and renal phenotypes was confirmed through in vitro studies. To explore CV and renal damage mechanisms in lupus, HUVECs and renal HK2 cells were treated with serum from patients with cluster 1 and cluster 2 (Figure 5A). Cluster 1 serum induced significant increases in 29 CVD-related proteins—including inflammatory (IL-6, PTX3, IL-18), growth factors (SCF, HB_EGF, PDGFb), antioxidants (HO_1, SOD2), proteolytic enzymes (MMP7, CTSL1), signaling molecules (PAPR-1, SCR), and hemostatic regulators (TM, TF)—all linked to endothelial dysfunction and CV risk (Figure 5B and C). Similarly, renal cells treated with the serum of the cluster 1 of patients with LN displayed and altered expression of 34 inflammatory proteins compared with cells treated with the serum of the cluster 2 without LN. These altered proteins involved inflammatory cytokines (IL-17A, IL-13, IL-20, and IL-17C), growth factors (VEGFA, FGF-21, and FGF-19), immunomodulatory proteins (CSF-1, IL-15RA), chemokines (MCP-2, CCL4, CXCL9), markers of anti-inflammation (IL-10RA, IL-10RB, and LAP TGF-beta-1) and proteins involved in checkpoint pathways, critical in autoimmune responses (PD-L1 and CD244; Figure 5D and E). Moreover, some

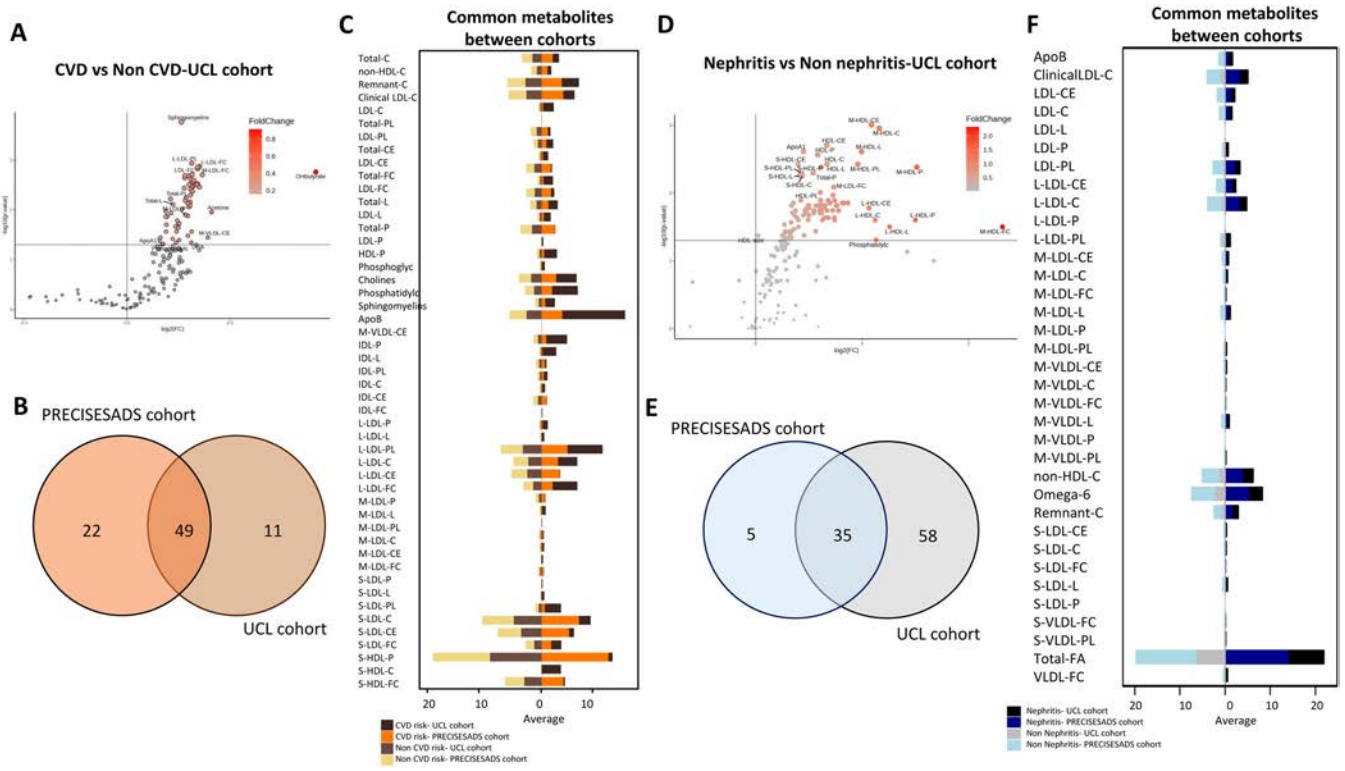


Figure 4. Validation of metabolic signatures in the University College London (UCL) cohort. (A) Volcano plot showing the differential metabolites between the groups with and without cardiovascular disease (CVD) risk in the UCL validation cohort. Significantly regulated metabolites are identified based on –log *P* values and log2 fold changes (FCs). (B) Venn diagram displaying the overlap among metabolites exclusive to the PRECISESADS cohort (orange) and the UCL cohort (brown), along with the common metabolites between both cohorts. (C) Likert scale plot showing the mean values of shared metabolites between the PRECISESADS and UCL cohorts, with specific colors assigned to each study group and cohort: dark brown for CVD risk$^-$ in UCL, orange for CVD risk$^-$ in PRECISESADS, brown for non-CVD risk in UCL, and yellow for non-CVD risk in PRECISESADS. (D) Volcano plot similar to (A) but focused on the lupus nephritis signature. (E) Venn diagram comparing metabolites exclusive to the PRECISESADS cohort (blue) and UCL cohort (gray) for lupus nephritis. (F) Likert scale plot showing the mean values of shared metabolites between the PRECISESADS and UCL cohorts for lupus nephritis, with color assignments as follows: dark black for CVD risk$^+$ in UCL, dark blue for CVD risk$^+$ in PRECISESADS, gray for non-CVD risk in UCL, and light blue for non-CVD risk in PRECISESADS. C, cholesterol; CE, cholesteryl ester; DHA, docosahexaenoic acid; FA, fatty acid; HDL, high-density lipoprotein; IDL, intermediate-density lipoprotein; L, large; LDL, low-density lipoprotein; M, medium; P, particle; PL, phospholipids; S, small; VLDL, very low–density lipoprotein. Color figure can be viewed in the online issue, which is available at http://onlinelibrary.wiley.com/doi/10.1002/art.70127/abstract.

of these proteins were further found altered in the serum of patients with lupus, such as MCP-2, IL-17C, CDCP1, CCL4, CCL25, CXCL9, and FGF-23 (Supplementary Figure 7A). Biologic enrichment analyses revealed clear similarity, especially in inflammation and immune response pathways like "proinflammatory and profibrotic mediators" and "IL-10 signaling" (Supplementary Figures 7B and C and 8), as well as significant enrichment of "cytokine–cytokine receptor interaction" in both data sets.

Ex vivo exposure of rat kidney slices to serum of patients with lupus revealed activation of inflammatory pathways, highlighting potential mechanisms underlying CV and renal damage. Lastly, to assess the ex vivo effects of altered serum proteomic and metabolomic profiles on CV and renal systems, rat kidney slices were exposed to serum from patients with SLE stratified as cluster 1, cluster 2, or HD. p65 expression was analyzed to evaluate NF-κB activation in renal arteries and tissue (Supplementary Figure 9A). Mean fluorescence intensity showed significantly higher p65 in vascular endothelium of slices treated with cluster 1 or cluster 2 serum versus HD (Supplementary Figure 9B) and were similarly elevated in glomeruli (Supplementary Figure 9C). Both groups in cluster 1 and cluster 2 had increased p65 compared to HDs, with significant differences in vascular (cluster 1 vs HD, $P = 0.05$; cluster 2 vs HD, $P = 0.03$) and glomerular compartments (cluster 1 vs HD, $P = 0.04$; cluster 2 vs HD, $P = 0.004$). Confocal microscopy detailed these effects (Supplementary Figures 9D and E and 10).

Although ex vivo comparisons between cluster 1 and cluster 2 did not reach statistical significance, a consistent trend toward higher inflammatory activation in cluster 1 was observed across vascular and glomerular compartments. To investigate whether these subtle differences reflected underlying molecular divergence, we performed targeted proteomic profiling using the Olink Mouse

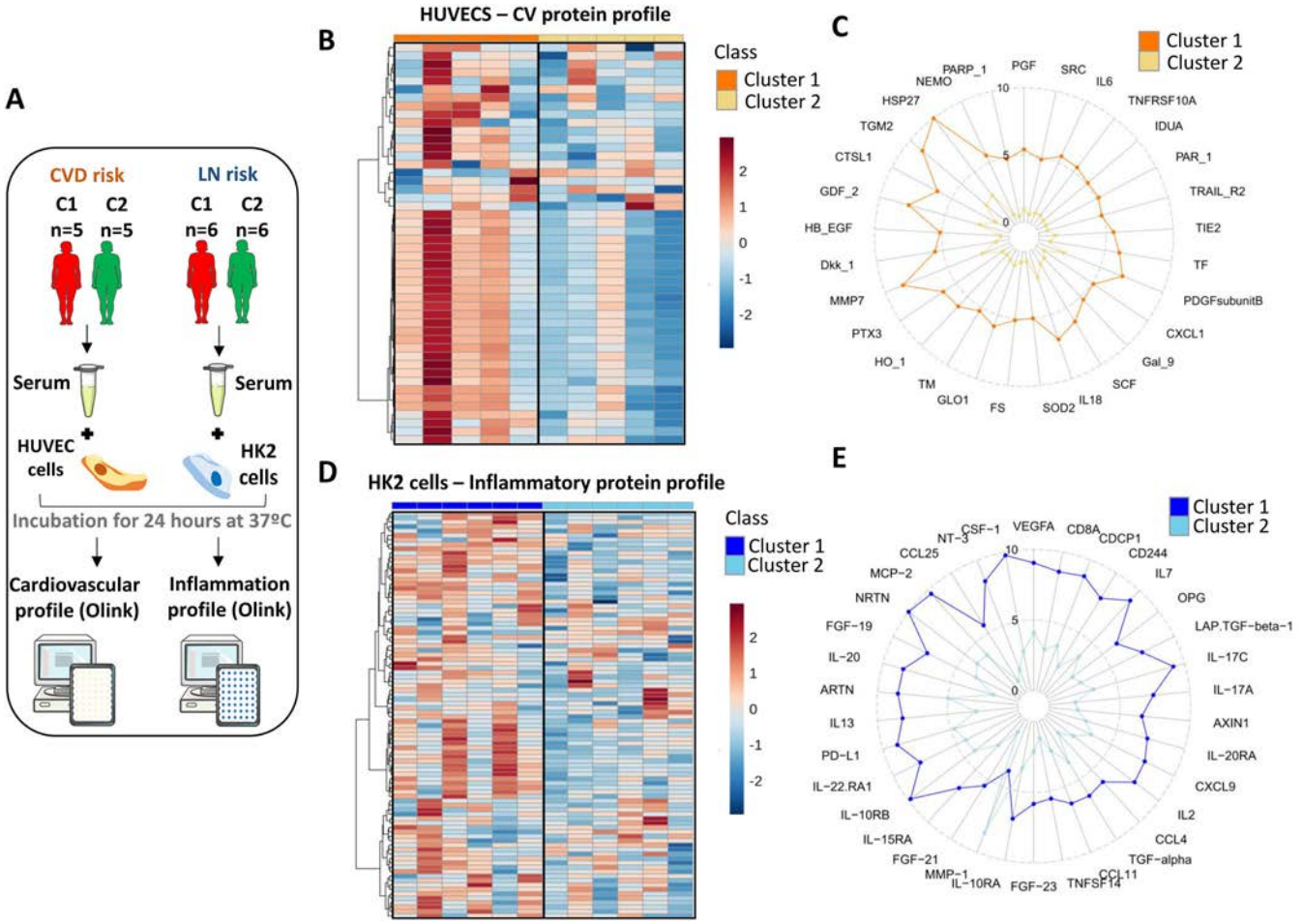


Figure 5. In vitro cellular models reveal proteomic signatures associated with cardiovascular disease (CVD) risk and lupus nephritis (LN). (A) Schematic image of the in vitro experimental setup in which serum samples from patients with or without CVD risk (cluster 1 [C1]/C2) and nephritis (C1/C2) were incubated with human umbilical vein endothelial cells (HUVECs) and kidney tubular cells (HK2) to study cellular responses related to CVD risk and LN. (B) Heatmap of all proteins measured in the CV Olink panel, expressed in HUVECs after a 24-hour incubation with serum from patients in C1 and C2, highlighting the proteomic profile studied for CVD risk. (C) Radar chart displaying the mean values of the significant proteins in the CV panel, scaled from 0 to 10 to facilitate visual comparison due to variability among proteins. The chart illustrates the increased expression of proteins in C1 compared to C2. (D) Heatmap of proteins measured in the inflammation-specific Olink panel, expressed in HK2 cells incubated with serum from patients in C1 and C2, used to study LN-related inflammation. (E) Radar chart showing the mean values of significant proteins from the inflammation-specific panel, scaled from 0 to 10, to visualize the differences in protein expression between the C1 and C2 in the context of LN. Color figure can be viewed in the online issue, which is available at http://onlinelibrary.wiley.com/doi/10.1002/art.70127/abstract.

Exploratory Panel on the same experimental system (Figure 6A). This analysis revealed that the average NPX values of the proteins included in the panel were significantly higher in cluster 1 than in cluster 2 ($P < 0.001$), indicating a globally increased inflammatory protein signature in cluster 1 (Figure 6B). Consistent with this, the heatmap (Figure 6C) demonstrated that most proteins showed higher expression levels in cluster 1 compared to cluster 2, further supporting the presence of distinct inflammatory signaling patterns among these serum-derived subgroups.

DISCUSSION

SLE is a highly heterogeneous autoimmune disease that complicates diagnosis and treatment. By integrating proteomic and metabolomic analyses, this study identified two distinct proteomic endotypes using unsupervised approaches, which were further supported by metabolomic alterations and associated clinical features. The more severe endotype was characterized by increased CV risk and renal involvement alongside dysregulated inflammatory mediators and metabolic disturbances. Overall, this multiomic and ML framework improves patient stratification and provides a basis for more personalized therapeutic strategies.

Among the 46 proteins up-regulated in cluster 1, both well-established inflammatory mediators and less-characterized proteins associated with NF-κB signaling and CVD were identified, underscoring their potential roles in SLE pathophysiology.[9] Notably, several of these proteins (eg, IL-6, tumor necrosis factor

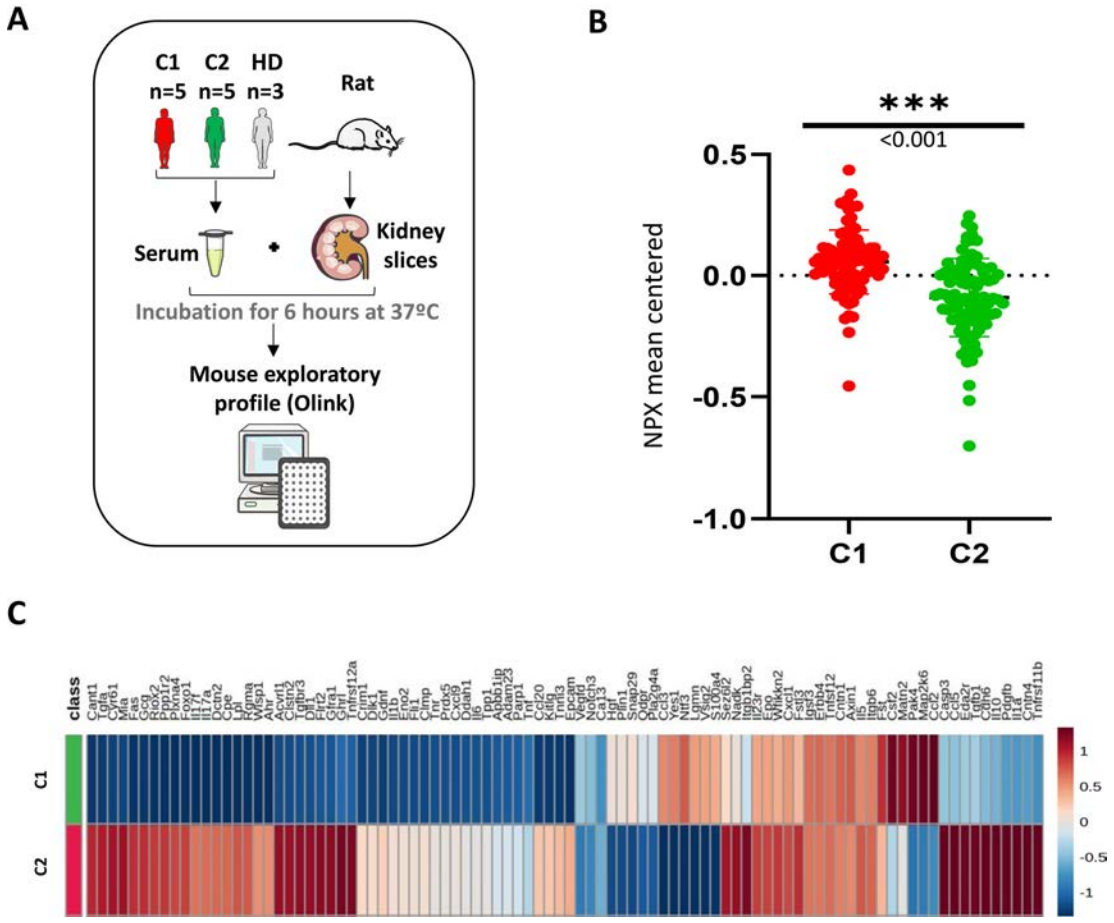


Figure 6. Ex vivo assessment of serum nephrotoxic potential of patients with lupus. (A) Schematic representation of the ex vivo experiment conducted to assess renal inflammation using kidney slices from male Wistar rats, incubated for six hours with 15% serum from healthy donors (HDs) and patients with lupus classified into cluster 1 (C1) and C2 subgroups. Finally, proteome assays were performed by PEA using the mouse cytokine panel compatible with rat samples. (B) Violin plots showing the distribution of mean-centered NPX values for all proteins included in this analysis, illustrating the global variability between groups C1 and C2 and providing supportive evidence for sections B through E. (C) Heatmap depicting the average mean-centered NPX values of the proteins shown in (B), summarizing group-level expression patterns between C1 and C2. NPX, normalized protein expression. Color figure can be viewed in the online issue, which is available at http://onlinelibrary.wiley.com/doi/10.1002/art.70127/abstract.

[TNF], IL-8, CXCL9/10/11, IL-18, and oncostatin M) have been linked to inflammatory processes beyond systemic inflammation, including tissue-specific alterations such as renal or hepatic involvement, among others, which may contribute to the molecular differences observed among the identified endotypes.

Previous studies have identified biomarkers of organ involvement in SLE, including CD163 and IL-16 for renal disease[10] and von Willebrand factor and GDF15 for CV risk.[11,12] Although some of these markers were not included in our analysis, our results revealed convergent biologic themes, such as enhanced myeloid/macrophage activation in LN and signatures of endothelial stress associated with CV risk. Differences among studies may reflect heterogeneity in patient populations, disease activity, and analytical platforms.

Consistent with our findings, Petrackova et al reported the up-regulation of several overlapping proteins in patients with SLE with organ damage or biopsy-proven active LN.[13] Similarly, Ruacho et al identified a subset of patients characterized by a systemic inflammatory state enriched in TNF, IL-6, chemokines, and interferon γ, which mirrors the cytokine profile observed in our cluster 1.[14] These mediators promote the recruitment of immunocompetent cells, reinforcing a pathogenic inflammatory loop driven in part by TNFα-induced chemokine expression.[15] The proteomic stratification was independently validated in an external cohort, in which it remained associated with key clinical features such as renal involvement and inflammation, with a high degree of overlap in dysregulated proteins across cohorts.

Metabolomic analyses revealed that cluster 1 exhibited elevated creatinine and citrate levels—markers of renal dysfunction and metabolic alterations—along with changes in LDL lipid profiles. Citrate links glycolysis and lipid metabolism and may contribute to enhanced inflammation in cluster 1,[16] whereas creatinine, beyond reflecting renal function, may indicate broader metabolic disturbances. In contrast, decreased isoleucine levels in cluster

1 are consistent with its role in regulating innate and adaptive immunity and key metabolic pathways.[17]

ML models integrating clinical and metabolomic data accurately discriminated cluster 1 from cluster 2, underscoring the added value of multiomic approaches for patient stratification. Logistic regression confirmed increased levels of citrate, creatinine, and LDL subclasses in cluster 1. In addition, alterations in acetoacetate were observed, a metabolite previously linked to rheumatoid arthritis and vascular disease through its capacity to promote oxidative stress and lipid peroxidation.[18,19]

In contrast to earlier studies that applied supervised ML to metabolomic data based on predefined clinical categories,[20,21] our approach identified a metabolomic signature using ML within unsupervised proteomic-derived clusters. Notably, the neural network highlighted citrate and isoleucine, together with clinical variables such as thrombosis and anti-dsDNA levels, as key contributors to a disrupted metabolic network involving energy metabolism, immune activation, and oxidative stress. Altered branched-chain amino acid metabolism, including reduced isoleucine levels, may further contribute to inflammatory and metabolic dysregulation in SLE through impaired ketogenesis and mitochondrial function.[22–25]

Lupus-associated dyslipidemia, characterized by elevated TGs and VLDL, is driven by imbalances in fatty acid saturation, with increased saturated fatty acids promoting inflammation and disease progression.[26] Although creatinine is not directly involved in energy metabolism, altered levels may reflect changes in protein metabolism or renal function, indirectly linking it to isoleucine metabolism.[27] These findings, supported by metabolite set enrichment analysis, enhance our understanding of lupus-related metabolic pathways and may aid diagnosis, endotype discrimination, and personalized therapeutic strategies.

To further extend our findings, we performed deeper integrated proteomic and untargeted metabolomic analyses in a smaller subset of patients, allowing a more detailed exploration of the connection among these omic layers. This approach recapitulated the inflammatory endotype identified in cluster 1 and uncovered additional dysregulated pathways consistent with immunometabolic reprogramming. Specifically, the convergence of inflammatory proteomic signals with metabolic alterations—particularly involving lipid metabolism, tryptophan/kynurenine pathways, and mitochondrial energy processes—supports a model in which immunometabolic dysregulation underlies a high-risk SLE phenotype. Dysregulated lipid metabolism has been implicated in immune cell hyperactivation and organ damage in SLE,[26] whereas enhanced kynurenine pathway activity has been associated with disease activity and renal involvement.[28] Mitochondrial dysfunction and oxidative stress, which promote reactive oxygen species production and inflammasome activation, are also recognized contributors to SLE pathogenesis.[29] Because there were no differences in steroid exposure, it is unlikely that differential protein and metabolite expression profiles identified were driven by pharmacologic effects of steroids. Together, these results reinforce the robustness of the identified endotypes and support immunometabolic coupling as a key pathophysiologic feature in SLE. Given the close link between the identified biomarkers and CV and renal involvement, we performed stratified analyses further characterize and contextualize the underlying molecular signatures.

CV risk in SLE was associated with a distinct molecular signature comprising inflammatory and immune-related proteins together with extensive lipid dysregulation. Key proteins involved in vascular inflammation and immune activation included MCP4, PDCD1, TNF, CXCL6, and CCL11, whereas regulators of lipid and energy metabolism such as PLIN1, PTN, and 4E-BP1 highlighted pathways linked to cholesterol handling and fat accumulation, central to atherosclerosis.[30–32] Additional proteins related to hormonal signaling, vascular regulation, and drug or lipid metabolism were also identified.[33–36] Metabolically, CV involvement was characterized by alterations across multiple lipoprotein subclasses, cholesterol, fatty acids, and apolipoproteins, all closely linked to CV dysfunction.[37] Integrative network analyses revealed strong connections between immune-related proteins and lipid metabolites, reinforcing immunometabolic dysregulation as a key contributor to CVD severity in SLE. These results highlight the need to consider CV risk when interpreting systemic molecular profiles in SLE because vascular comorbidities can significantly influence circulating proteomic and metabolomic signatures.

Renal involvement was associated with a distinct immunometabolic signature, characterized by dysregulated proteins involved in immune cell recruitment and renal damage, including CX3CL1, IL-2RB, CRH, MCP1, and TRANCE,[38–41] together with lipid alterations dominated by VLDL and LDL subclasses.[42,43] Integrative analyses revealed strong proteomic–metabolomic crosstalk, supporting coordinated immune and metabolic dysregulation in LN. These findings were validated in an independent cohort, indicating a persistent molecular footprint associated with renal involvement.

Despite the breadth of analyses performed across multiple omic layers and independent cohorts, our study converged on a robust proteomic and metabolomic signature composed of a defined set of molecules that consistently discriminated patient subgroups including the following: CCL20, IL-10, CXCL11, CDCP1, MCP-1, MCP-2, CXCL10, CCL4, IL-6, MCP-3, IL-8, EN-RAGE, citrate, creatinine, acetoacetate, large and medium LDL TGs, tryptophan/indole derivatives, bile acids, and lipid-mediated metabolites. These markers capture key biologic processes underlying disease heterogeneity and may serve as a valuable foundation for future mechanistic studies, biomarker validation efforts, and patient stratification approaches.

To investigate the functional relevance of the identified biomarkers, in vitro studies were performed in endothelial (HUVEC) and renal tubular (HK2) cells. Serum from patients with cluster

1 induced endothelial activation and dysfunction, characterized by increased inflammatory mediators, oxidative stress markers, and dysregulated angiogenic signaling, all processes implicated in CV risk in SLE.[44–46] These findings indicate that cluster 1 serum actively promotes endothelial injury and proatherogenic responses. Similarly, exposure of HK2 cells to serum from patients with LN, including those in cluster 1, triggered the up-regulation of multiple proteins involved in inflammation, immune cell recruitment, and fibrotic signaling. Key mediators associated with glomerular injury, Th17-driven inflammation, and fibrogenesis were identified, supporting a direct role of patient serum in promoting tubular dysfunction and LN progression.[47–51]

Ex vivo experiments using rat kidney tissue exposed to patient serum revealed increased expression of proteins related to inflammation, metabolic regulation, and tissue injury, accompanied by a trend toward activation of the NF-κB pathway as a potential contributing mechanism. These findings indicate that serum from patients with cluster 1 exerts a direct molecular impact on renal tissue, consistent with enhanced inflammatory and metabolic stress responses. Together, these data further support the notion that patients in cluster 1 display a systemic molecular profile capable of driving renal damage, linking circulating immunometabolic alterations to tissue-level pathology.[52,53] Overall, the functional analyses support that the identified molecular signatures have a direct biologic impact on vascular and renal tissues, linking immunometabolic dysregulation to organ-specific damage in SLE and reinforcing their relevance as mechanistic biomarkers and therapeutic targets.

The CV and renal molecular signatures identified in this study define a high-risk immunometabolic endotype in SLE, characterized by coordinated immune activation and metabolic dysregulation. Patients with increased CV risk and LN showed up-regulation of inflammatory cytokines and chemokines, Th17-related mediators, and broad alterations in atherogenic lipoproteins and inflammatory metabolic markers, reflecting pathways shared with nonautoimmune CVD and renal disease. Several key biomarkers overlapped with those linked to adverse outcomes in general and chronic kidney disease populations, supporting the relevance of these signatures beyond lupus-specific inflammation. Although limited by the cross-sectional design, the concordance with established CV risk profiles and the functional impact of high-risk SLE sera on endothelial and renal models suggest a biologically plausible link to future CV events that merits longitudinal validation.

Despite the strengths of this comprehensive multiomic study, some limitations should be acknowledged. The cohorts were of moderate size, predominantly European, and largely characterized by mild disease activity; however, the consistent replication of molecular signatures across independent cohorts supports the robustness of our findings. The cross-sectional design limits causal inference, highlighting the need for future longitudinal studies to assess prognostic value and clinical outcomes, as well as to validate these signatures in more diverse populations. Additionally, the presence or absence of nephrotic syndrome among patients with abnormal proteinuria may represent a potential confounder for the metabolomic profiles observed in this subgroup and should therefore be taken into account when interpreting these findings. Prospective studies with systematic characterization of nephrotic status will be required to clarify its specific impact on these metabolomic signatures.

Although HUVECs differ from the vascular endothelium lining arteries, microvasculature, or glomerular endothelial cells, and although rat kidney slices suffer from species differences, these are widely accepted models for exploratory studies investigating vascular inflammation and CV risk. This study identifies a robust immunometabolic stratification of SLE, linking distinct proteomic and metabolomic signatures to CV risk and LN. Integrating multiomic data, ML, and functional validation provides mechanistic insight into organ-specific damage and supports biomarker-driven patient stratification and personalized therapies.

ACKNOWLEDGMENT

We thank the patients who participated in the study. Funding for open access charge: Universidad de Córdoba / CBUA.

AUTHOR CONTRIBUTIONS

All authors contributed to at least one of the following manuscript preparation roles: conceptualization AND/OR methodology, software, investigation, formal analysis, data curation, visualization, and validation AND drafting or reviewing/editing the final draft. As corresponding authors, Drs Cerdó and Lopez-Pedrera confirm that all authors have provided the final approval of the version to be published, and take responsibility for the affirmations regarding article submission (eg, not under consideration by another journal), the integrity of the data presented, and the statements regarding compliance with institutional review board/Declaration of Helsinki requirements. All authors contributed to the investigation, formal analysis of the data, and writing, reviewing, and editing of the manuscript.

APPENDIX A: PRECISESADS CLINICAL CONSORTIUM

Members of the PRECISEADS Clinical Consortium are as follows: Lorenzo Beretta, Barbara Vigone, Jacques-Olivier Pers, Alain Saraux, Valérie Devauchelle-Pensec, Divi Cornec, Sandrine Jousse-Joulin, Bernard Lauwerys, Julie Ducreux, Anne-Lise Maudoux, Carlos Vasconcelos, Ana Tavares, Esmeralda Neves, Raquel Faria, Mariana Brandão, Ana Campar, António Marinho, Fátima Farinha, Isabel Almeida, Miguel Angel Gonzalez-Gay Mantecón, Ricardo Blanco Alonso, Alfonso Corrales Martínez, Ricard Cervera, Ignasi Rodríguez-Pintó, Gerard Espinosa, Rik Lories, Ellen De Langhe, Nicolas Hunzelmann, Doreen Belz, Torsten Witte, Niklas Baerlecken, Georg Stummvoll, Michael Zauner, Michaela Lehner, Eduardo Collantes, Ma Carmen Castro-Villegas, Norberto Ortego, María Concepción Fernández Roldán, Enrique Raya, Inmaculada Jiménez Moleón, Enrique de Ramon, Isabel Díaz Quintero, Pier Luigi Meroni, Maria Gerosa, Tommaso Schioppo, Carolina Artusi, Carlo Chizzolini, Aleksandra Zuber, Donatienne Wynar, Laszló Kovács, Attila Balog, Magdolna Deák, Márta Bocskai, Sonja Dulic, Gabriella Kádár, Falk Hiepe, Velia Gerl, Silvia Thiel,

Manuel Rodriguez Maresca, Antonio López-Berrio, Rocío Aguilar-Quesada, and Héctor Navarro-Linares.

REFERENCES

1. Aarts E, Ederveen THA, Naaijen J, et al. Gut microbiome in ADHD and its relation to neural reward anticipation. PLoS One 2017;12(9): e0183509.
2. Lopez-Pedrera C, Patiño-Trives A, Cerdó T, et al. Splicing machinery is profoundly altered in systemic lupus erythematosus and antiphospholipid syndrome and directly linked to key clinical features. J Autoimmun 2023;135:102990.
3. Patiño-Trives AM, Pérez-Sánchez C, Pérez-Sánchez L, et al. Anti-dsDNA antibodies increase the cardiovascular risk in systemic lupus erythematosus promoting a distinctive immune and vascular activation. Arterioscler Thromb Vasc Biol 2021;41(9):2417–2430.
4. Pérez-Sánchez C, Cecchi I, Barbarroja N, et al. Early restoration of immune and vascular phenotypes in systemic lupus erythematosus and rheumatoid arthritis patients after B cell depletion. J Cell Mol Med 2019;23(9):6308–6318.
5. Avasare R, Drexler Y, Caster DJ, et al. Management of lupus nephritis: new treatments and updated guidelines. Kidney360 2023;4(10): 1503–1511.
6. Aragón CC, Tafúr R-A, Suárez-Avellaneda A, et al. Urinary biomarkers in lupus nephritis. J Transl Autoimmun 2020;3:100042.
7. Mayr M, Chung Y-L, Mayr U, et al. Proteomic and metabolomic analyses of atherosclerotic vessels from apolipoprotein E-deficient mice reveal alterations in inflammation, oxidative stress, and energy metabolism. Arterioscler Thromb Vasc Biol 2005;25(10):2135–2142.
8. Aringer M, Costenbader K, Daikh D, et al. 2019 European League Against Rheumatism/American College of Rheumatology Classification Criteria for Systemic Lupus Erythematosus. Arthritis Rheumatol 2019;71(9):1400–1412.
9. Emilsson V, Jonsson BG, Austin TR, et al. Proteomic prediction of incident heart failure and its main subtypes. Eur J Heart Fail 2024; 26(1):87–102.
10. Fava A, Rao DA, Mohan C, et al. Urine proteomics and renal single-cell transcriptomics implicate interleukin-16 in lupus nephritis. Arthritis Rheumatol 2022;74(5):829–839.
11. Nossent JC, Raymond WD, Eilertsen GØ. Increased von Willebrand factor levels in patients with systemic lupus erythematosus reflect inflammation rather than increased propensity for platelet activation. Lupus Sci Med 2016;3(1):e000162.
12. Xu W-D, Huang Q, Yang C, et al. GDF-15: a potential biomarker and therapeutic target in systemic lupus erythematosus. Front Immunol 2022;13:926373.
13. Petrackova A, Smrzova A, Gajdos P, et al. Serum protein pattern associated with organ damage and lupus nephritis in systemic lupus erythematosus revealed by PEA immunoassay. Clin Proteomics 2017;14:32.
14. Ruacho G, Kvarnström M, Zickert A, et al. Sjögren syndrome in systemic lupus erythematosus: a subset characterized by a systemic inflammatory state. J Rheumatol 2020;47(6):865–875.
15. Ghafouri-Fard S, Shahir M, Taheri M, et al. A review on the role of chemokines in the pathogenesis of systemic lupus erythematosus. Cytokine 2021;146:155640.
16. Zhao Y, Liu X, Si F, et al. Citrate promotes excessive lipid biosynthesis and senescence in tumor cells for tumor therapy. Adv Sci (Weinh) 2022;9(1):e2101553.
17. Gu C, Mao X, Chen D, et al. Isoleucine plays an important role for maintaining immune function. Curr Protein Pept Sci 2019;20(7): 644–651.
18. Zabek A, Swierkot J, Malak A, et al. Application of 1H NMR-based serum metabolomic studies for monitoring female patients with rheumatoid arthritis. J Pharm Biomed Anal 2016;117:544–550.
19. Jain SK, Kannan K, Lim G. Ketosis (acetoacetate) can generate oxygen radicals and cause increased lipid peroxidation and growth inhibition in human endothelial cells. Free Radic Biol Med 1998;25(9):1083–1088.
20. Iperi C, Fernández-Ochoa Á, Pers J-O, et al. Integration of multi-omics analysis reveals metabolic alterations of B lymphocytes in systemic lupus erythematosus. Clin Immunol 2024;264:110243.
21. Kegerreis B, Catalina MD, Bachali P, et al. Machine learning approaches to predict lupus disease activity from gene expression data. Sci Rep 2019;9(1):9617.
22. Canfield C-A, Bradshaw PC. Amino acids in the regulation of aging and aging-related diseases. Transl Med Aging 2019;3:70–89.
23. Rojo-Sánchez A, Abuchaibe A, Carmona A, et al. Role of metabolomics in precision medicine in the context of systemic lupus erythematosus and lupus nephritis. In: Zhan X, ed. Personalized Medicine - New Perspectives. IntechOpen; 2024:149–158.
24. Hussain S, Keat S, Gelding SV. Ketosis-prone diabetes and SLE co-presenting in an African lady with previous gestational diabetes. Endocrinol Diabetes Metab Case Rep 2017;2017(1):17–0086.
25. Kimble LP, Khosroshahi A, Brewster GS, et al. Associations between TCA cycle plasma metabolites and fatigue in Black females with systemic lupus erythematosus: an untargeted metabolomics pilot study. Lupus 2024;33(9):948–961.
26. Sun W, Li P, Cai J, et al. Lipid metabolism: immune regulation and therapeutic prospectives in systemic lupus erythematosus. Front Immunol 2022;13:860586.
27. Shahbaz H, Rout P, Gupta M. Creatinine clearance. In: StatPearls. StatPearls Publishing; 2024.
28. Eryavuz Onmaz D, Tezcan D, Yilmaz S, et al. Altered kynurenine pathway metabolism and association with disease activity in patients with systemic lupus. Amino Acids 2023;55(12):1937–1947.
29. Yennemadi AS, Keane J, Leisching G. Mitochondrial bioenergetic changes in systemic lupus erythematosus immune cell subsets: contributions to pathogenesis and clinical applications. Lupus 2023; 32(5):603–611.
30. Cho KY, Miyoshi H, Nakamura A, et al. Lipid droplet protein PLIN1 regulates inflammatory polarity in human macrophages and is involved in atherosclerotic plaque development by promoting stable lipid storage. J Atheroscler Thromb 2023;30(2):170–181.
31. Li F, Tian F, Wang L, et al. Pleiotrophin (PTN) is expressed in vascularized human atherosclerotic plaques: IFN-γ/JAK/STAT1 signaling is critical for the expression of PTN in macrophages. FASEB J 2010; 24(3):810–822.
32. Pétremand J, Bulat N, Butty A-C, et al. Involvement of 4E-BP1 in the protection induced by HDLs on pancreatic β-cells. Mol Endocrinol 2009;23(10):1572–1586.
33. Choi J, Smitz J. Luteinizing hormone and human chorionic gonadotropin: distinguishing unique physiologic roles. Gynecol Endocrinol 2014;30(3):174–181.
34. Sreepada A, Tiwari M, Pal K. Adhesion G protein-coupled receptor gluing action guides tissue development and disease. J Mol Med (Berl) 2022;100(10):1355–1372.
35. Ruby MA, Massart J, Hunerdosse DM, et al. Human carboxylesterase 2 reverses obesity-induced diacylglycerol accumulation and glucose intolerance. Cell Rep 2017;18(3):636–646.
36. Yadav AK, Khan S, Chowdhry S, et al. State of adenosine deaminase in patients with dyslipidemia. Biotech Res Asia 2024;21(3):1137–1143.
37. Linton MF, Yancey PG, Davies SS, et al. The role of lipids and lipoproteins in atherosclerosis. In: Endotext. MDText.com; 2019.

38. Zhuang Q, Cheng K, Ming Y. CX3CL1/CX3CR1 axis, as the therapeutic potential in renal diseases: friend or foe? Curr Gene Ther 2017; 17(6):442–452.
39. Lieberman LA, Tsokos GC. The IL-2 defect in systemic lupus erythematosus disease has an expansive effect on host immunity. J Biomed Biotechnol 2010;2010(1):740619.
40. Schmitz MK, Botte DA, Sotto MN, et al. Increased corticotropin-releasing hormone (CRH) expression in cutaneous lupus lesions. Lupus 2015;24(8):854–861.
41. Kato I, Sato H, Kudo A. TRANCE together with IL-7 induces pre-B cells to proliferate. Eur J Immunol 2003;33(2):334–341.
42. Szabó MZ, Szodoray P, Kiss E. Dyslipidemia in systemic lupus erythematosus. Immunol Res 2017;65:543–550.
43. Tall AR, Yvan-Charvet L. Cholesterol, inflammation and innate immunity. Nat Rev Immunol 2015;15(2):104–116.
44. Ding J, Su S, You T, et al. Serum interleukin-6 level is correlated with the disease activity of systemic lupus erythematosus: a meta-analysis. Clinics (Sao Paulo) 2020;75:e1801.
45. Moschetti L, Piantoni S, Vizzardi E, et al. Endothelial dysfunction in systemic lupus erythematosus and systemic sclerosis: a common trigger for different microvascular diseases. Front Med (Lausanne) 2022;9:849086.
46. Kümpers P, David S, Haubitz M, et al. The Tie2 receptor antagonist angiopoietin 2 facilitates vascular inflammation in systemic lupus erythematosus. Ann Rheum Dis 2009;68(10):1638–1643.
47. Hong S, Healy H, Kassianos AJ. The emerging role of renal tubular epithelial cells in the immunological pathophysiology of lupus nephritis. Front Immunol 2020;11:578952.
48. Schrijvers BF, Flyvbjerg A, De Vriese AS. The role of vascular endothelial growth factor (VEGF) in renal pathophysiology. Kidney Int 2004; 65(6):2003–2017.
49. Jakiela B, Kosałka J, Plutecka H, et al. Facilitated expansion of Th17 cells in lupus nephritis patients. Clin Exp Immunol 2018;194(3):283–294.
50. Kim KK, Sheppard D, Chapman HA. TGF-β1 signaling and tissue fibrosis. Cold Spring Harb Perspect Biol 2018;10(4):a022293.
51. Ding Q, Lu P, Xia Y, et al. CXCL9: evidence and contradictions for its role in tumor progression. Cancer Med 2016;5(11):3246–3259.
52. Guo Q, Jin Y, Chen X, et al. NF-κB in biology and targeted therapy: new insights and translational implications. Signal Transduct Target Ther 2024;9(1):53.
53. Brennan E, Kantharidis P, Cooper ME, et al. Pro-resolving lipid mediators: regulators of inflammation, metabolism and kidney function. Nat Rev Nephrol 2021;17(11):725–739.

Check for updates

American College of Rheumatology
Empowering Rheumatology Professionals

Arthritis & Rheumatology
Vol. 78, No. 10, October 2026, pp 2138–2148
DOI 10.1002/art.70130
© 2026 American College of Rheumatology.

Subsets of Patients With Lupus Identified by Gene Expression Profiles Exhibit Differential Clinical Responsiveness to Baricitinib

Prathyusha Bachali, MS,[1,2] Amrie Grammer, PhD,[1,2] and Peter E. Lipsky, MD[1,2]

Objective. Baricitinib is a JAK1 inhibitor that showed efficacy in patients with systemic lupus erythematosus (SLE) in a phase 2 study but failed to meet the primary endpoint in phase 3 trials. To understand this discrepancy and identify patients with SLE who are responsive to baricitinib, we conducted baseline and longitudinal transcriptomic analysis in patients enrolled in the phase 2 trial.

Methods. Whole-blood samples from 272 patients with SLE were analyzed. Clinical response was assessed using SLE Responder Index-4 after 24 weeks of placebo or baricitinib (2 or 4 mg daily). Gene expression profiling was conducted using Gene Set Variation Analysis (GSVA) of 32 immune-related gene modules.

Results. Eight distinct molecular endotypes (A–H) were identified from baseline GSVA scores, with progressively increasing immune disturbances. Baseline demographics were similar across endotypes, with modest but significant differences in anti–double-stranded DNA and complement levels but no SLE Disease Activity Index differences. Significant clinical responses to baricitinib were confined to endotypes D and G ($P = 0.004$ and 0.048 vs placebo, with effect sizes of 41.54% and 31.89%, respectively). Importantly, patient clustering based on clinical features failed to identify treatment-responsive subsets. Endotype G demonstrated the most pronounced treatment-related transcriptional modulation, with dose-dependent suppression of interferon, JAK1/JAK2/TYK2 signaling, immunoproteasome, and inflammatory pathways evident as early as week 2 and sustained through week 24. Transcriptional changes in response to baricitinib were largely confined to clinical responders in endotype G. Feature importance analysis identified the interferon and Treg cell signatures as major predictors of response.

Conclusion. Transcriptomic analysis identified subsets of patients with SLE responsive to baricitinib.

INTRODUCTION

Systemic lupus erythematosus (SLE) is a complex, multisystem autoimmune disorder characterized by diverse clinical manifestations and unpredictable disease trajectories, including episodic flares and progressive organ damage.[1–3] The marked clinical and immunologic heterogeneity of SLE, together with limitations in predictive biomarkers, poses significant challenges in predicting individual patient responses to therapeutic interventions.[4–6] Previous work from our group demonstrated that patients with SLE can be stratified into molecularly distinct subsets based on their peripheral blood gene expression signatures, with each subset exhibiting a unique clinical prognosis and differential responsiveness to standard therapies.[7] These transcriptomically defined subgroups displayed characteristic molecular profiles despite having overlapping clinical phenotypes and laboratory parameters, implying the presence of underlying disease endotypes driven by distinct immunopathogenic mechanisms.

Baricitinib is an orally administered inhibitor of JAK1 and has received regulatory approval for the treatment[8–10] of rheumatoid arthritis, atopic dermatitis, alopecia areata, and COVID-19. By targeting the JAK-STAT signaling pathway, baricitinib interferes with cytokine-mediated processes implicated in SLE, including interferon (IFN) and other inflammatory cytokines.[10–13] In a phase 2 randomized trial (NCT02708095), treatment with baricitinib produced modest clinical benefits, particularly in patients with involvement of the skin and joints, with the 4-mg daily dose

Supported by the RILITE Foundation.
[1]AMPEL BioSolutions, Charlottesville, Virginia; [2]RILITE Research Institute, Charlottesville, Virginia.
Additional supplementary information cited in this article can be found online in the Supporting Information section (https://acrjournals.onlinelibrary.wiley.com/doi/10.1002/art.70130).

Author disclosures and graphical abstract are available at https://onlinelibrary.wiley.com/doi/10.1002/art.70130.
Address correspondence via email to Peter E. Lipsky, MD, at peterlipsky@comcast.net.
Submitted for publication October 7, 2025; accepted in revised form January 15, 2026.

yielding an effect size of 16.8% compared with placebo, whereas the 2-mg daily dose showed no statistically significant effect.[12] Subsequent phase 3 trials (NCT03616964 and NCT03616912) showed mixed results, with only one meeting its primary endpoint in the 4-mg group and neither achieving any secondary endpoints, underscoring the need for improved patient selection and the identification of predictive biomarkers to guide therapy.[14–16]

One possible explanation for the disparate results in the phase 2 and 3 trials could relate to the possibility that only subsets of patients are responsive to this agent and that the distribution of these subsets differed in the trials. In the present study, we therefore employed analysis of gene expression profiles of the phase 2 baricitinib trial study subjects to determine whether there were subsets of patients with SLE with particular responsiveness to baricitinib. We employed a previously validated machine-learning (ML) algorithm trained on transcriptomic data from over 3,000 patients with lupus. Our goals were to (1) determine the gene expression–based endotypes of the subjects who were responsive to baricitinib treatment, (2) analyze the impact of this JAK inhibitor on gene expression profiles over the 24 weeks of the trial, and (3) identify molecular features that predict clinical response to baricitinib therapy using feature importance analysis. This approach aims to advance precision medicine in lupus by identifying biomarkers that can guide therapeutic decisions and improve patient outcomes.[13,17]

MATERIALS AND METHODS

Study design and participants. Whole-blood samples were obtained from participants in the phase 2 clinical trial of baricitinib in patients with SLE, which was conducted at multiple sites globally (ClinicalTrials.gov NCT02708095).[11] Trial participants were adults (age ≥18 years) with a diagnosis of SLE based on the updated American College of Rheumatology SLE classification criteria[18] and with active disease as determined by an SLE Disease Activity Index 2000 (SLEDAI-2K)[19] score ≥6, with involvement of skin and joints. Patients were randomly assigned to receive placebo or one of two doses of baricitinib (2 mg or 4 mg once daily) administered for 24 weeks.

Baseline and longitudinal whole-blood samples (weeks 2, 4, 12, and 24) were profiled using Affymetrix microarrays and processed with standardized normalization and linear modeling approaches. Pathway activity was quantified using Gene Set Variation Analysis (GSVA) across validated gene modules. Classification of subsets based on transcriptomic profiles was done using a Random Forest classification framework[7] with GSVA enrichment scores as input. Clinical subsetting was performed using an unsupervised ML approach combining dimensionality reduction and clustering of standardized baseline demographic, serological, and disease activity features. Feature importance and pathway contributions to clinical response were assessed using Shapley Additive Explanations (SHAP). Detailed analytic approaches are described in the Supplementary Material. All participants provided written informed consent for the collection and use of their gene expression data.

Data availability. Data from this study is available in accordance with the data sharing policy. Requests can be made via https://www.vivil.org.

RESULTS

Molecular stratification of patients with SLE by baseline blood gene expression profile. Baseline whole-blood transcriptomic profiling identified the eight anticipated molecular subsets (endotypes), labeled A through H, based on GSVA scores across 26 immune-related gene modules. These endotypes were derived using a previously developed and validated ML algorithm trained on transcriptomic data from 3,166 patients with SLE across 17 independent datasets.[7,20]

Among the eight identified molecular endotypes, endotype A was characterized by markedly reduced enrichment (GSVA score <0) of gene modules associated with the IFN gene signature (IGS), tumor necrosis factor (TNF), interleukin-1 (IL-1), anti-inflammatory pathways, plasma cells, and Ig chains. In contrast, this endotype showed increased enrichment (GSVA score >0) in modules related to B cells, Treg cells, T cells, and T cell receptors (including α-, β-, and δ-chains), suggesting a relatively quiescent or "least abnormal" immunologic profile. At the opposite end of the spectrum, endotype H displayed the highest enrichment of proinflammatory gene modules along with decreases in lymphocyte modules indicative of lymphopenia and was defined as the "most abnormal" endotype. The intermediate endotypes (B–G) exhibited a range of immunologic activity patterns.

Figure 1B presents the same patient heatmap, annotated with enrichment scores for gene modules representing JAK signaling and glucocorticoid (GC) response signatures. The JAK modules include the target of baricitinib (JAK1), whereas the GC modules comprise a number of gene modules, all reflecting GC-induced gene signatures.[11,21,22] Expression of JAK-related modules was predominantly elevated in endotypes G, H, C, and D, aligning with higher inflammatory activity and potential sensitivity to JAK inhibition. In contrast, GC module enrichment was most pronounced in endotype H, as well as C, F, and G. The immediate targets of baricitinib, JAK1 and JAK2, did not differ in their expression across the various subsets (Supplemental Figures S1A and S1B).

Distinct disease activity and serological profiles across molecular endotypes in patients with lupus at baseline. Figure 2 displays the distribution of important serological markers across the eight molecular endotypes (A–H) identified at baseline.[7] Significant differences were observed for several markers. Anti–double-stranded DNA (dsDNA) levels (Figure 2A)

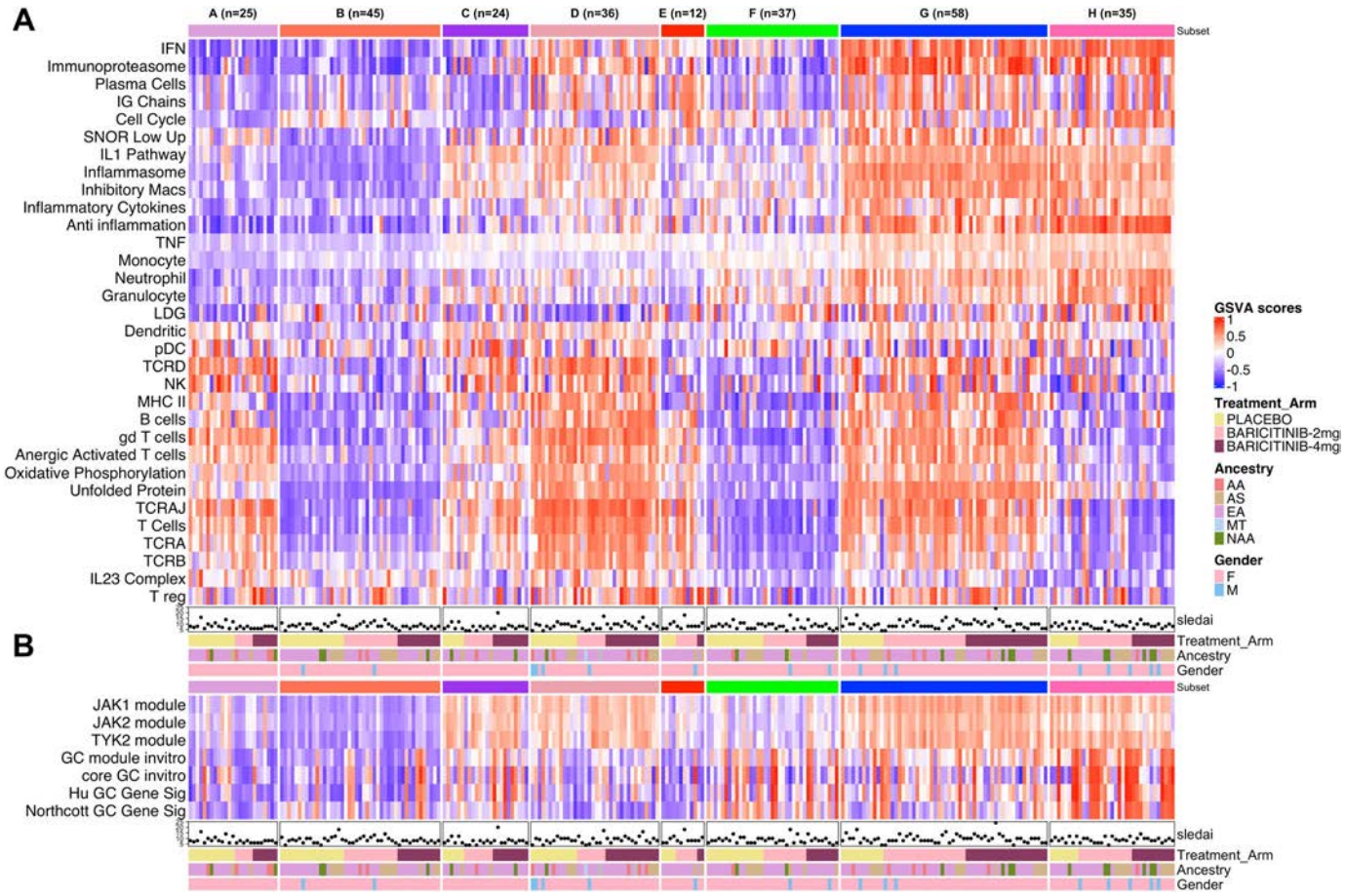


Figure 1. Random Forest classifier identified eight distinct systemic lupus erythematosus subsets from 272 baseline samples across 17 datasets. (A) Gene Set Variation Analysis (GSVA) score clustering based on 32 gene modules ordered by immunologic activity abnormality across the eight molecular endotypes: A (n = 25), B (n = 45), C (n = 24), D (n = 36), E (n = 12), F (n = 37), G (n = 58), and H (n = 35). (B) Subset visualization using JAK1/JAK2/TYK2 and glucocorticoid activity gene modules. AA, African American; AS, Asian; EA, European; F, female; GC, glucocorticoid; IFN, interferon; IL1, interleukin-1; LDG, low-density granulocyte; M, male; MHC, major histocompatibility complex; MT, multiple; NAA, Native American; NK, natural killer; pDC, plasmacytoid dendritic cell; SLEDAI, Systemic Lupus Erythematosus Disease Activity Index; TNF, tumor necrosis factor.

were significantly higher in endotypes E and H compared to C (Bonferroni-adjusted $P < 0.05$), with the lowest levels observed in endotype A and the highest in E and H. Complement C4 levels (Figure 2C) also varied significantly, with lowest values in endotypes E and H and highest in A. In contrast, SLEDAI-2K scores[19] and complement C3 levels (Figures 2B and 2D) did not differ significantly across the endotypes. However, both IgA and IgG levels (Figures 2E and 2F) showed significant variation, with the lowest levels in endotypes A and C and the highest in D, E, G, and H.

Molecular endotyping predicts therapeutic response to baricitinib. Treatment response to baricitinib was assessed using the SLE Responder Index-4 (SRI-4) at week 24, the primary endpoint of the clinical trial.[11] Stratification of patients by transcriptome-derived molecular endotypes revealed that endotypes D and G exhibited the highest frequency of clinical responses to baricitinib, particularly in the 4-mg daily dose group (Figure 3). Response frequencies for endotypes D and G were significantly greater than placebo (false discovery rate [FDR]–adjusted $P = 0.004$ for endotype D and 0.048 for endotype G, one tailed t-test), with effect sizes of 41.54% and 31.89%, respectively.

Although endotype H was defined as the most immunologically abnormal based on global transcriptomic profiles, including high enrichment of the IGS and the GC response modules, it did not exhibit a significant therapeutic response to baricitinib. Instead, the strongest clinical responses were observed in endotype G, which also displayed elevated IGS expression, increased plasma cell and Ig chain module activity, and notably high expression of immunoproteasome genes. JAK1/2/TYK2 gene signatures were also prominently enriched in endotype G, whereas the GC response modules were not elevated in this group.

In contrast, endotype D, which also showed significant response to baricitinib, was characterized by moderately increased IGS activity and strong enrichment of plasma cell and

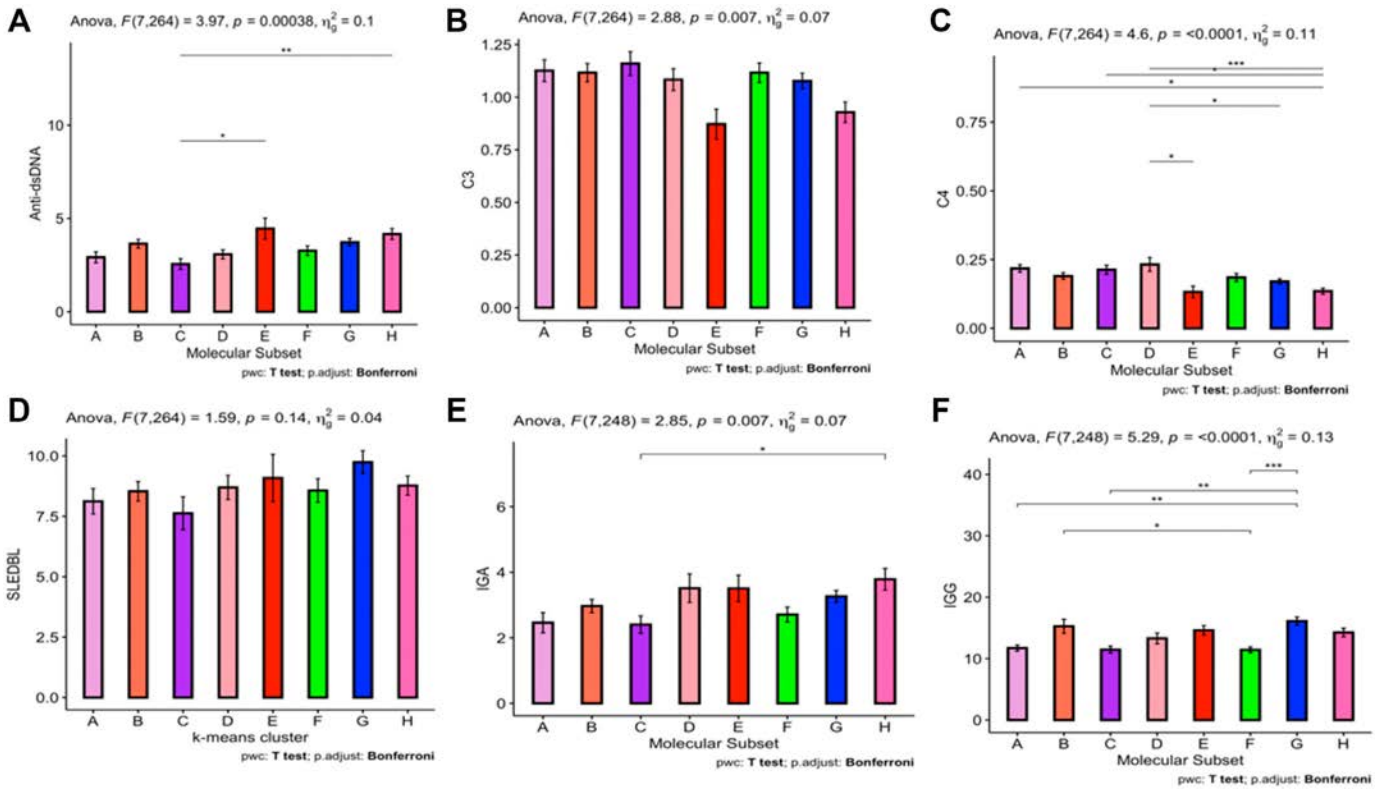


Figure 2. Baseline clinical characteristics across eight subsets. Molecular subsets arranged by immunologic abnormality order. Distributions of specific serological and clinical markers across the eight subsets (A-F) are shown: (A) anti double stranded DNA (dsDNA) antibody levels; (B) complement C3 levels; (C) complement C4 levels; (D) Systemic Lupus Erythematosus Disease Activity Index (SLEDAI); (E) immunoglobulin A (IGA) (F) immunoglobulin G (IGG) levels. Welch's analysis of varaiance (ANOVA) assessed associations between subset A ("least abnormal") and other clusters. *$P < 0.05$, **$P < 0.01$, ***$P < 0.001$, ****$P < 0.0001$.

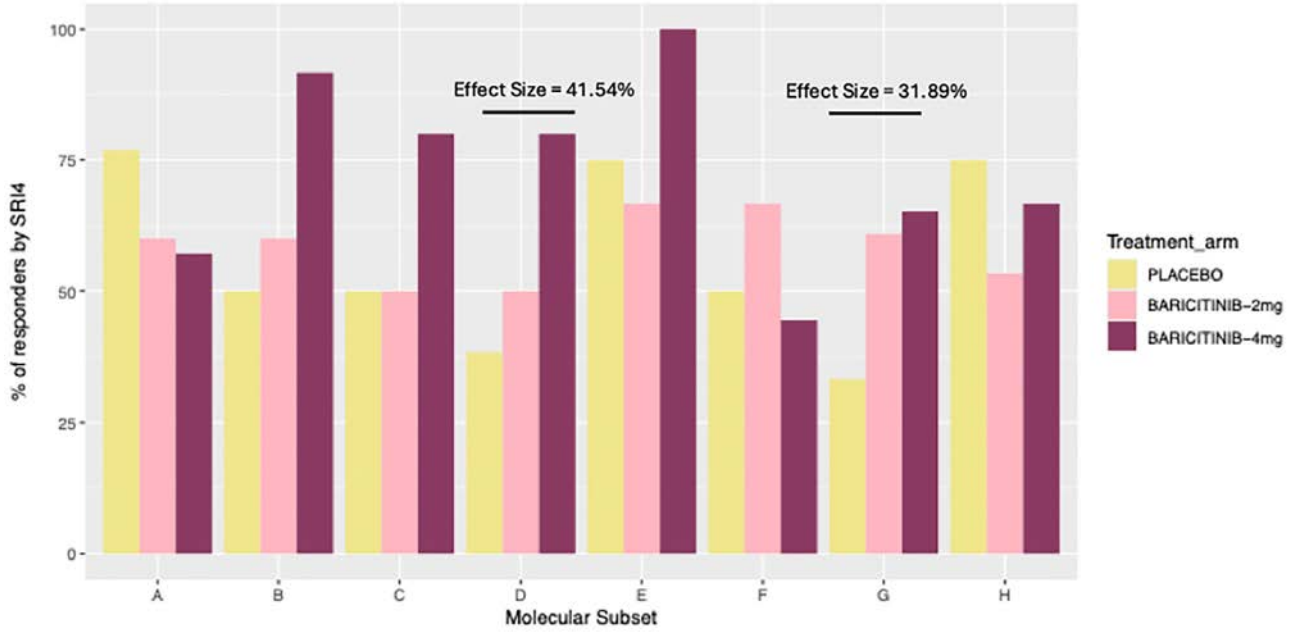


Figure 3. Clinical responses by gene expression–defined endotypes using SRI-4 at week 24. Baricitinib showed significant response improvement in endotype D (false discovery rate–adjusted $P = 0.004$, effect sizes = 41.54%) and endotype G versus placebo (false discovery rate–adjusted $P = 0.048$; effect sizes = 31.89%). SRI-4, Systemic Lupus Erythematosus Responder Index-4.

GC gene modules. Importantly, across the remaining six endotypes (A–H), higher placebo SRI-4 response rates were observed, and no statistically significant difference was seen between active treatment and placebo groups.

Because some of the subsets were relatively small, significant clinical responsiveness may have been missed. To address this, we combined subsets based upon either expression of the IGS/IFN (D, E, G, and H) or enrichment of the JAK1 pathway (C, D, G, and H) because JAK1 is the immediate target of baricitinib and is central in type 1 IFN signaling. Significant clinical responses were observed in the IGS^+/IFN^+ and JAK^+ aggregated molecular subsets treated with baricitinib 4 mg (effect sizes: $IGS^+ = 27.5\%$, $P = 0.042$; $JAK^+ = 31\%$; $P = 0.003$), whereas IGS^-/IFN^- (A, B, C, and F) and JAK^- (A, B, E, and F) subsets showed minimal or no significant clinical response (Supplemental Figure S2). Treatment with 2 mg baricitinib did not produce significant responses in any of the four molecular subsets. Notably, the effect sizes in the aggregated responsive subsets were lower than those noted in the individual responsive molecular subsets (D and G)

Longitudinal gene expression analysis of baricitinib treatment across endotypes. Longitudinal gene expression analysis was conducted to investigate the molecular effects of baricitinib across A through H endotypes (Figure 4). Endotype G demonstrated pronounced transcriptional modulation in response to both doses of baricitinib, with high-dose treatment inducing the most sustained and consistent changes. Both baricitinib 2 mg and 4 mg daily led to significant down-regulation of key immune pathways as early as week 2, with stronger and more persistent effects observed at weeks 12 and 24 in the 4-mg daily group.

Treatment with both doses of baricitinib resulted in rapid (week 2) reduction of the IGS, IL-1 signaling, inflammasome, inhibitory macrophage, unfolded protein response, and anergic activated T cells JAK2, JAK3, and TYK2 gene signatures. On the other hand, high-dose baricitinib (4 mg daily) uniquely reduced expression of natural killer (NK) cell, T cell, and γδ T cell gene signatures at weeks 12 and 24, as well as immunoproteasome-associated genes, which were unaffected in the low-dose cohort.

In contrast, placebo-treated subjects exhibited no significant changes, with only significant changes in IL-1, inflammasome, TNF, and γδ T cell pathways at week 12 or later. In contrast to endotype G, endotype D exhibited a markedly narrower transcriptional response, confined exclusively to high-dose (4 mg daily) baricitinib and only at week 4. Specifically, only a transient reduction in JAK1, JAK2, and TYK2 gene signatures, but not the IGS or immunoproteasome module, was detected.

Similarly, gene expression changes over time were also examined in the aggregated IFN^+/IFN^- and JAK^+/JAK^- subsets across all treatment arms (placebo, 2 mg, and 4 mg), including both clinical responders and nonresponders (Supplemental Figure S3). Across both the IFN^+ and JAK^+ subsets, baricitinib induced the most extensive and sustained transcriptomic suppression with clear dose dependence. Treatment with 4 mg baricitinib resulted in down-regulation of numerous inflammatory and immune pathways, as shown in Supplemental Figure S3. In contrast, the 2-mg dose produced more limited effects, characterized by minimal early gene expression changes that expanded

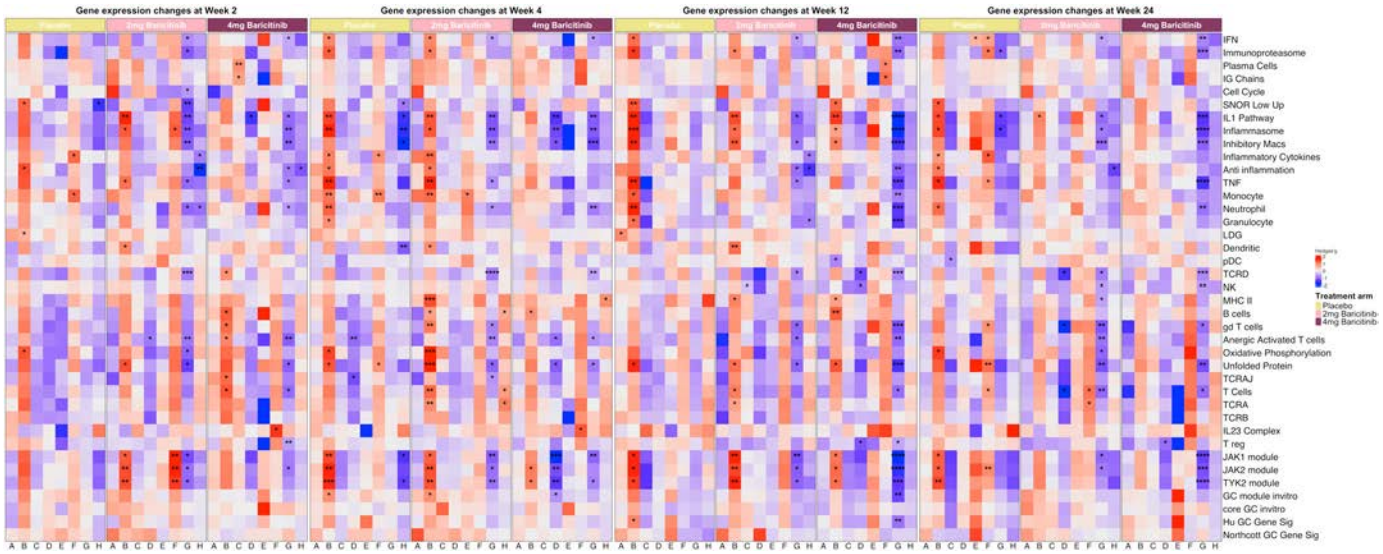


Figure 4. Longitudinal baricitinib impact on gene expression across systemic lupus erythematosus endotypes (weeks 2, 4, 12, and 24). Heatmap shows Gene Set Variation Analysis score changes for immune pathways across treatment groups, stratified by endotype. Hedges' g quantified transcriptional modulation from baseline. GC, glucocorticoid; IFN, interferon; IL1, interleukin-1; LDG, low-density granulocyte; MHC, major histocompatibility complex; NK, natural killer; pDC, plasmacytoid dendritic cell; TNF, tumor necrosis factor.

modestly between week 12 and week 24. In contrast, IFN⁻ and JAK⁻ subsets showed a reverse transcriptional trend, characterized by progressive upregulation of inflammatory and immune pathways over time, regardless of treatment assignment.

Transcriptional profiling reveals treatment-linked responses in clinically responsive subjects. To investigate the relationship between gene expression changes and clinical response in greater detail, transcriptional profiles were analyzed in clinical responders and nonresponders across different endotypes (Figures 5A and 5B). Endotypes B, D, E, and H were excluded from the primary nonresponder analysis because of insufficient sample sizes for statistical comparison.

In endotype G, pharmacodynamic effects following treatment with low-dose and high-dose baricitinib were primarily observed in clinical responders (Figure 5A). The most significant and consistent gene expression changes were evident at weeks 12 and 24, particularly with the 4-mg daily dose. Reduced expression of the IGS was consistently observed at all time points (weeks 2, 4, 12, and 24), exclusively in clinical responders treated with high-dose baricitinib. In addition to the IGS, clinical responders in endotype G also exhibited decreased expression of the JAK1, JAK2, and TYK2 gene modules at week 24. Of note, expression of JAK1 and JAK2 were comparable between responders and nonresponders at baseline and after 24 weeks of treatment (Supplemental Figure S4).

In endotype D, a transient reduction in JAK1, JAK2, TYK2, IL-1 pathway, inflammasome, and inhibitory macrophage gene signatures was observed at week 12 following treatment with 4-mg daily baricitinib. However, these changes were not accompanied by modulation of key responder-associated modules, such as the IGS or immunoproteasome. In contrast, gene expression changes were less pronounced in the 2-mg daily group (Figure 5A; Supplemental Figure S5), and no significant

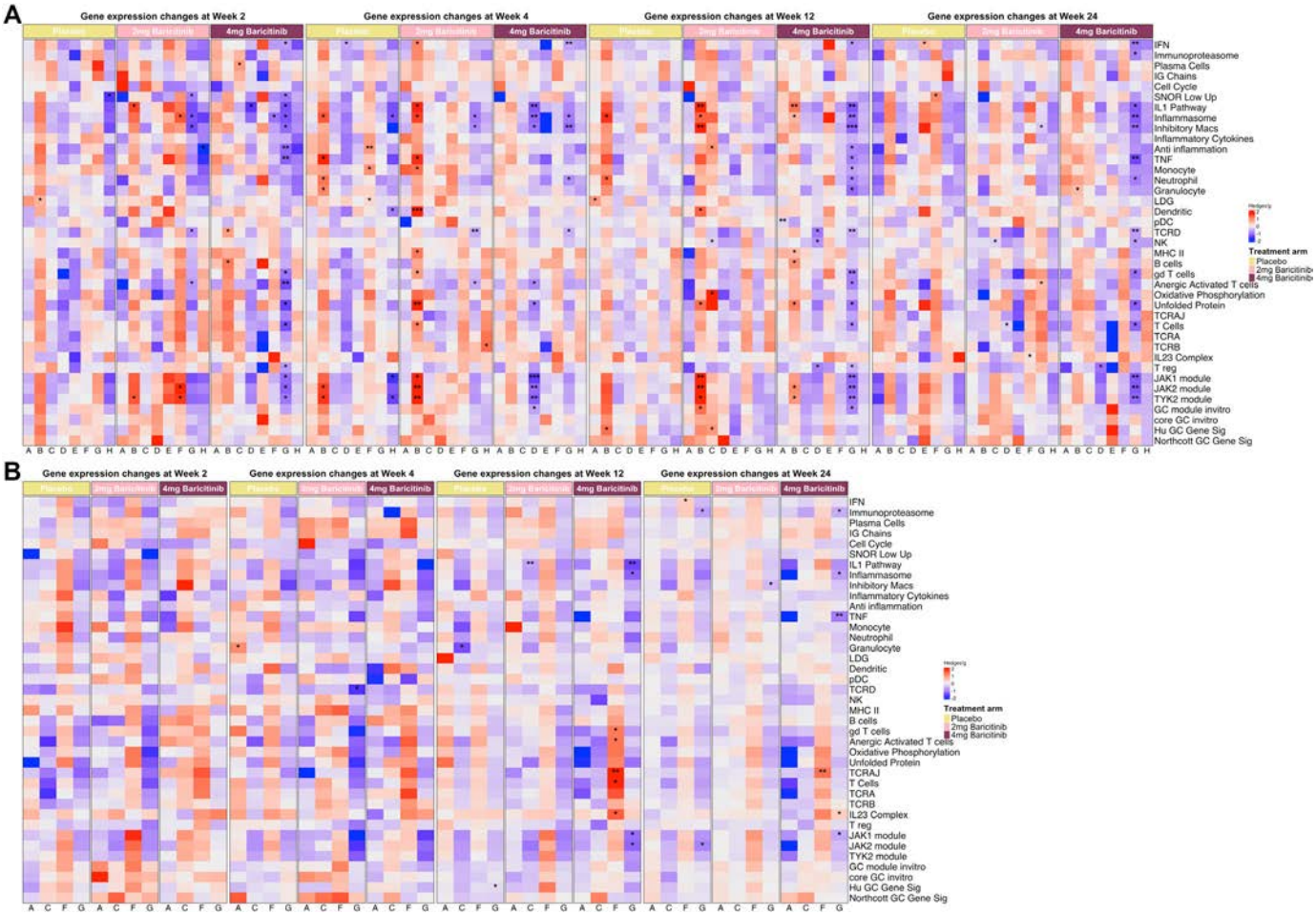


Figure 5. Treatment-linked responses in (A) clinical responders and (B) nonresponders. Heatmaps display Gene Set Variation Analysis score differences across treatments, with Hedges' g measuring transcriptional shifts reveal to baseline. Statistical significance of changes at each time point and treatment arm is indicated by asterisks, derived from paired *t*-tests and false discovery rate–adjusted *P* values. **P* < 0.05, ***P* < 0.01, ****P* < 0.001, *****P* < 0.0001. Transcriptional profiles were analyzed across molecular subsets (endotypes), with endotypes B, D, E, and H excluded from nonresponder analyses due to small sample sizes. GC, glucocorticoid; IFN, interferon; IL1, interleukin-1; LDG, low-density granulocyte; MHC, major histocompatibility complex; NK, natural killer; pDC, plasmacytoid dendritic cell; TNF, tumor necrosis factor.

transcriptional alterations were detected in responders receiving placebo.

Clinical responders in the aggregated IFN$^+$ and JAK$^+$ subsets demonstrated broad, dose-dependent suppression of immune pathways and inflammatory modules (Supplemental Figure S6A). IFN$^+$ responders treated with 4 mg baricitinib showed early and sustained down-regulation of numerous pathways, with effects peaking at week 12 and persisting through week 24. A dose of 2 mg baricitinib induced only modest early changes, with no sustained suppression of JAK-STAT pathway components and IGS expression. No meaningful gene expression changes were observed in placebo-treated responders beyond a transient effect at week 4. Conversely, aggregated IFN$^-$ and JAK$^-$ responders displayed a progressive upregulation of inflammatory modules and immune pathways. Nonresponders showed limited gene expression changes, largely confined to week 12 (Supplemental Figure S6B).

Feature importance analysis delineates dose-dependent immunologic correlates of clinical response in endotype G. To assess the gene expression features most associated with clinical response in endotype G, SHAP analysis was conducted. In patients treated with 4-mg daily baricitinib, the top features associated with response included the IGS, Treg cell, oxidative phosphorylation, low-density granulocyte (LDG), anti-inflammatory, and plasmacytoid dendritic cell (pDC) signatures (Figure 6C). Notably, both the IGS and Treg cell signature were among the strongest predictors of response in this group.

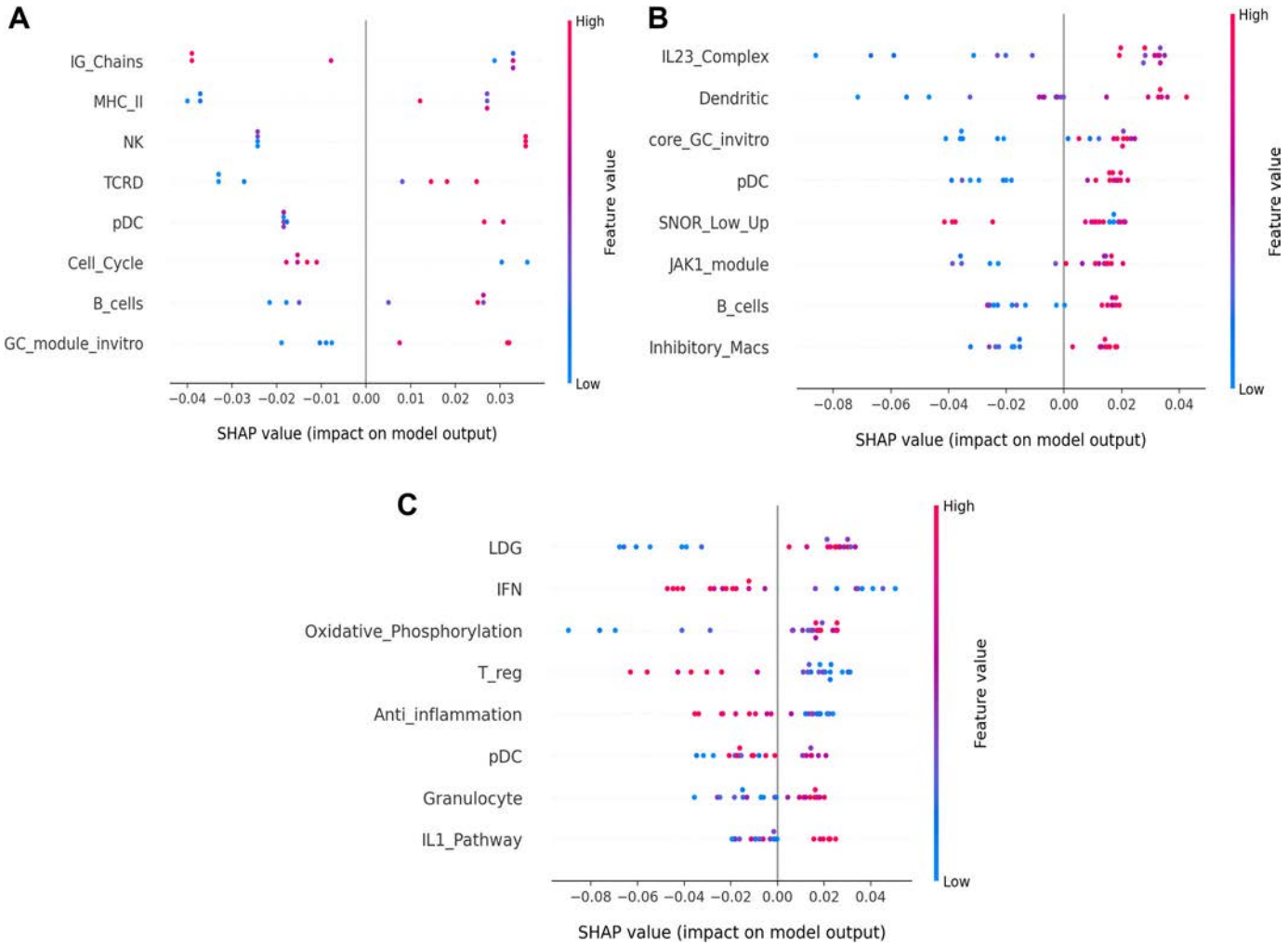


Figure 6. SHAP analysis identifies dose-dependent transcriptional predictors in endotype G. SHAP analysis comparing responders and nonresponders across (A) placebo, (B) low-dose, and (C) high-dose baricitinib identifies dose-dependent predictive features. Top predictors in 4-mg group included IFN gene signature, Treg cells, oxidative phosphorylation, LDG, and anti-inflammation signatures, whereas IFN gene signature and Treg cell pathways were not among the top features at 2-mg baricitinib. GC, glucocorticoid; IFN, interferon; IL23, interleukin-23; LDG, low-density granulocyte; MHC, major histocompatibility complex; NK, natural killer; pDC, plasmacytoid dendritic cell; SHAP, Shapley Additive Explanations.

In contrast, neither the GC nor the JAK1, JAK2, or TyK2 signatures were important predictors of clinical responses.

In contrast, in the 2-mg daily baricitinib cohort, top features include IL-23 complex, dendritic cells, in vitro GC signature, small nucleolar RNA low-upregulated transcripts, JAK1 signaling, and pDC. Although these features suggest immune down-regulation, IFN and Treg cell pathways were not among the top contributors, indicating a potentially incomplete or less effective immunoregulatory response at the lower dose. In the placebo group, top features differentiating responders from nonresponders included Ig chains, major histocompatibility complex class II, NK cells, T cell receptor-δ, and pDC, reflecting fluctuations in innate and adaptive immune variation in the absence of treatment beyond standard of care.

Unsupervised clustering of patients with lupus based on clinical features reveals diverse groups unrelated to baricitinib efficacy. To determine whether clinical characteristics could be employed to identify clinically responsive subsets, we employed baseline clinical features as input into a variational autoencoder algorithm to determine clinical groups. Three distinct clinical groups were identified from clinical and demographic data collected at baseline (Supplemental Figure S7). Group 0 (n = 84) was the most clinically and serologically active subgroup, with the highest SLEDAI (mean ∼9.6), markedly elevated dsDNA (∼186), higher Cutaneous Lupus Erythematosus Disease Area and Severity Index Activity/Cutaneous Lupus Erythematosus Disease Area and Severity Index Damage scores, lower complement levels, higher physician global assessment (physicianGA) score (∼58.6), and greater fatigue burden (Brief Fatigue Inventory [BFI] ∼6.2), reflecting active inflammation. The group was primarily composed of patients from the United States and Mexico and was predominantly of European ancestry. Group 1 (n = 144) represented an intermediate clinical phenotype, with moderate dsDNA (∼96), the lowest complement levels, intermediate SLEDAI (∼8.8), and low skin activity. Patient-reported burden was comparatively lower (BFI ∼5.7, Patient Global Assessment [PatientGA] ∼1.95, physicianGA ∼47). This group included the largest proportion of patients with Asian ancestry and substantial representation from Japan. Group 2 (n = 44) was the oldest subgroup (mean age ∼53) and exhibited the lowest serologic and clinical activity, including the lowest dsDNA (∼31) and SLEDAI (∼7.2). Despite lower objective activity, this cluster reported higher patient-perceived global impact (PGA ∼2.4, BFI ∼6.1). Members were predominantly of European ancestry.

No significant differences in the frequency of response were observed between placebo and baricitinib (2 mg or 4 mg daily) within any of the groups (Supplemental Figure S8). The placebo and treatment response frequencies were comparable across all three clinically defined groups, indicating that patient groups determined by clinical features did not capture treatment-responsive endotypes. As expected, each of the clinically defined groups contained patients from all of the molecularly defined subsets.

DISCUSSION

We classified patients with lupus from the phase 2 baricitinib trial into discrete endotypes using baseline blood samples and informative immune pathway and cellular gene modules[7,23] and monitored the treatment responses of each endotype over time. This approach identified subsets of subjects with distinct molecular profiles[24] that were preferentially responsive to baricitinib, with effect sizes in the responsive subsets (32%–42%) substantially greater than those noted in the entire population of treated patients. Longitudinal transcriptomic analysis revealed that clinical responders exhibited substantial modulation of specific gene clusters, whereas nonresponders showed minimal changes. These findings indicate that baseline gene expression profiles can help predict clinical responsiveness, whereas the pharmacodynamic impact of baricitinib varies between individuals even within responsive endotypes.

Using our previously validated ML-based approach employing transcriptomic data from over 3,000 patients with lupus,[7] we delineated the anticipated eight lupus endotypes (A–H) in the baricitinib trial cohort, each characterized by a distinct molecular profile.[7,20] The identification of representatives of each of the eight molecular endotypes among patients with SLE in the baricitinib trial confirms the substantial immunologic heterogeneity that underlies the clinical variability of lupus, even among patients meeting inclusion criteria in a clinical trial.[6] Importantly, only two endotypes (D and G) demonstrated significant clinical responses to baricitinib, representing approximately 25% to 30% of the study population.[11] This finding has important implications for understanding why JAK inhibition shows only modest overall efficacy in unselected SLE populations[11,14,16] while potentially providing substantial benefit to patients of specific molecularly defined endotypes. These results indicate that molecular endotyping not only deconvolutes the heterogeneity inherent in SLE[7,17] but also holds substantial promise for predicting therapeutic responses in subsets of patients with SLE.[7,24]

Endotype G emerged as the most baricitinib-responsive subset, characterized by elevated IGS,[13] JAK pathway activity, and immunoproteasome expression. This molecular profile suggests a lupus subset driven primarily by type I IFN signaling,[10,13] a pathway directly targeted by JAK1 inhibition.[9] Importantly, transcriptional changes in endotype G were both robust and sustained, with dose-dependent reductions in IGS, JAK1/JAK2/TYK2 signaling, immunoproteasome, and inflammatory pathways detectable as early as week 2 and persisting through week 24.[11] Using SHAP analysis, the gene modules that were the strongest contributors to clinical response to baricitinib in endotype G were pinpointed.[25] In

responders, key features included the IGS, as well as Treg cell, oxidative phosphorylation, LDGs, and anti-inflammatory signatures. These findings highlight the molecular features underlying the therapeutic efficacy and support the potential of these signatures to predict patient response.[13,17] The sustained and dose-dependent transcriptional responses observed in endotype G, including consistent down-regulation of IGS and JAK signaling pathways, provide molecular evidence for on-target drug activity and suggest that these patients have lupus pathophysiology most amenable to JAK inhibition.[11]

The JAK1, JAK2, and TYK2 gene signature modules employed in this analysis were originally derived and validated by Dörner et al.[11] Here, we validated these JAK pathway signatures within a molecular endotyping framework,[7] confirming their use for tracking on-target pharmacodynamic effects in different patient subsets. It is important to emphasize that neither enrichment of the JAK modules nor the IGS was sufficient to predict maximal responsiveness to baricitinib. Although the clinically responsive subsets had these modules enriched, other nonresponsive subsets also exhibited enrichment of these modules. Rather than expression of individual modules, the overall profile of gene expression seems to be essential to predict clinical responsiveness.

Endotype D, although also demonstrating significant clinical response to baricitinib, exhibited a more restricted transcriptional response pattern compared to endotype G. This endotype was distinguished by elevated plasma cell and Ig chain gene modules with moderate IGS activity, suggesting a lupus subset characterized by prominent B cell and antibody-mediated pathophysiology. Although endotype D showed clinical improvement with baricitinib treatment, the molecular changes were more limited and transient, primarily involving JAK pathway suppression without the broader downstream immune network modulation observed in endotype G. This suggests that although JAK inhibition provides clinical benefit in endotype D, the underlying disease mechanisms may be more complex and less dependent on sustained IFN pathway suppression.[13] Moreover, it is also possible that baricitinib suppressed JAK pathway activity in secondary lymphoid organs or affected tissues that was not detected in analysis of blood and, thereby, suppressed clinical activity.

Subset H also manifested an increased IGS and JAK1 signature, but there was no clinical response to baricitinib in the subset. The reason for this is uncertain. It is notable that the pharmacodynamic effect of baricitinib was inconsistent in this subset and that patients with subset H had an increased steroid signature at baseline with little change throughout the trial. Whether these features contribute to clinical unresponsiveness is unknown at this time.

The temporal dynamics of JAK inhibition revealed distinct patterns of transcriptional modulation. Our feature importance analysis suggests that both the IGS and JAK1 contribute to baricitinib response, highlighting the central role of IFN-JAK pathway suppression. In the 2-mg arm, incomplete suppression of the IGS likely limits overall pathway inhibition, which may explain the reduced clinical efficacy observed at this dose compared with 4 mg. The early response (week 2) in endotype G, including rapid suppression of IFN and inflammatory pathways, demonstrated that JAK inhibition can quickly impact core lupus pathophysiology[9,10] in appropriately selected patients. The sustained effects through week 24, particularly with high-dose baricitinib, suggest that continuous pathway suppression may be necessary for optimal clinical outcomes. The dose-dependent effects observed support the concept that adequate JAK pathway inhibition requires sufficient drug exposure and may inform dosing strategies in responsive molecular subsets.

To further contextualize our findings, we compared our results with prior studies that have applied transcriptome-based stratification to identify treatment-responsive molecular subsets. Notably, molecular endotyping of patients with SLE treated with iberdomide using the same ML algorithm applied here identified one endotype (H) with significant clinical response.[26] Although iberdomide acts through a different mechanism (cereblon modulation) and does not directly target the JAK pathway, it has been shown to decrease IFN secretion from pDC as well as modifying T cell and B cell function by decreasing expression of the transcription factors Ikaros and Aiolos.[26] The multiple targets of iberdomide may explain its capacity to provide clinical benefit in subset H, but the reason for the lack of responsiveness of patients in other IGS-positive patient subsets is uncertain.

The ineffectiveness of clinical features to predict baricitinib responsiveness, as demonstrated by the autoencoder analysis, underscores the limitations of traditional clinical measures for predicting treatment response in SLE[4] and their inability to capture the underlying molecular complexity of lupus.[6] Three distinct clinical groups were identified, but none showed differential treatment responses, highlighting that clinical and demographic data alone are insufficient to identify patient subsets that benefit from baricitinib. Importantly, there was minimal overlap between the groups identified by clinical features and those defined by gene expression profiles. This finding raises questions about current approaches to patient stratification in lupus clinical trials and supports the development of molecular diagnostics for treatment selection.[13,17] Although we included all the clinical features that were available in the study, it remains possible that inclusion of additional clinical features could alter the effectiveness of clinical-based patient clustering, as has been suggested.[27]

The primary limitation of this study was the relatively small sample size, which restricted our ability to perform robust statistical analyses across all molecular endotypes. Additionally, this study analyzed samples from a single phase 2 trial, and validation in independent cohorts with larger sample sizes is necessary to confirm these findings.

This comprehensive molecular analysis of baricitinib treatment in SLE demonstrates that baseline gene expression profiling can identify patient subsets with differential therapeutic

responses. The findings provide a molecular explanation for the heterogeneous responses observed in lupus clinical trials and offer a framework for implementing precision medicine approaches.[13,28] By identifying molecular endotypes that predict treatment responsiveness, this work represents an important step toward optimizing therapeutic outcomes in SLE through patient stratification and personalized treatment selection.

ACKNOWLEDGMENT

We thank Matt Linnik of Eli Lilly for making the clinical data and transcriptomics data available for this analysis.

AUTHOR CONTRIBUTIONS

All authors contributed to at least one of the following manuscript preparation roles: conceptualization AND/OR methodology, software, investigation, formal analysis, data curation, visualization, and validation AND drafting or reviewing/editing the final draft. As corresponding author, Dr Lipsky confirms that all authors have provided the final approval of the version to be published and takes responsibility for the affirmations regarding article submission (eg, not under consideration by another journal), the integrity of the data presented, and the statements regarding compliance with institutional review board/Declaration of Helsinki requirements.

ADDITIONAL DISCLOSURES

All authors are employees of AMPEL BioSolutions, LLC.

REFERENCES

1. Fanouriakis A, Tziolos N, Bertsias G, et al. Update on the diagnosis and management of systemic lupus erythematosus. Ann Rheum Dis 2021;80(1):14–25. doi:https://doi.org/10.1136/annrheumdis-2020-218272
2. Kaul A, Gordon C, Crow MK, et al. Systemic lupus erythematosus. Nat Rev Dis Primers 2016;2(1):16039. doi:https://doi.org/10.1038/nrdp.2016.39
3. Tsokos GC. Systemic lupus erythematosus. N Engl J Med 2011;365(22):2110–2121. doi:https://doi.org/10.1056/NEJMra1100359
4. Parodis I, Gomez A, Lustig Y, et al. Predicting treatment response in systemic lupus erythematosus: current challenges and future goals. Autoimmun Rev 2019;18(11):102371.
5. Durcan L, O'Dwyer T, Petri M. Management strategies and future directions for systemic lupus erythematosus in adults. Lupus 2019;28(1):6–17.
6. Catalina MD, Bachali P, Yeo AE, et al. Patient ancestry significantly contributes to molecular heterogeneity of systemic lupus erythematosus. JCI Insight 2020;5(15):e140380. doi:https://doi.org/10.1172/jci.insight.140380
7. Hubbard EL, Bachali P, Kingsmore KM, et al. Analysis of transcriptomic features reveals molecular endotypes of SLE with clinical implications. Genome Med 2023;15(1):84. doi:https://doi.org/10.1186/s13073-023-01237-9
8. O'Shea JJ, Kontzias A, Yamaoka K, et al. Janus kinase inhibitors in autoimmune diseases. Nat Rev Rheumatol 2015;11(4):234–243. doi:https://doi.org/10.1038/nrrheum.2015.8
9. Kubo S, Nakayamada S, Yoshikawa M, et al. Janus kinase inhibitors and their potential in the treatment of autoimmune diseases. J Autoimmun 2021;117:102590. doi:https://doi.org/10.1016/j.jaut.2020.102590
10. Banerjee S, Biehl A, Gadina M, et al. JAK–STAT signaling as a target for inflammatory and autoimmune diseases: current and future prospects. Drugs 2017;77(5):521–546. doi:https://doi.org/10.1007/s40265-017-0701-9
11. Dörner T, Tanaka Y, Petri MA, et al. Baricitinib-associated changes in global gene expression during a 24-week phase II clinical systemic lupus erythematosus trial implicates a mechanism of action through multiple immune-related pathways. Lupus Sci Med 2020;7(1):e000424. doi:https://doi.org/10.1136/lupus-2020-000424
12. Wallace DJ, Furie RA, Tanaka Y, et al. Baricitinib for systemic lupus erythematosus: a randomised, double-blind, placebo-controlled, phase 3 trial. Lancet 2018;392(10143):222–231. doi:https://doi.org/10.1016/S0140-6736(18)31363-1
13. Catalina MD, Bachali P, Geraci NS, et al. Gene expression analysis delineates the potential roles of multiple interferons in systemic lupus erythematosus. Commun Biol 2019;2(1):140. doi:https://doi.org/10.1038/s42003-019-0382-x
14. Morand E, Furie R, Tanaka Y, et al. Trial of anifrolumab in active systemic lupus erythematosus. Lancet 2023;401:1001–1010. doi:https://doi.org/10.1016/S0140-6736(22)02607-1
15. Petri M, Bruce IN, Dörner T, et al. Efficacy and safety of anifrolumab in systemic lupus erythematosus: a double-blind, randomized, placebo-controlled, phase 3 trial (SLE-BRAVE-II). Lancet 2023;401(10381):1011–1019. doi:https://doi.org/10.1016/S0140-6736(22)02546-6
16. Furie R, Khamashta M, Merrill JT, et al. Efficacy and safety of baricitinib in systemic lupus erythematosus: results of two phase 3 trials. Arthritis Rheumatol 2023;75(4):574–585.
17. Hubbard EL, Grammer AC, Lipsky PE. Transcriptomics data: pointing the way to subclassification and personalized medicine in systemic lupus erythematosus. Curr Opin Rheumatol 2021;33(6):579–585. doi:https://doi.org/10.1097/BOR.0000000000000833
18. Hochberg MC. Updating the American College of Rheumatology revised criteria for the classification of systemic lupus erythematosus. Arthritis Rheum 1997;40(9):1725. doi:https://doi.org/10.1002/art.1780400928
19. Gladman DD, Ibañez D, Urowitz MB. Systemic lupus erythematosus disease activity index 2000. J Rheumatol 2002;29(2):288–291.
20. Hubbard E, Bachali P, Grammer AC, et al. Validation of eight endotypes of lupus based on whole-blood RNA profiles. Lupus Sci Med 2025;12(1):e001526. doi:https://doi.org/10.1136/lupus-2025-001526
21. Northcott M, Gearing LJ, Nim HT, et al. Glucocorticoid gene signatures in systemic lupus erythematosus and the effects of type I interferon: a cross-sectional and in-vitro study. Lancet Rheumatol 2021;3(5):e357–e370. doi:https://doi.org/10.1016/S2665-9913(21)00006-0
22. Hu Y, Carman JA, Holloway D, et al. Development of a molecular signature to monitor pharmacodynamic responses mediated by in vivo administration of glucocorticoids. Arthritis Rheumatol 2018;70(8):1331–1342. doi:https://doi.org/10.1002/art.40476
23. Guthridge JM, Lu R, Tran LT, et al. Adults with systemic lupus exhibit distinct molecular phenotypes in a cross-sectional study. EClinicalMedicine 2020;20:100291. doi:https://doi.org/10.1016/j.eclinm.2020.100291
24. Garantziotis P, Nikolakis D, Doumas S, et al. Molecular taxonomy of systemic lupus erythematosus through data-driven patient stratification: molecular endotypes and cluster-tailored drugs. Front Immunol 2022;13:860726. doi:https://doi.org/10.3389/fimmu.2022.860726
25. Lundberg SM, Lee SI. A unified approach to interpreting model predictions. Proceedings of the 31st International Conference on Neural Information Processing Systems (NIPS '17); Red Hook, NY. 4768–4777. https://dl.acm.org/doi/10.5555/3295222.3295230

26. Bachali P, Daamen A, Korish S, et al. Responsiveness of systemic lupus erythematosus subjects to iberdomide based on molecular endotypes. Ann Rheum Dis 2025;84(6):1001–1010. 2025 doi: 10.1016/j.ard.2025.01.044

27. Parodis I, Lindblom J, Tsoi A, et al. Trajectories of disease evolution upon treatment initiation in systemic lupus erythematosus: results from four clinical trials of belimumab. Rheumatology (Oxford) 2025;64(5):2697–2705. doi:https://doi.org/10.1093/rheumatology/keae575

28. Toro-Domínguez D, Martorell-Marugán J, Goldman D, et al. Stratification of systemic lupus erythematosus patients into three groups of disease activity progression according to longitudinal gene expression. Arthritis Rheumatol 2018;70(12):2025–2035. doi:https://doi.org/10.1002/art.40653

Check for updates

Arthritis & Rheumatology
Vol. 78, No. 10, October 2026, pp 2149–2159
DOI 10.1002/art.70146
© 2026 The Author(s). *Arthritis & Rheumatology* published by Wiley Periodicals LLC on behalf of American College of Rheumatology.
This is an open access article under the terms of the Creative Commons Attribution-NonCommercial-NoDerivs License, which permits use and distribution in any medium, provided the original work is properly cited, the use is non-commercial and no modifications or adaptations are made.

American College of Rheumatology
Empowering Rheumatology Professionals

A Rare *RIPK3* Variant Enhances Necroptosis and Promotes Inflammation in a Still Disease–Like Autoinflammatory Syndrome

Longfang Chen, MD,[1] Qihua Dai, MD,[1] Yu Xiao, MD,[1] Jialin Dai, MD,[2,3] Mengyan Wang, MD,[1] Yuning Ma, MD,[1] Yujie Shen, MD,[1] Zhimo Xu, MD,[1] Jianfen Meng, MD,[1] Xia Chen, MD,[1] Da Yi, MD,[1] Yue Sun, PhD,[1] Hui Shi, MD,[1] Honglei Liu, MD,[1] Xiaobing Cheng, MD,[1] Yutong Su, MD,[1] Junna Ye, MD,[1] Huihui Chi, MD,[1] Zhuochao Zhou, MD,[1] Tingting Liu, MD,[1] Jialin Teng, MD,[1] Chengde Yang, MD,[1] Jinchao Jia, MD,[1] and Qiongyi Hu, MD[1]

Objective. Still disease represents a prototypical polygenic systemic autoinflammatory disease, characterized by recurrent systemic inflammation and dysregulation of innate immunity. Despite extensive clinical characterization, familial clustering Still disease remains unreported. This study investigates a novel variant underlying a distinct Still disease–like autoinflammatory syndrome.

Methods. Whole-exome sequencing was performed in a three-generation family with three affected individuals. Functional analyses were conducted to assess the impact of the receptor-interacting protein kinase 3 (*RIPK3*) p.Q134K variant on kinase activity, necroptosis, and inflammatory signaling. Transcriptomic profiling of peripheral blood mononuclear cells (PBMCs) and in vitro cytokine assays were used to characterize inflammatory responses.

Results. A heterozygous *RIPK3* p.Q134K variant was identified in all affected individuals. Functional analyses demonstrated that this variant exhibits gain-of-function activity, characterized by enhanced RIPK3 kinase activity and increased RIPK3 self-association, which in turn promote mixed-lineage kinase domain-like protein phosphorylation and necroptosis. RNA sequencing of PBMCs from one patient revealed marked up-regulation of NF-κB and MAPK signaling pathways and elevated expression of interleukin-6, and tumor necrosis factor-α, which was effectively suppressed by pharmacologic inhibition of RIPK3.

Conclusion. This study describes a familial Still disease–like autoinflammatory syndrome caused by a gain-of-function *RIPK3* variant. Our findings establish aberrant RIPK3 activation as a driver of autoinflammation and expand the spectrum of human RIPK3-associated diseases.

INTRODUCTION

Systemic autoinflammatory diseases (SAIDs) comprise a group of complex disorders characterized by recurrent systemic inflammation arising from dysregulation of the innate immune system. Still disease represents a prototypical polygenic SAID characterized by spiking fever, evanescent salmon-colored rash, arthritis, and markedly elevated inflammatory cytokines. Unlike autoimmune diseases, which are mediated by adaptive immune responses and autoantibodies, SAIDs are primarily driven by genetic mutations that alter the encoded protein and disrupt innate immune regulation, leading to uncontrolled inflammatory responses.[1,2] These pathogenic gene mutations often affect key signaling pathways, including interleukin-1β (IL-1β), IL-18, NF-κB, and type I interferon (IFN) pathways, which in turn results in diverse clinical manifestations such as recurrent fever, rash, and

Supported by the National Natural Science Foundation of China (82471816, 82201969, and 82402090), Chinese National Key Technology R&D Program, Ministry of Science and Technology (2024YFC2510300), Shanghai Sailing Program (22YF1425600 and 23YF1424600), Postdoctoral Research Foundation of China (2023M732305), and Shanghai Jiao Tong University School of Medicine PhD Cultivation Fund for Science and Innovation (24KCPYYB006).

[1]Department of Rheumatology and Immunology, Ruijin Hospital, Shanghai Jiao Tong University School of Medicine, Shanghai, China; [2]Department of Rheumatology, Sir Run Run Shaw Hospital, Zhejiang University School of Medicine, Hangzhou, China; [3]Liangzhu Laboratory of Zhejiang University, Hangzhou, China.

Drs L. Chen, Q. Dai, and Y. Xiao contributed equally to this work.

Additional supplementary information cited in this article can be found online in the Supporting Information section (https://acrjournals.onlinelibrary.wiley.com/doi/10.1002/art.70146).

Author disclosures are available at https://onlinelibrary.wiley.com/doi/10.1002/art.70146.

Address correspondence via email to Chengde Yang, MD, at yangchengde@sina.com; Jinchao Jia, MD, at jiajinchao15@163.com; or to Qiongyi Hu, MD, at huqiongyi131@163.com.

Submitted for publication October 12, 2025; accepted in revised form February 24, 2026.

organ damage.[3–5] Despite these advances, familial clustering Still disease has not been previously reported. Within the expanding spectrum of SAIDs, we identified a family with three affected members presenting a classic Still disease–like phenotype that did not meet the full classification criteria. This distinct presentation defines a novel autoinflammatory syndrome.[6]

Building on these insights, >50 genes have now been identified as causative for SAIDs, many of which regulate inflammatory responses triggered by cell death pathways.[7] Among these, receptor-interacting protein kinase 3 (*RIPK3*), a member of the RIPK family characterized by serine/threonine kinase activity, is best known for its essential role in mediating necroptosis, a regulated form of necrotic cell death.[8,9] In response to necroptotic stimuli, activated RIPK3 phosphorylates and facilitates the recruitment of mixed-lineage kinase domain-like protein (MLKL), leading to membrane rupture and the release of damage-associated molecular patterns, thereby amplifying inflammation.[9] Dysregulated RIPK3 signaling has been implicated in the pathogenesis of multiple inflammatory diseases, including ischemic injury, tumor necrosis factor-α (TNF-α)–induced systemic inflammatory response syndrome, and organ-specific inflammatory diseases affecting the liver, lungs, kidneys, and intestines.[10–15] Furthermore, pharmacologic inhibition of RIPK3 has been shown to attenuate excessive inflammation and mitigate lung damage in severe influenza infections, highlighting its potential as a therapeutic target in inflammatory disorders.[16]

Despite increasing evidence demonstrating the critical role of cell death–related gene mutations in autoinflammation, including variations or deficiencies in *RIPK1*, disease-associated *RIPK3* variants remain undocumented in familial Still disease–like syndromes. Recent studies, including our work on the JAK-STAT pathway in patients with refractory macrophage activation syndrome, have highlighted the importance of genetic variants in autoinflammatory phenotypes.[17] These observations raise the possibility that rare, functionally relevant variants in other key immune regulators, such as *RIPK3*, may underlie certain undiagnosed SAIDs.

PATIENTS AND METHODS

Study design. Whole-exome sequencing (WES) was first performed on three patients with systemic inflammatory symptoms to identify potential pathogenic genes. Subsequently, we validated the function of the mutant by examining the expression and function of wild-type (WT) or mutant *RIPK3* proteins through transient transfection into HeLa cells as well as the expression and function of *RIPK3* in primary peripheral blood mononuclear cells (PBMCs) from the patients. Finally, to investigate the specific pathogenic mechanisms of *RIPK3* mutations, we examined the expression of known MAPK and NF-κB pathways in HeLa cells transfected with the mutant and further evaluated the therapeutic potential of inhibitors of these pathways in the disease.

Patients. This study was conducted following the Declaration of Helsinki and Good Clinical Practice guidelines. Ethical approval was granted by the Institutional Research Ethics Committee of Ruijin Hospital in Shanghai, China (approval ID: 2023-273), and the patient assessments were conducted in accordance with the approved protocol. All participants provided written informed consent before participating in the study.

WES. Genomic DNA was isolated from peripheral blood samples and evaluated for quality using agarose gel electrophoresis and quantified using a Qubit fluorometer. WES was conducted on affected individuals to identify potential pathogenic variants. Libraries were prepared through enzymatic or ultrasonic DNA fragmentation into 150- to 250-bp fragments followed by end repair, adapter ligation, and polymerase chain reaction (PCR) amplification. Target regions were enriched using a liquid-phase hybridization capture method with biotin-labeled RNA probes specific to exonic regions. Enriched libraries were quantified and assessed for quality before high-throughput sequencing on a NovaSeq 6000 platform (Illumina). Data analysis included quality filtering of raw reads, alignment to the reference genome (GRCh38), and annotation of variants.

Sanger sequencing. Candidate variants detected by WES were confirmed through Sanger sequencing. Corresponding primers were employed to amplify the genomic regions flanking the variants via PCR. The PCR products were then purified and subjected to bidirectional sequencing on an ABI 3730 DNA Analyzer. Phred/Phrap software was used to analyze the sequence data, confirming the presence of the variants and their segregation within the family.

RNA sequencing. PBMCs were isolated using Polymorphprep (1895, Serumwerk Bernburg AG) for RNA extraction. Messenger RNA was enriched using oligo(dT) magnetic beads, fragmented, and complementary DNA synthesis with random hexamer primers. Libraries were constructed, circularized, amplified into DNA nanoballs, and sequenced on the BGISEQ G400 platform (BGI-Shenzhen). Differentially expressed genes were identified using DESeq2 ($|\log2 \text{ fold change}| > 1$, $P < 0.05$). Pathway enrichment was performed using KEGG, and gene set enrichment analysis (GSEA) was conducted. Data visualization was generated using ggplot2.

Cell culture and stimulation. Hela cells were obtained from the ATCC. The total white blood cells (WBCs) were acquired by processing peripheral blood with a red blood cell lysis buffer (G2015, Servicebio) following the manufacturer's protocol. HeLa cells were maintained in Dulbecco Modified Eagle Medium (Servicebio) supplemented with 10% fetal bovine serum (FBS; S711, Lonsera) and penicillin-streptomycin (G4003, Servicebio). PBMCs and WBCs were cultured in RPMI 1640 medium

containing 10% FBS and the same concentration of penicillin-streptomycin. For stimulation, cells were treated with TNF-α (30001A, PeproTech), SM164 (S7089, Selleck), Z-VAD-FMK (S7023, Selleck), and GSK872 (S8465, Selleck) under appropriate conditions as specified for each experimental setup.

Plasmid construction and transfection. Human WT *RIPK3* and the K50A, Q134K, Q134H, and Q134R mutants were cloned into the cytomegalovirus promoter–based vector. Site-directed mutagenesis was then used to generate the mutant plasmids. After plasmids were confirmed by Sanger sequencing, transfection was conducted using Lipofectamine 3000 (L3000, Thermo Fisher Scientific) as per the manufacturer's protocol.

Western blotting. Hela cells and PBMCs were stimulated as described above and then lysed with radioimmunoprecipitation assay lysis buffer (P0013, Beyotime) containing phosphatase inhibitor cocktails (4906845001, Roche) and protease inhibitor cocktails (4693116001, Roche). The separation of nuclear and cytoplasmic proteins was performed using the Nuclear and Cytoplasmic Protein Extraction Kit (KGB5302, Keygen Biotech) following the manufacturer's protocol. Protein concentration was measured using a BCA protein assay kit (ZJ101, Epizyme). Immunoblotting was performed using primary antibodies diluted at 1:1,000, unless otherwise indicated, following previously described methods.[18] Antibodies against GAPDH (GB11002) and Flag (AB3058) were purchased from Servicebio and Beyotime, respectively. Other antibodies listed below were obtained from Cell Signaling Technology: MLKL (14993), phospho-MLKL (91689), RIPK3 (13526), phospho-RIPK3 (93654), phospho-p38 (4511), p38 (8690), phospho-ERK (4370), ERK (4695), phospho-JNK (4668), JNK (9258), NFκB p65 (8242), phospho-NFκB p65 (3033), and RIPK1 (14993).

Lactate dehydrogenase release assay. The lactate dehydrogenase (LDH) release assay was conducted using the LDH Cytotoxicity Assay Kit (C0016, Beyotime). Cells were treated as indicated, and 10% LDH release reagent was added to control wells 1 hour before measurement. Plates were centrifuged at 400*g* for 5 minutes, and 120 μL of the supernatants was transferred to a new 96-well plate. After addition of 60 μL of LDH detection solution, samples were incubated at room temperature in the dark for 30 minutes, and absorbance was measured at 490 nm.

Cell death assay. An Annexin V-FITC/PI Apoptosis Detection Kit (KGA1102, Keygen Biotech) was used to evaluate cell death. After the aforementioned treatments, cells were resuspended in 500 μL of binding buffer, then incubated with 5 μL of FITC-conjugated Annexin V and 5 μL of PI for 10 minutes at room temperature in the dark. Apoptotic and necrotic cells were subsequently analyzed using a FACS Calibur flow cytometer (BD Biosciences).

Cytokine detection. Plasma levels of IFN-α, IFN-γ, IL-1β, IL-2, IL-4, IL-5, IL-6, IL-8, IL-10, IL-12p70, IL-17, IL-18, and TNF-α were determined using a cytometric bead array (BD Biosciences) following the manufacturers' instructions. Additionally, the concentrations of TNF-α, IL-1β, and IL-6 in the cell supernatants were quantified by enzyme-linked immunosorbent assay (DY210, DY201, and DY206, R&D systems), according to the respective manufacturer's guidelines.

ADP-Glo kinase assay. The kinase activity of WT and Q134K mutant RIPK3 was assessed using the ADP-Glo Kinase Assay (Promega, V6930) according to the manufacturer's instructions. Recombinant human WT RIPK3 (MCE, HY-P71855), Q134K RIPK3 (custom synthesized, MCE, HYP7S2531), and MLKL protein (MCE, HY-P702574) were reconstituted in kinase reaction buffer (40 mM Tris-HCl, pH 7.5; 20 mM $MgCl_2$; 0.1 mg/mL BSA) with ATP (20 μM) at room temperature for 1 hour. The reaction was terminated with ADP-Glo Reagent, followed by Kinase Detection Reagent, and luminescence was measured using a microplate luminometer.

Blue native Western blotting. To assess whether the *RIPK3* Q134K mutation affects RIPK3 self-dimerization, HeLa cells were stimulated as described above and lysed on ice for 15 minutes in a native lysis buffer containing 5% Digitonin (BN20061, Invitrogen). Lysates were clarified by centrifugation at 20,000*g* for 30 minutes at 4°C. Equal amounts of protein were then mixed with nondenaturing loading buffer (BN20041, Invitrogen) and subjected to blue native PAGE using precast gels (P0546S, Beyotime). Proteins were subsequently transferred to PVDF membranes and analyzed by immunoblotting using standard procedures.

Co-immunoprecipitation. To examine the interaction between RIPK1 and RIPK3 in WT and Q134K mutant, clarified cell lysates were incubated with anti-Flag magnetic beads (90 μL, resuspended in 1 × Tris-buffered saline [TBS]; Beyotime) overnight at 4°C on a rotator. Beads were captured using a magnetic rack and washed four times with 1 × TBS. Bound proteins were eluted in 1× SDS-PAGE sample buffer by heating at 95°C for 5 minutes and subsequently analyzed by Western blotting.

Dual-luciferase reporter assay. NF-κB– and AP-1–dependent transcriptional activity was assessed using dual-luciferase reporter assays. HeLa cells were cotransfected with pNFκB-TA-luc (D2207, Beyotime), pAP1-TA-luc (D2109, Beyotime), and pRL-TK (D2760, Beyotime) in 96-well plates and treated as indicated. Following stimulation, cells were lysed with Dual-Lumi Firefly Luciferase Reporter Cell Lysis Buffer (RG126S,

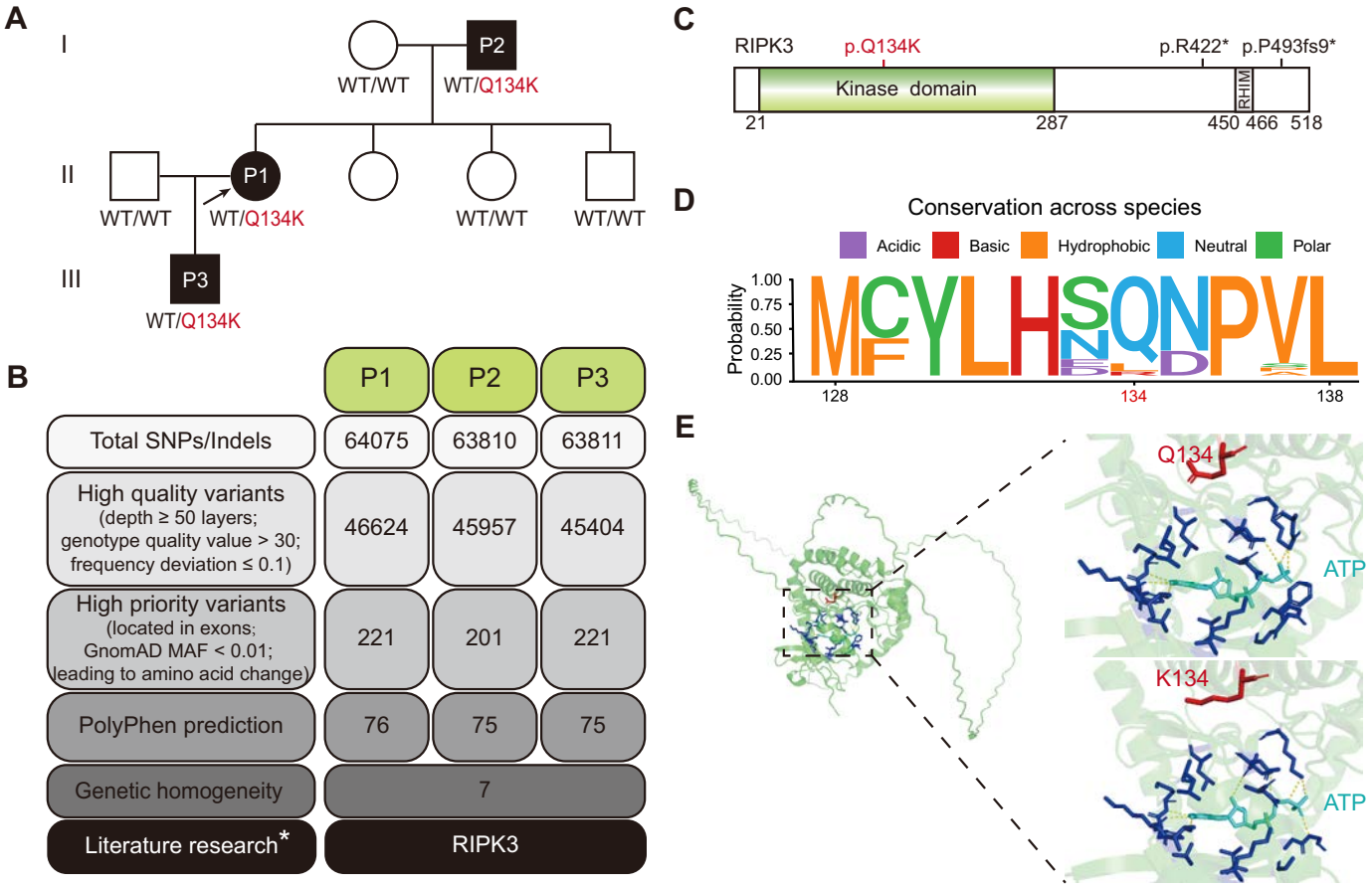


Figure 1. A rare heterozygous variant of *RIPK3* identified in a family with Still disease–like autoinflammatory syndrome. (A) Pedigrees of the family with variants in RIPK3. Black solid symbols represent individuals affected with a hemizygous RIPK3 variant. Genotypes are indicated below the symbols. Squares indicate male family members and circles female members. Roman numerals indicate generations. (B) Whole-exome sequencing data-filtering approach under the assumption of genetic homogeneity. (C) Schematic showing the protein domain of RIPK3 with the position of Q134K marked. Pathogenic variants associated with viral encephalitis (shown in black font) are included for comparison. (D) Conservation analysis of the RIPK3 p.Gln134 residue across species. Amino acids are colored according to physicochemical properties. (E) The structure of ATP interacting with RIPK3 and expanded view of the effects of WT and Q134K mutation on ATP and RIPK3 interactions. Protein and small-molecule interaction structure predictions were performed using AlphaFold3, and structural analysis was executed with PyMOL. Light blue represents ATP, dark blue represents amino acids in RIPK3 protein interacting with ATP, yellow represents hydrogen bonds, and red represents amino acid position 134 in RIPK3 protein. *Genes associated with autoimmunity and autoinflammation. MAF, minor allele frequency; P, patient; RHIM: RIP homotypic interaction motif; RIPK3, receptor-interacting protein kinase 3; SNP, single-nucleotide polymorphism; WT, wild-type.

Beyotime), and luciferase activity was measured using the Dual-Lumi Luciferase Reporter Assay Kit (RG088S, Beyotime) according to the manufacturer's instructions. Firefly luciferase activity was normalized to Renilla luciferase activity and expressed as relative luciferase units.

Statistical analysis. Statistical analysis was performed using R v4.3 or GraphPad Prism v9.0. Quantitative data are presented as the mean ± SD. For data with a Gaussian distribution, an unpaired two-sided *t*-test or one-way analysis of variance was used, and nonparametric data were analyzed with the Mann-Whitney *U* test. A *P* value <0.05 was considered statistically significant. All experiments were performed with at least three independent biologic replicates. Each experiment included three technical replicates. The data that support the findings of this study are available from the corresponding author upon reasonable request.

RESULTS

Case presentations and identification of the *RIPK3* variant. All three patients (Figure 1A; Table 1) exhibited a spectrum of Still disease–like symptoms. The proband (P1), a 34-year-old female, presented with recurrent fever, rash, arthritis, and diarrhea. Laboratory tests revealed elevated C-reactive protein (117 mg/L, normal range <10 mg/L) and a raised erythrocyte sedimentation rate (75 mm/h, normal range <20 mm/h). Autoimmune-related antibody test results, including antinuclear

Table 1. Baseline characteristics of the three patients affected by a Still disease–like syndrome*

Characteristic	P1	P2	P3
Sex	Female	Male	Male
Age at onset, y	34	50	8
Fever >39°C	Y	Y	Y
Rash	Y	Y	N
Sore throat	Y	Y	N
Arthralgia	Y	Y	N
Pleuritis	N	N	N
Pneumonia	N	N	N
Pericarditis	N	N	N
Hepatomegaly	N	N	N
Splenomegaly	N	N	N
Lymphadenopathy	Y	Y	N
Myalgia	N	Y	N
Diarrhea	Y	Y	N
ANA	Neg	1:320	–
RF	Neg	Neg	–
ACPA	Neg	Neg	–
ALT, U/L	20	130	–
AST, U/L	22	103	–
ESR, mm/h	75	28	–
CRP, mg/L	117	17	–
Ferritin, ng/mL	>1,500	391.4	–

* ACPA, anticitrullinated protein antibody; ALT, alanine aminotransferase; ANA, antinuclear antibody; AST, aspartate aminotransferase; CRP, C-reactive protein; ESR, erythrocyte sedimentation rate; N, no; Neg, negative; P, patient; RF, rheumatoid factor; Y, yes.

antibody (ANA), extractable nuclear antigen (ENA), antineutrophil cytoplasmic antibody, rheumatoid factor (RF), and cyclic citrullinated peptide antibody, were all negative. Comprehensive imaging studies and bone marrow evaluation excluded infection, malignancy, and hematologic disorders. P2, a 57-year-old male and the father of P1, experienced similar symptoms of recurrent fever, rash, arthritis, diarrhea, and myalgia at the age of 50 years. Laboratory findings included an increased erythrocyte sedimentation rate and an ANA titer of 1:320, whereas ENA and RF results were negative. Imaging examinations revealed diffuse lymphadenopathy. Both P1 and P2 received methylprednisolone treatment, resulting in marked alleviation of symptoms. P3, a 9-year-old male and the son of P1, developed a fever of unknown origin refractory to antimicrobial therapy but responsive to glucocorticoids at the age of 7 years.

We performed WES on the three patients and their family members. By filtering for mutation quality and priority under the assumption of genetic homogeneity, we identified a heterozygous mutation in *RIPK3* (c.400C>A, p.Gln134Lys) in all three patients (Figure 1A and B; Supplementary Table S1). The variant was extremely rare in population databases (gnomAD v4.1.0 minor allele frequency = 6.2×10^{-7}) and absent in the East Asian subpopulation. In silico analyses predicted a deleterious effect (Combined Annotation Dependent Depletion 12.2; PolyPhen "probably damaging"; Functional Analysis through Hidden Markov Models "deleterious"; missense tolerance ratio = 0.93), supporting functional constraint (Table 2). Segregation was confirmed by Sanger sequencing, which detected the variant exclusively in affected family members (Supplementary Figure S1A).

The p.Q134K variant localizes to the kinase domain of RIPK3 (Figure 1C). Evolutionary conservation analysis revealed that residue Q134 is relatively conserved across species but not across the RIPK family, suggesting a RIPK3-specific regulatory role (Figure 1D; Supplementary Figure S1B). AlphaFold3 modeling predicted that the Q134K mutation alters the local ATP-binding environment and hydrogen-bonding network, indicating a potential effect on ATP-dependent kinase activity (Figure 1E).

The *RIPK3* Q134K mutation enhances RIPK3 kinase activity and sensitizes HeLa cells to TSZ-mediated necroptosis. To investigate the functional impact of the *RIPK3* Q134K mutation, we transfected HeLa cells—which lack endogenous *RIPK3* expression—with plasmids encoding WT, kinase-dead mutant K50A, or Q134K *RIPK3*. Considering the critical role of the RIPK3 kinase domain in necroptosis, we induced necroptosis in HeLa cells by cotreatment with TNF-α, second mitochondrial-derived activator of caspases mimetic SM-164, and the pancaspase inhibitor Z-VAD-FMK (TSZ). Notably, compared with the WT, the Q134K mutant exhibited significantly elevated phosphorylated RIPK3 (p-RIPK3) and phosphorylated MLKL (p-MLKL, a biomarker for necroptosis) levels in HeLa cells (Figure 2A and B). Furthermore, these elevated phosphorylation levels were effectively suppressed by the low concentrations of RIPK3 inhibitor GSK872 (Figure 2C and D), confirming RIPK3 dependency. Importantly, ADP-Glo assay demonstrated that Q134K RIPK3 exhibited higher kinase activity in the presence of the MLKL substrate compared with WT RIPK3 (Figure 2E), indicating a gain-of-function effect at the kinase level.

Missense variants at residue 134 (Q134H and Q134R) are present in population databases without reported disease associations. To assess the functional sensitivity of this site, we generated Q134H and Q134R mutants. Upon TSZ stimulation, both mutants induced p-RIPK3 and p-MLKL more strongly than WT but less than Q134K, indicating an intermediate activation phenotype (Supplementary Figure S2A). These differences likely reflect distinct physicochemical properties of the substituted residues that differentially modulate local kinase activation.

To further investigate the mechanism of the *RIPK3* Q134K variant, we examined RIPK3 dimerization. Blue native PAGE revealed enhanced RIPK3 homodimerization in Q134K-expressing cells compared with WT, particularly upon TSZ stimulation (Figure 2F). In contrast, co-immunoprecipitation showed comparable RIPK3–RIPK1 interactions between WT and Q134K (Figure 2G). Consistently, inhibition of RIPK1 with necrostatin-1s only modestly reduced the levels of p-RIPK3 and p-MLKL in Q134K-expressing cells (Supplementary Figure S2B). Together, these data indicate that the Q134K mutation preferentially

enhances RIPK3 self-association, thereby promoting RIPK3 activation independently of RIPK1.

Subsequently, Annexin V/PI staining was performed to examine cell death. Following TSZ treatment, the Q134K mutant group exhibited a significant increase in Annexin/PI double-positive late apoptotic/necrotic cells compared with WT, which was markedly reduced by GSK872 (Figure 2H). In contrast, the Annexin V^+PI^- (early apoptotic) population showed variable changes across conditions (Supplementary Figure S2D). This variability may reflect the transient nature of early apoptosis under strong necroptotic stimulation. To further assess cell necroptosis, we conducted an LDH release assay. Similarly, the mutant group showed significantly higher LDH release, which was markedly reduced by GSK872 (Figure 2I). Because activation of necroptosis is known to induce a strong inflammatory response, including the release of pro-inflammatory cytokines such as IL-6,[19] we measured IL-6 levels in the supernatant of HeLa cells. The mutant group exhibited significantly higher IL-6 secretion in response to TSZ stimulation compared with the WT group, which was effectively inhibited by GSK872 (Figure 2J). In addition, we also measured the levels of TNF-α in the supernatant of HeLa cells to explore whether the Q134K mutation leads to increased TNF-α release following necroptosis, thereby establishing a positive feedback loop that further promotes necroptosis. Consistent with our hypothesis, the Q134K mutant group exhibited significantly higher TNF-α levels in the supernatant after TSZ stimulation in comparison with the WT group (Figure 2J). In summary, the reduction of inflammatory signaling through RIPK3 inhibition further supports that the Q134K mutation enhances the sensitivity of HeLa cells to TSZ-induced necroptosis, thereby exacerbating inflammation.

Enhanced necroptosis response of PBMCs in the patient. Subsequently, we examined the inflammatory response in the patient. A marked increase in the levels of pro-inflammatory cytokines, including TNF-α, IL-1β, IL-6, and IL-8 was detected in the patients' serum, especially in P3 (Figure 3A; Supplementary Figure S3). Consistent with the findings observed in HeLa cells, PBMCs from P3 treated with TSZ showed significantly elevated levels of p-RIPK3 and p-MLKL compared with those of healthy controls, both of which were effectively suppressed by the RIPK3 inhibitor GSK872 (Figure 3B and C). Annexin V/PI staining and LDH release assays were subsequently conducted to assess cell death in PBMCs. Upon TSZ stimulation, PBMCs from P3 showed a marked increase in Annexin V^+PI^+ late apoptotic/secondary necrotic cells compared with healthy controls, whereas the Annexin V^+PI^- (early apoptotic) population did not show a consistent increase (Figure 3D; Supplementary Figure S4B). Quantification of total Annexin V–positive cells revealed a concordant increase following TSZ stimulation, which was effectively suppressed by GSK872 (Supplementary Figure S4C). In parallel, LDH release was significantly elevated in P3 PBMCs and reduced

Table 2. *RIPK3* mutation identified in Still disease–like autoinflammatory syndrome family*

Gene	Chromosome	Position	Consequence	MAF[a]	MAF_eas	CADD	Polyphen	FATHMM	ChinaMAP	MTR
RIPK3	14	24,339,086	c.400C>A:p.Gln134Lys	0.00000062	0	12.2	Probably damaging	Deleterious	0	0.93

* CADD, Combined Annotation Dependent Depletion; FATHMM, Functional Analysis through Hidden Markov Models; MAF, minor allele frequency; MAF_eas, minor allele frequency in the East Asian subpopulation; MTR, missense tolerance ratio; RIPK3, receptor-interacting protein kinase 3.
[a] MAF in gnomAD v4.1.0.

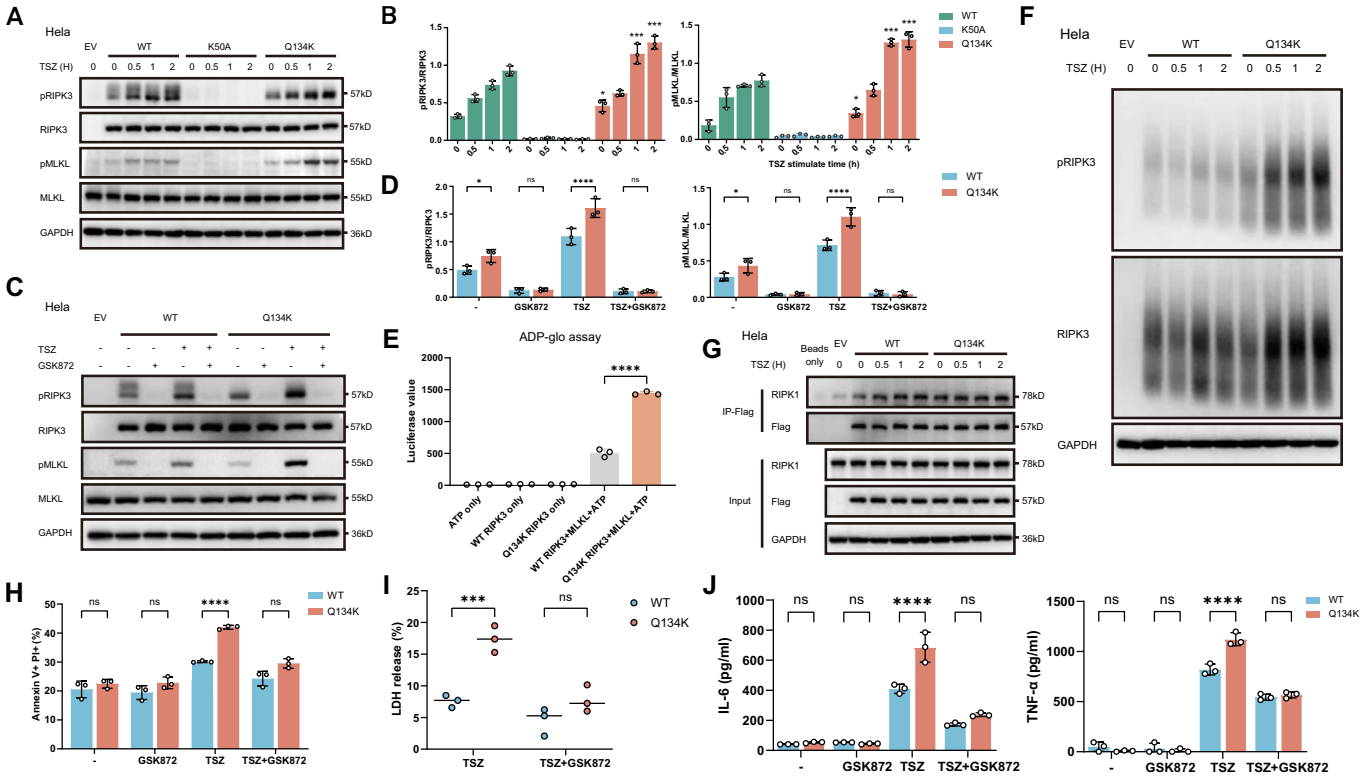


Figure 2. Legend on next page.

by GSK872 (Figure 3E). Additionally, we quantified the levels of TNF-α, IL-1β, and IL-6 in the supernatants of PBMCs stimulated with TSZ. The results revealed that PBMCs from the patient secreted significantly higher levels of TNF-α, IL-1β, and IL-6 when contrasted with those of healthy individuals. Importantly, GSK872 effectively suppressed the secretion of these cytokines (Figure 3F). These findings provide additional evidence that RIPK3 activity is enhanced in the patient's immune cells, with the Q134K variant potentially contributing to RIPK3-associated necroptosis.

***RIPK3* variant promotes inflammation through the NF-κB and MAPK signaling pathways.** To gain additional insight into the molecular mechanisms underlying the inflammatory phenotype observed in the patient's PBMCs, RNA sequencing was performed on PBMCs from P3 and four healthy individuals. KEGG analysis showed significant enrichment of inflammatory pathways, most prominently the MAPK signaling pathway, along with the IL-17 signaling pathway, Toll-like receptor signaling pathway, and TNF signaling pathway (Figure 4A). Notably, IL-17 pathway enrichment was driven mainly by downstream NF-κB/MAPK target genes (eg, *FOS, FOSB, JUN, JUND, IL1B, TNF*, and *TRAF4*), whereas canonical Th17 differentiation markers (*RORC, IL17A*, and *IL21*) were not differentially expressed. Considering the pivotal role of the NF-κB pathway in necroptosis, GSEA was performed. Notably, a significant up-regulation of the NF-κB signaling pathway was observed in the patient's PBMCs (Figure 4B). Consistently, volcano plot analysis highlighted marked up-regulation of NF-κB– and MAPK-related genes (Figure 4C). In contrast, IFN-stimulated genes were not globally up-regulated, and no IFN-related pathways were enriched (Supplementary Figure S5). Together, these results suggest that the Q134K mutation may trigger activation of the NF-κB and MAPK pathways, thereby amplifying inflammatory responses.

Consistent with the transcriptomic findings, NF-κB– and AP-1–dependent luciferase reporter assays showed that the Q134K

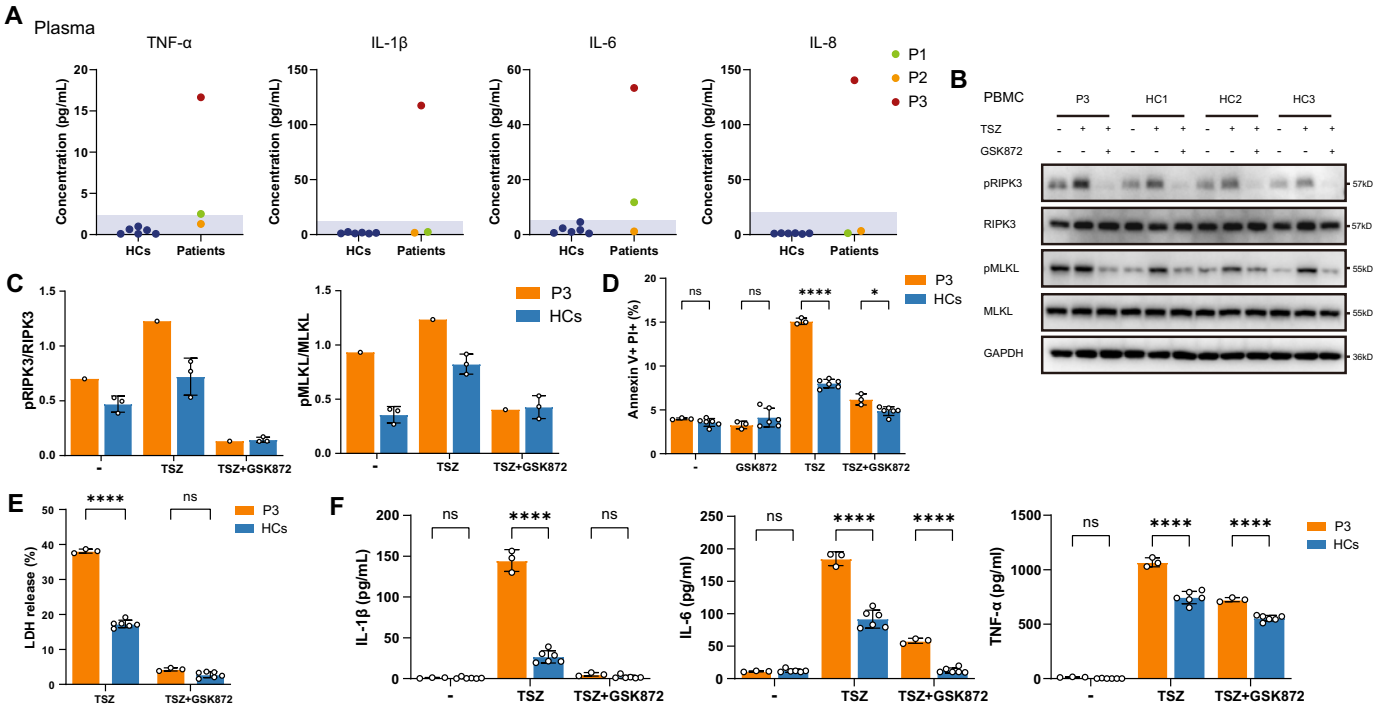


Figure 3. Patient PBMCs are sensitive to TSZ-induced necroptosis. (A) Serum levels of cytokines TNF-α, IL-1β, IL-6, and IL-8 in three patients and six HCs. Plasma samples from P1 and P2 were collected under treatment, whereas plasma from P3 was collected at baseline. (B) Western blots of PBMCs from P3 and HCs stimulated with TSZ for 2 hours in the presence or absence of GSK872. (C) Densitometric analysis of p-RIPK3/total RIPK3 and p-MLKL/total MLKL in Figure 3B. (D) Flow cytometric analysis of Annexin V/PI staining PBMCs treated as indicated, showing Annexin V^+/PI^+ populations. (E) LDH release was measured in PBMC supernatants stimulated with TSZ for 6 hours, with or without GSK872. (F) The concentrations of IL-1β, IL-6, and TNF-α in the supernatants of PBMCs at 4 hours after specific stimulation. *$p < 0.05$; ****$p < 0.0001$. HC, healthy control; IL, interleukin; LDH, lactate dehydrogenase; MLKL, mixed-lineage kinase domain-like protein; ns, not significant; p-, phosphorylated; P, patient; PBMC, peripheral blood mononuclear cell; RIPK3, receptor-interacting protein kinase 3; TNF-α, tumor necrosis factor α. Color figure can be viewed in the online issue, which is available at http://onlinelibrary.wiley.com/doi/10.1002/art.70146/abstract.

variant induced significantly higher NF-κB and AP-1 reporter activity compared with WT RIPK3, which was markedly suppressed by the GSK872 (Figure 4D and E). Immunoblot analysis further revealed increased phosphorylation of p65, p38, ERK, and JNK in Q134K-expressing cells following TSZ stimulation, and this effect was attenuated by GSK872 (Figure 4F and G). Moreover, inhibition of MAPK signaling (p38, ERK, or JNK) or treatment with prednisolone or dexamethasone significantly reduced IL-6 and TNF-α secretion in HeLa cells (Figure 4H and I). These findings not only further corroborate the role of the *RIPK3* Q134K mutation in the activation of the MAPK and NF-κB pathways but also align with the clinical efficacy of glucocorticoid therapy in the patient. This therapeutic effect may be attributed to the inhibitory action of prednisolone and dexamethasone on the NF-κB signaling pathway.[20,21]

DISCUSSION

In this study, we report a family case of a rare *RIPK3* variant associated with Still disease–like autoinflammatory syndrome and demonstrate that this variant exerts a gain-of-function effect on RIPK3 kinase activity. Functional analyses revealed that this mutation enhances RIPK3 homodimerization, MLKL activation, and necroptosis, subsequently activating the MAPK and NF-κB signaling pathways. This, in turn, promotes the production of proinflammatory cytokines, such as IL-1β, IL-6, and TNF-α, thereby establishing a positive feedback loop of cell death and inflammation. Our findings provide the first evidence linking a human *RIPK3* genetic variant to Still disease–like manifestations, suggesting a potential pathogenic mechanism involving enhanced RIPK3-driven necroptotic signaling and amplified inflammatory responses.

RIPK1 and RIPK3, both members of the RIPK family, share critical roles in pathways mediating inflammation and necroptosis through similar signaling cascades. During necroptosis, RIPK3 acts as a crucial downstream effector of RIPK1. Given their close functional relationship, we hypothesize that diseases caused by pathogenic variants in RIPK1 and RIPK3 may exhibit some overlapping features. Currently, two major categories of disorders associated with *RIPK1* pathogenic variants have been reported: *RIPK1* deficiency with autoinflammation[22,23] and cleavage-resistant *RIPK1*-induced autoinflammatory syndrome.[24,25] These disorders share certain clinical features with the condition

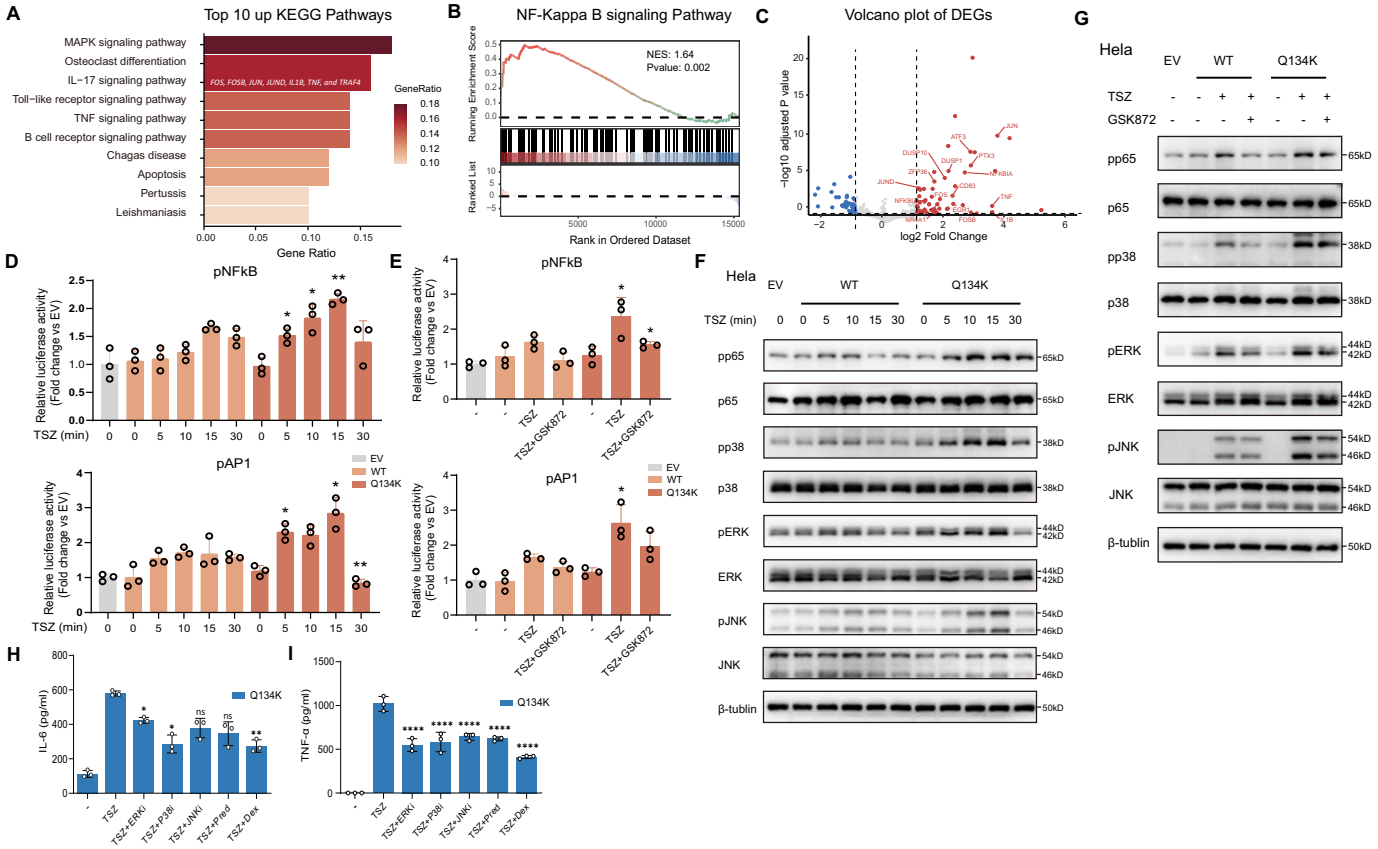


Figure 4. *RIPK3* Q134K variant induces inflammation through the NF-κB and MAPK signaling pathways. (A) KEGG enrichment analysis of up-regulated DEGs in P3 PBMCs compared with HCs. (B) Gene set enrichment analysis plot showing enrichment of the NF-κB pathway in P3 versus HCs. (C) Volcano plot showing DEGs in PBMCs from P3 compared with HCs. (D) NF-κB and AP-1 luciferase reporter activity in HeLa cells expressing EV, WT, or Q134K RIPK3 following TSZ stimulation. (E) Luciferase reporter activity in HeLa cells treated with TSZ in the presence or absence of GSK872. (F) Western blots of Hela cells transfected with the indicated RIPK3 constructs treated with TSZ for the indicated times. (G) Western blots of Hela cells transfected with the indicated RIPK3 constructs treated with TSZ with or without GSK872 at 0.5 hours after specific stimulation. (H and I) The concentrations of IL-6 and TNF-α in the supernatants of Hela cells at 4 hours after specific stimulation. Statistical comparisons were performed relative to the TSZ group. $^{*}p < 0.05$; $^{**}p < 0.01$; $^{****}p < 0.0001$. DEG, differentially expressed gene; EV, empty vector; HC, healthy control; IL, interleukin; NES, normalized enrichment score; ns, not significant; P, patient; PBMC, peripheral blood mononuclear cell; RIPK3, receptor-interacting protein kinase 3; TNF-α, tumor necrosis factor α; WT, wild-type. Color figure can be viewed in the online issue, which is available at http://onlinelibrary.wiley.com/doi/10.1002/art.70146/abstract.

described here, such as recurrent fever and systemic inflammation, suggesting partial phenotypic overlap among RIPK family–associated diseases. However, our mechanistic data indicate that the *RIPK3* Q134K variant acts through a pathway distinct from RIPK1-driven disease mechanisms. We found that the Q134K variant neither enhanced RIPK3-RIPK1 heterodimerization nor rendered RIPK3 or MLKL phosphorylation sensitive to RIPK1 inhibition. Instead, it preferentially promoted RIPK3 self-association and kinase activation, indicating a RIPK3-intrinsic mechanism of signal amplification. Together, our results refine the current framework of RIPK-associated autoinflammatory diseases and highlight that perturbations at different nodes of the necroptotic pathway can give rise to overlapping yet mechanistically distinct clinical phenotypes.

Hitherto, pathogenic mutations in >50 genes have been implicated in the development of SAIDs.[7] Several SAIDs and inborn errors of immunity (IEIs) have been linked to defects in necroptotic signaling, including *RIPK1* deficiency,[22] *RIPK1* cleavage resistance,[24,25] linear ubiquitin chain assembly complex deficiency,[26–28] ovarian tumor deubiquitinase with linear linkage specificity deficiency,[29] and *TBK1* deficiency,[30] giving rise to a broad clinical spectrum ranging from early-onset arthritis and systemic vasculitis to organ-specific inflammation and immune dysregulation. Increasing evidence also supports a genetic contribution to Still disease, suggesting a shared genetic basis with Still disease–like autoinflammatory syndromes.[31] In this study, analysis based on the updated 2024 International Union of Immunological Societies classification did not identify additional variants in known IEI- or SAID-associated genes beyond *RIPK3* p.Q134K, supporting a primary role for aberrant RIPK3 signaling. In terms of treatment, it remains individualized because of the absence of standardized guidelines. High-dose glucocorticoids

are often effective, and biologic therapies targeting IL-1β, IL-6, and TNF-α pathways are increasingly used. Additionally, hematopoietic stem cell transplantation has demonstrated partial efficacy in certain cases.[32] In our study, the patients exhibited systemic inflammation with elevated cytokine production, consistent with excessive cytokine release downstream of RIPK3-driven necroptotic signaling and supporting the idea that cytokine-targeted therapies may represent rational therapeutic options.

Previous studies of *RIPK3* mutations predominantly investigate their functional impacts and pro-inflammatory mechanisms, where these genetic alterations are typically introduced experimentally in cellular or animal models. To date, only one report has associated *RIPK3* mutations (*RIPK3* R422* and P493fs9*) with human disease, which impair cell death-dependent regulation of herpes simplex virus-1 in cortical neurons independent of type I IFN immunity, thereby increasing susceptibility to herpes simplex encephalitis.[33] In contrast, our study associates a *RIPK3* variant with Still disease–like autoinflammatory phenotypes. Although circulating IFN-α and IFN-γ levels showed a modest upward trend, they remained within the normal range, and transcriptomic analysis revealed no global induction of IFN-stimulated genes, indicating that the p.Q134K variant primarily promotes necroptotic and inflammatory signaling rather than IFN dysregulation. Together, our findings provide novel genetic and mechanistic insights into the pathogenesis of SAIDs and highlight the context-dependent effects of distinct *RIPK3* variants on immune signaling pathways.

RIPK3 is broadly expressed across various immune cell types, exhibiting low immune cell specificity. Beyond immune cells, it is also expressed in a variety of tissues and organs, including the gastrointestinal tract, spleen, kidneys, bone marrow, lymphoid tissues, skin, and soft tissues (https://proteinatlas.org/). Given its ubiquitous expression, *RIPK3* variants may affect multiple organ systems throughout the body, potentially accounting for the systemic manifestations observed in our patients. Moreover, the infiltration of activated immune cells into different tissues may further lead to the heterogeneity of clinical presentations.

A limitation of this study is that comprehensive segregation analysis within the extended family could not be completed, as the genotype of the proband's healthy sister was unavailable. Therefore, incomplete penetrance or variable expressivity associated with the *RIPK3* p.Q134K variant cannot be formally excluded. Additional cases will be required to further define the penetrance and phenotypic spectrum of *RIPK3*-associated autoinflammatory disease.

In summary, our study identifies a familial clustering of a Still disease–like autoinflammatory syndrome associated with a rare variant in the *RIPK3* kinase domain. This variant enhances RIPK3 kinase activity, leading to aberrant necroptotic and inflammatory signaling, thereby providing mechanistic insight into the pathogenesis of Still disease–like inflammation. Accordingly, targeting RIPK3 and its downstream MAPK and NF-κB pathways, together with cytokine blockade, may represent a rational therapeutic strategy for RIPK3-associated autoinflammatory diseases.

ACKNOWLEDGMENTS

We sincerely thank our patients and their families as well as all the healthy individuals who participated in the study.

AUTHOR CONTRIBUTIONS

All authors contributed to at least one of the following manuscript preparation roles: conceptualization AND/OR methodology, software, investigation, formal analysis, data curation, visualization, and validation AND drafting or reviewing/editing the final draft. As corresponding authors, Drs Yang, Jia, and Hu confirm that all authors have provided the final approval of the version to be published and takes responsibility for the affirmations regarding article submission (eg, not under consideration by another journal), the integrity of the data presented, and the statements regarding compliance with institutional review board/Declaration of Helsinki requirements.

REFERENCES

1. Aksentijevich I, Schnappauf O. Molecular mechanisms of phenotypic variability in monogenic autoinflammatory diseases. Nat Rev Rheumatol 2021;17(7):405–425. doi:https://doi.org/10.1038/s41584-021-00614-1
2. Ozen S, Aksentijevich I. The past 25 years in paediatric rheumatology: insights from monogenic diseases. Nat Rev Rheumatol 2024;20(9):585–593. doi:https://doi.org/10.1038/s41584-024-01145-1
3. Sanchez GAM, Reinhardt A, Ramsey S, et al. JAK1/2 inhibition with baricitinib in the treatment of autoinflammatory interferonopathies. J Clin Invest 2018;128(7):3041–3052. doi:https://doi.org/10.1172/JCI98814
4. Martinon F, Burns K, Tschopp J. The inflammasome: a molecular platform triggering activation of inflammatory caspases and processing of proIL-beta. Mol Cell 2002;10(2):417–426. doi:https://doi.org/10.1016/S1097-2765(02)00599-3
5. Romano M, Arici ZS, Piskin D, et al. The 2021 EULAR/American College of Rheumatology points to consider for diagnosis, management and monitoring of the interleukin-1 mediated autoinflammatory diseases: cryopyrin-associated periodic syndromes, tumour necrosis factor receptor-associated periodic syndrome, mevalonate kinase deficiency, and deficiency of the interleukin-1 receptor antagonist. Arthritis Rheumatol 2022;74(7):1102–1121. doi:https://doi.org/10.1002/art.42139
6. Fautrel B, Mitrovic S, De Matteis A, et al. EULAR/PReS recommendations for the diagnosis and management of Still's disease, comprising systemic juvenile idiopathic arthritis and adult-onset Still's disease. Ann Rheum Dis 2024;83(12):1614–1627. doi:https://doi.org/10.1136/ard-2024-225851
7. Zhang J, Lee PY, Aksentijevich I, et al. How to build a fire: the genetics of autoinflammatory diseases. Annu Rev Genet 2023;57(1):245–274. doi:https://doi.org/10.1146/annurev-genet-030123-084224
8. Frank D, Garnish SE, Sandow JJ, et al. Ubiquitylation of RIPK3 beyond-the-RHIM can limit RIPK3 activity and cell death. iScience 2022;25(7):104632. doi:https://doi.org/10.1016/j.isci.2022.104632
9. Zhou Y, Xiang Y, Liu S, et al. RIPK3 signaling and its role in regulated cell death and diseases. Cell Death Discov 2024;10(1):200. doi:https://doi.org/10.1038/s41420-024-01957-w
10. Afonso MB, Rodrigues PM, Mateus-Pinheiro M, et al. RIPK3 acts as a lipid metabolism regulator contributing to inflammation and

carcinogenesis in non-alcoholic fatty liver disease. Gut 2021;70(12):2359–2372. doi:https://doi.org/10.1136/gutjnl-2020-321767

11. Huang HR, Cho SJ, Harris RM, et al. RIPK3 activates MLKL-mediated necroptosis and inflammasome signaling during *Streptococcus* infection. Am J Respir Cell Mol Biol 2021;64(5):579–591. doi:https://doi.org/10.1165/rcmb.2020-0312OC
12. Duprez L, Takahashi N, Van Hauwermeiren F, et al. RIP kinase-dependent necrosis drives lethal systemic inflammatory response syndrome. Immunity 2011;35(6):908–918. doi:https://doi.org/10.1016/j.immuni.2011.09.020
13. Welz PS, Wullaert A, Vlantis K, et al. FADD prevents RIP3-mediated epithelial cell necrosis and chronic intestinal inflammation. Nature 2011;477(7364):330–334. doi:https://doi.org/10.1038/nature10273
14. Hou B, Liu M, Chen Y, et al. Cpd-42 protects against calcium oxalate nephrocalcinosis-induced renal injury and inflammation by targeting RIPK3-mediated necroptosis. Front Pharmacol 2022;13:1041117. doi:https://doi.org/10.3389/fphar.2022.1041117
15. Zhang Y, Li M, Li X, et al. Catalytically inactive RIP1 and RIP3 deficiency protect against acute ischemic stroke by inhibiting necroptosis and neuroinflammation. Cell Death Dis 2020;11(7):565. doi:https://doi.org/10.1038/s41419-020-02770-w
16. Gautam A, Boyd DF, Nikhar S, et al. Necroptosis blockade prevents lung injury in severe influenza. Nature 2024;628(8009):835–843. doi:https://doi.org/10.1038/s41586-024-07265-8
17. Ma Y, Chen X, Wang M, et al. Ruxolitinib targets JAK-STAT signaling to modulate neutrophil activation in refractory macrophage activation syndrome. Blood 2025;146(5):612–627. doi:https://doi.org/10.1182/blood.2024024362
18. Jia J, Wang M, Meng J, et al. Ferritin triggers neutrophil extracellular trap-mediated cytokine storm through Msr1 contributing to adult-onset Still's disease pathogenesis. Nat Commun 2022;13(1):6804. doi:https://doi.org/10.1038/s41467-022-34560-7
19. Lawlor KE, Murphy JM, Vince JE. Gasdermin and MLKL necrotic cell death effectors: signaling and diseases. Immunity 2024;57(3):429–445. doi:https://doi.org/10.1016/j.immuni.2024.02.011
20. Guo Q, Jin Y, Chen X, et al. NF-κB in biology and targeted therapy: new insights and translational implications. Signal Transduct Target Ther 2024;9(1):53. doi:https://doi.org/10.1038/s41392-024-01757-9
21. Gong K, Guo G, Beckley NA, et al. Comprehensive targeting of resistance to inhibition of RTK signaling pathways by using glucocorticoids. Nat Commun 2021;12(1):7014. doi:https://doi.org/10.1038/s41467-021-27276-7
22. Li Y, Führer M, Bahrami E, et al. Human RIPK1 deficiency causes combined immunodeficiency and inflammatory bowel diseases. Proc Natl Acad Sci U S A 2019;116(3):970–975. doi:https://doi.org/10.1073/pnas.1813582116
23. Cuchet-Lourenço D, Eletto D, Wu C, et al. Biallelic *RIPK1* mutations in humans cause severe immunodeficiency, arthritis, and intestinal inflammation. Science 2018;361(6404):810–813. doi:https://doi.org/10.1126/science.aar2641
24. Lalaoui N, Boyden SE, Oda H, et al. Mutations that prevent caspase cleavage of RIPK1 cause autoinflammatory disease. Nature 2020;577(7788):103–108. doi:https://doi.org/10.1038/s41586-019-1828-5
25. Tao P, Sun J, Wu Z, et al. A dominant autoinflammatory disease caused by non-cleavable variants of RIPK1. Nature 2020;577(7788):109–114. doi:https://doi.org/10.1038/s41586-019-1830-y
26. Iwai K. LUBAC-mediated linear ubiquitination: a crucial regulator of immune signaling. Proc Jpn Acad Ser B Phys Biol Sci 2021;97(3):120–133. doi:https://doi.org/10.2183/pjab.97.007
27. Peltzer N, Darding M, Montinaro A, et al. LUBAC is essential for embryogenesis by preventing cell death and enabling haematopoiesis. Nature 2018;557(7703):112–117. doi:https://doi.org/10.1038/s41586-018-0064-8
28. Boisson B, Laplantine E, Prando C, et al. Immunodeficiency, autoinflammation and amylopectinosis in humans with inherited HOIL-1 and LUBAC deficiency. Nat Immunol 2012;13(12):1178–1186. doi:https://doi.org/10.1038/ni.2457
29. Spaan AN, Neehus AL, Laplantine E, et al. Human OTULIN haploinsufficiency impairs cell-intrinsic immunity to staphylococcal α-toxin. Science 2022;376(6599):eabm6380. doi:https://doi.org/10.1126/science.abm6380
30. Taft J, Markson M, Legarda D, et al. Human TBK1 deficiency leads to autoinflammation driven by TNF-induced cell death. Cell 2021;184(17):4447–4463.e20. doi:https://doi.org/10.1016/j.cell.2021.07.026
31. Shen Y, Jia J, Teng J, et al. Advancing personalised precision treatment for Still's disease based on molecular characteristics and disease progression. Lancet Rheumatol 2025;7(2):e127–e140. doi:https://doi.org/10.1016/S2665-9913(24)00225-X
32. Savic S, Caseley EA, McDermott MF. Moving towards a systems-based classification of innate immune-mediated diseases. Nat Rev Rheumatol 2020;16(4):222–237. doi:https://doi.org/10.1038/s41584-020-0377-5
33. Liu Z, Garcia Reino EJ, Harschnitz O, et al. Encephalitis and poor neuronal death-mediated control of herpes simplex virus in human inherited RIPK3 deficiency. Sci Immunol 2023;8(82):eade2860. doi:https://doi.org/10.1126/sciimmunol.ade2860

Check for updates

Arthritis & Rheumatology
Vol. 78, No. 10, October 2026, pp 2160–2170
DOI 10.1002/art.70149
© 2026 The Author(s). *Arthritis & Rheumatology* published by Wiley Periodicals LLC on behalf of American College of Rheumatology.
This is an open access article under the terms of the Creative Commons Attribution-NonCommercial-NoDerivs License, which permits use and distribution in any medium, provided the original work is properly cited, the use is non-commercial and no modifications or adaptations are made.

American College of Rheumatology
Empowering Rheumatology Professionals

Validation of International Classification of Diseases Code–Based Case Definitions of Immune Checkpoint Inhibitor–Associated Inflammatory Arthritis From Administrative Health Data

Manar Elsayed, BSc,[1] Zoe Hsu, MSc,[2,3] Finlay A. McAlister, MD, MSc,[1] William D. Leslie, MD, MSc,[4] Lisa M. Lix, PhD,[4] Sasha Bernatsky, MD, PhD,[5] Suzanne N. Morin, MD, MSc,[5] Michelle M. Graham, MD,[1] Aurore Fifi-Mah, MD,[6] Shahin Jamal, MD,[7] Janet Roberts, MD, MPH,[8] and Carrie Ye, MD, MPH[1]

Objective. Immune checkpoint inhibitors (ICIs) for cancer can lead to immune-related adverse events, including ICI-associated inflammatory arthritis (ICI-IA). There are no validated *International Classification of Diseases* (ICD) code–based case definitions for ICI-IA.

Methods. We conducted a validation study using the Canadian Research Group of Rheumatology in Immuno-Oncology (CanRIO) database. Rheumatologist-confirmed ICI-IA was the reference standard, defined as new onset of at least one swollen joint on examination or synovitis on imaging following ICI exposure, without another cause or pre-existing IA. We compared ICD-9 (714.x and 696.0) and ICD-10 (M05.x, M06.x, and M07.x) IA diagnostic codes against the reference standard. Seven core case definitions of different combinations of ICD codes from the Physician Claims Database (PCD) and the Discharge Abstract Database were tested. Results were stratified by sex. Sensitivity testing with additional criteria was also evaluated.

Results. We included 228 patients in the final analysis: 100 with ICI-IA and 128 without ICI-IA. Sensitivity of the tested case definitions ranged from 1.0% to 88.0%, whereas specificity ranged from 86.7% to 100.0%. The case definition with at least one PCD IA code achieved the best balance of sensitivity (88.0%, 95% confidence interval [CI] 81.6%–94.4%) and specificity (86.7%, 95% CI 80.8%–92.6%). Case definition performances were similar between sexes. Additional criteria minimally improved specificity but sacrificed sensitivity.

Conclusion. ICD code–based case definitions of ICI-IA can accurately detect ICI-IA and can be used to support ICI-IA surveillance and research with administrative health data.

INTRODUCTION

Immune checkpoint inhibitors (ICIs) are now widely used to treat numerous malignancies, with immunotherapy representing the fourth pillar of cancer therapies alongside chemotherapy, radiation, and surgery.[1] ICIs function by blocking immune regulatory checkpoints, such as programmed death 1 (PD-1); its ligand, programmed death ligand 1 [PD-L1]; and cytotoxic T-lymphocyte–associated antigen 4 (CTLA-4), thereby enhancing the immune system to attack tumor cells and ultimately prolonging survival in many patients.[2] Although ICIs offer significant clinical benefits, they can cause off-target

The interpretation and conclusions contained herein are those of the researchers and do not represent the views of the Government of Alberta or Alberta Health Services. Neither the Government of Alberta nor Alberta Health Services express any opinion in relation to this study.

Carrie Ye was supported by a Canadian Institutes of Health Research Early Career Research Award [PJF 198655]. This project was supported by the Canadian Institutes of Health Research [PJT197771]. The provincial administrative datasets used and analyzed during the current study were accessed from and are currently stored in the Alberta Health Services Enterprise Data Warehouse with support provided by the Alberta Strategy for Patient-Oriented Research (SPOR) Support for People and Patient-Oriented Research and Trials (SUPPORT) Unit Data and Research Services team (https://absporu.ca).

[1]University of Alberta, Edmonton, Alberta, Canada; [2]Provincial Research Data Services, Alberta Health Services, Edmonton, Alberta, Canada; [3]Data and Research Services, Alberta SPOR SUPPORT Unit, Edmonton, Canada; [4]University of Manitoba, Winnipeg, Manitoba, Canada; [5]McGill University, Montreal, Quebec, Canada; [6]University of Calgary, Calgary, Alberta, Canada; [7]University of British Columbia, Vancouver, British Columbia, Canada; [8]Dalhousie University, Halifax, Nova Scotia, Canada.

Additional supplementary information cited in this article can be found online in the Supporting Information section (https://acrjournals.onlinelibrary.wiley.com/doi/10.1002/art.70149).

Author disclosures are available at https://onlinelibrary.wiley.com/doi/10.1002/art.70149.

Address correspondence via email to Carrie Ye, MD, MPH, at cye@ualberta.ca.

Submitted for publication September 23, 2025; accepted in revised form February 2, 2026.

effects known as immune-related adverse events (irAEs), which may affect multiple organs.[3]

Among these, rheumatic irAEs have been increasingly recognized in small case series and observational studies, though they remain poorly described in randomized controlled trials.[4–10] ICI-associated inflammatory arthritis (ICI-IA), the most common rheumatic irAE, is estimated to occur in 1% to 11% of ICI users.[11–14] However, the true incidence is unknown as most of the reported data on ICI-IA come from clinical case series, and ICI clinical trials tend to report symptoms, such as arthralgias and myalgias, and not the underlying cause of these symptoms (ie, osteoarthritis vs IA vs soft tissue disorders vs metastatic cancer).[11,14,15] Additionally, the reporting of irAE in ICI clinical trials is generally completed by the oncology team, and not rheumatologists, making accurate incidence rates for ICI-IA difficult to ascertain.

Although studies have been done for detection of irAEs in general using administrative health data and electronic health records,[16,17] *International Classification of Diseases* (ICD) code–based case definitions for rheumatic irAEs have not been validated, an important standard for use of ICD code–based case definitions in administrative database research.[18] Despite this, several administrative database studies have been published examining the frequency and predictors and outcomes of rheumatic irAEs, including ICI-IA, making the validity of these studies difficult to assess.[13,19–21] This underscores the urgent need to validate ICD code–based case definitions for rheumatic irAEs.

One of the challenges of validating administrative case definitions for rheumatic irAEs is that it requires a relatively large cohort of confirmed cases and confirmed noncases. The Canadian Research Group of Rheumatology in Immuno-Oncology (CanRIO) database is a national database of ICI users referred to rheumatology for assessment of possible rheumatic irAEs, which includes rheumatologist-confirmed cases (and noncases) of ICI-IA.[8] By leveraging the CanRIO database, our study aims to validate ICD code–based case definitions of the most common rheumatic irAE: ICI-IA.

METHODS

Data sources. We conducted a validation study analyzing data from the Alberta cohort of the CanRIO database (CanRIO-AB). Alberta is the fourth most populous province in Canada, with an estimated population of 4.9 million people in 2024.[22] Every resident of Alberta is assigned a unique personal health number that provides universal access to all health services in the province and can be used to track individual health care use across settings (outpatient clinics, emergency departments, hospitalizations, laboratories, diagnostic imaging, pharmacies). These identifiers were used to link individuals in CanRIO-AB to their Alberta provincial health administrative records.

Baseline patient characteristics including demographics and cancer- and ICI-related data were ascertained from CanRIO-AB. IA ICD codes were ascertained from the Physician Claims Database (PCD) and the Discharge Abstract Database (DAD) from three years before ICI initiation up to July 31, 2024, death, or loss of registration, whichever came sooner. The PCD employs ICD, Ninth Revision, Clinical Modification (ICD-9-CM) codes, whereas the DAD (which captures all hospitalizations) uses ICD, Tenth Revision, Canadian Enhancements (ICD-10-CA) codes. Deaths were ascertained from Vital Statistics, which captures all births and deaths in Alberta. The study was approved by the Health Research Ethics Board for the University of Alberta (Pro00118986), which granted a waiver for individual consent as investigators were only supplied with data after de-identification. We followed the Strengthening the Reporting of Observational Studies in Epidemiology (STROBE) reporting guidelines for observational cohort studies.[23] Patients or the public were not involved in the planning or conduct of this research study.

CanRIO database. CanRIO is a network of rheumatologists from 11 institutions across Canada specializing in rheumatic irAEs. The retrospective CanRIO database was established in January 2019 and includes patients assessed between January 2013 to May 30, 2024.[8,24] It includes all patients treated with ICIs referred to CanRIO rheumatologists for assessment of possible rheumatic irAEs or pre-existing rheumatic diseases. Chart review was conducted for each patient, and pertinent data, including patient demographics, history of pre-existing rheumatic diseases, oncologic history, irAE manifestations, treatments, and outcomes, were entered into the CanRIO database. All patients in CanRIO-AB with an ICI initiation date and final diagnosis were included. Patients who could not be linked to the provincial administrative databases were excluded.

ICI-IA reference cases. The reference standard for ICI-IA was rheumatologist-confirmed ICI-IA in the CanRIO database, defined as the new onset of at least one swollen joint on examination or synovitis on imaging following ICI exposure, without another cause or pre-existing IA. All other cases in CanRIO-AB (ie, patients referred to rheumatologists for assessment of rheumatologic symptoms but not confirmed by the rheumatologist to have met criteria for ICI-IA, including those with existing IA before ICI exposure) were classified as not having ICI-IA and considered noncases.

ICI-IA administrative data case definitions. There are no ICI-IA specific ICD codes. We selected ICD-9 and ICD-10 codes that represented IA. ICD-9 codes included rheumatoid arthritis and other IA (714.x) and psoriatic arthritis (696.0). ICD-10 codes included seropositive rheumatoid arthritis (M05.x), seronegative rheumatoid arthritis and other IA (M06.x), and psoriatic and inflammatory bowel disease–associated arthritis (M07.x).

IA ICD codes were ascertained three years before ICI initiation and any time post ICI initiation. In order to discriminate flares

of pre-existing IA from ICI-IA, an individual with an IA ICD code within three years before ICI initiation was classified as negative for ICI-IA, regardless of the presence of any IA codes ascertained after ICI initiation. We tested seven core case definitions that included different combinations of IA codes from PCD and DAD (Table 1). For our core set of case definitions, the first instance of IA code could occur any time after ICI initiation, but for all case definitions that required a minimum of at least two codes, the codes had to be within three years of the first code. Multiple records of IA codes registered for the same day for the same setting (PCD or DAD) were considered a single instance of IA code in that setting.

Sensitivity analysis. Nine sets of sensitivity analyses were conducted, each with additional criteria added to the core algorithms. (1) IA that develops years after ICI discontinuation may not be related to ICI exposure. Thus, we conducted a sensitivity analysis in which we reclassified reference ICI-IA cases with onset of symptoms beyond one year (365 days) after ICI discontinuation as not ICI-IA (ICI-IA n = 96, no ICI-IA n = 132), and correspondingly, first IA codes had to occur within the year of ICI discontinuation. (2) Because the vast majority of IA codes were rheumatoid arthritis codes (714.x, M05.x, and M06.x), we evaluated case definitions using only rheumatoid arthritis codes. (3) We restricted case definitions to IA codes from rheumatologists only or (4) to IA codes from internal medicine physicians and rheumatologists only. (5) We examined the addition of IA codes from the National Ambulatory Care Reporting System (NACRS). NACRS captures all emergency department visits using ICD-10-CA codes, which were treated as either PCD or DAD codes. Although Alberta has NACRS data for all institutions in the province, we did not include NACRS codes in our core case definition algorithms for this study because many other jurisdictions do not have NACRS data. (6) Case definitions requiring a minimum of at least two codes were restricted to multiple codes having to be within one year of the first code or (7) within two years of the first code. (8) We examined the addition of polymyalgia rheumatica (PMR) codes (ICD-9 725, ICD-10 M35.3) to the core algorithms. (9) We examined the addition of at least one filled prescription of a glucocorticoid or disease-modifying antirheumatic drug (DMARD) within 40 days (before or after) of the first code of ICI-IA (Supplementary Table 1).

Table 1. Case definitions*

Case definition	Abbreviation
≥1 Physician Claims Database code ICD-9 714.x or 696.0	≥1P
≥2 Physician Claims Database codes ICD-9 714.x or 696.0	≥2P
≥3 Physician Claims Database codes ICD-9 714.x or 696.0	≥3P
≥1 Discharge Abstract Database code ICD-10 M05.x, M06.x, or M07.x	≥1H
1 Discharge Abstract Database code ICD-10 M05.x, M06.x, or M07.x or 1 Physician Claims Database codes ICD-9 714.x or 696.0	≥1H or ≥1P
1 Discharge Abstract Database ICD-10 M05.x, M06.x, or M07.x or 2 Physician Claims Database codes ICD-9 714.x or 696.0	≥1H or ≥2P
1 Discharge Abstract Database code ICD-10 M05.x, M06.x, or M07.x or 3 Physician Claims Database codes ICD-9 714.x or 696.0	1H or ≥3P

* ICD, *International Classification of Diseases*; P, Physician Claims Database code, H, Discharge Abstract Database code.

Statistical analysis. Summary statistics were used to describe the baseline characteristics of the CanRIO-AB cohort, stratified by rheumatologist-confirmed ICI-IA status. For each of the seven core case definitions and for each of the sensitivity analyses, we estimated sensitivity (true positives/[true positives + false negatives]), specificity (true negatives/[true negatives + false positives]), positive predictive value (PPV = true positives/[true positives + false positives]), and negative predictive value (NPV = true negatives/[true negatives + false negatives]), along with their corresponding 95% confidence intervals (CIs) and C-statistic. For the seven core case definitions, with a sample size of 228 cases, including 100 ICI-IA cases, we could detect 0.9 sensitivity and 0.9 specificity (lower bound of 0.8), with power of 0.8 and alpha of 0.05.[25] Sex-stratified analysis was performed to test for sex differences in core case definitions. All analyses were conducted using SAS 9.4 (SAS Institute Inc).

Data availability statement. This study is based on data provided by Alberta Health and Alberta Health Services. We are not able to make our data set available to other researchers due to our contractual data disclosure agreement with Alberta Health Services, which is the data custodian, and the restrictions of the Alberta Health Information Act. Inquiries regarding access to the data can be made to health.resdata@gov.ab.ca.

RESULTS

There were a total of 233 individuals in the CanRIO-AB database as of May 30, 2024, all of whom had a final rheumatologist-assigned diagnosis (ICI-IA vs other diagnoses), but four did not have an ICI start date, and one did not have a provincial health registry record. The final study cohort included 228 individuals: 100 in the rheumatologist-confirmed ICI-IA group and 128 in the no ICI-IA group (control group; Figure 1).

The median age was similar between the two groups: 71.0 years (interquartile range [IQR] 63.0–77.0) in those with ICI-IA and 70.0 years (IQR 61.0–76.7) in those without (Table 2). A slightly higher proportion of men was observed in the ICI-IA group (61.0%) compared to the control group (53.1%). Smoking status and alcohol consumption were similar between the two groups. A higher percentage of patients in the control group had pre-existing autoimmune disease, as compared with the ICI-IA group (29.7% vs 16.0%), with 15.6% of the control group having

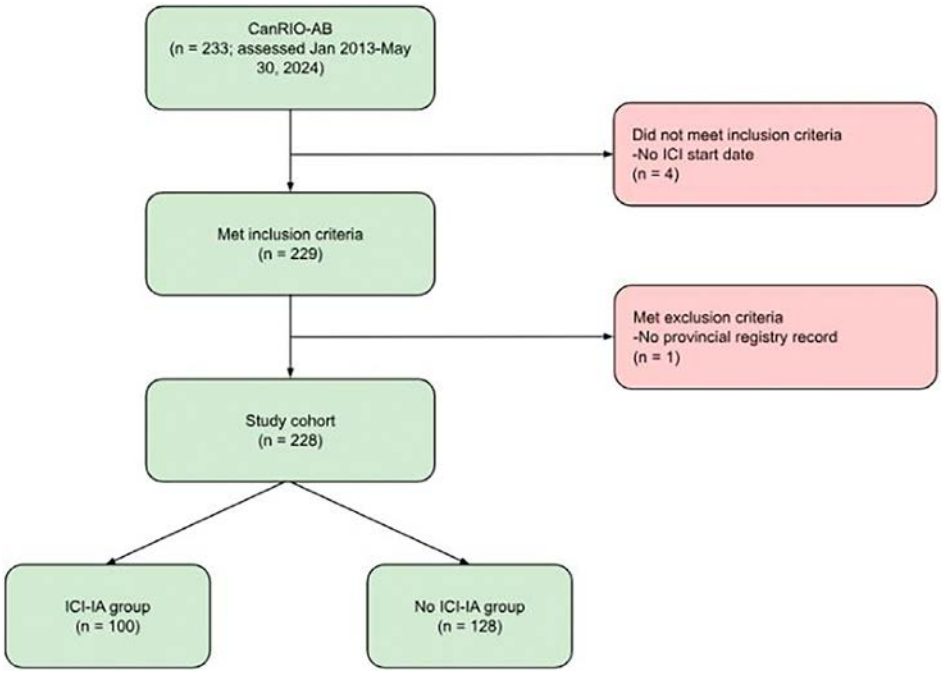


Figure 1. Cohort selection. CanRIO-AB, Canadian Research Group of Rheumatology in Immuno-Oncology Alberta; ICI, immune checkpoint inhibitor; ICI-IA, immune checkpoint inhibitor–associated inflammatory arthritis.

had pre-existing IA and, by definition, none of the ICI-IA group having had pre-existing IA.

Skin cancer and lung and bronchus cancer were the most common tumor groups, with the breakdown by tumor group appearing similarly in both ICI-IA and control groups. The majority of patients in both groups had stage IV cancer. PD-1/PD-L1 inhibitors were the most frequently administered ICI regimen, used in 76.0% of the ICI-IA group and 70.3% of the control group. More patients in the control group received concurrent chemotherapy, as compared with the ICI-IA group (18.0% vs 9.0%). The same percentage of patients in both groups developed non-rheumatologic irAEs (32.0%).

The median observation time in CanRIO-AB from ICI initiation was slightly longer in the ICI-IA group compared to the control group (33.9 months vs 24.0 months, Table 2), although IQRs overlapped. Similarly, the provincial registry observation time from ICI initiation period was longer in the ICI-IA cohort (34.4 vs 23.6 months), with overlapping IQRs. Despite the shorter observation period in the control group, the percentage of patients who died during the observation period was similar in both groups (39.0% vs 38.3%).

Of the 100 individuals with ICI-IA, the median time between ICI initiation and IA onset was 3.8 months (IQR 1.7–9.7, Table 3). At presentation, the median number of tender joints was 4.5 (IQR 1–12), and median number of swollen joints was 4 (IQR 2–12). The most common pattern of joint involvement was oligoarthritis, observed in 45 patients (45.0%), with most patients having symmetrical joint involvement (60.0%). Seropositivity for either rheumatoid factor (9.0%) and anti-cyclic citrullinated peptide antibodies (1.0%) was uncommon. The majority (64.0%) of ICI-IA cases were classified as being CTCAE (Common Terminology Criteria for Adverse Events) grade 2 severity (ie, moderate symptoms that limit activities of daily living[26]), and most were treated with conventional synthetic DMARDs (csDMARDs; 78.0%) and/or glucocorticoids (68.0%). ICI therapy was held in 37% of patients, was discontinued in 35%, was continued in 4%, or had already been discontinued before ICI-IA onset in 24%.

Of the 228 patients in the study cohort, 14 had at least one IA ICD code registered in the three years before ICI initiation, all of whom were classified as negative for ICI-IA by all of our ICD code–based case definitions. A total of 114 of 228 patients had at least one IA ICD code registered after ICI initiation, with a median time from ICI initiation to first IA code of 8.9 months (IQR 4.8–13.8). Of those who had more than one IA ICD code after ICI initiation, the median time between first and second IA ICD codes was 54 days (IQR 16–104). Among the 81 patients with two codes, 77 had the second code within one year of the first, 80 within two years, and one had an interval of more than three years between the first and second code. Among the 71 patients with three codes, 63 had the third code within one year of the first, 70 within two years, and one had an interval of more than three years between the first and third code. The specific IA codes registered at first, second, and third visits, by IA status, are shown in Supplementary Figure 1 and listed in Supplementary Table 2. The most frequently recorded IA code was 714.x.

Table 2. Baseline characteristics of the participants*

Variable	CanRIO-AB N = 228	
	ICI-IA n = 100	No ICI-IA n = 128
Age, median (IQR)	71.0 (63.0–77.0)	70.0 (61.0–76.7)
Sex, n (%)		
Women	39 (39.0)	60 (46.9)
Men	61 (61.0)	68 (53.1)
Smoking status, n (%)		
Smoked in the past	49 (49.0)	60 (46.9)
Never smoked	39 (39.0)	49 (38.3)
Current smoker	12 (12.0)	19 (14.8)
Alcohol consumption, n (%)		
<1 drink/week	71 (71.0)	106 (82.8)
1–7 drinks/week	26 (26.0)	18 (14.1)
>7 drinks/week	3 (3.0)	4 (3.1)
Pre-existing autoimmune diseases, n (%)	16 (16.0)	38 (29.7)
Pre-existing IA, n (%)	0 (0.0)[a]	20 (15.6)
Tumor group, n (%)		
Skin	39 (39.0)	42 (32.8)
Lung & bronchus	36 (36.0)	47 (36.7)
Genitourinary	15 (15.0)	17 (13.3)
Gastrointestinal	3 (3.0)	3 (2.3)
Gynecological	4 (4.0)	8 (6.2)
Endocrine & neuroendocrine	0 (0.0)	1 (0.8)
Primary unknown/other	4 (4.0)	10 (7.8)
ICI therapy, n (%)		
PD-1/PD-L1 inhibitor monotherapy	76 (76.0)	90 (70.3)
CTLA-4 inhibitor monotherapy	0 (0.0)	0 (0.0)
Combination ICI therapy	20 (20.0)	29 (22.7)
Unknown[b]	4 (4.0)	9 (7.0)
Concurrent chemotherapy, n (%)	9 (9.0)	23 (18.0)
Cancer stage, n (%)		
Stage I	0 (0.0)	1 (0.8)
Stage II	3 (3.0)	11 (8.6)
Stage III	34 (34.0)	39 (30.5)
Stage IV	63 (63.0)	77 (60.2)
Nonrheumatologic irAEs, n (%)	32 (32.0)	41 (32.0)
CanRIO-AB observation time from ICI initiation in months, median (IQR)	33.9 (20.2–46.9)	24.0 (12.3–50.3)
Provincial registry observation time from ICI initiation in months, median (IQR)	34.4 (20.1–55.2)	23.5 (12.0–50.9)
Death, n (%)	39 (39.0)	49 (38.3%)

* CanRIO-AB, Canadian Research Group of Rheumatology in Immuno-Oncology-Alberta Cohort; CTLA-4, cytotoxic T-lymphocyte–associated antigen 4; IA, inflammatory arthritis; ICI, immune checkpoint inhibitors; ICI-IA, immune checkpoint inhibitor–associated inflammatory arthritis; IQR, interquartile range; irAE, immune-related adverse events; PD-1, programmed death 1; PD-L1, programmed death ligand 1.
[a] Patients with pre-existing IA by definition could not have ICI-IA.
[b] Blinded clinical trial.

The performance of the core ICI-IA ICD code–based case definitions are presented in Table 4. Sensitivity estimates ranged from 1.0% (95% CI 0.0–3.0) to 88.0% (95% CI 81.6–94.4), specificity estimates ranged from 86.7% (95% CI 80.8–92.6) to 100.0% (95% CI 100.0–100.0), and C-statistics ranged from 0.51 to 0.87 across all tested case definitions. The simplest case definition, requiring at least one PCD IA code had sensitivity of 88.0%, specificity of 86.7%, and C-statistic of 0.87. Sensitivity estimates decreased and specificity estimates increased when additional PCD codes were required. The case definition requiring at least one DAD IA code demonstrated high specificity (100.0%, 95% CI 100.0%–100.0%) but very low sensitivity (1.0%, 95% CI 0.0%–3.0%). The addition of DAD codes to any of the PCD-based case definitions did not enhance the performance of the corresponding PCD code–only case definition. Sex-stratified performance estimates for the seven core case definitions were similar between men and women (Table 4).

Sensitivity analysis of additional case definitions criteria are shown in Table 5. The addition of the requirement that IA onset be within 365 days of ICI discontinuation to the core case definitions minimally reduced all performance measures. Restricting to rheumatoid arthritis ICD codes, or to only IA codes by either rheumatologists or internal medicine physicians, essentially did not change performance of the case definitions. However, restricting to only IA codes by rheumatologists increased specificity but reduced sensitivity across all case definitions. Inclusion of NACRS IA codes did not change the performance of any of the case definitions. Restricting multiple IA codes to being within one or two years of the first IA code reduced sensitivity without any improvement in specificity. The addition of PMR codes did not appreciably improve sensitivity but reduced specificity. The addition of glucocorticoid or DMARD prescription fill reduced sensitivity but slightly improved specificity.

DISCUSSION

In this study, we evaluated the performance of ICD code–based administrative case definitions of ICI-IA against rheumatologist-confirmed ICI-IA cases and noncases in the CanRIO-AB database. We found that a simple case definition requiring at least one PCD IA ICD code has a good balance of sensitivity (88%) and specificity (87%) for identifying ICI-IA, and performance of the various case definitions was similar between men and women. Higher specificity could be achieved with algorithms that required more than one PCD IA code (up to 96%), but with loss of sensitivity (lowest sensitivity 61%). The addition of hospital (DAD) and emergency department (NACRS) based codes did not improve the performance of PCD-based case definitions. The algorithms requiring at least one code in DAD or NACRS data had extremely low sensitivity as expected, given that ICI-IA is usually managed in the outpatient setting. Highest specificity was achieved when IA codes were restricted to rheumatologists.

The baseline characteristics of our ICI-IA group were similar to other reported contemporaneous ICI-user and ICI-IA cohorts. The breakdown by tumor type in our cohort (majority being skin

Table 3. ICI-IA phenotype and treatment*

Variable	ICI-IA n = 100
ICI initiation to symptom onset, median (IQR), months	3.8 (1.7–9.7)
Tender joints, median (IQR)	4.5 (1–12)
Swollen joints, median (IQR)	4 (2–12)
Pattern of joint involvement, n (%)	
Oligoarthritis	45 (45.0)
Polyarthritis	41 (41.0)
Monoarthritis	14 (14.0)
Axial	1 (1.0)
Symmetric joint distribution, n (%)	60 (60.0)
Associated symptoms, n (%)	
None	89 (89.0)
Bursitis	7 (7.0)
Tenosynovitis	2 (2.0)
Enthesitis	2 (2.0)
PMR onset symptoms	2 (2.0)
Inflammatory back pain	1 (1.0)
Achilles tendonitis	0 (0.0)
Patient global assessment (0–10 scale[a]), median (IQR)	7.0 (5.0–8.0)
Physician global assessment (0–10 scale[a]), median (IQR)	7.0 (5.7–8.0)
Morning stiffness, n (%)	
≤1 h	37 (37.0)
>1 h	16 (16.0)
None	9 (9.0)
Positive RF, n (%)	9 (9.0)
Positive anti-CCP, n (%)	1 (1.0)
CRP, median (IQR)	47.3 (11.1–112.2)
Joint irAE grading at its worst (CTCAE grade[b]), n (%)	
Grade 1	7 (7.0)
Grade 2	64 (64.0)
Grade 3	27 (27.0)
Grade ≥4	0 (0.0)
Joint symptoms improved by activity, n (%)	12 (12.0)
Inability to make a fist, n (%)	12 (12.0)
Decreased function, n (%)	20 (20.0)
Reduced range of motion hips, n (%)	5 (5.0)
Reduced range of motion shoulders, n (%)	10 (10.0)
Glucocorticoids, n (%)	68 (68.0)
Oral glucocorticoid	62 (62.0)
Intra-articular glucocorticoids	5 (5.0)
IM glucocorticoids	1 (1.0)
IV glucocorticoids	0 (0.0)
Narcotics, n (%)	5 (5.0)
Conventional synthetic DMARDs, n (%)	78 (78.0)
Hydroxychloroquine	73 (73.0)
Methotrexate	27 (27.0)
Sulfasalazine	8 (8.0)
Leflunomide	3 (3.0)
Mycophenolate	0 (0.0)
Azathioprine	0 (0.0)
Other	0 (0.0)
Biologic DMARDs, n (%)	2 (2.0)
Targeted synthetic DMARDs, n (%)	0 (0.0)
ICI management after ICI-IA, n (%)	
ICI held	37 (37.0)
ICI discontinued	35 (35.0)
ICI continued	4 (4.0)
Not on ICI at ICI-IA onset	24 (24.0)

* Missing data: morning stiffness (38), RF (20), anti-CCP (23), CRP (3), patient global at initial assessment (17), physician global at initial assessment (40), joint symptoms improved by activity (79), decreased function (38), inability to make a fist (36), reduced range of motion hips (28), and reduced range of motion shoulders (22). anti-CCP, anti–cyclic citrullinated peptide antibodies; CRP, C-reactive protein; CTCAE, Common Terminology Criteria for Adverse Events; DMARD, disease-modifying antirheumatic drug; ICI, immune checkpoint inhibitor; ICI-IA, immune checkpoint inhibitor–associated inflammatory arthritis; IM, intramuscular; IQR, interquartile range; irAE, immune-related adverse event; IV, intravenous; PMR, polymyalgia rheumatica; RF, rheumatoid factor.
[a] Patient and physician global assessments were recorded on a 0–10 scale: 0 = no disease activity, 10 = maximum disease activity.[42]
[b] CTCAE: grade 1 = asymptomatic or mild symptoms; grade 2 = moderate symptoms that limit instrumental activity daily living; grade 3 = severe symptoms that limit self-care activity daily living, persistent or significant disability; grade 4 = life threatening; grade 5 = death directly related to adverse event.[26]

and lung cancer) was consistent with recent irAE studies reporting lung cancer and melanoma each making up roughly one-third of the ICI users, and PD-1/PD-L1 being the most frequently used ICI.[27,28] The median time from ICI initiation to joint symptom onset in the ICI-IA group of 3.7 months was similar to that reported by Cappelli et al (5 months),[29] Roberts et al (6.5 months),[30] and Chan et al (2.8 months).[31] Nearly all patients with ICI-IA in our cohort were seronegative for rheumatoid factor and anti–cyclic citrullinated peptide, consistent with previous studies which have highlighted the seronegative nature of ICI-IA.[8,24,29,32–34] The majority of patients with ICI-IA in CanRIO-AB received glucocorticoids and csDMARDs, most commonly hydroxychloroquine, consistent with the ICI-IA treatment patterns reported in the full CanRIO database.[8,24] Use of biologic DMARDs was very low in our cohort (2%), as compared with studies from other countries, likely reflecting, at least in part, drug-coverage differences.[13,33,35]

Although ICI-IA case definitions have not been previously validated, ICD-based case definitions for similar IAs such as rheumatoid arthritis and psoriatic arthritis have been evaluated. Two Canadian validation studies found that an algorithm requiring a single outpatient physician claim for rheumatoid arthritis yielded high sensitivity and specificity (both in the 90% range), similar to our findings.[36,37] They also found that hospital- and/or emergency department–based case definitions were not sensitive but highly specific for rheumatoid arthritis and that algorithms requiring multiple rheumatoid arthritis codes showed high specificity but sacrificed sensitivity. Another Canadian validation study examined the performance of ICD code–based case definitions for psoriatic arthritis and found that although all algorithms had excellent specificity (97%–100%), there was overall lower sensitivity (34%–72%) as compared with previous rheumatoid arthritis

Table 4. Performance of ICI-IA core case definitions with 95% confidence intervals for the full cohort and by sex*

Case definition	Sensitivity	Specificity	PPV	NPV	C-statistic
Full cohort, N = 228					
≥1P	88.0 (81.6–94.4)	86.7 (80.8–92.6)	83.8 (76.8–90.9)	90.2 (85.0–95.5)	0.87 (0.83–0.92)
≥2P	68.0 (58.9–77.1)	93.8 (89.6–97.9)	89.5 (82.6–96.4)	78.9 (72.5–85.4)	0.81 (0.76–0.86)
≥3P	61.0 (51.4–70.6)	96.1 (92.7–99.5)	92.4 (86.0–98.8)	75.9 (69.3–82.5)	0.79 (0.73–0.84)
≥1H	1.0 (0.0–3.0)	100.0 (100.0–100.0)	100.0 (100.0–100.0)	56.4 (49.9–62.8)	0.51 (0.49–0.51)
≥1H or ≥1P	88.0 (81.6–94.4)	86.7 (80.8–92.6)	83.8 (76.8–90.9)	90.2 (85.0–95.5)	0.87 (0.83–0.92)
≥1H or ≥2P	68.0 (58.9–77.1)	93.8 (89.6–97.9)	89.5 (82.6–96.4)	78.9 (72.5–85.4)	0.81 (0.76–0.86)
≥1H or ≥3P	61.0 (51.4–70.6)	96.1 (92.7–99.5)	92.4 (86.0–98.8)	75.9 (69.3–82.5)	0.79 (0.73–0.84)
Women, n = 99					
≥1P	87.2 (76.7–97.7)	88.3 (80.2–96.5)	82.9 (71.4–94.4)	91.4 (84.2–98.6)	0.88 (0.81–0.94)
≥2P	74.4 (60.7–88.1)	95.0 (89.5–100.0)	90.6 (80.5–100.0)	85.1 (76.5–93.6)	0.85 (0.77–0.92)
≥3P	66.7 (51.9–81.5)	96.7 (92.1–100.0)	92.9 (83.3–100.0)	81.7 (72.7–90.7)	0.82 (0.74–0.90)
≥1H	2.6 (0.0–7.5)	100.0 (100.0–100.0)	100.0 (100.0–100.0)	61.2 (51.6–70.9)	0.51 (0.49–0.54)
≥1H or ≥1P	87.2 (76.7–97.7)	88.3 (80.2–96.5)	82.9 (71.4–94.4)	91.4 (84.2–98.6)	0.88 (0.81–0.94)
≥1H or ≥2P	74.4 (60.7–88.1)	95.0 (89.5–100.0)	90.6 (80.5–100.0)	85.1 (76.5–93.6)	0.85 (0.77–0.92)
≥1H or ≥3P	66.7 (51.9–81.5)	96.7 (92.1–100.0)	92.9 (83.3–100.0)	81.7 (72.7–90.7)	0.82 (0.74–0.90)
Men, n = 129					
≥1P	88.5 (80.5–96.5)	85.3 (76.9–93.7)	84.4 (75.5–93.3)	89.2 (81.7–96.8)	0.87 (0.81–0.93)
≥2P	63.9 (51.9–76.0)	92.6 (86.4–98.9)	88.6 (79.3–98.0)	74.1 (64.8–83.4)	0.78 (0.71–0.85)
≥3P	57.4 (45.0–69.8)	95.6 (90.7–100.0)	92.1 (83.5–100.0)	71.4 (62.1–80.7)	0.76 (0.70–0.83)
≥1H	–	–	–	–	–
≥1H or ≥1P	88.5 (80.5–96.5)	85.3 (76.9–93.7)	84.4 (75.5–93.3)	89.2 (81.7–96.8)	0.87 (0.81–0.93)
≥1H or ≥2P	63.9 (51.9–76.0)	92.6 (86.4–98.9)	88.6 (79.3–98.0)	74.1 (64.8–83.4)	0.78 (0.71–0.85)
≥1H or ≥3P	57.4 (45.0–69.8)	95.6 (90.7–100.0)	92.1 (83.5–100.0)	71.4 (62.1–80.7)	0.76 (0.70–0.83)

* "–" denotes case definitions for which no patients met the case definition. H, Discharge Abstract Database code; ICI-IA, immune checkpoint inhibitor–associated inflammatory arthritis; NPV, negative predictive value; P, Physician Claims Database code; PPV, positive predictive value.

studies.[38] In our study, the overall performance of ICD code–based case definitions of ICI-IA seems to fall somewhere between those reported for rheumatoid arthritis and psoriatic arthritis and confirms that like other IAs, ICI-IA is predominantly managed in the outpatient setting. Oftentimes, more specific case definitions, such as definitions requiring a minimum of two instances of a target IA ICD code, are used. However, ICI-IA differs from rheumatoid arthritis or psoriatic arthritis in many aspects that may make a case definition requiring only a single instance of an IA ICD code favorable: it is not uncommon that ICI-IA resolves; ICI-IA is often managed by oncology, even after an initial visit with a rheumatologist, and patients with ICI-IA may die of their cancer before a follow-up visit with their rheumatologist.

There are currently no widely accepted or validated classification criteria for ICI-IA, although this work is in progress.[39] One major point of contention when defining ICI-IA is how long after ICI cessation new onset IA can be attributed to ICI therapy and be classified as ICI-IA. In our primary analysis, we included all rheumatologist-confirmed cases of ICI-IA in CanRIO-AB, regardless of the timing of IA symptom onset in relation to ICI cessation. However, in anticipation of future classification criteria having exposure restriction, we also conducted a sensitivity analysis in which patients who developed ICI-IA more than 365 days after ICI discontinuation were reclassified as not having ICI-IA. This resulted in only a slight decrease in performance measures. The decline in sensitivity may be partially attributed to the observed approximate five-month lag between patient-reported IA symptom onset in CanRIO-AB and subsequent first IA-coded health care visit. This observed lag and corresponding attenuation in sensitivity should inform the use of ICD code–based definitions of ICI-IA that are meant to reflect IA symptom onset in relation to ICI use. For example, if the clinical criteria for ICI-IA requires that IA onset is within one year of ICI cessation, the ICD code–based case definition of ICI-IA may require that the first IA code be coded within 18 months of ICI cessation to account for the lag observed between IA symptom onset and first IA-coded visit.

In our core set of algorithms that required multiple IA codes, we chose to apply a liberal time restriction of maximum three years between codes because patients with ICI-IA are often followed by oncologists, who are less likely to enter ICI-IA codes versus cancer-related codes for their visit diagnosis (even though in Alberta a physician can enter up to three diagnostic codes for any outpatient visit, most only enter one). Applying a more restrictive one-year or two-year time restriction between multiple IA codes only decreased sensitivity without increasing specificity. Although similar findings have been reported for rheumatoid arthritis, with sensitivity of 77% to 84% when a one-year or two-year time restriction was applied between codes, compared to a sensitivity of 90% if there was no time restriction,[36] the drop in sensitivity was more pronounced for ICI-IA. These findings highlight that strict time restrictions between multiple IA codes can result in missing true ICI-IA cases, without improving specificity. Using rheumatoid arthritis–only ICD codes did not change the performance measures, so the core case definitions could be

Table 5. Performance of additional criteria for ICI-IA case definitions with 95% confidence intervals, N = 228*

Case definition	Sensitivity	Specificity	PPV	NPV	C-statistic
IA onset within 365 days after ICI discontinuation					
≥1P	87.5 (80.9–94.1)	84.1 (77.9–90.3)	80.0 (72.3–87.7)	90.2 (85.0–95.5)	0.86 (0.81–0.90)
≥2P	67.7 (58.4–77.1)	91.7 (87.0–96.4)	85.5 (77.6–93.4)	79.6 (73.2–86.0)	0.80 (0.74–0.85)
≥3P	60.4 (50.6–70.2)	93.9 (89.9–98.0)	87.9 (80.0–95.8)	76.5 (70.0–83.1)	0.77 (0.72–0.83)
≥1H	–	–	–	–	–
≥1H or ≥1P	87.5 (80.9–94.1)	84.1 (77.9–90.3)	80.0 (72.3–87.7)	90.2 (85.0–95.5)	0.86 (0.81–0.90)
≥1H or ≥2P	67.7 (58.4–77.1)	91.7 (87.0–96.4)	85.5 (77.6–93.4)	79.6 (73.2–86.0)	0.80 (0.74–0.85)
≥1H or ≥3P	60.4 (50.6–70.2)	93.9 (89.9–98.0)	87.9 (80.0–95.8)	76.5 (70.0–83.1)	0.77 (0.72–0.83)
Rheumatoid arthritis ICD codes only (714.x, M05.x, M06.x)					
≥1P	88.0 (81.6–94.4)	86.7 (80.8–92.6)	83.8 (76.8–90.9)	90.2 (85.0–95.5)	0.87 (0.83–0.92)
≥2P	68.0 (58.9–77.1)	93.8 (89.6–97.9)	89.5 (82.6–96.4)	78.9 (72.5–85.4)	0.81 (0.76–0.86)
≥3P	59.0 (49.4–68.6)	95.3 (91.7–99.0)	90.8 (83.7–97.8)	74.8 (68.2–81.5)	0.77 (0.72–0.82)
≥1H	1.0 (0.0–3.0)	100.0 (100.0–100.0)	100.0 (100.0–100.0)	56.4 (49.9–62.8)	0.51 (0.49–0.51)
≥1H or ≥1P	88.0 (81.6–94.4)	86.7 (80.8–92.6)	83.8 (76.8–90.9)	90.2 (85.0–95.5)	0.87 (0.83–0.92)
≥1H or ≥2P	68.0 (58.9–77.1)	93.8 (89.6–97.9)	89.5 (82.6–96.4)	78.9 (72.5–85.4)	0.81 (0.76–0.86)
≥1H or ≥3P	59.0 (49.4–68.6)	95.3 (91.7–99.0)	90.8 (83.7–97.8)	74.8 (68.2–81.5)	0.77 (0.72–0.82)
IA code by rheumatologist only					
≥1P	45.0 (35.2–54.8)	94.5 (90.6–98.5)	86.5 (77.3–95.8)	68.8 (61.9–75.6)	0.70 (0.64–0.75)
≥2P	23.0 (14.8–31.2)	97.7 (95.0–100.0)	88.5 (76.2–100.0)	61.9 (55.2–68.6)	0.60 (0.56–0.65)
≥3P	14.0 (7.2–20.8)	98.4 (96.3–100.0)	87.5 (71.3–100.0)	59.4 (52.8–66.0)	0.56 (0.53–0.60)
≥1H	1.0 (0.0–3.0)	100.0 (100.0–100.0)	100.0 (100.0–100.0)	56.4 (49.9–62.8)	56.4 (49.9–62.8)
≥1H or ≥1P	45.0 (35.2–54.8)	94.5 (90.6–98.5)	86.5 (77.3–95.8)	68.8 (61.9–75.6)	0.70 (0.64–0.75)
≥1H or ≥2P	24.0 (15.6–32.4)	97.7 (95.0–100.0)	88.9 (77.0–100.0)	62.2 (55.5–68.9)	0.61 (0.56–0.65)
≥1H or ≥3P	15.0 (8.0–22.0)	98.4 (96.3–100.0)	88.2 (72.9–100.0)	59.7 (53.1–66.3)	0.57 (0.53–0.60)
IA code by rheumatologist or internal medicine physician only					
≥1P	88.0 (81.6–94.4)	88.3 (82.7–93.9)	85.4 (78.6–92.2)	90.4 (85.2–95.6)	0.88 (0.84–0.92)
≥2P	67.0 (57.8–76.2)	93.8 (89.6–97.9)	89.3 (82.3–96.3)	78.4 (71.9–84.9)	0.80 (0.75–0.85)
≥3P	59.0 (49.4–68.6)	96.1 (92.7–99.5)	92.2 (85.6–98.8)	75.0 (68.4–81.6)	0.78 (0.72–0.83)
≥1H	1.0 (0.0–3.0)	100.0 (100.0–100.0)	100.0 (100.0–100.0)	56.4 (49.9–62.8)	0.51 (0.49–0.51)
≥1H or ≥1P	88.0 (81.6–94.4)	88.3 (82.7–93.9)	85.4 (78.6–92.2)	90.4 (85.2–95.6)	0.88 (0.84–0.92)
≥1H or ≥2P	67.0 (57.8–76.2)	93.8 (89.6–97.9)	89.3 (82.3–96.3)	78.4 (71.9–84.9)	0.80 (0.75–0.85)
≥1H or ≥3P	59.0 (49.4–68.6)	96.1 (92.7–99.5)	92.2 (85.6–98.8)	75.0 (68.4–81.6)	0.78 (0.72–0.83)
Including NACRS IA codes as either P or H codes					
≥1P	88.0 (81.6–94.4)	86.7 (80.8–92.6)	83.8 (76.8–90.9)	90.2 (85.0–95.5)	0.87 (0.83–0.92)
≥2P	68.0 (58.9–77.1)	93.8 (89.6–97.9)	89.5 (82.6–96.4)	78.9 (72.5–85.4)	0.81 (0.76–0.86)
≥3P	61.0 (51.4–70.6)	96.1 (92.7–99.5)	92.4 (86.0–98.8)	75.9 (69.3–82.5)	0.79 (0.73–0.84)
≥1H	2.0 (0.0–4.7)	100.0 (100.0–100.0)	100.0 (100.0–100.0)	56.6 (50.2–63.1)	0.51 (0.50–0.52)
≥1H or ≥1P	88.0 (81.6–94.4)	86.7 (80.8–92.6)	83.8 (76.8–90.9)	90.2 (85.0–95.5)	0.87 (0.83–0.92)
≥1H or ≥2P	68.0 (58.9–77.1)	93.8 (89.6–97.9)	89.5 (82.6–96.4)	78.9 (72.5–85.4)	0.81 (0.76–0.86)
≥1H or ≥3P	61.0 (51.4–70.6)	96.1 (92.7–99.5)	92.4 (86.0–98.8)	75.9 (69.3–82.5)	0.79 (0.73–0.84)
Multiple IA codes must be within 1 y of first IA code					
≥2P	65.0 (55.7–74.3)	93.8 (89.6–97.9)	89.0 (81.9–96.2)	77.4 (70.8–84.0)	0.79 (0.74–0.85)
≥3P	48.0 (38.2–57.8)	96.1 (92.7–99.5)	90.6 (82.7–98.4)	70.3 (63.5–77.1)	0.72 (0.67–0.77)
≥1H or ≥2P	65.0 (55.7–74.3)	93.8 (89.6–97.9)	89.0 (81.9–96.2)	77.4 (70.8–84.0)	0.79 (0.74–0.85)
≥1H or ≥3P	48.0 (38.2–57.8)	96.1 (92.7–99.5)	90.6 (82.7–98.4)	70.3 (63.5–77.1)	0.72 (0.67–0.77)
Multiple IA codes must be within 2 y of the first IA code					
≥2P	68.0 (58.9–77.1)	93.8 (89.6–97.9)	89.5 (82.6–96.4)	78.9 (72.5–85.4)	0.81 (0.76–0.86)
≥3P	58.0 (48.3–67.7)	96.1 (92.7–99.5)	92.1 (85.4–98.7)	74.5 (67.9–81.2)	0.77 (0.72–0.82)
≥1H or ≥2P	68.0 (58.9–77.1)	93.8 (89.6–97.9)	89.5 (82.6–96.4)	78.9 (72.5–85.4)	0.81 (0.76–0.86)
≥1H or ≥3P	58.0 (48.3–67.7)	96.1 (92.7–99.5)	92.1 (85.4–98.7)	74.5 (67.9–81.2)	0.77 (0.72–0.82)
Addition of PMR codes					
≥1P	88.0 (81.6–94.4)	75.8 (68.4–83.2)	73.9 (66.1–81.8)	89.0 (83.1–94.9)	0.82 (0.77–0.87)
≥2P	68.0 (58.9–77.1)	85.2 (79.0–91.3)	78.2 (69.5–86.8)	77.3 (70.4–84.2)	0.77 (0.71–0.82)
≥3P	61.0 (51.4–70.6)	88.3 (82.7–93.9)	80.3 (71.3–89.2)	74.3 (67.4–81.3)	0.75 (0.69–0.80)
≥1H	1.0 (0.0–3.0)	98.4 (96.3–100.0)	33.3 (0.0–86.7)	56.0 (49.5–62.5)	0.50 (0.49–0.52)

(Continued)

Table 5. (*Cont'd*)

Case definition	Sensitivity	Specificity	PPV	NPV	C-statistic
≥1H or ≥1P	88.0 (81.6–94.4)	75.8 (68.4–83.2)	73.9 (66.1–81.8)	89.0 (83.1–94.9)	0.82 (0.77–0.87)
≥1H or ≥2P	68.0 (58.9–77.1)	85.2 (79.0–91.3)	78.2 (69.5–86.8)	77.3 (70.4–84.2)	0.77 (0.71–0.82)
≥1H or ≥3P	61.0 (51.4–70.6)	88.3 (82.7–93.9)	80.3 (71.3–89.2)	74.3 (67.4–81.3)	0.75 (0.69–0.80)
Addition of at least one filled prescription of glucocorticoid or DMARD within 40 days (before or after) of the first code of ICI-IA					
≥1P	77.0 (68.8–85.2)	89.8 (84.6–95.1)	85.6 (78.3–92.8)	83.3 (77.1–89.6)	0.83 (0.79–0.88)
≥2P	63.0 (53.5–72.5)	93.8 (89.6–97.9)	88.7 (81.4–96.1)	76.4 (69.8–83.1)	0.78 (0.73–0.84)
≥3P	57.0 (47.3–66.7)	96.1 (92.7–99.5)	91.9 (85.2–98.7)	74.1 (67.4–80.8)	0.77 (0.71–0.82)
≥1H	1.0 (0.0–3.0)	100.0 (100.0–100.0)	100.0 (100.0–100.0)	56.4 (49.9–62.8)	0.51 (0.49–0.51)
≥1H or ≥1P	77.0 (68.8–85.2)	89.8 (84.6–95.1)	85.6 (78.3–92.8)	83.3 (77.1–89.6)	0.83 (0.79–0.88)
≥1H or ≥2P	63.0 (53.5–72.5)	93.8 (89.6–97.9)	88.7 (81.4–96.1)	76.4 (69.8–83.1)	0.78 (0.73–0.84)
≥1H or ≥3P	57.0 (47.3–66.7)	96.1 (92.7–99.5)	91.9 (85.2–98.7)	74.1 (67.4–80.8)	0.77 (0.71–0.82)

* "–" denotes case definitions for which no patients met the case definition. DMARD, disease-modifying antirheumatic drug; H, Discharge Abstract Database code; IA, inflammatory arthritis; ICD, *International Classification of Diseases*; ICI, immune checkpoint inhibitor; ICI-IA, immune checkpoint inhibitor–associated inflammatory arthritis; NACRS, National Ambulatory Care Reporting System; NPV, negative predictive value; P, Physician Claims Database code; PMR, polymyalgia rheumatica; PPV, positive predictive value.

further simplified to only rheumatoid arthritis ICD codes without losing accuracy. The best PPVs were achieved when restricting to IA codes by rheumatologists, and thus, these additional criteria may be beneficial when identifying ICI-IA cases from cohorts with low ICI-IA prevalence.

Strengths of this study include the relatively large sample size of rheumatologist-confirmed cases of ICI-IA versus controls. Cancer diagnoses were ascertained from the Alberta Cancer Registry, which has been validated and received gold star certification from the North American Association of Central Cancer Registries, with more than 95% case ascertainment.[40,41] ICIs are covered in Alberta under the provincial health plan and are administered in a hospital setting, ensuring a high ascertainment rate of ICI therapy at the population level. Similarly, physician, hospital, and emergency department visits are covered by the provincial health plan, and thus, all visits within the province are captured in the provincial health administrative databases. Using these databases, we were able to look back three years before the ICI initiation date to evaluate pre-existing IA to ensure that our case definitions were able to discriminate those with a flare of pre-existing IA from true ICI-IA. We conducted a sex-stratified analysis, although ICI-IA does not appear to have a sex predilection unlike most rheumatic diseases, and the analysis showed that estimates of performance were similar between women and men, with overlapping 95% CIs, providing reassurance that our case definitions can be used across sexes.

We acknowledge that this study has limitations. The CanRIO-AB database only includes patients referred to rheumatologists, which may bias our sample toward patients with better access to rheumatology care and/or those with persistent or more severe joint symptoms. Thus, the performance of the case definitions tested in this study may not generalize to ICI users who experience mild or transient joint symptoms or to those with limited access to rheumatologists. Additionally, the PPV and NPV estimates reported in this study will vary depending on the prevalence of ICI-IA of the population to which these case definitions are applied. Similarly, the choice of the "best" case definition(s) will depend on whether sensitivity or specificity is the priority for a given use case. A recent study examined the incidence rate of ICI-IA using various unvalidated ICD code–based case definitions and found that the incidence rate ranged from two to seven per 100 person-years depending on the case definition used,[13] underscoring the importance of evaluating the attributes of all case definitions that are being used. Finally, although this study validated the case definitions using population-level data in Alberta, external validation is required to assess the performance of these case definitions in other regions.

In conclusion, ICD code–based case definitions can accurately detect ICI-IA in administrative health data, and a simple algorithm of at least one IA PCD code demonstrated a good balance of sensitivity and specificity in both sexes. However, the selection of the ICI-IA ICD code–based case definition for use in a given study will depend on the use setting and the relative importance of optimizing PPV versus NPV. Development of a specific ICD code for ICI-IA would likely improve the accuracy of ICI-IA case detection using administrative health data, but in its absence, this study supports the use of currently available ICD code–based case definitions of ICI-IA for disease surveillance and research using administrative health data.

AUTHOR CONTRIBUTIONS

All authors contributed to at least one of the following manuscript preparation roles: conceptualization AND/OR methodology, software, investigation, formal analysis, data curation, visualization, and validation AND drafting or reviewing/editing the final draft. As corresponding author, Dr Ye confirms that all authors have provided the final approval of the version to be published and takes responsibility for the affirmations regarding article submission (eg, not under consideration by another journal), the integrity of the data presented, and the statements regarding compliance with institutional review board/Declaration of Helsinki requirements.

REFERENCES

1. Siamof CM, Goel S, Cai W. Moving beyond the pillars of cancer treatment: perspectives from nanotechnology. Front Chem 2020;8:598100. doi:10.3389/fchem.2020.598100
2. Wang SJ, Dougan SK, Dougan M. Immune mechanisms of toxicity from checkpoint inhibitors. Trends Cancer 2023;9(7):543–553. doi:10.1016/j.trecan.2023.04.002
3. Ramos-Casals M, Brahmer JR, Callahan MK, et al. Immune-related adverse events of checkpoint inhibitors. Nat Rev Dis Primers 2020;6(1):38. doi:10.1038/s41572-020-0160-6
4. Cappelli LC, Gutierrez AK, Baer AN, et al. Inflammatory arthritis and sicca syndrome induced by nivolumab and ipilimumab. Ann Rheum Dis 2017;76(1):43–50. doi:10.1136/annrheumdis-2016-209595
5. Kuswanto WF, MacFarlane LA, Gedmintas L, et al. Rheumatologic symptoms in oncologic patients on PD-1 inhibitors. Semin Arthritis Rheum 2018;47(6):907–910. doi:10.1016/j.semarthrit.2017.10.018
6. Belkhir R, Burel SL, Dunogeant L, et al. Rheumatoid arthritis and polymyalgia rheumatica occurring after immune checkpoint inhibitor treatment. Ann Rheum Dis 2017;76(10):1747–1750. doi:10.1136/annrheumdis-2017-211216
7. Calabrese C, Kirchner E, Kontzias A, et al. Rheumatic immune-related adverse events of checkpoint therapy for cancer: case series of a new nosological entity. RMD Open 2017;3(1):e000412. doi:10.1136/rmdopen-2016-000412
8. Roberts J, Ennis D, Hudson M, et al. Rheumatic immune-related adverse events associated with cancer immunotherapy: a nationwide multi-center cohort. Autoimmun Rev 2020;19(8):102595. doi:10.1016/j.autrev.2020.102595
9. Hoa S, Laaouad L, Roberts J, et al. Preexisting autoimmune disease and immune-related adverse events associated with anti-PD-1 cancer immunotherapy: a national case series from the Canadian Research Group of Rheumatology in Immuno-Oncology. Cancer Immunol Immunother 2021;70(8):2197–2207. doi:10.1007/s00262-021-02851-5
10. Lee K, Elahi S, Mashhouri S, et al. Gout presenting as a chronic inflammatory arthritis from immune checkpoint inhibitors: case series. Rheumatology (Oxford) 2021;60(12):e441–e443. doi:10.1093/rheumatology/keab608
11. Shen P, Deng X, Hu Z, et al. Rheumatic manifestations and diseases from immune checkpoint inhibitors in cancer immunotherapy. Front Med (Lausanne) 2021;8:762247. doi:10.3389/fmed.2021.762247
12. Cappelli LC, Gutierrez AK, Bingham CO III, et al. Rheumatic and musculoskeletal immune-related adverse events due to immune checkpoint inhibitors: a systematic review of the literature. Arthritis Care Res (Hoboken) 2017;69(11):1751–1763. doi:10.1002/acr.23177
13. Bass AR, Xie F, Jannat-Khah D, et al. Incidence of checkpoint inhibitor-associated inflammatory arthritis, immunomodulation and mortality in cancer patients on immunotherapy: a retrospective cohort study. Rheumatology (Oxford) 2025;64(4):1637–1642. doi:10.1093/rheumatology/keae343
14. Roberts J, Barmettler S, Murray J, et al. Musculoskeletal immune-related adverse events of PD-(L)1 inhibitors in melanoma: a systematic review and meta-analysis. Immunotherapy 2024;16(20–22):1247–1254. doi:10.1080/1750743X.2024.2436838
15. Angelopoulou F, Bogdanos D, Dimitroulas T, et al. Immune checkpoint inhibitor-induced musculoskeletal manifestations. Rheumatol Int 2021;41(1):33–42. doi:10.1007/s00296-020-04665-7
16. Heyward JS, Segal JB, Mehta HB, et al. Validation of immune-related adverse event (irAE) case definitions in a real-world lung cancer population. Pharmacoepidemiol Drug Saf 2025;34(2):e70100. doi:10.1002/pds.70100
17. Bejan CA, Wang M, Venkateswaran S, et al. irAE-GPT: leveraging large language models to identify immune-related adverse events in electronic health records and clinical trial datasets. medRxiv Preprint posted online March 6, 2025. doi:10.1101/2025.03.05.25323445
18. Bernatsky S, Lix L, O'Donnell S, et al; CANRAD Network. Consensus statements for the use of administrative health data in rheumatic disease research and surveillance. J Rheumatol 2013;40(1):66–73. doi:10.3899/jrheum.120835
19. Kalinich M, Murphy W, Wongvibulsin S, et al. Prediction of severe immune-related adverse events requiring hospital admission in patients on immune checkpoint inhibitors: study of a population level insurance claims database from the USA. J Immunother Cancer 2021;9(3):e001935. doi:10.1136/jitc-2020-001935
20. Tang K, Seo J, Tiu BC, et al. Association of cutaneous immune-related adverse events with increased survival in patients treated with anti-programmed cell death 1 and anti-programmed cell death ligand 1 therapy. JAMA Dermatol 2022;158(2):189–193. doi:10.1001/jamadermatol.2021.5476
21. Xia T, Brucker AJ, McGeehan B, et al. Risk of non-infectious uveitis or myasthenia gravis in patients on checkpoint inhibitors in a large healthcare claims database. Br J Ophthalmol 2022;106(1):87–90. doi:10.1136/bjophthalmol-2020-317060
22. Government of Canada. Population estimates, quarterly. Statistics Canada. 2024. Accessed January 30, 2025. https://www150.statcan.gc.ca/t1/tbl1/en/tv.action?pid=1710000901
23. STROBE Checklists. STROBE. Accessed December 17, 2024.
24. Ladouceur A, Jamal S, Saltman A, et al. Chronicity of immune checkpoint inhibitor-associated inflammatory arthritis after immunotherapy discontinuation: results from the Canadian Research Group of Rheumatology in Immuno-Oncology database. ACR Open Rheumatol 2025;7(2):e70002. doi:10.1002/acr2.70002
25. Bujang MA, Adnan TH. Requirements for minimum sample size for sensitivity and specificity analysis. J Clin Diagn Res 2016;10(10):YE01–YE06. doi:10.7860/JCDR/2016/18129.8744
26. National Cancer Institute. CTCAE and Adverse Event Reporting. 2025. Accessed September 12, 2025. https://dctd.cancer.gov/research/ctep-trials/for-sites/adverse-events.
27. Gougis P, Jochum F, Abbar B, et al. Clinical spectrum and evolution of immune-checkpoint inhibitors toxicities over a decade-a worldwide perspective. EClinicalMedicine 2024;70:102536. doi:10.1016/j.eclinm.2024.102536
28. Braaten TJ, Brahmer JR, Forde PM, et al. Immune checkpoint inhibitor-induced inflammatory arthritis persists after immunotherapy cessation. Ann Rheum Dis 2020;79(3):332–338. doi:10.1136/annrheumdis-2019-216109
29. Cappelli LC, Brahmer JR, Forde PM, et al. Clinical presentation of immune checkpoint inhibitor-induced inflammatory arthritis differs by immunotherapy regimen. Semin Arthritis Rheum 2018;48(3):553–557. doi:10.1016/j.semarthrit.2018.02.011
30. Roberts J, Smylie M, Walker J, et al. Hydroxychloroquine is a safe and effective steroid-sparing agent for immune checkpoint inhibitor-induced inflammatory arthritis. Clin Rheumatol 2019;38(5):1513–1519. doi:10.1007/s10067-019-04451-2
31. Chan KK, Tirpack A, Vitone G, et al. Higher checkpoint inhibitor arthritis disease activity may be associated with cancer progression: results from an observational registry. ACR Open Rheumatol 2020;2(10):595–604. doi:10.1002/acr2.11181
32. Cappelli LC, Bingham CO, Forde PM, et al. Anti-RA33 antibodies are present in a subset of patients with immune checkpoint inhibitor-induced inflammatory arthritis. RMD Open 2022;8(2):e002511. doi:10.1136/rmdopen-2022-002511
33. Ghosh N, Tiongson MD, Stewart C, et al. Checkpoint inhibitor-associated arthritis: a systematic review of case reports and case series. J Clin Rheumatol 2021;27(8):e317–e322. doi:10.1097/RHU.0000000000001370

34. Ladouceur A, Ezdoglian A, Sparks JA, et al. The utility of laboratory investigations for the assessment and management of rheumatic immune related adverse events. Rheum Dis Clin North Am 2024; 50(2):181–199. doi:10.1016/j.rdc.2024.01.003
35. Bass AR, Abdel-Wahab N, Reid PD, et al. Comparative safety and effectiveness of TNF inhibitors, IL6 inhibitors and methotrexate for the treatment of immune checkpoint inhibitor-associated arthritis. Ann Rheum Dis 2023;82(7):920–926. doi:10.1136/ard-2023-223885
36. Widdifield J, Bombardier C, Bernatsky S, et al. An administrative data validation study of the accuracy of algorithms for identifying rheumatoid arthritis: the influence of the reference standard on algorithm performance. BMC Musculoskelet Disord 2014;15(1):216. doi:10.1186/1471-2474-15-216
37. Widdifield J, Bernatsky S, Paterson JM, et al. Accuracy of Canadian health administrative databases in identifying patients with rheumatoid arthritis: a validation study using the medical records of rheumatologists. Arthritis Care Res (Hoboken) 2013;65(10):1582–1591. doi:10.1002/acr.22031
38. Eder L, Widdifield J, Rosen CF, et al. Identifying and characterizing psoriasis and psoriatic arthritis patients in Ontario administrative data: a population-based study from 1991 to 2015. J Rheumatol 2020; 47(11):1644–1651. doi:10.3899/jrheum.190659
39. Ghosh N, Jivanelli B, Couette N, et al. The need for classification criteria of immune checkpoint inhibitor-induced inflammatory arthritis: a scoping review. Rheum Dis Clin North Am 2024;50(2):325–335. doi:10.1016/j.rdc.2024.02.006
40. Cairncross ZF, Nelson G, Shack L, et al. Validation in Alberta of an administrative data algorithm to identify cancer recurrence. Curr Oncol 2020;27(3):e343–e346. doi:10.3747/co.27.5861
41. The 2019 Report on Cancer Statistics in Alberta. Alberta Health Services; 2019.
42. Harrington JT. The uses of disease activity scoring and the physician global assessment of disease activity for managing rheumatoid arthritis in rheumatology practice. J Rheumatol 2009;36(5):925–929. doi:10.3899/jrheum.081046

Check for updates

Arthritis & Rheumatology
Vol. 78, No. 10, October 2026, pp 2171–2178
DOI 10.1002/art.70132
© 2026 The Author(s). *Arthritis & Rheumatology* published by Wiley Periodicals LLC on behalf of American College of Rheumatology.
This is an open access article under the terms of the Creative Commons Attribution License, which permits use, distribution and reproduction in any medium, provided the original work is properly cited.

American College of Rheumatology
Empowering Rheumatology Professionals

Coverage Generosity of Novel Antirheumatic Drugs in Medicare Advantage and Stand-Alone Part D Plans

Youngmin Kwon, PhD,[1] Robert W. Corty, MD, PhD,[2] and Stacie B. Dusetzina, PhD[1]

Objective. We examine coverage of self-administered disease-modifying antirheumatic drugs (DMARDs) in Medicare Part D.

Methods. Using 2022–2026 Part D formulary data, we assessed coverage of the following DMARD classes that treat relapsed rheumatoid arthritis (RA): tumor necrosis factor (TNF) inhibitors, T cell costimulatory modulator, interleukin-6 (IL-6) inhibitors, and JAK inhibitors. We measured (1) coverage of individual DMARDs and (2) the generosity of coverage between classes (the share of plans covering at least one drug in each class) and within classes (the share of covered drugs within each class).

Results. We included 26,915 plan-year observations, representing 217.6 million enrolled beneficiaries from 2022 to 2026. In the five-year period, coverage was relatively complete (>94%) for etanercept and adalimumab (TNF inhibitors) and upadacitinib (JAK inhibitor). However, coverage was lower for golimumab and certolizumab (TNF inhibitors), abatacept (the sole T cell costimulatory modulator), sarilumab (IL-6 inhibitor), and baricitinib (JAK inhibitor). Moreover, only 10.4% and 37.6% of stand-alone and Medicare Advantage (MA) Part D plans, respectively, covered all mechanisms of action, mostly due to low coverage of abatacept. In 2026, only 0.3% and 21.2% of stand-alone and MA Part D plans, respectively, covered abatacept. On the other hand, coverage increased for IL-6 inhibitors, likely due to the availability of biosimilar drugs for tocilizumab in 2024.

Conclusion. The growing exclusions of self-administered DMARDs across several mechanisms of action and heterogeneity in coverage by plan type suggest potential barriers to accessing optimal RA treatments. Further monitoring of formulary adequacy and research into the clinical impacts of formulary exclusions are warranted.

INTRODUCTION

Clinical management of rheumatoid arthritis (RA) has been greatly improved by the introduction of novel disease-modifying antirheumatic drugs (DMARDs), including biologic DMARDs and targeted-synthetic DMARDs. These novel therapies reduce symptom burden and improve health-related quality of life by delaying joint damage in patients with an inadequate response to conventional synthetic DMARDs that are commonly prescribed as first-line treatment.[1,2]

Because not all novel DMARDs are equally efficacious or safe for each patient, finding a suitable treatment often involves switching to a DMARD with a different mechanism of action or cycling within the same drug class.[3] This suggests that having access to a broad range of DMARDs is crucial for optimal RA management. However, the high costs of DMARDs have led health insurers to restrict coverage. For example, in prior studies of coverage in the Medicare Part D program (which administers prescription drug benefits for Medicare beneficiaries), between 69% and 79% of all DMARDs were covered by Part D plans and nearly all drugs were subjected to utilization restrictions, such as prior authorization.[4,5] Restrictive coverage of DMARDs has fueled concerns that Medicare beneficiaries may face inadequate access to DMARDs,[6] which may exacerbate the burden of RA among older adults.[7]

Medicare coverage of novel DMARDs is further complicated by the fact that coverage for a specific drug may vary by its route

The content is solely the responsibility of the authors and does not necessarily represent the official views of Arnold Ventures, Commonwealth Fund, Institute for Clinical and Economic Review, or the Medicare Payment Advisory Commission.

Supported by grants from Arnold Ventures and the Commonwealth Fund (principal investigator: Dr Dusetzina).

[1]Department of Health Policy, Vanderbilt University Medical Center, Nashville, Tennessee; [2]Division of Rheumatology and Immunology, Department of Medicine, Vanderbilt University Medical Center, Nashville, Tennessee.

Additional supplementary information cited in this article can be found online in the Supporting Information section (https://acrjournals.onlinelibrary.wiley.com/doi/10.1002/art.70132).

Author disclosures are available at https://onlinelibrary.wiley.com/doi/10.1002/art.70132.

Address correspondence via email to Youngmin Kwon, PhD, at Youngmin.kwon@vumc.org.

Submitted for publication October 16, 2025; accepted in revised form February 26, 2026.

of administration and whether a beneficiary is enrolled in traditional Medicare (TM) versus Medicare Advantage (MA).[8] Many DMARDs are self-administered medications, which are covered under Medicare's pharmacy benefit (Part D), whereas other clinician-administered DMARDs are covered under Medicare's outpatient medical benefit (Part B).[9] In TM, Part D benefits are separately administered and reimbursed through "stand-alone" private plans, whereas Part B benefits are reimbursed by the federal Medicare program. In contrast, Part B and Part D benefits are integrated within MA, with reimbursement through a single private MA plan. Given differences in benefit design and preferences for clinician-administered versus self-administered medications between MA and stand-alone plans,[10,11] coverage of DMARDs may differ by the type of plan in which beneficiaries are enrolled.

Given mounting concerns about inadequate access to novel DMARDs in Medicare, we provide recent insights into self-administered DMARD coverage in Medicare Part D and compare DMARD coverage across plan types (stand-alone vs. MA Part D plans). Importantly, our analysis spans years following the Part D benefit redesign under the Inflation Reduction Act (IRA),[12] which may have generated additional financial pressure to exclude coverage by sharply increasing Part D plans' responsibility for catastrophic drug costs beyond a newly instituted $2,000 cap on out-of-pocket costs. Given the importance of breadth in DMARD coverage, we measured the generosity of coverage by examining how broadly plans cover DMARDs between and within mechanisms of action.

MATERIALS AND METHODS

Data and study population. We analyzed Part D plan formulary data from 2022 to 2026,[13] characterizing coverage of DMARDs in the first quarter of each year, separately by stand-alone and MA Part D plans. Our study population included plan-year observations for each stand-alone or MA Part D plan (identified using unique combinations of the contract and plan identifiers) that were available at any point during this period and contributing to the plan formulary data (data for certain plans are suppressed in the formulary data due to plan requests or data quality issues; see the Supplement for further details). To account for the share of beneficiaries represented by each plan, we also obtained plan enrollment data from the monthly Part D enrollment data. Institutional review board approval was waived because we analyzed publicly available plan-level data. We analyzed the data from March 2025 to January 2026.

Eligible DMARDs. We examined coverage of drugs belonging to the following classes of DMARDs that are guideline-recommended treatments for relapsed RA[2]: tumor necrosis factor (TNF) inhibitors (etanercept, adalimumab, golimumab, and certolizumab pegol), T cell costimulation modulator (abatacept), interleukin-6 (IL-6) inhibitors (tocilizumab and sarilumab), and JAK inhibitors (tofacitinib, baricitinib, and upadacitinib). These drugs are available as either subcutaneous or oral formulations, and some also have clinician-administered formulations. For each plan, we identified coverage for each unique ingredient, dose, and formulation for these products using their RxNorm concept unique identifiers listed in the US Centers for Medicare and Medicaid Services (CMS) Part D formulary reference file[14,15] (see e-Table 1 in the Supplement). Two other DMARDs, infliximab and rituximab, were excluded because they are primarily clinician-administered medications covered under Part B and are no longer listed in the formulary reference file as of 2020. For drugs with biosimilars (adalimumab and tocilizumab), we considered coverage of either the originator or the biosimilar as coverage for that product (we examined the sensitivity of our results to excluding biosimilar coverage from the analysis).

Outcomes. We initially determined per-plan coverage of each individual DMARD. Then, we constructed two measures of coverage generosity. First, we calculated the share of plans covering at least one drug in each class to examine the generosity of coverage across mechanisms of action (ie, between-class). Second, we calculated the share of drugs covered within each mechanism of action to ascertain the within-class coverage generosity. For this measure, we divided the number of covered drugs in the class (numerator) by the total number of drugs in the class (denominator).

As another measure of within-class coverage generosity, we determined the share of plans that cover at least two drugs in each class. For the T cell costimulatory modulator class, which included only a single drug (abatacept), we determined the share of plans covering abatacept. This latter evaluation assesses the adequacy of coverage by "simulating" the Part D formulary requirement that at least two different drugs be covered in each therapeutic class.[16]

Statistical analysis. We calculated regression-adjusted differences in outcomes between stand-alone and MA Part D plans, controlling for year fixed effects, reflecting the average across the six-year period. All estimates were weighted by plan enrollment in May of each year (up-weighing plans with a larger number of beneficiaries),[17] and standard errors were clustered at the plan level to account for within-plan clustering of outcomes across years. We also compared annual trends in outcomes across plans separately for stand-alone and MA Part D plans. We analyzed the data using SAS Studio and STATA MP 14.

We conducted several sensitivity analyses. First, we reanalyzed the data for plans available throughout the study period to account for insurer exits from the Part D market, especially following the Part D benefit redesign.[18] Second, we further excluded Special Needs Plans and regional plans from the sample to focus on representative plans that were available to all Medicare

beneficiaries. Third, we replicated the analysis but included two drugs (anakinra and rilonacept[19,20]) belonging to an additional drug class—IL-1 inhibitor—which is less commonly used and often prescribed as off-label treatment for RA (we note that canakinumab is another drug in this category but was not included in Part D formularies during the study period). Third, we assessed the use of other formulary restrictions, including utilization management (prior authorization, step therapy, or quantity limits) and placement on a specialty tier, conditional on coverage.

RESULTS

Overall pooled differences in DMARDs coverage generosity between stand-alone and MA Part D plans from 2022 to 2026. We included 26,915 plan-year observations, representing 217.6 million enrolled beneficiaries from 2022 to 2026 (weighted proportions were 58.2% and 41.8% for stand-alone and MA Part D plans, respectively). During the five-year period we examined, we found varying DMARD coverage across regimens and plan types (Table 1). Coverage was nearly universal for etanercept, adalimumab, and upadacitinib (>94% of plans providing coverage). However, coverage was lower for other DMARDs, including golimumab and certolizumab (TNF inhibitors), abatacept (T cell costimulatory modulator), sarilumab (IL-6 inhibitor), and baricitinib (JAK inhibitor).

In terms of coverage generosity, 10.4% and 37.6% of stand-alone and MA Part D plans, respectively, covered all mechanisms of action (Table 2). Among stand-alone plans, the mean coverage share was 48.5% for TNF inhibitors, 19.4% for T cell costimulatory modulators, 31.3% for IL-6 inhibitors, and 53.4% for JAK inhibitors. Among MA Part D plans, the mean coverage share was 61.7% for TNF inhibitors, 44.8% for T cell costimulatory modulators, 42.7% for IL-6 inhibitors, and 60.5% for JAK inhibitors.

Table 1. Mean coverage of specific disease-modifying therapy for relapsed rheumatoid arthritis by stand-alone and MA Part D plans during 2022–2026*

Coverage, %[a]	Stand-alone plans, mean (95% CI)	MA plans, mean (95% CI)
TNF inhibitors		
Etanercept	93.9 (92.5–95.4)	96.1 (95.6–96.6)
Adalimumab	100 (100–100)	100 (100–100)
Golimumab	0.1 (0–0.2)	23.8 (21.6–26)
Certolizumab	0.1 (0–0.2)	26.8 (24.6–29)
T cell costimulatory modulator		
Abatacept	19.4 (16.4–22.3)	44.8 (42.1–47.5)
IL-6 inhibitors		
Tocilizumab	47.9 (44.3–51.5)	58.1 (55.8–60.4)
Sarilumab	14.6 (12.5–16.8)	27.4 (25.3–29.5)
JAK inhibitors		
Tofacitinib	64.9 (61.4–68.4)	73.1 (70.9–75.4)
Baricitinib	0.1 (0–0.2)	9.1 (6.8–11.5)
Upadacitinib	95.1 (93.3–96.9)	99.4 (99.1–99.6)

* CI, confidence interval; IL-6, interleukin-6; MA, Medicare Advantage; TNF, tumor necrosis factor.
[a] The pooled yearly average of plans covering each drug, separately shown for stand-alone and MA plans, adjusting for secular trends (via year fixed effects) from 2022 to 2026. All estimates were clustered at the plan level to account for within-plan clustering over the study period and were weighted by plan enrollment in May of each year, giving plans with a larger number of beneficiaries greater weight.

Trends in DMARDs coverage by plan type. In examining trends in coverage for specific DMARDs, we observed a changing coverage landscape for all DMARDs except etanercept, adalimumab, and upadacitinib in both stand-alone and MA plans (Figure 1). Among stand-alone plans, coverage was essentially null for golimumab, certolizumab, and baricitinib throughout 2022 to 2026. The trend in coverage was more volatile for abatacept, sarilumab, and tofacitinib. On the other hand, MA plans had more consistent coverage throughout this period.

At the same time, several notable trends emerged in the later years of the study. For instance, there were large drops in coverage of golimumab, certolizumab, abatacept, sarilumab, and baricitinib in 2025 and 2026. For both stand-alone and MA plans, tocilizumab coverage increased progressively, reaching near-universal coverage in 2026.

When analyzing the trends in coverage generosity measures, we note that the share of plans covering all mechanisms of action sharply dropped from 11.7% to 0.3% for stand-alone plans and 42.3% to 21.2% for MA Part D plans, due to many plans excluding abatacept from their formularies from 2025 to 2026 (Figure 2). The trend in coverage share was relatively stable for TNF inhibitors or progressively increasing for IL-6 inhibitors.

Sensitivity analyses. Our results were robust to limiting the sample to plans available throughout the study period (eTable 2) and to representative plans only (eTable 3). Although excluding biosimilars from the analysis did not change our main conclusions, we found that biosimilars accounted for the substantial increase in tocilizumab coverage (eTable 4).

Our finding on between-class coverage generosity remained consistent when IL-1 inhibitors were included in our analysis (eTable 5). Because essentially all plans covered at least one IL-1 inhibitor, inclusion of IL-1 inhibitors did not impact the estimate of plans covering all mechanisms of action. Notably, there was a sharp increase in coverage of anakinra from 0.3% to 84.1% among stand-alone plans and 13.3% to 68.6% among MA plans from 2025 to 2026.

Although the use of other formulary restrictions was high across plan types, stand-alone plans were more likely to apply utilization management and place DMARDs on specialty tiers than MA plans (eTable 6). We also detected some regional variations in coverage; plans operating in the West and Northeast had more generous coverage than plans operating in the Midwest and South (eTable 7).

When applying the minimum threshold of two drugs per class to determine within-class generosity, we found

Table 2. Coverage generosity of disease-modifying therapy for relapsed rheumatoid arthritis in stand-alone and MA Part D plans, 2022–2026*

Coverage generosity measures[a]	Stand-alone plans, mean (95% CI)	MA plans, mean (95% CI)
Covering all mechanism of action, %[b]	10.4 (8.4–12.5)	37.6 (34.9–40.2)
Coverage share of TNF inhibitors (4), %[c,d]	48.5 (48.2–48.9)	61.7 (60.5–62.8)
Coverage share of T cell costimulatory modulator (1), %[c,e]	19.4 (16.4–22.3)	44.8 (42.1–47.5)
Coverage share of IL-6 inhibitors (2), %[c,f]	31.3 (29.5–33.1)	42.7 (41.2–44.3)
Coverage share of JAK inhibitors (3), %[c,g]	53.4 (52.1–54.6)	60.5 (59.3–61.8)

* CI, confidence interval; IL-6, interleukin-6; MA, Medicare Advantage; TNF, tumor necrosis factor.
[a] The table displays the pooled yearly average of the coverage generosity measure for stand-alone and MA plans, adjusting for secular trends (via year fixed effects) from 2022 to 2026. All estimates were clustered at the plan level to account for within-plan clustering over the study period and were weighted by plan enrollment in May of each year, giving plans with a larger number of beneficiaries greater weight.
[b] Proportion of plans covering at least one drug belonging to each mechanism of action.
[c] Coverage share for each plan was determined by dividing the number of covered drugs in each mechanism of action (numerator) by the total number of drugs belonging to each class (denominator), which is indicated by the number in parentheses.
[d] TNF inhibitors included etanercept, adalimumab (or its biosimilar), golimumab, or certolizumab pegol.
[e] Abatacept is the only T cell costimulatory modulator included in the analysis.
[f] IL-6 inhibitors included tocilizumab (or its biosimilar drug) and sarilumab.
[g] JAK inhibitors included tofacitinib, baricitinib, and upadacitinib.

comparatively high levels of coverage generosity between stand-alone and MA plans for TNF inhibitors (93.9% and 96.1%, respectively) and JAK inhibitors (60.0% and 72.5%, respectively; e-Table 8). For JAK inhibitors, tofacitinib and upadacitinib were the preferred drugs, with virtually no plans covering baricitinib. The share of plans covering both IL-6 inhibitors was low for both stand-alone plans (0.1%) and MA plans (9.0%), with most plans exclusively covering tocilizumab rather than sarilumab.

DISCUSSION

In this national study of Medicare Part D plan formularies, we observed general trends of reduced coverage of novel, self-administered DMARDs treating relapsed RA from 2022 to 2026. In 2026, there was a noticeable drop in plans covering abatacept, the sole T cell costimulatory inhibitor, which considerably reduced the share of plans covering all mechanisms of action (with few to no stand-alone plans covering abatacept in 2026). Moreover, we found low shares of plans covering golimumab and certolizumab (TNF inhibitors), sarilumab (IL-6 inhibitor), and baricitinib (JAK inhibitor). In contrast, coverage of tocilizumab has substantially increased in 2026, likely driven by the launch of its biosimilar in 2024.[21] In general, the coverage of DMARDs was more generous among MA plans as opposed to stand-alone plans, both across and within classes.

This declining coverage of DMARDs, as well as the differential coverage across plan types, has access implications for beneficiaries who need such treatments. In clinical practice, switching to alternative DMARDS between and within drug classes to address treatment failure and nonresponse or to avoid contraindicated medications is increasingly common.[22,23] As such, formularies that restrict access to a wide range of DMARDs can limit physicians' and patients' autonomy in selecting the optimal care regimen. Moreover, beneficiaries who must switch from self-administered to clinician-administered DMARDs (due to Part D coverage exclusions) may face the time burden of regular infusions at physician practices and high out-of-pocket costs, especially if they are in TM without supplemental coverage.[24] Broadly, limited coverage of self-administered DMARDs may circumvent the goal of the Part D benefit redesign under the IRA to provide financial relief for Medicare beneficiaries filling high-cost drugs. Because the newly enacted $2,000 cap on out-of-pocket costs only applies to drugs covered by Part D formularies,[25] beneficiaries treated with DMARDs not covered by their plans may still experience access and affordability problems.

Given these observed changes in coverage, it is imperative that beneficiaries compare Part D plan options during open enrollment to ensure their plan includes the preferred DMARDs.[26] However, because most beneficiaries do not shop for plans after their initial enrollment decisions[12,27,28] and the number of available plans offering comprehensive coverage has decreased, many beneficiaries may remain in plans that may not provide optimal coverage. The search for optimal coverage is further complicated by the fact that patients may not know which DMARD(s) will be indicated for their use in the year(s) ahead. Given these facts, future studies should continue to examine how the Part D formulary evolves over time and illuminate any potential barriers to access and their impacts on patient outcomes.

Our study—focusing specifically on gaps in RA drug coverage—has larger implications for the adequacy of Part D formularies. The finding that plans issued narrowed coverage for RA drugs comports with the general trend of Part D plans covering fewer drugs over time (among all drugs eligible for Part D coverage), with the share of covered drugs decreasing from 73% in 2010 to 54% in 2024.[29] In providing additional evidence of this fact, we also highlight the differential trends in coverage generosity between stand-alone and MA plans. It is possible that these trends reflect diverging plan preferences for self-administered versus clinician-administered drugs, especially given clinical exchangeability between these formulations.[10,30] For instance, stand-alone plans may prefer less generous coverage of self-administered DMARDs in Part D to shift beneficiaries toward

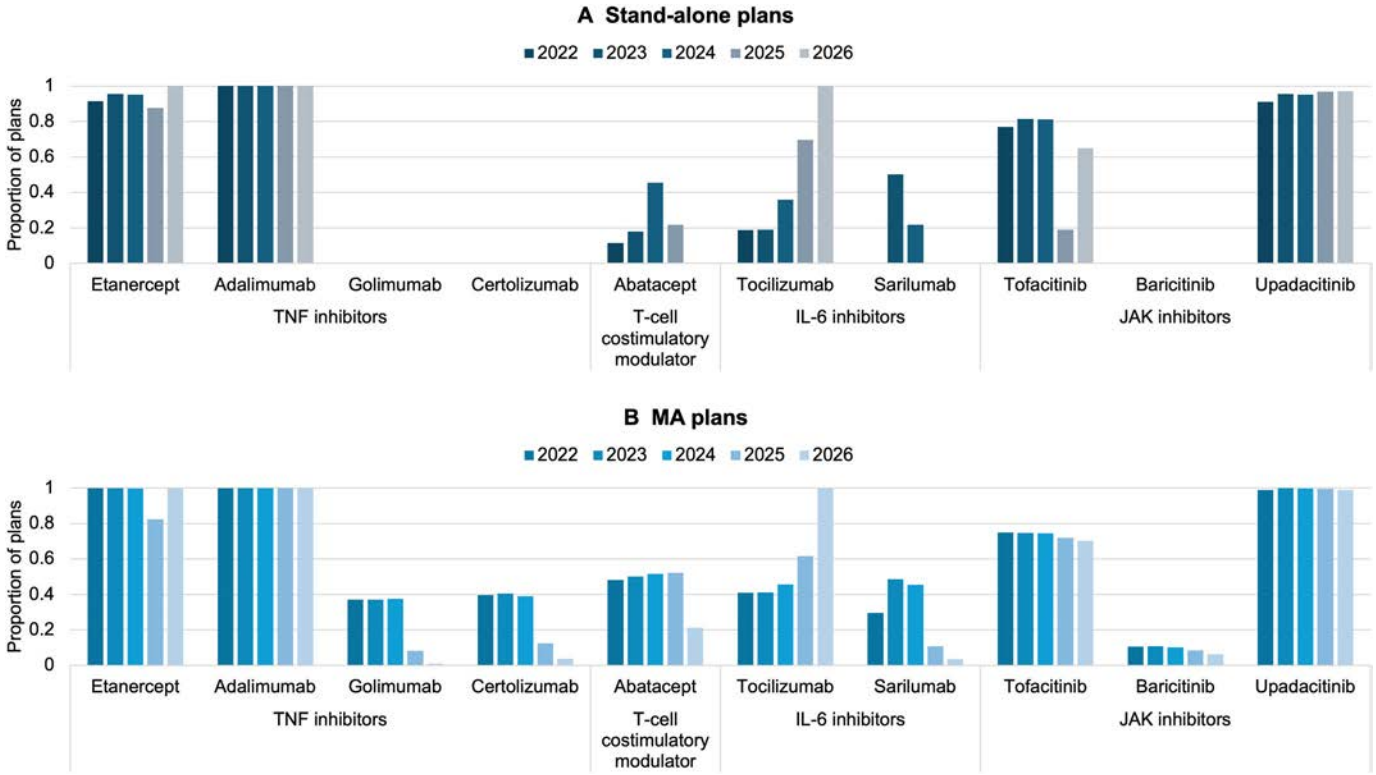


Figure 1. Trends in coverage of specific disease-modifying therapy for relapsed rheumatoid arthritis in stand-alone and MA Part D plans. The figure shows yearly trends in coverage for each DMARD under stand-alone Part D plans (A) and MA Part D plans (B). All estimates were clustered at the plan level to account for within-plan clustering over the study period and were weighted by plan enrollment in May of each year, giving plans with a larger number of beneficiaries greater weight. DMARD, disease-modifying antirheumatic drug; IL-6, interleukin-6; MA, Medicare Advantage; TNF, tumor necrosis factor.

clinician-administered drugs because they are only financially responsible for managing the pharmacy benefit. On the other hand, MA plans manage spending for both pharmacy and medical benefits and may prefer self-administered medications to reduce the administrative costs associated with infusions. In addition to these financial factors, MA plans may be weighing the safety and efficacy of clinician-administered versus self-administered medications, as well as preferences for different formulations, within their respective patient populations and among providers participating in their network.[10,31] With an increasing number of therapeutically equivalent medications that vary by routes of administration (eg, Ig treatments and interferon therapies for multiple sclerosis),[10,32] we may expect further heterogeneity in formulary coverage between stand-alone and MA Part D plans for these drugs. This underscores the need for additional research examining potential variations in coverage across plan types and the causal mechanisms underlying these variations.

Addressing the trend toward restrictive formularies may require regulators to revisit how they ascertain formulary adequacy. Statutorily, a key requirement of Part D formularies is the mandate to cover at least two drugs within therapeutic categories and classes. This provides some floor for coverage and allows CMS to identify formularies with egregious coverage gaps.[33,34] At the same time, plans have ample latitude in defining therapeutic categories and classes[35]; outside the six protected drug classes in which plans are required to cover "all or substantially all" drugs,[36] plans retain considerable freedom in determining the scope of coverage. To illustrate this issue in our context, we note that all included drugs in our study are listed under a very broad therapeutic category ("immunological agents" or "immunosuppressant") in the US Pharmacopeia, one of the drug classification systems used in formulary reviews.[16] Because this category encompasses many biologic medications, not all of which treat the same condition (like RA), the requirement to cover at least two drugs in this category does not necessarily translate into comprehensive coverage of RA drugs. Hypothetically, if drugs were categorized by their exact mechanisms of action (eg, T cell costimulatory modulator) for a particular condition, such as RA, as we have done in our simulation analysis, then formularies may face stricter minimum coverage requirements. Thus, the definition for therapeutic categories and classes may need to be reviewed to ensure adequate coverage for distinct conditions.

However, there are important trade-offs to mandating more comprehensive DMARD coverage. Imposing a requirement for

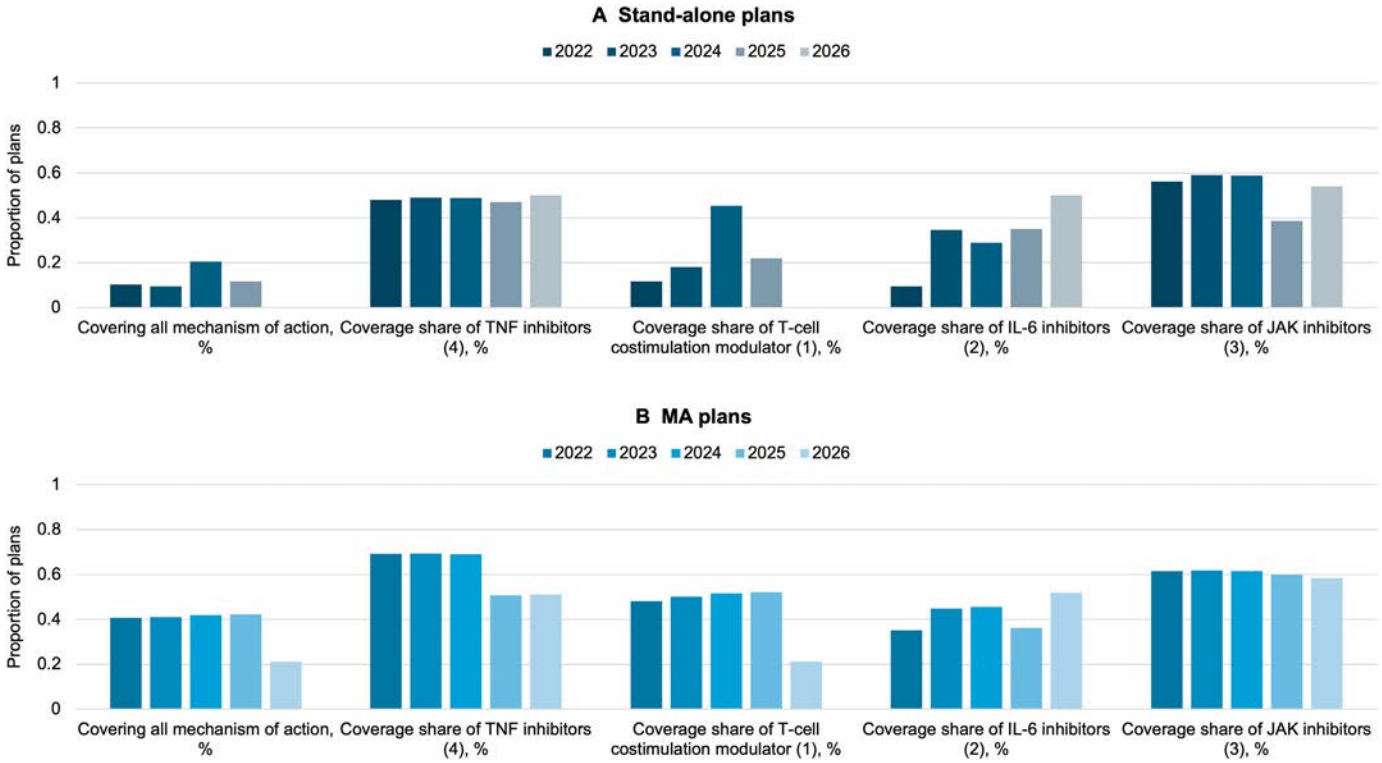


Figure 2. Trends in coverage generosity of disease-modifying therapy for relapsed rheumatoid arthritis between stand-alone and MA Part D plans, 2022–2025. The figure presents yearly trends in coverage generosity measures for stand-alone Part D plans (A) and MA Part D plans (B). To measure the breadth of coverage, we examined the share of plans covering at least one drug in each mechanism of action (TNF inhibitors, T cell costimulatory inhibitors, IL-6 inhibitors, and JAK inhibitors). We then calculated coverage share for each plan by dividing the number of covered drugs in each mechanism of action (numerator) by the total number of drugs in each class (denominator), as indicated by the number in parentheses. All estimates were clustered at the plan level to account for within-plan clustering over the study period and were weighted by plan enrollment in May of each year, giving plans with a larger number of beneficiaries greater weight. IL-6, interleukin-6; MA, Medicare Advantage; TNF, tumor necrosis factor. Color figure can be viewed in the online issue, which is available at http://onlinelibrary.wiley.com/doi/10.1002/art.70132/abstract.

broader coverage may preclude plans from using the prospect of formulary exclusion as leverage when negotiating price concessions from manufacturers. In a prior study, the average amount of rebates (ie, price discounts) for drugs belonging to the protected classes in Part D is lower than that for drugs in non-protected classes,[36] suggesting that more generous coverage of high-cost specialty medications such as DMARDs may come at the expense of increased drug spending by Medicare and its beneficiaries. This may also run counter to the desire of Part D plans to more tightly control formularies,[37,38] especially in the post-IRA period when plans are responsible for a greater share of catastrophic drug spending,[12] and may induce further volatility in the Part D market.[18] At the same time, it is necessary to account for the nuances of specific clinical contexts when ascertaining and weighting such trade-offs. In RA, exclusion of a single product could be clinically consequential because patients often receive multiple lines of therapy,[39] providing a stronger clinical rationale for ensuring broader coverage relative to other therapeutic areas featuring more substitutable treatments. Taken together, a more targeted, granular assessment of formulary adequacy may be needed to inform efforts to optimize coverage across drug classes.

We acknowledge several limitations. First, the descriptive nature of the study precludes any causal explanations for why stand-alone and MA Part D plans may cover self-administered DMARDs differently. Instead, the goal of this research was to generate hypotheses behind variations in coverage. Second, whether the observed coverage differences translate into actual differences in utilization and patient outcomes remains unknown but is a fruitful avenue for future research. Third, we did not estimate the costs of DMARDs across plan options and were unable to compare costs by treatment because they depend on specific plan benefit structure and the decision to use self-administered versus clinician-administered DMARDs. Fourth, because our results may not generalize to other therapeutic contexts, future studies investigating coverage disparities for other high-cost medications are needed to provide a more comprehensive understanding of formulary adequacy in Part D.

In this national study of Medicare Part D formularies, we found reductions in coverage of novel self-administered DMARDs in several mechanisms of action in recent periods and heterogeneity in coverage generosity between stand-alone and MA Part D plans, which may impact patient access to and affordability of RA treatment. Our findings underscore the importance of monitoring the adequacy of Part D formularies more closely, especially considering recent policy changes, such as the IRA, that have significantly impacted the Part D program.

AUTHOR CONTRIBUTIONS

All authors contributed to at least one of the following manuscript preparation roles: conceptualization AND/OR methodology, software, investigation, formal analysis, data curation, visualization, and validation AND drafting or reviewing/editing the final draft. As corresponding author, Dr Kwon confirms that all authors have provided the final approval of the version to be published and takes responsibility for the affirmations regarding article submission (eg, not under consideration by another journal), the integrity of the data presented, and the statements regarding compliance with institutional review board/Declaration of Helsinki requirements.

REFERENCES

1. Boytsov NN, Bhattacharya R, Saverno K, et al. Health care effect of disease-modifying antirheumatic drug use on patients with rheumatoid arthritis. J Manag Care Spec Pharm 2019;25(8):879–887. doi:https://doi.org/10.18553/jmcp.2019.25.8.879
2. Fraenkel L, Bathon JM, England BR, et al. 2021 American College of Rheumatology guideline for the treatment of rheumatoid arthritis. Arthritis Care Res (Hoboken) 2021;73(7):924–939. doi:https://doi.org/10.1002/acr.24596
3. Villeneuve E, Haraoui B. To switch or to change class—the biologic dilemma in rheumatoid arthritis. Nat Rev Rheumatol 2010;6(5):301–305. doi:https://doi.org/10.1038/nrrheum.2010.45
4. Polinski JM, Mohr PE, Johnson L. Impact of Medicare Part D on access to and cost sharing for specialty biologic medications for beneficiaries with rheumatoid arthritis. Arthritis Rheum 2009;61(6):745–754. doi:https://doi.org/10.1002/art.24560
5. Yazdany J, Dudley RA, Chen R, et al. Coverage for high-cost specialty drugs for rheumatoid arthritis in Medicare Part D. Arthritis Rheumatol 2015;67(6):1474–1480. doi:https://doi.org/10.1002/art.39079
6. Howlett J, Tamayo A. Arthritis patients resort to an inconvenient Medicare workaround to avoid pricey drugs. STAT. August 15, 2024. Accessed June 12, 2025. https://www.statnews.com/2024/08/15/medicare-coverage-gap-arthritis-drugs-humira-xeljanz-infliximab/
7. Chen CI, Wang L, Wei W, et al. Burden of rheumatoid arthritis among US Medicare population: co-morbidities, health-care resource utilization and costs. Rheumatol Adv Pract 2018;2(1):rky005. doi:https://doi.org/10.1093/rap/rky005
8. Cubanski J. A current snapshot of the Medicare Part D prescription drug benefit. KFF. October 9, 2024. Accessed June 26, 2025. https://www.kff.org/medicare/issue-brief/a-current-snapshot-of-the-medicare-part-d-prescription-drug-benefit/
9. Duddy-Tenbrunsel R, Sullivan M, OLaughlin C. Over half of Medicare Advantage beneficiaries enrolled in plans that require step therapy for new starts of Part B RA biologics in 2019. Avalere Health. July 1, 2019. Accessed August 15, 2025. https://advisory.avalerehealth.com/insights/over-half-of-medicare-advantage-beneficiaries-enrolled-in-plans-that-require-step-therapy-for-new-starts-of-part-b-ra-biologics-in-2019
10. Epstein RS. Payer perspectives on intravenous versus subcutaneous administration of drugs. Clinicoecon Outcomes Res 2021;13:801–807. doi:https://doi.org/10.2147/CEOR.S317687
11. Levine AA, Panzer AD, Kauf TL, et al. Specialty drug coverage varies between health plans' medical and pharmacy benefit policies. J Manag Care Spec Pharm 2023;29(6):607–613. doi:https://doi.org/10.18553/jmcp.2023.29.6.607
12. Dusetzina SB, Kwon Y, Keating NL, et al. Medicare Part D redesign savings may be lower for beneficiaries with spending below the out-of-pocket cap. Health Aff (Millwood) 2025;44(6):650–658. doi:https://doi.org/10.1377/hlthaff.2024.01527
13. US Centers for Medicare and Medicaid Services. Quarterly prescription drug plan formulary, pharmacy network, and pricing information. May 22, 2025. Accessed June 11, 2025. https://data.cms.gov/provider-summary-by-type-of-service/medicare-part-d-prescribers/quarterly-prescription-drug-plan-formulary-pharmacy-network-and-pricing-information
14. US Centers for Medicare and Medicaid Services. Formulary guidance. August 8, 2025. Accessed August 21, 2025. https://www.cms.gov/medicare/coverage/prescription-drug-coverage/formulary-guidance
15. Nelson SJ, Zeng K, Kilbourne J, et al. Normalized names for clinical drugs: RxNorm at 6 years. J Am Med Inform Assoc 2011;18(4):441–448. doi:https://doi.org/10.1136/amiajnl-2011-000116
16. USP Model Guidelines Expert Committee, US Pharmacopeia Staff. Narrative review: the U.S. Pharmacopeia and model guidelines for Medicare Part D formularies. Ann Intern Med 2006;145(6):448–453. doi:https://doi.org/10.7326/0003-4819-145-6-200609190-00008
17. US Centers for Medicare and Medicaid Services. Medicare Advantage/Part D contract and enrollment data. February 27, 2025. Accessed August 21, 2025. https://www.cms.gov/data-research/statistics-trends-and-reports/medicare-advantagepart-d-contract-and-enrollment-data
18. Cai CL, Kesselheim AS, Bhaskar A, et al. Insurer exits after the Inflation Reduction Act Part D redesign. JAMA 2025;334(4):360–362. doi:https://doi.org/10.1001/jama.2025.7289
19. McDermott MF. Rilonacept in the treatment of chronic inflammatory disorders. Drugs Today (Barc) 2009;45(6):423–430. doi:https://doi.org/10.1358/dot.2009.45.6.1378935
20. Cohen SB. The use of anakinra, an interleukin-1 receptor antagonist, in the treatment of rheumatoid arthritis. Rheum Dis Clin North Am 2004;30(2):365–380. doi:https://doi.org/10.1016/j.rdc.2004.01.005
21. Goll GL, Kvien TK. Biosimilar tocilizumab—better access and lower cost? Lancet Rheumatol 2024;6(1):e6–e8. doi:https://doi.org/10.1016/S2665-9913(23)00268-0
22. Desai RJ, Solomon DH, Jin Y, et al. Temporal trends in use of biologic DMARDs for rheumatoid arthritis in the United States: a cohort study of publicly and privately insured patients. J Manag Care Spec Pharm 2017;23(8):809–814. doi:https://doi.org/10.18553/jmcp.2017.23.8.809
23. Rubbert-Roth A, Szabó MZ, Kedves M, et al. Failure of anti-TNF treatment in patients with rheumatoid arthritis: the pros and cons of the early use of alternative biological agents. Autoimmun Rev 2019;18(12):102398. doi:https://doi.org/10.1016/j.autrev.2019.102398
24. O'Malley K. The Inflation Reduction Act and its Medicare Part B problem. Health Affairs Forefront. November 20, 2023. doi:https://doi.org/10.1377/forefront.20231117.71714
25. National Organization for Rare Disorders. Changes to Medicare for 2025 and beyond: important information for the rare disease community ahead of open enrollment. September 16, 2024. Accessed June 30, 2025. https://rarediseases.org/medicare-ira-changes/

26. Nguyen A, Li D. Being in the wrong Medicare Part D plan could cost over $800 per year. December 1, 2022. Accessed July 1, 2025. https://www.goodrx.com/healthcare-access/research/medicare-part-d-unrealized-savings
27. Ochieng N, Cubanski J, Freed M, et al. Nearly 7 in 10 Medicare beneficiaries did not compare plans during Medicare's open enrollment period. KFF. September 26, 2024. Accessed June 30, 2025. https://www.kff.org/medicare/nearly-7-in-10-medicare-beneficiaries-did-not-compare-plans-during-medicares-open-enrollment-period/
28. Bruine de Bruin W, Hodson N, Rabinovich L, et al. Medicare Part D beneficiaries' self-reported barriers to switching plans and making plan comparisons at all. Health Aff Sch 2024;2(11):qxae141. doi: https://doi.org/10.1093/haschl/qxae141
29. Marsh T, Li D. The big pinch: fewer medications covered, more restrictions on covered drugs. June 26, 2024. Accessed July 1, 2025. https://www.goodrx.com/insurance/health-insurance/the-big-pinch-fewer-prescription-drugs-covered-more-insurance-restrictions
30. Hwang TJ, Jain N, Lauffenburger JC, et al. Analysis of proposed Medicare Part B to Part D shift with associated changes in total spending and patient cost-sharing for prescription drugs. JAMA Intern Med 2019;179(3):374–380. doi:https://doi.org/10.1001/jamainternmed.2018.6417
31. American Journal of Managed Care. Cost considerations for self- vs HCP-administered agents. October 12, 2020. Accessed January 16, 2026. https://www.ajmc.com/view/cost-considerations-for-self-vs-hcp-administered-agents
32. Bittner B, Richter W, Schmidt J. Subcutaneous administration of biotherapeutics: an overview of current challenges and opportunities. BioDrugs 2018;32(5):425–440. doi:https://doi.org/10.1007/s40259-018-0295-0
33. Naci H, Kyriopoulos I, Feldman WB, et al. Coverage of new drugs in Medicare Part D. Milbank Q 2022;100(2):562–588. doi:https://doi.org/10.1111/1468-0009.12565
34. US Centers for Medicare and Medicaid Services. Medicare prescription drug benefit manual. January 15, 2016. Accessed June 28, 2025. https://www.cms.gov/medicare/prescription-drug-coverage/prescriptiondrugcovcontra/downloads/part-d-benefits-manual-chapter-6.pdf
35. Huskamp HA, Keating NL. The new Medicare drug benefit: potential effects of pharmacy management tools on access to medications. July 2004. Accessed June 28, 2025. https://www.kff.org/wp-content/uploads/2013/01/the-new-medicare-drug-benefit-potential-effects-of-pharmacy-management-tools-on-access-to-medications.pdf
36. Kakani P, Kyle MA, Chandra A, et al. Medicare Part D protected-class policy is associated with lower drug rebates. Health Aff (Millwood) 2024;43(10):1420–1427. doi:https://doi.org/10.1377/hlthaff.2024.00273
37. Medicare Access for Patient Rx. Hope for the best, prepare for the worst: the Inflation Reduction Act's unintended consequences for Medicare Part D in 2025 and 2026. August 23, 2024. Accessed November 23, 2024. https://maprx.info/wp-content/uploads/2024/08/MAPRx_whitepaper_2024-08-15_Final.pdf
38. EVERSANA. Special Report: Inflation Reduction Act sets Part D stakeholders scrambling. September 28, 2022. Accessed June 28, 2025. https://www.eversana.com/2022/09/28/special-report-inflation-reduction-act-sets-part-d-stakeholders-scrambling/
39. Lampner C. Switch or swap: strategies for anti-TNF failure in rheumatoid arthritis. Rheumatology Advisor. December 20, 2019. Accessed January 13, 2026. https://www.rheumatologyadvisor.com/features/switch-or-swap-strategies-for-anti-tnf-failure-in-rheumatoid-arthritis/

Check for updates

Arthritis & Rheumatology
Vol. 78, No. 10, October 2026, pp 2179–2182
© 2026 American College of Rheumatology

American College of Rheumatology
Empowering Rheumatology Professionals

LETTER

DOI 10.1002/art.70199

Entering the era of somatic variant sequencing in immune dysregulation: comment on the article by Fu et al

To the Editor:

We read with great interest the study by Fu et al, who systematically reanalyzed existing exome sequencing data for somatic variant analysis in 2,912 patients with genetically unresolved immune dysregulation.[1] This study represents a landmark contribution to the growing recognition of mosaic genetic errors of immunity (MEI) and provides a robust framework for large-scale somatic variant discovery.[2,3] Despite increasing awareness of this entity and its underlying mechanisms, the overall contribution of mosaic genetic variation in patients with nondiagnostic germline testing has remained uncertain. Addressing this gap, Fu et al report a diagnostic yield of 1.35% in adults and 0.98% in children, confirming that mosaicism is clinically relevant but accounts for only a modest fraction of unresolved disease.

Here, we aim to place the report by Fu et al in the context of two recent complementary US cohort studies with a similar design, published shortly beforehand. (Table 1).[4,5] Despite differences in cohort composition and age distribution, sequencing strategies, variant calling, and filtering approaches, all three studies converge on a comparable yield of (likely) causative and actionable variants. This highlights a reproducible diagnostic contribution of somatic mosaicism across the globe. Ghosh et al, using a similar whole exome sequencing (WES) re-analysis strategy, reported a yield of 1.4%, whereas Schmitz et al, applying high-depth targeted sequencing, reported an effective yield of ∼3%, despite a stringent VAF cutoff of 25%. Although these yields seem modest, they are clinically meaningful with potential therapeutic and prognostic relevance.

Table 1. Comparative overview of three large-scale studies of somatic variants in immune dysregulation*

	Fu et al 2026[1]	Ghosh et al 2026[5]	Schmitz et al 2026[4]
Cohort			
Patients, n	2,912	2,296	452
Included phenotypes	Autoinflammation (43%), autoimmunity (46.5%), immunodeficiency (10.5%)	Immune dysregulation or hematologic phenotypes (90%), bronchiectasis (10%)	Autoinflammation (14.6%), bone marrow failure (1.3%), immunodeficiency (29%), immune dysregulation (37.4%), lymphoproliferation (12.2%), malignancy (2.4%), unknown (3.1%)
Top 5 HPO terms	NR	Skin rash, asthma, allergic rhinitis, pneumonia, recurrent infections	Fever, lymphadenopathy, fatigue, splenomegaly, asthma
Healthy reference population	No	Yes, n = 359	Yes, n = 154
Demographics	China	United States	United States
Age distribution	< 18 y: n = 1,136 ≥18 y: n = 1,776	Blood samples: 36.1 y (median) Saliva samples: 49.9 y (median)	19.4 y (mean, range: 2 mo–68 y)
Sequencing approach			
DNA source	Peripheral blood	Blood and/or saliva	Peripheral blood (in some cases PBMC, PMN, monocytes or bone marrow)
Technique	WES (+ *in silico* 185-gene panel)	WES (+ *in silico* IEI panel)	TPS (71- and/or 101-gene panel)
Reported depth	∼100×	∼62× (blood), ∼87× (saliva)	∼3000–6000×
Variant callers used	Mutect2, HaplotypeCaller	LoFreq2, Mutect2	Mutect, DoCM, Varscan
VAF thresholds for somatic variant calling	<44.1% (autosomal genes) <100% (X-linked genes)	≤10th percentile of germline VAFs (∼0.35%)	1–25% (autosomal genes) <50% (X-linked genes)
Reported limit of detection, VAF, %	NR	≥3%	≥1%
Validation of mosaic variants	TPS	Sanger, ddPCR, TPS	ddPCR, TPS

(Continued)

Table 1. (*Cont'd*)

	Fu et al 2026[1]	Ghosh et al 2026[5]	Schmitz et al 2026[4]
Pathogenicity/clinical relevance scoring	Formal ACMG-based classification (P/LP); literature & manual expert curation	Curated gene list of known IEI genes; focus on previously reported pathogenic variants	Literature & manual expert curation; tailored scoring system: UMS, LMB, LMP, MP
Diagnostic yield			
(Likely) pathogenic/causal variants	1.35% (adults), 0.97% (children)	1.4%	∼3%
Reported genes[a]	*UBA1* (n = 12); ***KRAS*** (n = 10); ***TNFAIP3*** (n = 4); ***NRAS*** (n = 3); ***NLRP3*** (n = 2); ***CARD14*** (n = 1); NFKBIA (n = 1); NLRC4 (n = 1); STING1 (n = 1)	*KIT* (n = 11); ***NLRP3*** (n = 5); *JAK2* (n = 3); ***STAT3*** (n = 3); *NOD2* (n = 1); *JAK1* (n = 2); *TLR8* (n = 1); *STAT1* (n = 1); ***KRAS*** (n = 1); *ITGB2* (n = 1)	***STAT3*** (n = 5); ***TNFAIP3*** (n = 3); *FAS* (n = 3); *OAS1* (n = 2); ***NLRP3*** (n = 2); *SAMD9L* (n = 1); ***NRAS*** (n = 1); *TP53* (n = 1); *TLR8* (n = 1)
Reported VAF range, %	Autosomal genes: ∼1.32%–41.40% (autosomal genes); X-linked genes (*UBA1*): ∼3.63%–93.97%	Autosomal genes: ∼4.6%–37%; X-linked genes (*TLR8*): 12%	Autosomal genes: ∼1.1%–13%; X-linked genes (*TLR8*): ∼14.4%

* ACMG, American College of Medical Genetics and Genomics; ddPCR, droplet digital polymerase chain reaction; HPO, human phenotype ontology; IEI, inborn errors of immunity; LMB, likely mosaic benign; LMP, likely mosaic pathogenic; LP, likely pathogenic; MP, mosaic pathogenic; NR, not reported; P, pathogenic; PBMC, peripheral mononuclear blood cells; PMN, polymorphonuclear cells; TPS, targeted panel sequencing; UMS, uncertain mosaic significance; VAF, variant allele fraction; WES, whole exome sequencing.
[a] Overlapping genes reported in ≥2 studies are highlighted in bold. *TLR8* was not considered an overlapping gene, as the case reported by Schmitz et al[4] and Ghosh et al[5] represent the same patient.

At the biologic level, implicated genes vary across studies but consistently converge on *KRAS/NRAS*, *NLRP3*, *CARD14*, and *STAT3*, highlighting shared pathway vulnerabilities and pointing to additional MEI beyond the currently recognized set of ∼30 genes.[2,3] Notably, mosaic A20 haploinsufficiency emerges as a novel MEI across two cohorts, including cases of gonosomal transmission to offspring.[1,4] Emerging literature further supports more complex disease models, including digenic or multihit mechanisms and interactions with clonal hematopoiesis, suggesting that somatic variants act within broader clonal evolutionary contexts rather than as isolated events. Interestingly, Fu et al further provide longitudinal analyses of clonal dynamics in two patients with *NLRC4* and *KRAS* gain-of-function variants, respectively, suggesting gene-dosage effects and links between clonal burden and phenotype. Integrating these observations with existing literature, particularly on driver–passenger mechanisms and determinants of clonal expansion, may further advance insight into these processes.[2,6–9]

These comparisons highlight key technical trade-offs: exome-based approaches offer breadth but may miss low-VAF variants, whereas targeted deep sequencing improves sensitivity at the cost of genomic scope. All studies are further constrained by their focus on predefined gene sets, largely limited to known genes associated with monogenic immune dysregulation and dominant inheritance, potentially overlooking unknown or novel genes and alternative mechanisms such as somatic loss of heterozygosity. In addition, reliance on short-read sequencing may miss chromosomal alterations such as trisomy 8–associated autoinflammatory disease, as recently described.[10]

Collectively, these findings support a shift toward integrated germline–somatic approaches but also highlight the technical challenges and complexities in interpretation and clinical translation that must be addressed before routine implementation.

Dr Roosens is a fellow of the Fonds Wetenschappelijk Onderzoek–Vlaanderen National Fund for Scientific Research (FWO; 11PDZ24N). Dr Schrijvers' work was supported by an FWO Senior Clinical Investigator Fellowship (1805523N) and was a recipient of an FWO Junior Research Project Grant (G054022N, G0AHL25N). Dr Meyts is Senior Clinical Investigator at the Research Foundation FWO—Flanders and is supported by the Commonwealth Serum Laboratories Behring Chair of Primary Immunodeficiencies through KU Leuven, by the FWO grants G0C8517N, G0B5120N, and G0E8420N, and by the Jeffrey Modell Foundation.

Author disclosures are available at https://onlinelibrary.wiley.com/doi/10.1002/art.70199.

Willem Roosens, MD
Catho Colson, MD
KU Leuven, Department of Microbiology, Immunology and Transplantation, Allergy and Clinical Immunology Research Group
Leuven, Belgium
Isabelle Meyts, MD, PhD
KU Leuven, Department of Microbiology, Immunology and Transplantation, Laboratory of Inborn Errors of Immunity and UZ Leuven, Department of Pediatrics
Leuven, Belgium
Rik Schrijvers, MD, PhD
Rik.Schrijvers@uzleuven.be
KU Leuven, Department of Microbiology, Immunology and Transplantation, Allergy and Clinical Immunology Research Group and UZ Leuven, Department of Internal Medicine
Leuven, Belgium

1. Fu J, Fu Q, Wang J, et al. Landscape of somatic mutations in a large cohort of Chinese patients with immune dysregulations. Arthritis

Rheumatol 2026;78(9):1975–1988. doi:https://doi.org/10.1002/art.70126

2. Roosens W, Demeulemeester J, Legius E, et al. Emerging insights into mosaic errors of immunity. Trends Immunol 2026;47(2):130–146. doi:https://doi.org/10.1016/j.it.2025.09.003
3. Schmitz EG, Griffith M, Griffith OL, et al. Identifying genetic errors of immunity due to mosaicism. J Exp Med 2025;222(5):e20241045. doi:https://doi.org/10.1084/jem.20241045
4. Schmitz EG, Paul AJ, Ghosh R, et al. Targeted deep sequencing identifies mosaicism in patients with immune dysregulation. J Allergy Clin Immunol 2026;157(5):1179–1194. doi:https://doi.org/10.1016/j.jaci.2026.01.023
5. Ghosh R, Fazal Z, Oler AJ, et al; NIAID Centralized Sequencing Program. Clinical relevance of mosaic variants detected by exome sequencing. J Allergy Clin Immunol 2026;157(5):1195–1205. doi:https://doi.org/10.1016/j.jaci.2026.02.011
6. Forkgen J, Masle-Farquhar E, Fontaine Y, et al. Mosaic variants in KRAS and STAT5B associated with a mixed phenotype of 2 acquired errors of immunity. J Allergy Clin Immunol 2026;157(5):1218–1223.E3. doi:https://doi.org/10.1016/j.jaci.2026.01.018
7. De Langhe E, Van Loo S, Malengier-Devlies B, et al. TET2-Driver and NLRC4-passenger variants in adult-onset autoinflammation. N Engl J Med 2023;388(17):1626–1629. doi:https://doi.org/10.1056/NEJMc2212928
8. Shinar Y, Tohami T, Livneh A, et al. Acquired familial Mediterranean fever associated with a somatic MEFV mutation in a patient with JAK2 associated post-polycythemia myelofibrosis. Orphanet J Rare Dis 2015;10(1):86. doi:https://doi.org/10.1186/s13023-015-0298-6
9. Bonet N, Mascaro JM Jr, Hurtado-Navarro L, et al. Novel insights into the clinical features, genetic spectrum and clonal evolution of patients carrying NLRP3 mosaicism. J Clin Immunol 2025;45(1):134. doi:https://doi.org/10.1007/s10875-025-01922-x
10. Manthiram K, Xu Q, Wu Z, et al. Trisomy 8-associated autoinflammatory disease (TRIAD) is characterized by dysregulated myeloid cells. J Immunol 2023;210(S1):155.07. doi:https://doi.org/10.4049/jimmunol.210.Supp.155.07

DOI 10.1002/art.70226

Reply

To the Editor:

We sincerely thank Roosens et al for their positive evaluation of our study[1] and for recognizing the important role of somatic mutations in immune dysregulation. This comment systematically compares three recent cohort studies on somatic mutations, reporting diagnostic yields of approximately 1% to 3% obtained using different sequencing approaches, thereby highlighting the impact of sequencing methodologies on the detection rate of somatic mutations.[1–3]

Conventional whole-exome sequencing provides comprehensive coverage; however, somatic mutations may be missed by standard sequencing approaches if they are present in small clones. In contrast, targeted sequencing offers excellent sensitivity for detecting very low-frequency somatic variants.[4] Nevertheless, targeted approaches require restricting analysis to a predefined set of candidate genes, which may lead to the omission of potentially causative genes. In addition, structural variations require whole-genome sequencing (WGS) or other methods for reliable detection, whereas high-depth WGS remains prohibitively expensive. Therefore, the respective advantages and limitations of different sequencing strategies can significantly influence the diagnostic yield of somatic mutations. The widespread adoption of single-cell sequencing and the reduction in its cost will surely open up more possibilities in the mosaic genetic errors of immunity era.

The dynamic expansion and reduction of somatic mutations is of particular interest. Previous studies have suggested that driver mutations may promote the expansion of mutant clones, leading to an increased variant allele fraction[5]; however, the mechanisms underlying their decline remain unclear. In our study, we observed in one patient a marked increase in the proportion of somatic mutations during flare phases, followed by a clear decrease during nonflare periods. The factors driving this phenomenon warrant further investigation.

Currently, there are no established guidelines for determining whether somatic mutations are causative of monogenic immune dysregulation disorders. Although somatic variants are widespread in the human body, the vast majority are not pathogenic.[6] In our study, in conjunction with American College of Medical Genetics criteria, we applied a relatively stringent filtering strategy for somatic mutations, including only those variants with prior evidence of somatic pathogenicity or clear functional validation in the confirmed diagnosis category, whereas variants with uncertain functional significance were classified as secondary findings. Therefore, there is an urgent need for standardized guidelines to evaluate the role of somatic mutations in monogenic immune dysregulation disorders.

In a recent study, Nicola et al employed multiple sequencing approaches to demonstrate that somatic mutations in autoimmune lymphocytes may allow them to escape tolerance constraints through a polyclonal cascade of somatic evolution, providing new insights into the molecular basis of autoimmune disease.[4] This study suggests that somatic mutations play a role not only in monogenic immune disorders but potentially in a broad spectrum of immune diseases, highlighting the critical role of somatic mutations in disease pathogenesis.

We sincerely thank the editors and researchers for their recognition of our work. We hope that advances in the study of somatic mutations will enable more patients to receive timely diagnosis and appropriate treatment.

Author disclosures are available at https://onlinelibrary.wiley.com/doi/10.1002/art.70226.

Check for updates

Rheumatol 2026;78(9):1975–1988. doi:https://doi.org/10.1002/art.70126

2. Roosens W, Demeulemeester J, Legius E, et al. Emerging insights into mosaic errors of immunity. Trends Immunol 2026;47(2):130–146. doi:https://doi.org/10.1016/j.it.2025.09.003
3. Schmitz EG, Griffith M, Griffith OL, et al. Identifying genetic errors of immunity due to mosaicism. J Exp Med 2025;222(5):e20241045. doi:https://doi.org/10.1084/jem.20241045
4. Schmitz EG, Paul AJ, Ghosh R, et al. Targeted deep sequencing identifies mosaicism in patients with immune dysregulation. J Allergy Clin Immunol 2026;157(5):1179–1194. doi:https://doi.org/10.1016/j.jaci.2026.01.023
5. Ghosh R, Fazal Z, Oler AJ, et al; NIAID Centralized Sequencing Program. Clinical relevance of mosaic variants detected by exome sequencing. J Allergy Clin Immunol 2026;157(5):1195–1205. doi:https://doi.org/10.1016/j.jaci.2026.02.011
6. Forkgen J, Masle-Farquhar E, Fontaine Y, et al. Mosaic variants in KRAS and STAT5B associated with a mixed phenotype of 2 acquired errors of immunity. J Allergy Clin Immunol 2026;157(5):1218–1223.E3. doi:https://doi.org/10.1016/j.jaci.2026.01.018
7. De Langhe E, Van Loo S, Malengier-Devlies B, et al. TET2-Driver and NLRC4-passenger variants in adult-onset autoinflammation. N Engl J Med 2023;388(17):1626–1629. doi:https://doi.org/10.1056/NEJMc2212928
8. Shinar Y, Tohami T, Livneh A, et al. Acquired familial Mediterranean fever associated with a somatic MEFV mutation in a patient with JAK2 associated post-polycythemia myelofibrosis. Orphanet J Rare Dis 2015;10(1):86. doi:https://doi.org/10.1186/s13023-015-0298-6
9. Bonet N, Mascaro JM Jr, Hurtado-Navarro L, et al. Novel insights into the clinical features, genetic spectrum and clonal evolution of patients carrying NLRP3 mosaicism. J Clin Immunol 2025;45(1):134. doi:https://doi.org/10.1007/s10875-025-01922-x
10. Manthiram K, Xu Q, Wu Z, et al. Trisomy 8-associated autoinflammatory disease (TRIAD) is characterized by dysregulated myeloid cells. J Immunol 2023;210(S1):155.07. doi:https://doi.org/10.4049/jimmunol.210.Supp.155.07

DOI 10.1002/art.70226

Reply

To the Editor:

We sincerely thank Roosens et al for their positive evaluation of our study[1] and for recognizing the important role of somatic mutations in immune dysregulation. This comment systematically compares three recent cohort studies on somatic mutations, reporting diagnostic yields of approximately 1% to 3% obtained using different sequencing approaches, thereby highlighting the impact of sequencing methodologies on the detection rate of somatic mutations.[1–3]

Conventional whole-exome sequencing provides comprehensive coverage; however, somatic mutations may be missed by standard sequencing approaches if they are present in small clones. In contrast, targeted sequencing offers excellent sensitivity for detecting very low-frequency somatic variants.[4] Nevertheless, targeted approaches require restricting analysis to a predefined set of candidate genes, which may lead to the omission of potentially causative genes. In addition, structural variations require whole-genome sequencing (WGS) or other methods for reliable detection, whereas high-depth WGS remains prohibitively expensive. Therefore, the respective advantages and limitations of different sequencing strategies can significantly influence the diagnostic yield of somatic mutations. The widespread adoption of single-cell sequencing and the reduction in its cost will surely open up more possibilities in the mosaic genetic errors of immunity era.

The dynamic expansion and reduction of somatic mutations is of particular interest. Previous studies have suggested that driver mutations may promote the expansion of mutant clones, leading to an increased variant allele fraction[5]; however, the mechanisms underlying their decline remain unclear. In our study, we observed in one patient a marked increase in the proportion of somatic mutations during flare phases, followed by a clear decrease during nonflare periods. The factors driving this phenomenon warrant further investigation.

Currently, there are no established guidelines for determining whether somatic mutations are causative of monogenic immune dysregulation disorders. Although somatic variants are widespread in the human body, the vast majority are not pathogenic.[6] In our study, in conjunction with American College of Medical Genetics criteria, we applied a relatively stringent filtering strategy for somatic mutations, including only those variants with prior evidence of somatic pathogenicity or clear functional validation in the confirmed diagnosis category, whereas variants with uncertain functional significance were classified as secondary findings. Therefore, there is an urgent need for standardized guidelines to evaluate the role of somatic mutations in monogenic immune dysregulation disorders.

In a recent study, Nicola et al employed multiple sequencing approaches to demonstrate that somatic mutations in autoimmune lymphocytes may allow them to escape tolerance constraints through a polyclonal cascade of somatic evolution, providing new insights into the molecular basis of autoimmune disease.[4] This study suggests that somatic mutations play a role not only in monogenic immune disorders but potentially in a broad spectrum of immune diseases, highlighting the critical role of somatic mutations in disease pathogenesis.

We sincerely thank the editors and researchers for their recognition of our work. We hope that advances in the study of somatic mutations will enable more patients to receive timely diagnosis and appropriate treatment.

Author disclosures are available at https://onlinelibrary.wiley.com/doi/10.1002/art.70226.

Jinjian Fu, BS
Xiaomin Yu, PhD
yuxiaomin78@gmail.com
Life Sciences Institute, Zhejiang University, Department of Rheumatology, The Second Affiliated Hospital, Zhejiang University School of Medicine
and Liangzhu Laboratory of Zhejiang University, Department of Rheumatology,
Sir Run Run Shaw Hospital, Zhejiang University School of Medicine
Hangzhou, China
Jun Wang, PhD
Liangzhu Laboratory of Zhejiang University, Department of Rheumatology, Sir Run Run Shaw Hospital, Zhejiang University School of Medicine
Hangzhou, China
Qing Zhou, PhD
Life Sciences Institute, Zhejiang University, Department of Rheumatology, The Second Affiliated Hospital, Zhejiang University School of Medicine
Liangzhu Laboratory of Zhejiang University, Department of Rheumatology, Sir Run Run Shaw Hospital, Zhejiang University School of Medicine
Hangzhou, China
and State Key Laboratory of Common Mechanism Research for Major Diseases, Institute of Basic Medical Sciences & School of Basic Medicine, Chinese Academy of Medical Sciences & Peking Union Medical College
Beijing, China
Qiong Fu, MD
Department of Rheumatology, Renji Hospital, Shanghai Jiao Tong University School of Medicine
and Shanghai Immune Therapy Institute
Shanghai, China

1. Fu J, Fu Q, Wang J, et al. Landscape of somatic mutations in a large cohort of Chinese patients with immune dysregulations. Arthritis Rheumatol 2026;78(9):1975–1988. doi:https://doi.org/10.1002/art.70126
2. Ghosh R, Fazal Z, Oler AJ, et al; NIAID Centralized Sequencing Program. Clinical relevance of mosaic variants detected by exome sequencing. J Allergy Clin Immunol 2026;157(5):1195–1205. doi:https://doi.org/10.1016/j.jaci.2026.02.011
3. Schmitz EG, Paul AJ, Ghosh R, et al. Targeted deep sequencing identifies mosaicism in patients with immune dysregulation. J Allergy Clin Immunol 2026;157(5):1179–1194. doi:https://doi.org/10.1016/j.jaci.2026.01.023
4. Nicola PA, Lawson ARJ, Tidd A, et al. Polyclonal selection of immune checkpoint mutations in thyroid autoimmunity. Nature 2026. doi:https://doi.org/10.1038/s41586-026-10493-9
5. De Langhe E, Van Loo S, Malengier-Devlies B, et al. *TET2*-Driver and *NLRC4*-passenger variants in adult-onset autoinflammation. N Engl J Med 2023;388(17):1626–1629. doi:https://doi.org/10.1056/NEJMc2212928
6. Martincorena I, Campbell PJ. Somatic mutation in cancer and normal cells. Science 2015;349(6255):1483–1489. doi:https://doi.org/10.1126/science.aab4082